CATALYTIC NITRENE REACTIONS ENABLED BY DINUCLEAR NICKEL CATALYSTS

by

John M Andjaba

A Dissertation

Submitted to the Faculty of Purdue University

In Partial Fulfillment of the Requirements for the degree of

Doctor of Philosophy

Department of Chemistry

West Lafayette, Indiana

August 2021

THE PURDUE UNIVERSITY GRADUATE SCHOOL
STATEMENT OF COMMITTEE APPROVAL

Dr. Christopher Uyeda, Chair

Department of Chemistry

Dr. Suzanne Bart

Department of chemistry

Dr. Corey Thompson

Department of Chemistry

Dr. Jianguo Mei

Department of Chemistry

Approved by:

Dr. Christine Hrycyna

To my family

Pops, Mum, Mama C, David, Monica and Junior

"There's beauty in the struggle and ugliness in the success."
-Jermaine Cole

ACKNOWLEDGMENTS

I would preemptively like to say if I forget anyone in my acknowledgements—my bad, I appreciate you too! My family is the main source of inspiration and support in my life and I would not be anywhere near where I am without their guidance and patience. They are amazing and I thank them for everything they've helped me through. I would also like to acknowledge Dr. Christopher A. Bradley, my undergraduate research professor and my first mentor. He took a chance on mentoring me as a college freshman, knowing very well I knew nothing. He spent many hours explaining chemistry concepts and teaching me how to be a proficient synthetic organometallic chemist. I will not soon forget how the group would wait to hear the crack of a new soda to find out your location in the lab and the summers we carpooled together up to the The Mount. We shared great life stories and talked at length about hip-hop; but most importantly you convinced me to attend graduate school. Dr. Bradley is the reason why I grew to love chemistry and why this dissertation exists—so thank you Dr. Bradley.

I would also like to thank my graduate advisor Chris Uyeda. Chris has over the past five years showed an unimaginable amount of patience for me but has also set a high standard for me to aim for in being a world class scientist. As he knows, I came into grad school not doing too hot but somehow he believed in me and cultivated me into a strong scientist. While Chris doesn't often share his personal side, he has been there for me at my lowest lows (at the hospital with my teeth knocked in–woof) and at my highest highs (probably this). I will forever be in debt to you as a mentor and I truly aspire to be like him as a scientist. After all these years I will finally be able to use an en dash appropriately–I hope. Also, I promise choosing to work with two Chris' was not part of the plan.

I'd like to thank my fellow labmates and postdocs that have helped and supported me throughout the years: You-Yun, Arnab, Houng, Qiang Talia, Doug, Sudipta, Colby, Heather, Mike, Annah, Sourish, Vibha, Kristen, Kohei, Kyle, Wen, Mingxin, Courtney and Hayden. I'd particularly like to show my appreciation and shout out my graduate student mentor Ian Powers. His guidance through my first few years of graduate school put me on the research trajectory that I'm on and my success is largely in part due to him. Additionally, Conner, Shawn and Jake were great friends and labmates that I could share deeply personal things with as well as were great

examples of what a model scientist is. You guys are dope. I'd like to also thank all the people I've mentored as well: Chris (yes, there's a third Chris) the graduate student in the lab that helped me finish my main thesis work. I couldn't have finished it without you and you helped set me up for my future—I hope NapBithOx (NapButt) makes it. The two undergraduate students that worked with me: Kate and Allen, were instrumental in helping me learn how to mentor, patience and also how to make sure I actually knew what I was talking about. All the time spent in lab and the laughs we shared were the best.

The street dance community of Indiana has also been instrumental in my success in graduate school. Without the ability to express my happiness, sadness, success, and failures through breakdance I would have had a much more difficult time these past five years. Thank you to my OG Seoul for creating a space for us as dancers in Indiana to come, communicate, and grow as well as for all the lessons you taught me. I would lastly like to thank my closest friends, Isaac, Colin, Katie, Alisha, Micky, Mason, Anthony and Daniel. I've spent most of my years in graduate school away from my family and it was incredibly difficult. You all have been family to me and your support throughout the years of graduate school have helped me cope through the hard times and helped me succeed in ways you may or may not know—I love you all dearly.

TABLE OF CONTENTS

LIST OF TABLES

LIST OF FIGURES

ABSTRACT

Nitrenes are reactive intermediates that are known to generate high interest organic molecules. Due to their inherent instability, nitrenes are often stabilized by introducing them to transition metal complexes. Many transition metal stabilized nitrenes ($M=NR_2$) have been reported and some of these complexes have been shown to control nitrene reactivity and selectivity. Transition metal nitrene reactivity can be categorized into two main groups: bond-insertion and group transfer reactions. In the reference to the former, chapter one of this dissertation highlights using unique dinuclear Ni catalysts to generate nitrenes from aromatic azides. These Ni_2 nitrenes are used towards selective $C(sp^2)$−H bond amination in order to generate indole and carbazole derivatives. This work highlights the unique properties of the Ni_2 imide that enable a 1,2-addition pathway, which contrasts known bimetallic nitrene insertion reactions. A detailed mechanistic study, primarily using density functional theory (DFT) is the focus of this chapter.

Chapter two of this dissertation focuses on nitrene group transfer. In particular, this chapter highlights the ability of the dinuclear Ni catalyst $[^{i\text{-Pr}}NDI]Ni_2(C_6H_6)$ to react with aromatic azides to perform N=N coupling. A large scope of functional groups are tolerated in high yield with short reaction times. Catalyst comparison studies, studies on relevant catalytic intermediates for N=N coupling and reaction kinetics are shown in this chapter. Lastly, chapter three showcases the expansion of the nitrene group transfer ability of $[^{i\text{-Pr}}NDI]Ni_2(C_6H_6)$ to generate high molecular weight azopolymers from aromatic diazides. These azopolymers are generated from monomers often used in organic semi-conducting materials. End group control and post polymer functionalization are highlighted in this chapter. Lastly, this work showcases a new polymer, polyazoisoindigo, as the first organic semiconducting material that reversibly transitions from a colored to colorless state upon reduction.

CHAPTER 1. CATALYTIC C(SP^2)−H AMINATION REACTIONS USING DINICKEL IMIDES

1.1 Abstract

C−H amination reactions are valuable transformations for the construction of C−N bonds. Due to their relatively high bond dissociation energies, C(sp^2)−H bonds are generally not susceptible toward direct nitrene insertion, necessitating alternative mechanisms for C−H activation. Here, we report that cationic dinuclear (NDI)Ni_2 (NDI = naphthyridine−diimine) complexes catalyze intramolecular nitrene insertions into aryl and vinyl C(sp^2)− H bonds. Mechanistic studies suggest that a bridging imido ligand supported at a Ni_2 site induces C−H activation by a 1,2-addition pathway to generate an azametallacyclic intermediate. This organometallic mechanism contrasts with the electrocyclization/1,2-shift mechanism proposed for analogous transformations using Rh_2 catalysts. The implications of these mechanistic differences for the stereoselectivity and chemoselectivity of C−H amination are described.

1.2 Introduction

Cytochrome P450 enzymes promote C−H oxidation reactions using high-valent metal oxo species. The aza analogue of this process is unknown in biology but is of interest to synthetic chemists as a route to complex alkaloids and nitrogen-rich pharmaceutical compounds. In 1983, Breslow reported that Rh_2 catalysts promote the intramolecular amination of benzylic C−H bonds using nitrene equivalents derived from iminoiodinanes. This reaction is mechanistically related to Rh_2- catalyzed carbene transfer reactions4 and is proposed to access Rh_2=NR complexes as key intermediates (Figure 1). Two limiting pathways for C−H bond cleavage have been advanced: one that proceeds through a concerted three centered transition state and the other stepwise, involving an initial H atom abstraction followed by radical rebound to form the C−N bond. In both mechanisms, there is a correlation between the strength of a C−H bond and its propensity to undergo nitrene insertion.

Driver reported that Rh_2 catalysts also promote nitrene insertions into aromatic C−H bonds. This finding is notable due to the significantly higher bond dissociation energies of C(sp^2)−H vs C(sp^3)−H bonds, likely rendering the direct insertion and H atom abstraction pathways inaccessible. Indeed, mechanistic studies revealed that these reactions proceed by a different pathway, wherein the putative Rh_2=NAr intermediate undergoes a 4π-electrocyclic ring closure to first form the C−N bond. A rapid 1,2-hydride shift restores aromaticity and yields the product. This mechanism takes advantage of the electrophilic character of Rh_2=NR species in order to generate carbocation character at the position undergoing C−N bond formation.

Recently, we found that dinickel complexes can access an alternative mechanism for the intramolecular C−H amination reaction of biaryl azides. The Ni_2(μ-NAr) complex 1 was synthesized using m-terphenylazide as an imido precursor. Upon the addition of an exogenous ligand, such as t-BuNC or pyridine, a C−H bond of one of the phenyl substituents is activated to form a stable Ni_2(aryl)(μ-amido) species. This cyclometalated intermediate then undergoes C−N reductive elimination at elevated temperatures to yield 1-phenyl-9*H*-carbazole, the product of a net C−H amination process.

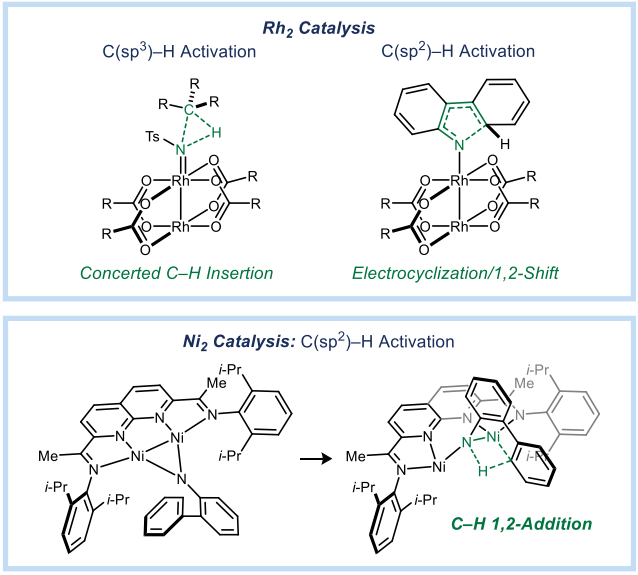

Figure 1.1 Mechanisms of C(sp^3)−H and C(sp^2)−H activation using Rh_2 and Ni_2 catalysts.

At the time, we were unable to render this process catalytic due to decomposition of the (NDI)Ni_2 system (NDI = naphthyridine−diimine) when it was heated in the presence of t-BuNC

or pyridine. Here, we report that (NDI)Ni_2 complexes in higher oxidation states function as efficient catalysts for C(sp^2)−H amination in the absence of ligand additives. Mechanistic studies indicate that C−H bond cleavage proceeds by a 1,2-addition mechanism rather than a 4π-electrocyclization/1,2-shift, as was observed for Rh_2 complexes. This difference in mechanism leads to differences in the selectivity profiles for these two classes of catalysts.

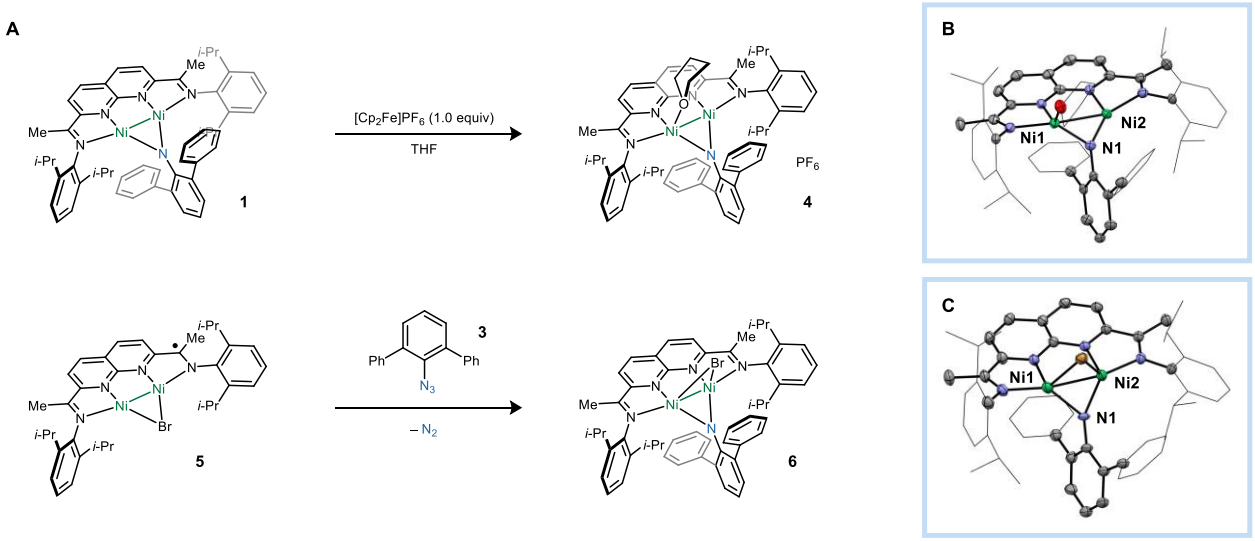

Figure 1.2. (a) Syntheses of S = 1/2 Ni_2(NAr) complexes. Selected bond distances for 1. Ni1–Ni2: 2.3415(9) Å, Ni1–N1: 1.768(2) Å, Ni2–N2: 1.784(3) Å. Σ of angles about N: 345°. (b) Selected bond distances for **4**. Ni1–Ni2: 2.515(1) Å, Ni1–N1: 1.885(4) Å, Ni2–N2: 1.735(4) Å. Σ of angles about N: 340°. (c) Selected bond distances for **6**: Ni1–Ni2: 2.430(1) Å, Ni1–N1: 1.973(6) Å, Ni2–N2: 1.996(6) Å. Σ of angles about N: 349°.

1.3 Preparation of Dinickel Imido Complexes Varying in Oxidation State and Charge

We began our studies by preparing a series of Ni_2(μ-NAr) (Ar = m-terphenyl) complexes with the goal of examining their relative ability to undergo intramolecular C–H amination (Figure 2a). The previously described ($^{i\text{-Pr}}$NDI)Ni_2(μ-NAr) complex **1** was synthesized from a reaction between ($^{i\text{-Pr}}$NDI)Ni_2(C_6H_6) (**2**) and m-terphenylazide (**3**). Cyclic volt-ammetry measurements of Ni_2(μ-NAr) **1** in THF (containing 0.3 M [n-Bu_4N]PF_6) indicate that it undergoes a reversible oxidation at potentials that are cathodic of the Cp_2Fe/Cp_2Fe^+ couple ($E_{1/2}$ = –1.9 V vs. Cp_2Fe/Cp_2Fe^+, ΔE_p = 140 mV). Accordingly, the cationic Ni_2(μ-NAr) complex **4** is accessible from its neutral counterpart using [Cp_2Fe]PF_6 (1.0 equiv) as a chemical oxidant.

The green paramagnetic cation **4** was precipitated from saturated THF solutions and yielded single crystalline material suitable for XRD analysis (Figure 1.2b). The solid-state structure of **4** features a THF ligand bound to Ni1. The most significant structural changes to the $Ni_2(\mu\text{-N})$ core upon oxidation are expansions in the Ni1–Ni2 and Ni1–N1 distances. The imido N also becomes moderately more pyramidalized as determined by the sum of the angle about N of 340° (vs. 345° in the neutral complex **1**). All of these metrical changes are consistent with a disruption in the three-centered/two-electron π-bonding in the $Ni_2(\mu\text{-N})$ fragment.

We were unable to obtain a reliable bulk measurement of the magnetic moment for **4** due to its decomposition to high-spin products during isolation. However, complex **4** displays a well-defined axial EPR signal that is suggestive of an $S = 1/2$ ground state (Figure 1.3b). The high degree of anisotropy in the frozen solution spectrum and the large shift in g_{avg} from that of the free electron are characteristic features of a Ni-centered radical. DFT models (BP86/6-311G(d,p) level of theory) corroborate this assignment. The $S = 1/2$ state is calculated to be more stable than the alternative $S = 3/2$ state by 9.8 kcal/mol, and the spin density plot for **4** (Figure 3a) shows that the unpaired electron is predominantly associated with the Ni atom bearing the THF ligand (92% of the total spin population).

The related charge-neutral $Ni_2(\mu\text{-NAr})Br$ complex **6** (Figure 1.2c) was prepared by a different synthetic route from the Ni_2Br complex **5** and *m*-terphenylazide (**3**). Like cation **4**, the $Ni_2(\mu\text{-NAr})Br$ complex **6** possesses an $S = 1/2$ ground state, assigned on the basis of its EPR spectrum. In the solid-state structure of **6**, both the imide and the Br ligands occupy a symmetrically bridging position between the two Ni atoms and are displaced above and below the $[NDI]Ni_2$ plane (Figure 1.2c).

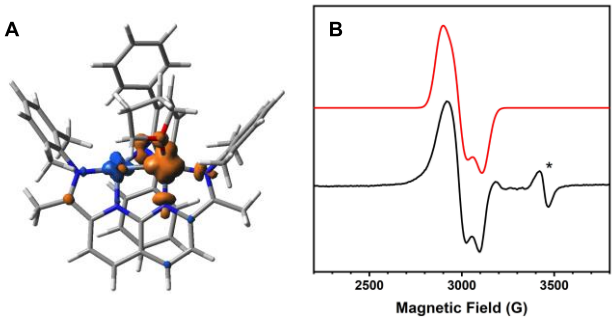

Figure 1.3. (a) Calculated spin density plot for [($^{i\text{-Pr}}$NDI)Ni_2(μ-Ar)(thf)]PF_6 complex **4**. (b) X-band EPR spectrum (black) and simulation (red) for **4** (THF, 5.9 K, g = [2.341, 2.206]). The asterisk denotes an S = 1/2 impurity in the sample.

1.4 Stoichiometric C–H Amination Reactions of Ni_2(μ-NAr) Complexes.

The redox pair of dinickel imido complexes exhibits divergent thermal reactivities (Figure 1.4). Extended heating of Ni_2(μ-NAr) complex **1** in C_6D_6 (80 °C, 16 h) induces its decomposition to carbazole **7** in a relatively low yield of 24%. The $Ni_2(C_6D_6)$ complex **2** is regenerated in 10% yield. The majority of the remaining mass balance appeared to be a new paramagnetic blue complex, which was identifiable by an isotropic signal at g = 2.07 in the room temperature EPR spectrum. We hypothesized that this S = 1/2 product might be a Ni_2(μ-NHAr) complex formed by a H-atom abstraction process that competes with the desired C–H amination. This proposal was corroborated by matching the EPR spectrum of the imido decomposition product to that of the authentic Ni_2(μ-NHAr) complex **8**, which was independently synthesized from a salt metathesis reaction between Ni_2Br complex **5** and potassium *m*-terphenylanilide (**9**) (Figure 1.5a). In the solid state structure of **8**, the *N*-H atom could be located in the difference map, and its presence was further inferred by the highly pyramidalized N (Σ of angles = 317°). The Ni_2(μ-NHAr) complex **8** possesses a rhombic EPR spectrum in frozen solution (Figure 1.5b), and DFT calculations suggest that the radical is delocalized between the two Ni atoms and the NDI π-system (Figure 5c).

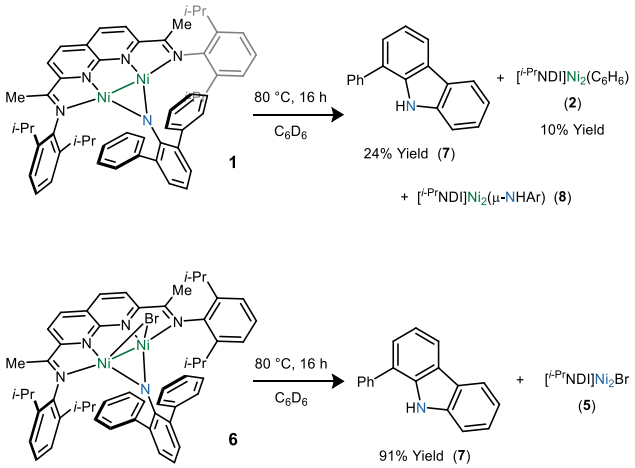

Figure 1.4. Relative C–H amination reactivities of ($^{i\text{-Pr}}$NDI)Ni_2(μ-NAr) (**1**) and ($^{i\text{-Pr}}$NDI)Ni_2(μ-NAr)Br (**6**).

In contrast to the Ni_2(μ-NAr) complex **1**, the oxidized Ni_2(μ-NAr)Br complex **6** undergoes high-yielding carbazole formation (91% yield) when heated at 80 °C for 16 h. The Ni_2Br complex **5** was detected by EPR spectroscopy as the primary metal-containing product. Overall, the oxidation state dependence in carbazole yield suggested that oxidized (NDI)Ni_2 complexes may serve as more viable platforms for the development of catalytic C–H amination reactions.

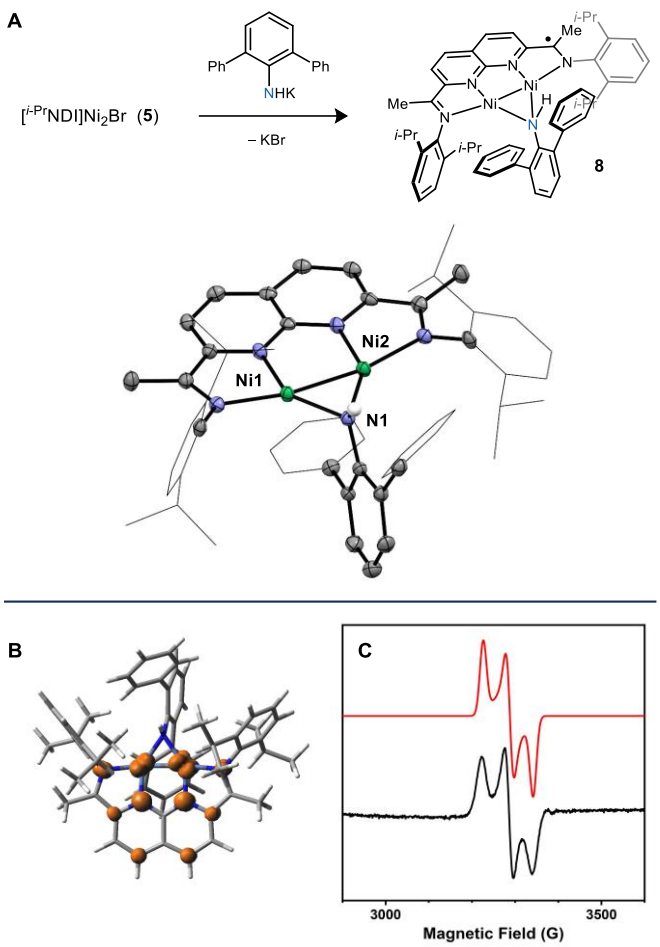

Figure 1.5. (a) Independent synthesis of ($^{i\text{-Pr}}$NDI)Ni$_2$(μ-NHAr) complex **8**. Selected bond distances for **8**. Ni1–Ni2: 2.2481(7) Å, Ni1–N1: 1.924(3) Å, Ni2–N1: 1.921(3) Å. Σ of angles about N: 317°. (b) Calculated spin density plot for complex 8. (c) X-band EPR spectrum (black) and simulation (red) for **8** (THF, 108 K, g = [2.105, 2.066, 2.032]).

1.5 Catalytic C–H Amination Reactions of Ni$_2$(μ-NAr) Complexes

Accordingly, we next examined the relative catalytic activities of the different Ni$_2$(μ-NAr) complexes using *m*-terphenylazide (**3**) as a model substrate (Table 1.1). At 10 mol% loading of **1** (80 °C, 72 h), carbazole **7** is formed in a low yield of 39% (entry 1). The major byproduct is aniline **10**, which represents 33% of the product mixture. Notably, Ni$_2$(μ-NHAr) complex **8** also provides comparable catalytic activity, suggesting that the amide can undergo a second H-atom abstraction to generate free aniline and re-enter the catalytic cycle (entry 2).

The Ni$_2$(μ-NAr)Br complex **5** is a substantially more efficient catalyst, providing carbazole **7** in 77% yield, with only 16% of competing aniline formation (entry 3). During catalysis, the

appearance of the paramagnetic ($^{i\text{-Pr}}$NDI)Ni_2Br_2 complex was observed by ^{1}H NMR, suggesting that a competing redox disproportionation may be a limiting factor in the C–H amination yield. Consistent with this observation, the halide-free cationic imido complex (**4**) proved to be the highest yielding catalyst. By increasing the reaction temperature to 110 °C, the yield was further optimized to 96%, even at a lower catalyst loading of 5 mol% (entry 5). The oxidized catalyst may also be generated *in situ* by reacting the $Ni_2(C_6H_6)$ precatalyst **2** with *m*-terphenylazide then oxidizing with $[Cp_2Fe]PF_6$. In addition to carbazole formation, the Ni_2 catalyst **4** is also efficient at forming indoles (**11** and **12**) through vinyl C–H activation processes.

Table 1.1. Ni_2-catalyzed C–H amination reactions of *m*-terphenyl azide (**3**).[a]

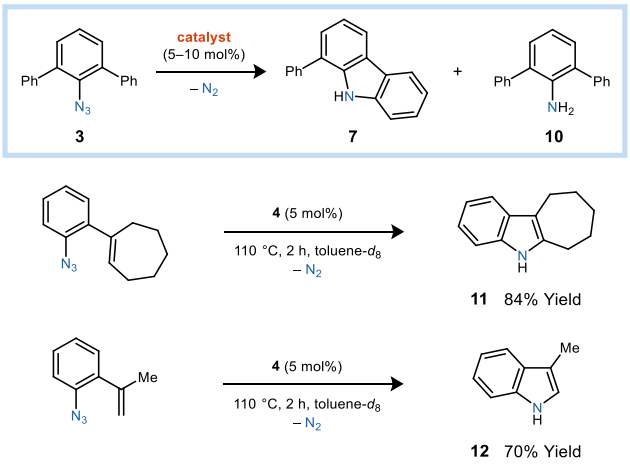

entry	catalyst	Yield of **7**	Yield of **10**
1	Ni_2(μ-NAr) **1**	39%	33%
2	Ni_2(μ-NHAr) **8**	44%	39%
3	Ni_2(μ-Br) **5**	77%	16%
4	$[Ni_2(\mu\text{-NAr})(thf)]^+$ **4**	89%	6%
5[b]	$[Ni_2(\mu\text{-NAr})(thf)]^+$ **4**	96%	<2%

[a]Reaction conditions: 10 mol% catalyst loading at 80 °C for 72 h. Yields of **7** and **10** were determined by 1H NMR integration against an internal standard. bReaction conditions: 5 mol% catalyst loading at 110 °C for 24 h.

1.6 Kinetic Isotope Effects

Kinetic isotope effect measurements (k_H/k_D) are used extensively to probe the mechanisms of C–H functionalization reactions. The deuterium-labelled competition substrate **3-*d*$_5$** was prepared and examined in the C–H amination catalyzed by **4** (Figure 1.6). The catalytic conversion of **3-*d*$_5$** displays a normal primary kinetic isotope effect of 4.3. By comparison, Driver previously examined a similar H/D competition substrate in the Rh_2-catalyzed process and found a k_H/k_D value of 1.01 due to the C–H bond cleavage occurring in a fast 1,2-shift following a slow and product-determining electrocyclization.

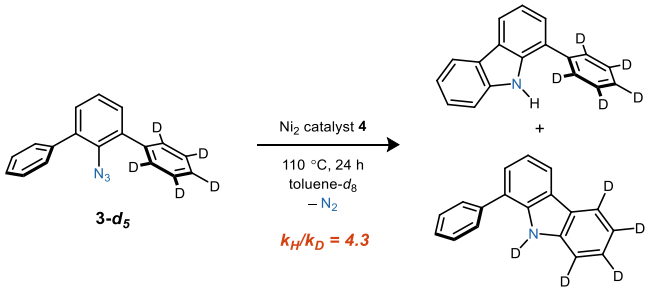

Figure 1.6. Kinetic isotope effects study. Catalytic amination of **3-*d*$_5$**.

1.7 Experiments Distinguishing Between Electrocyclization and 1,2-Addition Mechanisms

One unique feature of the electrocyclization mechanism in Rh_2 catalysis is that substrates such as **13**, which possess a substituent blocking the position that would undergo C(sp^2)–H activation, can still undergo cyclization (Figure 1.7a). For example, $Rh_2(esp)_2$ promotes the conversion of **13** to **14** by inducing a 1,2-shift of the ester substituent. An examination of substrate **13** under the Ni_2 catalyzed conditions revealed that none of product **14** is obtained after 2 h of reaction time at 110 °C, consistent with the inaccessibility of an electrocyclization mechanism.

Another hallmark of the electrocyclization mechanism is that vinyl C–H activations are insensitive to the stereochemistry of the alkene (Figure 1.7b).[8] For example, **15-*E*** and **15-*Z*** are converted to 2-phenylindole using Rh_2 catalysts in similar yields of 93% and 95%. By contrast, the Ni_2-catalyzed process is only viable when the C–H bond is in an appropriate orientation to undergo activation by the catalyst (*E*-stereochemistry of the alkene).

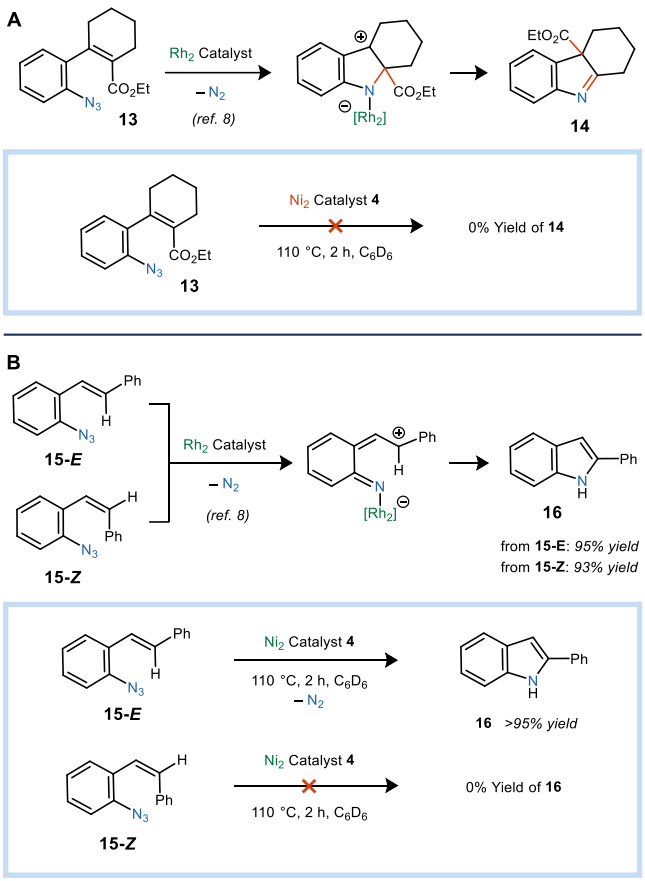

Figure 1.7. Experiments distinguishing between electrocyclization and 1,2-addition mechanisms. (a) Reactions of substrates in which nitrene C–H insertion is blocked by an ester substituent. (b) Experiments probing the stereospecificity of the nitrene insertion reactions.

1.8 Calculated Mechanisms for C–H Amination

The experiments described above indicate that the Ni_2 catalyzed amination occurs by a different mechanism than the previously described electrocyclization mechanism using Rh_2 catalysts. Thus, DFT calculations were performed in order to examine the detailed mechanism of C–H activation from the $[(^{i\text{-Pr}}\text{NDI})Ni_2(\mu\text{-NAr})(thf)]^+$ complex **4** (Figure 1.8). We identified an isomeric structure **4A** in which the Ni–Ni distance elongates to 3.16 Å, opening up a coordination site for the phenyl ring to bind in an η^2 fashion. This π-complex can further isomerize to a C–H σ-complex (**4B**), which was also found to be a local minimum on the potential energy surface. Consistent with the fact that neither **4A** nor **4B** were observed experimentally, their energies were calculated to lie above that of **4** (+11.8 kcal/mol and +13.6 kcal/mol, respectively).

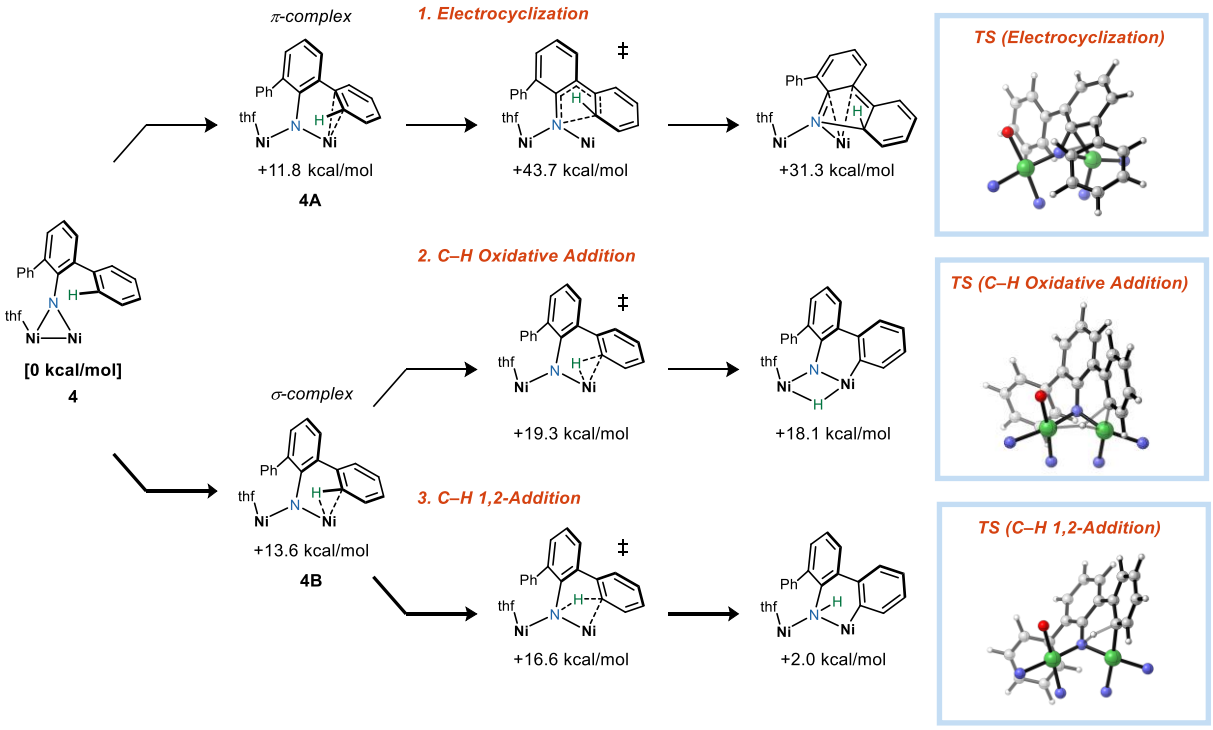

Figure 1.8. DFT models for the C–H activation mechanism from the [($^{i\text{-Pr}}$NDI)Ni$_2$(μ-NAr)(thf)]$^+$ complex **4**. Energies are ΔG values at 383 K relative to that of **4** in the *S* = 1/2 spin state (PCM(toluene)-BP86/6-311G(d,p)//BP86/6-311G(d,p) level of theory). *i*-Pr groups on the catalyst were truncated to Me groups in the model.

From here, we considered three pathways for C–H bond cleavage. The first pathway is akin to that of the Rh$_2$-catalyzed reaction and involves initial C–N bond-formation followed by a 1,2-hydride shift. A transition state for the electrophilic addition of the imido ligand to the phenyl group could be located but was found to be prohibitively high in energy. The calculated activation barrier for this step is 43.7 kcal/mol, which is inconsistent with the observed experimental rate of the reaction. By contrast, the C–H oxidative addition transition state is considerably lower in energy and possesses an activation barrier of only 19.3 kcal/mol. The product of this step contains a bridging hydride and a terminal aryl ligand. The C–H oxidative addition is calculated to be endothermic by 18.1 kcal/mol. Thus, to the extent that this process might be kinetically accessible, it is likely to be reversible.

The most favorable calculated mechanism for C–H activation was determined to be a 1,2-addition pathway in which an Ar–Ni bond is formed concurrently with deprotonation of the C–H bond by the imide. This mechanism is related to the concerted metalation–deprotonation processes that have been observed for other aromatic C–H activation reactions but has yet to be proposed for

a nitrene insertion. The calculated kinetic isotope effect for this step is 3.2, which is qualitatively in line with the experimental value of 4.3.

1.9 C(sp^2)–H Bond Chemoselectivity

In order to examine C(sp^2)–H bond chemoselectivity, the competition substrate **17** was synthesized (Figure 1.9a). Using $Rh_2(esp)_2$ as a catalyst, a 1:1.6 mixture of vinyl carbazole **19** to phenyl indole **18** was obtained, indicating a modest preference for vinyl C–H amination. By contrast, Ni_2 catalyst **4** afforded a >20:1 selectivity for phenyl indole (**18**) formation. This high degree of selectivity was reproduced in DFT calculations, and the 1,2-addition transition state for vinyl C–H activation was predicted to be 9.1 kcal/mol more favorable than that for aryl C–H activation (Figure 1.9b).

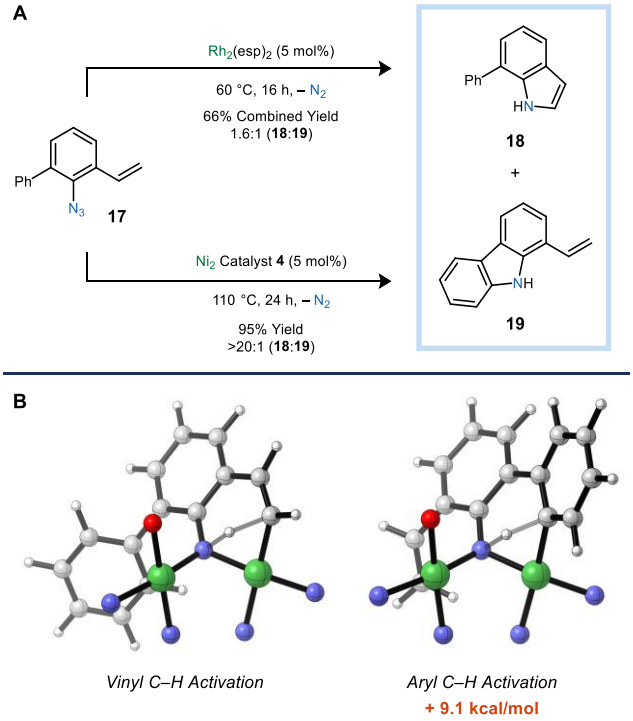

Figure 1.9. (a) Comparison of vinyl vs. aryl C–H amination using Rh_2 and Ni_2 catalysts. (b) DFT models for vinyl vs. aryl C–H activation using Ni_2 catalyst **4** (*S* = 1/2 surface). Relative energies of the two transition states are ΔG values at 383 K (BP86/6-311G(d,p) level of theory).

1.10 Conclusion

In summary, Ni_2 imido complexes activate C(sp^2)–H bonds by a distinct organometallic mechanism that differs from the electrocyclization processes previously described for Rh_2-catalyzed reactions. These mechanisms may be distinguished experimentally by kinetic isotope effect measurements, alkene stereoselectivity studies, and probes for 1,2-migration events. Additionally, the C–H 1,2-addition process enables highly selective nitrene insertions into olefinic C–H bonds in the presence of competing aromatic C–H bonds.

1.11 Acknowledgements

This research was supported by the U.S. National Science Foundation (CHE-1554787). I.G.P. is an NSF Graduate Re-search Fellow. J.M.A. is a Purdue University Department of Chemistry Charles H. Viol Memorial Fellow. C.U. is an Alfred. P. Sloan Research Fellow and a Camille Dreyfus Teacher–Scholar.

1.12 References

(1) (a) Meunier, B.; de Visser, S. P.; Shaik, S. "Mechanism of oxidation reactions catalyzed by cytochrome P450 enzymes" *Chem. Rev.* **2004**, *104*, 3947-3980; (b) Rittle, J.; Green, M. T. "Cytochrome P450 compound I: Capture, characterization, and C-H bond activation kinetics" *Science* **2010**, *330*, 933-937; (c) Poulos, T. L. "Heme enzyme structure and function" *Chem. Rev.* **2014**, *114*, 3919-3962.

(2) (a) Collet, F.; Dodd, R. H.; Dauban, P. "Catalytic C-H amination: Recent progress and future directions" *Chem. Commun.* **2009**, 5061-5074; (b) Dequirez, G.; Pons, V.; Dauban, P. "Nitrene chemistry in organic synthesis: Still in its infancy?" *Angew. Chem., Int. Ed.* **2012**, *51*, 7384-7395; (c) Yamaguchi, J.; Yamaguchi, A. D.; Itami, K. "C-H bond functionalization: Emerging synthetic tools for natural products and pharmaceuticals" *Angew. Chem., Int. Ed.* **2012**, *51*, 8960-9009; (d) Roizen, J. L.; Harvey, M. E.; Du Bois, J. "Metal-catalyzed nitrogen-atom transfer methods for the oxidation of aliphatic C–H bonds" *Acc. Chem. Res.* **2012**, *45*, 911-922; (e) Shin, K.; Kim, H.; Chang, S. "Transition-metal-catalyzed C–N bond forming reactions using organic azides as the nitrogen source: A journey for the mild and versatile C–H amination" *Acc. Chem. Res.* **2015**, *48*, 1040-1052.

(3) Breslow, R.; Gellman, S. H. "Intramolecular nitrene carbon-hydrogen insertions mediated by transition-metal complexes as nitrogen analogs of cytochrome P-450 reactions" *J. Am. Chem. Soc.* **1983**, *105*, 6728-6729.

(4) (a) Nakamura, E.; Yoshikai, N.; Yamanaka, M. "Mechanism of C−H bond activation/C−C bond formation reaction between diazo compound and alkane catalyzed by dirhodium tetracarboxylate" *J. Am. Chem. Soc.* **2002**, *124*, 7181-7192; (b) Berry, J. F. "The role of three-center/four-electron bonds in superelectrophilic dirhodium carbene and nitrene catalytic intermediates" *Dalton Trans.* **2012**, *41*, 700-713.

(5) Varela-Álvarez, A.; Yang, T.; Jennings, H.; Kornecki, K. P.; Macmillan, S. N.; Lancaster, K. M.; Mack, J. B. C.; Du Bois, J.; Berry, J. F.; Musaev, D. G. "Rh_2(II,III) catalysts with chelating carboxylate and carboxamidate supports: Electronic structure and nitrene transfer reactivity" *J. Am. Chem. Soc.* **2016**, *138*, 2327-2341.

(6) (a) King, E. R.; Hennessy, E. T.; Betley, T. A. "Catalytic C−H bond amination from high-spin iron imido complexes" *J. Am. Chem. Soc.* **2011**, *133*, 4917-4923; (b) Laskowski, C. A.; Miller, A. J. M.; Hillhouse, G. L.; Cundari, T. R. "A two-coordinate nickel imido complex that effects C−H amination" *J. Am. Chem. Soc.* **2011**, *133*, 771-773; (c) Wiese, S.; McAfee, J. L.; Pahls, D. R.; McMullin, C. L.; Cundari, T. R.; Warren, T. H. "C–H functionalization reactivity of a nickel–imide" *J. Am. Chem. Soc.* **2012**, *134*, 10114-10121; (d) Aguila, M. J. B.; Badiei, Y. M.; Warren, T. H. "Mechanistic insights into C–H amination via dicopper nitrenes" *J. Am. Chem. Soc.* **2013**, *135*, 9399-9406; (e) Hennessy, E. T.; Betley, T. A. "Complex N-heterocycle synthesis via iron-catalyzed, direct C–H bond amination" *Science* **2013**, *340*, 591-595.

(7) (a) Stokes, B. J.; Dong, H.; Leslie, B. E.; Pumphrey, A. L.; Driver, T. G. "Intramolecular C−H amination reactions: Exploitation of the Rh_2(II)-catalyzed decomposition of azidoacrylates" *J. Am. Chem. Soc.* **2007**, *129*, 7500-7501; (b) Stokes, B. J.; Jovanović, B.; Dong, H.; Richert, K. J.; Riell, R. D.; Driver, T. G. "Rh_2(II)-catalyzed synthesis of carbazoles from biaryl azides" *J. Org. Chem.* **2009**, *74*, 3225-3228.

(8) Stokes, B. J.; Richert, K. J.; Driver, T. G. "Examination of the mechanism of Rh_2(II)-catalyzed carbazole formation using intramolecular competition experiments" *J. Org. Chem.* **2009**, *74*, 6442-6451.

(9) Powers, I. G.; Kiattisewee, C.; Mullane, K. C.; Schelter, E. J.; Uyeda, C. "A 1,2-addition pathway for C(sp^2)−H activation at a dinickel imide" *Chem.-Eur. J.* **2017**, *23*, 7694-7697.

(10) (a) Jiao, J.; Murakami, K.; Itami, K. "Catalytic methods for aromatic C–H amination: An ideal strategy for nitrogen-based functional molecules" *ACS Catal.* **2016**, *6*, 610-633; (b) Tsang, W. C. P.; Zheng, N.; Buchwald, S. L. "Combined C−H functionalization/C−N bond formation route to carbazoles" *J. Am. Chem. Soc.* **2005**, *127*, 14560-14561; (c) Jordan-Hore, J. A.; Johansson, C. C. C.; Gulias, M.; Beck, E. M.; Gaunt, M. J. "Oxidative Pd(II)-catalyzed C−H bond amination to carbazole at ambient temperature" *J. Am. Chem. Soc.* **2008**, *130*, 16184-16186; (d) Takamatsu, K.; Hirano, K.; Satoh, T.; Miura, M. "Synthesis of carbazoles by copper-catalyzed intramolecular C–H/N–H coupling" *Org. Lett.* **2014**, *16*, 2892-2895; (e) Alt, I. T.; Plietker, B. "Iron-catalyzed intramolecular C(sp^2)−H amination" *Angew. Chem., Int. Ed.* **2016**, *55*, 1519-1522.

(11) (a) Walsh, P. J.; Hollander, F. J.; Bergman, R. G. "Generation, alkyne cycloaddition, arene carbon-hydrogen activation, nitrogen-hydrogen activation and dative ligand trapping reactions of the first monomeric imidozirconocene (Cp_2Zr:NR) complexes" *J. Am. Chem. Soc.* **1988**, *110*, 8729-8731; (b) Cummins, C. C.; Baxter, S. M.; Wolczanski, P. T. "Methane and benzene activation via transient (tert-$Bu_3SiNH)_2Zr$:NSi-tert-Bu_3" *J. Am. Chem. Soc.* **1988**, *110*, 8731-8733; (c) Bennett, J. L.; Wolczanski, P. T. "Selectivities in hydrocarbon activation: Kinetic and thermodynamic investigations of reversible 1,2-Rh-elimination from $(silox)_2(tBu_3SiNH)TiR$ (silox = tBu_3SiO)" *J. Am. Chem. Soc.* **1997**, *119*, 10696-10719; (d) Schaller, C. P.; Cummins, C. C.; Wolczanski, P. T. "Hydrocarbon activation via reversible 1,2-RH-elimination from $(tBu_3SiNH)_3ZrR$: Synthetic, structural, and mechanistic investigations" *J. Am. Chem. Soc.* **1996**, *118*, 591-611; (e) Cundari, T. R.; Grimes, T. V.; Gunnoe, T. B. "Activation of carbon−hydrogen bonds via 1,2-addition across M−X (X = OH or NH_2) bonds of d^6 transition metals as a potential key step in hydrocarbon functionalization: A computational study" *J. Am. Chem. Soc.* **2007**, *129*, 13172-13182; (f) Pierpont, A. W.; Cundari, T. R. "Computational study of methane C−H activation by first-row late transition metal $L_nM{=}E$ (M: Fe, Co, Ni) complexes" *Inorg. Chem.* **2010**, *49*, 2038-2046.

(12) Zhou, Y.-Y.; Hartline, D. R.; Steiman, T. J.; Fanwick, P. E.; Uyeda, C. "Dinuclear nickel complexes in five states of oxidation using a redox-active ligand" *Inorg. Chem.* **2014**, *53*, 11770-11777.

(13) Lin, C.-Y.; Power, P. P. "Complexes of Ni(I): A “rare” oxidation state of growing importance" *Chem. Soc. Rev.* **2017**, *46*, 5347-5399.

(14) Kong, C.; Driver, T. G. "Rh_2(II)-catalyzed ester migration to afford 3H-indoles from trisubstituted styryl azides" *Org. Lett.* **2015**, *17*, 802-805.

(15) (a) Gorelsky, S. I.; Lapointe, D.; Fagnou, K. "Analysis of the concerted metalation-deprotonation mechanism in palladium-catalyzed direct arylation across a broad range of aromatic substrates" *J. Am. Chem. Soc.* **2008**, *130*, 10848-10849; (b) David, L.; Keith, F. "Overview of the mechanistic work on the concerted metallation–deprotonation pathway" *Chemistry Letters* **2010**, *39*, 1118-1126; (c) Ackermann, L. "Carboxylate-assisted transition-metal-catalyzed C−H bond functionalizations: Mechanism and scope" *Chem. Rev.* **2011**, *111*, 1315-1345.

CHAPTER 2. CATALYTIC AZOARENE SYNTHESIS FROM ARYL AZIDES ENABLED BY A DINUCLEAR NI COMPLEX

2.1 Abstract

Azoarenes are valuable chromophores that have been extensively incorporated as photoswitchable elements in molecular machines and biologically active compounds. Here, we report a catalytic nitrene dimerization reaction that provides access to structurally and electronically diverse azoarenes. The reaction utilizes aryl azides as nitrene precursors and generates only gaseous N_2 as a byproduct. By circumventing the use of a stoichiometric redox reagent, a broad range of organic functional groups are tolerated, and common byproducts of current methods are avoided. A catalyst featuring a Ni—Ni bond is found to be uniquely effective relative to those containing only a single Ni center. The mechanistic origins of this nuclearity effect are described.

2.2 Introduction

Azoarenes represent an important class of organic chromophores distinguished for their ability to function as photoswitches.[1] At equilibrium in the dark, azoarenes reside predominantly in their thermodynamically preferred *trans* geometry; however, upon excitation at their π–π* or n–π* absorption bands, a substantial fraction of the less stable *cis* form can be generated.[2] This isomerization has been utilized in molecular machines, probes, and therapeutics as a mechanism to trigger conformational changes using incident visible or UV light.[3] While early physical studies of azoarene photoswitching behavior were conducted on simple model compounds, including azobenzene itself,[2a] the motivation to incorporate these functionalities into more complex systems necessitates the development of new synthetic methods that ideally achieve N=N coupling under mild conditions, in high yield, and with broad substrate scope.

Certain classes of azoarenes are accessible by substitution reactions between nucleophilic arenes and electrophilic diazonium ions; however, symmetrical azoarenes are more commonly

prepared by homodimerization methods that involve an oxidation state adjustment of a nitrogen-containing precursor, which then induces N=N bond formation.[4] For example, anilines can be oxidized with reagents such as $KMnO_4$, MnO_2, Ag_2O, or O_2/KO*t*-Bu to form azoarenes.[5] Alternatively, nitroarenes can be reductively coupled using Zn or a hydride source.[6] Despite this diversity of redox-based approaches, N=N coupling is commonly a low-yielding step in the preparation of highly functionalized photoswitches. Furthermore, the limitations of current methods can necessitate that additional synthetic manipulations be performed following installation of the N=N bond to reach a given target molecule.[7]

In principle, many of these challenges may be addressed by considering an alternative redox-neutral dimerization of a nitrene precursor. Free aryl nitrenes can be liberated from the photolysis or pyrolysis of aryl azides.[8] Singlet aryl nitrenes predominantly decompose by ring-expansion to form unstable dehydroazepines, which then undergo poorly defined polymerization reactions. In competition with this process, intersystem crossing generates triplet nitrenes, which can dimerize by N=N coupling but are often sufficiently reactive to abstract H-atoms from the reaction medium to form anilines.

Transition metal catalysis provides an avenue to achieve selective N=N coupling through the intermediacy of metal-stabilized nitrenes (Figure 2.1). While M=NR complexes have been extensively studied over the past few decades,[9] systems that catalytically generate azoarenes are rare, and methods that achieve broad scope and high efficiency have yet to emerge.[10,11] Many transition metal imides react with aryl azides to form tetrazene complexes that are resistant to N_2 loss.[12] Cenini first noted that azoarenes were generated as minor byproducts of benzylic C–H amination reactions catalyzed by Co(porphyrin) complexes. Peters subsequently demonstrated that an Fe catalyst bearing a trisphosphinesilyl (SiP_3) ligand could achieve improved selectivities for N=N coupling (up t0 57% yield) over C–H abstraction for electronically neutral or electron-rich aryl azides.[10b] Additionally, Groysman reported a $Fe(OC$*t*$-Bu_2Ph)_2$ complex, which promotes the dimerization of ortho-disubstituted aryl azides (e.g., mesityl azide or 2,6-diethylphenyl azide).[10d] Less hindered substrates form dimeric $M_2(\mu\text{-}NAr)_2$ complexes that do not undergo N=N coupling.

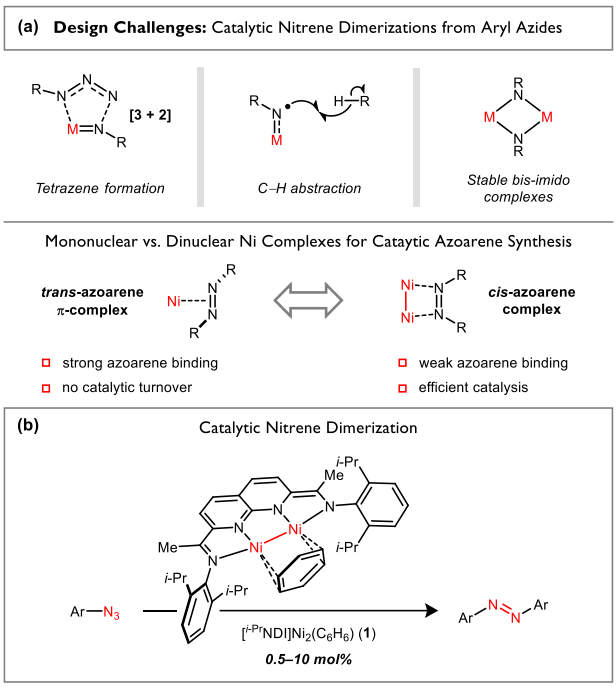

Figure 2.1. (a) Design challenges associated with transition metal-catalyzed nitrene dimerization reactions. (b) The identification of a dinuclear Ni catalyst for the conversion of aryl azides to azoarenes.

We postulated that Ni complexes might be capable of promoting the catalytic coupling of aryl azides based on reactivity studies reported by Hillhouse. The (dtbpe)Ni=NMes complex (dtbpe = 1,2-bis(di-*tert*-butylphosphino)ethane) was shown to react with mesityl azide at room temperature to form azomesitylene.[13] Despite the high yield of this stoichiometric process, the strong binding of the Ar_2N_2 product to Ni(0) precluded catalytic turnover. Here, we report that a dinuclear Ni complex (**1**)[14] is capable of overcoming this challenge associated with product inhibition, leading to the development of a general method for the catalytic dimerization of aryl nitrenes.

2.3 Comparison of Mononuclear and Dinuclear Ni Catalysts for Aryl Nitrene Dimerization.

We initiated our studies by surveying Ni catalysts (Table 2.1) for the dimerization of a model aryl azide substrate (**2**). Zero-valent Ni complexes bearing monodentate phosphine or NHC ligands (entries 3–4) were found to be unsuitable as catalysts due to competing nitrene transfer to the ligand. For example, $Ph_3P/Ni(COD)_2$ promoted significant conversion of aryl azide **2** but yielded none of the desired azoarene. NMR analysis of the resulting reaction mixture revealed the

formation of a new organic species, which was assigned as the Ph_3P=NAr product (Ar = 4-trifluoromethylphenyl; ^{31}P = 3.29 ppm)[15] by comparison to an authentic sample prepared from Ph_3P and **2** in the absence of Ni. Similar observations were made using the IPr ligand.

Table 2.1. Catalyst Comparison Studies[a]

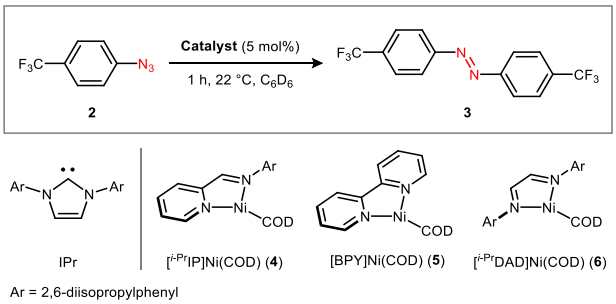

entry	catalyst	conversion	yield
1	none	<2%	<2%
2	$Ni(COD)_2$	24%	<2%
3[b]	$Ni(COD)_2$ + PPh_3	35%	<2%
4[c]	$Ni(COD)_2$ + IPr	32%	<2%
5	[$^{i\text{-Pr}}$IP]Ni(COD) (**4**)	24%	13%
6	[BPY]Ni(COD) (**5**)	23%	13%
7	[$^{i\text{-Pr}}$DAD]Ni(COD) (**6**)	<2%	<2%
8	[$^{i\text{-Pr}}$NDI]$Ni_2(C_6H_6)$ (**1**)	>98%	90%
9[d]	[$^{i\text{-Pr}}$NDI]$Ni_2(C_6H_6)$ (**1**)	>98%	96%

[a]Conversions of **2** and yields of **3** were determined by ^1H NMR integration against an internal standard. [b]5 mol% $Ni(COD)_2$ and 28 mol% PPh_3. [c]5 mol% $Ni(COD)_2$ and 14 mol% IPr. [d]0.5 mol% catalyst **1**.

Measurable yields of azoarene **3** were obtained using Ni complexes of bidentate N-donor ligands (Table 2.1, entries 5–6). For example, the [$^{i\text{-Pr}}$IP]Ni(COD) catalyst (**4**) provided **3** in 13% yield after 1 h at room temperature (76% recovery of starting material). There is no additional conversion after this time, even after heating at 80 °C for 1 h, suggesting that the catalyst is susceptible to rapid inactivation. Accordingly, the catalytic reaction with [$^{i\text{-Pr}}$IP]Ni(COD) (**4**)

produces a new diamagnetic Ni complex (**7**), which could be independently synthesized in a stoichiometric reaction between **4** (1.0 equiv) and aryl azide **2** (2.0 equiv). The identity of **7** was assigned by XRD analysis as an azoarene π-complex (Figure 2.2). The bound azoarene adopts its more stable *trans* geometry (□C–N=N–C = 156.6(2)°), and the N=N distance (1.403(3) Å) is elongated from the characteristic bond length of a free azoarene (N=N distance for azobenzene: 1.26 Å),[16] suggesting a high degree of π-back-bonding from the electron-rich Ni center. Consistent with studies reported by Hillhouse using the (dtbpe)Ni system,[13] the stability of this π-complex prevents catalytic turnover. When isolated [$^{i\text{-Pr}}$IP]Ni(Ar_2N_2) **7** is treated with **2** (20 equiv), no consumption of the aryl azide is observed.

The dinuclear Ni catalyst **1** bears a structurally and electronically related nitrogen-based donor set to complexes **4**–**6** but exhibits substantially higher catalytic efficiency for nitrene dimerization. At 5 mol% loading, full conversion of aryl azide **2** to azoarene **3** (90% yield) is achieved after 1 h at 22 °C. The catalyst loading can also be decreased to 0.5 mol% without sacrificing catalytic efficiency (96% yield after 1 h at 22 °C).

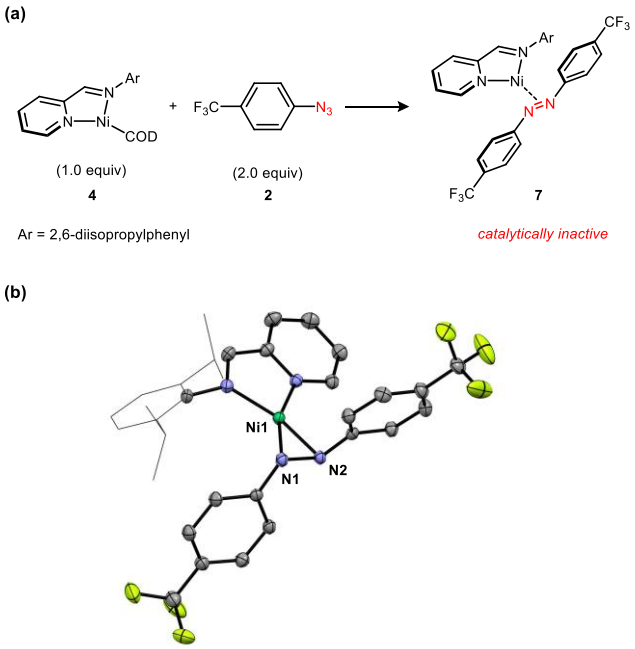

Figure 2.2. (a) Synthesis and (b) solid-state structure of **7**. Ni1–N1: 1.893(3) Å; Ni1–N2: 1.889(2) Å; N1–N2: 1.403(3) Å.

2.4 Substrate Scope for the Ni_2-Catalyzed Nitrene Dimerization.

The substrate scope of the catalytic nitrene dimerization reaction is illustrated in Table 2.2. Both electron-rich and electron-deficient substrates undergo N=N coupling, with the rate of reaction being accelerated by the presence of electron-withdrawing substituents. The presence of strongly donating substituents (e.g. **12** and **22**) has a moderately detrimental effect on yield. A variety of common redox-sensitive functional groups are tolerated, including tertiary amines, aryl halides, carbonyl derivatives, boronate esters, internal alkynes, electron-rich heterocycles, and a ferrocene group. Mesityl azide represents the limit of steric hindrance that is tolerated by the catalyst, requiring elevated temperatures and longer reaction times to reach full conversion (100 °C for 4 h). Azoarenes derived from amino acid[17] or terpene[18] frameworks (e.g. **26**–**28**) are accessible by this method. Finally, the diazide starting material **29** undergoes selective intramolecular N=N coupling to generate benzo[*c*]cinnoline (**30**) in 80% yield. Of note, the conversion of **29** to **30** was previously carried out under photolysis conditions but required that the reaction be conducted in a solid matrix to avoid competing C–H insertion and intermolecular coupling.[19]

Table 2.2. Substrate Scope for the Catalytic N=N Coupling Reaction[a]

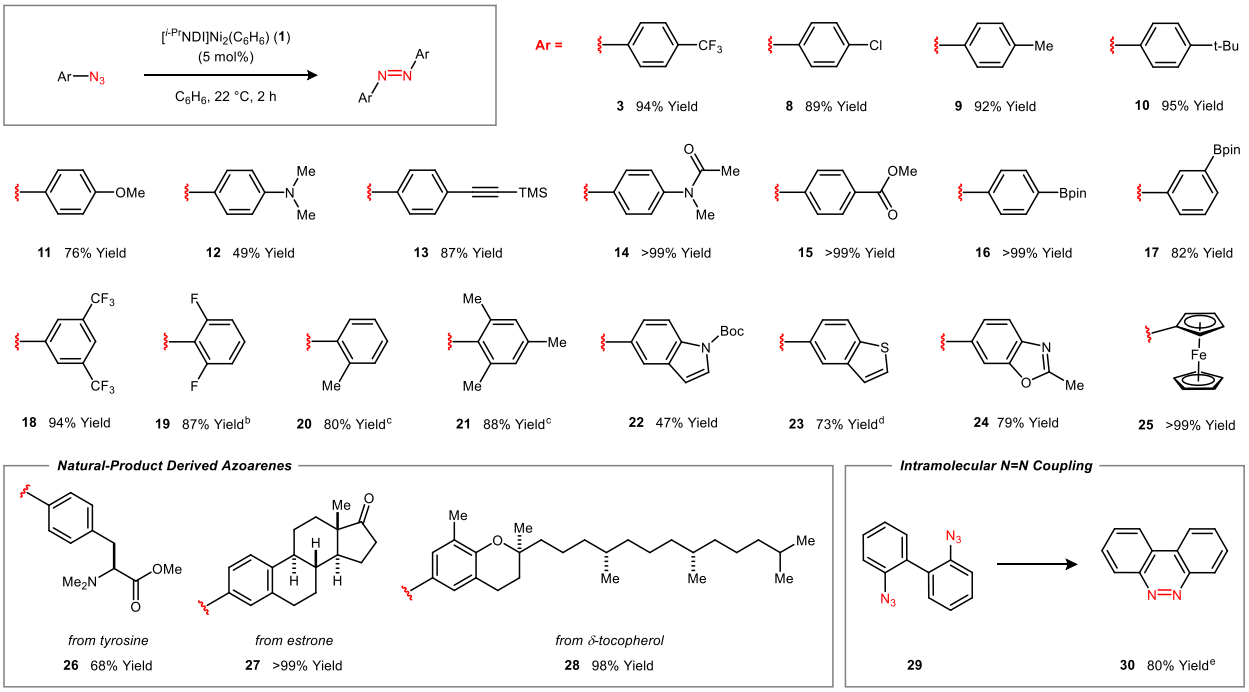

[a]Standard reaction conditions: 22 °C for 2 h, 5 mol% of **1**. Isolated yields were determined following purification and are averaged over two runs. See Supporting Information for experimental details. [b]Modifications from standard reaction conditions: 80 °C. [c]Modifications from standard reaction conditions: 100 °C for 4 h. [d]Modifications from standard reaction conditions: 10 mol% of **1**. [e]NMR yield.

Several of the results obtained by the catalytic nitrene dimerization protocol represent significant improvements in yield over reported syntheses. For example, azoferrocene **25** was studied as a light-switchable redox center[20] and was prepared from lithioferrocene and N_2O in a low yield of 7%.[21] By contrast, the dimerization of known azidoferrocene proceeds in >99% yield using **1**. The 2,6-difluoro-substituted azoarene **19**, a high-performance photoswitch exhibiting near quantitative isomerization, was previously synthesized by the oxidation of 2,6-difluoroaniline with $KMnO_4$ in 24% yield.[5e] Catalyst **1** affords **19** in 87% yield.

2.5 Applications to the Synthesis of Azoarene Polymers.

Polymers containing azoarenes have been investigated as photoresponsive materials for imaging, data storage, and electro-optic applications.[22] A majority of azo polymers reported in the literature incorporate the azoarene subunit as part of the polymer side chains. Materials containing

main-chain azo linkages, while less common, are attractive in that the conjugated azoarenes can form highly conductive π-systems.[23] Additionally, c*is–trans* isomerization enables light stimuli to be used to trigger long-range conformational changes in the polymer. Due to the synthetic challenge associated with utilizing N=N bond formation as a chain propagation step,[24] most main-chain azo polymers are synthesized by alternative coupling strategies that rely on monomer units containing the pre-generated azoarene functionality.[25]

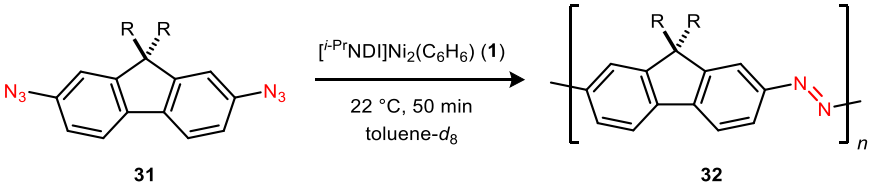

31

R = *n*-$C_{12}H_{25}$–

32

1 (2 mol%): M_n = 18.1 kDa, PDI = 2.48
1 (5 mol%): M_n = 41.1 kDa, PDI = 3.23

Figure 2.3. Polymerization of **31** using catalyst **1**.

In order to examine the polymerization activity of catalyst **1**, we selected the diazide **31** as a model substrate (Figure 2.3). A related dinitrofluorene derivative was previously used to synthesize an azopolymer by a reductive method.[24b] Addition of **31** to solutions of **1** (2 or 5 mol%) in toluene-d_8 led to rapid monomer consumption and the formation of a deep red polymeric material (**32**), which was isolated in high yield by precipitation from MeOH (76% yield at 2 mol% loading of **1**). The molecular weight distribution of polymer **32** is sensitive to catalyst loading; for example, the average molecular weight is 18.1 kDa (PDI = 2.48) at 2 mol% but approximately doubles to 41.4 kDa (PDI = 3.23) at 5 mol%. This result highlights the potential for catalytic nitrene dimerization to be leveraged as a strategy to access tunable photo-responsive polymers containing main-chain azo bonds.

2.6 Synthesis and Stoichiometric N=N Coupling Reactivity of a Ni_2(μ-NAr) Complex.

We next turned our attention to identifying catalytically relevant intermediates with the goal of understanding the unique effectiveness of the Ni_2 catalyst in the nitrene dimerization reaction. Hindered aryl azides bearing large ortho substituents are ineffective as substrates for the catalytic N=N coupling but provided an opportunity to characterize stable $Ni_2(NAr)_x$ complexes.

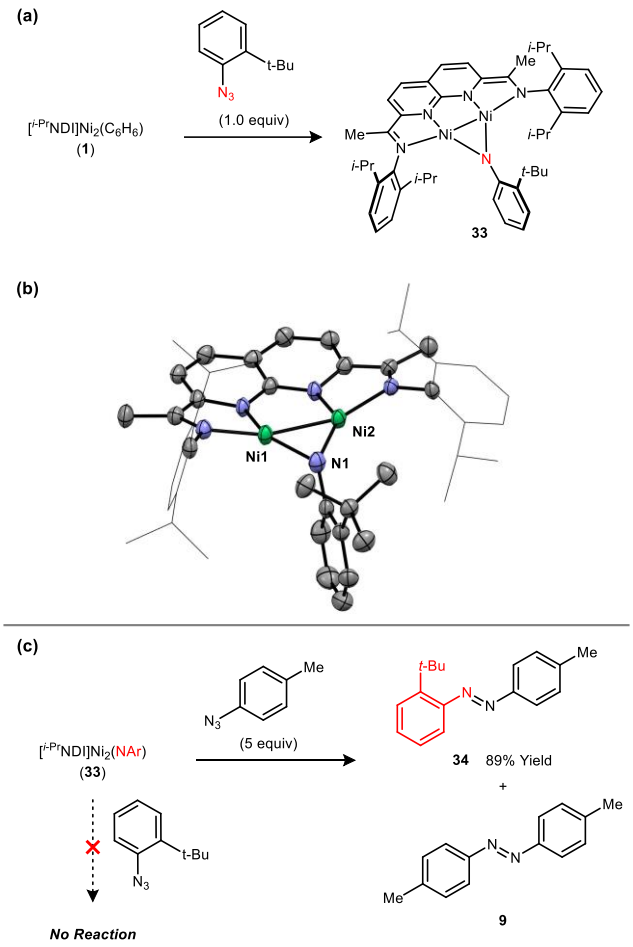

Figure 2.4. (a) Synthesis and (b) solid-state structure of **33**. Ni1–Ni2: 2.3356(7) Å; Ni1–N1: 1.777(3) Å; Ni1–N2: 1.775(3) Å. (c) Stoichiometric reactions of **33** with aryl azides.

Treatment of **1** with 2-*tert*-butylphenyl azide (1.0 equiv) in C_6D_6 causes an immediate evolution of N_2 gas, accompanied by the formation of a new paramagnetic brown species (**33**) observable by ^{1}H NMR spectroscopy (Figure 2.4a). Complex **33** undergoes gradual decomposition when stored in solution at room temperature but is sufficiently stable at –30 °C to allow for crystallization from a pentane/toluene solvent mixture. XRD analysis confirmed the identity of **33** as a μ-NAr complex (Figure 2.4b). The Ni–N distances are relatively short (1.777(3) and 1.775(3) Å), and the μ-N atom adopts a nearly planar geometry (Σ of the angles about N = 340.8(2)°). At room temperature, **33** exhibits a magnetic moment (μ = 1.77 μ_B by Evans method) that is intermediate between the expected values for a singlet and a triplet state.[26] Variable-temperature studies indicate that the ^{1}H NMR chemical shifts become increasingly paramagnetically shifted at lower temperatures with modest deviations from simple Curie behavior. Taken together, the

magnetic moment and VT data suggest that both the $S = 0$ and $S = 1$ states are sufficiently close in energy to be populated at room temperature.[27] According to DFT models (BP86/6-31G(d,p) level of theory), the triplet state is calculated to be lower in energy by only 2.1 kcal/mol relative to the singlet state.

The μ-NAr complex **33** is sufficiently hindered that it does not react with additional equivalents of 2-*tert*-butylphenyl azide (Figure 2.4c); however, treatment of **33** with a smaller reaction partner, 4-tolyl azide (5 equiv), provides the heterocoupled azoarene product **34** in 89% yield. Excess quantities of 4-tolyl azide are required in this reaction to reach high yields of **34** due to the concurrent catalytic formation of homodimer **9** (81% yield, corresponding to 98% total mass balance of converted 4-tolyl azide).

A key challenge associated with achieving efficient catalytic azoarene formation is the propensity for mid-to-late transition metal imides to undergo competing H-atom abstraction from the reaction medium.[27b,28] This side process results in aniline products and may also decompose the catalyst through the formation of inactive M(NHAr) complexes. For example, the (SiP_3)Fe catalyst studied by Peters dimerizes 4-tolyl azide in 57% yield but generates 8% of toluidine as a byproduct.[10b] Additionally, the isolable (SiP_3)Fe(NAr) complex (Ar = 4-tolyl) was found to react rapidly with H-atom donors such as 9,10-dihydroanthracene to yield mixtures of the corresponding (SiP_3)Fe(NHAr) complex and free $ArNH_2$.

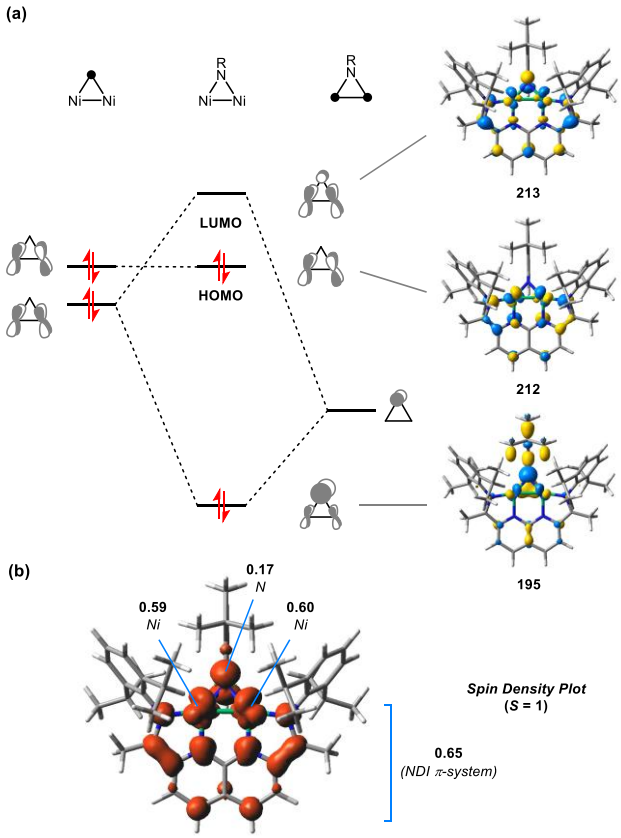

Figure 2.5. (a) Qualitative orbital interaction diagram highlighting three-centered π-bonding in the Ni_2(μ-NAr) fragment of **33**. Molecular orbitals are shown for the S = 0 state. The labelled HOMO and LUMO for the S = 0 state correspond to the two SOMOs in the S = 1 state. (b) Mulliken spin density plot for **33** in the S = 1 state (BP86/6-31G(d,p)).

A notable feature of the Ni_2(μ-NAr) complex **33** is its resistance toward undergoing H-atom abstraction reactions. While complex **33** is only metastable at room temperature, the rate of its decomposition is unaffected by the presence of 9,10-dihydroanthracene. Additionally, no detectable amounts of $ArNH_2$ side products were observed in any of the catalytic N=N coupling reactions shown in Table 2.2.

The ability of a M(NAr) complex to engage in H-atom abstraction is often correlated with significant imidyl radical character. For example, the (SiP_3)Fe(NAr) complex in its intermediate spin S = 3/2 state was calculated by DFT to localize a significant fraction of its total spin density on the imido N-atom (0.82 electons).[10b] In the case of the Ni_2(μ-NAr) complex **33** (Figure 2.5a), an orbital corresponding to the μ-NAr lone pair could be located by DFT at HOMO–17 (195). The relatively low energy of this orbital is attributed to the stabilizing influence of π-bonding between

the Ni–Ni fragment and the N p-orbital. The corresponding anti-bonding combination is unfilled (LUMO), indicating a net three-centered, two-electron interaction. The calculated π-bonding interaction is corroborated experimentally by the short Ni–N(Ar) distances and the planar geometry of the μ-imido N atom observed in the XRD structure of **33**. In the *S* = 1 state, the two unpaired electrons are delocalized across the NDI π-system, the Ni–Ni bond, and the μ-NAr fragment such that only 9% of the total spin density is associated with the imido N-atom (Figure 2.5b).

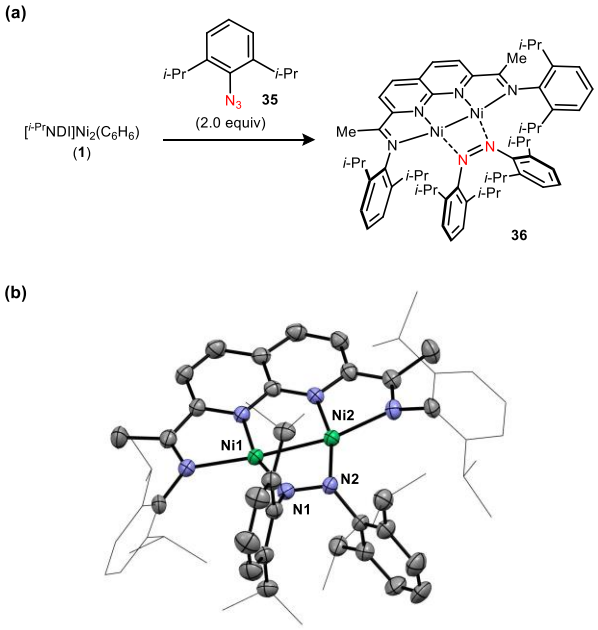

Figure 2.6. (a) Synthesis and (b) solid-state structure of **36**. Ni1–Ni2: 2.3751(7) Å; Ni1–N1: 1.815(2) Å; Ni1–N2: 1.814(2) Å; N1–N2: 1.378(3) Å.

2.7 Characterization of a $Ni_2(\mu\text{-}N_2Ar_2)$ Complex and Implications for Product Inhibition.

The sterically hindered 2,6-diisopropylphenyl azide reagent **35** reacts in a 2:1 stoichiometry with **1** to generate a diamagnetic product (**36**), which was identified as an azoarene adduct by XRD analysis (Figure 2.6a). Attempts to carry out the same reaction using a 1:1 ratio of **35** and **1** led to the formation of azoarene complex **36** in approximately 50% yield with the remainder of the mass balance being recovered **1**. This result indicates that the putative imido intermediate is either more reactive than **1** with azide **35** or is unstable toward disproportionation. Due to its steric hindrance, complex **36** does not react with additional equivalents of **35** to catalytically release free azoarene.

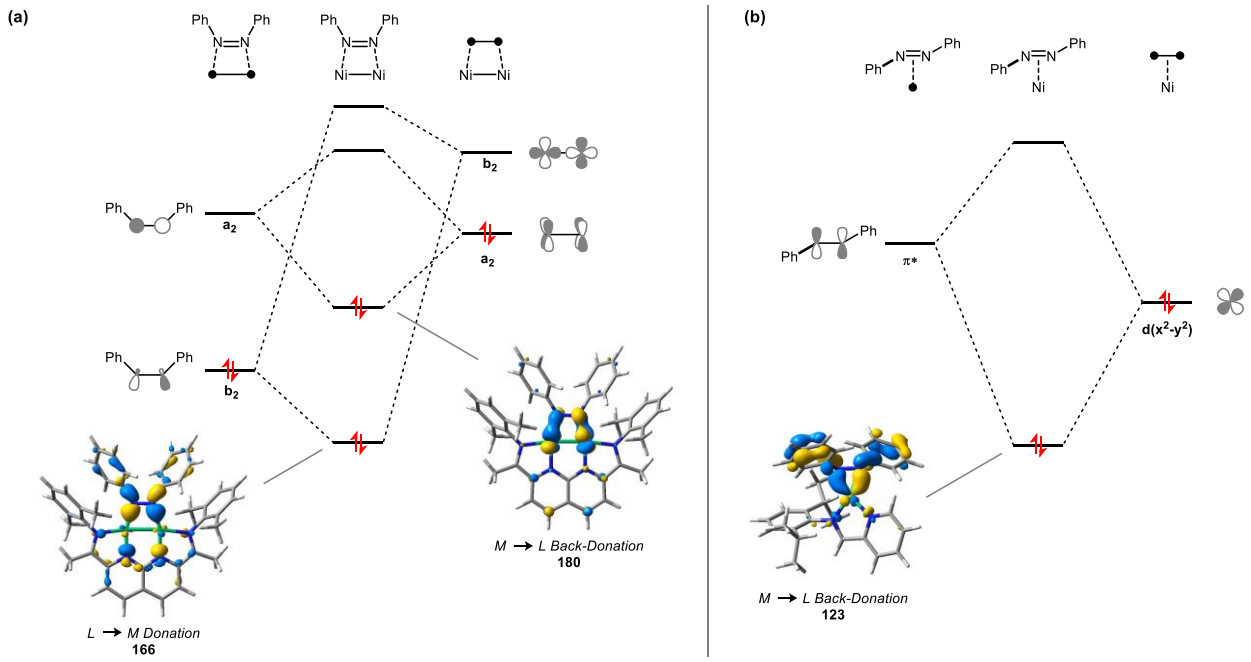

Figure 2.7. A comparison of qualitative orbital interaction diagrams highlighting two-electron interactions between the Ar_2N_2 and Ni_x fragments for (a) the dinuclear $Ni_2(\mu\text{-}N_2Ar_2)$ complex **36** and (b) the mononuclear $Ni(N_2Ar_2)$ complex **7**

Azoarenes generally interact with low-valent late transition metals by adopting their more stable *trans* configuration and forming π-complexes.[29] In this context, the structure of **36** (Figure 2.6b) is unusual in that the azoarene is constrained to be in its higher energy *cis* geometry (∠C–N=N–C = 52.2(3)˚) and binds through the two nitrogen lone pairs. The N–N bond distance (1.378(3) Å) is significantly elongated relative to free azobenzene (N=N distance for azobenzene: 1.26 Å[16]; N–N distance for N,N'-diphenylhydrazine: 1.39 Å[30]), suggesting that there is significant back-donation from the Ni_2 fragment into the π* orbital of the azoarene. Previous examples of azoarene binding in the *cis* orientation are associated with d^0 early transition-metal complexes formulated as metalladiaziridines.[31,32]

DFT calculations using a model azobenzene complex provided further insight into the nature of the interaction between the bound Ar_2N_2 fragment and the Ni–Ni bond in **36** (Figure 2.7a). HOMO–22 (166) corresponds to the anti-symmetric combination of nitrogen lone pairs, which has appropriate symmetry to donate into the unfilled σ* orbital of the d^9–d^9 Ni–Ni bond. Slightly higher in energy (180), a back-bonding interaction can be identified from a filled Ni–Ni δ* orbital into the π* orbital of the azoarene. The net effect of these interactions is a significant reduction in

the N=N bond order (Wiberg bond index = 1.18). By contrast, the metal–ligand interactions in the monometallic Ni azoarene complex **7** are dominated by back-bonding between the Ni d(x^2–y^2) and azoarene π* orbitals (Figure 2.7b).

2.8 Computational Studies of an N=N Coupling Pathway from a $Ni_2(\mu\text{-}NAr)_2$ Intermediate.

The N=N coupling step of the catalytic mechanism may proceed through a variety of possible pathways, including external attack of a $Ni_2(\mu\text{-}NAr)$ species by an aryl azide or the formation of a $Ni_2(\mu\text{-}N_4Ar_2)$ intermediate that undergoes N_2 extrusion. Alternatively, a common mode of reactivity for transition metal complexes and aryl azides is the formation of dimeric bridging imido complexes.[33] For example, a $Fe(OC\textit{t}\text{-}Bu_2Ph)_2$ complex studied by Groysman catalyzes the dimerization of mesityl azide; however, less hindered substrates, such as phenyl azide, formed stable $Fe_2(\mu\text{-}NAr)_2$ complexes that do not undergo N=N coupling.[10d] In light of these results, we considered whether the constrained environment of the $[NDI]Ni_2$ system, which enforces a significantly shorter metal–metal distance, would promote effective N=N bond formation from a bis(imido) intermediate.

By DFT (Figure 2.8), the putative $Ni_2(\mu\text{-}NAr)_2$ intermediate **A** was calculated to be modestly higher in energy (3.7 kcal/mol in the S = 0 state) relative to its isomeric azoarene product **C**. A transition state corresponding to N=N coupling was located on both the singlet and triplet surfaces leading to a perpendicularly coordinated azoarene intermediate **B**, which then rotates to its more stable parallel orientation **C**, the geometry that is observed experimentally in complex **20**. The barrier to N=N coupling is remarkably low (10.1 kcal/mol), consistent with this process being a fast step in the catalytic cycle. The initial bis(imido) species **A** and the transition state for N=N coupling are lower in energy on the singlet surface, but a spin-crossing event generates the more stable triplet complex **B**. Rotation of the azoarene ligand is then accompanied by a second spin-state change to yield the diamagnetic, parallel-coordinated azoarene adduct **C**.

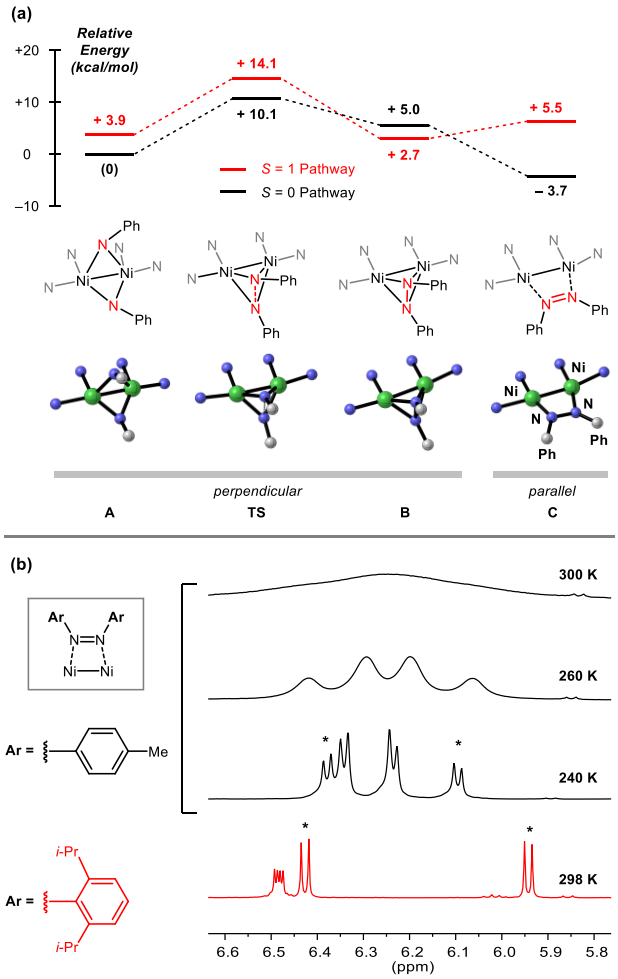

Figure 2.8. (a) Calculated mechanism for N=N Bond-formation from a putative bis(imido) intermediate (**A**) to generate the [NDI]$Ni_2(Ar_2N_2)$ complex **C**. Structures were modeled for Ar = Ph. Energies are relative to the **A** in the singlet state. (b) ^{1}H NMR spectra for the [$^{i\text{-}Pr}$NDI]$Ni_2(Ar_2N_2)$ complex: Ar = 4-tolyl (top, black); Ar = 2,6-diisopropylphenyl (bottom, red). Signals corresponding to the naphthyridine doublets of the NDI ligand are indicated by asterisks.

While endothermic relative to **C** (+6.4 kcal/mol), the paramagnetic perpendicularly coordinated azoarene adduct **B** is expected to be populated to a minor extent at room temperature based on calculated thermodynamics. Accordingly, the ^{1}H NMR spectrum for the azoarene complex derived from 4-azotoluene (**9**) is broad at room temperature but resolves into a set of well-defined peaks at temperatures below 250 K (Figure 2.8b). The energy gap between the parallel and perpendicular rotamers can also be tuned through the introduction of *ortho*-substituents to the bound azoarene. For example, the 2,6-diisopropylphenyl derivative **36** is strictly diamagnetic at room temperature with no evidence of fluxional behavior. By DFT, the addition of

ortho-methyl groups to the bound azoarene causes the parallel orientation to be favored by 14.3 kcal/mol.

2.9 Catalyst Resting State, Kinetics and Thermodynamics of Ligand Substitution.

The reactivity studies using 2,6-diisopropylphenyl azide suggest that the limiting factor preventing the catalytic coupling of hindered substrates is displacement of the bound azoarene product, rather than slow N=N coupling. In order to further probe this ligand substitution step, we conducted kinetics experiments using a catalytically competent substrate, mesityl azide, which forms azomesitylene (**21**) at a sufficiently slow rate to allow for convenient reaction monitoring.

The homocoupling of mesityl azide proceeds to full conversion in the presence of 10 mol% **1** in C_6D_6 after 2 h at 75 °C. Throughout the reaction time course, the primary catalyst resting state is a C_2-symmetric diamagnetic species, which was assigned as the azoarene adduct by analogy of its ^{1}H NMR spectrum to that of **36**. The reaction exhibits a strictly zero-order rate dependence on mesityl azide up to approximately 70% conversion, after which, substrate depletion results in a positive order regime. This kinetic behavior is consistent with a solvent-assisted ligand substitution process being favored over direct substitution of bound product by the azide starting material (Figure 2.9).

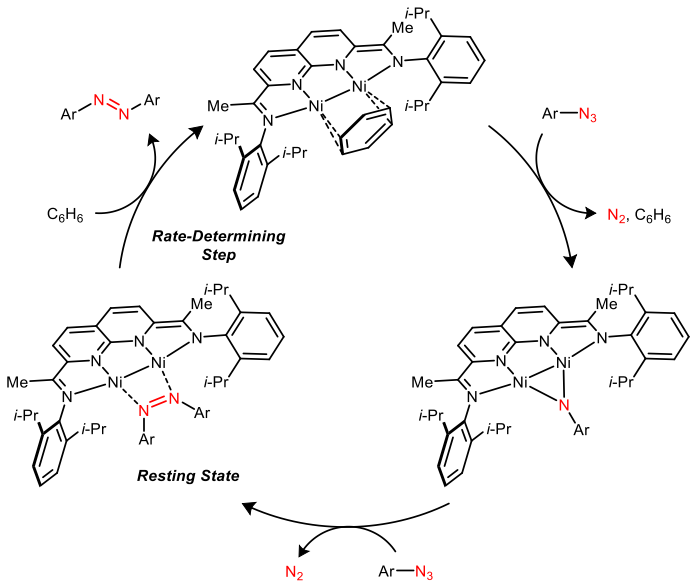

Figure 2.9. Proposed mechanism for the catalytic N=N coupling reaction.

Given the resistance of the mononickel azoarene adduct **7** to undergoing ligand substitution, it was of interest to compare the thermodynamics of azoarene displacement for the dinickel system. According to DFT models, the initial substitution of bound azoarene by C_6H_6 to form free *cis*-azoarene is endothermic by 17.2 kcal/mol (Figure 2.10a); however, the ability of the *cis* azoarene to isomerize to its more stable *trans* form recovers all but 3.3 kcal/mol of this energy. Consequently, the overall substitution is nearly thermoneutral. This step of the mechanism could be examined experimentally in the reverse direction by treating the $Ni_2(C_6H_6)$ complex **1** with a stoichiometric amount of azoarene **21** (Figure 2.10b). In accordance with the calculated thermodynamics of this process, the ligand substitution to generate azoarene adduct **37** is favorable and reaches full conversion. Due to the high thermal barrier for *trans*-to-*cis* isomerization, the substitution requires heating and long reaction times (30 days at 80 °C). By contrast, when mixtures of **1** and **21** are irradiated using a 254 nm light source, conditions known to induced *cis*-*trans* isomerization, ligand substitution proceeds more rapidly (within 90 min at room temperature). Collectively, these studies suggest that product inhibition is avoided in the catalytic cycle due to (1) the inability of the more stable *trans* form of the azoarene to bind to the catalyst and (2) the high barrier for thermal isomerization.

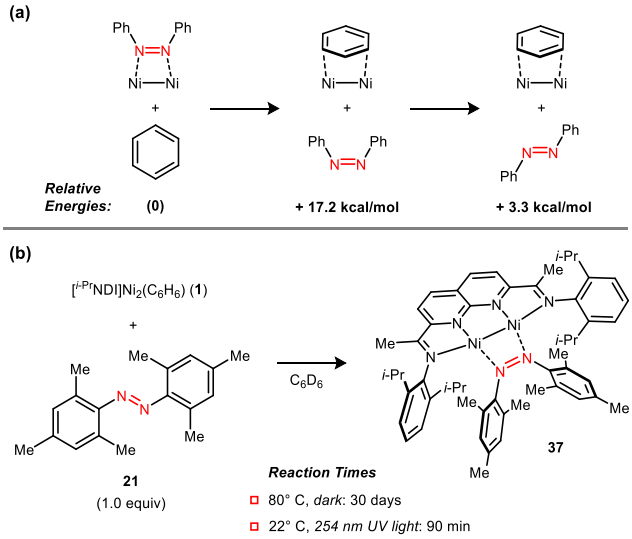

Figure 2.10. (a) Calculated energetics of C_6H_6/Ph_2N_2 ligand substitution on the $[NDI]Ni_2$ platform. (b) Ligand substitution using azomesitylene in the dark and under illumination in a photobox (254 nm light source).

2.10 Conclusions.

In summary, the dinuclear Ni complex **1** promotes the selective catalytic dimerization of aryl azides to form azoarene products. This method requires no stoichiometric redox reagents and generates only N_2 as a byproduct, allowing functional groups sensitive to reduction or oxidation to be tolerated. Mechanistic studies are consistent with the initial formation of a μ-NAr intermediate, which then reacts with a second equivalent of an aryl azide to generate a μ-N_2Ar_2 adduct. The structure and reactivity of these putative intermediates suggest two key features of the dinickel active site critical for efficient catalytic turnover. First, the reactive imido intermediate is stabilized by π-interactions with the Ni–Ni bond, suppressing undesired H-atom abstraction reactions. Second, the azoarene product is weakly coordinated to the Ni–Ni bond due to an enforced high-energy *cis*-conformation. Ongoing studies are directed at exploiting the unique electronic properties of dinuclear nitrene intermediates to address other challenges in selective group transfer catalysis.

2.11 Acknowledgements.

This research was supported by the NSF (CHE-1554787) and by Purdue University. XRD data were collected using instruments funded by the NSF (CHE-1625543). This work used the Extreme Science and Engineering Discovery Environment (XSEDE), which is supported by National Science Foundation grant number ACI-1548562 (Comet supercomputing cluster, allocation number TG-CHE150051). We thank Dr. Matthias Zeller for assistance with XRD experiments. C.U. is an Alfred P. Sloan Research Fellow and I.G.P. is an NSF graduate research fellow (DGE-1333468).

2.12 References.

(1) (a) Griffiths, J. *Chem. Soc. Rev.* **1972**, *1*, 481-493; (b) Rau, H. *Angew. Chem., Int. Ed.* **1973**, *12*, 224-235.

(2) (a) Hartley, G. S. *Nature* **1937**, *140*, 281; (b) Fliegl, H.; Köhn, A.; Hättig, C.; Ahlrichs, R. *J. Am. Chem. Soc.* **2003**, *125*, 9821-9827.

(3) (a) Browne, W. R.; Feringa, B. L. *Nat. Nanotech.* **2006**, *1*, 25; (b) Kay, E. R.; Leigh, D. A.; Zerbetto, F. *Angew. Chem., Int. Ed.* **2007**, *46*, 72-191; (c) Yagai, S.; Kitamura, A. *Chem. Soc. Rev.* **2008**, *37*, 1520-1529; (d) Beharry, A. A.; Woolley, G. A. *Chem. Soc. Rev.* **2011**, *40*, 4422-4437; (e) Merino, E.; Ribagorda, M. *Beilstein J. Org. Chem.* **2012**, *8*, 1071-1090; (f) Bandara, H. M. D.; Burdette, S. C. *Chem. Soc. Rev.* **2012**, *41*, 1809-1825; (g) Mura, S.; Nicolas, J.; Couvreur, P. *Nat. Mater.* **2013**, *12*, 991-1003; (h) Dong, M.; Babalhavaeji, A.; Samanta, S.; Beharry, A. A.; Woolley, G. A. *Acc. Chem. Res.* **2015**, *48*, 2662-2670; (i) Bléger, D.; Hecht, S. *Angew. Chem., Int. Ed.* **2015**, *54*, 11338-11349; (j) Erbas-Cakmak, S.; Leigh, D. A.; McTernan, C. T.; Nussbaumer, A. L. *Chem. Rev.* **2015**, *115*, 10081-10206.

(4) (a) Hamon, F.; Djedaini-Pilard, F.; Barbot, F.; Len, C. *Tetrahedron* **2009**, *65*, 10105-10123; (b) Merino, E. *Chem. Soc. Rev.* **2011**, *40*, 3835-3853.

(5) Examples of functional photoswitching molecules synthesized by the oxidative dimerization of anilines: (a) Shinkai, S.; Minami, T.; Kusano, Y.; Manabe, O. *J. Am. Chem. Soc.* **1983**, *105*, 1851-1856; (b) Norikane, Y.; Tamaoki, N. *Org. Lett.* **2004**, *6*, 2595-2598; (c) Muraoka, T.; Kinbara, K.; Aida, T. *Nature* **2006**, *440*, 512; (d) Beharry, A. A.; Sadovski, O.; Woolley, G. A. *J. Am. Chem. Soc.* **2011**, *133*, 19684-19687; (e) Bléger, D.; Schwarz, J.; Brouwer, A. M.; Hecht, S. *J. Am. Chem. Soc.* **2012**, *134*, 20597-20600; (f) Samanta, S.; Beharry, A. A.; Sadovski, O.; McCormick, T. M.; Babalhavaeji, A.; Tropepe, V.; Woolley, G. A. *J. Am. Chem. Soc.* **2013**, *135*, 9777-9784.

(6) Examples of functional photoswitching molecules synthesized by the reductive dimerization of nitroarenes: (a) Shinkai, S.; Nakaji, T.; Ogawa, T.; Shigematsu, K.; Manabe, O. *J. Am. Chem. Soc.* **1981**, *103*, 111-115; (b) Rakotondradany, F.; Whitehead, M. A.; Lebuis, A.-M.; Sleiman, H. F. *Chem.–Eur. J.* **2003**, *9*, 4771-4780; (c) Tamaoki, N.; Wada, M. *J. Am. Chem. Soc.* **2006**, *128*, 6284-6285; (d) Siewertsen, R.; Neumann, H.; Buchheim-Stehn, B.; Herges, R.; Näther, C.; Renth, F.; Temps, F. *J. Am. Chem. Soc.* **2009**, *131*, 15594-15595; (e) Basheer, M. C.; Oka, Y.; Mathews, M.; Tamaoki, N. *Chem.–Eur. J.* **2010**, *16*, 3489-3496.

(7) Konrad, D. B.; Frank, J. A.; Trauner, D. *Chem.–Eur. J.* **2016**, *22*, 4364-4368.

(8) (a) Leyva, E.; Platz, M. S.; Persy, G.; Wirz, J. *J. Am. Chem. Soc.* **1986**, *108*, 3783-3790; (b) Borden, W. T.; Gritsan, N. P.; Hadad, C. M.; Karney, W. L.; Kemnitz, C. R.; Platz, M. S. *Acc. Chem. Res.* **2000**, *33*, 765-771; (c) Schuster, G. B.; Platz, M. S. Photochemistry of Phenyl Azide. *Adv. Photochem.* **1992**, *17*, 69-143.

(9) Reviews of mid-to-late transition metal imides: (a) Eikey, R. A.; Abu-Omar, M. M. *Coord. Chem. Rev.* **2003**, *243*, 83-124; (b) Berry, J. F. *Comments Inorg. Chem.* **2009**, *30*, 28-66; (c) Saouma, C. T.; Peters, J. C. *Coord. Chem. Rev.* **2011**, *255*, 920-937; (d) Ray, K.; Heims, F.; Pfaff, F. F. *Eur. J. Inorg. Chem.* **2013**, *2013*, 3784-3807.

(10) (a) Ragaini, F.; Penoni, A.; Gallo, E.; Tollari, S.; Li Gotti, C.; Lapadula, M.; Mangioni, E.; Cenini, S. *Chem.–Eur. J.* **2003**, *9*, 249-259; (b) Mankad, N. P.; Müller, P.; Peters, J. C. *J. Am. Chem. Soc.* **2010**, *132*, 4083-4085; (c) Heyduk, A. F.; Zarkesh, R. A.; Nguyen, A. I. *Inorg. Chem.* **2011**, *50*, 9849-9863; (d) Bellow, J. A.; Yousif, M.; Cabelof, A. C.; Lord, R. L.; Groysman, S. *Organometallics* **2015**, *34*, 2917-2923.

(11) Catalytic conversions of aryl azides to azoarenes proposed to proceed through free nitrene intermediates: (a) Takaoka, A.; Moret, M.-E.; Peters, J. C. *J. Am. Chem. Soc.* **2012**, *134*, 6695-6706; (b) Harman, W. H.; Lichterman, M. F.; Piro, N. A.; Chang, C. J. *Inorg. Chem.* **2012**, *51*, 10037-10042.

(12) (a) Overbosch, P.; Van Koten, G.; Overbeek, O. *J. Am. Chem. Soc.* **1980**, *102*, 2091-2093; (b) Trogler, W. C. *Acc. Chem. Res.* **1990**, *23*, 426-431.

(13) Harrold, N. D.; Waterman, R.; Hillhouse, G. L.; Cundari, T. R. *J. Am. Chem. Soc.* **2009**, *131*, 12872-12873.

(14) (a) Zhou, Y.-Y.; Hartline, D. R.; Steiman, T. J.; Fanwick, P. E.; Uyeda, C. *Inorg. Chem.* **2014**, *53*, 11770-11777; (b) Steiman, T. J.; Uyeda, C. *J. Am. Chem. Soc.* **2015**, *137*, 6104-6110.

(15) Foster, R. S.; Adams, H.; Jakobi, H.; Harrity, J. P. A. *J. Org. Chem.* **2013**, *78*, 4049-4064.

(16) Harada, J.; Ogawa, K.; Tomoda, S. *Acta Crystallogr., Sect. B* **1997**, *53*, 662-672.

(17) (a) Renner, C.; Moroder, L. *ChemBioChem* **2006**, *7*, 868-878; (b) Mart, R. J.; Allemann, R. K. *Chem. Commun.* **2016**, *52*, 12262-12277.

(18) Katritzky, A. R.; Tala, S. R.; Abo-Dya, N. E.; Abdel-Samii, Z. K. *Synthesis* **2009**, *2009*, 1708-1714.

(19) (a) Yabe, A.; Honda, K. *Tetrahedron Lett.* **1975**, *16*, 1079-1082; (b) Akira, Y.; Koichi, H. *Bull. Chem. Soc. Jpn.* **1976**, *49*, 2495-2499.

(20) Kurihara, M.; Matsuda, T.; Hirooka, A.; Yutaka, T.; Nishihara, H. *J. Am. Chem. Soc.* **2000**, *122*, 12373-12374.

(21) Kurosawa, M.; Nankawa, T.; Matsuda, T.; Kubo, K.; Kurihara, M.; Nishihara, H. *Inorg. Chem.* **1999**, *38*, 5113-5123.

(22) (a) Nuyken, O.; Scherer, C.; Baindl, A.; Brenner, A. R.; Dahn, U.; Gärtner, R.; Kaiser-Röhrich, S.; Kollefrath, R.; Matusche, P.; Voit, B. *Prog. Polym. Sci.* **1997**, *22*, 93-183; (b) Delaire, J. A.; Nakatani, K. *Chem. Rev.* **2000**, *100*, 1817-1846; (c) Natansohn, A.; Rochon, P. *Chem. Rev.* **2002**, *102*, 4139-4176; (d) Yesodha, S. K.; Sadashiva Pillai, C. K.; Tsutsumi, N. *Prog. Polym. Sci.* **2004**, *29*, 45-74; (e) Wang, D.; Wang, X. *Prog. Polym. Sci.* **2013**, *38*, 271-301.

(23) Xue, X.; Zhu, J.; Zhang, Z.; Zhou, N.; Tu, Y.; Zhu, X. *Macromolecules* **2010**, *43*, 2704-2712.

(24) (a) Nguyen, H. T.; Coulembier, O.; Gheysen, K.; Martins, J. C.; Dubois, P. *Macromolecules* **2012**, *45*, 9547-9550; (b) Wang, L.; Pan, X.; Zhao, Y.; Chen, Y.; Zhang, W.; Tu, Y.; Zhang, Z.; Zhu, J.; Zhou, N.; Zhu, X. *Macromolecules* **2015**, *48*, 1289-1295.

(25) Select examples of azoarene polymers synthesized using pre-generated azoarene monomers: (a) Izumi, A.; Teraguchi, M.; Nomura, R.; Masuda, T. *Macromolecules* **2000**, *33*, 5347-5352; (b) Wu, Y.; Natansohn, A.; Rochon, P. *Macromolecules* **2001**, *34*, 7822-7828; (c) Sapich, B.; Vix, A. B. E.; Rabe, J. P.; Stumpe, J. *Macromolecules* **2005**, *38*, 10480-10486; (d) Xue, X.; Zhu, J.; Zhang, W.; Zhang, Z.; Zhu, X. *Polymer* **2009**, *50*, 4512-4519; (e) Ding, L.; Zhang, L.; Han, H.; Huang, W.; Song, C.; Xie, M.; Zhang, Y. *Macromolecules* **2009**, *42*, 5036-5042; (f) Bléger, D.; Liebig, T.; Thiermann, R.; Maskos, M.; Rabe, J. P.; Hecht, S. *Angew. Chem., Int. Ed.* **2011**, *50*, 12559-12563; (g) Heo, J.; Kim, Y. J.; Seo, M.; Shin, S.; Kim, S. Y. *Chem. Commun.* **2012**, *48*, 3351-3353; (h) Ding, L.; Qiu, J.; Li, J.; Wang, C.; Wang, L. *Macromol, Rapid Commun.* **2015**, *36*, 1578-1584; (i) Kumar, K.; Knie, C.; Bléger, D.; Peletier, M. A.; Friedrich, H.; Hecht, S.; Broer, D. J.; Debije, M. G.; Schenning, A. P. H. J. *Nat. Commun.* **2016**, *7*, 11975.

(26) Powers, I. G.; Kiattisewee, C.; Mullane, K. C.; Schelter, E. J.; Uyeda, C. *Chem.–Eur. J.* **2017**, *23*, 7694-7697.

(27) Examples of late transition metal imides exhibiting spin-crossover behavior: (a) Bowman, A. C.; Milsmann, C.; Bill, E.; Turner, Z. R.; Lobkovsky, E.; DeBeer, S.; Wieghardt, K.; Chirik, P. J. *J. Am. Chem. Soc.* **2011**, *133*, 17353-17369; (b) King, E. R.; Sazama, G. T.; Betley, T. A. *J. Am. Chem. Soc.* **2012**, *134*, 17858-17861.

(28) Examples of late transition metal imides that exhibit *C*-H abstraction reactivity: (a) Kogut, E.; Wiencko, H. L.; Zhang, L.; Cordeau, D. E.; Warren, T. H. *J. Am. Chem. Soc.* **2005**, *127*, 11248-11249; (b) Lucas, R. L.; Powell, D. R.; Borovik, A. S. *J. Am. Chem. Soc.* **2005**, *127*, 11596-11597; (c) Eckert, N. A.; Vaddadi, S.; Stoian, S.; Lachicotte, R. J.; Cundari, T. R.; Holland, P. L. *Angew. Chem., Int. Ed.* **2006**, *45*, 6868-6871; (d) King, E. R.; Hennessy, E. T.; Betley, T. A. *J. Am. Chem. Soc.* **2011**, *133*, 4917-4923; (e) Wiese, S.; McAfee, J. L.; Pahls, D. R.; McMullin, C. L.; Cundari, T. R.; Warren, T. H. *J. Am. Chem. Soc.* **2012**, *134*, 10114-10121; (f) Aguila, M. J. B.; Badiei, Y. M.; Warren, T. H. *J. Am. Chem. Soc.* **2013**, *135*, 9399-9406; (g) Zhang, L.; Liu, Y.; Deng, L. *J. Am. Chem. Soc.* **2014**, *136*, 15525-15528; (h) Du, J.; Wang, L.; Xie, M.; Deng, L. *Angew. Chem., Int. Ed.* **2015**, *54*, 12640-12644; (i) Wang, L.; Hu, L.; Zhang, H.; Chen, H.; Deng, L. *J. Am. Chem. Soc.* **2015**, *137*, 14196-14207.

(29) (a) Dickson, R. S.; Ibers, J. A. *J. Am. Chem. Soc.* **1972**, *94*, 2988-2993; (b) Klein, H.-F.; Helwig, M.; Koch, U.; Flörke, U.; Haupt, H.-J. *Z. Naturforsch. B Chem. Sci.* **1993**, *48*, 778; (c) Fedotova, Y. V.; Kornev, A. N.; Sushev, V. V.; Kursky, Y. A.; Mushtina, T. G.; Makarenko, N. P.; Fukin, G. K.; Abakumov, G. A.; Zakharov, L. N.; Rheingold, A. L. *J. Organomet. Chem.* **2004**, *689*, 3060-3074; (d) Sadique, A. R.; Gregory, E. A.; Brennessel, W. W.; Holland, P. L. *J. Am. Chem. Soc.* **2007**, *129*, 8112-8121; (e) Field, L. D.; Li, H. L.; Dalgarno, S. J.; Turner, P. *Chem. Commun.* **2008**, 1680-1682; (f) Zurita, D. A.; Flores-Alamo, M.; Garcia, J. J. *Dalton Trans.* **2016**, *45*, 10389-10401.

(30) Pestana, D. C.; Power, P. P. *Inorg. Chem.* **1991**, *30*, 528-535.

(31) (a) Walsh, P. J.; Hollander, F. J.; Bergman, R. G. *J. Am. Chem. Soc.* **1990**, *112*, 894-896; (b) Durfee, L. D.; Hill, J. E.; Fanwick, P. E.; Rothwell, I. P. *Organometallics* **1990**, *9*, 75-80; (c) Aubart, M. A.; Bergman, R. G. *Organometallics* **1999**, *18*, 811-813; (d) Kaleta, K.; Arndt, P.; Spannenberg, A.; Rosenthal, U. *Inorg. Chim. Acta* **2011**, *370*, 187-190; (e) Gilbert, Z. W.; Hue, R. J.; Tonks, I. A. *Nat. Chem.* **2015**, *8*, 63.

(32) A Fe_2 complex featuring an azoarene ligand bound in a *cis* geometry: Hansert, B.; Vahrenkamp, H. *J. Organomet. Chem.* **1993**, *459*, 265-269.

(33) (a) Hashimoto, T.; Hoshino, R.; Hatanaka, T.; Ohki, Y.; Tatsumi, K. *Organometallics* **2014**, *33*, 921-929; (b) Dai, X.; Kapoor, P.; Warren, T. H. *J. Am. Chem. Soc.* **2004**, *126*, 4798-4799; (c) Tsai, Y.-C.; Wang, P.-Y.; Chen, S.-A.; Chen, J.-M. *J. Am. Chem. Soc.* **2007**, *129*, 8066-8067; (d) Nguyen, A. I.; Zarkesh, R. A.; Lacy, D. C.; Thorson, M. K.; Heyduk, A. F. *Chem. Sci.* **2011**, *2*, 166-169; (e) Bellows, S. M.; Arnet, N. A.; Gurubasavaraj, P. M.; Brennessel, W. W.; Bill, E.; Cundari, T. R.; Holland, P. L. *J. Am. Chem. Soc.* **2016**, *138*, 12112-12123.

CHAPTER 3. CATALYTIC SYNTHESIS OF CONJUGATED AZOPOLYMERS FROM AROMATIC DIAZIDES

3.1 Abstract

Conjugated polymers containing main chain azoarene repeat units are synthesized by a dinickel catalyzed N=N coupling reaction of aromatic diazides. The polymerization exhibits broad substrate scope and is compatible with heterocycles commonly featured in high performance organic materials, including carbazole, thiophene, propylenedioxythiophene (ProDOT), diketopyrrolopyrrole (DPP), and isoindigo. Copolymerizations can be carried out using monomer mixtures, and monoazide chain stoppers can be used to install well-defined end groups. Azopolymers possess unique properties owing to the functionality of the azo linkages. For example, protonation at nitrogen results in LUMO lowering and red-shifted absorption bands. Additionally, N=N bonds possess low-lying π^* levels, allowing azopolymers to be reversibly reduced under mild conditions.

3.2 Introduction

Conjugated polymers have numerous applications in light capture, energy storage, sensing, and flexible electronic devices.[1] Transition metal catalyzed cross-coupling reactions are the dominant methods for synthesizing high performance conjugated polymers (Figure 1).[2] Despite the success of this approach, cross-coupling reactions can suffer from competing protodemetallation, reductive dehalogenation, and homodimerization processes, which become particularly problematic when using highly functionalized, heteroaromatic, or hindered monomers.[3] These side reactions lead to low average molecular weight polymers and structural defects that negatively impact optical and electronic performance. Additionally, metal byproducts of cross-coupling reactions, particularly organotin halides formed in Stille cross-couplings,[2c] must be carefully separated during purification. It would therefore be valuable to develop alternative

catalytic polymerization reactions that form conjugated π-systems in high yield, ideally without stoichiometric waste.

Azo bonds are an underexplored linkage in conjugated polymers with the potential to manifest useful photochemical and electrochemical properties. As compared to C=C bonds, N=N bonds have smaller HOMO–LUMO gaps,[4] resulting in light absorption at longer wavelengths and redox activity at milder potentials. Initial investigations of N=N bond formation in polymer synthesis have centered on the oxidative coupling of bis(aniline)[5] or reductive coupling of bis(nitroarene)[6] monomers. One drawback associated with these strategies is the formation of undesired azoxy groups due to overoxidation or under-reduction. Additionally, the redox reagents used in these reactions can be incompatible with sensitive functional groups, resulting in low yields of N=N coupling.[7] Due to these limitations, most of the syntheses of azoarene-containing polymers rely on C–C cross-coupling reactions with monomers containing the pre-installed azo unit.[8]

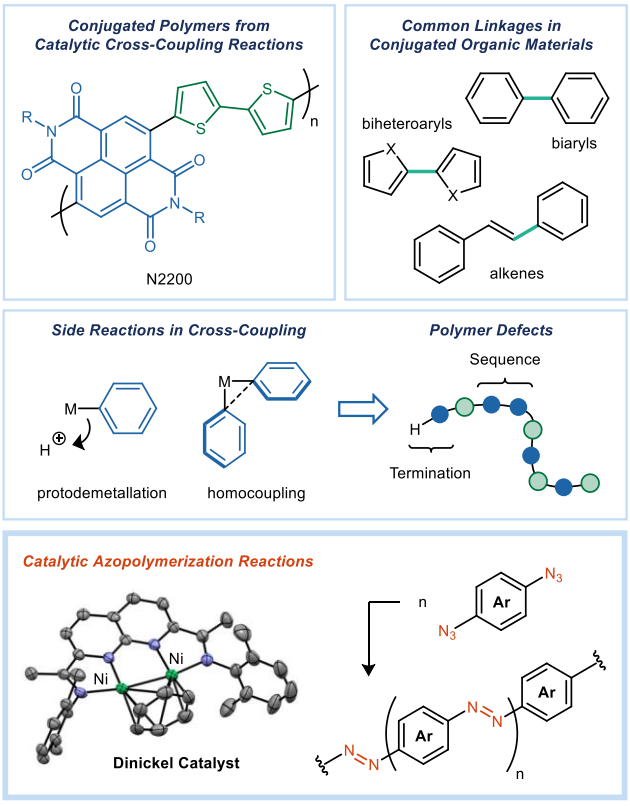

Figure 3.1. High performance conjugated polymers generated using C–C cross-coupling reactions. Synthesis of conjugated azopolymers through catalytic N=N bond formation.

Recently, we found that dinickel catalysts could promote the dimerization of aryl azides to form azoarenes.[9] The reaction does not require any additional reagents, and it produces gaseous N_2 as the only stoichiometric byproduct. Because N=N bond formation occurs in a redox neutral fashion through nitrene dimerization, there is no competing formation of azoxy or hydrazine linkages. Here, we report the application of this reaction to the synthesis of conjugated azopolymers (Figure 3.1). The reaction is compatible with heterocycles such as carbazole, thiophene, isoindigo, and diketopyrrolopyrrole (DPP), which are often featured in high performance organic materials.

3.3 Catalytic Synthesis of PolyAzoCarbazole

Diazidocarbazole **2** was selected as a model substrate for our initial reaction development studies.[10] When the ($^{i\text{-Pr}}$NDI)$Ni_2(C_6H_6)$ catalyst **1**[11] (3 mol%) was added to a toluene solution containing monomer **2**, effervescence of N_2 was observed, and the solution turned deep red over

the course of 30 min at room temperature (Table 3.1, entry 1). After 2 h, the crude polymer (**3**) was precipitated from the reaction mixture by addition of 1:1 MeOH/CH_2Cl_2. PolyAzoCarbazole (**3**) is soluble in toluene-d_8 at 100 °C and possesses all of the ^{1}H NMR resonances expected for the carbazole repeat unit (aromatic region: 8.47 (s, 2H), 8.16 (d, J = 8.4 Hz, 2H), 8.09 (d, J = 8.3 Hz, 2H)). ATR-IR analysis of solid samples revealed that nearly all of the azide from the starting material was consumed in the polymerization. However, a small residual stretch at 2106 cm^{-1} was detectable, indicating that unreacted aryl azides are present in the polymer chain ends. By GPC, a number average molecular weight (M_n) of 20.5 kg/mol was calculated (entry 1). This value corresponds to an average of 38 repeat units (X_n). The dispersity ($Đ_M$) for polymer **3** is 2.9. Therefore, the polymerization likely proceeds by a step-growth process as expected based on the catalytic mechanism.[9]

Table 3.1. Effect of Reaction Parameters on the Polymerization of 2.

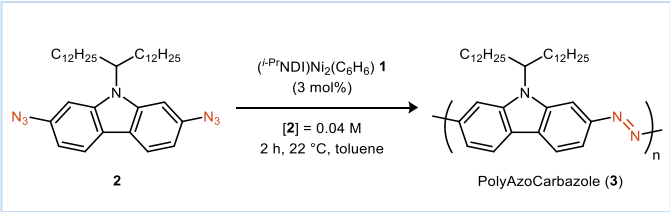

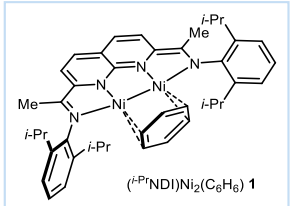

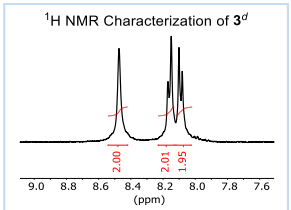

entry	deviation from Standard Conditions[a]	conversion of **2**	M_n (kg/mol)[c]	M_w (kg/mol)[c]	$Đ_M$[c]	X_n[c]
1	none	>99%	20.5	58.7	2.9	38
2	purification by Soxhlet extraction (C_6H_5Cl)[b]	>99%	42.1	92.5	2.2	77
3	1 mol% of **1**	31%	–	–	–	–
4	5 mol% of **1**	>99%	28.2	98.5	3.5	52
5	[**2**] = 0.02 M	79%	–	–	–	–
6	[**2**] = 0.08 M	>99%	35.2	104.2	3.0	65
7	60 °C	>99%	69.0	295.9	4.3	127
8	THF instead of toluene	>99%	8.6	18.6	2.1	16

[a]Standard Conditions: monomer **2** (0.017 mmol), ($^{i\text{-Pr}}$NDI)$Ni_2(C_6H_6)$ (**1**) (3 mol%), toluene (0.3 mL), 2 h, rt. Polymers were precipitated from the reaction mixtures using 1:1 MeOH/CH_2Cl_2 and isolated by filtration. [b]Polymer **3** was washed with MeOH, hexanes, and $CHCl_3$ then extracted with C_6H_5Cl in a Soxhlet apparatus. [c]Average molecular weights and $Đ_M$ values were determined by high temperature gel permeation chromatography (HT-GPC) (1,2,4-trichlorobenzene at 180 °C). [d]Aromatic region of the ^{1}H NMR for the purified polymer (entry 2).

Polymer **3** was further purified in a Soxhlet apparatus by continuous washing with MeOH, hexanes, and $CHCl_3$ then by continuous extraction with C_6H_5Cl (entry 2). Purification in this manner resulted in a higher average molecular weight polymer (M_n = 42.1 kg/mol, $Đ_M$ = 2.2), consistent with the removal of low molecular weight fractions. The IR band at 2106 cm^{-1} was absent in the Soxhlet purified polymer, presumably due to thermal decomposition of the end group azides.

Higher molecular weight polymers (M_n = 28.2–69.0 kg/mol) could be obtained by increasing the catalyst loading to 5 mol% (entry 4), increasing the reaction concentration two-fold (entry 6), or increasing the temperature to 60 °C (entry 7). Conversely, lower catalyst loadings (entry 3) or lower reaction concentrations (entry 5) resulted in incomplete monomer conversion and no high molecular weight products. Aromatic solvents were found to be critical for reaction efficiency. For example, a polymerization conducted in THF produced low molecular weight material (M_n = 8.6 kg/mol) (entry 8). Previously, we observed that the primary catalyst resting state for the N=N

coupling is the azoarene adduct and that the reaction is zero order in aryl azide.[9] Therefore, the observation of a pronounced solvent effect is consistent with a mechanism involving rate-limiting product displacement by toluene.

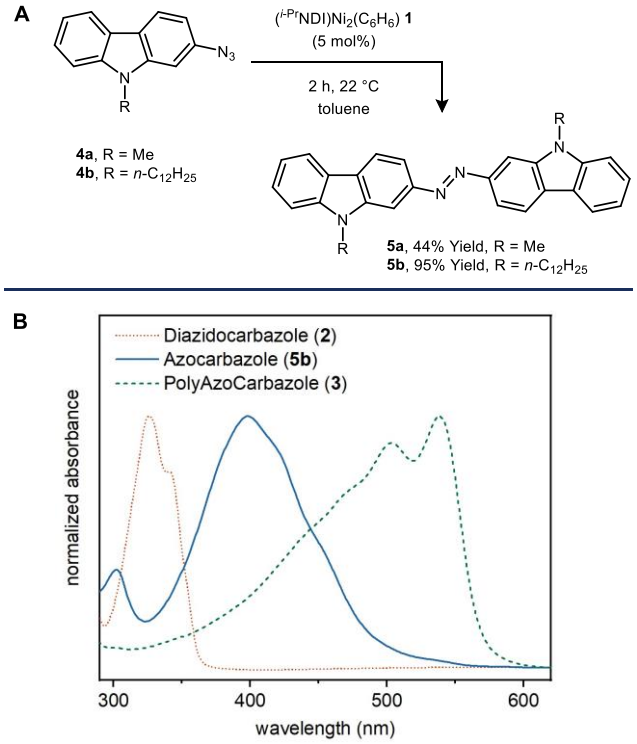

Figure 3.2. (A) Dinickel catalyzed dimerization of 2-azido carbazole **4**. (B) UV–vis spectra for diazido carbazole **2**, azocarbazole **5b**, and PolyAzoCarbazole **3**.

In order to assess the optical properties of PolyAzoCarbazole **3**, the corresponding azocarbazoles **5a** and **5b** were prepared as reference compounds (Figure 3.2A). Catalytic dimerizations provided **5a** and **5b** in 44% and 95% yield, respectively (5 mol% of **1**, 2 h, rt). Azocarbazole **5b** displays absorption maxima at 302 nm and 398 nm (Figure 3.2B). The lower energy band was assigned as a π–π* transition on the basis of TD-DFT models (B3LYP/6-31G(d,p)-PCM(C_6H_5Cl)). The UV-vis bands for PolyAzoCarbazole **3** are significantly red-shifted from those of **5b**, consistent with a higher degree of conjugation. Polymer **3** features absorption maxima at 503 nm and 538 nm, with shoulders extending to 350 nm. Polymers containing azo bonds are expected to have smaller HOMO–LUMO gaps than corresponding polymers containing

vinylene linkages. Accordingly, 2,7-carbazolene vinylene polymers possess absorption maxima at approximately 400–450 nm.[12]

Table 3.2. Scope of Azopolymers

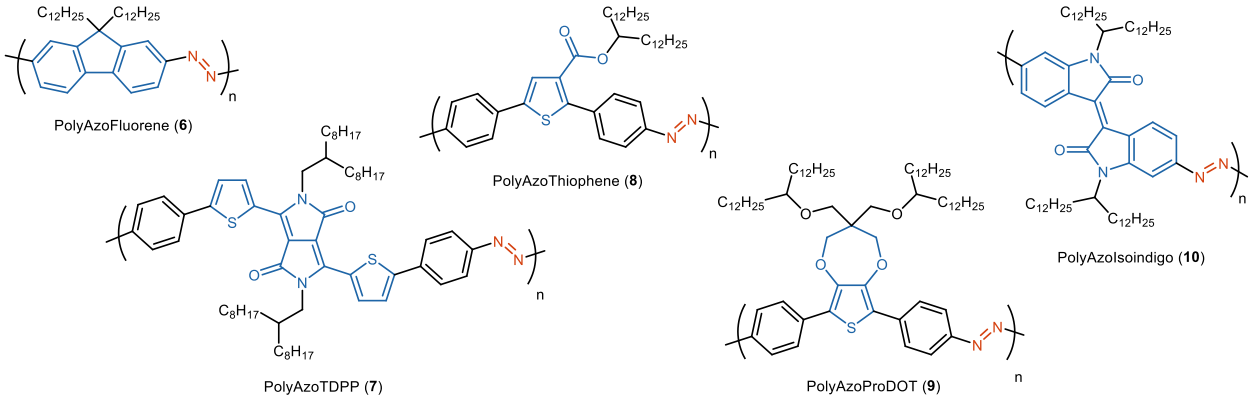

entry	polymer	M_n[b] (kg/mol)	M_w[b] (kg/mol)	$Đ_M$[b]	X_n[b]	selected λ_{max} values
1	PolyAzoFluorene (**6**)	101.9	336.9	3.3	192	484 (17,000), 520 (18,000)
2	PolyAzoTDPP (**7**)	6.4	12.5	2.0	6.5	426 (3,500), 664 (8,600)
3	PolyAzoThiophene (**8**)	39.4	122.9	3.1	60	427 (15,000)
4	PolyAzoProDOT (**9**)	60.4	143.3	2.4	55	514 (20,000), 543 (sh)
5	PolyAzoIsoindigo (**10**)[c]	18.2	48.1	2.6	18	481 (17,000), 664 (25,000), 709 (26,000)
6	PolyAzoProDOT/TDPP (1:1 **9**/**7**) (**11**)	50.4	118.6	2.4	–	442 (sh), 534 (7,900), 659 (sh), 710 (13,000)
7	PolyAzoProDOT/TDPP (3:1 **9**/**7**) (**12**)	97.9	246.4	2.5	–	521 (11,000), 644 (sh), 692 (6,300)

[a]Reaction Conditions: monomer (100 mg scale), ($^{i\text{-Pr}}$NDI)$Ni_2(C_6H_6)$ (**1**) (3 mol%), toluene (0.04 M), 2 h, rt. Polymers were precipitated from the reaction mixtures using MeOH and purified in a Soxhlet apparatus. [b]Average molecular weights and $Đ_M$ values were determined by HT- GPC (1,2,4-trichlorobenzene at 180 °C). [c]Reaction was carried out using 10 mol% of **1**.

Azocarbazole **5b** photoisomerizes to its *Z* form when irradiated with a 395 nm violet LED.[13,14] During irradiation, the intense band at 398 nm bleaches, and new features grow in at shorter wavelengths (λ_{max} = 303 and 324 nm). When stored in the dark at room temperature, **5b** undergoes isosbestic conversion back to its *E* form with a half-life of 4.1 min. In comparison to the well-defined photoswitching behavior of azocarbazole **5b**, PolyAzoCarbazole **3** exhibits minimal changes in its absorption spectrum when irradiated at the 538 nm band (555 nm green LED). This finding is in accordance with previous studies showing that photoswitching[15] is suppressed when two azo units are placed in conjugation through a central π-system–for example,

in a *para*-bis(azo)benzene.[16] Azobenzene photoisomerization requires a significant reduction in the N=N bond order upon population of the π* excited state. Thus, the lack of photoswitching in polymer **3** is indicative of a highly delocalized excited state electronic structure, where the N=N π* character is distributed over several azo units.

3.4 Substrate Scope Studies

With optimized reaction conditions in hand, we next examined the substrate scope of the azopolymerization (Table 3.2). PolyAzoFluorene (**6**) was generated with M_n = 101.9 kg/mol (X_n = 192), which is a notably high average molecular weight relative to conjugated main chain azopolymers that have been synthesized by other N=N coupling methods.[5a,6] Polymerizations of thiophene-containing monomers proceeded efficiently to form yellow polymer **8** and orange polymer **9**. Finally, azopolymers of different absorption wavelengths could be obtained by incorporating various chromophores into the repeat units. For example, PolyAzoIsoindigo (**10**) and PolyAzoTDPP (**7**) are both green polymers obtained with M_n = 18.2 kg/mol and 6.4 kg/mol, respectively. The relatively low molecular weight of PolyAzoTDPP (**7**) is likely due to the limits of solubility rather than inefficient N=N coupling. When polymerizations yielding **7** were run at higher catalyst loadings, we obtained copious amounts of precipitate that could not be redissolved in $CHCl_3$ or C_6H_5Cl.

3.5 Copolymerization of a Monomer Mixture

Copolymerization experiments were carried out using a mixture of TDPP and ProDOT monomers. PolyAzoProDOT (**9**) is an orange polymer with an absorption maximum at 514 nm (ε = 20,000 M^{-1} cm^{-1}), and PolyAzoTDPP (**7**) is a green polymer with absorption maxima at 664 nm (ε = 8,600 M^{-1} cm^{-1}) and 426 nm (ε = 3,500 M^{-1} cm^{-1}) (Figure 3). Copolymer **11** obtained using a 1:1 mixture of TDPP and ProDOT monomers is purple and absorbs across most of the visible spectrum (400–800 nm). ^{1}H NMR integration indicates that the copolymer contains a near 1:1 ratio of ProDOT and TDPP repeat units, matching the monomer feed ratio. Whereas the PolyAzoTDPP homopolymer (**7**) has limited solubility and could only be obtained in low molecular weight, copolymer **11** had a higher average molecular weight (M_n = 50.4 kg/mol), approaching that of the more soluble ProDOT homopolymer (**9**). The UV–vis spectrum of **11** contain the primary

absorption bands of the two homopolymers: 442 (sh), 534, 659 (sh), and 710 nm. When the ratio of monomers is adjusted to 3:1 (ProDOT/TDPP), the relative intensities of these features change in a manner that is consistent with a higher fraction of the ProDOT repeat unit.

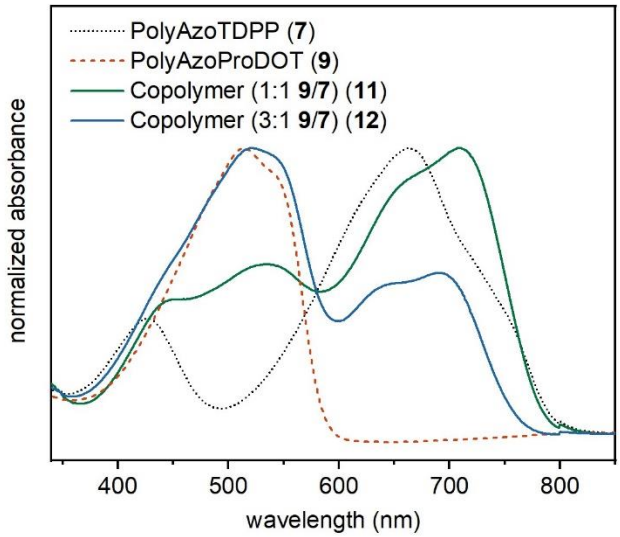

Figure 3.3. UV–vis spectra for PolyAzoProDOT/TDPP copolymers (**11** and **12**) and comparisons to homopolymers **7** and **9**.

3.6 Incorporation of End Groups into Azopolymers

Monofunctional chain stoppers can be used in step-growth polymerizations to control average molecular weight and to incorporate well-defined end groups. Carbazole diazide **2** was polymerized in the presence of carbazole monoazide **4b** (0.05 equiv) under the standard catalytic conditions (Table 3.3, entry 1). Consistent with the monofunctional azide promoting chain termination, the average molecular weight of polymer **13** (M_n = 14.1 kg/mol) was lower than that of polymer **3**, obtained in the absence of the chain stopper (M_n = 20.5 kg/mol). In the high-temperature ^{1}H NMR spectrum of **13**, there is a distinct resonance that can be assigned to the end groups at 4.02 ppm (*C*-H groups of the alkyl side chain immediately adjacent to the carbazole ring). By integrating this signal against that of the internal repeat units (4.70 ppm), we calculated an average ratio of 34 repeat units for every two end groups, which is similar to the X_n = 26 obtained from GPC analysis.

Other end groups could also be readily incorporated into azopolymers. Polymers containing 2-CF_3Ph (**13**), ferrocene (**14**), and isoindigo (**15**) chain ends were obtained with average molecular

weights ranging from 17.6–16.5 kg/mol (entries 2–4). In all cases, the end groups could be clearly detected in the high temperature ^{1}H NMR spectra of the isolated polymers. For polymer **13**, there is a ^{19}F NMR signal at –58.8 ppm, assigned to the 2-CF_3 group. Finally, a thin film of the ferrocene-capped polymer (**14**) dropcasted onto a glassy carbon electrode displayed a low-intensity reversible redox event at +0.02 V vs. free Fc/Fc^{+}.[17]

Table 3.3. End Group Incorporation into Azopolymers.

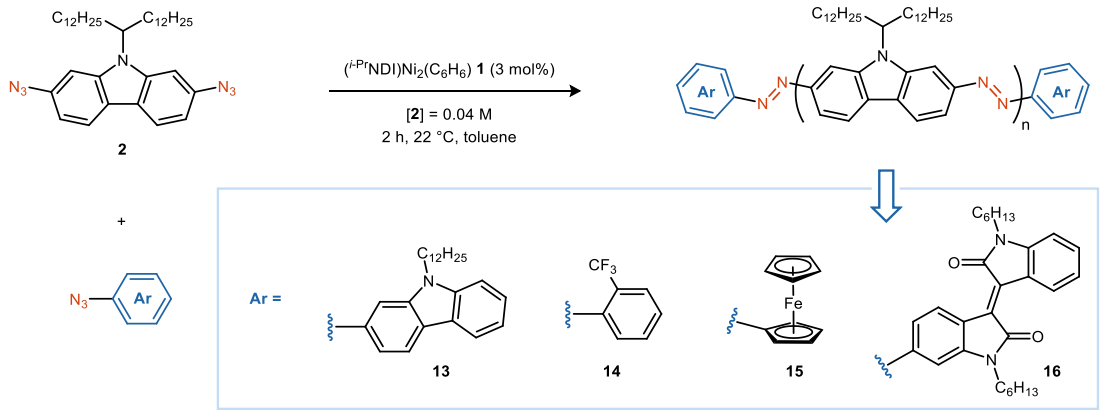

entry	end group	M_n[b] (kg/mol)	M_w[b] (kg/mol)	$Đ_M$[b]	X_n[b]	Observable NMR signals for the end group
1	carbazole (**13**)	14.1	28.5	2.0	26	^{1}H NMR: δ 7.97 (d, *J* = 7.9 Hz, 1H), 4.02 (br s, 2H),
2	2-(CF_3)Ph (**14**)	16.5	41.8	2.5	30	^{1}H NMR: δ 7.79 (d, *J* = 8.2 Hz, 1H), 7.58 (d, *J* = 7.7 Hz, 1H); ^{19}F NMR: δ –58.8
3	ferrocene (**15**)	17.0	41.3	2.4	31	^{1}H NMR: δ 5.15 (t, *J* = 2.0 Hz, 2H), 4.31 (t, *J* = 2.0 Hz, 2H), 4.10 (s, 5H)
4	isoindigo (**16**)	17.6	46.0	2.6	32	^{1}H NMR: δ 9.83 (br s, 1H), 9.62 (br s, 1H), 3.65 (br s, 2H)

[a]Reaction Conditions: monomer **2** (0.025 mmol, 1.0 equiv), monoazide (0.05 equiv), ($^{i\text{-Pr}}$NDI)$Ni_2(C_6H_6)$ (**1**) (3 mol%), toluene (0.63 mL), 2 h, rt. Polymers were precipitated from the reaction mixtures using MeOH and washed with Et_2O and CH_2Cl_2. [b]Average molecular weights and $Đ_M$ values were determined by HT-GPC (1,2,4-trichlorobenzene at 180 °C).

3.7 Protonation of Azopolymers

Azoarenes are Brønsted[18] and Lewis basic,[8j,19] and association of an acid results in a lowering of the π* LUMO level. Accordingly, addition of $B(C_6F_5)_3$ to solutions of azocarbazole **5b** in C_6H_5Cl resulted in an immediate color change from pale yellow to deep blue (Figure 3.4A). By UV–vis spectroscopy, the adduct **17b** possesses a π–π* transition that is red-shifted by 228 nm (Figure 3.4C). In order to characterize the nature of the interaction between $B(C_6F_5)_3$ and azocarbazole **5a**, single crystals of the adduct were obtained from C_6H_5Cl/pentane solutions (Figure 3.4B). The borane does not directly coordinate to the N=N bond, presumably due to prohibitive steric hindrance. Rather, $B(C_6F_5)_3$ and azocarbazole **5a** act as a frustrated Lewis pair and split adventitious water.[20] The product (**17a**) is a protonated diazenium ion bearing a $HOB(C_6F_5)_3$ counteranion. In the solid state structure, the diazenium *N*-H group is hydrogen-bonded to the anion with a *N*-H–O distance of 1.90 Å.

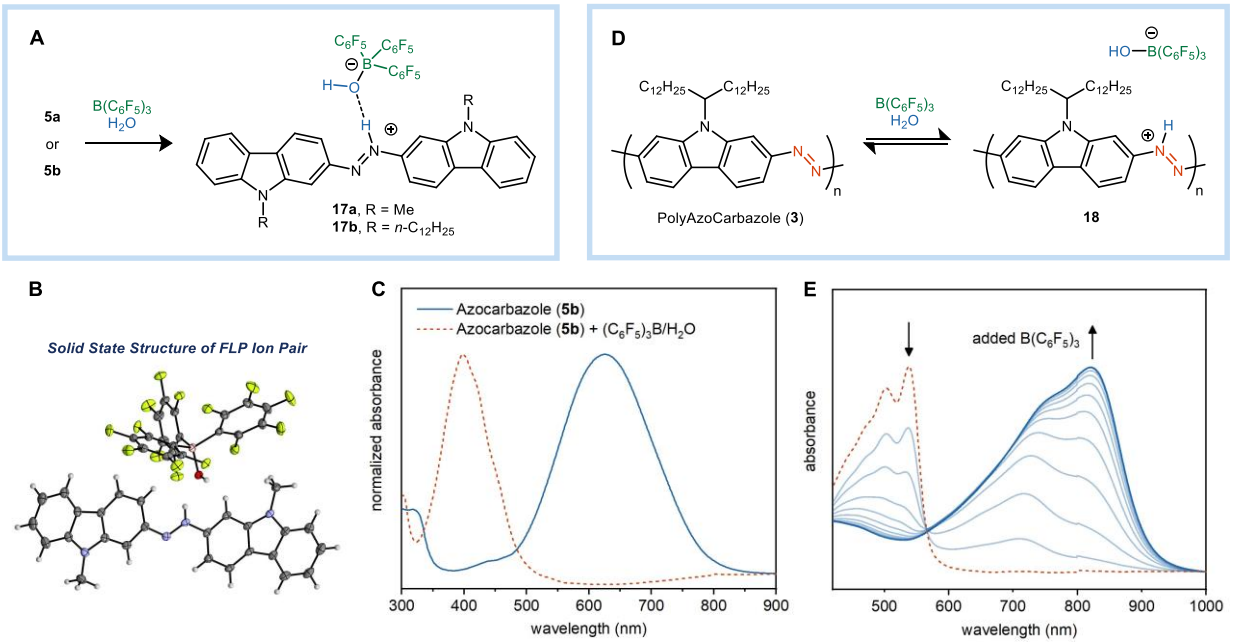

Figure 3.4. (A) Protonation of azocarbazole **5a** and **5b** using $B(C_6F_5)_3/H_2O$ (B) Solid state structure of the protonated azocarbazole (**17a**). (C) UV–vis spectra for **5b** with and without $(C_6F_5)_3B/H_2O$. (D) Protonation of PolyAzoCarbazole **3** using $B(C_6F_5)_3/H_2O$. (E) UV–vis titration experiment of PolyAzoCarbazole **3** in C_6H_5Cl (containing H_2O) with $B(C_6F_5)_3$.

We reasoned that protonation may provide an operationally straightforward approach to post-synthetically tuning the band gap of an azopolymer. A solution of PolyAzoCarbazole **3** dissolved in C_6H_5Cl was titrated with $B(C_6F_5)_3$ (Figure 3.4D). As $B(C_6F_5)_3$ was added, absorbance features in the 400–560 nm region decreased in intensity, and there was a corresponding growth of new bands spanning 600–950 nm (Figure 3.4E). Upon closer inspection, there is an initial band at 740 nm that appears at low $B(C_6F_5)_3$ concentrations. However, at higher concentrations of $B(C_6F_5)_3$, a longer wavelength band at 821 nm predominates. This lower energy feature may signify protonation of adjacent azo units at higher acid concentrations. The protonation of the azopolymer is fully reversible. Adding a drop of pyridine to the solution restores the initial red color and UV–vis spectrum of the neutral polymer.

3.8 Azopolymers as n-Type Materials

In contrast to p-type conjugated polymers, there is a dearth of high-performance n-type polymers, and many of them possess complex heterocycles that are challenging to synthesize.[21]

We hypothesized that azopolymers might be intrinsically suitable as n-type materials due to the N=N π* LUMO level being low-lying.[22]

To that end, we examined the electrochemical properties of PolyAzoIsoindigo (**10**), which contains an electron-deficient heterocycle as the repeat unit.[23] An FTO substrate was spin-coated with a thin film of **10**. Cyclic voltammetry experiments under an N_2 atmosphere showed a reduction event at $E_{1/2}$ = –0.62 V vs. Ag/AgCl (–0.52 V reduction onset: LUMO ~ –4.1 eV) (Figure 3.5A). Notably, this potential is approximately 150 mV more anodic than the reduction potential for the analogous vinylene isoindigo polymer.[23]

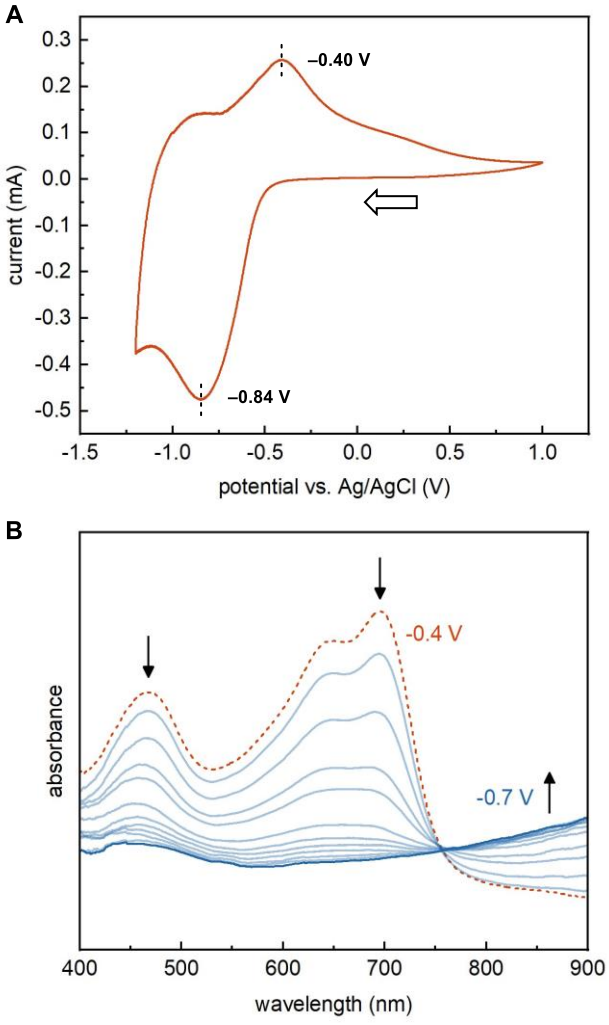

Figure 3.5. (A) Cyclic voltammetry data for a thin film of PolyAzoIsoindigo (**10**) deposited on FTO (N_2 atmosphere, 50 mV/s scan rate, 0.2 M $TBAPF_6$ in PC). (B) Spectroelectrochemical data: potentials stepped from –0.4 V to –0.7 V in 20 mV increments.

Spectroelectrochemical data were obtained by stepping the potential from –0.40 to –0.70 V in 20 mV increments (Figure 3.5B). Upon reduction, the absorption bands at 466 nm and 696 nm bleach, and there are polaron and bipolaron peaks in the NIR region that grow in. An isosbestic point at 755 nm indicates that the reduction is reversible. The polymer film proved to be stable over repeated redox cycles, suggesting that there is minimal degradation of the reduced state or delamination of the film. In contrast to the large number of p-type polymers that exhibit colored-to-transmissive switching upon oxidation, it is unusual to observe such electrochromic behavior in an n-type polymer.

3.9 Conclusions

The Ni_2 catalyzed nitrene dimerization provides synthetic entry into an underexplored class of conjugated polymers containing N=N linkages. Polymerizations proceed at room temperature, do not require any additional stoichiometric reagents, and are compatible with a broad scope of heterocycles. As compared to conjugated polymers prepared through cross-coupling reactions, azopolymers possess unique properties owing the functionality of the N=N bonds. For example, they can be protonated or associate Lewis acids, resulting in band-gap lowering. Azoarenes are also intrinsically electron-deficient due to their low-lying π^* LUMO levels. Consequently, azopolymers can be reversibly reduced under mild conditions, and, in the case of PolyAzoIsoindigo, reduction causes a bleaching of the absorption bands in the visible region. Future efforts will be directed at exploring the materials properties of conjugated azopolymers.

3.10 Acknowledgements

This research was supported by the NSF (CHE-1554787). X-ray diffraction data were collected using an instrument funded by the NSF (CHE-1625543). We thank Matthias Zeller for assistance with X-ray crystallography and Xuyi Luo for assistance with HT-GPC. C.U. acknowledges support from a Camille Dreyfus Teacher–Scholar award. J.M. and Z.W. are grateful for an unrestricted gift from Ambilight Inc.

3.11 References.

(1) (a) Thomas, S. W.; Joly, G. D.; Swager, T. M. "Chemical sensors based on amplifying fluorescent conjugated polymers" *Chem. Rev.* **2007**, *107*, 1339-1386; (b) Grimsdale, A. C.; Leok Chan, K.; Martin, R. E.; Jokisz, P. G.; Holmes, A. B. "Synthesis of light-emitting conjugated polymers for applications in electroluminescent devices" *Chem. Rev.* **2009**, *109*, 897-1091; (c) Cheng, Y.-J.; Yang, S.-H.; Hsu, C.-S. "Synthesis of conjugated polymers for organic solar cell applications" *Chem. Rev.* **2009**, *109*, 5868-5923; (d) Facchetti, A. "Π-conjugated polymers for organic electronics and photovoltaic cell applications" *Chem. Mater.* **2011**, *23*, 733-758; (e) Zhu, C.; Liu, L.; Yang, Q.; Lv, F.; Wang, S. "Water-soluble conjugated polymers for imaging, diagnosis, and therapy" *Chem. Rev.* **2012**, *112*, 4687-4735; (f) Muench, S.; Wild, A.; Friebe, C.; Häupler, B.; Janoschka, T.; Schubert, U. S. "Polymer-based organic batteries" *Chem. Rev.* **2016**, *116*, 9438-9484; (g) Ostroverkhova, O. "Organic optoelectronic materials: Mechanisms and applications" *Chem. Rev.* **2016**, *116*, 13279-13412.

(2) (a) Sakamoto, J.; Rehahn, M.; Wegner, G.; Schlüter, A. D. "Suzuki polycondensation: Polyarylenes à la carte" *Macromol. Rapid Commun.* **2009**, *30*, 653-687; (b) Kiriy, A.; Senkovskyy, V.; Sommer, M. "Kumada catalyst-transfer polycondensation: Mechanism, opportunities, and challenges" *Macromol. Rapid Commun.* **2011**, *32*, 1503-1517; (c) Carsten, B.; He, F.; Son, H. J.; Xu, T.; Yu, L. "Stille polycondensation for synthesis of functional materials" *Chem. Rev.* **2011**, *111*, 1493-1528; (d) Pouliot, J.-R.; Grenier, F.; Blaskovits, J. T.; Beaupré, S.; Leclerc, M. "Direct (hetero)arylation polymerization: Simplicity for conjugated polymer synthesis" *Chem. Rev.* **2016**, *116*, 14225-14274; (e) Leone, A. K.; Mueller, E. A.; McNeil, A. J. "The history of palladium-catalyzed cross-couplings should inspire the future of catalyst-transfer polymerization" *J. Am. Chem. Soc.* **2018**, *140*, 15126-15139.

(3) (a) Lundgren, R. J.; Stradiotto, M. "Addressing challenges in palladium-catalyzed cross-coupling reactions through ligand design" *Chem.-Eur. J.* **2012**, *18*, 9758-9769; (b) Campeau, L.-C.; Hazari, N. "Cross-coupling and related reactions: Connecting past success to the development of new reactions for the future" *Organometallics* **2019**, *38*, 3-35; (c) Leone, A. K.; McNeil, A. J. "Matchmaking in catalyst-transfer polycondensation: Optimizing catalysts based on mechanistic insight" *Acc. Chem. Res.* **2016**, *49*, 2822-2831.

(4) Fliegl, H.; Köhn, A.; Hättig, C.; Ahlrichs, R. "Ab initio calculation of the vibrational and electronic spectra of trans- and cis-azobenzene" *J. Am. Chem. Soc.* **2003**, *125*, 9821-9827.

(5) (a) Nguyen, H. T.; Coulembier, O.; Gheysen, K.; Martins, J. C.; Dubois, P. "Copper-catalyzed dehydrogenative polycondensation of a bis-aniline hexylthiophene-based monomer: A kinetically controlled air-tolerant process" *Macromolecules* **2012**, *45*, 9547-9550; (b) Arab, P.; Rabbani, M. G.; Sekizkardes, A. K.; İslamoğlu, T.; El-Kaderi, H. M. "Copper(i)-catalyzed synthesis of nanoporous azo-linked polymers: Impact of textural properties on gas storage and selective carbon dioxide capture" *Chem. Mater.* **2014**, *26*, 1385-1392.

(6) Wang, L.; Pan, X.; Zhao, Y.; Chen, Y.; Zhang, W.; Tu, Y.; Zhang, Z.; Zhu, J.; Zhou, N.; Zhu, X. "A straightforward protocol for the highly efficient preparation of main-chain azo polymers directly from bisnitroaromatic compounds by the photocatalytic process" *Macromolecules* **2015**, *48*, 1289-1295.

(7) (a) Hamon, F.; Djedaini-Pilard, F.; Barbot, F.; Len, C. "Azobenzenes—synthesis and carbohydrate applications" *Tetrahedron* **2009**, *65*, 10105-10123; (b) Merino, E. "Synthesis of azobenzenes: The coloured pieces of molecular materials" *Chem. Soc. Rev.* **2011**, *40*, 3835-3853.

(8) Recent examples of conjugated azopolymers synthesized by C–C cross-coupling: (a) Bléger, D.; Liebig, T.; Thiermann, R.; Maskos, M.; Rabe, J. P.; Hecht, S. "Light-orchestrated macromolecular "accordions": Reversible photoinduced shrinking of rigid-rod polymers" *Angew. Chem., Int. Ed.* **2011**, *50*, 12559-12563; (b) Zhang, W.; Yoshida, K.; Fujiki, M.; Zhu, X. "Unpolarized-light-driven amplified chiroptical modulation between chiral aggregation and achiral disaggregation of an azobenzene-alt-fluorene copolymer in limonene" *Macromolecules* **2011**, *44*, 5105-5111; (c) Anwar, N.; Willms, T.; Grimme, B.; Kuehne, A. J. C. "Light-switchable and monodisperse conjugated polymer particles" *ACS Macro Lett.* **2013**, *2*, 766-769; (d) Yan, Z.; Sun, B.; Guo, C.; Li, Y. "Synthesis and properties of azothiazole based π-conjugated polymers" *J. Mater. Chem. C* **2014**, *2*, 7096-7103; (e) Cheng, H. L.; Tang, M. T.; Tuchinda, W.; Enomoto, K.; Chiba, A.; Saito, Y.; Kamiya, T.; Sugimoto, M.; Saeki, A.; Sakurai, T.; Omichi, M.; Sakamaki, D.; Seki, S. "Reversible control of radius and morphology of fluorene-azobenzene copolymer nanowires by light exposure" *Adv. Mater. Interfaces* **2015**, *2*, 1400450; (f) Gon, M.; Tanaka, K.; Chujo, Y. "A highly efficient near-infrared-emissive copolymer with a N=N double-bond π-conjugated system based on a fused azobenzene–boron complex" *Angew. Chem., Int. Ed.* **2018**, *57*, 6546-6551; (g) Wang, K.; Yin, L.; Miu, T.; Liu, M.; Zhao, Y.; Chen, Y.; Zhou, N.; Zhang, W.; Zhu, X. "Design and synthesis of a novel azobenzene-containing polymer both in the main- and side-chain toward unique photocontrolled isomerization properties" *Mater. Chem. Front.* **2018**, *2*, 1112-1118; (h) Otaki, M.; Kumai, R.; Sagayama, H.; Goto, H. "Synthesis and properties of chiral polyazobenzenes with photoinduced change in optical activity" *Macromolecules* **2019**, *52*, 2340-2348; (i) Otaki, M.; Kumai, R.; Goto, H. "Synthesis of methyl-substituted azobenzene–carbazole conjugated copolymers with photoinduced structural changes" *J. Polym. Sci., Part A: Polym. Chem.* **2019**, *57*, 1756-1764; (j) Wakabayashi, J.; Gon, M.; Tanaka, K.; Chujo, Y. "Near-infrared absorptive and emissive poly(p-phenylene vinylene) derivative containing azobenzene–boron complexes" *Macromolecules* **2020**, *53*, 4524-4532.

(9) Powers, I. G.; Andjaba, J. M.; Luo, X.; Mei, J.; Uyeda, C. "Catalytic azoarene synthesis from aryl azides enabled by a dinuclear ni complex" *J. Am. Chem. Soc.* **2018**, *140*, 4110-4118.

(10) Additional safety notes for organoazides are included in the Supporting Information. For information about organoazide hazard assessment: (a) Kolb, H. C.; Finn, M. G.; Sharpless, K. B. "Click chemistry: Diverse chemical function from a few good reactions" *Angew. Chem., Int. Ed.* **2001**, *40*, 2004-2021; (b) Bräse, S.; Gil, C.; Knepper, K.; Zimmermann, V. "Organic azides: An exploding diversity of a unique class of compounds" *Angew. Chem., Int. Ed.* **2005**, *44*, 5188-5240; (c) Keicher, T.; Löbbecke, S. Lab-Scale Synthesis of Azido Compounds: Safety Measures and Analysis. In *Organic Azides* Bräse, S.; Banert, K., Eds.; John Wiley and Sons, Ltd: Chichester, U.K., 2010, pp 1-27; (d) Zhu, H.-T.; Arosio, L.; Villa, R.; Nebuloni, M.; Xu, H. "Process safety assessment of the iron-catalyzed direct olefin diazidation for the expedient synthesis of vicinal primary diamines" *Org. Process Res. Dev.* **2017**, *21*, 2068-2072.

(11) Zhou, Y.-Y.; Hartline, D. R.; Steiman, T. J.; Fanwick, P. E.; Uyeda, C. "Dinuclear nickel complexes in five states of oxidation using a redox-active ligand" *Inorg. Chem.* **2014**, *53*, 11770-11777.

(12) (a) Morin, J.-F.; Drolet, N.; Tao, Y.; Leclerc, M. "Syntheses and characterization of electroactive and photoactive 2,7-carbazolenevinylene-based conjugated oligomers and polymers" *Chem. Mater.* **2004**, *16*, 4619-4626; (b) Drolet, N.; Morin, J.-F.; Leclerc, N.; Wakim, S.; Tao, Y.; Leclerc, M. "2,7-carbazolenevinylene-based oligomer thin-film transistors: High mobility through structural ordering" *Adv. Funct. Mater.* **2005**, *15*, 1671-1682; (c) Leclerc, N.; Michaud, A.; Sirois, K.; Morin, J.-F.; Leclerc, M. "Synthesis of 2,7-carbazolenevinylene-based copolymers and characterization of their photovoltaic properties" *Adv. Funct. Mater.* **2006**, *16*, 1694-1704.

(13) (a) Hartley, G. S. "The cis-form of azobenzene" *Nature* **1937**, *140*, 281; (b) Schultz, T.; Quenneville, J.; Levine, B.; Toniolo, A.; Martínez, T. J.; Lochbrunner, S.; Schmitt, M.; Shaffer, J. P.; Zgierski, M. Z.; Stolow, A. "Mechanism and dynamics of azobenzene photoisomerization" *J. Am. Chem. Soc.* **2003**, *125*, 8098-8099; (c) Cembran, A.; Bernardi, F.; Garavelli, M.; Gagliardi, L.; Orlandi, G. "On the mechanism of the cis−trans isomerization in the lowest electronic states of azobenzene: S0, S1, and T1" *J. Am. Chem. Soc.* **2004**, *126*, 3234-3243; (d) Wang, X. Azo Polymer Syntheses. In *Azo polymers: Synthesis, functions and applications*; Springer Berlin Heidelberg: Berlin, Heidelberg, 2017, p 19-56.

(14) (a) Bandara, H. M. D.; Burdette, S. C. "Photoisomerization in different classes of azobenzene" *Chem. Soc. Rev.* **2012**, *41*, 1809-1825; (b) Dong, M.; Babalhavaeji, A.; Samanta, S.; Beharry, A. A.; Woolley, G. A. "Red-shifting azobenzene photoswitches for in vivo use" *Acc. Chem. Res.* **2015**, *48*, 2662-2670; (c) Bléger, D.; Hecht, S. "Visible-light-activated molecular switches" *Angew. Chem., Int. Ed.* **2015**, *54*, 11338-11349.

(15) (a) Kumar, G. S.; Neckers, D. C. "Photochemistry of azobenzene-containing polymers" *Chem. Rev.* **1989**, *89*, 1915-1925; (b) Natansohn, A.; Rochon, P. "Photoinduced motions in azo-containing polymers" *Chem. Rev.* **2002**, *102*, 4139-4176; (c) Mahimwalla, Z.; Yager, K. G.; Mamiya, J.-I.; Shishido, A.; Priimagi, A.; Barrett, C. J. "Azobenzene photomechanics: Prospects and potential applications" *Polym. Bull.* **2012**, *69*, 967-1006.

(16) Cisnetti, F.; Ballardini, R.; Credi, A.; Gandolfi, M. T.; Masiero, S.; Negri, F.; Pieraccini, S.; Spada, G. P. "Photochemical and electronic properties of conjugated bis(azo) compounds: An experimental and computational study" *Chem.-Eur. J.* **2004**, *10*, 2011-2021.

(17) Kurihara, M.; Matsuda, T.; Hirooka, A.; Yutaka, T.; Nishihara, H. "Novel photoisomerization of azoferrocene with a low-energy mlct band and significant change of the redox behavior between the cis- and trans-isomers" *J. Am. Chem. Soc.* **2000**, *122*, 12373-12374.

(18) (a) Jaffé, H. H.; Yeh, S.-J.; Gardner, R. W. "The electronic spectra of azobenzene derivatives and their conjugate acids" *J. Mol. Spectrosc.* **1958**, *2*, 120-136; (b) Collins, J. H.; Jaffe, H. H. "The structures of the conjugate acids of cis- and trans-azobenzenes" *J. Am. Chem. Soc.* **1962**, *84*, 4708-4712; (c) Hoefnagel, M. A.; van Veen, A.; Wepster, B. M. "Protonation of azo-compounds. Part II: The structure of the conjugate acid of trans-azobenzene" *Recl. Trav. Chim. Pays-Bas* **1969**, *88*, 562-572.

(19) (a) Fraleoni-Morgera, A.; Giorgini, L.; Zanirato, P. "[arylazobenzene–BF_3] dyes: Electronic absorption and nmr spectroscopic evidence for a novel class of dyes stable in aprotic solvents" *Dyes and Pigments* **2008**, *76*, 394-399; (b) Yang, Y.; Hughes, R. P.; Aprahamian, I. "Visible light switching of a BF_2-coordinated azo compound" *J. Am. Chem. Soc.* **2012**, *134*, 15221-15224; (c) Yang, Y.; Hughes, R. P.; Aprahamian, I. "Near-infrared light activated azo-BF_2 switches" *J. Am. Chem. Soc.* **2014**, *136*, 13190-13193.

(20) Stephan, D. W. "Frustrated lewis pairs" *J. Am. Chem. Soc.* **2015**, *137*, 10018-10032.

(21) (a) Sui, Y.; Deng, Y.; Du, T.; Shi, Y.; Geng, Y. "Design strategies of n-type conjugated polymers for organic thin-film transistors" *Mater. Chem. Front.* **2019**, *3*, 1932-1951; (b) Jia, H.; Lei, T. "Emerging research directions for n-type conjugated polymers" *J. Mater. Chem. C* **2019**, *7*, 12809-12821; (c) Genene, Z.; Mammo, W.; Wang, E.; Andersson, M. R. "Recent advances in n-type polymers for all-polymer solar cells" *Adv. Mater.* **2019**, *31*, 1807275.

(22) Sadler, J. L.; Bard, A. J. "Electrochemical reduction of aromatic azo compounds" *J. Am. Chem. Soc.* **1968**, *90*, 1979-1989.

(23) Stalder, R.; Mei, J.; Subbiah, J.; Grand, C.; Estrada, L. A.; So, F.; Reynolds, J. R. "N-type conjugated polyisoindigos" *Macromolecules* **2011**, *44*, 6303-6310.

APPENDIX A. SUPPORTING INFORMATION FOR CHAPTER 1.

1. Spectroscopic and Cyclic Voltammetric Data for Dinickel Complexes

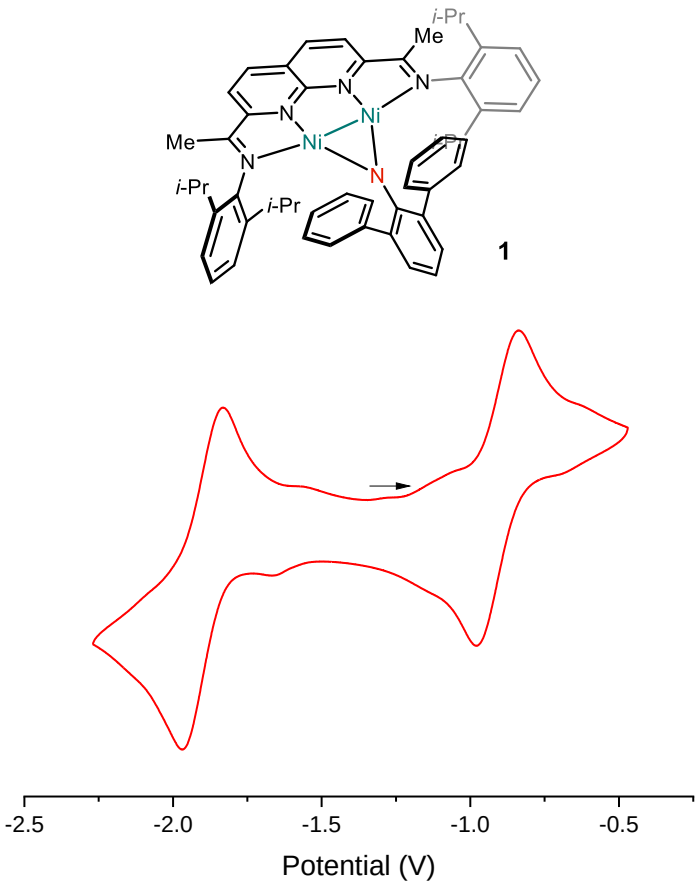

Figure S1. Cyclic voltammogram for ($^{i\text{-Pr}}$NDI)Ni_2(μ-NAr) (**1**) (0.3 M [*n*-Bu_4N][PF_6] supporting electrolyte in THF, glassy carbon working electrode, 100 mV/s scan rate). The scan begins at the open circuit potential and proceeds in the indicated direction.

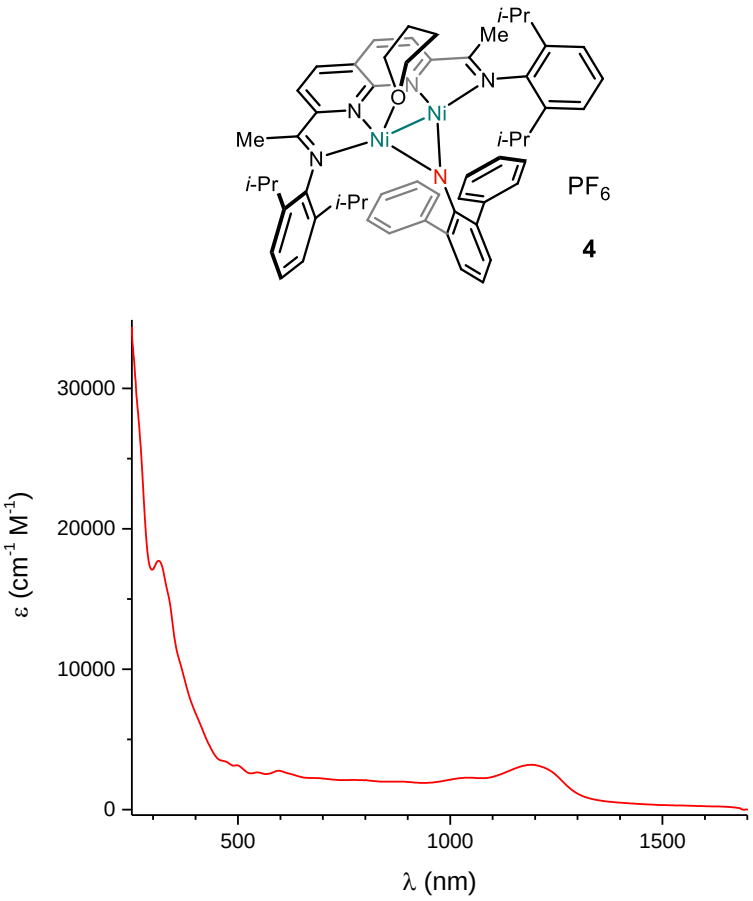

Figure S2. UV–vis–NIR spectrum of **4** in THF (0.128 mM).

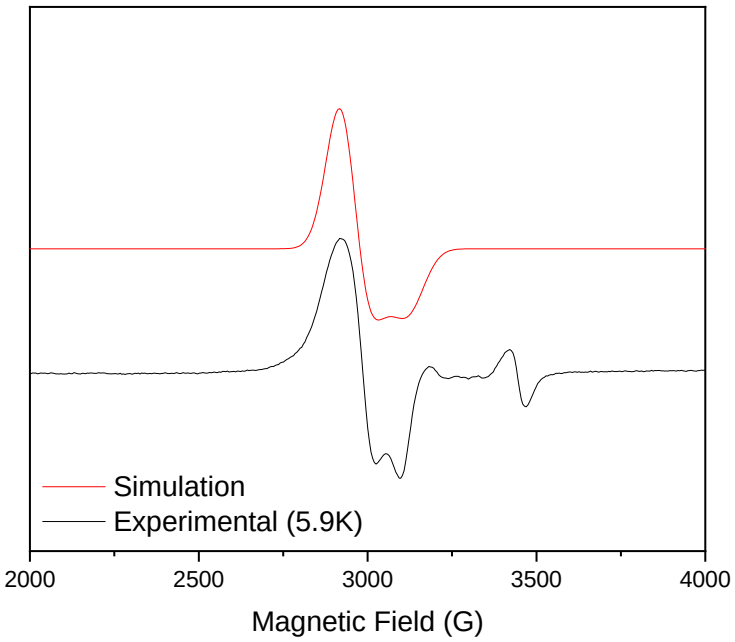

Figure S3. Frozen solution (5.9 K, THF) X-band EPR spectrum for **4**. Simulated parameters: g_1 = 2.341, g_2 = 2.206. $g_{max} - g_{min}$ = 0.135. The signal at g = 2.0 is attributed to an uncharacterized *S* = 1/2 impurity.

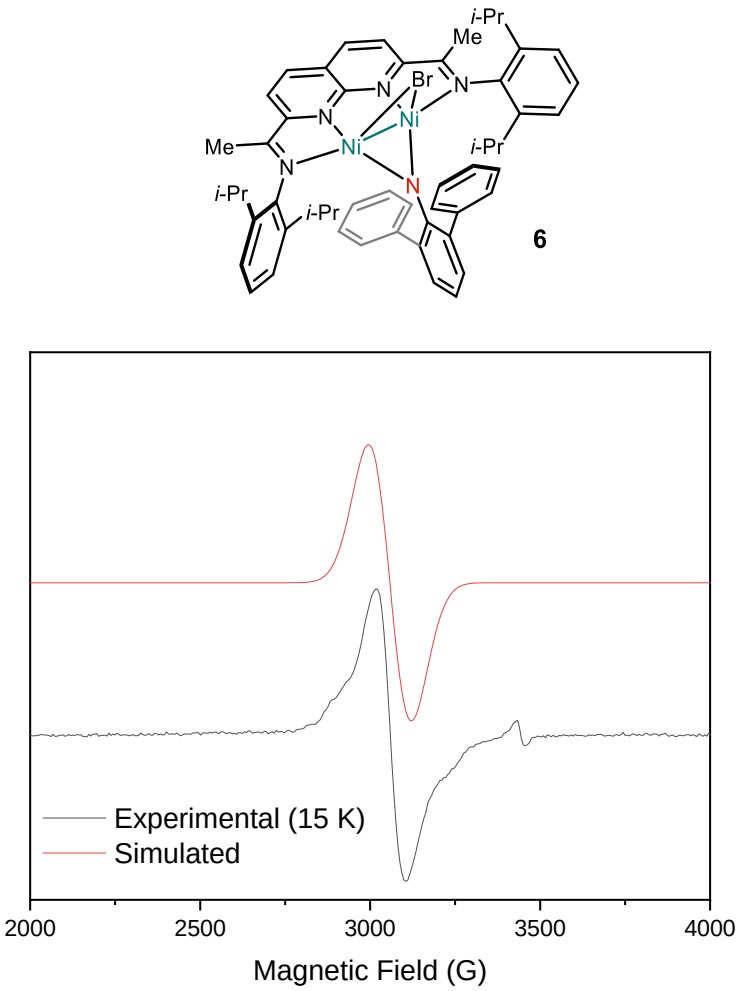

Figure S4. Frozen solution (15 K, THF) X-band EPR spectrum for **6**. Simulated parameters: g_1 = 2.254.

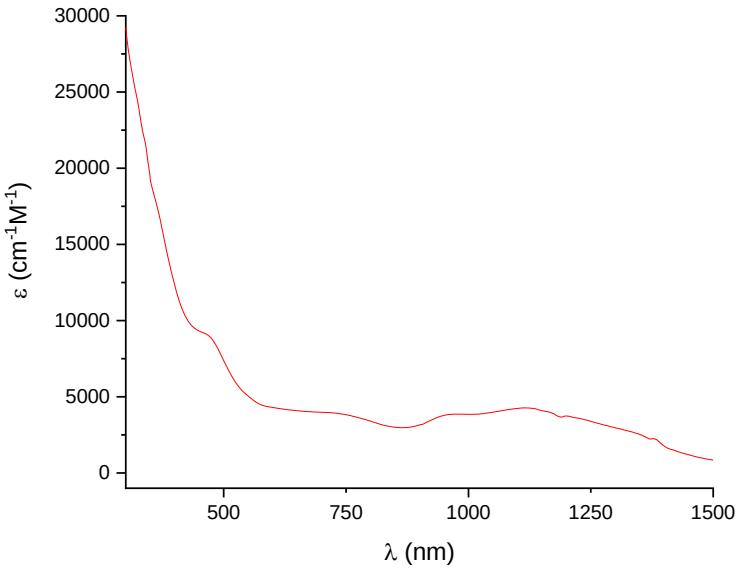

Figure S5. UV-vis-NIR spectrum of **6** in THF (0.057 mM).

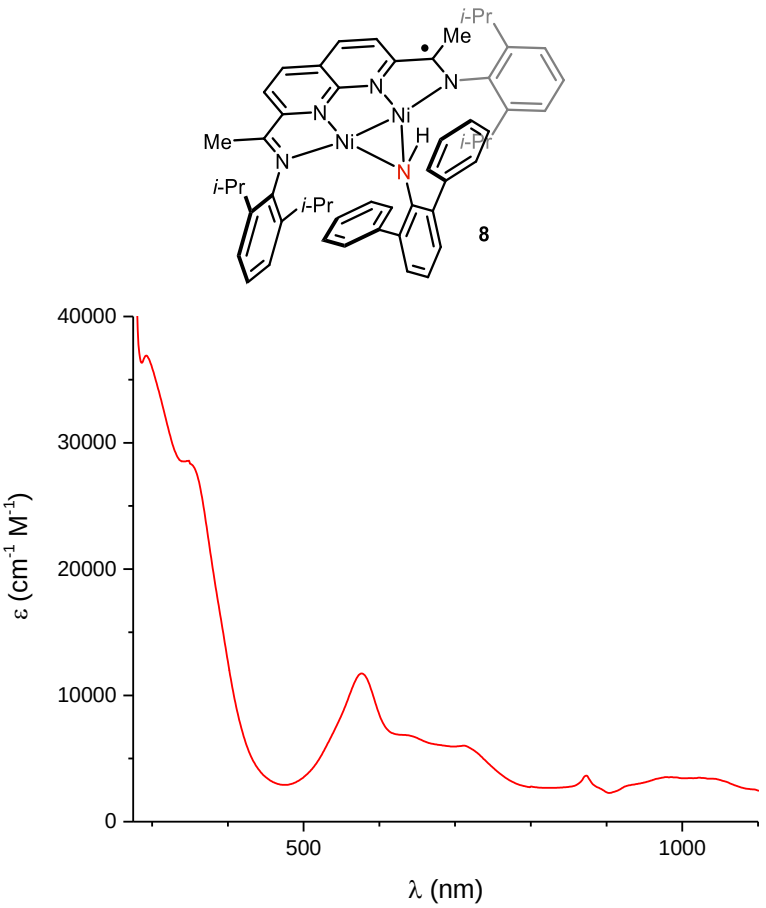

Figure S6. UV-Vis-NIR spectrum of **8** in C_6H_6 (0.067 mM).

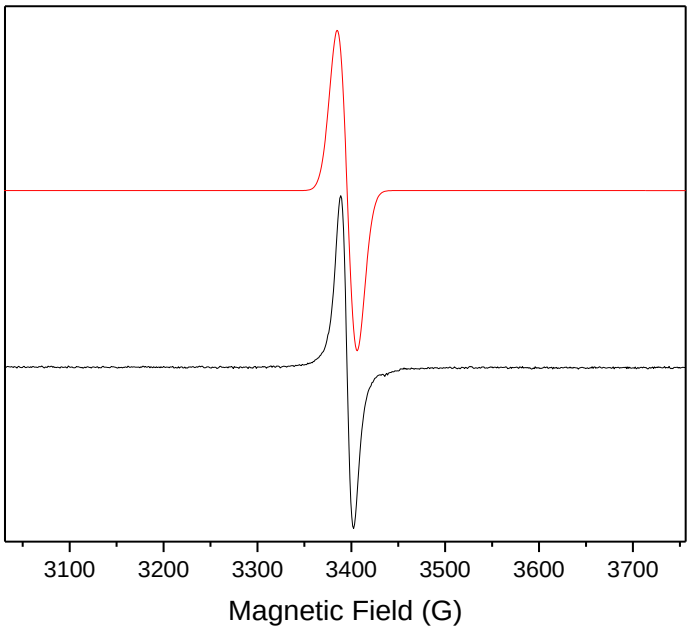

Figure S7. Solution (298 K, toluene) X-band EPR spectrum for **8**. Simulated parameters: g_{iso} = 2.071.

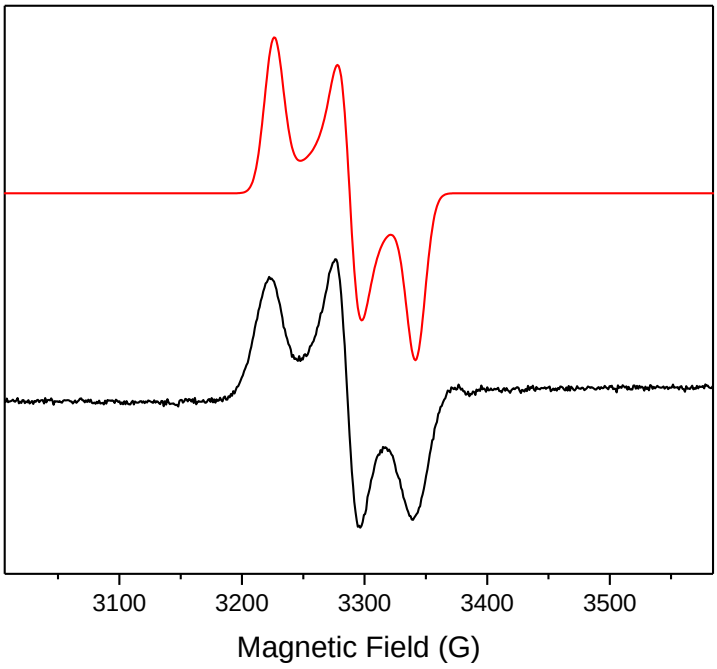

Figure S8. Frozen solution (108 K, toluene) X-band EPR spectrum for **8**. Simulated parameters: $g_1 = 2.032$ $g_2 = 2.066$ $g_3 = 2.105$. $g_{max} - g_{min} = 0.073$.

2. Stoichiometric Decomposition Reactions of Dinickel Complexes

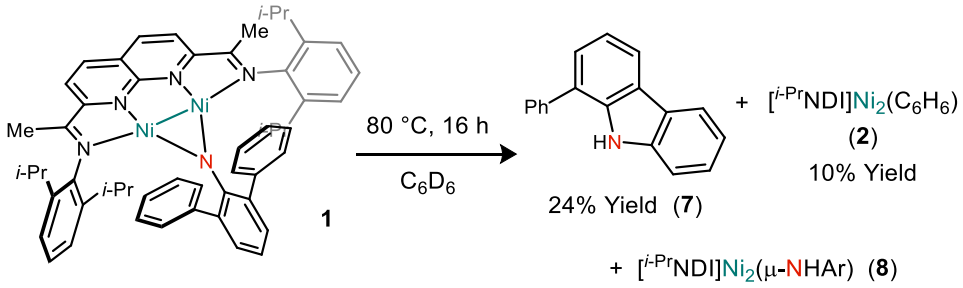

Stoichiometric decomposition of Compound 1. In an N_2 filled glovebox, a J-Young NMR tube was charged with **1** (12.5 mg, 0.014 mmol, 1.0 equiv), *m*-terphenylazide (3.7 mg, 0.014 mmol, 1.0 equiv), and C_6D_6, along with 1,3,5-trimethoxybenzene (2.1 mg, 0.013 mmol) as an internal standard. After mixing for 10 min, the brown reaction mixture was heated at 80 °C for 16 h resulting in a color change to dark blue. The yields of 1-phenyl-9-H-carbazole (**7**) and recovered **2** were determined by ^{1}H NMR integration against the internal standard (24% and 10%, respectively). Complex **8** was identified as the major S = 1/2 compound by EPR and UV-Vis.

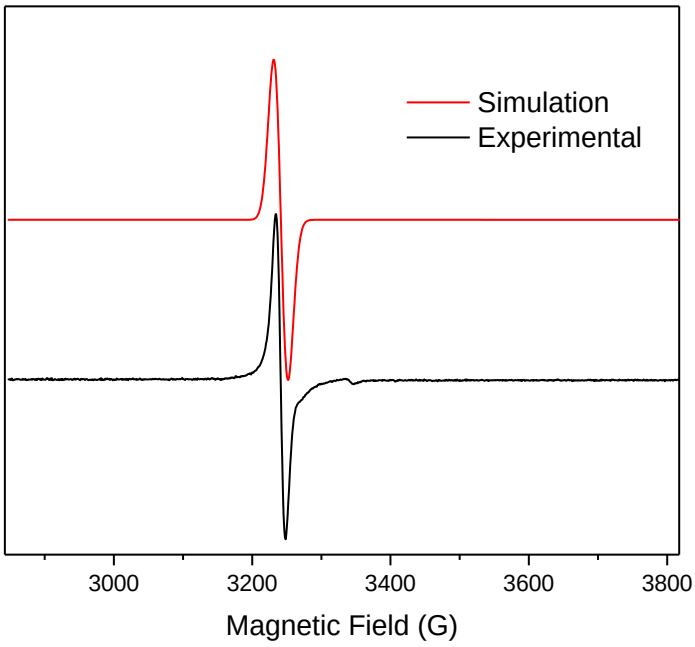

Figure S9. EPR spectrum for the decomposition of **1** (298 K, C_6H_6). Simulated parameters g_{iso} = 2.068.

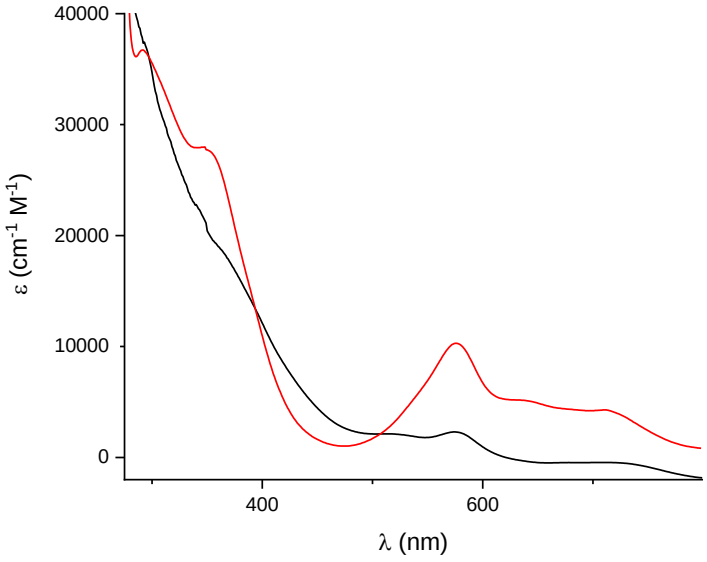

Figure S10. UV-Vis spectrum for the decomposition of **1** in C_6H_6 (0.073 mM) in black overlaid with spectrum of isolated **8** in C_6H_6 (0.067 mM) in red.

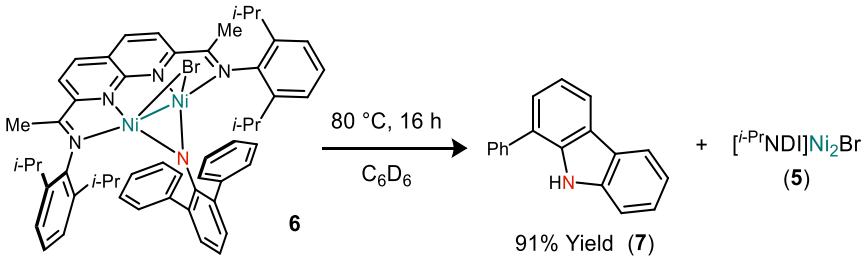

Stoichiometric decomposition of Compound 6. In an N_2 filled glovebox, a J-Young NMR tube was charged with **6** (9.4 mg, 0.0097 mmol) and C_6D_6 (1.0 mL) along with 1,3,5-trimethoxybenzene (2.2 mg, 0.013 mmol) as an internal standard. After mixing for 10 min, the reaction mixture was heated at 80 °C for 16 h. The yield of 1-phenyl-9-H-carbazole (**7**) was determined to be 91% by ^{1}H NMR integration against the internal standard. Complex **5** was identified as the primary S = 1/2 product by EPR.

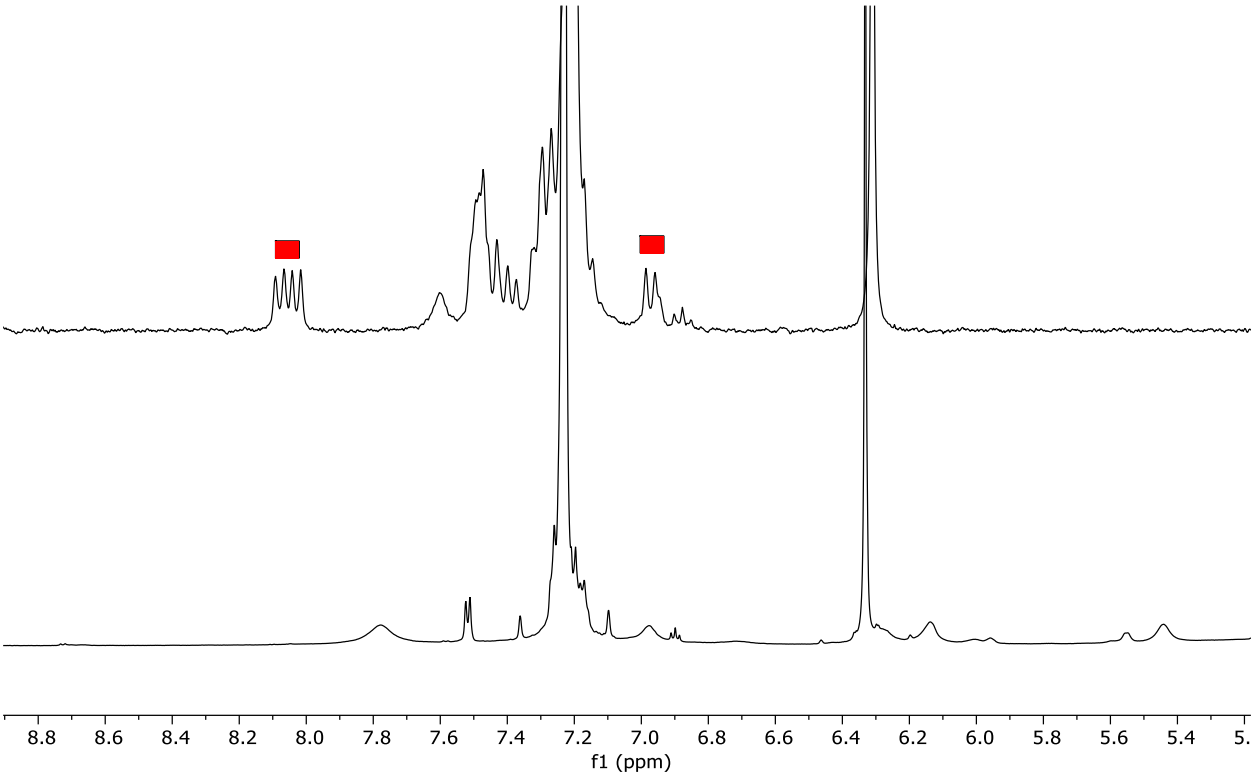

Figure S11. Initial ^{1}H NMR spectrum of **6** (bottom) and of **6** after heating at 80 °C for 16 h (top). Red squares indicate peaks corresponding to **7.**

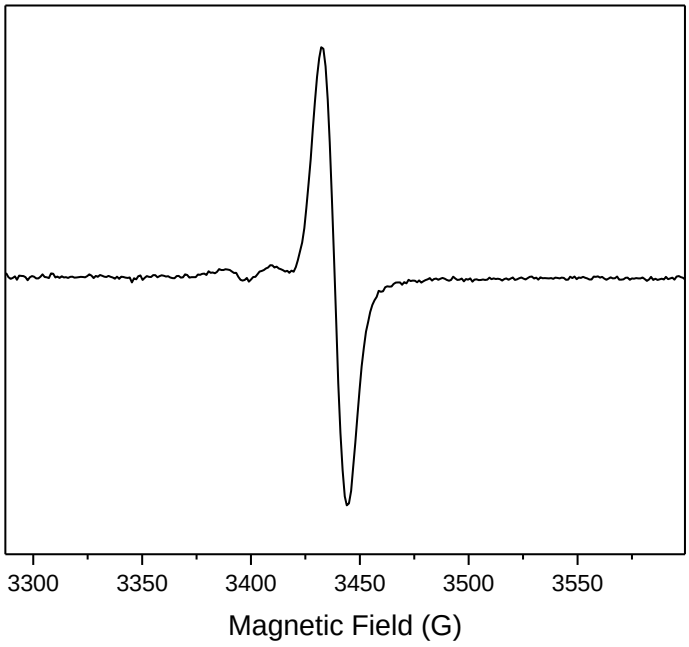

Figure S12. EPR spectrum after heating **6** at 80 °C for 16 h. Simulated parameters g_{iso} = 2.04.

3. Catalytic C–H Amination Reactions of 3

General Procedure. In an N_2 filled glovebox, a J-Young NMR tube was charged with catalyst (10 mol%), *m*-terphenylazide (3.0 mg, 0.011 mmol) 1,3,5-trimethoxybenzene (1.9 mg, 0.011 mmol) as an internal standard, and toluene-d_8 (700 µL). The reaction was heated at 80 °C for 72 h. The yields of indole **7** and aniline **10** were determined by ^{1}H NMR integration against the internal standard.

Procedure for entry 5. In an N_2 filled glovebox, a J-Young NMR tube was charged with **2** (0.95 mg, 0.0013mmol, 5 mol%), $[Cp_2Fe]PF_6$ (0.43 mg, 1.0 equiv), *m*-terphenylazide (3.0 mg, 0.011 mmol), 1,3,5-trimethoxybenzene (1.9 mg, 0.011 mmol) as an internal standard, and toluene-d_8 (700 µL). The reaction was heated at 110 °C for 24 hours. The yields of indole **7** and aniline **10** were determined by ^{1}H NMR integration against the internal standard.

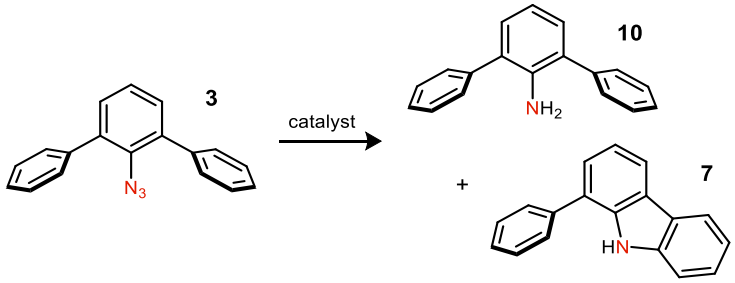

entry	catalyst	Yield of **7**	Yield of **10**
1	Ni_2(µ-NAr) **1**	39%	33%
2	Ni_2(µ-NHAr) **8**	44%	39%
3	Ni_2(µ-Br) **5**	77%	16%
4	$[Ni_2(\mu\text{-NAr})(thf)]^+$ **4**	89%	6%
5[a]	$[Ni_2(\mu\text{-NAr})(thf)]^+$ **4**	87%	6%
6[b]	$[Ni_2(\mu\text{-NAr})(thf)]^+$ **4**	96%	<2%

Figure S13. [a]See procedure above. [b]Reaction conditions: 5 mol% catalyst at 110 °C for 24 h.

4. Synthesis of Azide Compounds and C–H amination Reactions

Safety Note. Though no specific safety concerns arose during our studies, organoazide compounds are high energy molecules, and they are known to be thermally unstable and shock sensitive. In order to minimize explosion hazards, general care should be taken to avoid organoazides with low C-to-N ratios, limit scale to the extent possible, and store organoazides in solution.

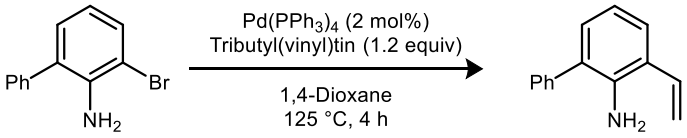

3-vinyl-[1,1'-biphenyl]-2-amine. The following procedure was adapted from a previously reported method.[1] In an N_2 filled glovebox, a Schlenk flask was charged with 3-bromo-[1,1'-biphenyl]-2-amine (298 mg, 1.2 mmol), $Pd(PPh_3)_4$ (2.8 mg, 0.024 mmol, 2 mol %), tributyl(vinyl)tin (0.42 mL, 1.45 mmol), and anhydrous 1,4-dioxane (9 mL). The reaction vessel was sealed, removed from the glovebox, and heated at 125 °C. After 4 h, the reaction mixture was cooled to room temperature, and 10% KF (aq) solution (0.08 M, 22.5 mL) was added. The mixture was allowed to stand for 2 h then filtered through a pad of celite. The filtrate was extracted with 2 × 10 mL of ether, and the combined organic phases were washed with sat. NaCl (aq) (10 mL), dried over Na_2SO_4, and concentrated under reduced pressure. The crude product was directly loaded onto a SiO_2 column for purification (2.5:97.5 EtOAc: hexane). The product was isolated as a yellow oil (0.212 g, 92% yield).

^{1}H NMR (300 MHz, $CDCl_3$) δ 7.27 (s, 2H), 7.23 – 7.04 (m, 4H), 6.89 (dd, *J* = 7.4, 1.6 Hz, 1H), 6.72 – 6.57 (m, 2H), 5.49 (dt, *J* = 17.4, 1.5 Hz, 1H), 5.18 (dd, *J* = 10.9, 1.5 Hz, 1H), 3.67 (s, 2H).

^{13}C{^{1}H} NMR (201 MHz, $CDCl_3$) δ 141.0, 139.6, 133.3, 130.1, 129.4, 129.0, 128.6, 128.4, 127.4, 126.9, 124.7, 122.0, 120.2, 118.6, 116.5, 29.9

HRMS(ESI): calcd for $C_{14}H_{13}N^+$: 196.1121; found: 196.1123

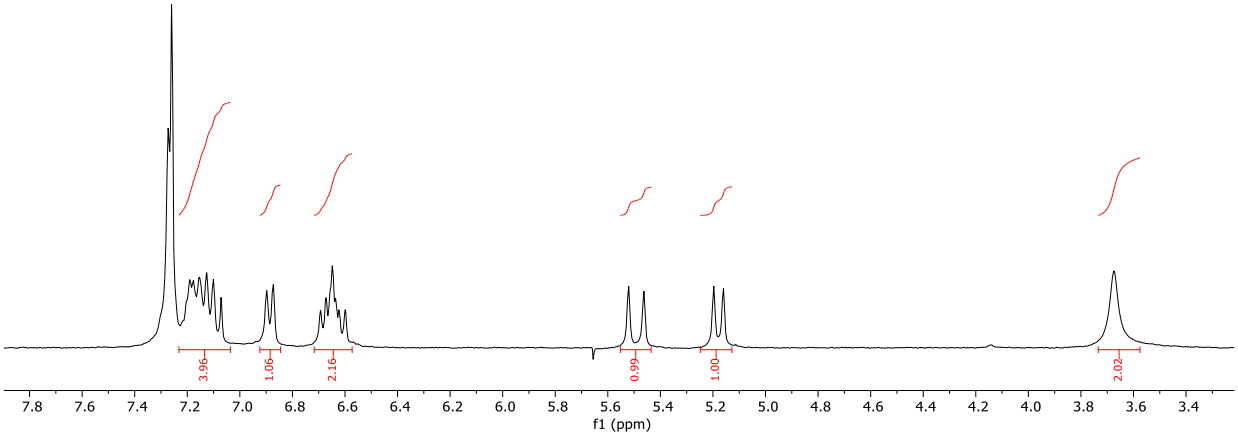

Figure S14. ^{1}H NMR spectrum for 3-vinyl-[1,1'-biphenyl]-2-amine in $CDCl_3$.

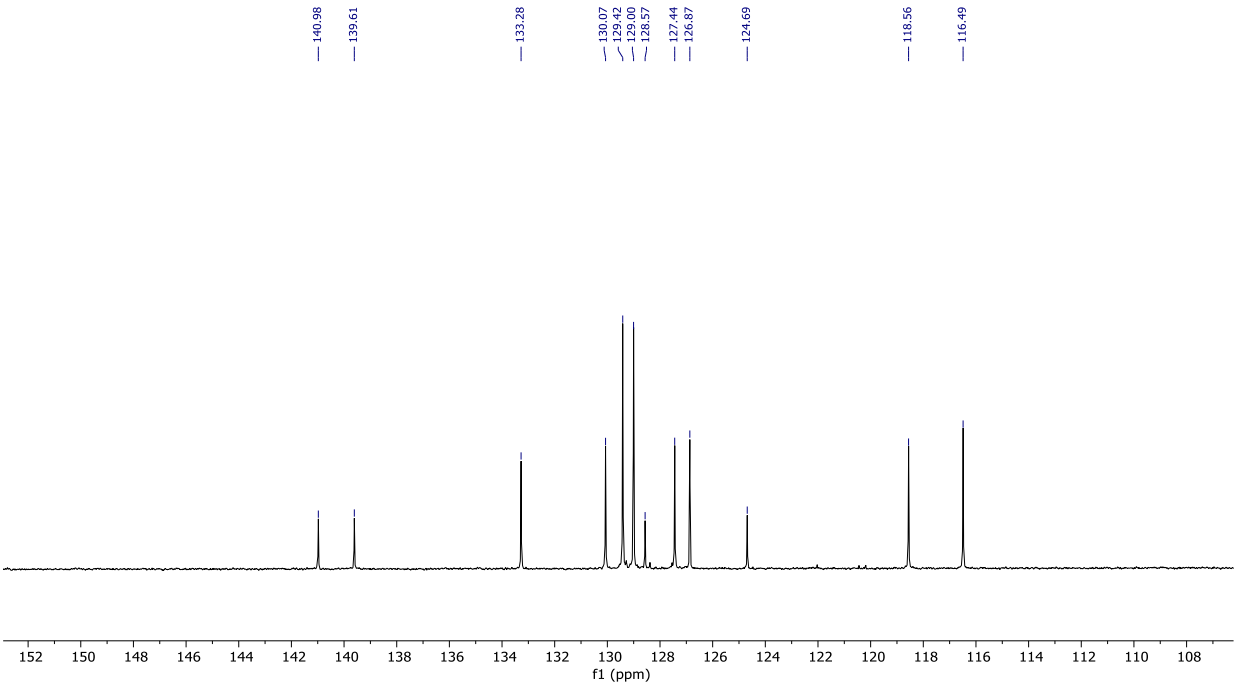

Figure S15. $^{13}C\{^{1}H\}$ NMR spectrum for 3-vinyl-[1,1'-biphenyl]-2-amine in $CDCl_3$.

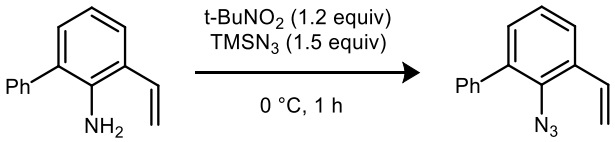

2-azido-3-vinyl-1,1'-biphenyl (17). A solution of 3-vinyl-[1,1'-biphenyl]-2-amine (330 mg, 1.69 mmol, 1.0 equiv) in CH_3CN (8.5 mL) was cooled to 0 °C. *t*-$BuNO_2$ (0.303 mL, 1.2 equiv) and $TMSN_3$ (0.27mL, 1.5 equiv) were added sequentially. The reaction mixture was vigorously stirred at room temperature under air for 1 h. The mixture was concentrated to dryness under reduced pressure. The crude product was directly loaded onto a SiO_2 column for purification (100% hexanes). The product was isolated as a yellow oil (97 mg, 26% yield).

^{1}H NMR (800 MHz, $CDCl_3$) δ 7.52 (dd, *J* = 6.4, 2.9 Hz, 1H), 7.47 (d, *J* = 5.5 Hz, 3H), 7.40 (tt, *J* = 5.7, 3.1 Hz, 1H), 7.24 – 7.19 (m, 2H), 7.11 (dd, *J* = 17.6, 10.9 Hz, 1H), 5.77 (d, *J* = 17.5 Hz, 1H), 5.40 (d, *J* = 11.0 Hz, 1H).

^{13}C{^{1}H} NMR (201 MHz, $CDCl_3$) δ 138.1, 136.8, 134.6, 132.4, 132.2, 130.8, 129.2, 128.6, 127.9, 125.8, 125.7, 116.5.

HRMS(ESI): calcd for $C_{14}H_{12}N^+$: 194.0964; found: 194.0965.

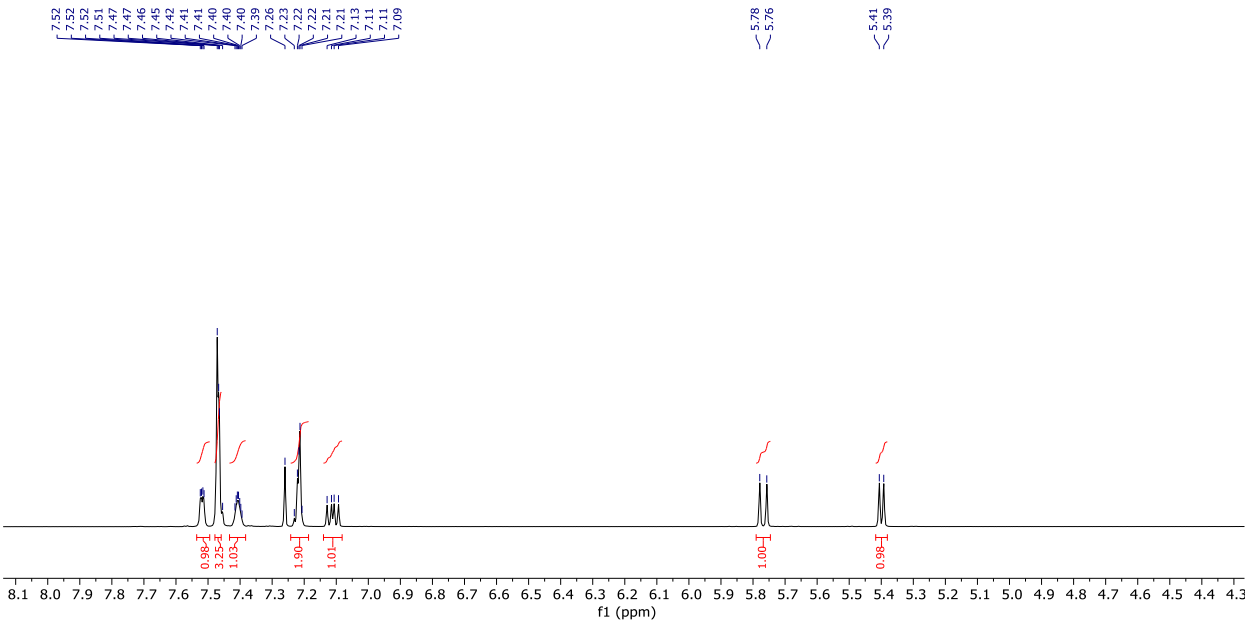

Figure S16. ^{1}H NMR spectrum for **17** in $CDCl_3$.

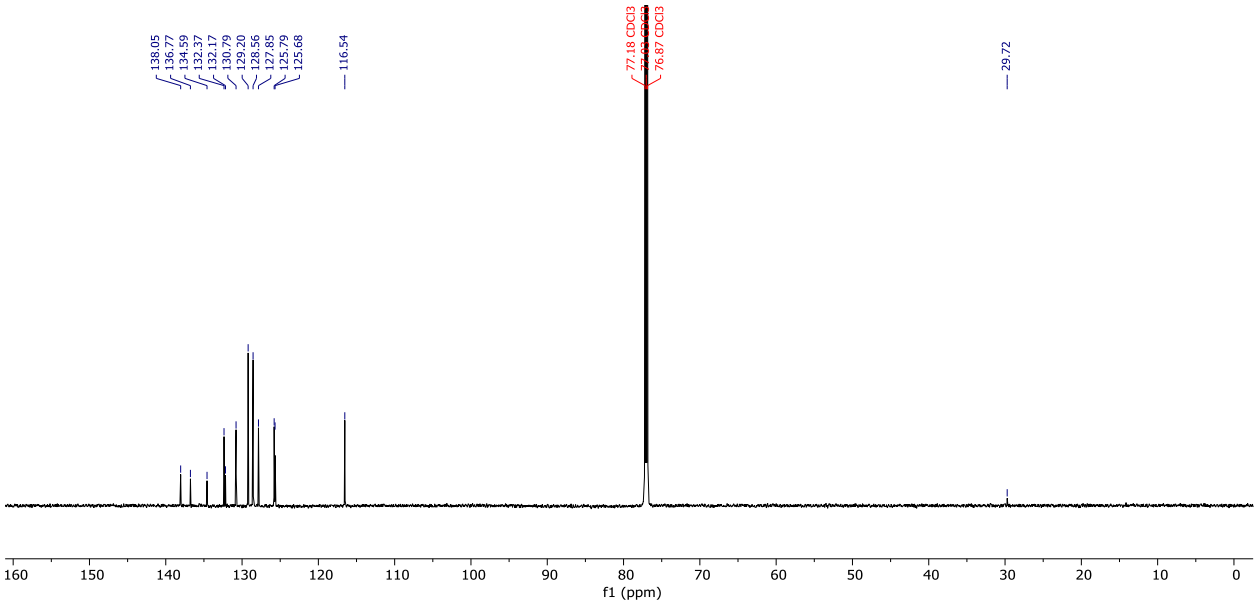

Figure S17. $^{13}C\{^{1}H\}$ NMR spectrum for **17** in $CDCl_3$.

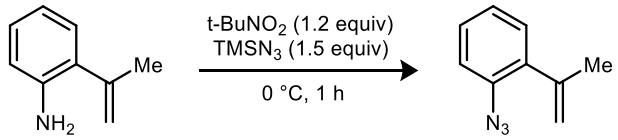

1-Azido-2-(prop-1-en-2-yl)benzene. A solution of 2-(prop-1-en-2-yl)aniline (2.0 g, 15.0 mmol, 1.0 equiv) in CH_3CN (75 mL) was cooled to 0 °C. *t*-$BuNO_2$ (2.69 mL, 1.2 equiv) and $TMSN_3$ (2.39 mL, 1.5 equiv) were added sequentially. The reaction mixture was vigorously stirred at room temperature under air for 1 h. The mixture was concentrated to dryness under reduced pressure. The crude product was directly loaded onto a SiO_2 column for purification (100% hexanes). The product was isolated as a yellow oil (2.39 g, >99% yield).

^{1}H NMR (800 MHz, $CDCl_3$) δ 7.33 (t, *J* = 7.7 Hz, 1H), 7.23 (d, *J* = 7.7 Hz, 1H), 7.18 (d, 1H), 7.13 (t, *J* = 7.7 Hz, 1H), 5.23 (s, 1H), 5.03 (s, 1H), 2.14 (s, 3H).

^{13}C{^{1}H} NMR (201 MHz, $CDCl_3$) δ 143.4, 136.7, 135.8, 129.8, 128.4, 124.8, 118.5, 116.2, 23.6.

HRMS(ESI): calcd for $C_9H_{10}N^+$: 132.0813; found: 132.0805

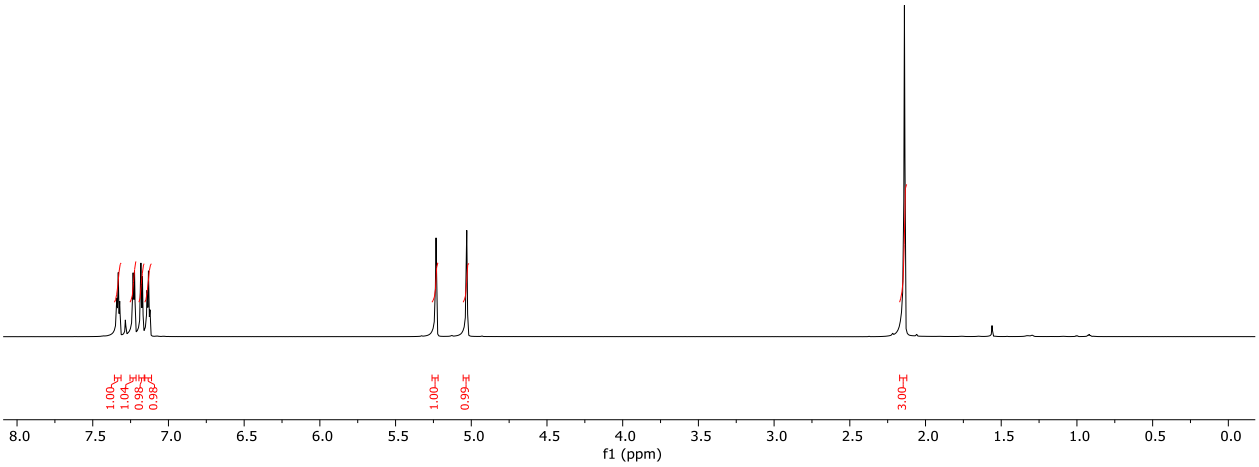

Figure S18. ^{1}H NMR spectrum for 1-azido-2-(prop-1-en-2-yl)benzene in $CDCl_3$.

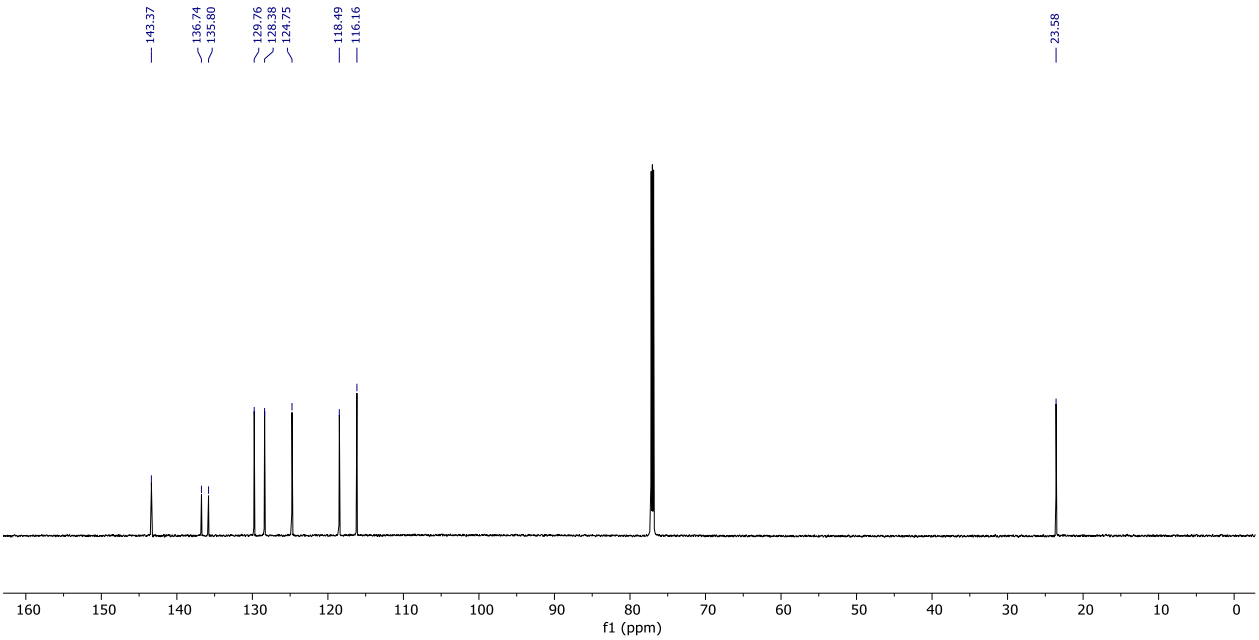

Figure S19. $^{13}C\{^{1}H\}$ NMR spectrum for 1-azido-2-(prop-1-en-2-yl)benzene in $CDCl_3$.

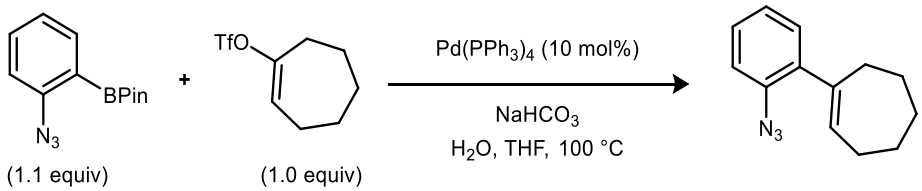

(1-(2-azidophenyl)cyclohept-1-ene). The following procedure was adapted from a previously reported method.[2] In an N_2 filled glovebox, a Schlenk flask was charged with cyclohept-1-en-1-yl trifluoromethanesulfonate (428 mg, 1.8 mmol, 1.0 equiv), 2-azidoarylboronic acid pinacol ester (495 mg, 2.0 mmol, 1.1 equiv), $Pd(PPh_3)_4$ (25 mg, 0.022 mmol, 10 mol %), and 25 mL THF. The flask was sealed, removed from the glovebox, and 6.0 mL of sat. $NaHCO_3$ (aq) was added by syringe. The reaction mixture was heated at 75 °C. After 1 h, the mixture was cooled to room temperature and diluted with 5 mL of water. The solution was extracted with 2 × 10 mL of Et_2O. The combined organic phases were washed with 10 mL of sat. NaCl (aq), dried over Na_2SO_4, and concentrated under reduced pressure. The crude product was directly loaded onto a SiO_2 column for purification (3:97 to 5:95 EtOAc: hexane). The product was isolated as a yellow oil. (300 mg, 80% yield).

^{1}H NMR (800 MHz, $CDCl_3$) δ 7.24 (t, J = 7.6, 1.6 Hz, 1H), 7.13 (d, J = 7.5, 1.6 Hz, 1H), 7.10 (d, J = 8.0, 1.1 Hz, 1H), 7.06 (t, J = 7.5, 1.2 Hz, 1H), 5.84 (t, J = 6.5 Hz, 1H), 2.48 – 2.43 (m, 2H), 2.29 – 2.24 (m, 2H), 1.84 – 1.79 (m, 2H), 1.69 – 1.64 (m, 2H), 1.61 – 1.55 (m, 2H).

^{13}C{^{1}H} NMR (201 MHz, $CDCl_3$) δ 143.7, 138.5, 136.7, 132.8, 130.0, 127.7, 124.7, 118.4, 34.5, 32.7, 29.1, 27.0, 26.9.

HRMS(ESI): calcd for $C_{13}H_{16}N^+$: 186.1283; found: 186.1277

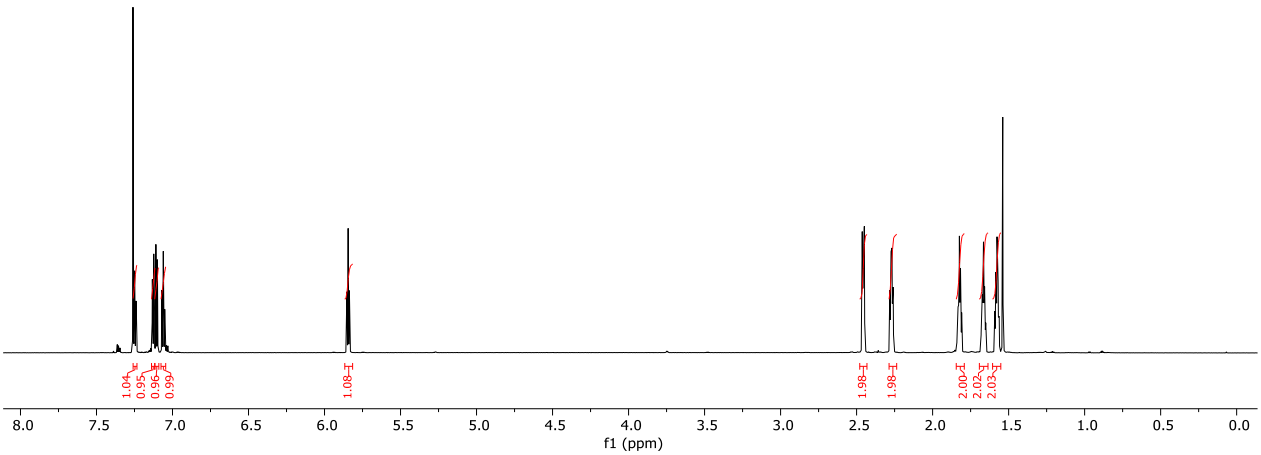

Figure S20. ^{1}H NMR spectrum for (1-(2-azidophenyl)cyclohept-1-ene) in $CDCl_3$.

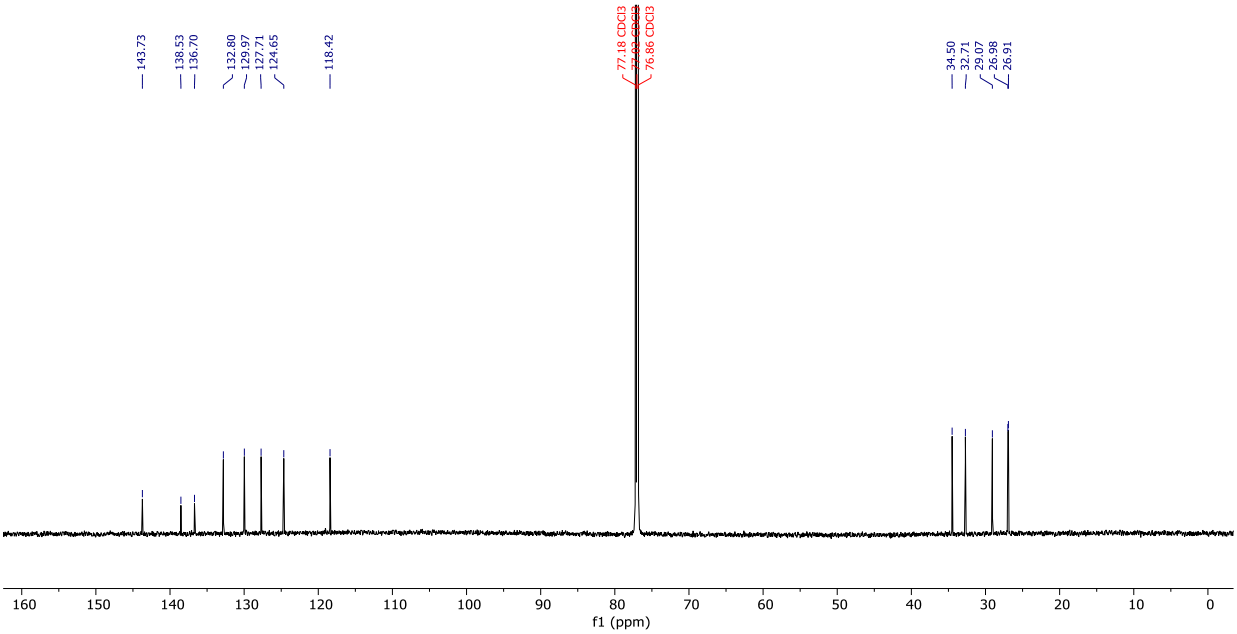

Figure S21. $^{13}C\{^{1}H\}$ NMR spectrum for (1-(2-azidophenyl)cyclohept-1-ene) in $CDCl_3$.

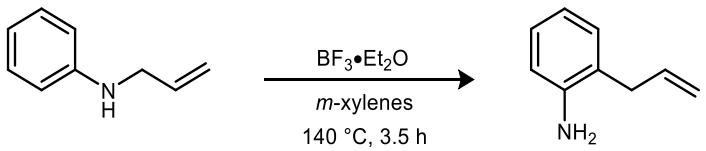

2-allylaniline. The following procedure was adapted from a previously reported method. In an N_2 filled glovebox, a Schlenk tube was charged with N-allylaniline (532 mg, 4 mmol, 1.0 equiv) and *m*-xylenes (10 mL). The Schlenk tube was sealed, removed from the glovebox and BF_3•Et_2O (490 uL, 4 mmol, 1.0 equiv) was added by syringe. The reaction mixture was heated at 140 °C. After 3 h, the mixture was cooled to room temperature and diluted with 10 mL of aqueous NaOH. The solution was extracted with 3 × 10 mL of EtOAc. The combined organic phases were washed with 10 mL of sat. NaCl (aq), dried over Na_2SO_4, and concentrated under reduced pressure. The product was isolated as a yellow oil. (370 mg, 70% yield). The spectral data match those previously reported.[3]

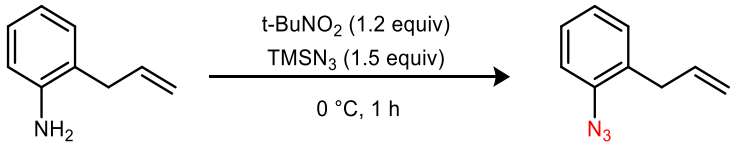

1-allyl-2-azidobenzene. A solution of 2-allylaniline (0.370 g, 2.7 mmol, 1.0 equiv) in CH_3CN (5 mL) was cooled to 0 °C. *t*-$BuNO_2$ (0.5 mL, 1.2 equiv) and $TMSN_3$ (0.45 mL, 1.5 equiv) were added sequentially. The reaction mixture was vigorously stirred at room temperature under air for 1 h. The mixture was concentrated to dryness under reduced pressure. The crude product was directly loaded onto a SiO_2 column for purification (50:50 DCM:hexanes). The product was isolated as a yellow oil (0.380 g, 86% yield). The spectral data match those previously reported.[3]

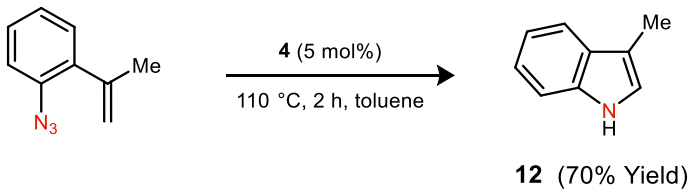

12 (70% Yield)

Catalytic amination of 1-azido-2-(prop-1-en-2-yl)benzene with 4. In an N_2 filled glovebox, a J-Young NMR tube was charged with **4** (1.4 mg, 0.0013 mmol, 5 mol%), 1-azido-2-(prop-1-en-2-yl)benzene (4.0 mg, 0.026 mmol), 1,3,5-trimethoxybenzene (1.0 mg, 0.006 mmol) as an internal standard, and toluene-d_8 (700 µL). The reaction was heated at 110 °C for 2 h. The yield of indole was determined by ^{1}H NMR integration against the internal standard (70% yield). The spectral data match those previously reported.[4]

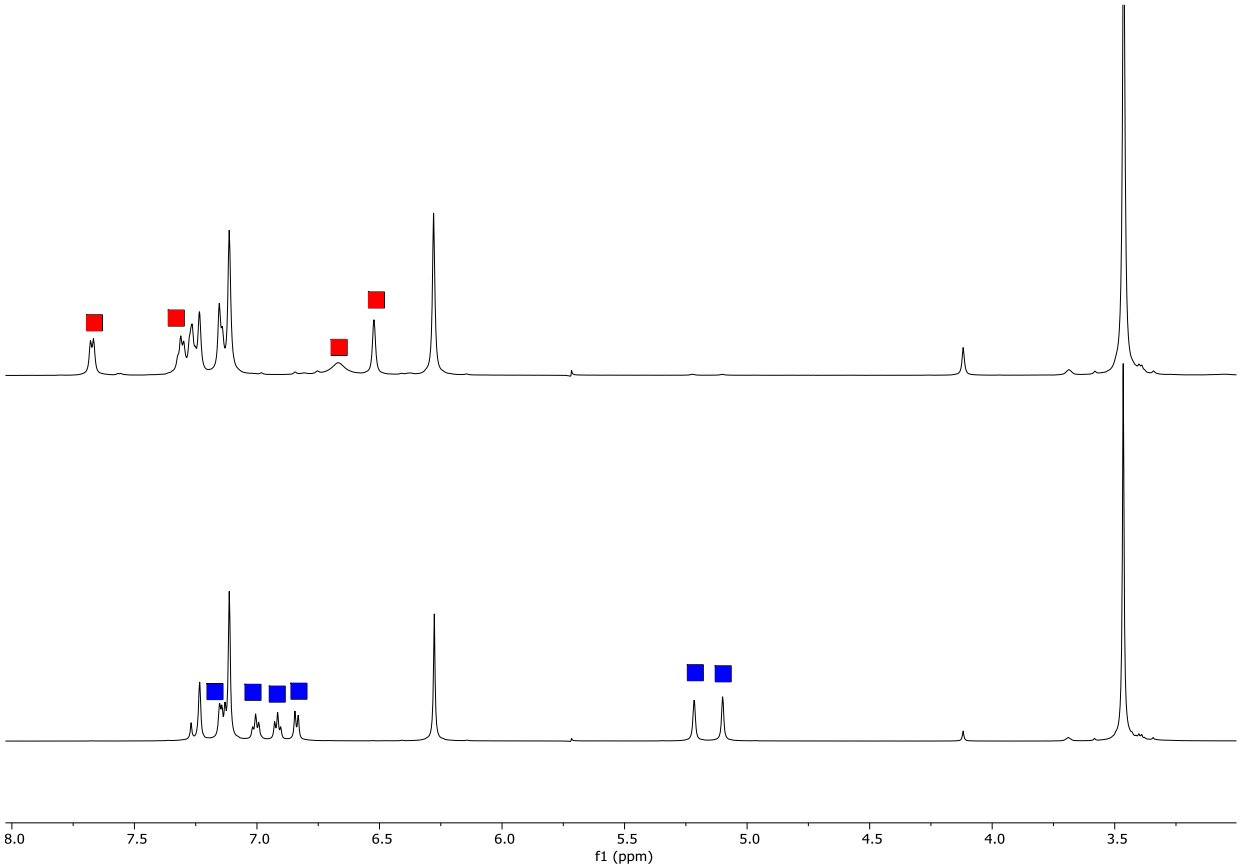

Figure S22. Bottom: ^{1}H NMR spectrum of 1-azido-2-(prop-1-en-2-yl)benzene. Top: ^{1}H NMR spectrum for the product mixture. Blue squares indicate starting material and red squares indicate **12**.

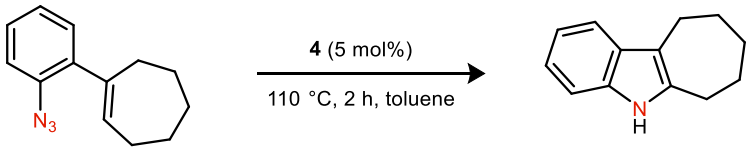

11 (84% Yield)

Catalytic amination of 1-(2-azidophenyl)cyclohept-1-ene with 4. In an N_2 filled glovebox, a J-Young NMR tube was charged with **4** (1.4 mg, 0.0013 mmol, 5 mol%), 1-(2-azidophenyl)cyclohept-1-ene (5.4 mg, 0.026 mmol), 1,3,5-trimethoxybenzene (1.0 mg, 0.006 mmol) as an internal standard, and toluene-d_8 (700 µL). The reaction was heated to 110 °C for 2 h. The yield of indole was determined by ^{1}H NMR integration against the internal standard (84% yield). The spectral data match those previously reported.[5]

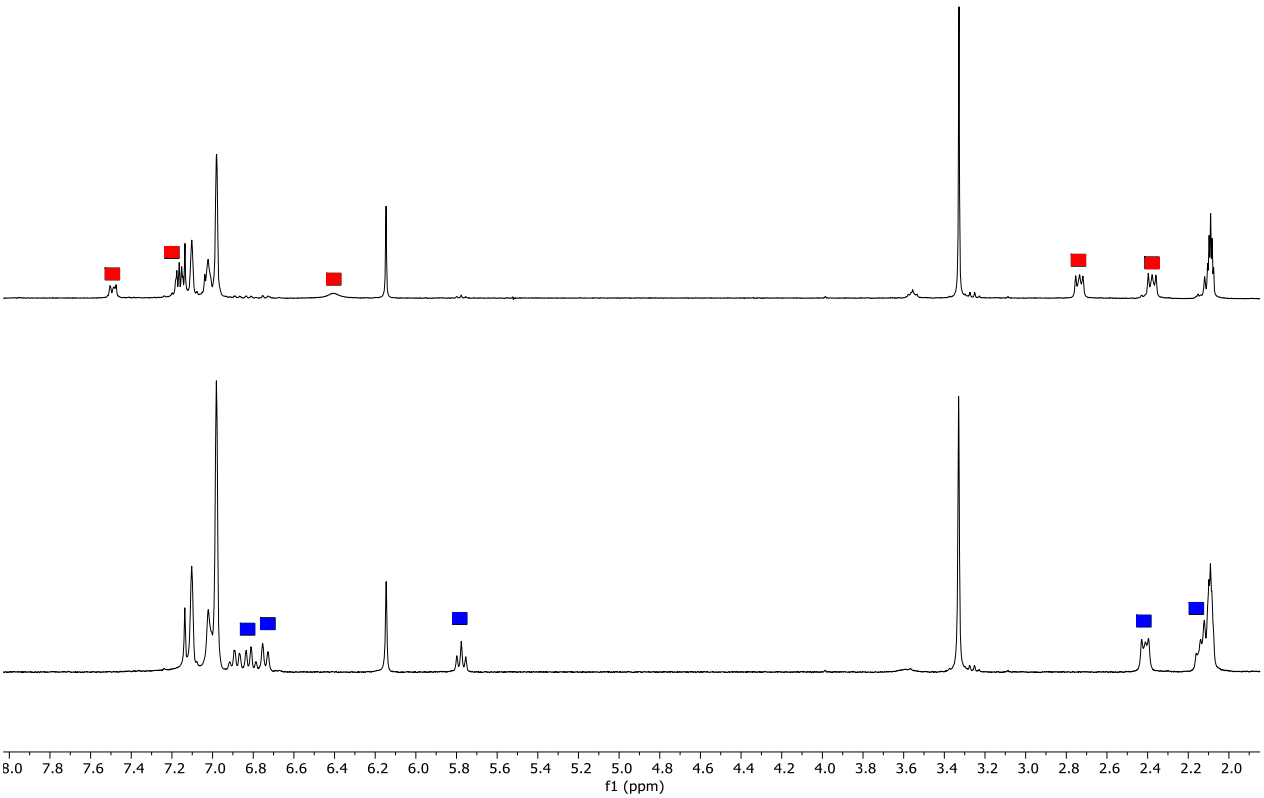

Figure S23. Bottom: ^{1}H NMR spectrum of 1-(2-azidophenyl)cyclohept-1-ene. Top: ^{1}H NMR spectrum of the product mixture. Blue squares indicate 1-(2-azidophenyl)cyclohept-1-ene and red squares indicate **11**.

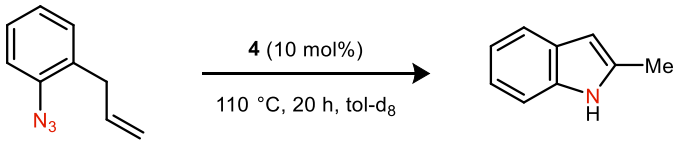

20 (61% Yield)

Catalytic amination of 1-allyl-2-azidobenzene with 4. In an N_2 filled glovebox, a J-Young NMR tube was charged with **4** (1.4 mg, 0.00126 mmol, 10 mol%), 1-allyl-2-azidobenzene (2.15 mg, 0.0135 mmol), 1,3,5-trimethoxybenzene (1.5 mg, 0.00892 mmol) as an internal standard, and toluene-d_8 (700 µL). The reaction was heated at 110 °C for 20 h. The yield of 2-methylindole was determined by ^{1}H NMR integration against the internal standard (61% yield). The spectral data match those previously reported.[6]

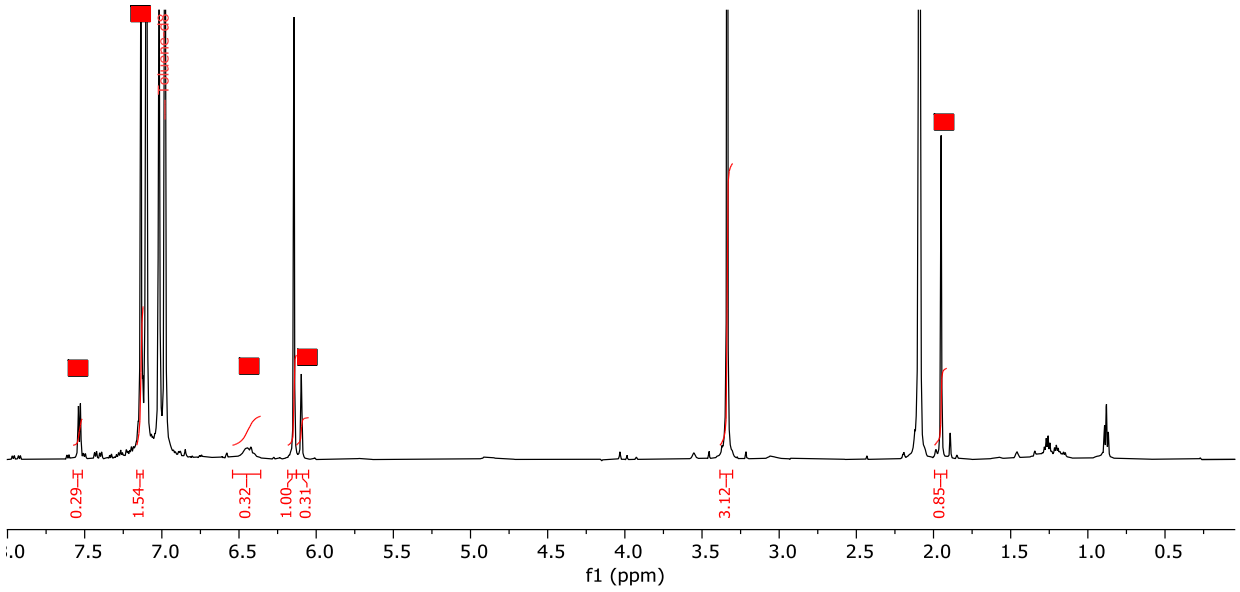

Figure S24. ^{1}H NMR spectrum of the product mixture. Red squares indicate **20**.

5. Mechanistic Experiments

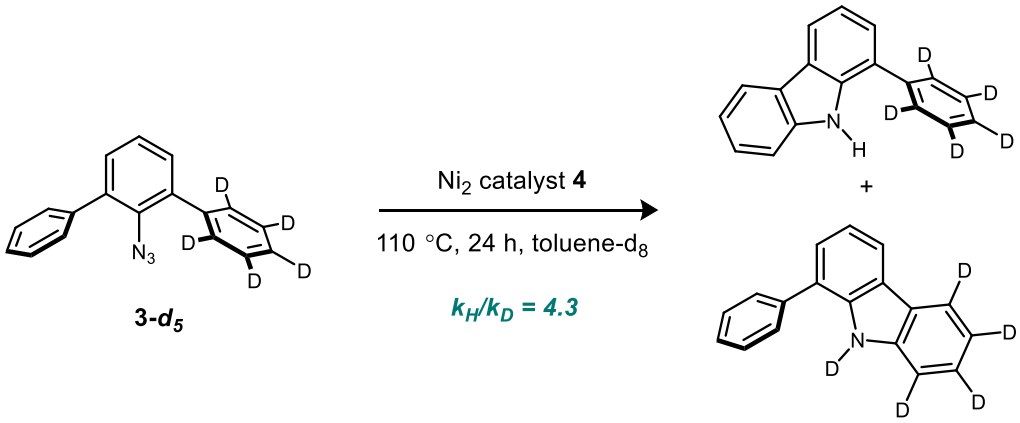

Catalytic amination of *m*-terphenylazide-d_5 with 4. In an N_2 filled glovebox, a J-Young NMR tube was charged with **4** (0.7 mg, 0.0007 mmol, 5 mol%), *m*-terphenylazide-d_5 (3.8 mg, 0.014 mmol, 1 equiv), and toluene-d_8 (700 µL). The reaction was heated at 110 °C for 24 h. The kinetic isotope effect was found to be 4.3 as determined by ^{1}H NMR integration. The spectral data match those previously reported.[7]

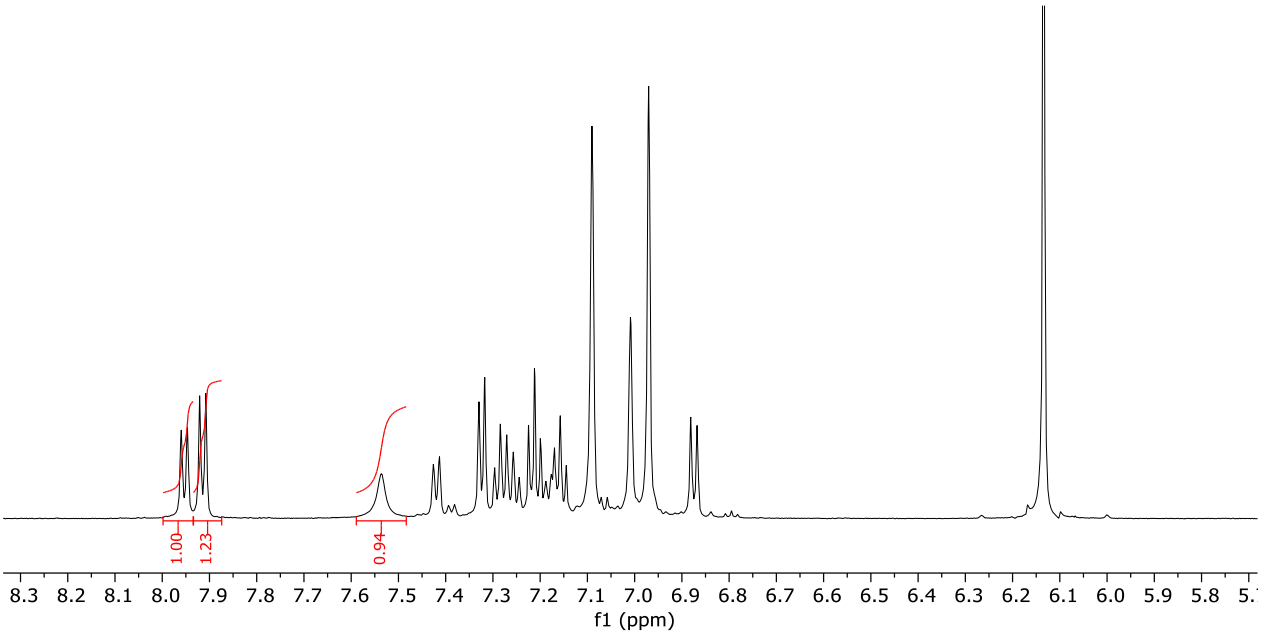

Figure S25. ^{1}H NMR spectrum of the amination of *m*-terphenylazide-d_5.

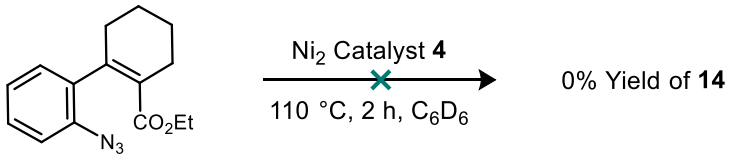

13

Catalytic amination of ethyl 2'-azido-3,4,5,6-tetrahydro-[1,1'-biphenyl]-2-carboxylate with 4. In an N_2 filled glovebox, a J-Young NMR tube was charged with **4** (1.4 mg, 0.0013 mmol, 10 mol%), **13** (3.4 mg, 0.013 mmol), 1,3,5-trimethoxybenzene (2.4 mg, 0.014 mmol) as an internal standard, and toluene-d_8 (825 µL).[8] The reaction was heated at 110 °C for 24 h. 15% conversion of azide **13** was observed, but **14** was not found in the reaction mixture.

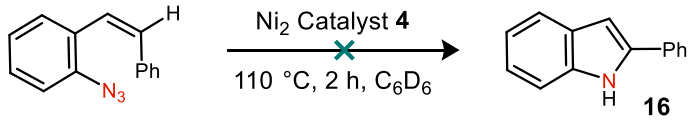

15-*Z* **16**

Catalytic amination of 15-*Z* with 4. In an N_2 filled glovebox, a J-Young NMR tube was charged with **4** (1.4 mg, 0.0013 mmol, 10 mol%), **15-*Z*** (2.8 mg, 0.013 mmol) 1,3,5-trimethoxybenzene (2.1 mg, 0.0013 mmol) as an internal standard, and toluene-d_8 (700 µL).[9] The reaction was heated at 110 °C for 2 h. The yield of indole was determined by ^{1}H NMR integration against the internal standard (0% yield).

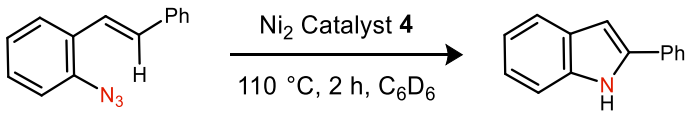

15-*E* **16**

Catalytic amination of 15-*E* with 4. In an N_2 filled glovebox, a J-Young NMR tube was charged with **4** (1.4 mg, 0.0013 mmol, 10 mol%), **15-*E*** (2.8 mg, 0.013 mmol), 1,3,5-trimethoxybenzene (2.1 mg, 0.0013 mmol) as an internal standard, and toluene-d_8 (700 µL). The reaction was heated at 110 °C for 2 h. The yield of indole was determined by ^{1}H NMR integration against the internal standard (>95% yield). The spectral data match those previously reported.[9]

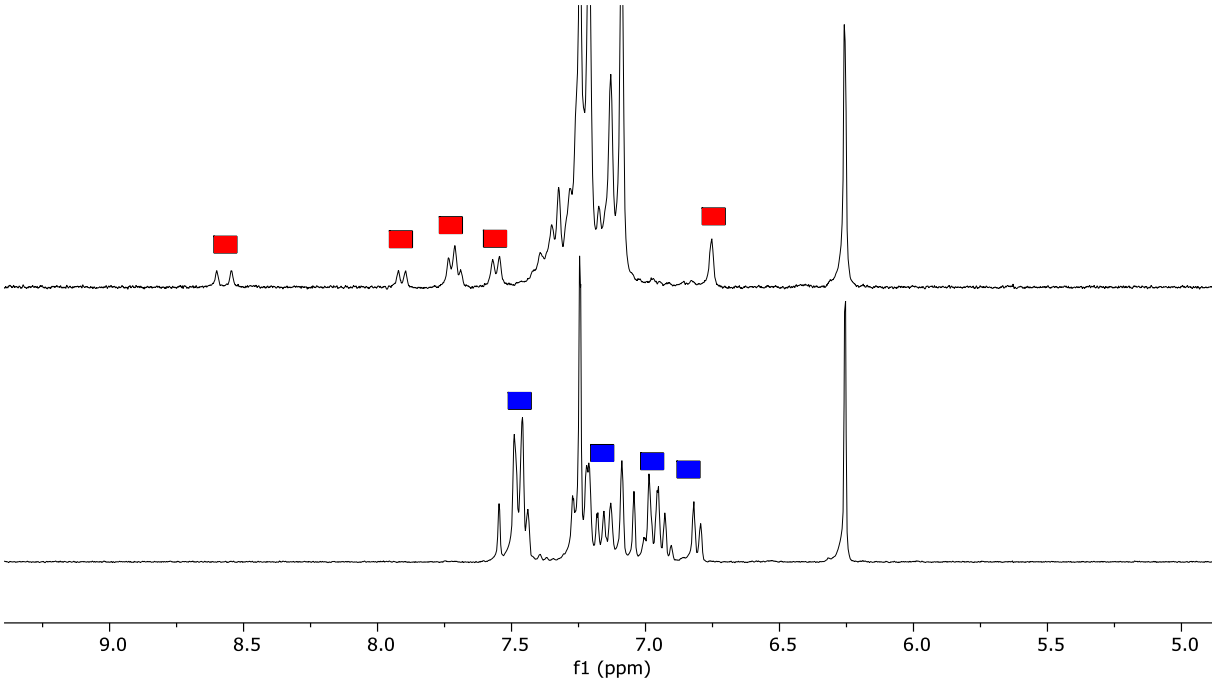

Figure S26. Bottom: ^{1}H NMR spectrum of **15-*E***. Top: ^{1}H NMR spectrum of product mixture. Blue squares indicate **15-E** and red squares indicate **16**.

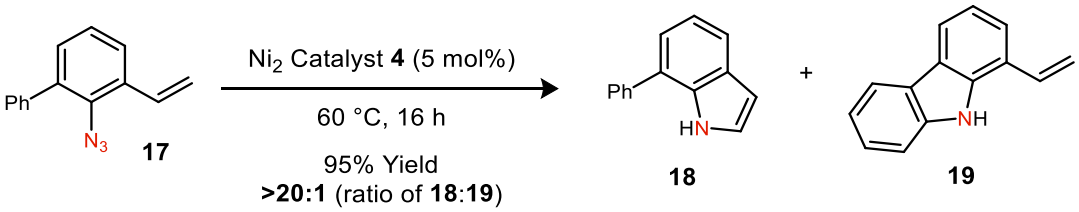

Catalytic amination of 17 with 4. In an N_2 filled glovebox, a J-Young NMR tube was charged with **4** (1.4 mg, 0.0013 mmol, 5 mol%), **17** (5.6 mg, 0.013 mmol), 1,3,5-trimethoxybenzene (2.1 mg, 0.0013 mmol) as an internal standard, and toluene-d_8 (700 µL). The reaction was heated at 110 °C for 2 h. The yield of indole was determined by ^{1}H NMR integration against the internal standard (95% yield). The spectral data match those previously reported.[10]

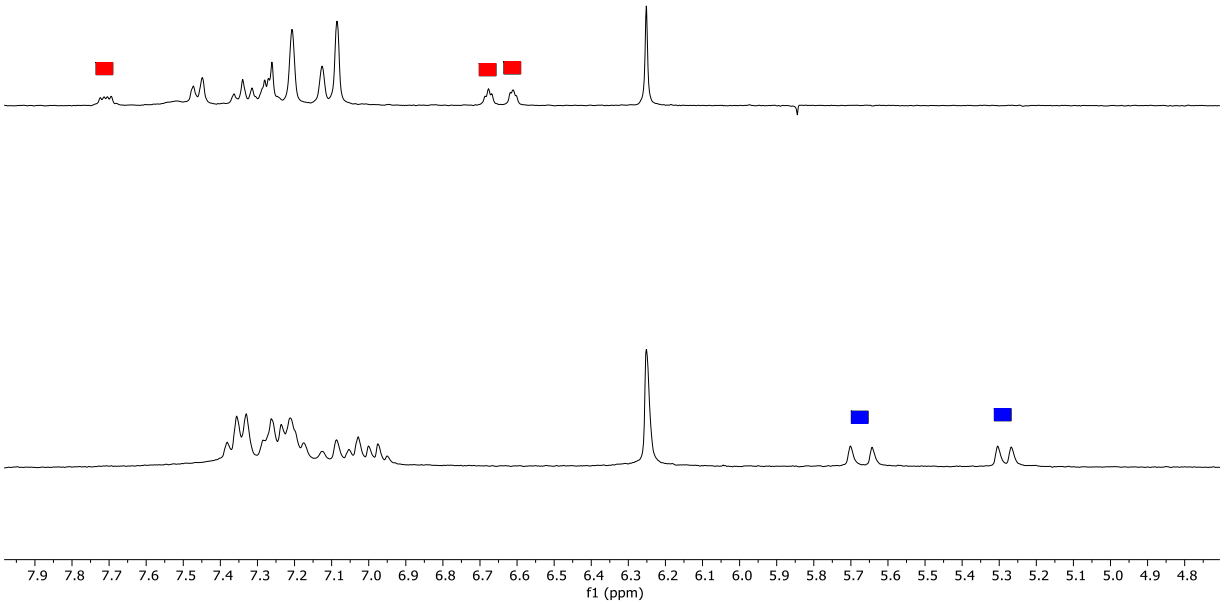

Figure S27. Bottom: ^{1}H NMR spectrum of **17**. Top: ^{1}H NMR spectrum of the product mixture. Blue squares indicate **17** and red squares indicate **18**.

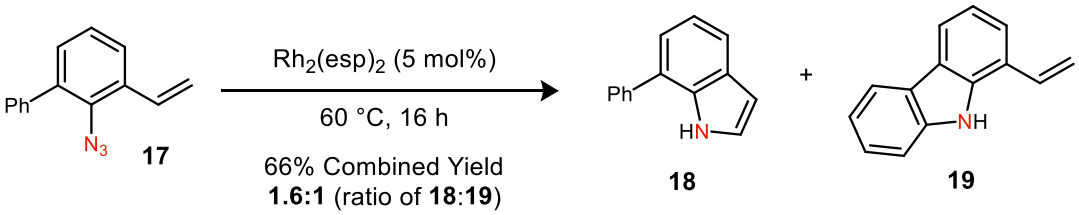

Catalytic amination of 17 with $Rh_2(esp)_2$ (5% loading). In an N_2 filled glovebox, a conical microwave vial was charged with $Rh_2(esp)_2$ (4.6 mg, 0.0061 mmol, 5 mol%), **17** (27 mg, 0.12 mmol), 1,3,5-trimethoxybenzene (2.1 mg, 0.0013 mmol) as an internal standard, and toluene (0.24 mL). The reaction was heated at 60 °C for 16 h after which the solvent was removed under reduced pressure. The yield of indole was determined by ^{1}H NMR integration against the internal standard (66% combined yield of **18** and **19** in a 1.6:1 ratio respectively). The spectral data match those previously reported.[11]

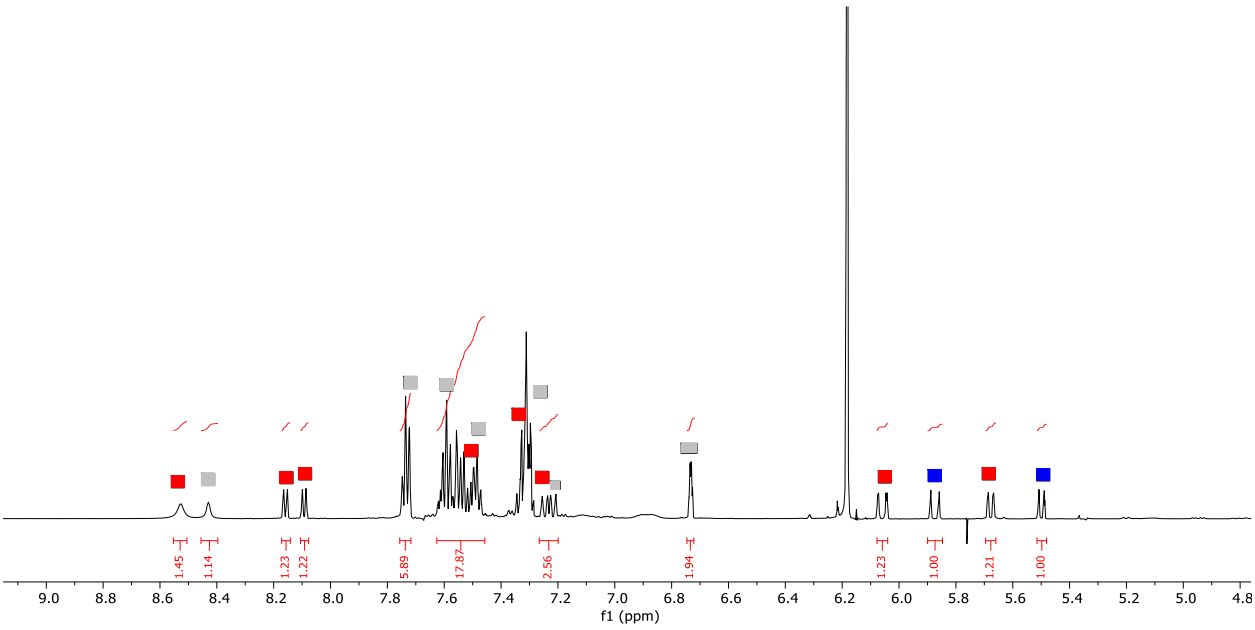

Figure S28. ^{1}H NMR spectrum of the product mixture. Blue squares indicate peaks corresponding to **17**, grey squares indicate peaks corresponding to **18** and red square indicates peaks corresponding to **19**.

6. X-Ray Diffraction Data

X-Ray Crystallography Data Processing. All data sets were processed using HKL3000 and data were corrected for absorption and scaled using Scalepack.[12] The space groups were assigned using XPREP from the Shelxtl suite of programs,[13] and structures were solved by direct methods using SHELXS and refined against F^2 on all data by full-matrix least-squares. The graphical user interface ShelXle[14] was used for refinement with the SHELXL program.[15] H-atoms attached to carbons were positioned geometrically and constrained to ride on their parent atoms, with carbon–hydrogen bond distances of 0.95 Å for and aromatic C–H, 1.00, 0.99 and 0.98 Å for aliphatic C–H, CH_2 and CH_3 moieties, respectively. Methyl H-atoms were allowed to rotate but not tip to best fit the experimental electron density. Positions of amine H-atoms were refined. U_{iso}(H) values were set to a multiple of U_{eq}(C/N) with 1.5 for CH_3, and 1.2 for C–H, CH_2 and N–H units, respectively. Complete crystallographic data, in CIF format, have been deposited with the Cambridge Crystallographic Data Centre. CCDC 1907259, 1907257, 1907253 contains the supplementary crystallographic data for this paper. These data can be obtained free of charge from The Cambridge Crystallographic Data Centre via www.ccdc.cam.ac.uk/data_request/cif.

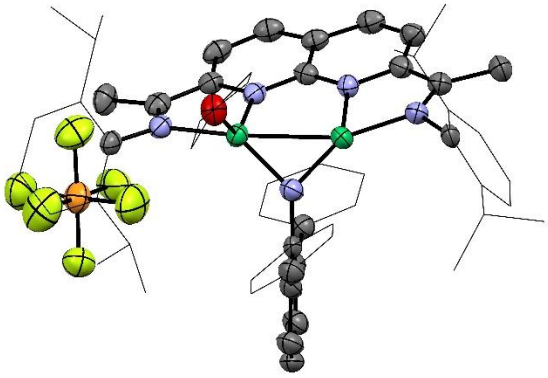

Compound 4

Crystal data	
Chemical formula	$C_{68}H_{85}F_6N_5Ni_2O_{3.50}P$
M_r	1290.79
Crystal system, space group	Monoclinic, $P2_1/n$
Temperature (K)	100
a, b, c (Å)	20.815 (4), 11.898 (2), 25.361 (5)
β (°)	94.16 (3)
V (Å^3)	6264 (2)
Z	4
Radiation type	Cu $K\alpha$
μ (mm^{-1})	1.56
Crystal size (mm)	0.60 × 0.20 × 0.02
Data collection	
Diffractometer	Rigaku Rapid II curved image plate diffractometer
Absorption correction	Multi-scan *SCALEPACK* (Otwinowski & Minor, 1997)
T_{min}, T_{max}	0.831, 0.969
No. of measured, independent and observed [$I > 2\sigma(I)$] reflections	64590, 11706, 7706
R_{int}	0.072
(sin θ/λ)$_{max}$ (Å^{-1})	0.617
Refinement	
$R[F^2 > 2\sigma(F^2)]$, $wR(F^2)$, S	0.078, 0.219, 1.07
No. of reflections	11706

No. of parameters	804
No. of restraints	10
H-atom treatment	H-atom parameters constrained
	$w = 1/[\sigma^2(F_o^2) + (0.0767P)^2 + 20.3456P]$ where $P = (F_o^2 + 2F_c^2)/3$
$\Delta\rho_{max}$, $\Delta\rho_{min}$ (e Å^{-3})	1.03, -0.63

*The three THF molecules were refined as disordered. One around an inversion center in a 1:1 ratio (that of O3). The other two (of O2 and O4) as disordered over two moieties in general positions. All disordered THF moieties were restrained to have similar geometries as that of a not disordered Ni-coordinated THF molecule. U^{ij} components of ADPs for disordered atoms closer to each other than 2.0 Angstrom were restrained to be similar. Subject to these conditions the occupancy ratio refined to 0.536(11) to 0.464(11) for the THF of oxygen O2, and to 0.724(9) to 0.276(9) for the THF of oxygen O4. Several reflections were located behind the beam stop, and were therefore omitted.

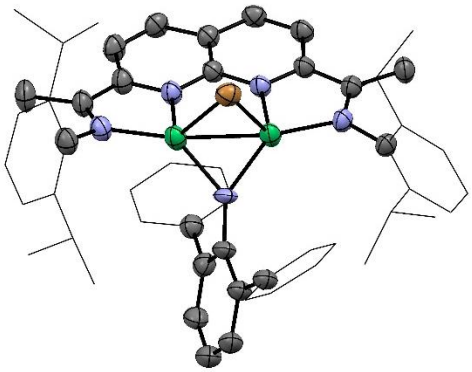

Compound 6

Crystal data	
Chemical formula	$0.8843(C_{56}H_{62}BrN_4Ni_2)\cdot 0.1157(C_{36}H_{57}Br_2N_5Ni_2)\cdot 2(C_4H_8O)$
M_r	1098.38
Crystal system, space group	Monoclinic, $P2_1/n$
Temperature (K)	100
a, b, c (Å)	18.650 (4), 27.977 (6), 21.577 (4)
β (°)	104.92 (3)
V (Å^3)	10879 (4)
Z	8
Radiation type	Cu $K\alpha$
μ (mm^{-1})	2.18
Crystal size (mm)	0.50 × 0.20 × 0.10
Data collection	
Diffractometer	Rigaku Rapid II curved image plate diffractometer
Absorption correction	Multi-scan *SCALEPACK* (Otwinowski & Minor, 1997)
T_{min}, T_{max}	0.831, 0.969
No. of measured, independent and observed [$I > 2\sigma(I)$] reflections	101438, 19994, 15997
R_{int}	0.089
$(\sin\theta/\lambda)_{max}$ (Å^{-1})	0.618
Refinement	
$R[F^2 > 2\sigma(F^2)]$, $wR(F^2)$, S	0.069, 0.186, 1.03
No. of reflections	19994

No. of parameters	1476
No. of restraints	772
H-atom treatment	H-atom parameters constrained
	$w = 1/[\sigma^2(F_o^2) + 33.1064P]$ where $P = (F_o^2 + 2F_c^2)/3$
$\Delta\rho_{max}$, $\Delta\rho_{min}$ (e Å^{-3})	1.29, -0.82

*The structure contains a number of disordered THF molecules. These molecules were refined with variable occupancies and restrained using SIMU and SAME commands.

The structure also contains a disorded Br atom due to cocrystallization with a dibromide species. The position of this atom was constrained with a SADI command to match the NiBr distances present for the nondisordered Br atom, and its occupancy was freely refined to a value of 0.1055(18).

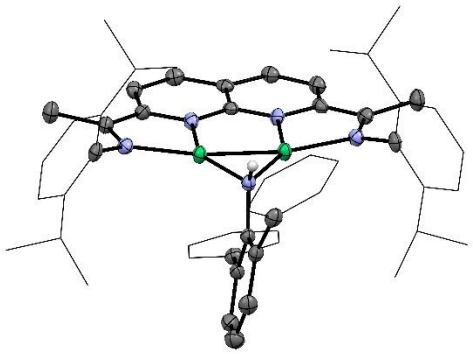

Compound 8

Crystal data	
Chemical formula	$C_{54}H_{58}N_5Ni_2 \cdot 3(C_6H_6)$
M_r	1128.79
Crystal system, space group	Triclinic, $P\bar{1}$
Temperature (K)	100
a, *b*, *c* (Å)	10.0447 (4), 16.2257 (6), 19.2830 (7)
α, β, γ (°)	86.007 (2), 75.110 (3), 78.833 (3)
V (Å^3)	2979.1 (2)
Z	2
Radiation type	Cu *K*α
μ (mm^{-1})	1.14
Crystal size (mm)	0.40 × 0.05 × 0.01
Data collection	
Diffractometer	Rigaku Rapid II curved image plate diffractometer
Absorption correction	Multi-scan *SCALEPACK* (Otwinowski & Minor, 1997)
T_{min}, T_{max}	0.750, 0.989
No. of measured, independent and observed [$I > 2\sigma(I)$] reflections	9411, 9411, 7497
R_{int}	0.076
$(\sin \theta/\lambda)_{max}$ (Å^{-1})	0.580
Refinement	
$R[F^2 > 2\sigma(F^2)]$, $wR(F^2)$, *S*	0.055, 0.152, 1.06
No. of reflections	9411

No. of parameters	725
No. of restraints	1
H-atom treatment	H atoms treated by a mixture of independent and constrained refinement
$\Delta\rho_{max}$, $\Delta\rho_{min}$ (e Å^{-3})	0.61, -0.50

7. DFT Calculations and Optimized Structures

Computational Methods. Geometry optimizations were performed using the Gaussian09 software package.[16] All geometries were fully optimized at the BP86/6-311G(d,p) level of DFT. Stationary points were verified by frequency analysis. Isopropyl groups on the catalyst were truncated to methyl groups. A polarizable continuum model (PCM) was used to apply solvent corrections for S = 1/2 compounds.

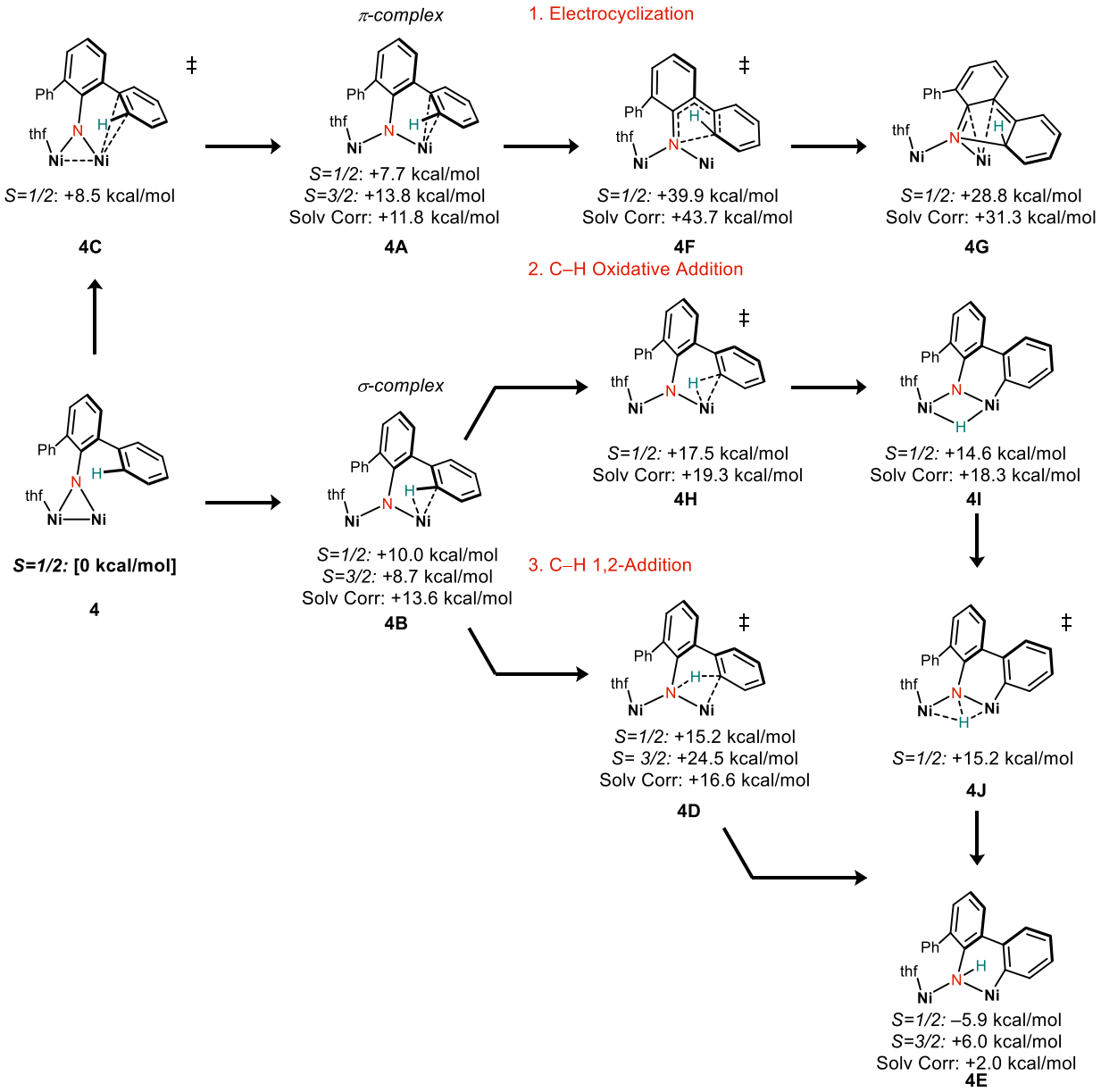

Figure S29. Reaction coordinate for electrocyclization, C–H oxidative addition and C–H 1,2-addition mechanisms of **4**. S=1/2 and S=3/2 spin states shown for C–H 1,2–Addition pathway (structures 4A-4E and 4J-4K). Energies are ΔG values at 383 K relative to that of **4** (BP86/6-31G(d,p) level of theory). Solvent corrections were applied to the S = 1/2 energies using the PCM(toluene) method.

Doublet:

Complex	NBO Ni 1	NBO Ni 2
4	9.19	9.05
4B	9.04	9.06
4D	9.04	9.16
4E	9.06	9.17

Figure S30. Natural Bond Orbital (NBO) analysis on Ni for each structure in the S=1/2 C–H 1,2-addition pathway. All complexes are best approximated as being Ni(I)/Ni(I).

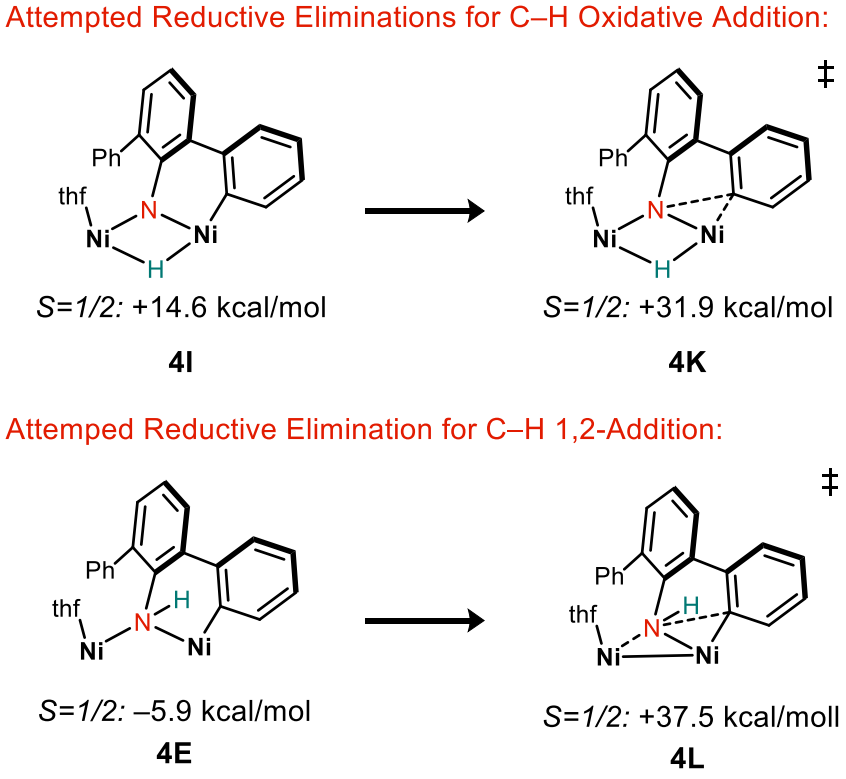

Figure S31. Reductive elimination transition states were located but found to be too high in energy to be relevant to the reaction. Energies are ΔG values at 383 K relative to that of **4** (BP86/6-31G(d,p) level of theory).

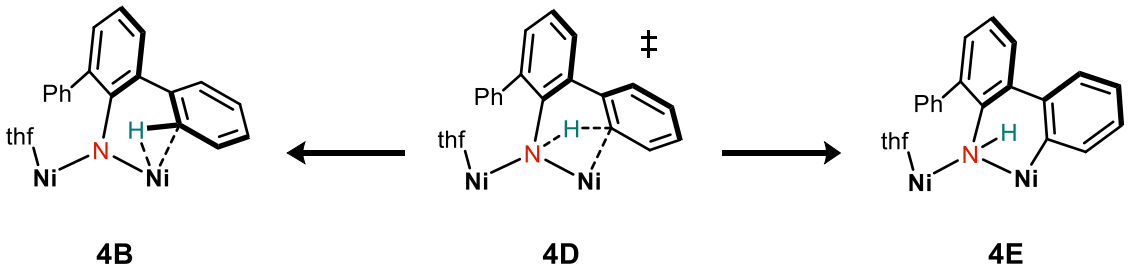

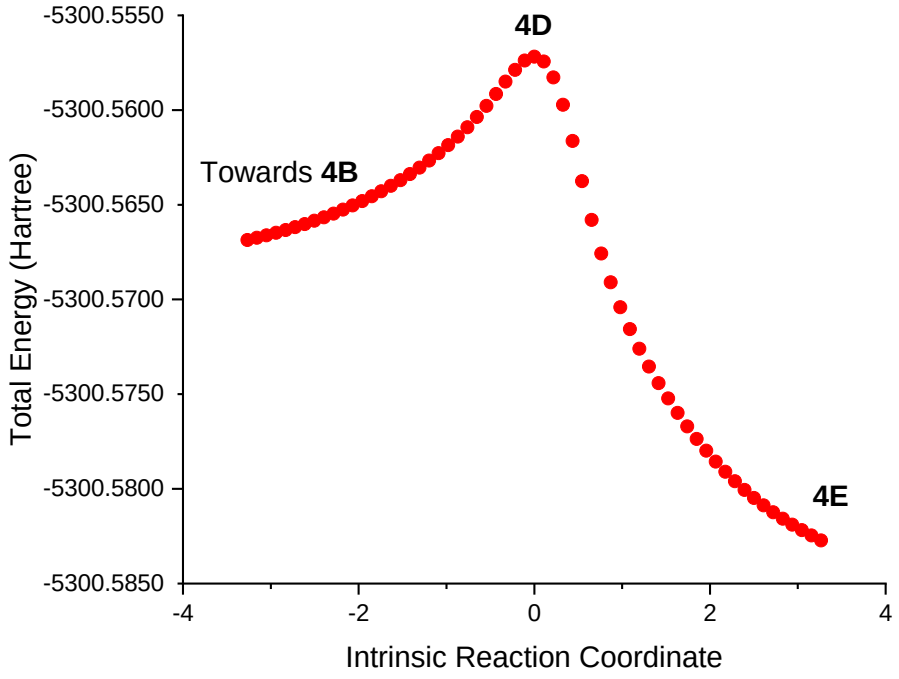

Figure S32. Intrinsic Reaction Coordinate (IRC) calculation for C–H 1,2-addition transition state **4D** with THF as ligand**.** Total energy of **4B** and **4E** are –5300.56918240 Hartrees and –5300.59440163 Hartrees respectively.

Complex 6

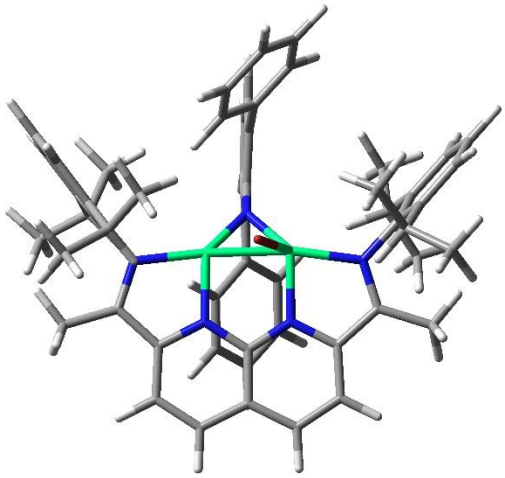

Charge: 0
Multiplicity: 2
Imaginary Frequencies: 0
Electronic Energy: –7640.314170 Hartrees
Gibbs Free Energy (353K): –7639.697760 Hartrees
Zero-Point Vibrational Energy: 1924830.3 J/mol

Charge: 0
Multiplicity: 4
Imaginary Frequencies: 0
Electronic Energy: –7640.297325 Hartrees
Gibbs Free Energy (353K): –7639.684274 Hartrees
Zero-Point Vibrational Energy: 1921737.5 J/mol

Complex 4

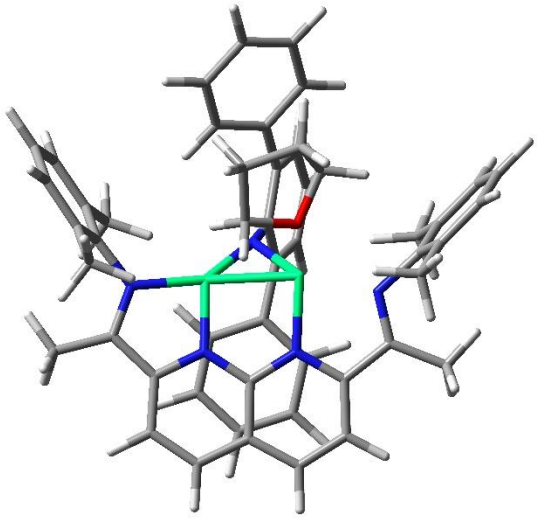

Charge: 1
Multiplicity: 2
Imaginary Frequencies: 0
Electronic Energy: –5300.58269527 Hartrees
Gibbs Free Energy (383K): –5299.869385 Hartrees
Zero-Point Vibrational Energy (H): 2230882.4 J/mol (D): 2222445.5 J/mol
Solvent Corrected Gibbs Free Energy (383K): –5299.900920 Hartrees

Charge: 1
Multiplicity: 4
Imaginary Frequencies: 0
Electronic Energy: –5300.56441855 Hartrees
Gibbs Free Energy (383K): –5299.854244 Hartrees
Zero-Point Vibrational Energy: 2228143.9 J/mol
Solvent Corrected Gibbs Free Energy (383K): –5299.882743 Hartrees

Complex 4C

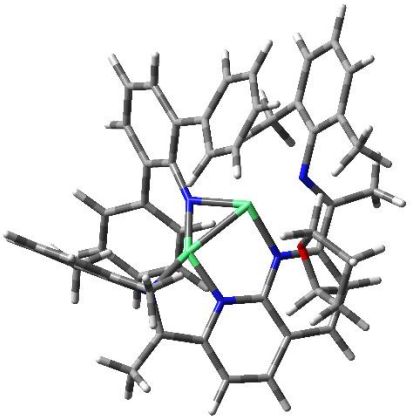

Charge: 1
Multiplicity: 2
Imaginary Frequencies: 1
Electronic Energy: –5300.561802 Hartrees
Gibbs Free Energy (383 K): –5299.855913 Hartrees
Zero-Point Vibrational Energy: 2227085.8 J/mol

Complex 4A

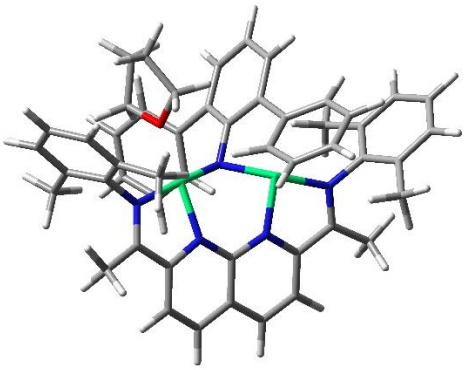

Charge: 1
Multiplicity: 2
Imaginary Frequencies: 0
Electronic Energy: –5300.57301636 Hartrees
Gibbs Free Energy (383 K): –5299.857033 Hartrees
Zero-Point Vibrational Energy (H): 2232449.1 J/mol (D): 2223974.0 J/mol
Solvent Corrected Gibbs Free Energy (383K): –5299.882143 Hartrees

Charge: 1
Multiplicity: 4
Imaginary Frequencies: 0
Electronic Energy: –5300.56208320 Hartrees
Gibbs Free Energy (383 K): –5299.847361 Hartrees
Zero-Point Vibrational Energy: 2231150.1 J/mol

Complex 4B

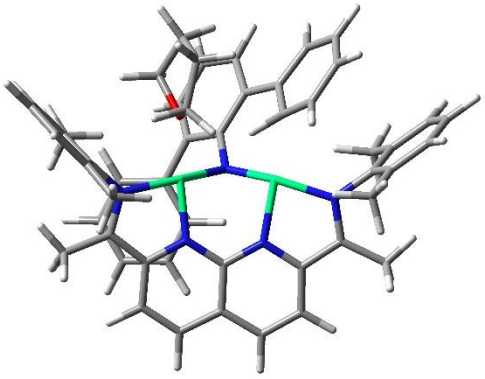

Charge: 1
Multiplicity: 2
Imaginary Frequencies: 0
Electronic Energy: –5300.56918240 Hartrees
Gibbs Free Energy (383 K): –5299.853418 Hartrees
Zero-Point Vibrational Energy: 2230811.4 J/mol
Solvent Corrected Gibbs Free Energy (383K): –5299.879253 Hartrees

Charge: 1
Multiplicity: 4
Imaginary Frequencies: 0
Electronic Energy: –5300.56649216 Hartrees
Gibbs Free Energy (383 K): –5299.855457 Hartrees
Zero-Point Vibrational Energy: 2229727.1 J/mol

Complex 4D

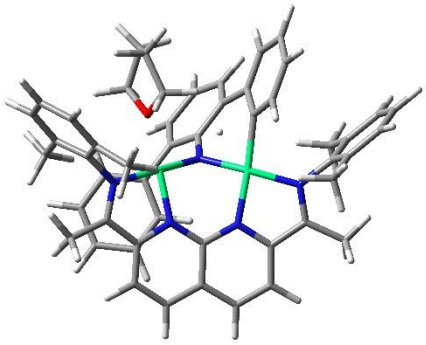

Charge: 1
Multiplicity: 2
Imaginary Frequencies: 1
Electronic Energy: –5300.55718006 Hartrees
Gibbs Free Energy (383 K): –5299.845158 Hartrees
Zero-Point Vibrational Energy (H): 2220379.6 J/mol (D): 2215647.6 J/mol
Solvent Corrected Gibbs Free Energy (383K): –5299.874423 Hartrees

Charge: 1
Multiplicity: 4
Imaginary Frequencies: 1
Electronic Energy: –5300.53754759 Hartrees
Gibbs Free Energy (383 K): –5299.830304 Hartrees
Zero-Point Vibrational Energy: 2215937.9 J/mol

Complex 4E

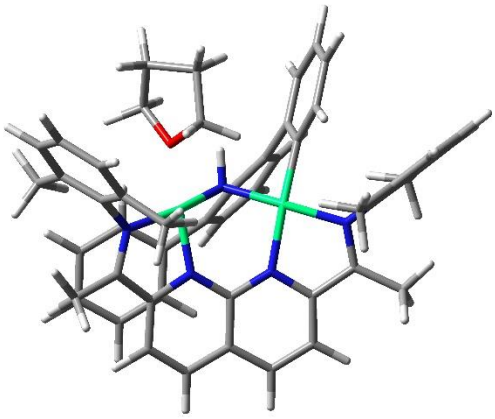

Charge: 1
Multiplicity: 2
Imaginary Frequencies: 0
Electronic Energy: –5300.59440163 Hartrees
Gibbs Free Energy (383 K): –5299.878758 Hartrees
Zero-Point Vibrational Energy: 2235482.2 J/mol
Solvent Corrected Gibbs Free Energy (383K): –5299.904157 Hartrees

Charge: 1
Multiplicity: 4
Imaginary Frequencies: 0
Electronic Energy: –5300.57471898 Hartrees
Gibbs Free Energy (383 K): –5299.859919 Hartrees
Zero-Point Vibrational Energy: 2232502.2 J/mol

Complex 4F

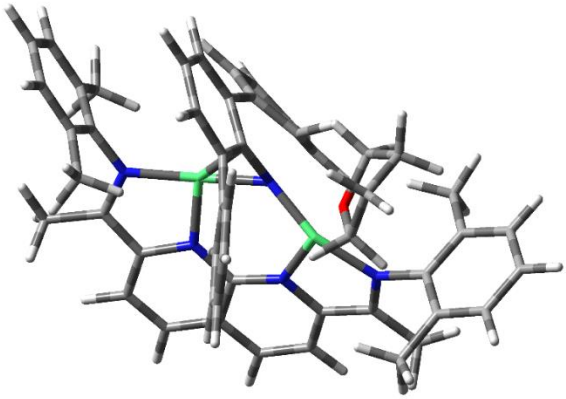

Charge: 1
Multiplicity: 2
Imaginary Frequencies: 1
Electronic Energy: -5300.524293 Hartrees
Gibbs Free Energy (383 K): –5299.805771 Hartrees
Zero-Point Vibrational Energy: 2229433.0 J/mol
Solvent Corrected Gibbs Free Energy (383K): – 5299.831341 Hartrees

Complex 4G

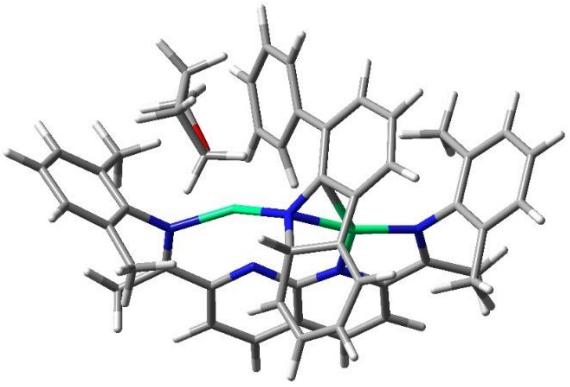

Charge: 1
Multiplicity: 2
Imaginary Frequencies: 0
Electronic Energy: –5300.53708234 Hartrees
Gibbs Free Energy (383 K): –5299.823556 Hartrees
Zero-Point Vibrational Energy: 2227739.6 J/mol
Solvent Corrected Gibbs Free Energy (383K): – 5299.850962 Hartrees

Complex 4H

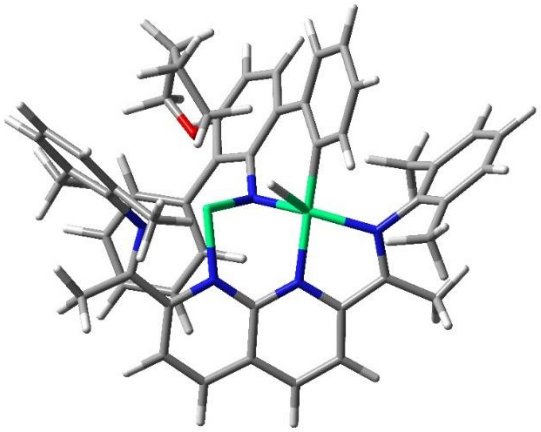

Charge: 1
Multiplicity: 2
Imaginary Frequencies: 1
Electronic Energy: –5300.55329722 Hartrees
Gibbs Free Energy (383 K): –5299.841473 Hartrees
Zero-Point Vibrational Energy: 2217681.3 J/mol
Solvent Corrected Gibbs Free Energy (383K): – 5299.870167 Hartrees

Complex 4I

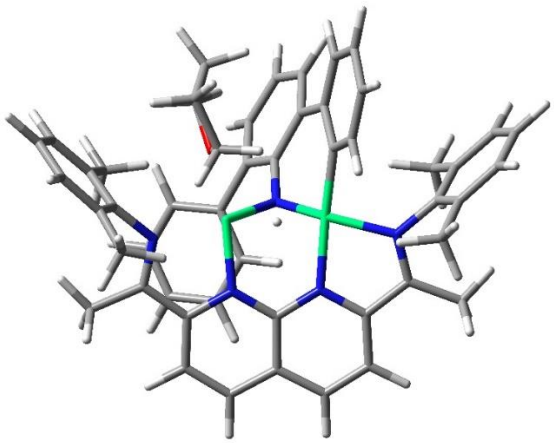

Charge: 1
Multiplicity: 2
Imaginary Frequencies: 0
Electronic Energy: –5300.55927500 Hartrees
Gibbs Free Energy (383 K): –5299.846078 Hartrees
Zero-Point Vibrational Energy: 2221073.4 J/mol
Solvent Corrected Gibbs Free Energy (383K): –5299.872011 Hartrees

Complex 4J

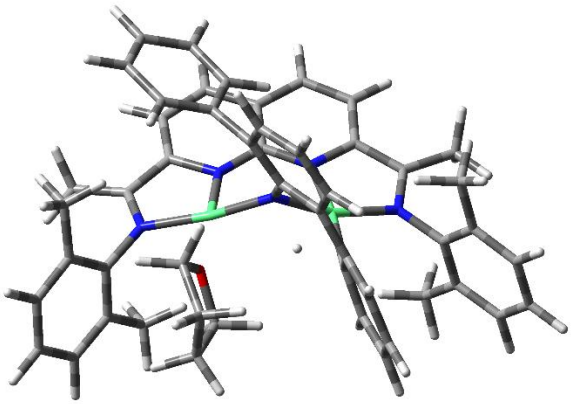

Charge: 1
Multiplicity: 2
Imaginary Frequencies: 1
Electronic Energy: –5300.557180 Hartrees
Gibbs Free Energy (383 K): –5299.845176 Hartrees
Zero-Point Vibrational Energy: 2220369.8J/mol
Solvent Corrected Gibbs Free Energy (383K): –5299.874486 Hartrees

Complex 4K

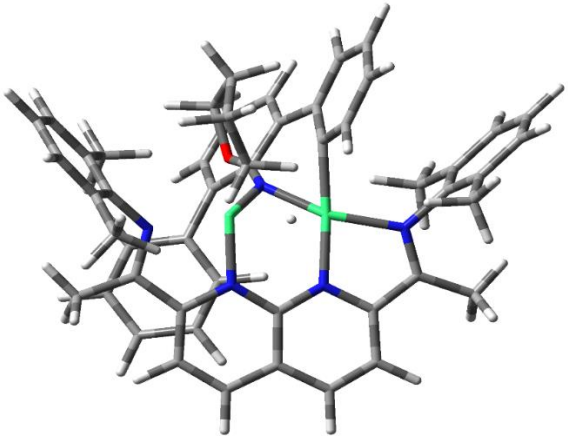

Charge: 1
Multiplicity: 2
Imaginary Frequencies: 1
Electronic Energy: –5300.530271 Hartrees
Gibbs Free Energy (383 K): –5299.818579 Hartrees
Zero-Point Vibrational Energy: 2219201.4 J/mol

Complex 4L

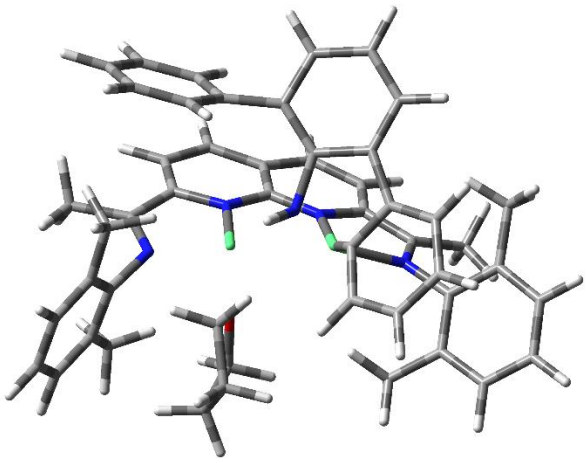

Charge: 1
Multiplicity: 2
Imaginary Frequencies: 1
Electronic Energy: –5300.523371 Hartrees
Gibbs Free Energy (383 K): – 5299.809567 Hartrees
Zero-Point Vibrational Energy: 2225778.3 J/mol

Charge: 1
Multiplicity: 4
Imaginary Frequencies: 1
Electronic Energy: –5300.523880 Hartrees
Gibbs Free Energy (383 K): –5299.809648 Hartrees
Zero-Point Vibrational Energy: 2226681.5 J/mol

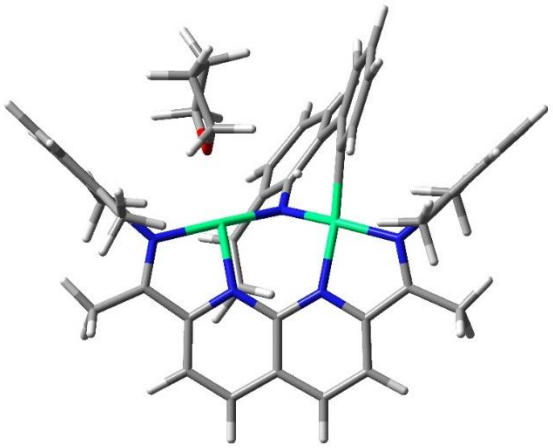

Charge: 1
Multiplicity: 2
Imaginary Frequencies: 1
Electronic Energy: –5146.89724466 Hartrees
Gibbs Free Energy (383.0 K): –5146.226867 Hartrees
Zero-Point Vibrational Energy: 2098137.0 J/mol

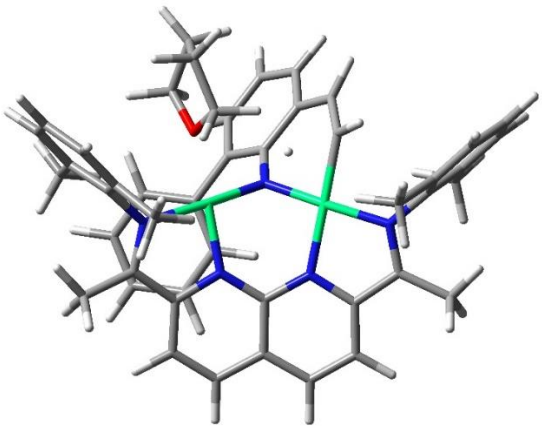

Charge: 1
Multiplicity: 2
Imaginary Frequencies: 1
Electronic Energy: –5146.91309061 Hartrees
Gibbs Free Energy (383.0 K): –5146.240588 Hartrees
Zero-Point Vibrational Energy: 2101424.1 J/mol

Complex 8

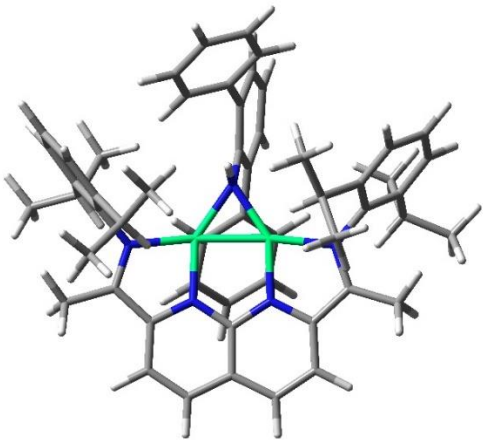

Charge: 0
Multiplicity: 2
Imaginary Frequencies: 0
Electronic Energy: –5383.40650269 Hartrees
Gibbs Free Energy (353 K): –5382.567691 Hartrees
Zero-Point Vibrational Energy: 2533082.6 J/mol

8. References

1. Youn, S. W.; Ko, T. Y.; Jang, M. J.; Jang, S. S. *Adv. Synth. Catal.* **2015**, *357*, 227–234.

2. Kong, C.; Jana, N.; Jones, C.; Driver, T. G. *J. Am. Chem. Soc.* **2016**, *138*, 13271–13280.

3. Brucelle, F.; Renaud, P. *Org. Lett.* **2012**, 14, 12, 3048–3051

4. He, K.-H.; Tan, F.-F.; Zhou, C.-Z.; Zhou, G.-J.; Yang, X.-L.; Li, Y.. *Angew. Chem., Int. Ed.* **2017**, *56*, 3080–3084.

5. Gore, S.; Baskaran, S.; König, B. *Org. Lett.* **2012**, *14* , 4568–4571.

6. Buil, M. L.; Esteruelas, M. A.; Gay, M. P.; Gomez-Gallego, M.; Nicasio, A. I.; Onate, E.; Santiago, A.; Sierra, M. A. *Organometallics* **2018**, 37, 4, 603–617

7. Powers, I. G.; Kiattisewee, C.; Mullane, K. C.; Schelter, E. J.; Uyeda, C. *Chem. Eur. J.* ***2017***, *23, 7694–7697*.

8. Kong, C.; Driver, T. G. *Org. Lett.* **2015**, *17*, 802–805.

9. Shen, M.; Leslie, B. E.; Driver, T. G. *Angew. Chem., Int. Ed.* **2008**, *47*, 5056–5059

10. Robbins, D. W.; Boebel, T. A.; Hartwig, J. F. *J. Am. Chem. Soc.* **2010**, *132*, 4068–4069.

11. Tsvelikhovsky, D.; Buchwald, S. L. *J. Am. Chem. Soc.* **2010**, *132*, 14048–14051.

12. Otwinowski, Z.; Minor, W. in: Methods Enzymol., 1997, pp. 307–326.

13. (a) SHELXTL (Version 6.14) (2000-2003) Bruker Advanced X-ray Solutions, Bruker AXS Inc., Madison, Wisconsin: USA. (b) Sheldrick, G. M. *Acta Cryst.* **2008**, A64, 112-122.

14. Hübschle, C. B.; Sheldrick, G. M.; Dittrich, B. *J. Appl. Crystallogr.* **2011**, *44*, 1281-1284.

15. Sheldrick, G. M. *Acta Crystallogr., Sect. C* **2015**, *71* 3-8.

16. Gaussian 09, Revision A.02, M. J. Frisch, G. W. Trucks, H. B. Schlegel, G. E. Scuseria, M. A. Robb, J. R. Cheeseman, G. Scalmani, V. Barone, G. A. Petersson, H. Nakatsuji, X. Li, M. Caricato, A. Marenich, J. Bloino, B. G. Janesko, R. Gomperts, B. Mennucci, H. P. Hratchian, J. V. Ortiz, A. F. Izmaylov, J. L. Sonnenberg, D. Williams-Young, F. Ding, F. Lipparini, F. Egidi, J. Goings, B. Peng, A. Petrone, T. Henderson, D. Ranasinghe, V. G. Zakrzewski, J. Gao, N. Rega, G. Zheng, W. Liang, M. Hada, M. Ehara, K. Toyota, R. Fukuda, J. Hasegawa, M. Ishida, T. Nakajima, Y. Honda, O. Kitao, H. Nakai, T. Vreven, K. Throssell, J. A. Montgomery, Jr., J. E. Peralta, F. Ogliaro, M. Bearpark, J. J. Heyd, E. Brothers, K. N. Kudin, V. N. Staroverov, T. Keith, R. Kobayashi, J. Normand, K. Raghavachari, A. Rendell, J. C. Burant, S. S. Iyengar, J. Tomasi, M. Cossi, J. M. Millam, M. Klene, C. Adamo, R. Cammi, J. W. Ochterski, R. L. Martin, K. Morokuma, O. Farkas, J. B. Foresman, and D. J. Fox, Gaussian, Inc., Wallingford CT, 2016.

APPENDIX B. SUPPORTING INFORMATION FOR CHAPTER 2.

1. General Information

General Considerations. All manipulations were carried out using standard Schlenk or glovebox techniques under an atmosphere of N_2. Solvents were dried and degassed by passing through a column of activated alumina and sparging with Ar gas. Deuterated solvents were purchased from Cambridge Isotope Laboratories, Inc., degassed, and stored over activated 3 Å molecular sieves prior to use. All other reagents and starting materials were purchased from commercial vendors and used without further purification unless otherwise noted. Liquid reagents were degassed and stored over activated 3 Å molecular sieves prior to use. Elemental analyses were performed by Midwest Microlab (Indianapolis, IN). The [$^{i\text{-Pr}}$NDI]$Ni_2(C_6H_6)$ complex (**1**), was prepared according to previously reported procedures.[1]

Physical Methods. ^{1}H NMR spectra were collected at room temperature on Varian INOVA 600 or 300 MHz or Bruker DRX 500 MHz spectrometers. ^{1}H and ^{13}C NMR spectra are reported in parts per million relative to tetramethylsilane, using the residual solvent resonances as an internal standard. GC/MS data was collected on a Shimadzu GC-2010/MS-QP2010 spectrometer containing a mini-bore capillary GC column and single quad EI detector. UV–vis measurements were acquired on a Perkin Elmer Lambda 950 UV–VIS–NIR spectrophotometer using a 1-cm two-window quartz cuvette. High-resolution mass data were obtained using a 6320 Ion Trap MS system.

X-Ray Crystallography. Single-crystal X-ray diffraction studies were carried out at the Purdue X-ray crystallography facility using a Rigaku Rapid II diffractometer or a Bruker AXS D8 Quest CMOS diffractometer.

Procedure for XRD data collected using the Rigaku Rapid II instrument. Single crystal X-ray measurements were conducted on a Rigaku Rapid II curved image plate diffractometer with a Cu-Kα X-ray microsource (λ = 1.54178 Å) with a laterally graded multilayer (Goebel) mirror for monochromatization. Single crystals were mounted on Mitegen microloop mounts using a trace of

mineral oil and cooled in-situ to 150(2) K for data collection. Data were collected using the dtrek option of CrystalClear-SM Expert 2.1 b32.[2] Data were processed using HKL3000 and data were corrected for absorption and scaled using Scalepack.[3]

Procedure for XRD data collected using the Bruker Quest instrument. Single crystals were coated with mineral oil or fomblin and quickly transferred to the goniometer head of a Bruker Quest diffractometer with kappa geometry, an I-μ-S microsource X-ray tube, laterally graded multilayer (Goebel) mirror single crystal for monochromatization, a Photon2 CMOS area detector and an Oxford Cryosystems low temperature device. Examination and data collection were performed with Cu Kα radiation (λ = 1.54178 Å) at 100 K. Data were collected, reflections were indexed and processed, and the files scaled and corrected for absorption using APEX3.[4]

Structure Solution and Refinement. The space groups were assigned and the structures were solved by direct methods using XPREP within the SHELXTL suite of programs[5] and refined by full matrix least squares against F^2 with all reflections using Shelxl2016[6] using the graphical interface Shelxle.[7] If not specified otherwise H atoms attached to carbon and nitrogen atoms were positioned geometrically and constrained to ride on their parent atoms, with carbon hydrogen bond distances of 0.95 Å for and aromatic C-H, 1.00, 0.99 and 0.98 Å for aliphatic C-H, CH_2 and CH_3 moieties, respectively. Methyl H atoms were allowed to rotate but not to tip to best fit the experimental electron density. U_{iso}(H) values were set to a multiple of U_{eq}(C) with 1.5 for CH_3, and 1.2 for C-H units, respectively. Additional data collection and refinement details, including description of disorder and/or twinning (where present) can be found in Section 9.

2. N=N Coupling Catalyst Comparison Studies

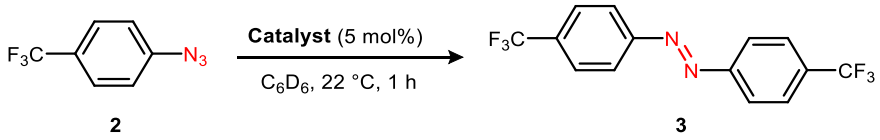

2 **3**

General procedure. In an N_2 filled glovebox, an NMR tube equipped with a J. Young valve was charged with catalyst (0.0015 mmol, 5 mol %) and C_6H_6 (550 µL). A solution of 4-trifluoromethylphenylazide **2** (50 µL of a 0.60 M stock solution in C_6D_6 containing 0.41 M 1,3,5-trimethoxybenzene, 0.3 mmol, 1.0 equiv) was added. The reaction components were allowed to react for 1 h, and the yield of the azoarene product was determined by ^{1}H NMR integration against 1,3,5-trimethoxybenzne as an internal standard. In all cases, no additional conversion or yield of azoarene was observed after 2 h or after heating for an additional hour at 80 °C. For entries 3 and 4, the catalyst was formed by mixing the corresponding ligand (28% and 14% for PPh_3 and $^{i\text{-Pr}}$IPr respectively) with $Ni(COD)_2$ (5 mol%). For entry 9, 0.5 mol% **1** was used.

entry	catalyst	conversion	yield
1	none	<2%	<2%
2	$Ni(COD)_2$	24%	<2%
3	$Ni(COD)_2$ + PPh_3	35%	<2%
4	$Ni(COD)_2$ + IPr	32%	<2%
5	[$^{i\text{-Pr}}$IP]Ni(COD) (**4**)	24%	13%
6	[BPY]Ni(COD) (**5**)	23%	13%
7	[$^{i\text{-Pr}}$DAD]Ni(COD) (**6**)	<2%	<2%
8	[$^{i\text{-Pr}}$NDI]$Ni_2(C_6H_6)$ (**1**)	>98%	90%
9	[$^{i\text{-Pr}}$NDI]$Ni_2(C_6H_6)$ (**1**)	>98%	96%

Identification of reaction products in entries 3 and 4. To determine the identity of the products formed in entries 3 and 4, **2** was reacted with the PPh_3 and IPr ligands respectively. Both reactions immediately evolved N_2 gas, leading to the formation of the respective nitrene transfer products, [$^{i\text{-Pr}}$IPr]=NAr and Ph_3P=NAr.[8] ^{1}H, ^{19}F, and ^{31}P (for entry 3) NMR spectra confirmed that the group transfer products formed in these stoichiometric reactions were the same as those formed in the catalytic reactions of entries 3 and 4.

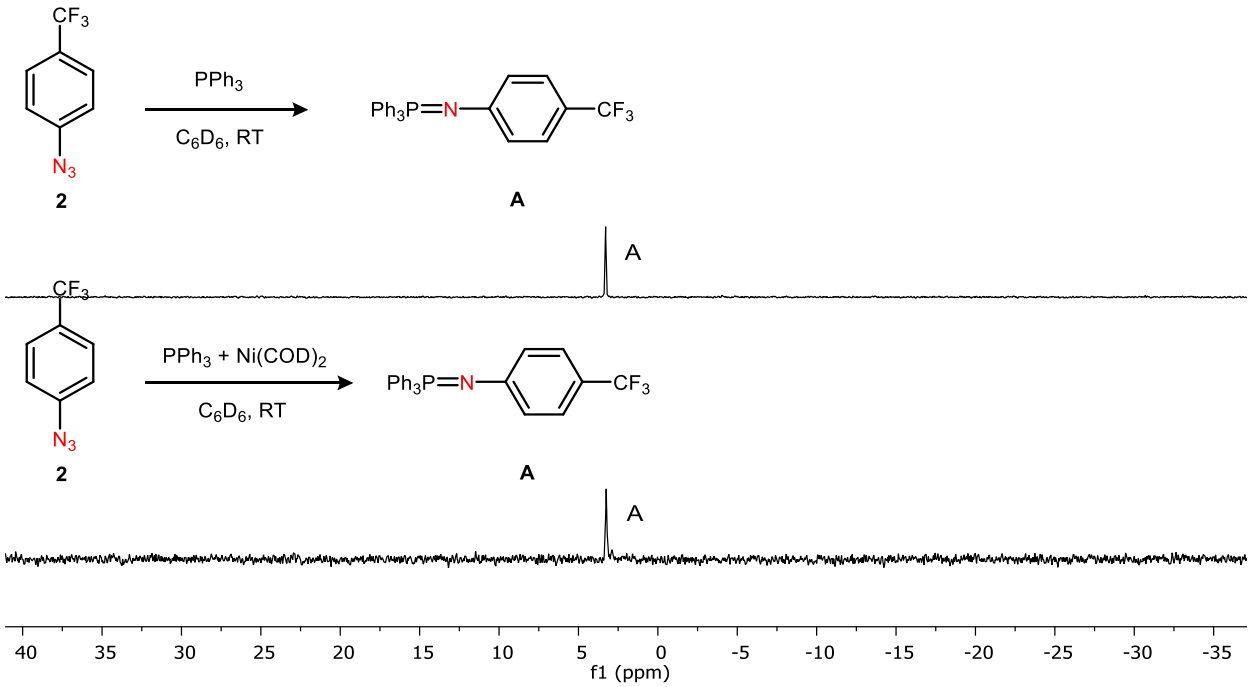

Figure S1. ^{31}P NMR comparison of the stoichiometric reaction between $^{i\text{-Pr}}$IPr and **2** (top) and the catalytic reaction mixture from entry 3 (bottom).

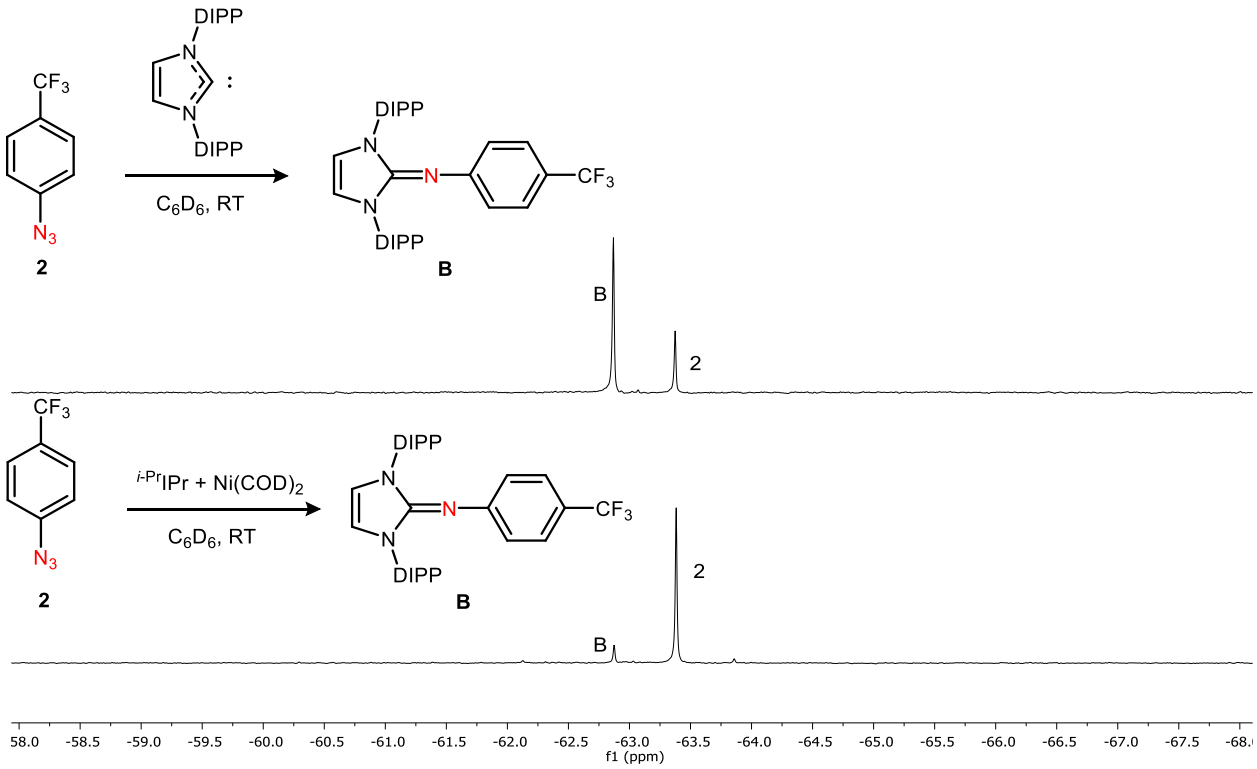

Figure S2. ^{19}F NMR comparison of the stoichiometric reaction between $^{i\text{-Pr}}$IPr and **2** (top) and the catalytic reaction mixture from entry 4 (bottom).

3. Synthesis of Azides and Characterization of Novel Azide Compounds

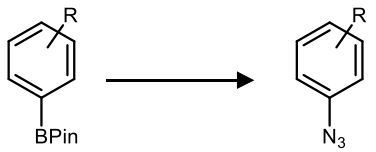

General Procedure for azidification of pinacolborane.[9] Pinacol boranes were synthesized from the corresponding aryl triflates according to a previously reported procedure.[10] To the aryl pinacol boronate (1.0 equiv) in MeOH (5 mL/mmol) was added NaN_3 (1.5 equiv) and $Cu(OAc)_2$ (0.1 equiv). The solution was vigorously stirred at 55 °C under air for 24 hours. The mixture was filtered through celite and concentrated. The residue was purified by silica gel column chromatography.

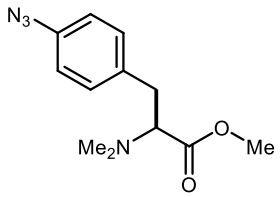

S1

Compound S1. Synthesized according to the general procedure using crude (*S*)-methyl 2-(dimethylamino)-3-(4-(4,4,5,5-tetramethyl-1,3,2-dioxaborolane)phenyl)propanoate (1.21 g, 3.63 mmol). Isolated yields were determined following column chromatography (SiO_2, 15% EtOAc/hexanes). The product was isolated as an orange solid. (0.187 g, 0.753 mmol 21% yield). ^{1}H NMR (800 MHz, $CDCl_3$) δ 7.18 (d, *J* = 8.0 Hz, 2H), 6.94 (d, *J* = 8.7 Hz, 2H), 3.61 (s, 3H), 3.38 (dd, *J* = 9.4, 5.8 Hz, 1H), 3.08 – 2.86 (m, 2H), 2.38 (s, 6H). ^{13}C{^{1}H} NMR (201 MHz, $CDCl_3$) δ 171.70, 138.18, 134.91, 130.42, 119.00, 69.50, 51.10, 41.84, 35.09. HRMS(ESI): calcd for $C_{12}H_{17}N_4O_2^+$: 249.1346; found: 249.1344.

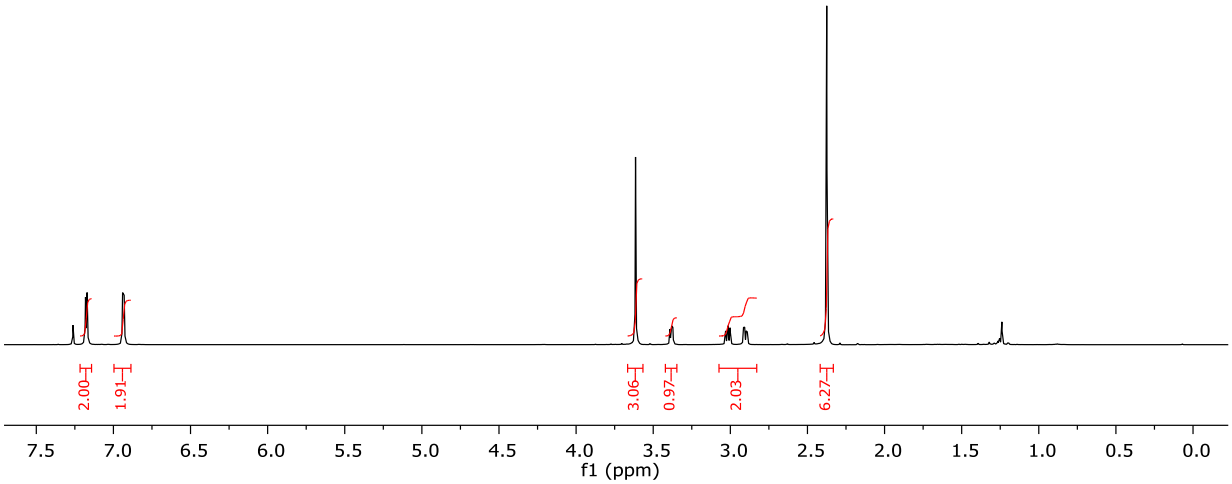

Figure S3. ^{1}H NMR spectrum of **S1** in $CDCl_3$.

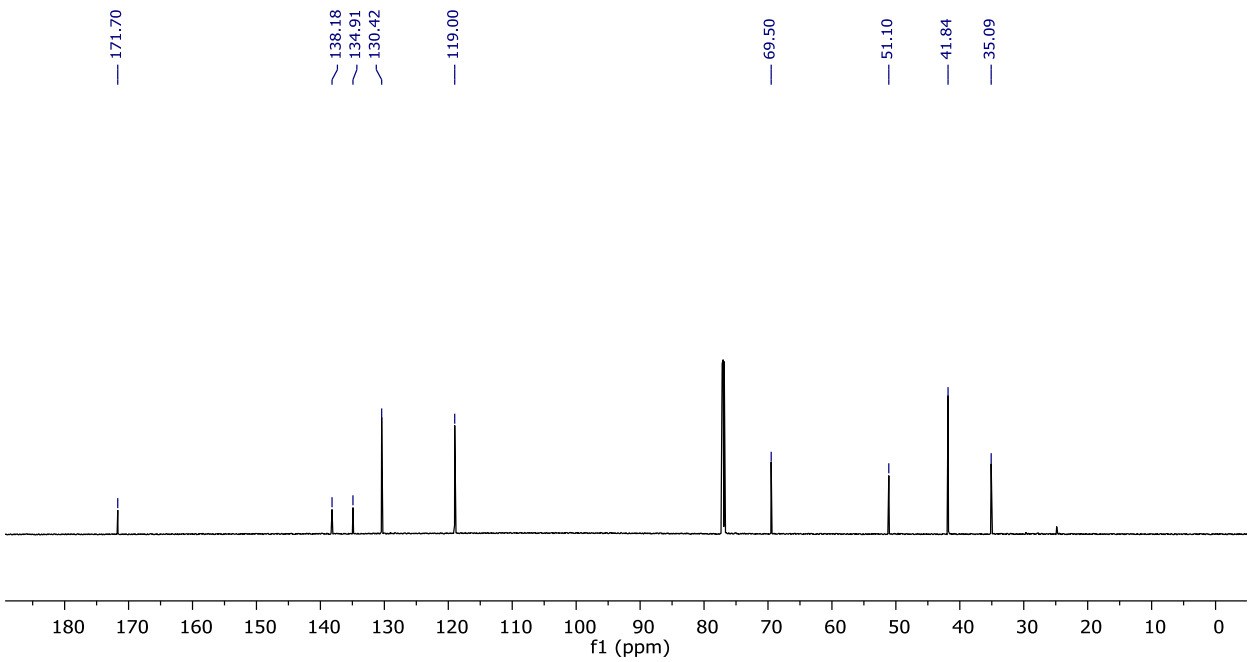

Figure S4. $^{13}C\{^{1}H\}$ NMR spectrum of **S1** in $CDCl_3$.

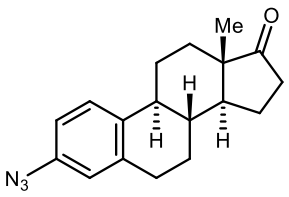

Compound S2. Synthesized according to the general procedure using 3-deoxyestrone-3-boronic acid pinacol ester (0.5267 g, 1.38 mmol). The isolated yield was determined following column chromatography (SiO_2, 10% EtOAc/hexanes) to yield a light-yellow oil (0.511g, >99% yield). ^{1}H NMR (800 MHz, $CDCl_3$) δ 7.27 (d, *J* = 8.1 Hz, 1H), 6.82 (dd, *J* = 8.5, 2.5 Hz, 1H), 6.76 (dd, *J* = 2.5, 1.2 Hz, 1H), 2.90 (dd, *J* = 9.2, 4.2 Hz, 2H), 2.51 (dd, *J* = 9.3, 8.7 Hz, 1H), 2.43 – 2.38 (m, 1H), 2.31 – 2.24 (m, 1H), 2.19 – 2.11 (m, 1H), 2.10 – 2.00 (m, 2H), 2.00 – 1.94 (m, 1H), 1.67 – 1.56 (m, 2H), 1.56 – 1.48 (m, 3H), 1.48 – 1.41 (m, 1H), 0.97 – 0.87 (m, 3H). ^{13}C{^{1}H} NMR (201 MHz, $CDCl_3$) δ 220.62, 138.31, 137.41, 136.67, 126.77, 119.11, 116.48, 50.40, 47.93, 44.12, 38.10, 35.82, 31.52, 29.37, 26.31, 25.79, 21.57, 13.83. HRMS(ESI): calcd for $C_{18}H_{22}N_3O^+$: 296.1757; found: 296.1760.

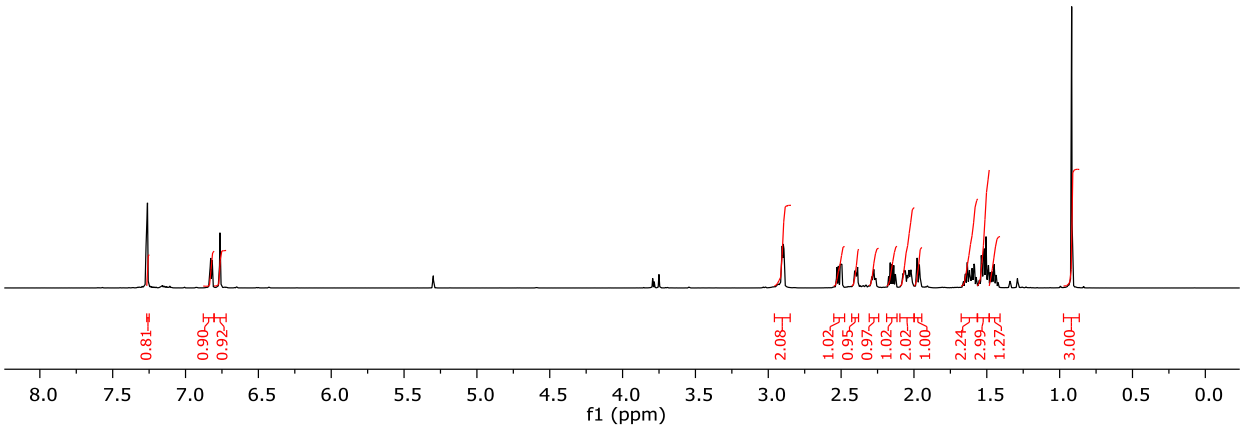

Figure S5. ^{1}H NMR spectrum of **S2** in $CDCl_3$.

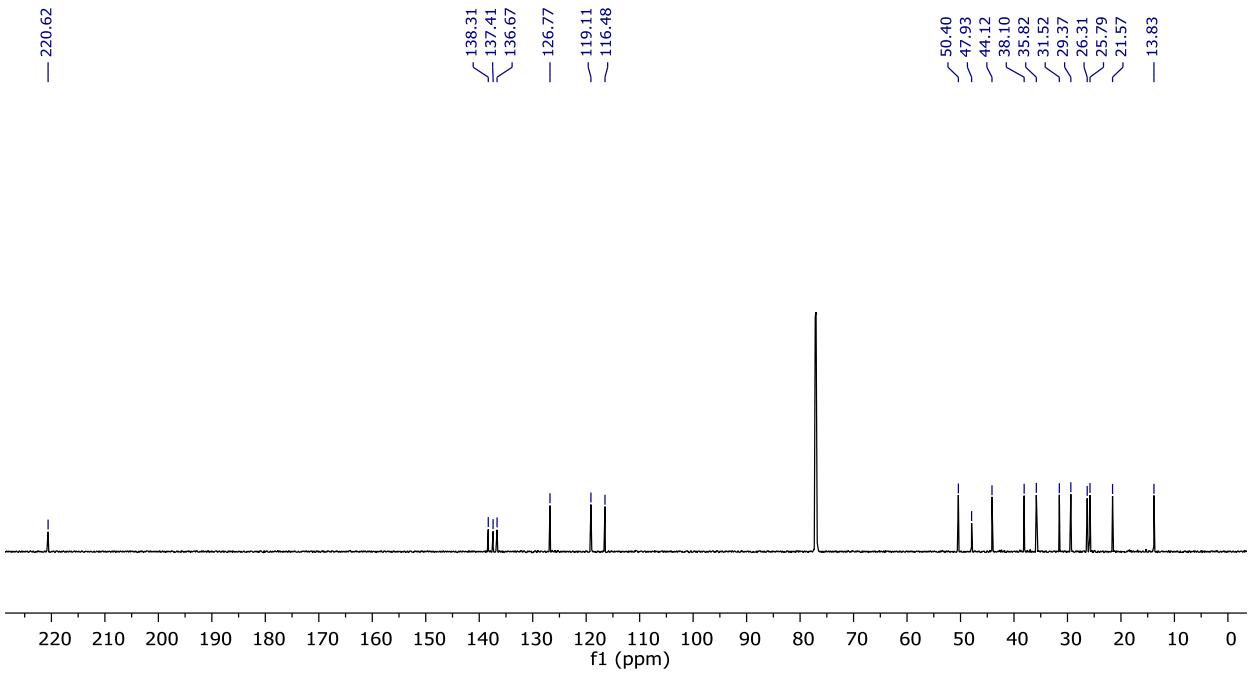

Figure S6. $^{13}C\{^{1}H\}$ NMR spectrum of **S2** in $CDCl_3$.

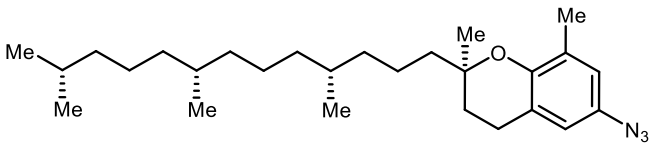

Compound S3. Synthesized according to the general procedure using crude 4,4,5,5-Tetramethyl-1,3,2-dioxaborolane δ-tocopherol (1.2 g, 2.34 mmol). Isolated yields were determined following column chromatography (SiO_2, 10% CH_2Cl_2/hexanes). The product was isolated as a colorless oil (0.624 g, 62% yield). ^{1}H NMR (800 MHz, C_6D_6) δ 6.61 (s, 1H), 6.50 (s, 1H), 2.32 (t, *J* = 6.9 Hz, 2H), 2.12 (s, 3H), 1.55 – 1.09 (m, 23H), 1.07 (s, 3H), 0.94 – 0.85 (m, 12H). ^{13}C{^{1}H} NMR (201 MHz, C_6D_6) δ 149.51, 130.47, 127.93, 121.50, 119.28, 117.14, 75.78, 39.94, 39.39, 37.54, 37.47, 37.43, 37.36, 32.88, 32.67, 30.82, 27.98, 24.92, 24.58, 23.70, 22.55, 22.46, 22.07, 20.92, 19.63, 19.51, 15.88. HRMS(ESI): calcd for [$C_{27}H_{45}N_3O^+$] - N_2 + H: 400.3574; found: 400.3572. The temperature required to vaporize the sample resulted in the loss of N_2 from the azide.

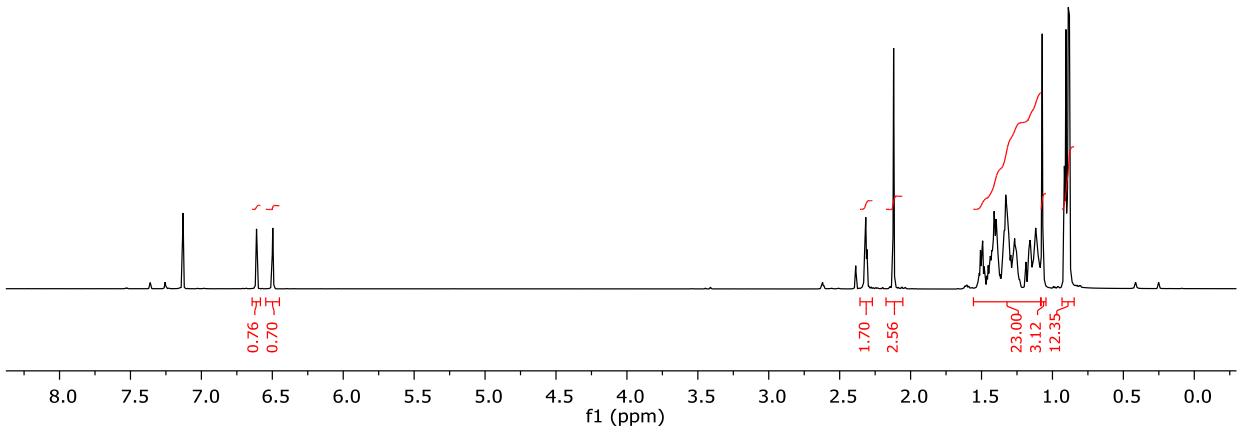

Figure S7. ^{1}H NMR spectrum for **S3** in $CDCl_3$.

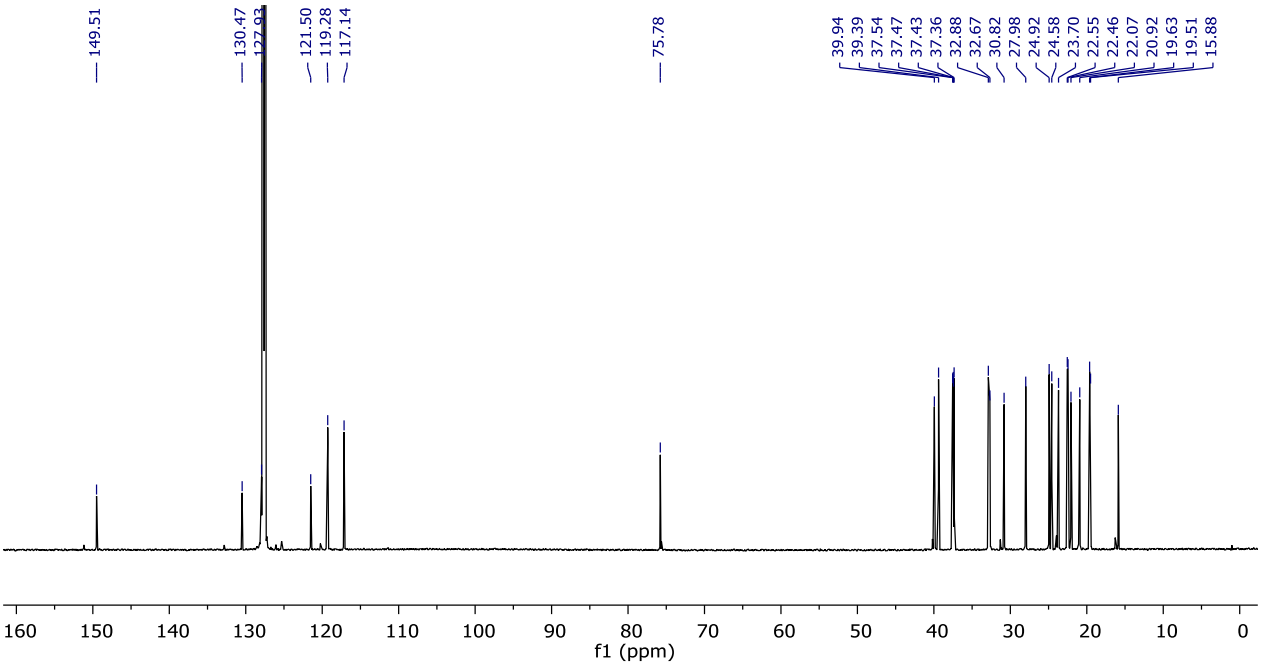

Figure S8. $^{13}C\{^{1}H\}$ NMR spectrum for **S3** in $CDCl_3$.

4. Catalytic N=N Coupling Reactions and Azoarene Characterization Data

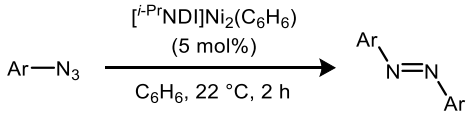

General procedure for the synthesis of azoarenes from aryl azides. In an N_2 filled glovebox, a 20-mL vial was charged with **1** (11.0 mg, 0.015 mmol, 5 mol%), C_6H_6 (3.0 mL), and a magnetic stir bar. A solution of the aryl azide (0.3 mmol, 1.0 equiv) dissolved in C_6H_6 (3.0 mL) was added. The vial was sealed, and the reaction mixture was stirred at room temperature. After 2 h, the reaction vial was opened to air and stirred for 30 min in order to quench the catalyst. The solution volume was reduced by half under reduced pressure, and the crude mixture was directly loaded onto a SiO_2 column. Isolated yields were determined following purification.

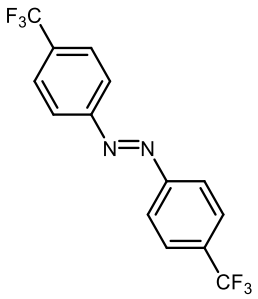

Azoarene 3.[11] The reaction was conducted according to the general procedure using 4-trifluoromethylphenyl azide (56.1 mg, 0.3 mmol, 1.0 equiv). Isolated yields were determined following column chromatography (SiO_2, 1% EtOAc/hexanes). The product was isolated as an orange solid. Run 1: 45.5 mg, 96% yield; Run 2: 43.6 mg, 92% yield. ^{1}H NMR (400 MHz, $CDCl_3$) δ 8.04 (d, *J* = 8.2 Hz, 4H), 7.81 (d, *J* = 8.3 Hz, 4H). ^{19}F NMR (300 MHz, $CDCl_3$) δ -63.85. ^{13}C{^{1}H} NMR (201 MHz, $CDCl_3$) δ 154.07, 132.97 (q, *J* = 32.6 Hz), 126.41 (q, *J* = 3.8 Hz), 123.79 (q, *J* = 272.4 Hz), 123.32.

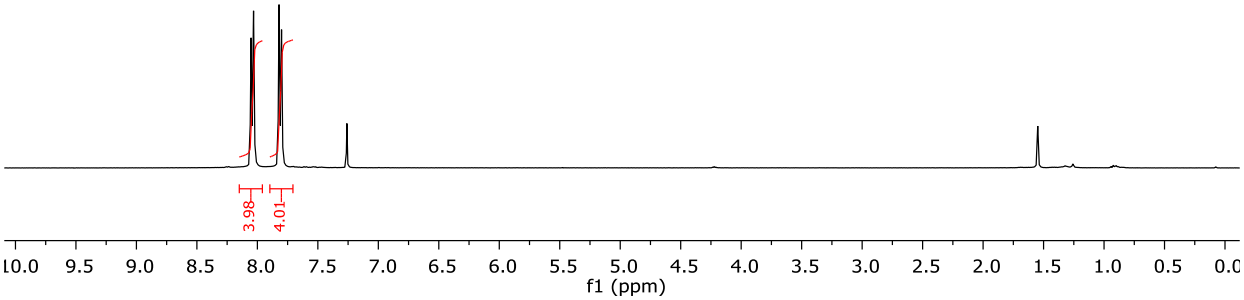

Figure S9. ^{1}H NMR spectrum for **3** in $CDCl_3$.

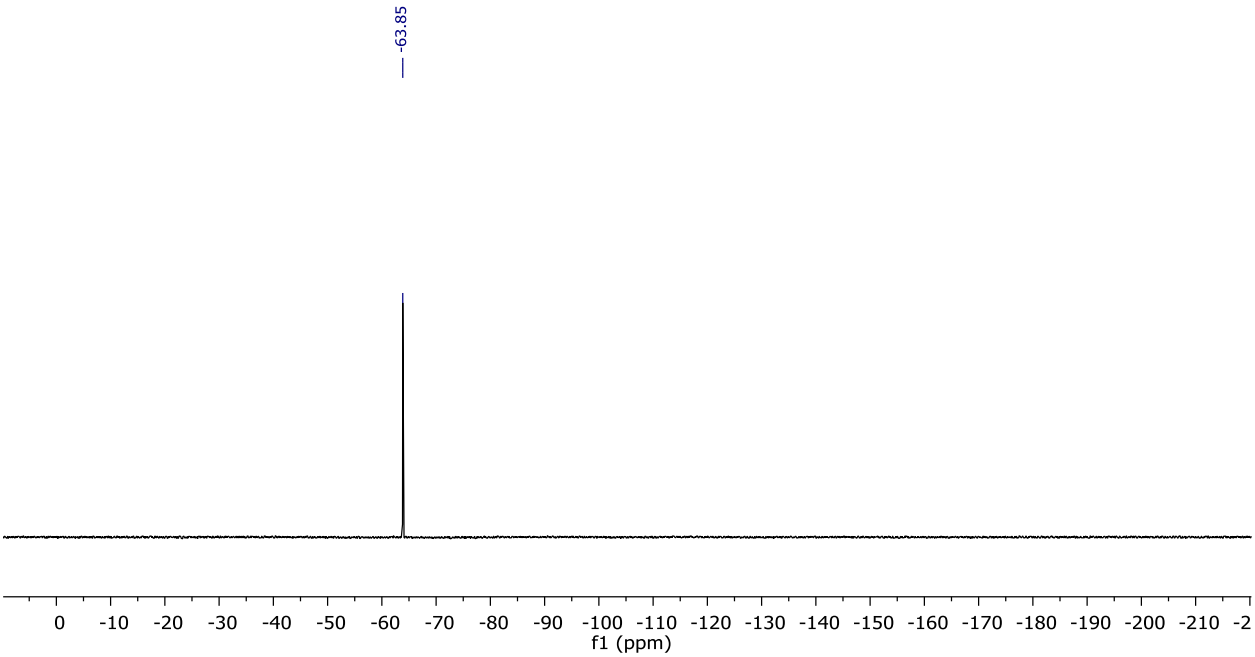

Figure S10. ^{19}F NMR spectrum for **3** in $CDCl_3$.

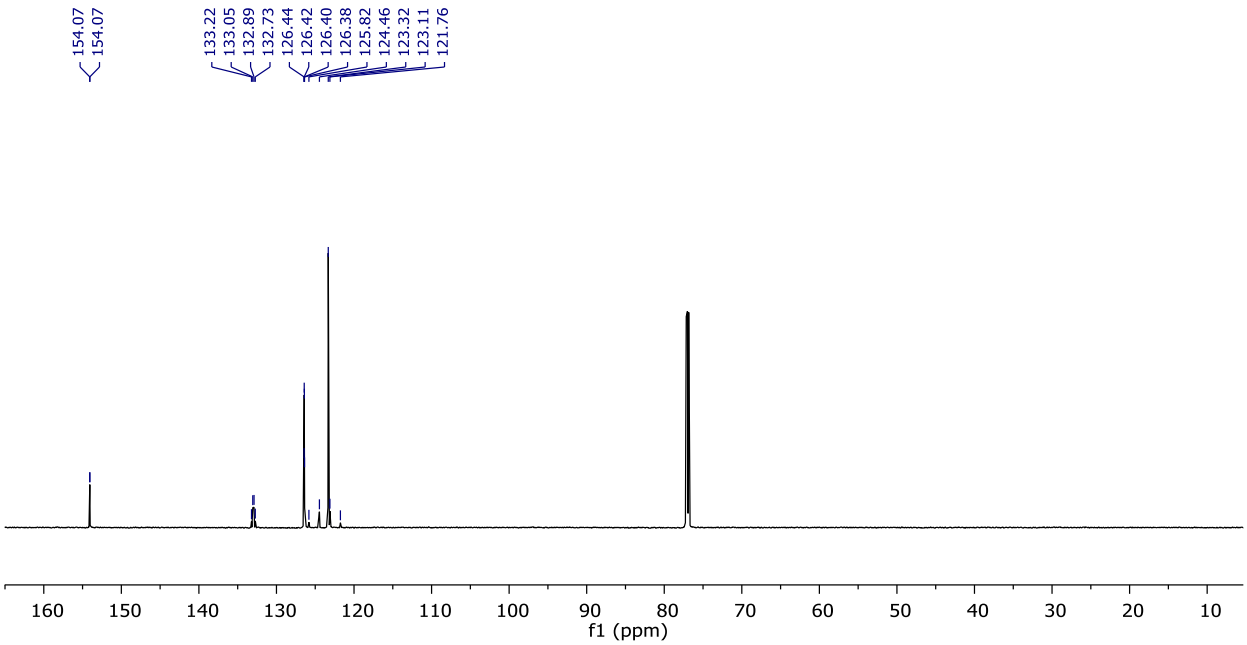

Figure S11. $^{13}C\{^{1}H\}$ NMR spectrum for **3** in $CDCl_3$.

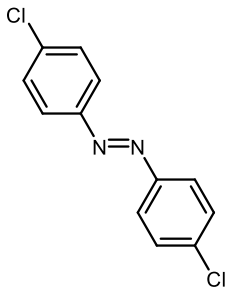

Azoarene 8.[Error! Bookmark not defined.] The reaction was conducted according to the general p rocedure using 4-chlorophenyl azide (46.1 mg, 0.3 mmol, 1.0 equiv). Isolated yields were determined following column chromatography (SiO_2, 0-3% EtOAc/hexanes). The product was isolated as an orange solid. Run 1: 34.7 mg, 92% yield; Run 2: 32.4 mg, 86% yield. ^{1}H NMR (300 MHz, $CDCl_3$) δ 7.86 (d, *J* = 8.8 Hz, 4H), 7.49 (d, *J* = 8.8 Hz, 4H). ^{13}C{^{1}H} NMR (101 MHz, $CDCl_3$) δ 150.68, 137.12, 129.29, 124.08.

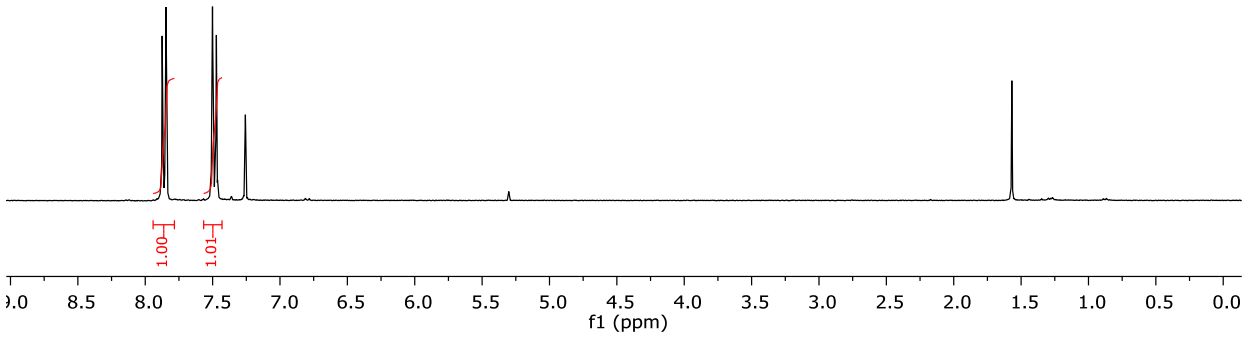

Figure S12. ^{1}H NMR spectrum for **8** in $CDCl_3$.

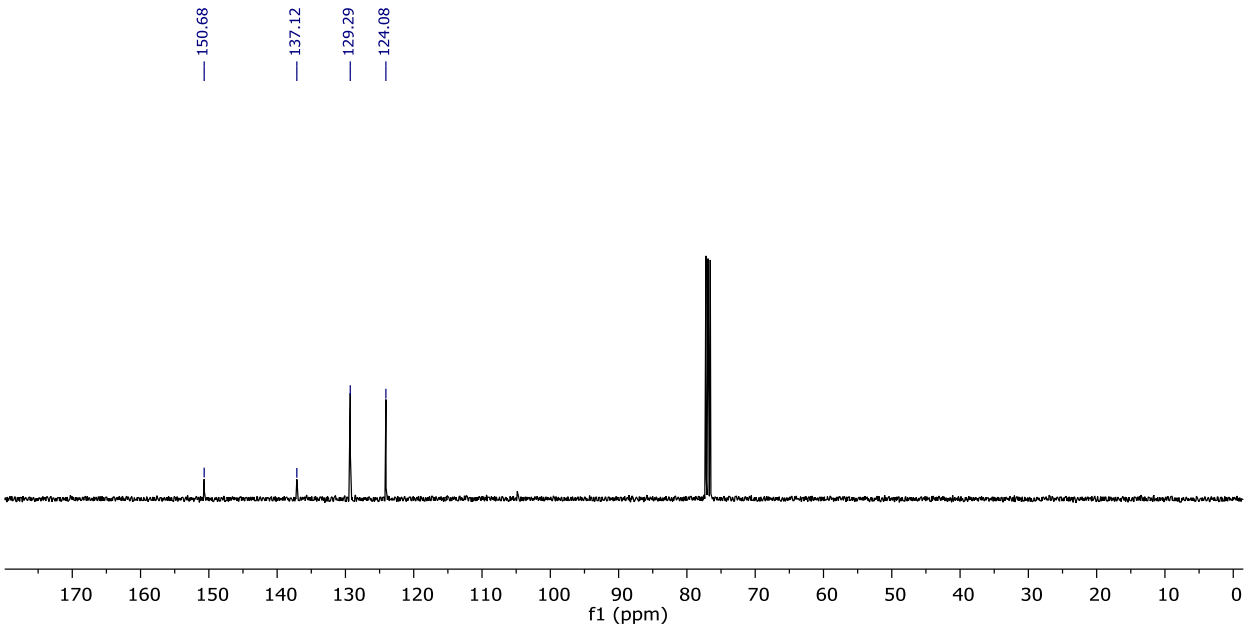

Figure S13. $^{13}C\{^{1}H\}$ NMR spectrum for **8** in $CDCl_3$.

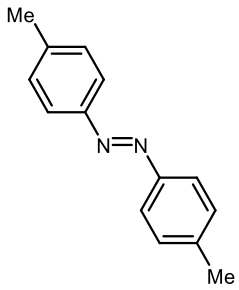

Azoarene 9.[Error! Bookmark not defined.] The reaction was conducted according to the general p rocedure using 4-methylphenyl azide (39.9 mg, 0.3 mmol, 1.0 equiv). Isolated yields were determined following column chromatography (hexanes). The product was isolated as an orange solid. Run 1: 29.3mg, 93% yield; Run 2: 28.7 mg, 91% yield. ^{1}H NMR (300 MHz, $CDCl_3$) δ 7.81 (d, *J* = 7.6 Hz, 4H), 7.31 (d, *J* = 7.8 Hz, 4H), 2.43 (s, 6H). $^{13}C\{^{1}H\}$ NMR (101 MHz, $CDCl_3$) δ 150.72, 141.08, 129.59, 122.60, 21.37.

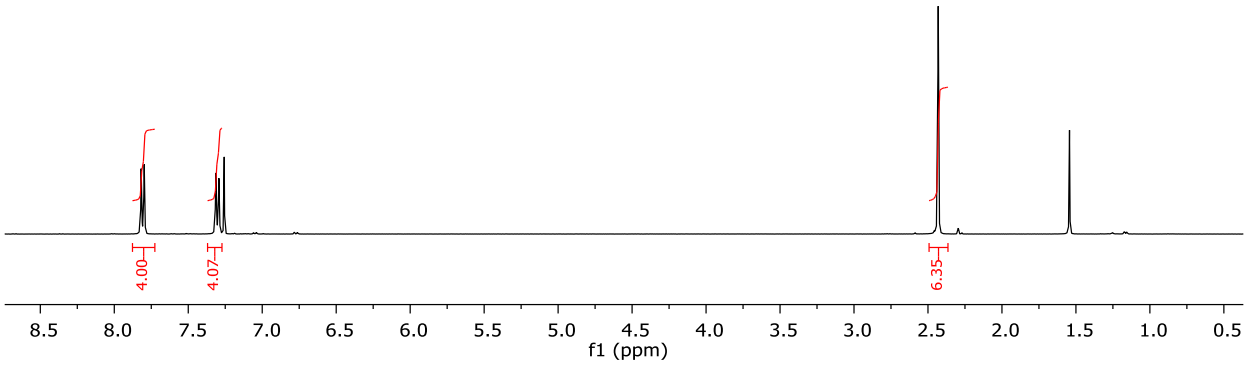

Figure S14. ^{1}H NMR spectrum for **9** in $CDCl_3$.

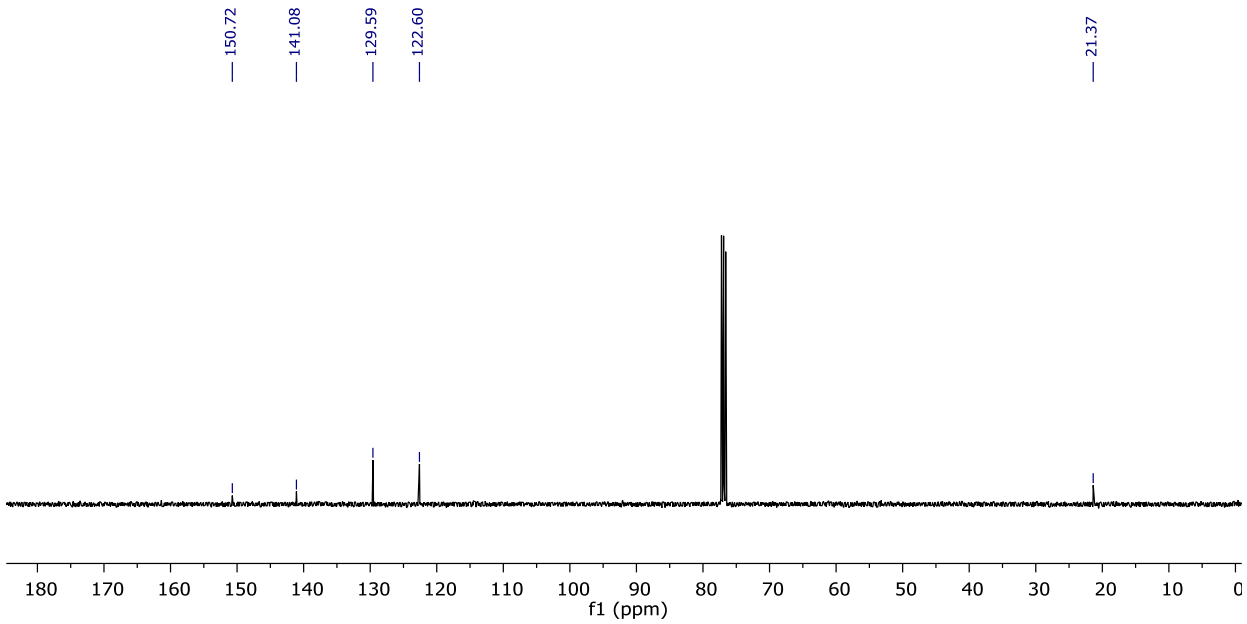

Figure S15. $^{13}C\{^{1}H\}$ NMR spectrum for **9** in $CDCl_3$.

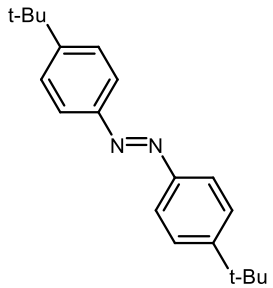

Azoarene 10.[12] The reaction was conducted according to the general procedure using 4-*tert*-butylphenyl azide (52.6 mg, 0.3 mmol, 1.0 equiv). Isolated yields were determined following column chromatography (SiO_2, 1% EtOAc/hexanes). The product was isolated as an orange solid. Run 1: 42.5mg, 96% yield; Run 2: 41.1 mg, 94% yield. ^{1}H NMR (300 MHz, $CDCl_3$) δ 7.85 (d, *J* = 8.9 Hz, 4H), 7.53 (d, *J* = 8.9 Hz, 4H), 1.38 (s, 18H). $^{13}C\{^1H\}$ NMR (101 MHz, $CDCl_3$) δ 154.11, 150.65, 125.85, 122.32, 34.88, 31.18.

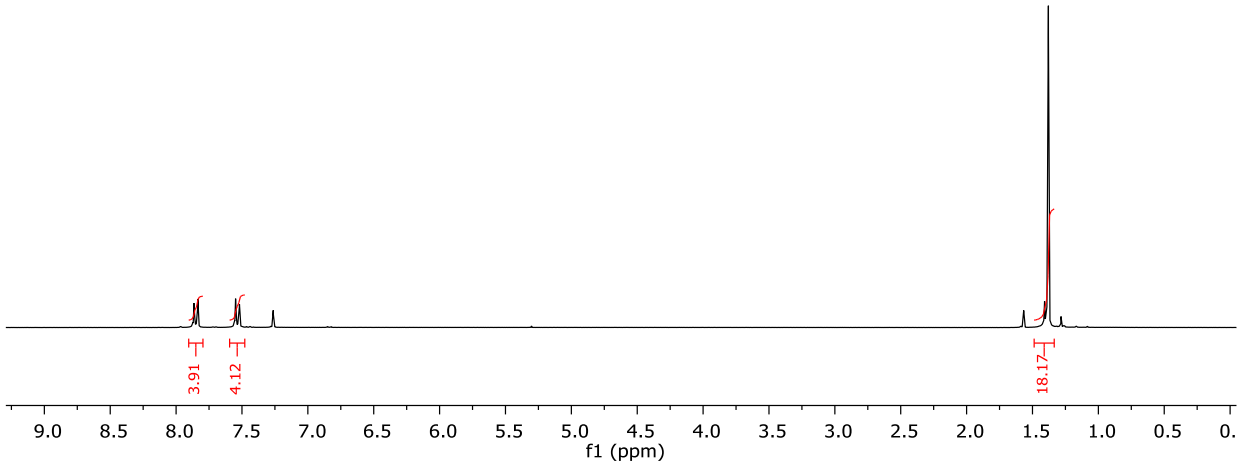

Figure S16. ^{1}H NMR spectrum for **10** in $CDCl_3$

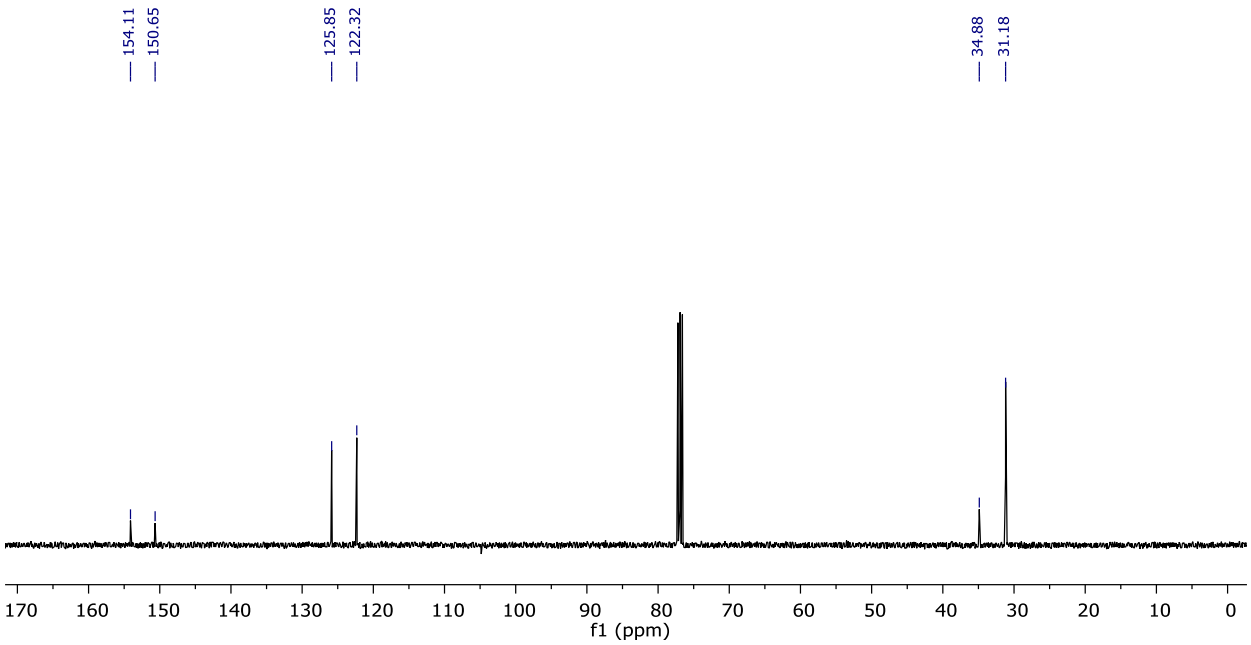

Figure S17. $^{13}C\{^{1}H\}$ NMR spectrum for **10** in $CDCl_3$.

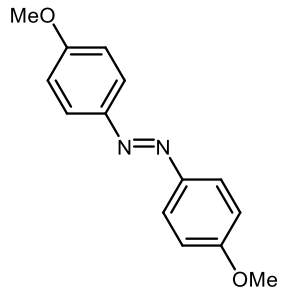

Azoarene 11.[13] The reaction was conducted according to the general procedure using 4-(methoxy)phenyl azide (44.7 mg, 0.3 mmol, 1.0 equiv). Isolated yields were determined following column chromatography (SiO_2, 0-3% EtOAc/hexanes). Run 1: 25 mg, 75% yield; Run 2: 28mg, 77% yield. ^{1}H NMR (300 MHz, $CDCl_3$) δ 7.89 (d, *J* = 9.0 Hz, 4H), 7.01 (d, *J* = 8.9 Hz, 4H), 3.89 (s, 6H). $^{13}C\{^1H\}$ NMR (101 MHz, $CDCl_3$) δ 161.47, 147.00, 124.25, 114.08, 55.47.

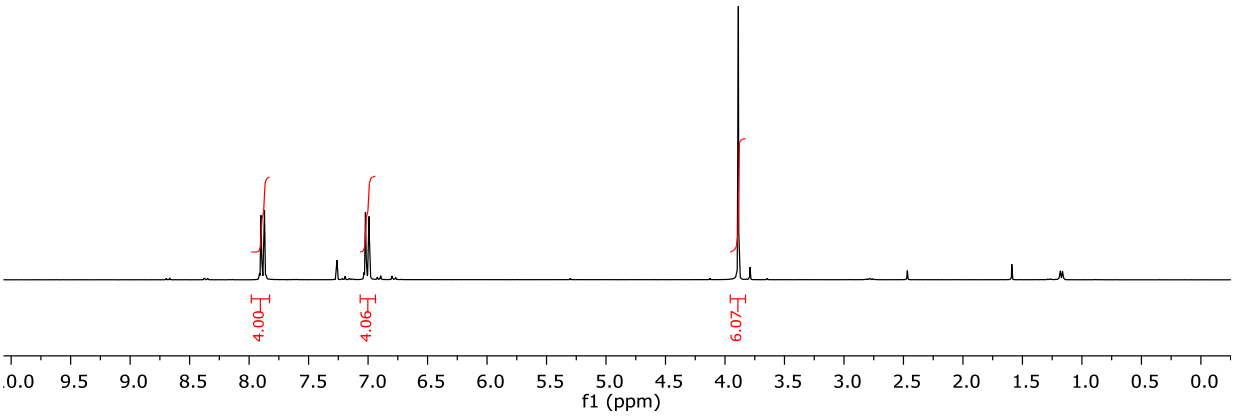

Figure S18. ^{1}H NMR spectrum for **11** in $CDCl_3$.

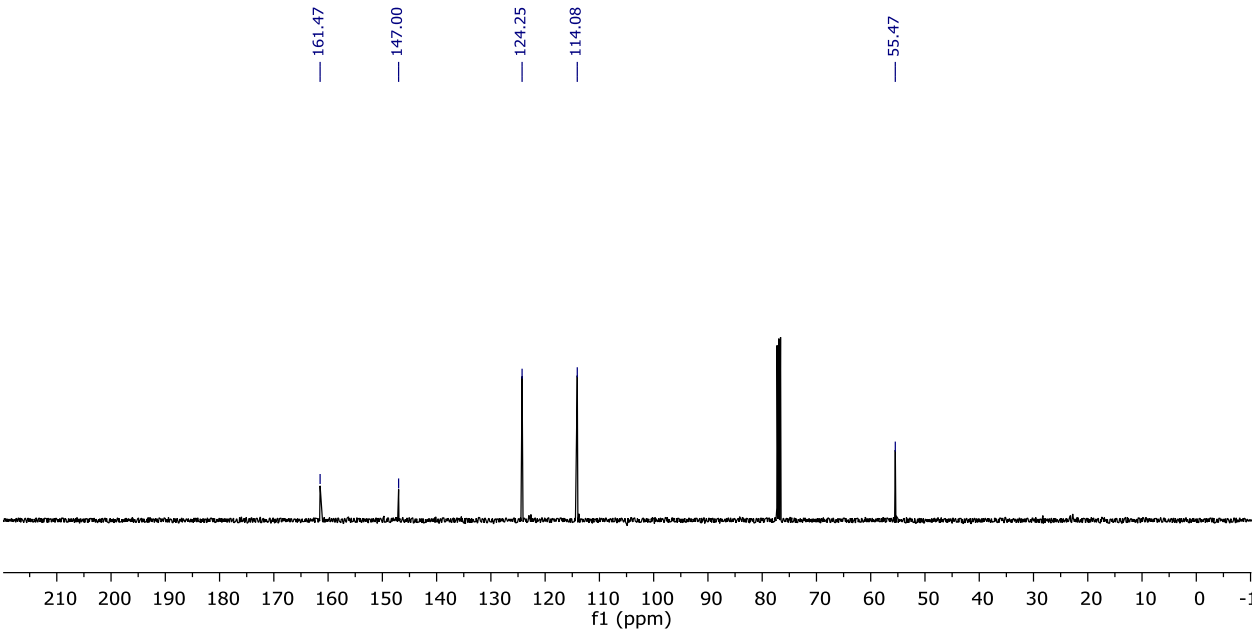

Figure S19. $^{13}C\{^{1}H\}$ NMR spectrum for **11** in $CDCl_3$.

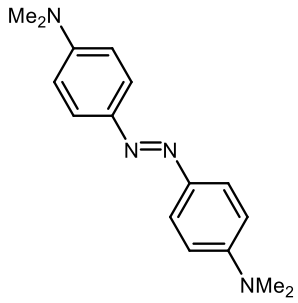

Azoarene 12.[14] The reaction was conducted according to the general procedure using 4-(N,N′-dimethyl)penyl azide (48.7 mg, 0.3 mmol, 1.0 equiv). Isolated yields were determined following column chromatography (SiO_2, 10% EtOAc/hexanes). Run 1: 20 mg, 50% yield; Run 2: 19 mg 48% yield. ^{1}H NMR (300 MHz, $CDCl_3$) δ 7.81 (d, *J* = 9.1 Hz, 4H), 6.76 (d, *J* = 9.2 Hz, 4H), 3.06 (d, *J* = 0.6 Hz, 12H). $^{13}C\{^1H\}$ NMR (201 MHz, $CDCl_3$) δ 151.50, 144.12, 123.97, 111.76, 40.43.

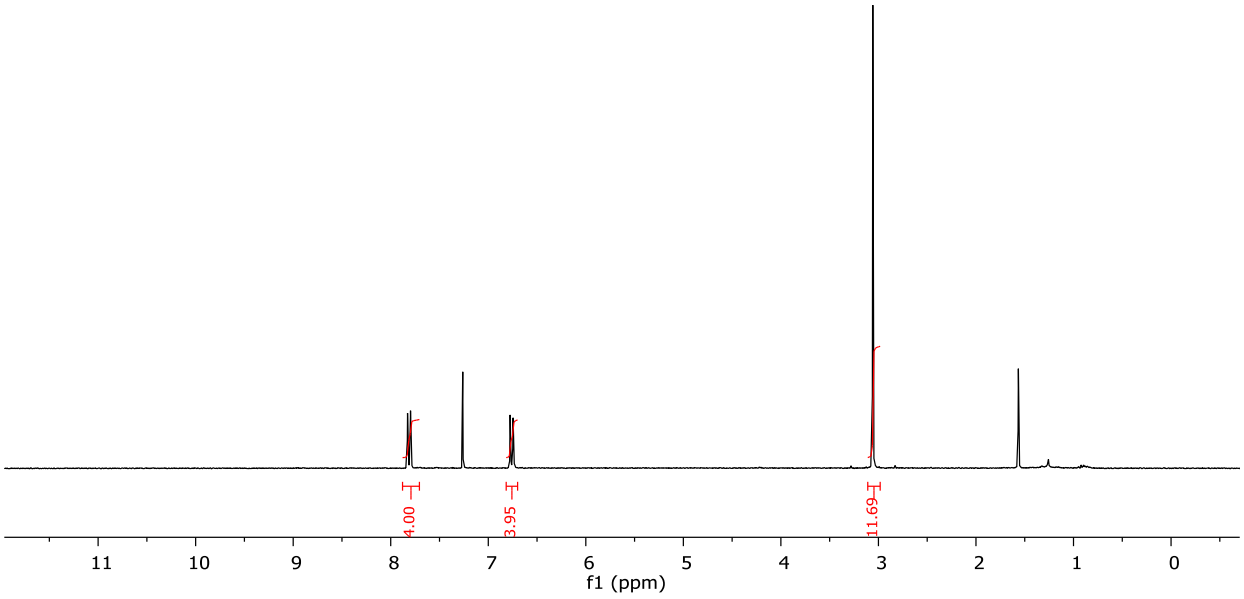

Figure S20. ^{1}H NMR spectrum for **12** in $CDCl_3$.

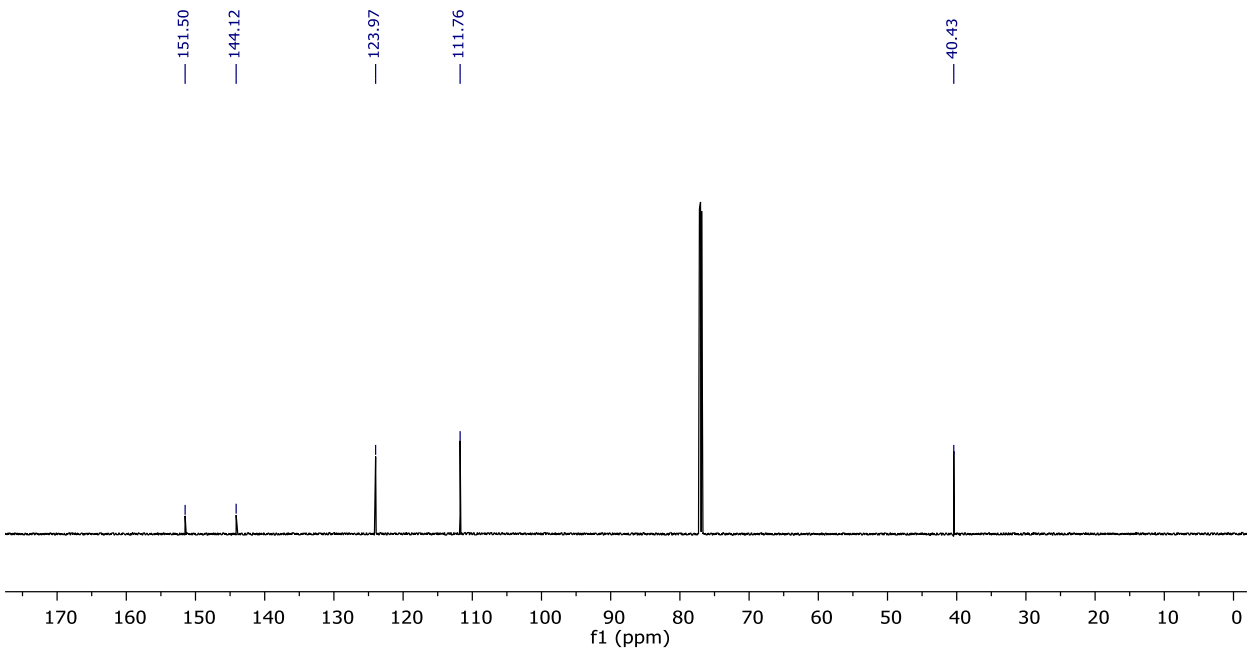

Figure S21. $^{13}C\{^{1}H\}$ NMR spectrum for **12** in $CDCl_3$.

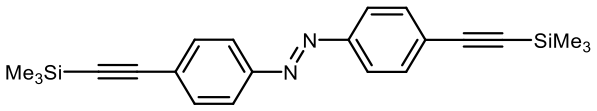

Azoarene 13.[15] The reaction was conducted according to the general procedure using 4-(trimethylsilylethynyl)phenyl azide (65 mg, 0.3 mmol, 1.0 equiv). Isolated yields were determined following column chromatography (SiO_2, 1% EtOAc/hexanes). Run 1: 46 mg, 82% yield; Run 2: 51 mg 91% yield. ^{1}H NMR (300 MHz, $CDCl_3$) δ 7.85 (d, *J* = 8.4 Hz, 4H), 7.60 (d, *J* = 8.5 Hz, 4H), 0.29 (s, 18H). $^{13}C\{^1H\}$ NMR (101 MHz, $CDCl_3$) δ 151.75, 132.71, 125.92, 122.76, 104.47, 97.22, -0.20.

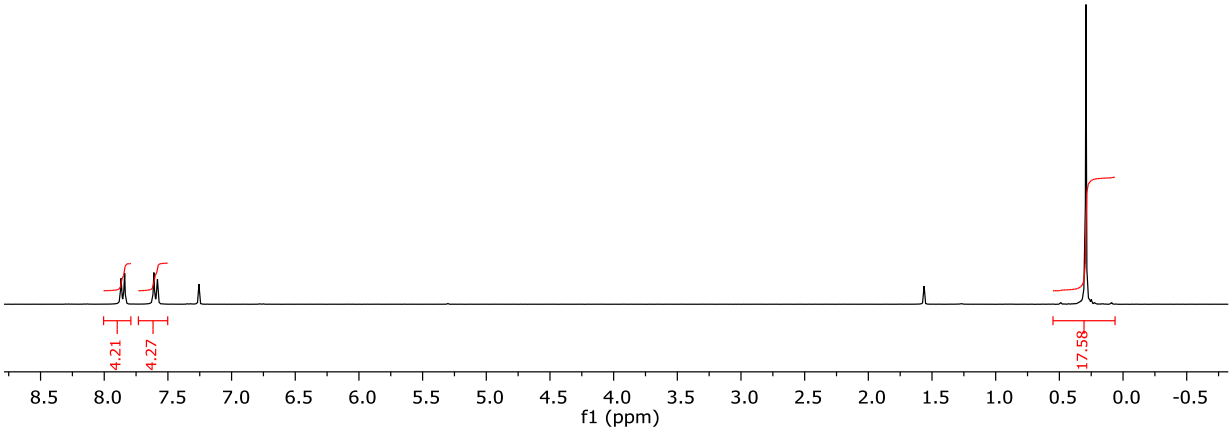

Figure S22. ^{1}H NMR spectrum for **13** in $CDCl_3$

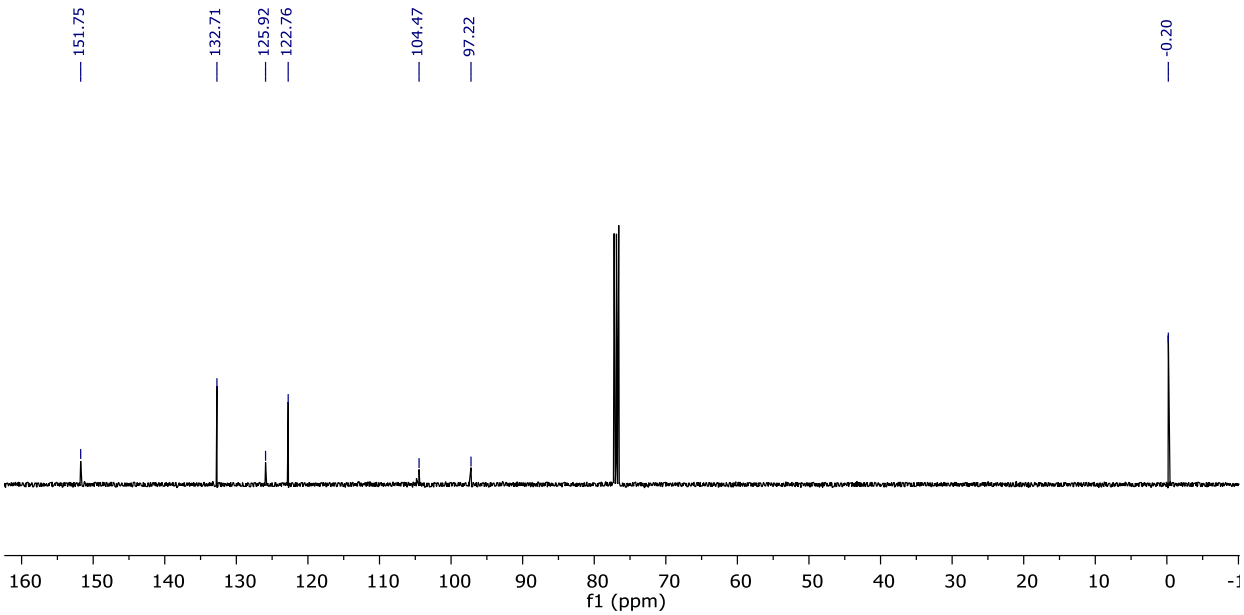

Figure S23. $^{13}C\{^{1}H\}$ NMR spectrum for **13** in $CDCl_3$.

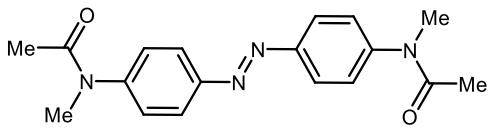

Azoarene 14. The reaction was conducted according to the general procedure using *N*-(4-azidophenyl)-*N*-methylacetamide (44.3 mg, 0.22 mmol, 1.0 equiv). The product was isolated without chromatography by the following workup procedure: after opening the vial to air and stirring, the solution was filtered through a glass fiber pad and the solvent was removed. The solid residue was then washed with 5 mL hexane and dried to yield a brown-orange solid. Run 1: 39.3 mg, >99% yield; Run 2: 41.0 mg, >99% yield. ^{1}H NMR (300 MHz, $CDCl_3$) δ 7.98 (d, *J* = 8.2 Hz, 4H), 7.36 (d, *J* = 8.7 Hz, 4H), 3.34 (s, 6H), 1.98 (s, 6H). $^{13}C\{^{1}H\}$ NMR (201 MHz, $CDCl_3$) δ 170.26, 151.23, 146.96, 127.75, 124.19, 37.14, 22.58. HRMS(ESI): calcd for $C_{26}H_{28}N_4O_4^+$: 325.1665; found: 325.1675.

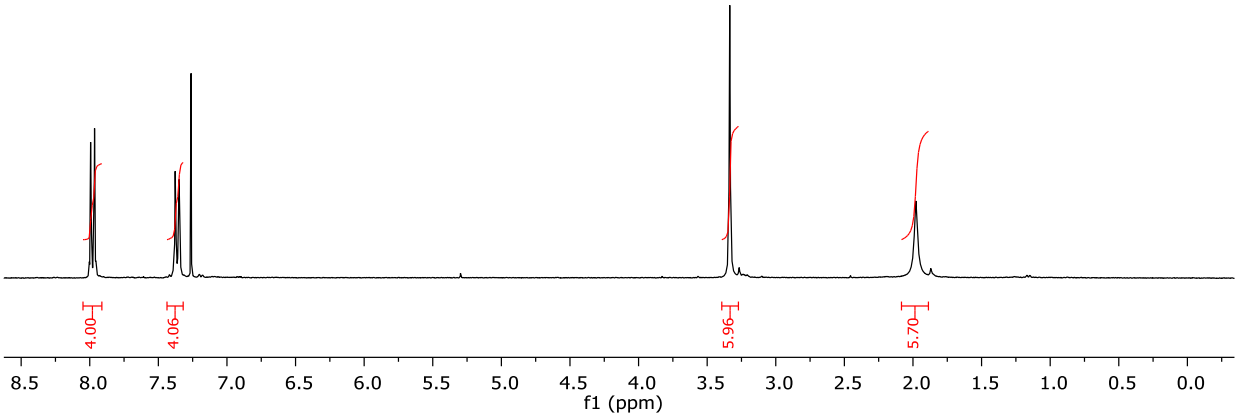

Figure S24. ^{1}H NMR spectrum for **14** in $CDCl_3$.

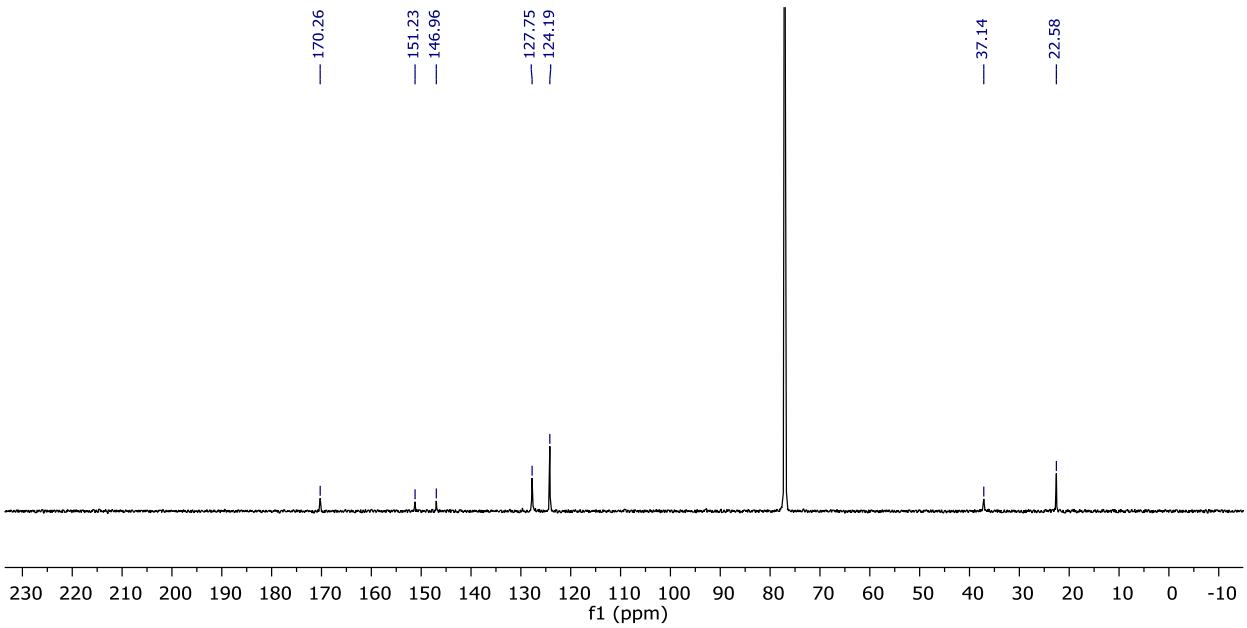

Figure S25. $^{13}C\{^{1}H\}$ NMR spectrum for **14** in $CDCl_3$.

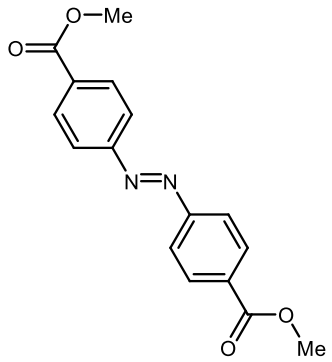

Azoarene 15.[Error! Bookmark not defined.] The reaction was conducted according to the general p rocedure using methyl 4-azidobenzoate (46.1 mg, 0.3 mmol, 1.0 equiv). The product was isolated without chromatography by the following workup procedure: after opening the vial to air and stirring, the solution was filtered through a glass fiber pad and the solvent was removed. The solid residue was then washed with 5 mL hexane and dried to yield a brown-orange solid. Run 1: 46.2 mg, >99% yield; Run 2: 45.4 mg, >99% yield. ^{1}H NMR (300 MHz, $CDCl_3$) δ 8.21 (d, *J* = 8.6 Hz, 4H), 7.99 (d, *J* = 8.3 Hz, 4H), 3.97 (s, 6H). $^{13}C\{^{1}H\}$ NMR (101 MHz, $CDCl_3$) δ 166.29, 154.81, 132.31, 130.57, 122.80, 52.30.

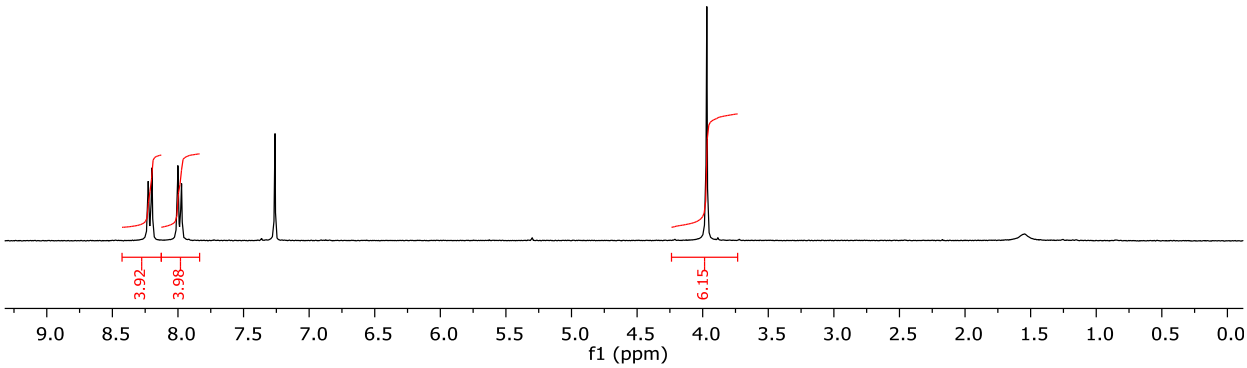

Figure S26. ^{1}H NMR spectrum for **15** in $CDCl_3$.

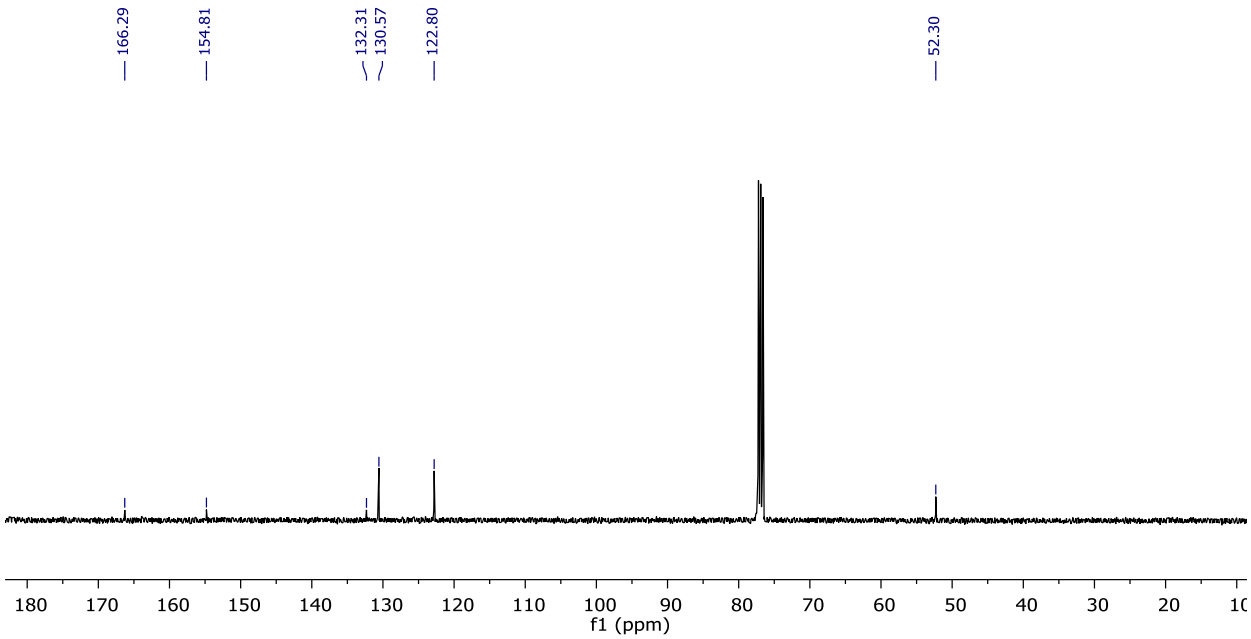

Figure S27. $^{13}C\{^{1}H\}$ NMR spectrum for **15** in $CDCl_3$.

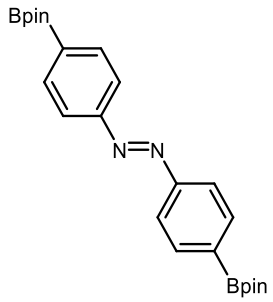

Azoarene 16.[16] The reaction was conducted according to the general procedure using 4-(pinacolboronato)phenyl azide (73.5 mg, 0.3 mmol, 1.0 equiv) and toluene as the solvent. The product was isolated without chromatography by the following workup procedure: after opening the vial to air and stirring, the solution was filtered through a glass fiber pad and the solvent was removed. The solid residue was then washed with 5 mL hexane and dried to yield a brown-orange solid. Run 1: 65.1 mg, >99% yield; Run 2: 65.0 mg, 99% yield. ^{1}H NMR (400 MHz, $CDCl_3$) δ 7.96 (d, *J* = 8.3 Hz, 4H), 7.90 (d, *J* = 8.2 Hz, 4H), 1.37 (s, 24H). $^{13}C\{^{1}H\}$ NMR (101 MHz, $CDCl_3$) δ 154.27, 135.52, 121.94, 83.97, 24.80.

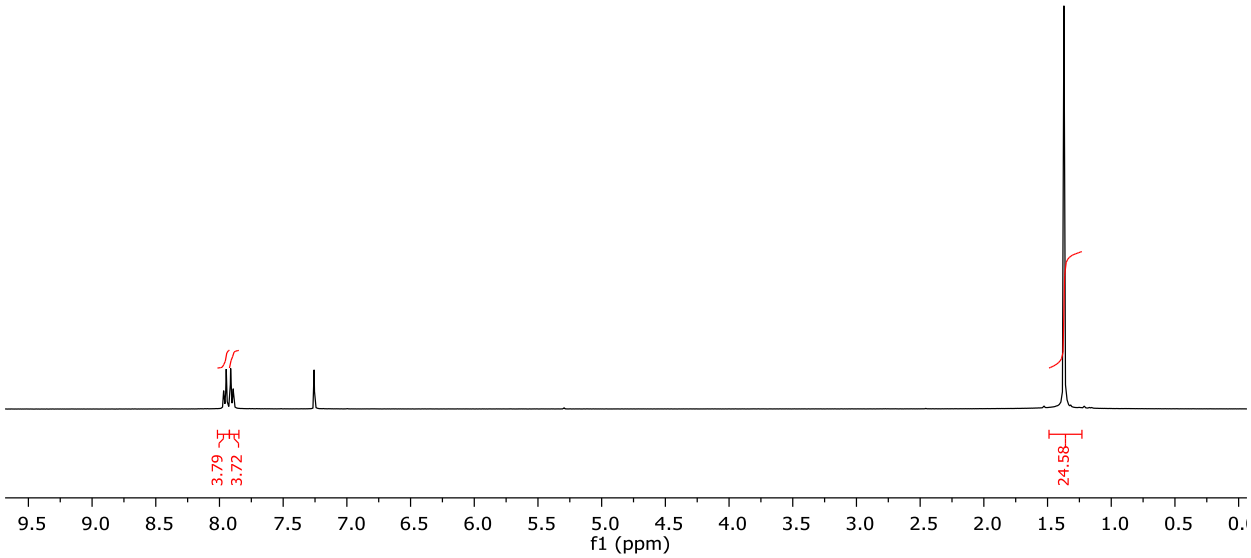

Figure S28. ^{1}H NMR spectrum for **16** in $CDCl_3$.

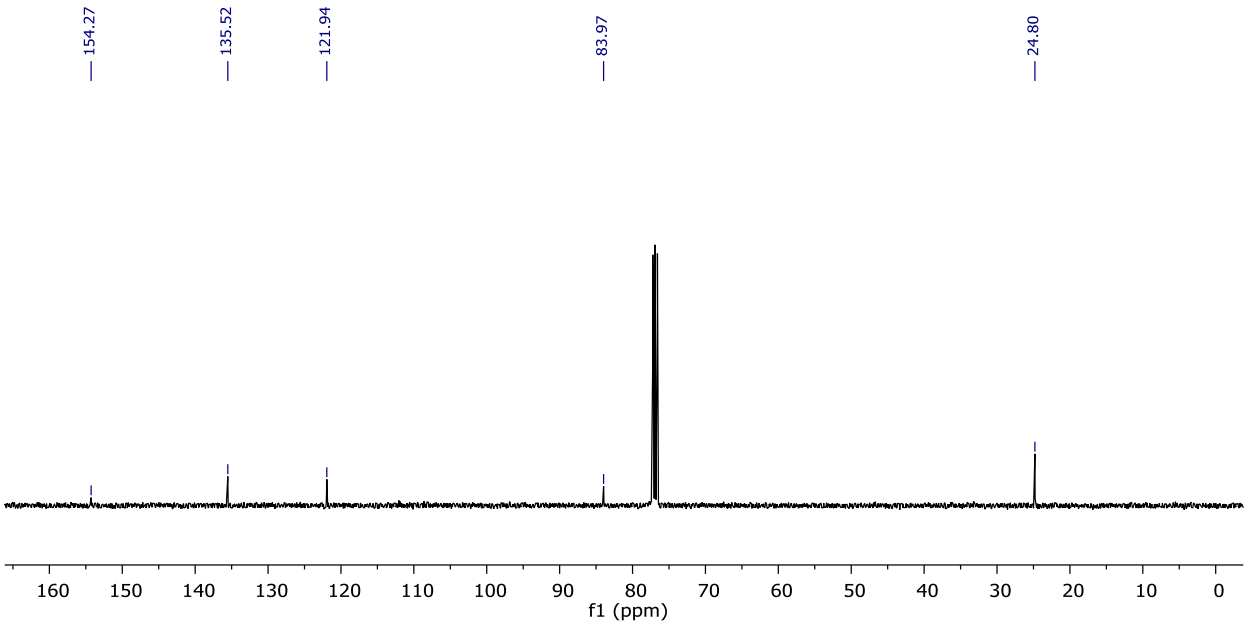

Figure S29. $^{13}C\{^{1}H\}$ NMR spectrum for **16** in $CDCl_3$.

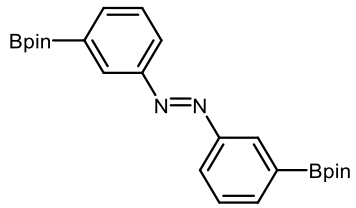

Azoarene 17.[Error! Bookmark not defined.] The reaction was conducted according to the general p rocedure using 3-(pinacolboronato)phenylazide (73.5 mg, 0.3 mmol, 1.0 equiv.) and toluene as the solvent. The product was isolated without chromatography by the following workup procedure: after opening the vial to air and stirring, the solution was filtered through a glass fiber pad and the solvent was removed. The solid residue was then washed with 5 mL hexane and dried to yield a brown-orange solid. Run 1: 53.0 mg, 81% yield; Run 2: 54.0 mg, 83% yield. ^{1}H (400 MHz, $CDCl_3$) δ 8.36 (s, 2H), 8.00 (d, *J* = 1.3 Hz, 2H), 7.90 (d, *J* = 1.3 Hz, 2H), 7.52 (t, *J* = 7.6 Hz, 2H), 1.37 (s, 24H). ^{13}C{H} NMR (101 MHz, CDCl3) δ 152.01, 137.05, 129.22, 128.42, 125.22, 83.94, 77.11, 24.81.

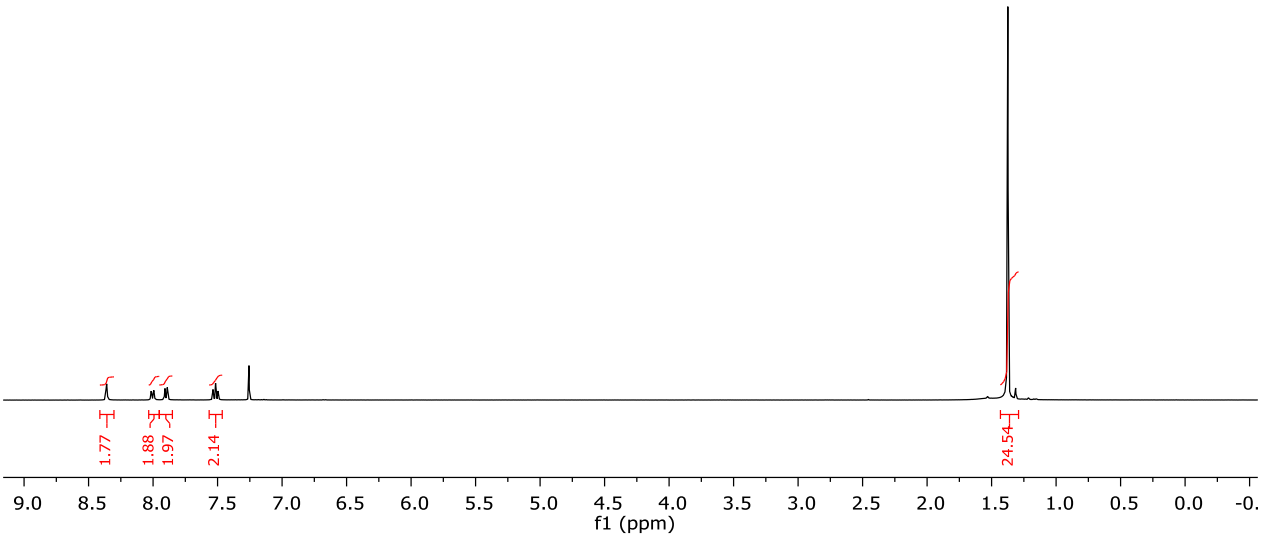

Figure S30. ^{1}H NMR spectrum for **17** in $CDCl_3$.

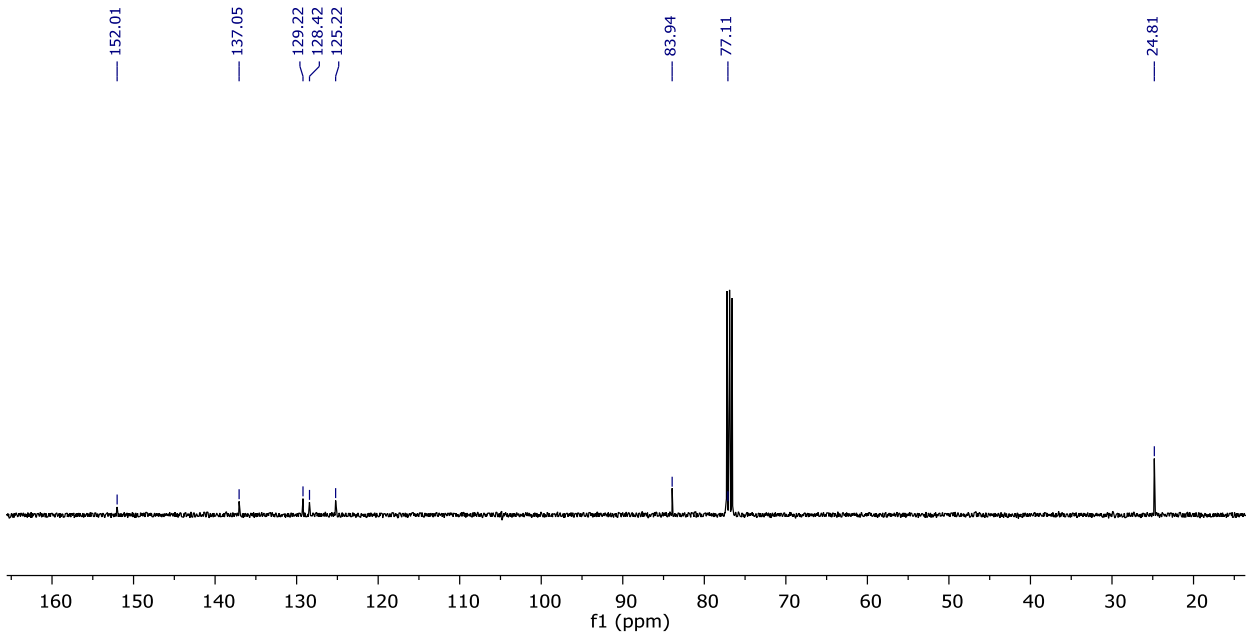

Figure S31. $^{13}C\{^{1}H\}$ NMR spectrum for **17** in $CDCl_3$.

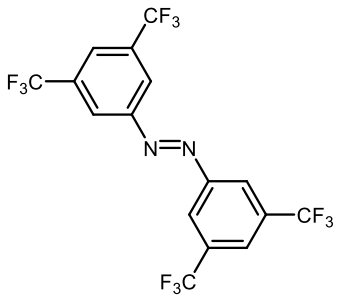

Azoarene 18.[17] The reaction was conducted according to the general procedure using 3,5-bis-trifluoromethylphenyl azide (68.1 mg, 0.27 mmol, 1.0 equiv). Isolated yields were determined following column chromatography (SiO_2, hexanes). The product was isolated as an orange solid. Run 1: 55 mg, 90% yield; Run 2: 58 mg, 97% yield. ^{1}H NMR (300 MHz, $CDCl_3$) δ 8.45 (d, *J* = 1.6 Hz, 4H), 8.06 (s, 2H). ^{19}F NMR (282 MHz, $CDCl_3$) δ -64.50. ^{13}C{^{1}H} NMR (201 MHz, $CDCl_3$) δ 152.12 , 133.13 (q, *J* = 34.2 Hz), 125.20 (hept, *J* = 4.1 Hz), 123.53 – 123.27 (m), 122.86 (q, *J* = 273.0 Hz).

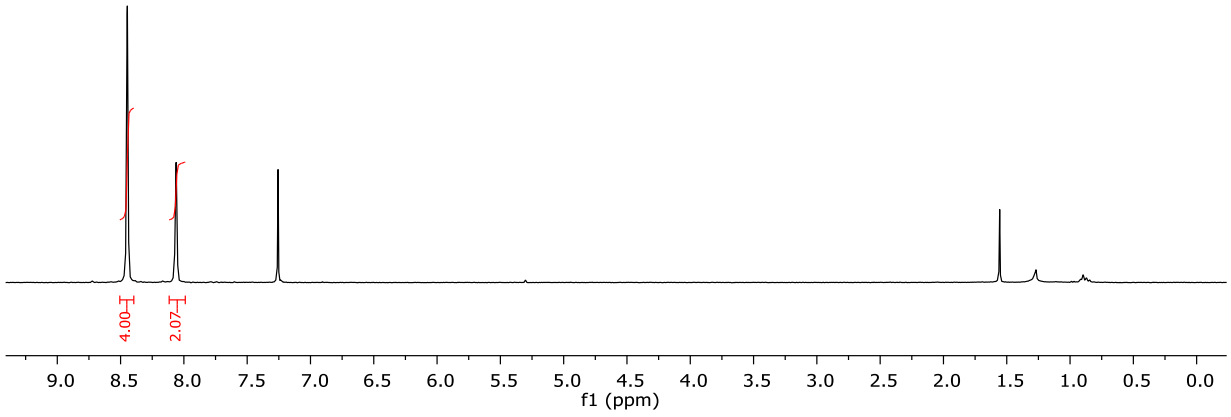

Figure S32. ^{1}H NMR spectrum for **18** in $CDCl_3$.

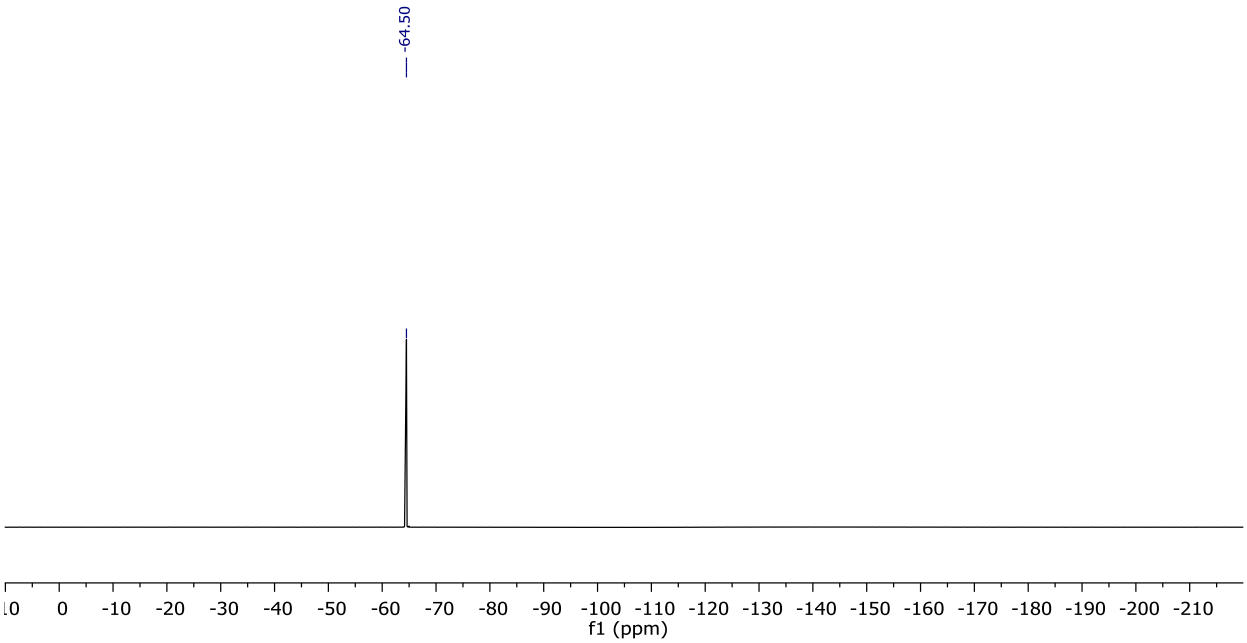

Figure S33. ^{19}F NMR spectrum for **18** in $CDCl_3$.

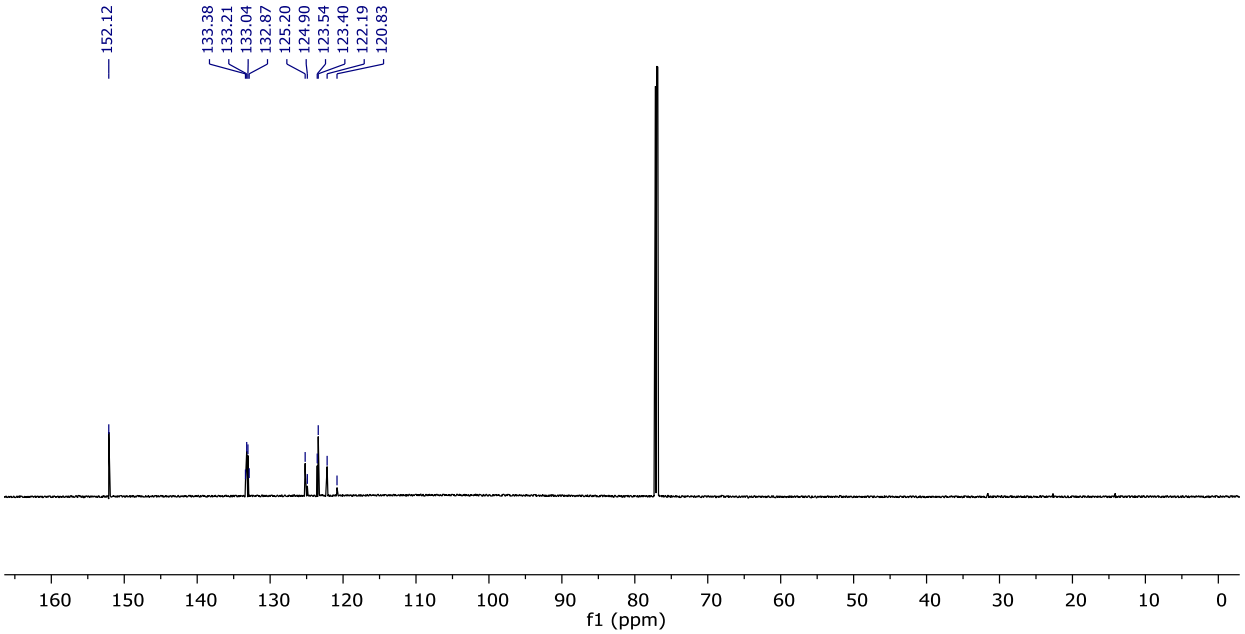

Figure S34. $^{13}C\{^{1}H\}$ NMR spectrum for **18** in $CDCl_3$.

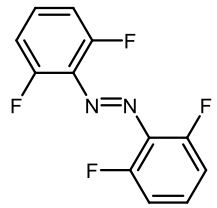

Azoarene 19.[18] The reaction was conducted according to the following modified general procedure using 2,6-difluorophenyl azide (46.5 mg, 0.3 mmol, 1.0 equiv): the reagents were mixed in a microwave vial, which was then sealed and heated to 80 °C for 2 h. Isolated yields were determined following column chromatography (SiO_2, 1% EtOAc/hexanes). The product was isolated as an orange solid in a 15:85 mixture of *Z* and *E* isomers. Run 1: 32.1 mg, 84% yield; Run 2: 34.2 mg, 90% yield. ^{1}H NMR (300 MHz, $CDCl_3$) *E* isomer: δ 7.47 – 7.31 (m, 2H), 7.12 – 7.00 (m, 4H); *Z* isomer: δ 7.24 – 7.14 (m, 2H), 6.95 – 6.75 (m, 4H). ^{19}F NMR (282 MHz, $CDCl_3$) *E* isomer: δ -122.81; Z isomer: δ -121.03. ^{13}C{^{1}H} NMR (101 MHz, $CDCl_3$) *E* isomer: δ 155.49 (d, *J* = 260.8 Hz), 131.70 (t, *J* = 9.3 Hz), 131.37 (t, *J* = 9.7 Hz), 112.54 (d, *J* = 24.1 Hz).

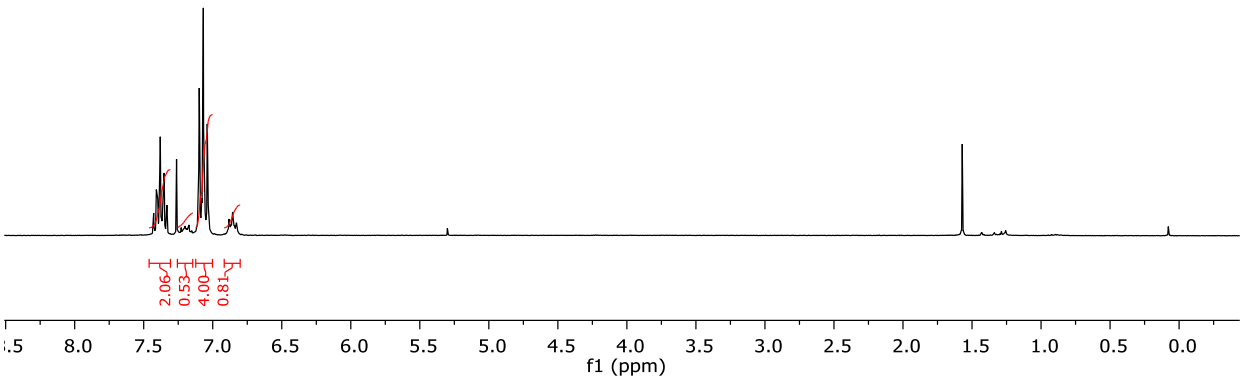

Figure S35. ^{1}H NMR spectrum for **19** in $CDCl_3$.

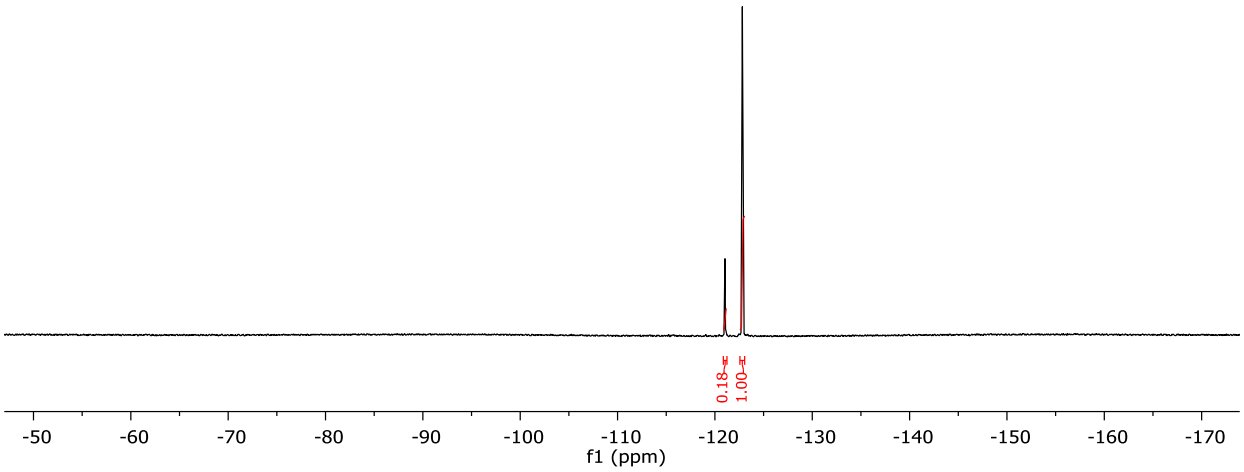

Figure S36. ^{19}F NMR spectrum for **19** in $CDCl_3$.

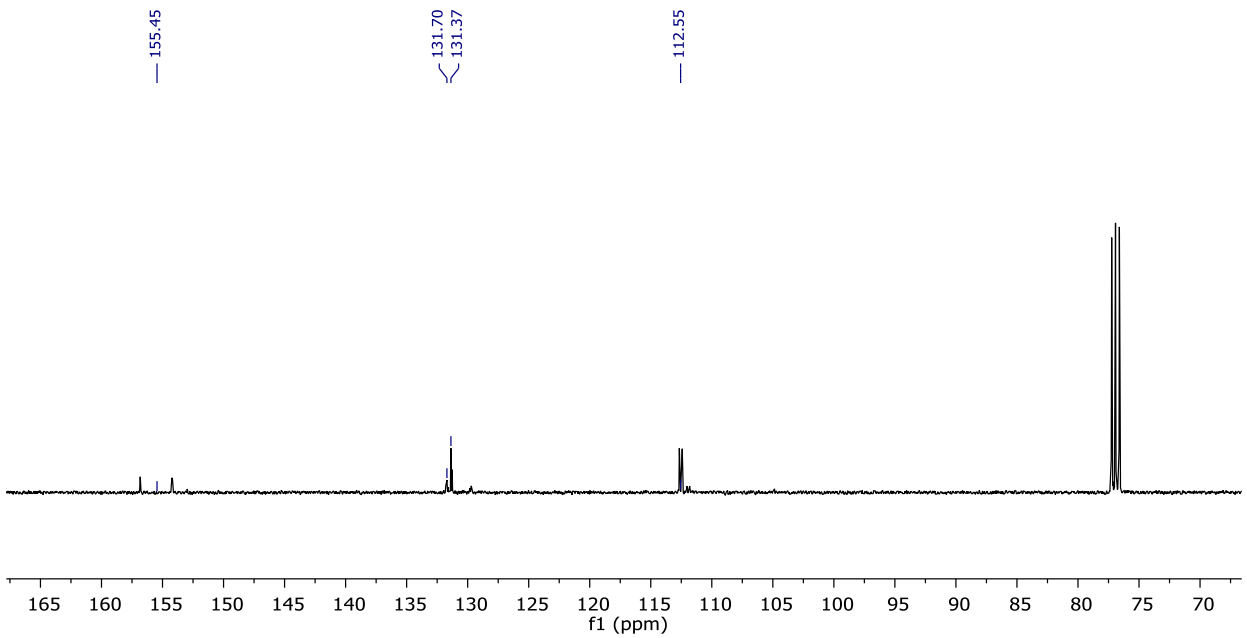

Figure S37. $^{13}C\{^{1}H\}$ NMR spectrum for **19** in $CDCl_3$.

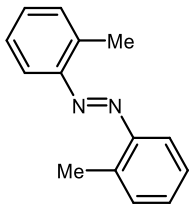

Azoarene 20.[Error! Bookmark not defined.] The reaction was conducted according to the following m odified general procedure using 2-tolyl azide (39.9 mg, 0.3 mmol, 1.0 equiv): the reagents were mixed in a microwave vial, which was then sealed and heated to 100 °C for 4 h. Isolated yields were determined following column chromatography (hexanes). The product was isolated as an orange oil. Run 1: 26.1 mg, 83% yield; Run 2: 24.3 mg, 77% yield. ^{1}H NMR (300 MHz, $CDCl_3$) δ 7.63 (d, *J* = 7.9 Hz, 2H), 7.44 – 7.32 (m, 4H), 7.31 – 7.22 (m, 2H), 2.76 (s, 6H). $^{13}C\{^{1}H\}$ NMR (101 MHz, $CDCl_3$) δ 151.01, 137.91, 131.17, 130.59, 126.27, 115.76, 17.54.

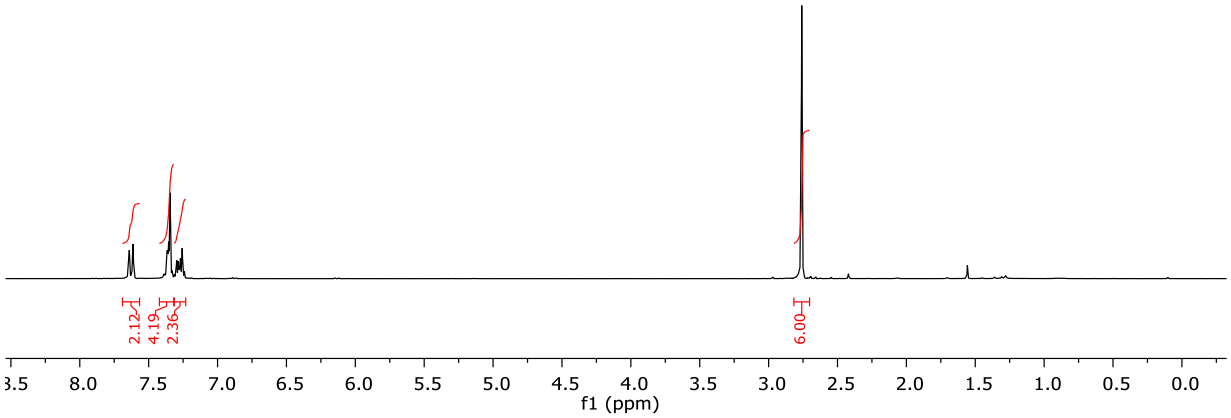

Figure S38. ^{1}H NMR spectrum for **20** in $CDCl_3$.

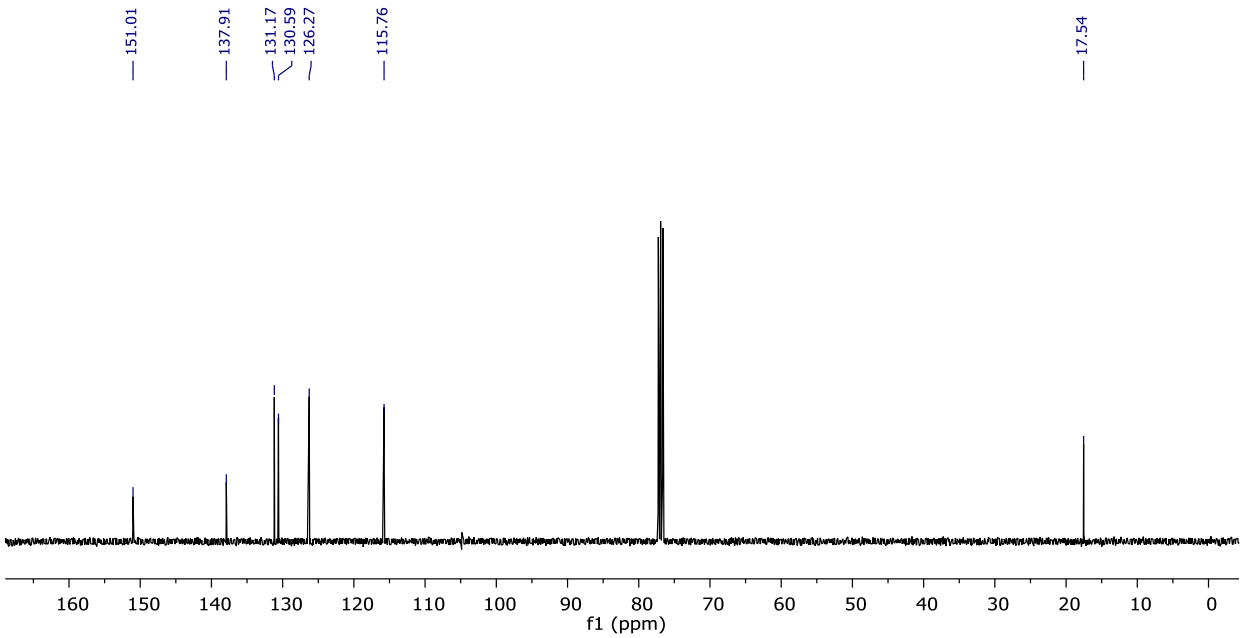

Figure S39. $^{13}C\{^{1}H\}$ NMR spectrum for **20** in $CDCl_3$.

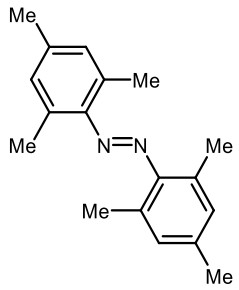

Azoarene 21.[19] The reaction was conducted according to the following modified general procedure using 2,4,6-trimethylphenyl azide (48.4 mg, 0.3 mmol, 1.0 equiv): the reagents were mixed in a microwave vial, which was then sealed and heated to 100 °C for 4 h. Isolated yields were determined following column chromatography (hexanes). The product was isolated as an orange solid. Run 1: 33 mg, 83% yield; Run 2: 37 mg, 93% yield. ^{1}H NMR (300 MHz, $CDCl_3$) δ 6.97 (s, 4H), 2.43 (s, 12H), 2.35 (s, 6H). $^{13}C\{^{1}H\}$ NMR (101 MHz, $CDCl_3$) δ 149.03, 138.23, 131.54, 129.97, 20.94, 19.92.

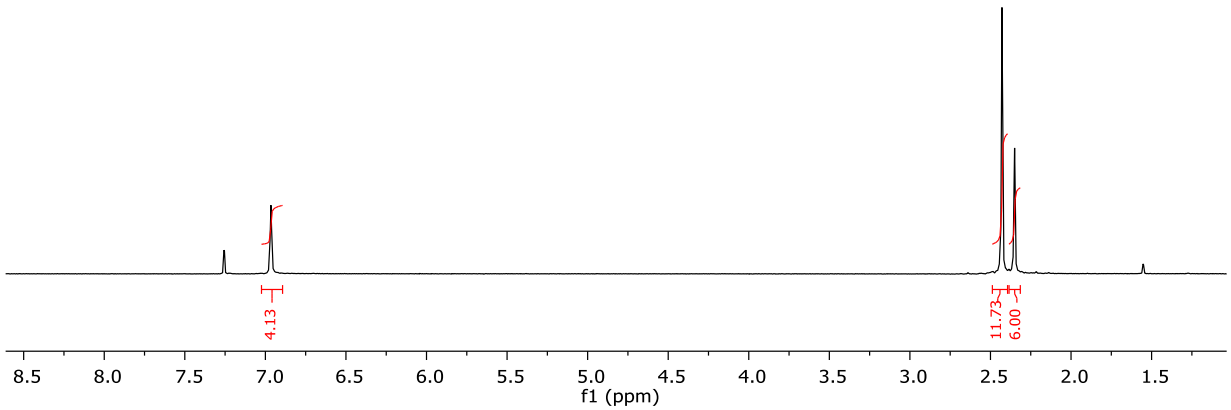

Figure S40. ^{1}H NMR spectrum for **21** in $CDCl_3$.

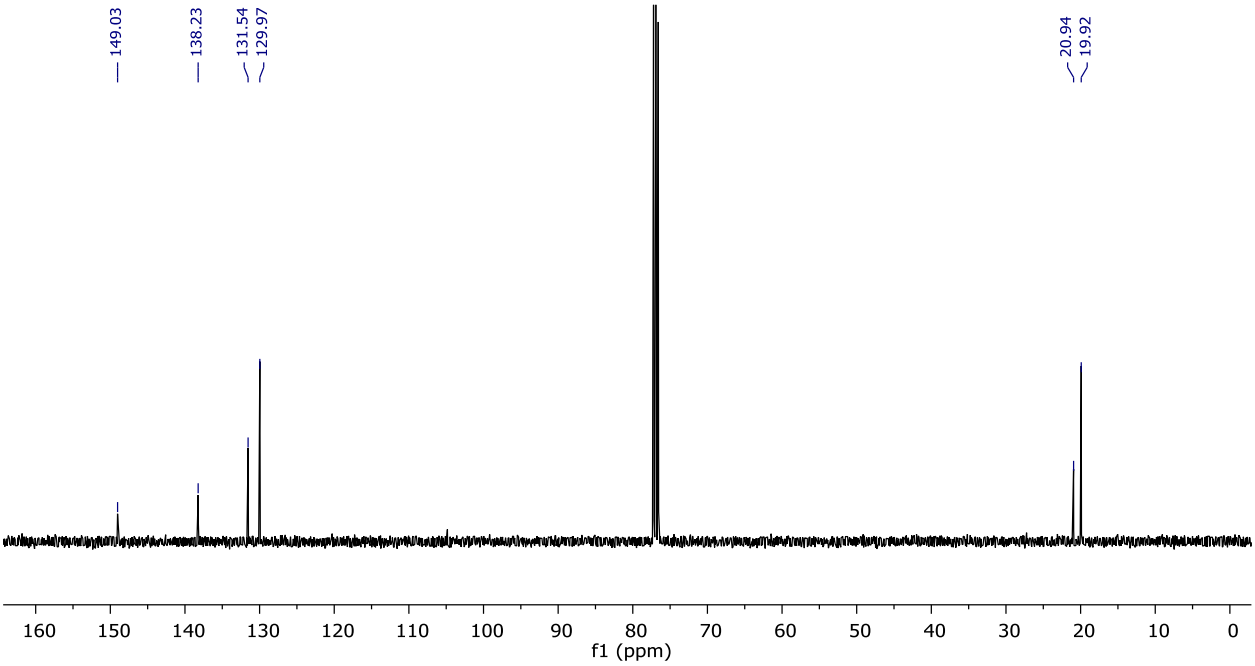

Figure S41. $^{13}C\{^{1}H\}$ NMR spectrum for **21** in $CDCl_3$.

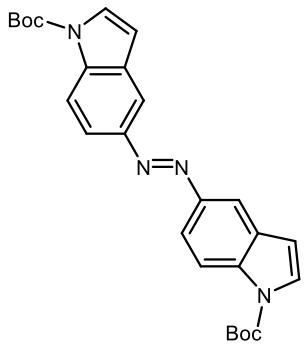

Azoarene 22. The reaction was conducted according to a modified general procedure using *tert*-butyl 5-azido-1*H*-indole-1-carboxylate (77.5 mg, 0.3 mmol, 1.0 equiv) and 5 mol% **1** (11.0 mg, 0.015 mmol). Isolated yields were determined following column chromatography (SiO_2, 0 – 3% EtOAc/Hexanes). The product was isolated as a yellow solid. Run 1: 30.9 mg, 45% yield; Run 2: 31.3 mg, 48% yield. ^{1}H NMR (300 MHz, $CDCl_3$) δ 8.26 (d, *J* = 8.9 Hz, 2H), 8.17 (d, *J* = 1.9 Hz, 2H), 7.98 (dd, *J* = 8.9, 2.0 Hz, 2H), 7.66 (d, *J* = 3.7 Hz, 2H), 6.70 (dd, *J* = 3.7, 0.7 Hz, 2H), 1.70 (s, 18H). ^{13}C{^{1}H} NMR (101 MHz, $CDCl_3$) δ 149.42, 148.71, 136.45, 130.92, 127.07, 118.74, 116.34, 115.35, 108.07, 84.04, 28.10. HRMS(ESI): calcd for $C_{26}H_{28}N_4O_4^+$: 461.2183; found: 461.2181.

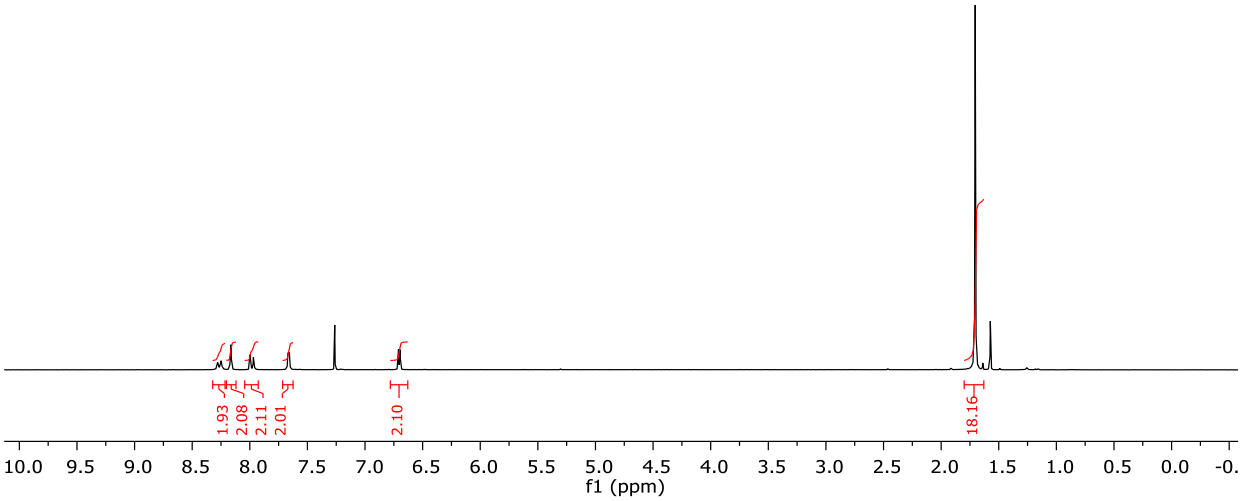

Figure S42. ^{1}H NMR spectrum for **22** in $CDCl_3$.

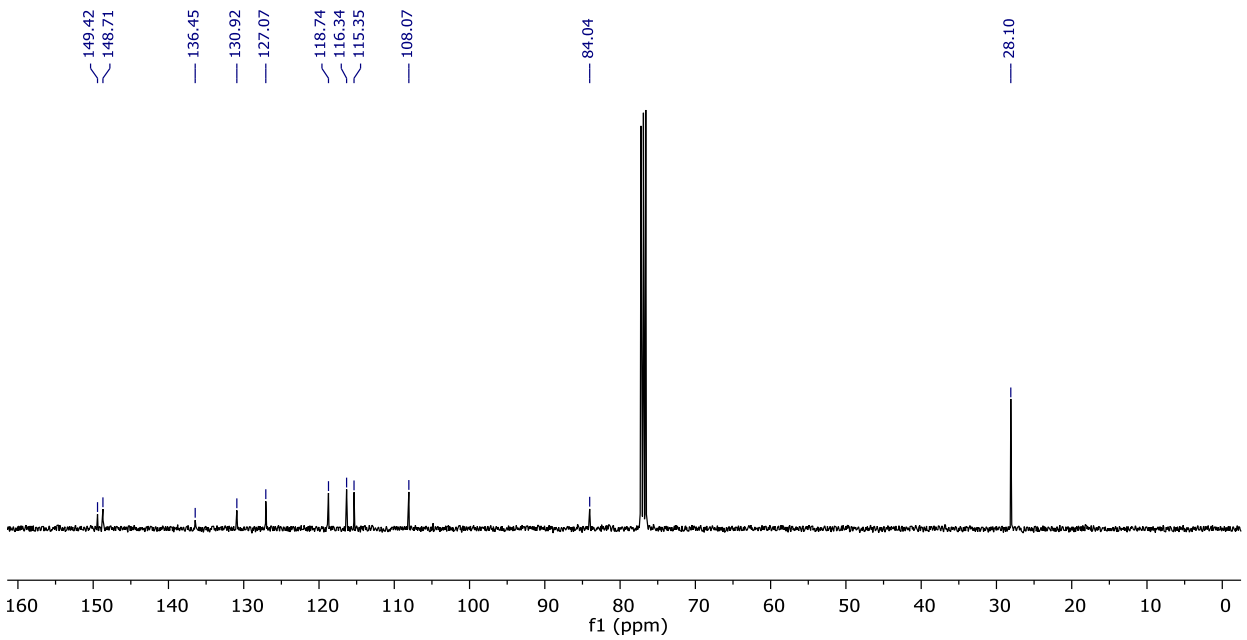

Figure S43. $^{13}C\{^{1}H\}$ NMR spectrum for **22** in $CDCl_3$.

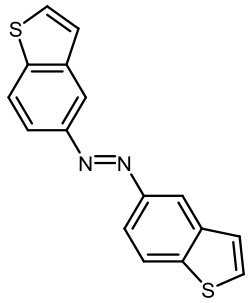

Azoarene 23.[20] The reaction was conducted according to a modified general procedure using 5-azidobenzo[*b*]thiophene (52.6 mg, 0.3 mmol, 1.0 equiv) and 5 mol% **1** (11.0 mg, 0.015 mmol), with an additional 5 mol% **1** added after one hour. Isolated yields were determined following column chromatography (SiO_2, 0 – 3% EtOAc/Hexanes). The product was isolated as a yellow solid. Run 1: 30 mg, 68% yield; Run 2: 34 mg, 77% yield. ^{1}H NMR (300 MHz, $CDCl_3$) δ 8.43 (dd, *J* = 1.7, 0.8 Hz, 2H), 8.06 – 7.93 (m, 4H), 7.55 (dd, *J* = 5.5, 0.4 Hz, 2H), 7.50 (dd, *J* = 5.5, 0.6 Hz, 2H). ^{13}C{^{1}H} NMR (201 MHz, $CDCl_3$) δ 150.16, 142.09, 140.12, 127.85, 124.80, 122.89, 120.29, 117.35.

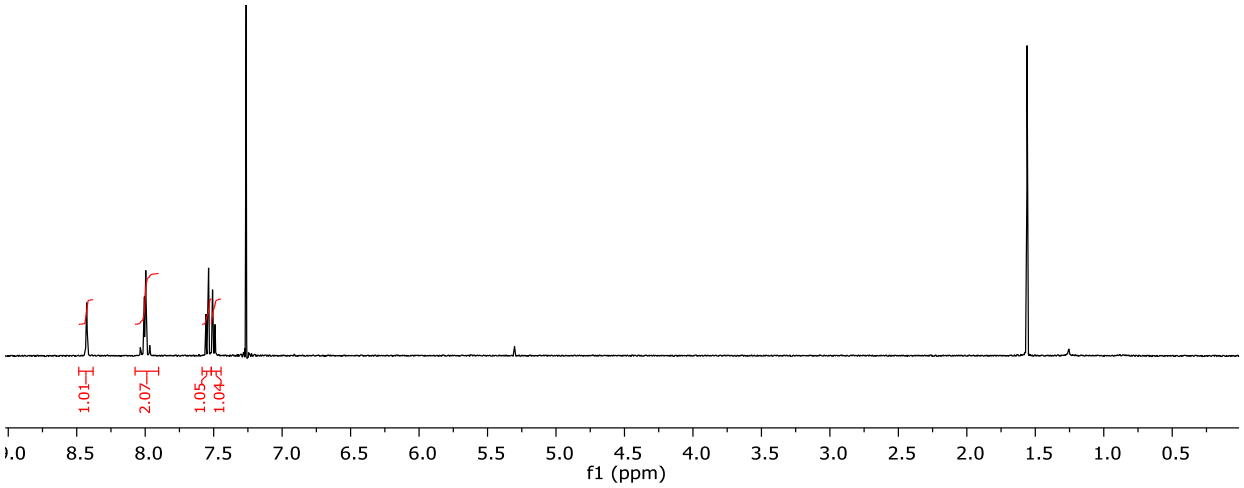

Figure S44. ^{1}H NMR spectrum for **23** in $CDCl_3$.

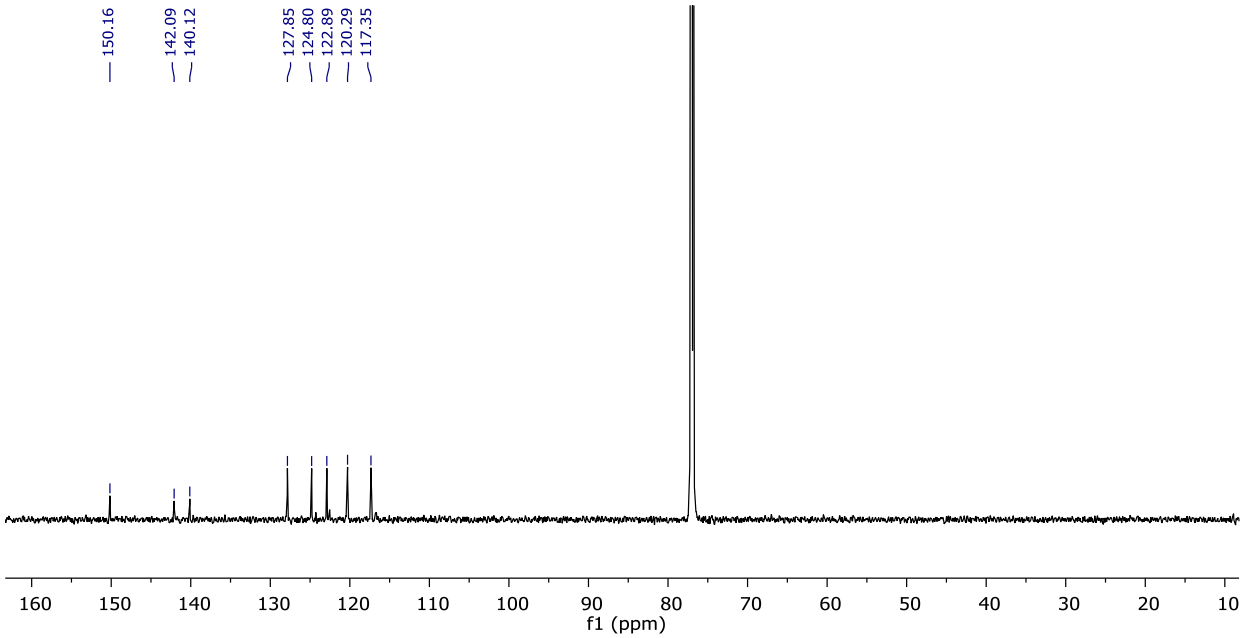

Figure S45. $^{13}C\{^{1}H\}$ NMR spectrum for **23** in $CDCl_3$.

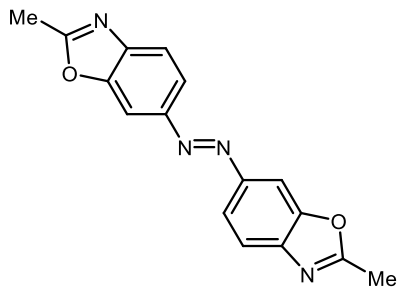

Azoarene 24. The reaction was conducted according to a modified general procedure using 5-azido-2-methylbenzo[*d*]oxazole (52.2 mg, 0.3 mmol, 1.0 equiv) and 5 mol% **1** (11.0 mg, 0.015 mmol). Isolated yields were determined following column chromatography (SiO_2, 0 – 1% CH_2Cl_2/MeOH). The product was isolated as a yellow solid. Run 1: 35.4 mg, 81% yield; Run 2: 33.8 mg, 77% yield. ^{1}H NMR (300 MHz, $CDCl_3$) δ 8.23 (d, *J* = 1.9 Hz, 2H), 7.99 (dd, *J* = 8.7, 1.9 Hz, 2H), 7.58 (dd, *J* = 8.6, 0.5 Hz, 2H), 2.68 (s, 6H). ^{13}C{^{1}H} NMR (101 MHz, $CDCl_3$) δ 165.24, 152.55, 149.80, 142.18, 120.09, 114.14, 110.24, 14.57. HRMS(ESI): calcd for $C_{16}H_{12}N_4O_2^+$: 293.1033; found: 293.1034.

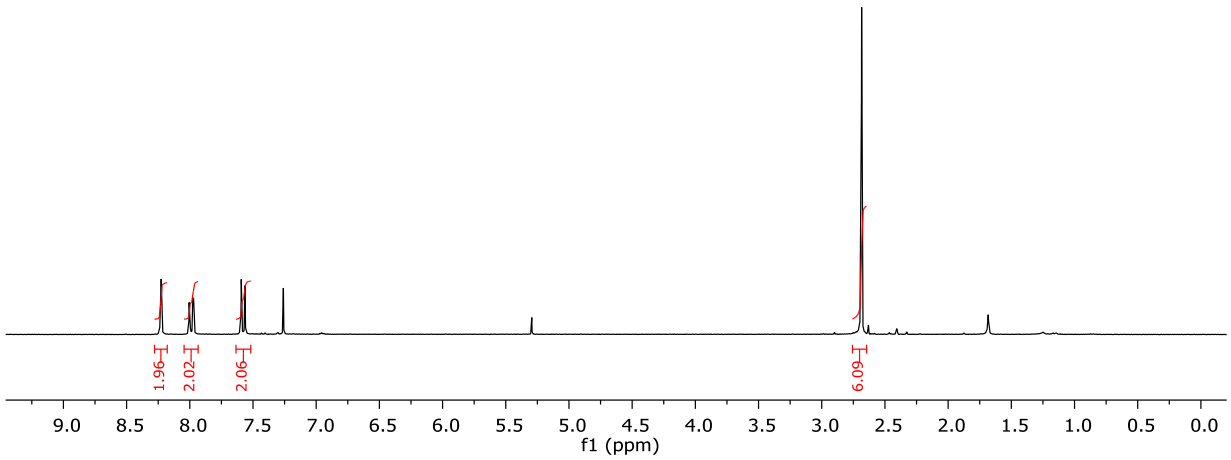

Figure S46. ^{1}H NMR spectrum for **24** in $CDCl_3$.

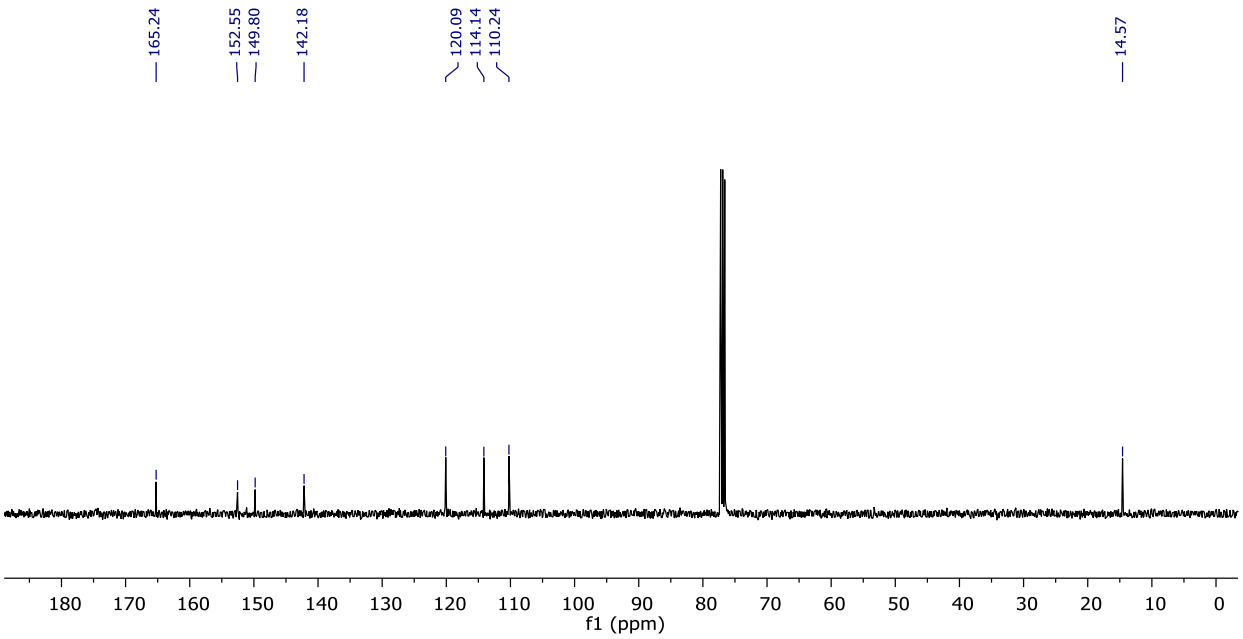

Figure S47. $^{13}C\{^{1}H\}$ NMR spectrum for **24** in $CDCl_3$.

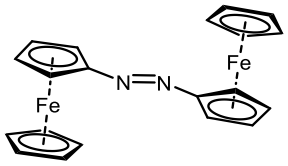

Azoarene 25.[21] The reaction was conducted according to a modified general procedure using 1-azidoferrocene (68.1 mg, 0.3 mmol, 1.0 equiv) and 5 mol% **1** (11.0 mg, 0.015 mmol). The product was isolated without chromatography by the following workup procedure: After opening the vial to air and stirring, the solution was filtered through a glass fiber pad, and residual solid product was washed through the filter with chloroform. The solvent was then removed, and the solid residue was washed with 2 x 5 mL hexane and dried to yield a purple solid. Run 1: 59.8 mg, >99% yield; Run 2: 59.7 mg, >99% yield. ^{1}H NMR (300 MHz, $CDCl_3$) δ 4.94 (t, *J* = 2.0 Hz, 2H), 4.49 (t, *J* = 2.0 Hz, 2H), 4.25 (s, 5H). $^{13}C\{^{1}H\}$ NMR (101 MHz, $CDCl_3$) δ 107.93, 69.64, 69.44, 64.01.

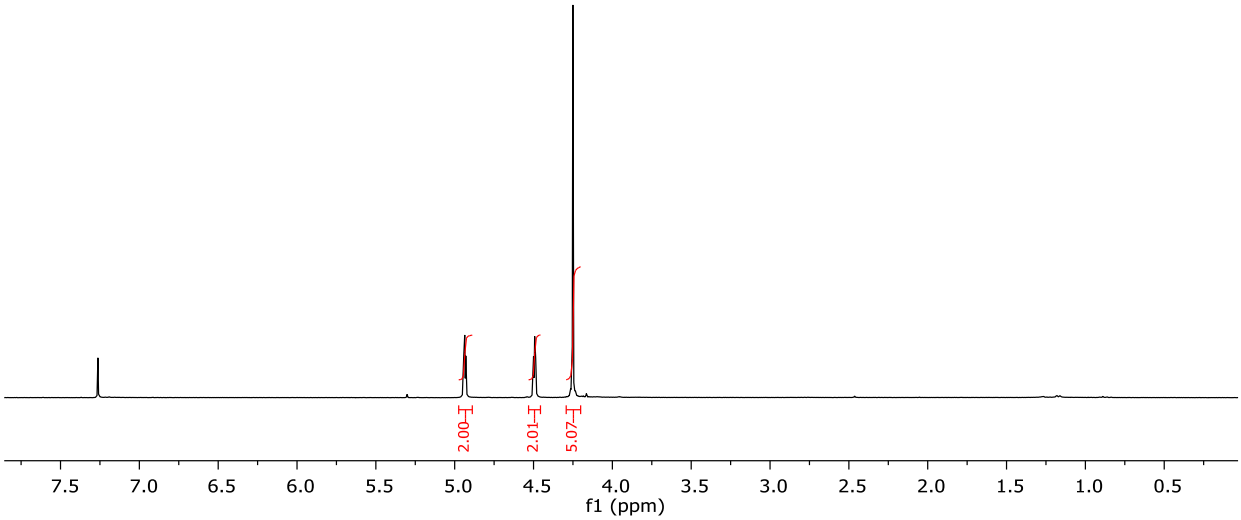

Figure S48. ^{1}H NMR spectrum for **25** in $CDCl_3$.

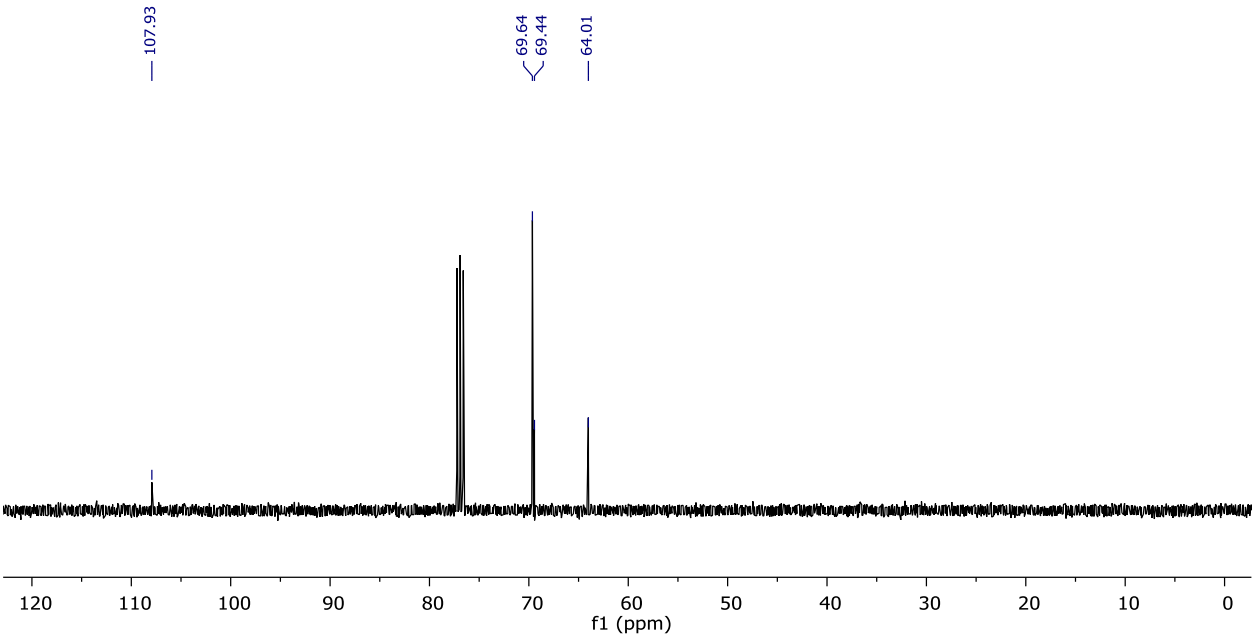

Figure S49. $^{13}C\{^{1}H\}$ NMR spectrum for **25** in $CDCl_3$.

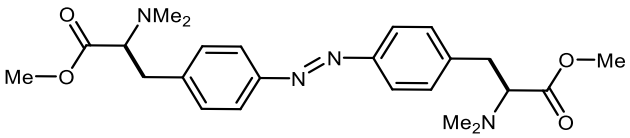

Azoarene 26. The reaction was conducted according to a modified general procedure using **S1** (57.1 mg, 0.3 mmol, 1.0 equiv) and 5 mol% **1** (11.0 mg, 0.015 mmol). The product was isolated without chromatography by the following workup procedure: After opening the vial to air and stirring, the solution was filtered through a glass fiber pad, and residual solid product was washed through the filter with chloroform. The solvent was then removed, and the solid residue was washed with 2 x 5 mL hexane and dried to yield a dark brown solid. Run 1: 31 mg, 67% yield; Run 2: 33 mg, 69% yield. ^{1}H NMR (300 MHz, $CDCl_3$) δ 7.81 (d, *J* = 8.0 Hz, 4H), 7.34 (d, *J* = 8.1 Hz, 4H), 3.62 (s, 6H), 3.46 – 3.39 (m, 2H), 3.22 – 2.90 (m, 4H), 2.40 (s, 12H). ^{13}C{^{1}H} NMR (201 MHz, $CDCl_3$) δ 171.68, 151.38, 141.49, 129.80, 122.83, 69.35, 51.15, 41.87, 35.56. HRMS(ESI): calcd for $C_{24}H_{33}N_4O_4^+$: 441.2496; found: 441.2494.

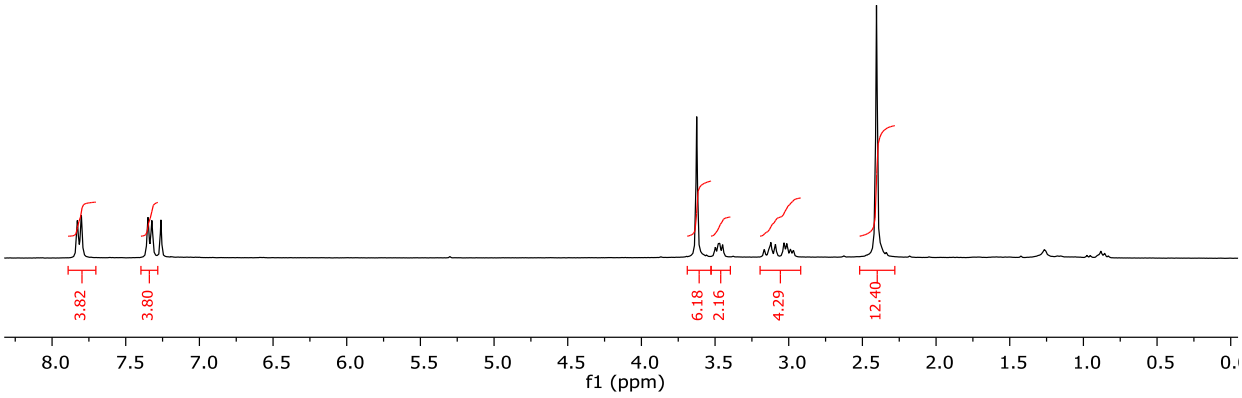

Figure S50. ^{1}H NMR spectrum for **26** in $CDCl_3$.

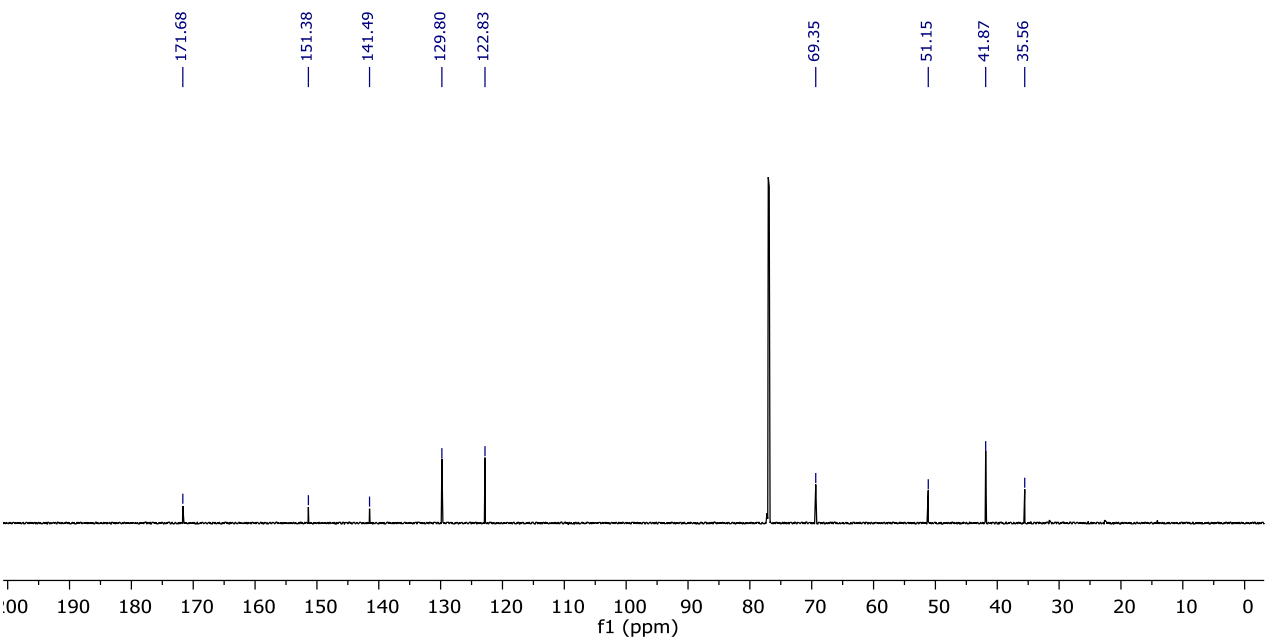

Figure S51. $^{13}C\{^{1}H\}$ NMR spectrum for **26** in $CDCl_3$.

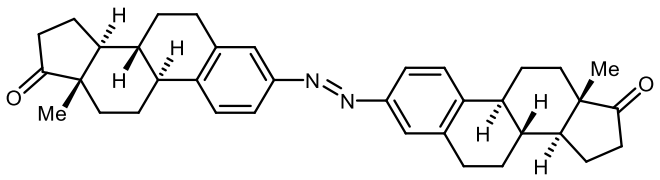

Azoarene 27. The reaction was conducted according to a modified general procedure using **S2** (88.6 mg, 0.30 mmol, 1.0 equiv) and 5 mol% **1** (11.0 mg, 0.015 mmol). The product was isolated without chromatography by the following workup procedure: after opening the vial to air and stirring, the solution was filtered through a glass fiber pad, and residual solid product was washed through the filter with dichloromethane. The solvent was then removed, and the solid residue was washed with 2 x 5 mL hexane and dried to yield a yellow solid. Run 1: 84 mg, >99% yield; Run 2: 83 mg, >99% yield. ^{1}H NMR (800 MHz, $CDCl_3$) δ 7.70 (d, *J* = 8.3 Hz, 2H), 7.65 (s, 2H), 7.44 (d, *J* = 8.4 Hz, 2H), 3.13 – 2.92 (m, 4H), 2.61 – 2.46 (m, 4H), 2.38 (td, *J* = 11.3, 4.2 Hz, 2H), 2.22 – 2.12 (m, 2H), 2.12 – 2.04 (m, 4H), 2.01 (dt, *J* = 13.4 Hz, 2H), 1.74 – 1.59 (m, 6H), 1.57 – 1.44 (m, 6H), 0.94 (s, 6H). ^{13}C{^{1}H} NMR (201 MHz, $CDCl_3$) δ 220.42, 150.92, 142.96, 137.43, 126.02, 122.87, 120.36, 50.63, 47.93, 44.74, 38.08, 35.82, 31.65, 29.44, 26.42, 25.77, 21.63, 13.86. HRMS(ESI): calcd for $C_{36}H_{42}N_2O_2^{+\cdot}$ 535.3319; found: 535.3323.

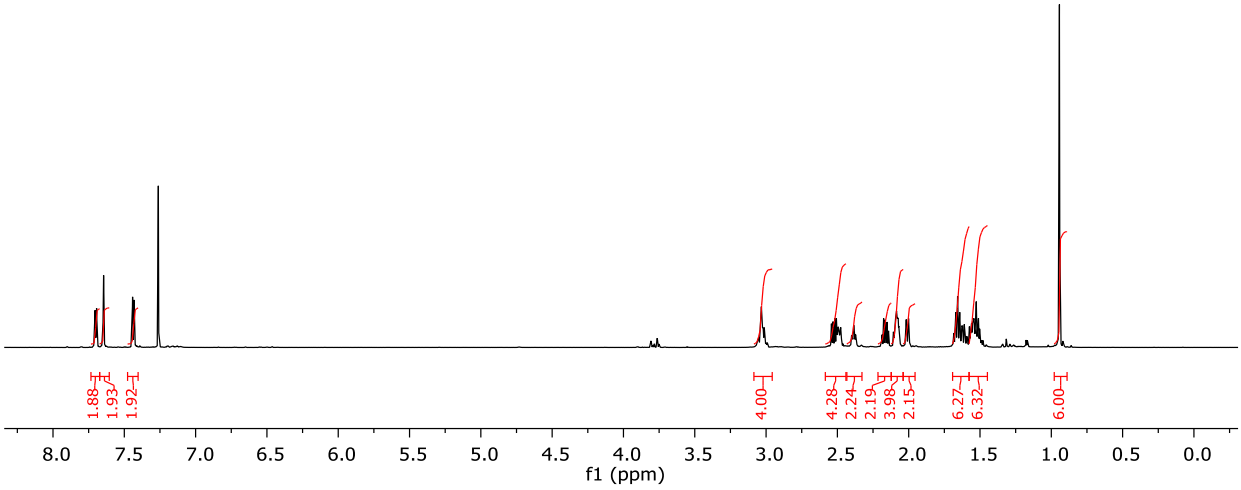

Figure S52. ^{1}H NMR spectrum for **27** in $CDCl_3$.

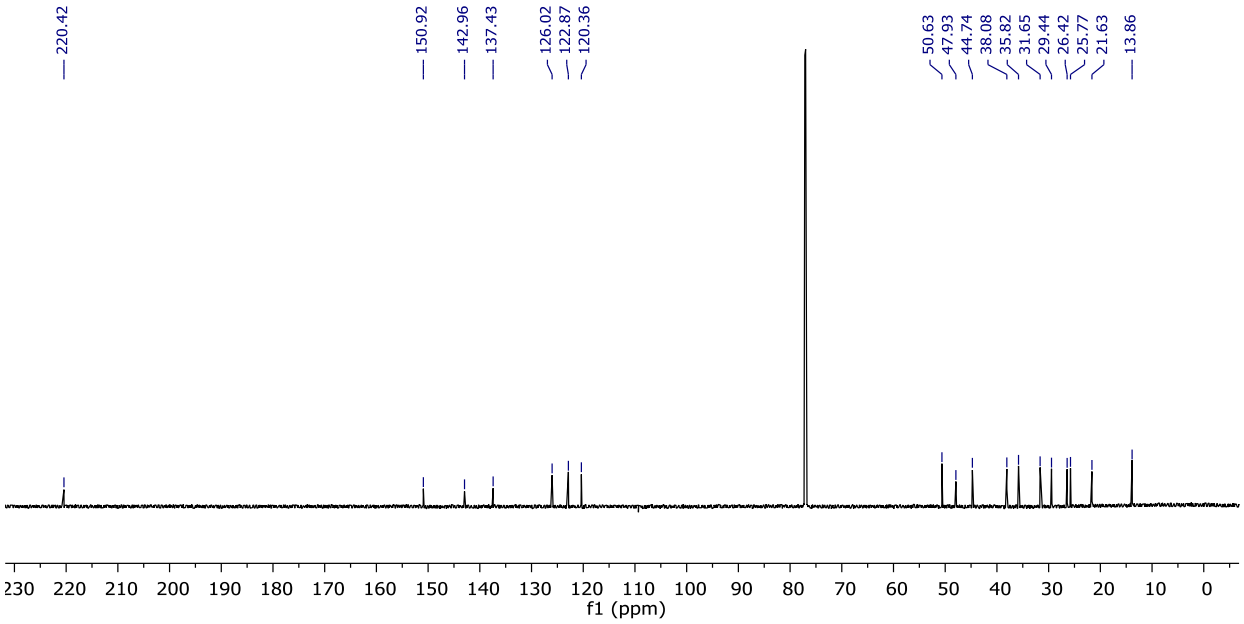

Figure S53. $^{13}C\{^{1}H\}$ NMR spectrum for **27** in $CDCl_3$.

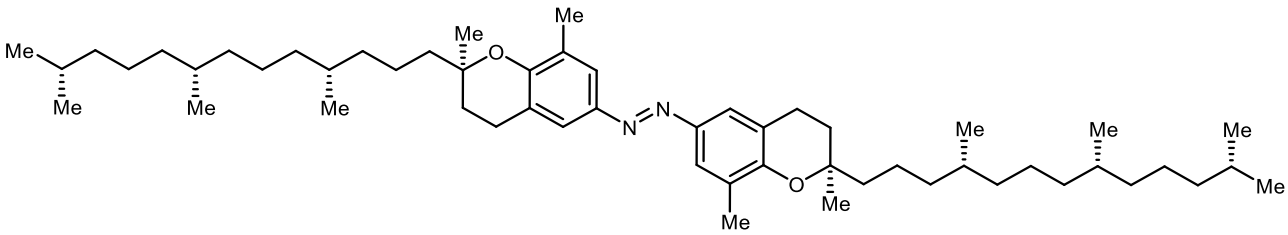

Azoarene 28. The reaction was conducted according to a modified general procedure using **S3** (128 mg, 0.30 mmol, 1.0 equiv) and 5 mol% **1** (11.0 mg, 0.015 mmol). Isolated yields were determined following column chromatography (SiO_2, 0 – 1% EtOAc/Hexanes). The product was isolated as a yellow oil. Run 1: 116 mg, 97% yield; Run 2: 117 mg, 98% yield. ^{1}H NMR (800 MHz, $CDCl_3$) δ 7.55 (d, *J* = 2.4 Hz, 2H), 7.48 (d, *J* = 2.4 Hz, 2H), 2.89 – 2.80 (m, 4H), 2.24 (s, 6H), 1.92 – 1.83 (m, 2H), 1.83 – 1.77 (m, 2H), 1.66 – 1.56 (m, 4H), 1.56 – 1.50 (m, 3H), 1.50 – 1.44 (m, 2H), 1.44 – 1.35 (m, 6H), 1.35 – 1.30 (m, 9H), 1.30 – 1.16 (m, 12H), 1.16 – 1.10 (m, 6H), 1.10 – 1.02 (m, 6H), 0.87 (d, *J* = 7.0 Hz, 18H), 0.85 (d, *J* = 6.7 Hz, 6H). ^{13}C{^{1}H} NMR (201 MHz, $CDCl_3$) δ 154.46, 145.69, 126.92, 122.44, 122.00, 120.65, 76.97, 40.17, 39.39, 37.46, 37.43, 37.30, 32.81, 32.69, 31.15, 28.00, 24.82, 24.47, 24.35, 22.74, 22.65, 22.40, 20.99, 19.77, 19.67, 16.21. HRMS(ESI): calcd for $C_{54}H_{90}N_2O_2^{+\cdot}$: 799.7075; found: 799.7068.

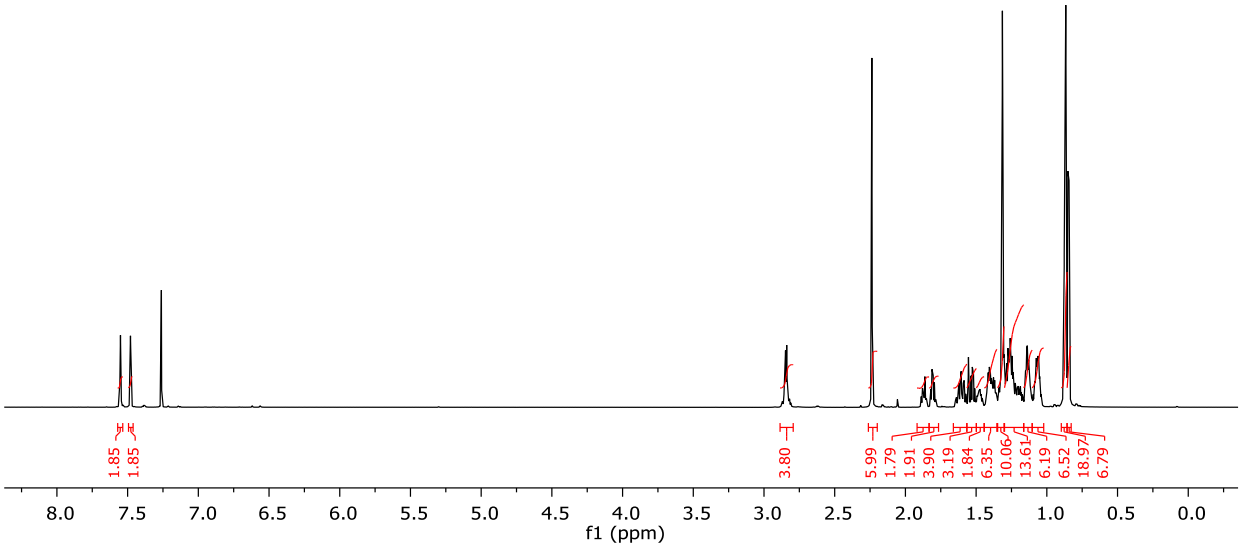

Figure S54. ^{1}H NMR spectrum for **28** in $CDCl_3$.

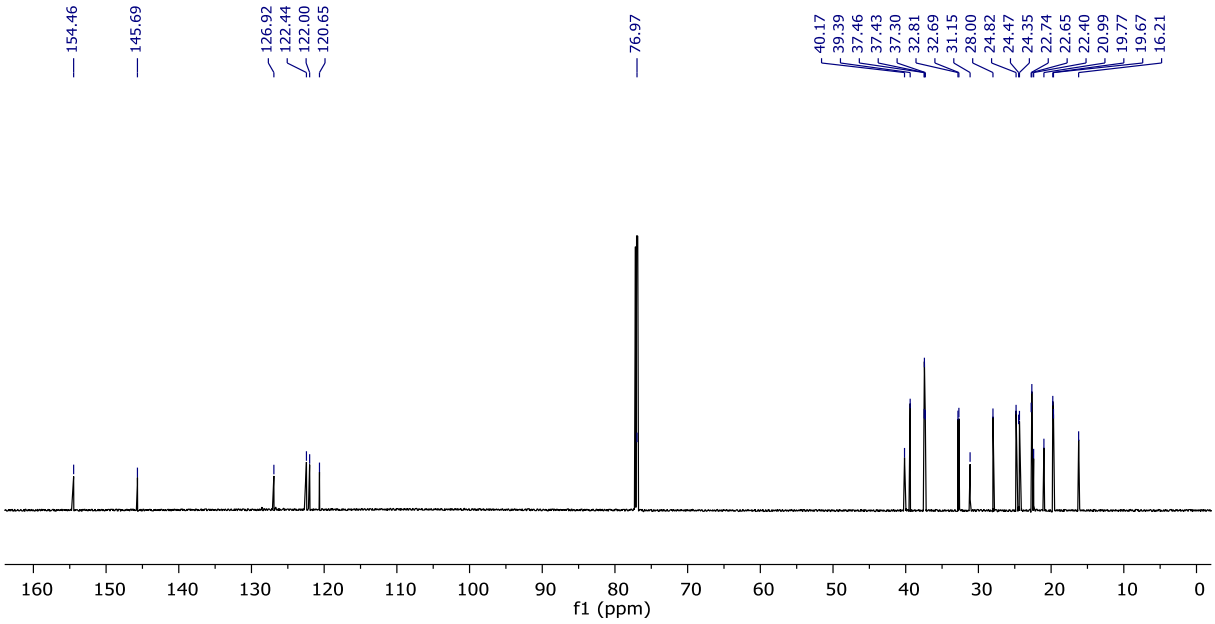

Figure S55. $^{13}C\{^{1}H\}$ NMR spectrum for **28** in $CDCl_3$.

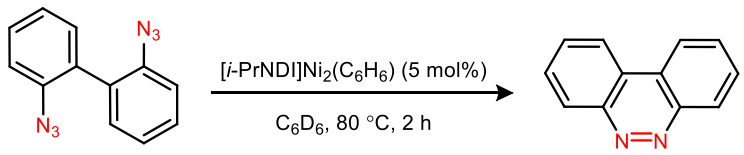

Intramolecular N=N Coupling. Under an atmosphere of N_2, an NMR tube equipped with a J. Young valve was charged with 2,2'-diazido-1,1'-biphenyl **29** (7.1 mg, 0.03 mmol, 1.0 equiv), **1** (2.2 mg, 0.003 mmol, 10 mol%) and C_6D_6 (600 µL), along with 1,3,5-trimethoxybenzene (2.0 mg, 0.012 mmol) as an internal standard. The mixture was then heated to 80 °C for 2 h, leading to the formation of **30** in 80% yield. The ^{1}H NMR spectrum of **30** was consistent with previous reports.**Error! Bookmark not defined.**

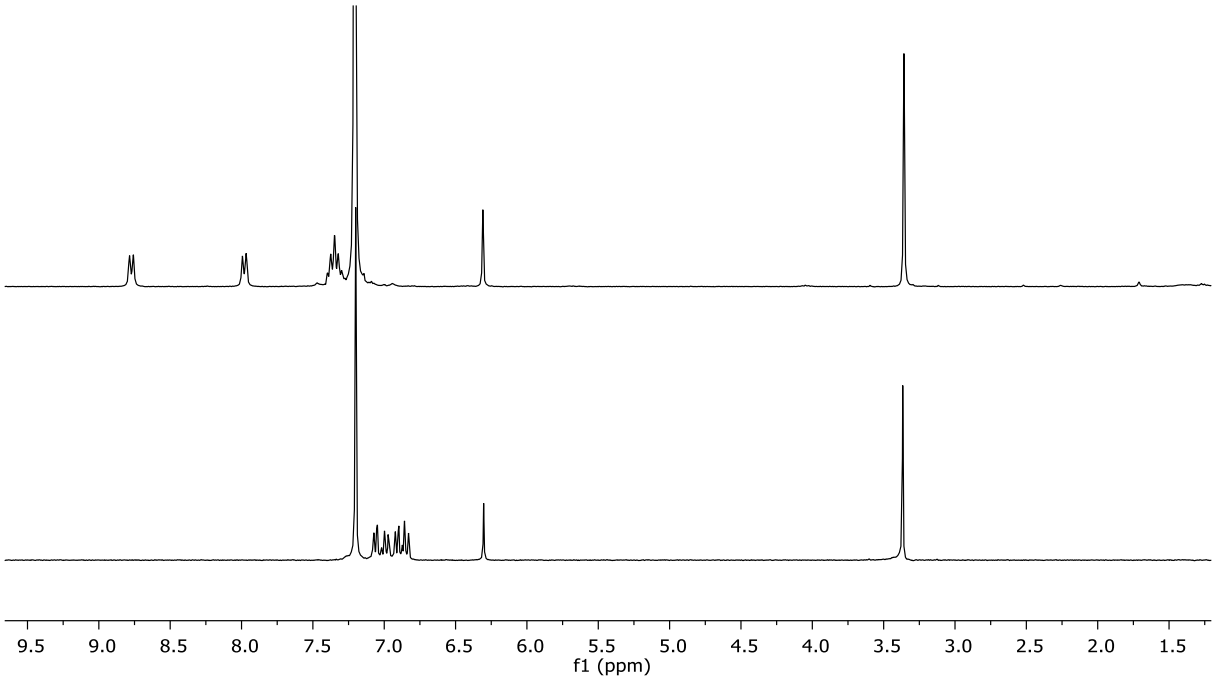

Figure S56. ^{1}H NMR spectrum for the intramolecular N=N coupling of **29** (bottom) to form **30** (top).

5. Polymerization Experiments

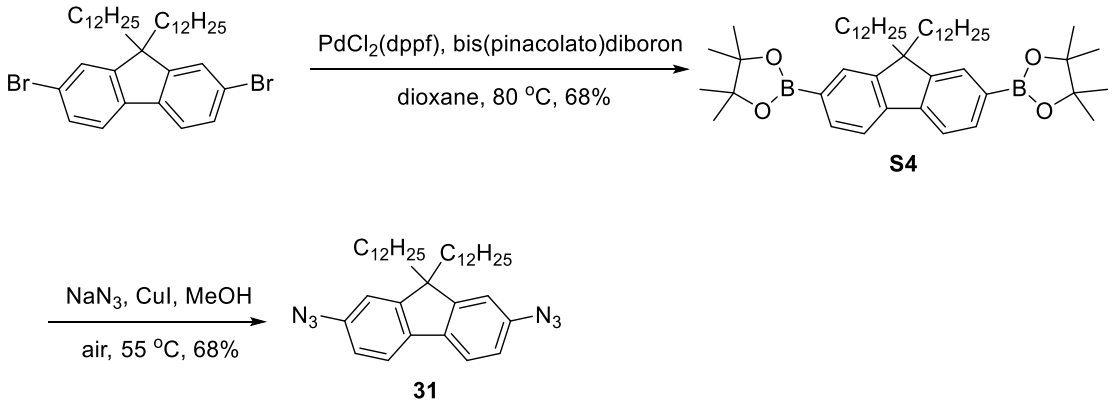

Figure S57. Synthetic route to the diazofluorene monomer **31**.

2,2'-(9,9-didodecyl-9H-fluorene-2,7-diyl)bis(4,4,5,5-tetramethyl-1,3,2-dioxaborolane) **S4** was synthesized according to previously reported methods.[22]

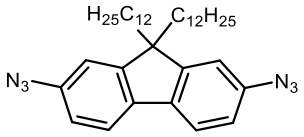

Synthesis of Compound 31. NaN_3 (139.6 mg, 2.147 mmol) and CuI (27.3 mg, 0.143 mmol) were added to a mixture of 2,2'-(9,9-didodecyl-9H-fluorene-2,7-diyl)bis(4,4,5,5-tetramethyl-1,3,2-dioxaborolane) **S4** (542.0 mg 0.718 mmol) and MeOH (40 mL). The resulting mixture was kept from light and bubbled with air at 50 °C for 8 h before being allowed to cool to room temperature. After removal of the solvent under reduced pressure, the residue was purified by silica gel chromatography (hexanes) to give the product **31** as a light yellow solid (285.0 mg, 68%). ^{1}H NMR (800 MHz, $CDCl_3$) δ 7.60 (dd, *J* = 8.0, 1.0 Hz, 2H), 7.00 (dd, *J* = 8.0, 2.2 Hz, 2H), 6.94 (d, *J* = 2.1 Hz, 2H), 1.93 – 1.89 (m, 4H), 1.27 (dt, *J* = 9.6, 4.8 Hz, 4H), 1.25 – 1.21 (m, 8H), 1.21 – 1.11 (m, 12H), 1.11 – 1.06 (m, 4H), 1.06 – 1.00 (m, 8H), 0.87 (d, *J* = 7.3 Hz, 6H), 0.60 – 0.54 (m, 4H). ^{13}C{^{1}H} NMR (201 MHz, $CDCl_3$) δ 152.55, 138.69, 137.57, 120.51, 117.84, 113.56, 109.31, 55.43, 40.35, 31.88, 29.88, 29.59, 29.54, 29.52, 29.31, 29.23, 23.64, 22.67, 14.10. HRMS(ESI):

calcd for $[C_{37}H_{56}N_6^+]$ - N_2 + H : 557.4578; found: 557.4571. The temperature required to vaporize the sample resulted in the loss of N_2 from the azide.

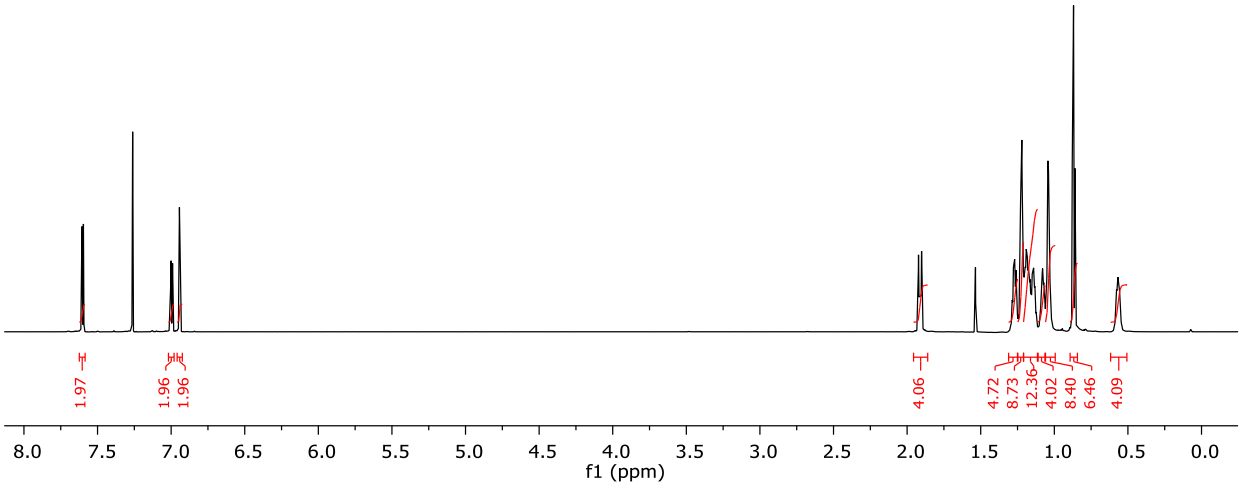

Figure S58. ^{1}H NMR spectrum for **31** in $CDCl_3$.

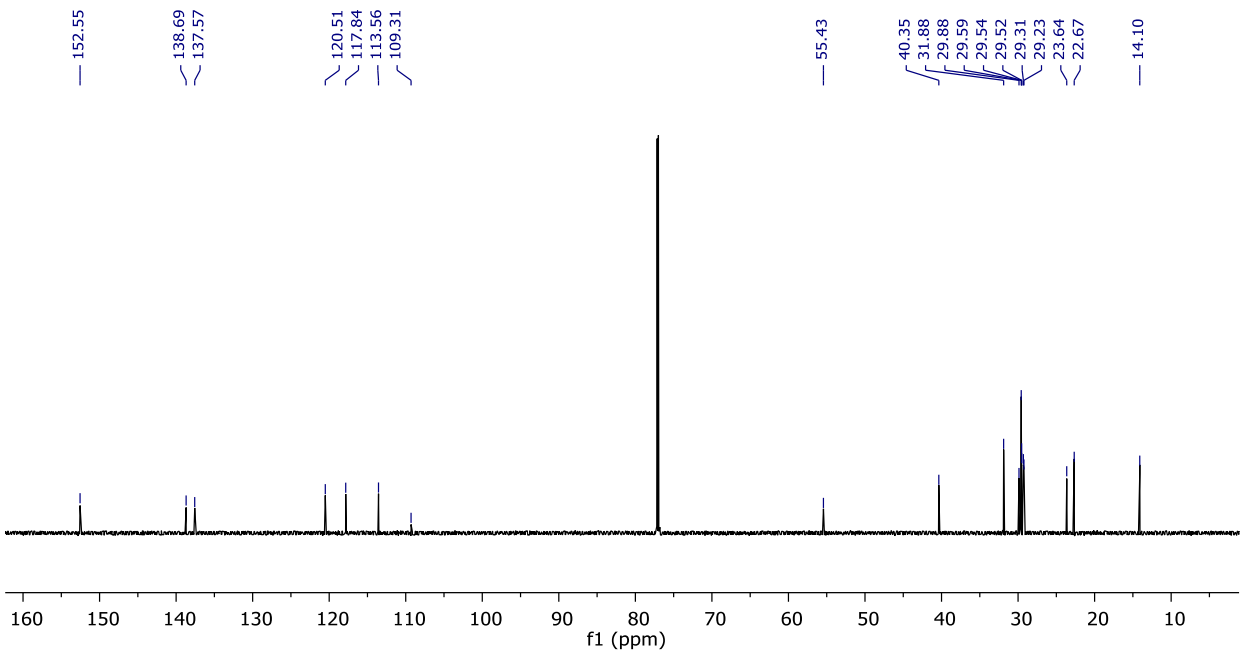

Figure S59. $^{13}C\{^{1}H\}$ NMR spectrum of **31** in $CDCl_3$.

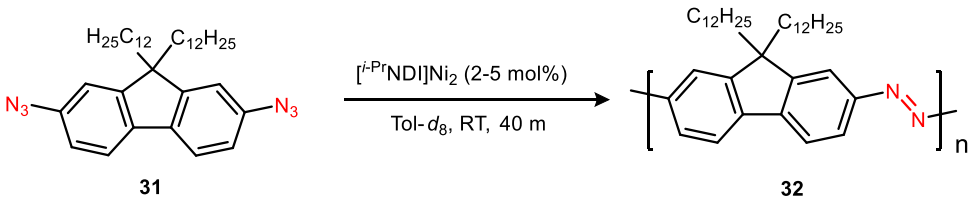

31 **32**

Catalytic Polymerization Procedure. Under an atmosphere of N_2, an NMR tube equipped with a J. Young valve was charged with **31** (29.0 mg, 0.050 mmol, 1.0 equiv), **1** (1.8 mg, 0.0025 mmol, 5 mol% or 0.7 mg, 0.001 mmol, 2 mol%), and toluene-d_8 (600 µL). Immediate gas evolution was observed, and the solution color turned from pale yellow to a deep red-orange. Over the course of 40 min at room temperature, complete consumption of the monomer was observed by ^{1}H NMR spectroscopy, and the solution darkened and became more viscous. The reaction was then quenched by opening the NMR tube to air. The polymeric material was removed from the tube using CH_2Cl_2 and added to methanol to precipitate the product. The precipitated solids were purified by Soxhlet extraction successively with acetone, hexane, and chloroform. The fraction extracted from chloroform was precipitated into methanol, filtered and dried at 60 °C under vacuum to afford the polymer.

32(2% loading). The first precipitation provided 17.1 mg (76% yield) of a dark orange solid. 12.2 mg of polymer was collected after Soxhlet extraction. ^{1}H NMR (300 MHz, toluene-*8d*, ppm) δ: 8.36 (s, 2H), 8.21 (d, *J* = 7.7 Hz, 2H), 7.63 (d, *J* = 7.8 Hz, 2H), 1.23-0.89 (m, *J* = 50H). 2% loading gives M_n of 18.1 kDa with a PDI of 2.48.

32(5% loading). The first precipitation provided 16.3 mg (72% yield) of a dark orange solid. 11.6 mg of polmer was collected after Soxhlet extraction. ^{1}H NMR (300 MHz, toluene-*8d*, ppm) δ: 8.36 (s, 2H), 8.21 (m, 2H), 7.65 (m, 2H), 1.23-0.89 (m, *J* = 50H). 5% loading gives M_n of 41.4 kDa with a PDI of 3.23.

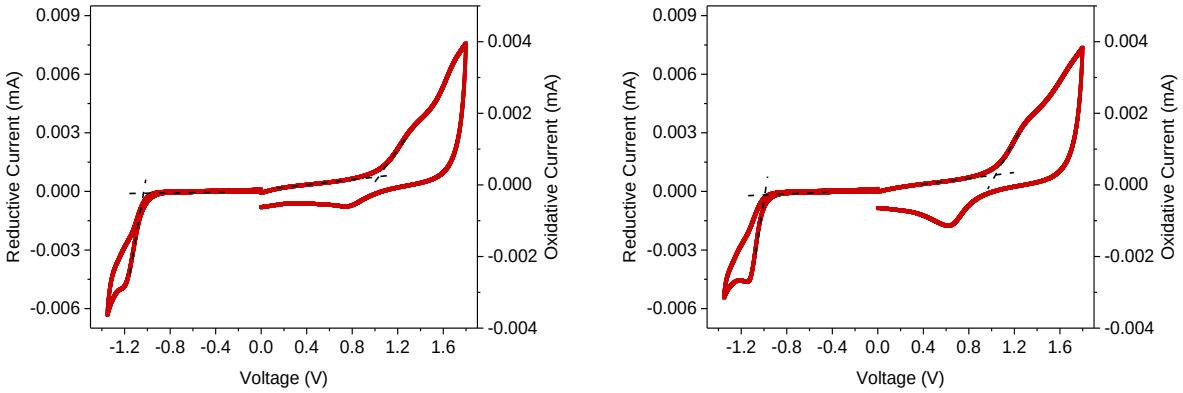

Figure S60. Cyclic voltammograms of **32(2% loading)** (left) and **32(5% loading)** (right) films in Propylene Carbonate with 0.2 M n-Bu_4NPF_6 as supporting electrolyte (scan rate: 20 mV s^{-1}).

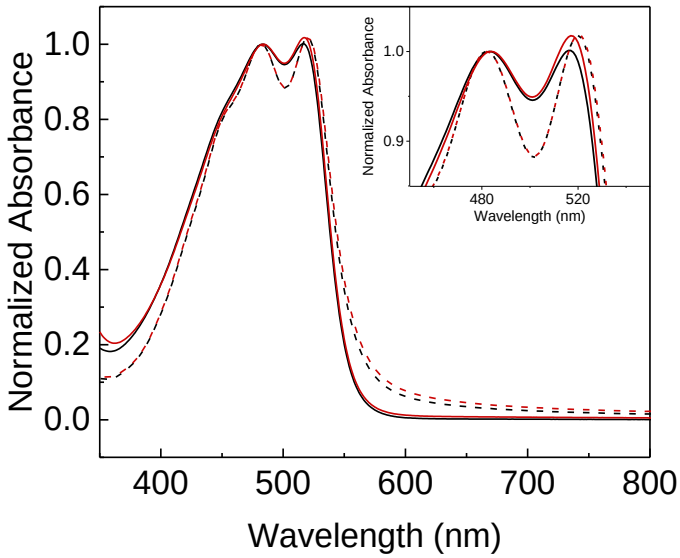

Figure S61. Absorption spectra of **32(2% loading)** (black) and **32(5% loading)** (red) in $CHCl_3$ solutions (solid lines) and as film (dashed lines).

The electrochemical properties of the azo-fluorene polymer were evaluated by cyclic voltammetry, shown in **Figure 1**. Azo polymer **32** exhibited an irreversible redox behavior. HOMO/LUMO levels were estimated around -5.52/-3.47 eV for the low M_n polymer and -5.53/-3.49 eV for the high M_n polymer. UV-Vis absorption spectra for the azo-fluorene polymers are shown in **Figure S60**. The peaks around 480 nm and 520 nm are attributed to intramolecular charge transfer peaks and aggregation peaks, respectively. The 520nm peak of **32(5% loading)** is

relatively more intense, indicative of a stronger aggregation in $CHCl_3$ solution owing to a higher molecular weight. Both thin films show slightly red-shifted absorption spectra, which is evidence of a stronger intermolecular interaction in films. Small CV and UV-Vis spectra difference two azo-fluorenes suggests that the molecular weight of azo-fluorenes has a negligible impact on their energy levels between this range.

Table 1. Molecular, Optical, and Electrochemical Properties

	Cat. Loading	Mn[a] (KDa)	PDI	HOMO [b] (eV)	LUMO [b] (eV)	E_g^{CV} [c] (eV)	E_g^{Opt} [d] (eV)
L	2%	18.1	2.48	-5.52	-3.47	2.05	2.20
H	5%	41.4	3.23	-5.53	-3.49	2.04	2.20

[a]Determined by GPC using polystyrene standards in THF. [b]The HOMO and LUMO energy levels are estimated from HOMO = − (4.80 + E_{ox} – E_{Fc/Fc^+}) and LUMO = − (4.80 + E_{red} – E_{Fc/Fc^+}), where E_{ox} and E_{red} are onsets of redox potentials. [c]Calculated from E_g = LUMO-HOMO. [d]Calculated from absorption band edge of the polymer films, $E_g = 1240/\lambda_{edge}$.

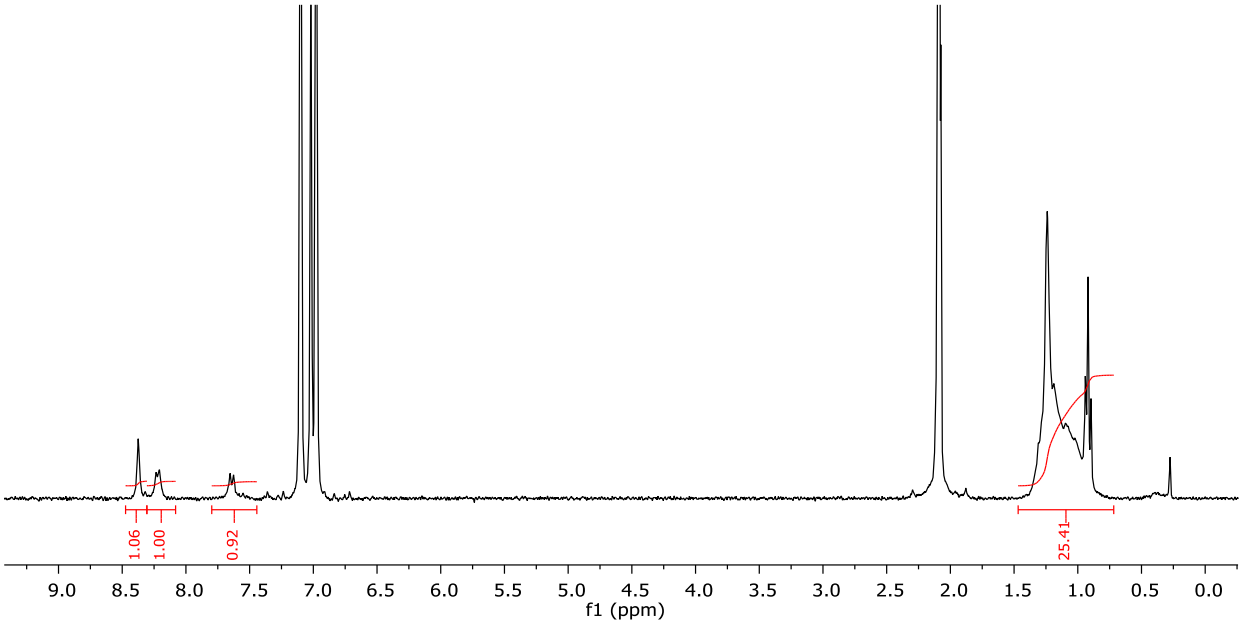

Figure S62. ^{1}H NMR spectrum for the polymerization of **31** using 2 mol% **1** (toluene-d_8).

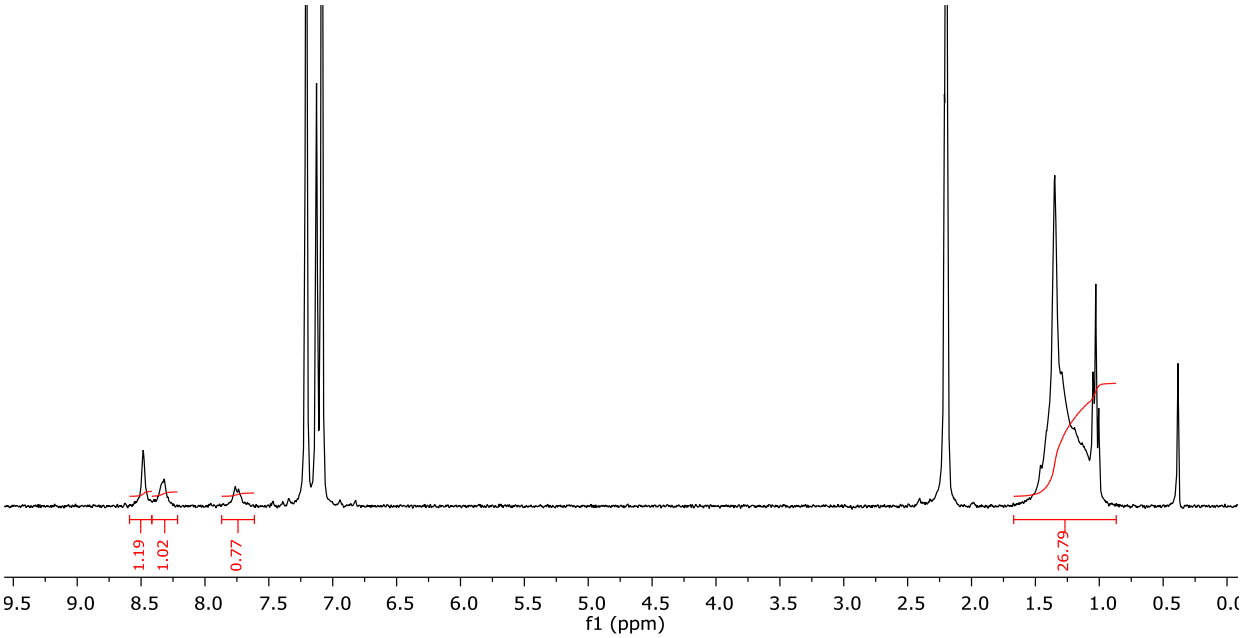

Figure S63. ^{1}H NMR spectrum for the polymerization of **31** using 5 mol% **1** (toluene-d_8).

6. Synthesis and Characterization of Nickel Complexes

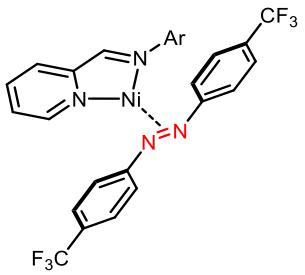

[$^{i\text{-Pr}}$IP]Ni(4,4′-bis-trifluoromethylazobenzene) (7). In an N_2 filled glovebox, a 20-mL vial was charged with **4** (50.0 mg, 0.115 mmol, 1.0 eq), C_6H_6 (2.0 mL), and a magnetic stir bar. A solution of 4-trifluoromethylphenyl azide (36 mg, 0.192 mmol, 1.7 equiv) in 2.0 mL C_6H_6 was added. Immediate gas evolution was observed, and the reaction solution turned from dark purple to dark blue-green. The reaction mixture was stirred at room temperature. After 5 min, the solvent was removed under reduced pressure. The solid residue was purified by recrystallization from a saturated pentane/toluene solution at –30 °C. Brown cube-like single crystals of **7** obtained by this procedure were suitable for X-ray diffraction studies (22 mg 44% yield). ^{1}H NMR (300 MHz, C_6D_6) δ 8.75 (d, *J* = 5.0 Hz, 1H), 7.81 (d, *J* = 8.2 Hz, 2H), 7.62 – 7.43 (m, 3H), 7.33 – 7.20 (m, 4H), 7.06 – 6.92 (m, 3H), 6.67 (t, *J* = 7.5 Hz, 1H), 6.45 (t, *J* = 6.4 Hz, 1H), 6.17 (d, *J* = 7.6 Hz, 1H), 4.32 (s, 1H), 2.28 (s, 1H), 1.77 (d, *J* = 6.6 Hz, 3H), 1.00 (d, *J* = 6.8 Hz, 3H), 0.78 (d, *J* = 6.6 Hz, 3H), 0.69 (d, *J* = 5.3 Hz, 3H). ^{13}C{^{1}H} NMR (201 MHz, C_6D_6) δ 162.09 , 161.32 , 159.83 , 152.58 , 150.46 , 144.91 , 140.54 , 139.29 , 135.39 , 127.94 , 127.73 (q, *J* = 39.2 Hz), 127.39 , 126.90 , 126.77 , 126.61 (q, *J* = 3.8 Hz), 126.42 (q, *J* = 3.8 Hz), 125.56 , 125.42 , 125.28 , 123.65 , 123.45 , 121.23 (q, *J* = 32.9 Hz), 120.74 (q, *J* = 31.9 Hz), 119.71 , 119.31 , 28.76 , 27.63 , 24.72 , 24.20 , 22.57 , 21.55. UV–Vis–NIR (C_6H_6, nm {M^{-1} cm^{-1}}): 326 {sh}, 386 {5200}, 549 {3700}, 656 {5700}. Anal. Calcd for $C_{32}H_{30}F_6N_4Ni$: C 59.75 H 4.70, N, 8.71; found: C 59.49 H 4.71 N 8.56.

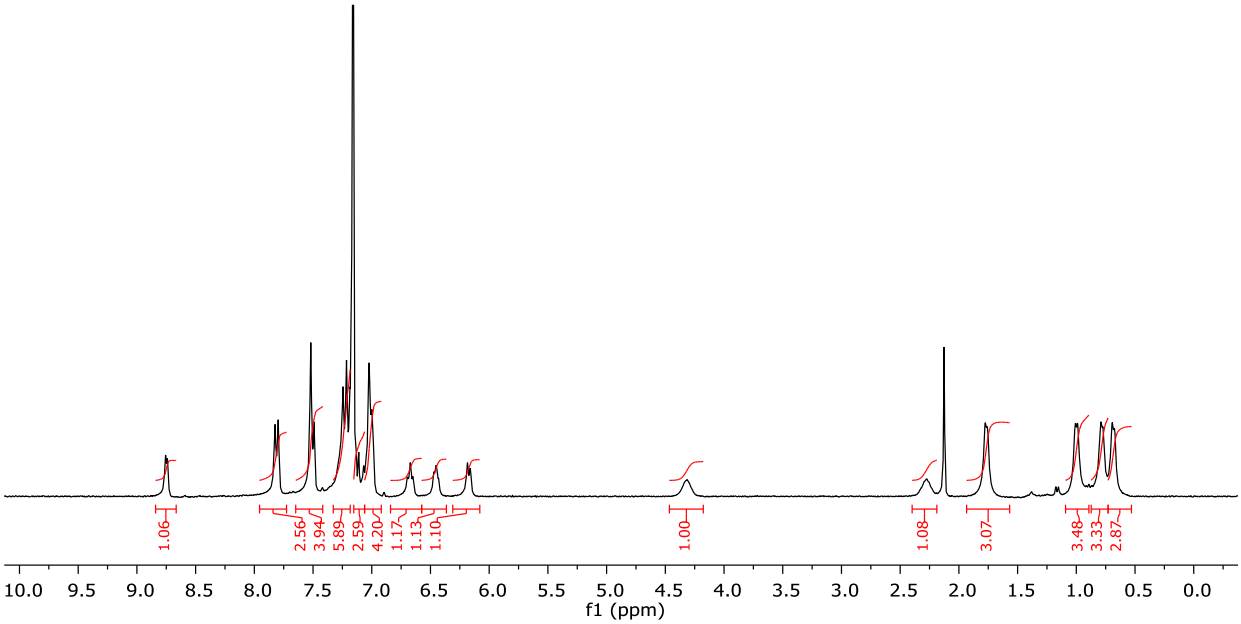

Figure S64. ^{1}H NMR spectrum of **7**.

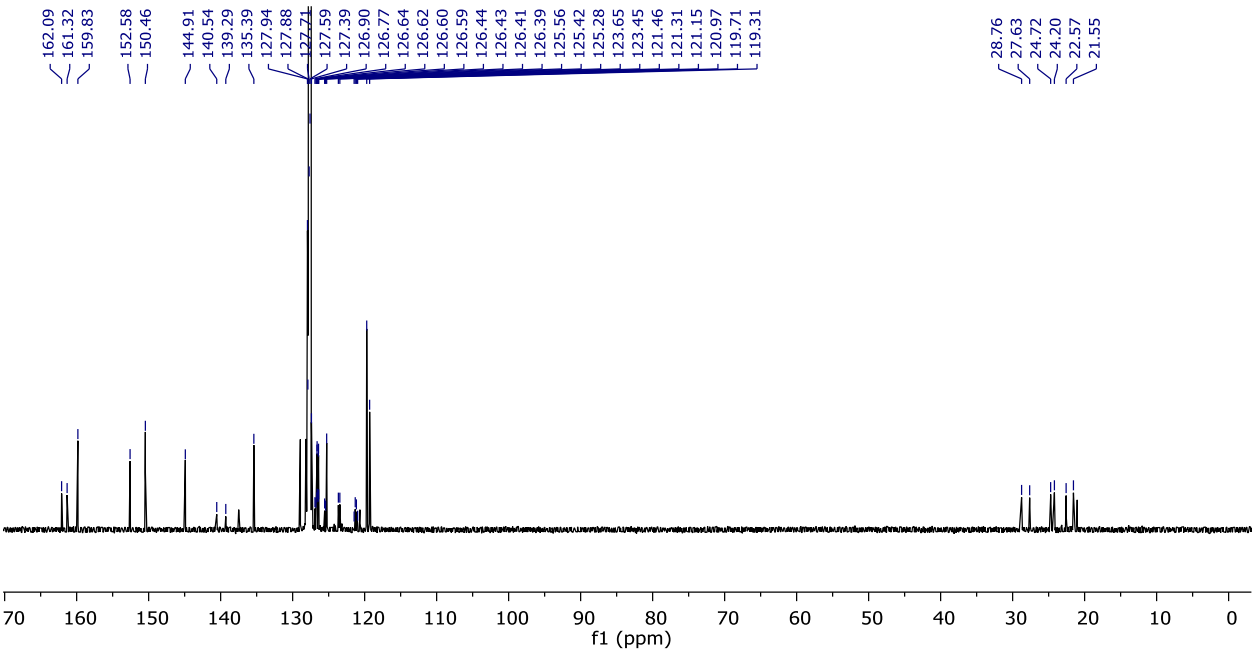

Figure S65. $^{13}C\{H\}$ NMR spectrum of **7** in C_6D_6.

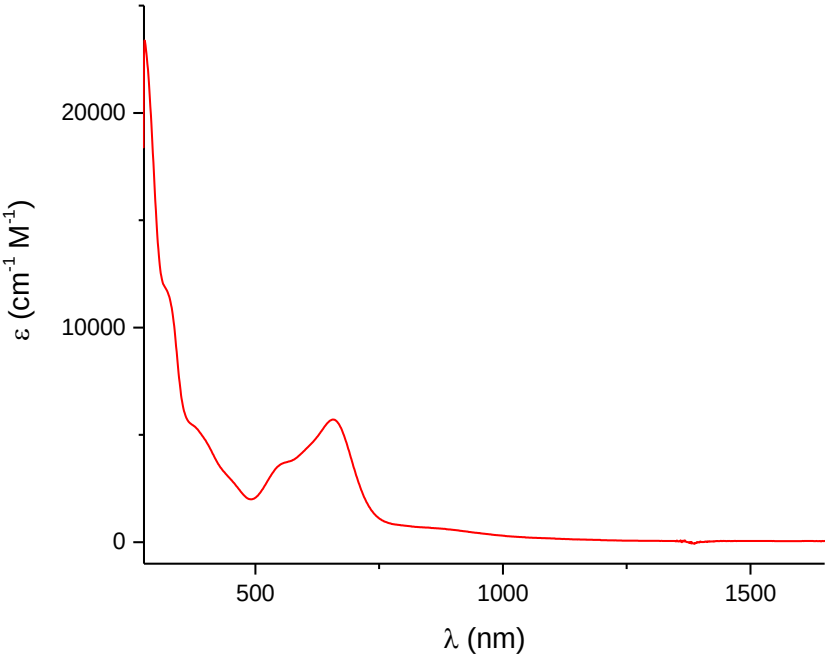

Figure S66. UV-Vis-NIR spectrum of **7** in C_6H_6 (0.012 mM).

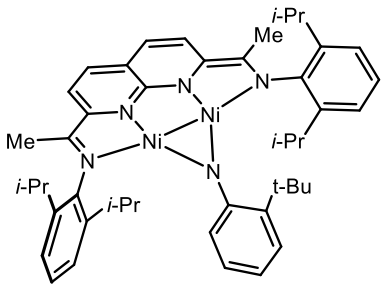

[$^{i\text{-Pr}}$NDI]Ni$_2$((2-C(CH$_3$)$_3$C$_6$H$_5$) (33). Under an atmosphere of N_2, a 20-mL vial was charged with [$^{i\text{-Pr}}$NDI]Ni$_2$(C_6H_6) (**1**) (15 mg, 0.021 mmol, 1.0 equiv.), 1-*tert*-butyl-phenyl azide (3.6 mg, 0.021 mmol, 1.0 equiv), and C_6D_6 (900 µL). Immediate gas evolution was observed, and the reaction mixture turned brown-purple. After 2 min, the solvent was then removed under reduced pressure. The solid residue was purified by recrystallization from a saturated 3:1 pentane/toluene solution at –30 °C. Brown plate-like single crystals of **33** obtained by this procedure were suitable for X-ray diffraction studies (8.7 mg 53% yield). ^{1}H NMR (800 MHz, C_6D_6) δ 45.54 (s, 6H), 29.19 (s, 1H), 26.39 (s, 1H), 19.22 (s, 2H), 13.74 (m, 4H), 10.87 (s, 1H), 7.11 – 6.81 (m, 4H), 4.13 (s, 9H), 3.38 (s, 2H), 2.33 (s, 12H), 1.90 (s, 12H), -3.63 (s, 1H), -102.45 (s, 2H). UV–Vis–NIR (C_6H_6, nm {M^{-1} cm^{-1}}): 288 {sh}, 342 {2300}, 516 {7500}, 707 {5900}, 812 {5600}, 979 {5700}. Anal. Calcd for $C_{46}H_{57}N_5Ni_2$: C 69.29 H 7.21, N, 8.78; found: C 68.86 H 7.28 N 8.47.

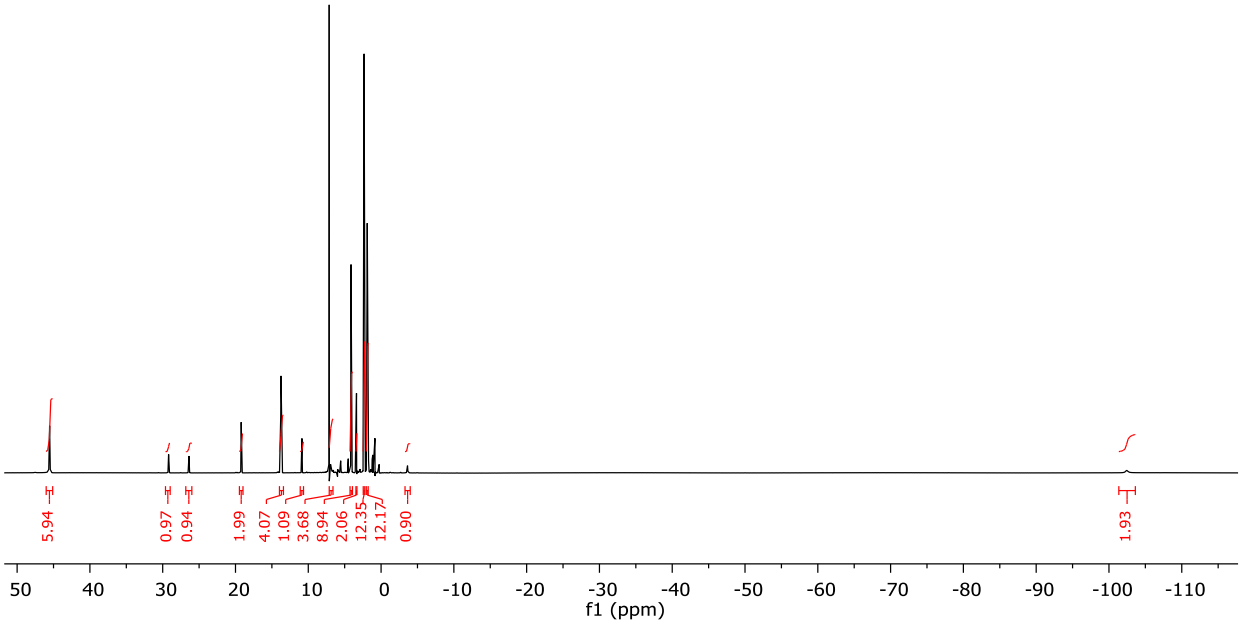

Figure S67. ^{1}H NMR spectrum of **33** in C_6D_6.

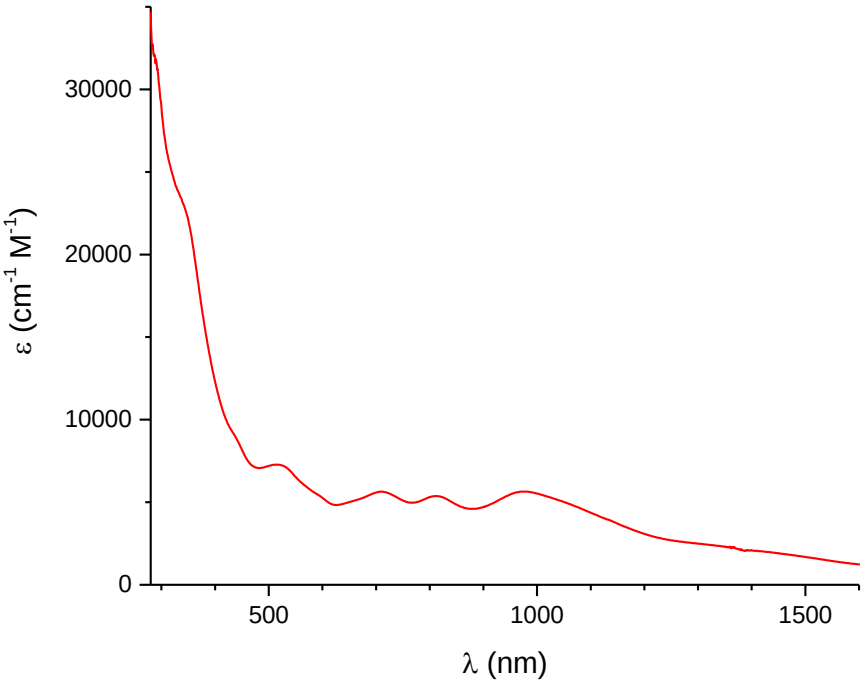

Figure S68. UV–Vis–NIR spectrum of **33** in C_6H_6 (0.13 mM).

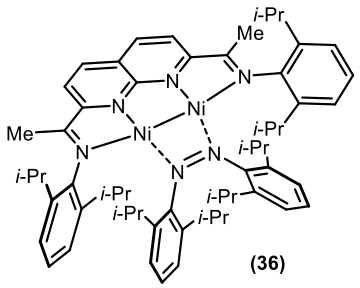

(36)

[*i*-PrNDI]Ni$_2$(N$_2$Ar$_2$) (36). Under an atmosphere of N_2, a 20-mL vial was charged with [*i*-PrNDI]Ni$_2$(C_6H_6) (**1**) (40 mg, 0.055 mmol, 1.0 equiv.), 2,6-diisopropylphenyl azide (23 mg, 0.11 mmol, 2.0 equiv.), and C_6H_6 (8.0 mL). Immediate gas evolution was observed, and the solution turned dark green-brown. After allowing the reactants to mix for 2 min, the mixture was filtered through a glass fiber pad, and the filtrate was evaporated under reduced pressure. The crude solid was washed with pentane (approx. 3 mL) and dried under vacuum. The solid residue was redissolved in C_6H_6 and lyophilized to yield **2** as a dark brown solid (43 mg, 78% yield). Single crystals suitable for XRD analysis were obtained from concentrated C_6H_6 solutions. ^{1}H NMR (500 MHz, C_6D_6) δ 7.15–7.12 (m, 2H), 7.07 (t, *J* = 7.7 Hz, 2H), 6.99 (d, *J* = 7.7 Hz, 1H), 6.87–6.82 (m, 4H), 6.48 (dd, *J* = 6.1, 3.2 Hz, 2H), 6.43 (d, *J* = 8.2 Hz, 2H), 5.94 (d, *J* = 8.2 Hz, 2H), 3.70 (hept, *J* = 6.2, 2H), 3.10 (hept, *J* = 6.6 Hz, 2H), 2.84 (hept, *J* = 6.6 Hz, 2H), 2.36 (hept, *J* = 6.3 Hz, 2H), 2.19 (d, *J* = 6.7 Hz, 6H), 1.75 (d, *J* = 6.8 Hz, 6H), 1.59 (s, 6H), 1.29 (d, *J* = 6.8 Hz, 6H), 1.16 (d, *J* = 6.8 Hz, 6H), 0.94 (d, *J* = 6.7 Hz, 6H), 0.69 (d, *J* = 6.8 Hz, 6H), 0.07 (d, *J* = 6.7 Hz, 6H), –0.19 (d, *J* = 6.6 Hz, 6H). ^{13}C{^{1}H} NMR (500 MHz, C_6D_6) δ 161.9, 150.0, 147.0, 142.1, 142.3, 141.7, 141.1, 137.3, 125.8, 125.7, 124.2, 123.9, 123.5, 123.4, 114.8, 29.6, 28.4, 28.4, 28.4, 28.0, 26.5, 24.5, 24.3, 24.2, 24.0, 23.9, 23.7, 23.2, 16.9. UV–Vis–NIR (C_6H_6, nm {M^{-1} cm^{-1}}): 284 {sh}, 338 {29300}, 446 {10500}, 506 {8000}, 704 {8700}, 969 {sh}, 1080 {10600}, 1329 {8200}. Anal. calcd for $C_{60}H_{78}N_6Ni_2$: C 73.48, H 7.85, N 7.79; found: C 73.27, H 7.76, N 7.76.

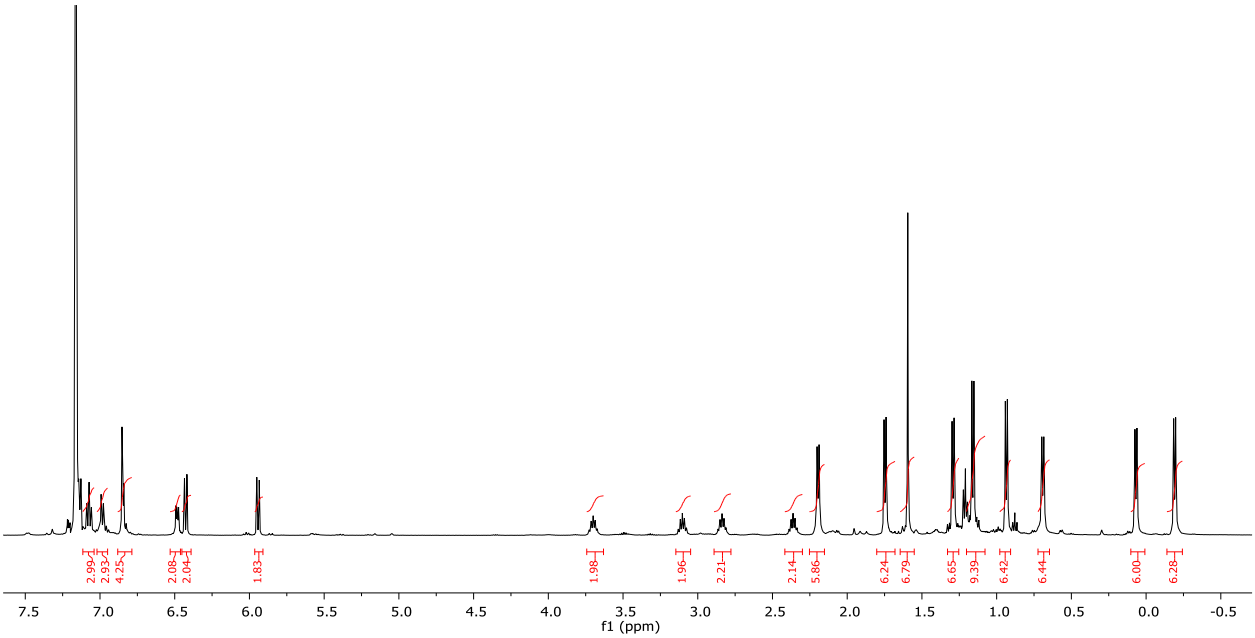

Figure S69. ^{1}H NMR spectrum of **36** in C_6D_6.

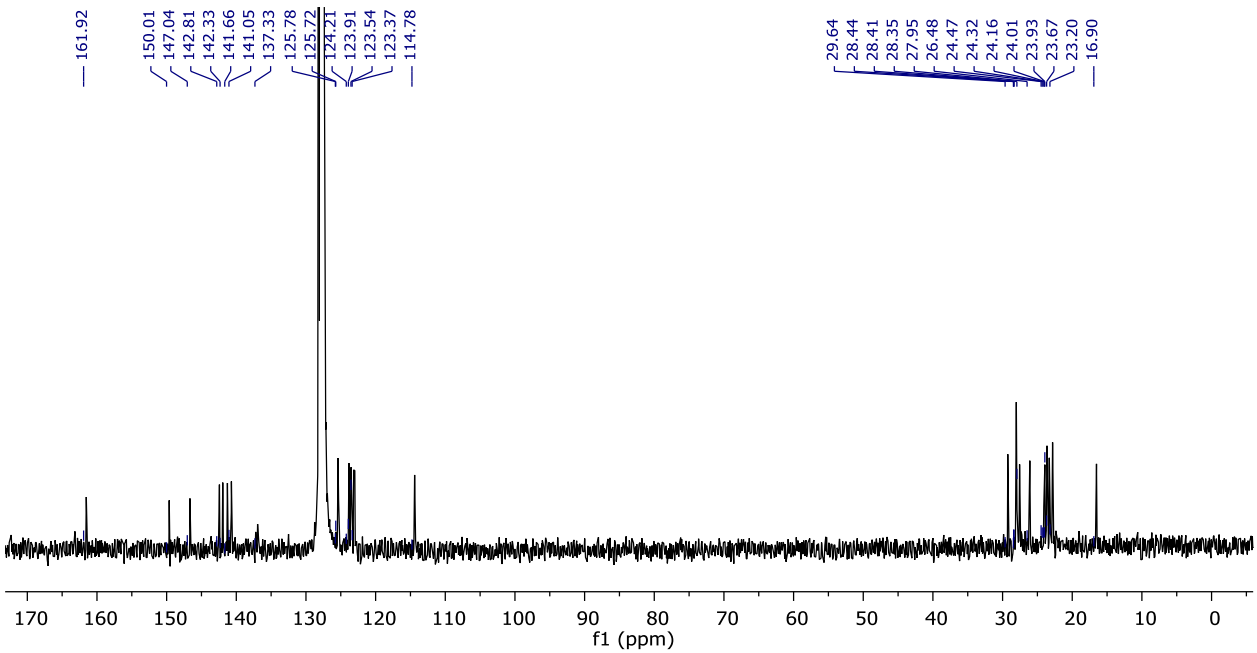

Figure S70. $^{13}C\{^{1}H\}$ NMR spectrum of **36** in C_6D_6.

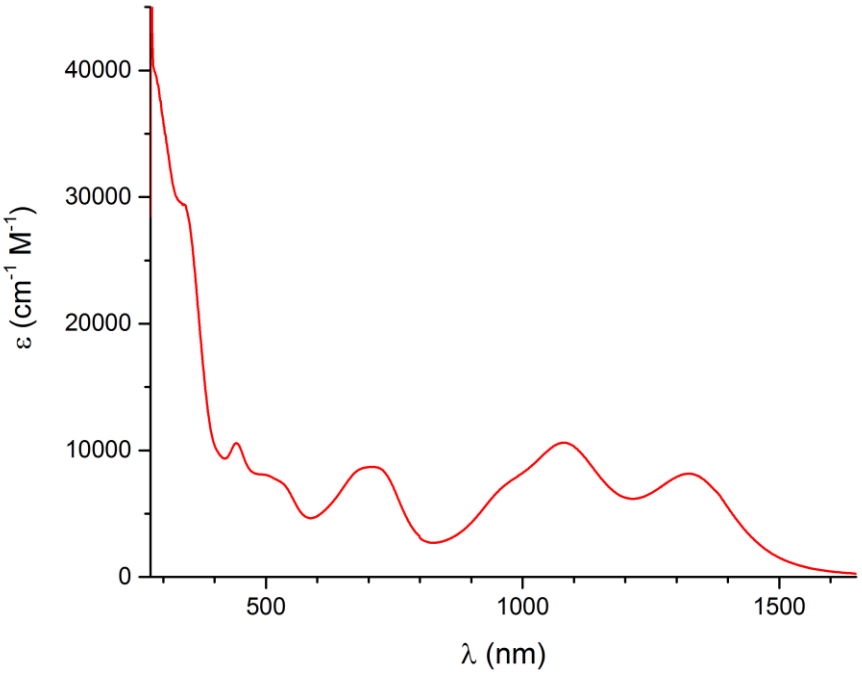

Figure S71. UV–Vis–NIR spectrum of **36** in C_6H_6 (0.10 mM).

7. Mechanistic Experiments

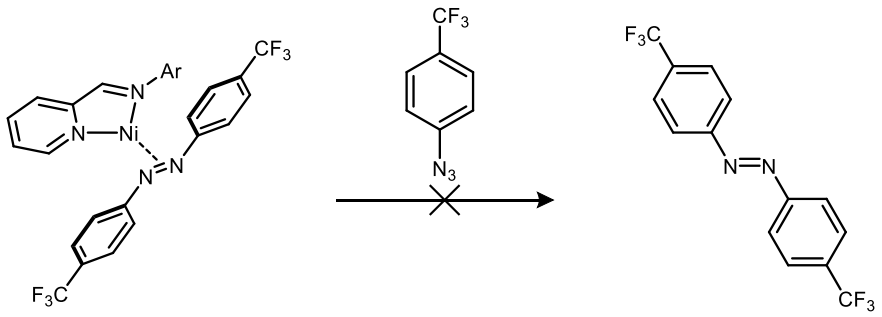

Reaction of 7 with 4-trifluoromethylphenyl azide. In an N_2 filled glovebox, an NMR tube equipped with a J. Young valve was charged with 4-trifluoromethylphenyl azide (**2**) (5.8 mg, 0.031 mmol, 1.0 equiv), C_6D_6 (500 µL), **7** (1.0 mg, 0.0015 mmol, 5 mol %), and 1,3,5-trimethoxybenzene (5.2 mg, 0.031mmol) as an internal standard. The reaction components were allowed to react for 1 h. No conversion of **2** was observed by ^{1}H NMR integration against 1,3,5-trimethoxybenzene as an internal standard. No additional conversion or yield of azoarene was observed after an additional 2 h at room temperature or after heating for 1 h at 80 °C.

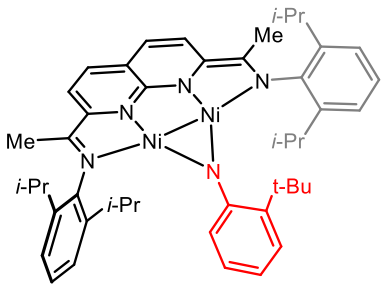

Variable temperature ^{1}H NMR data for 33.

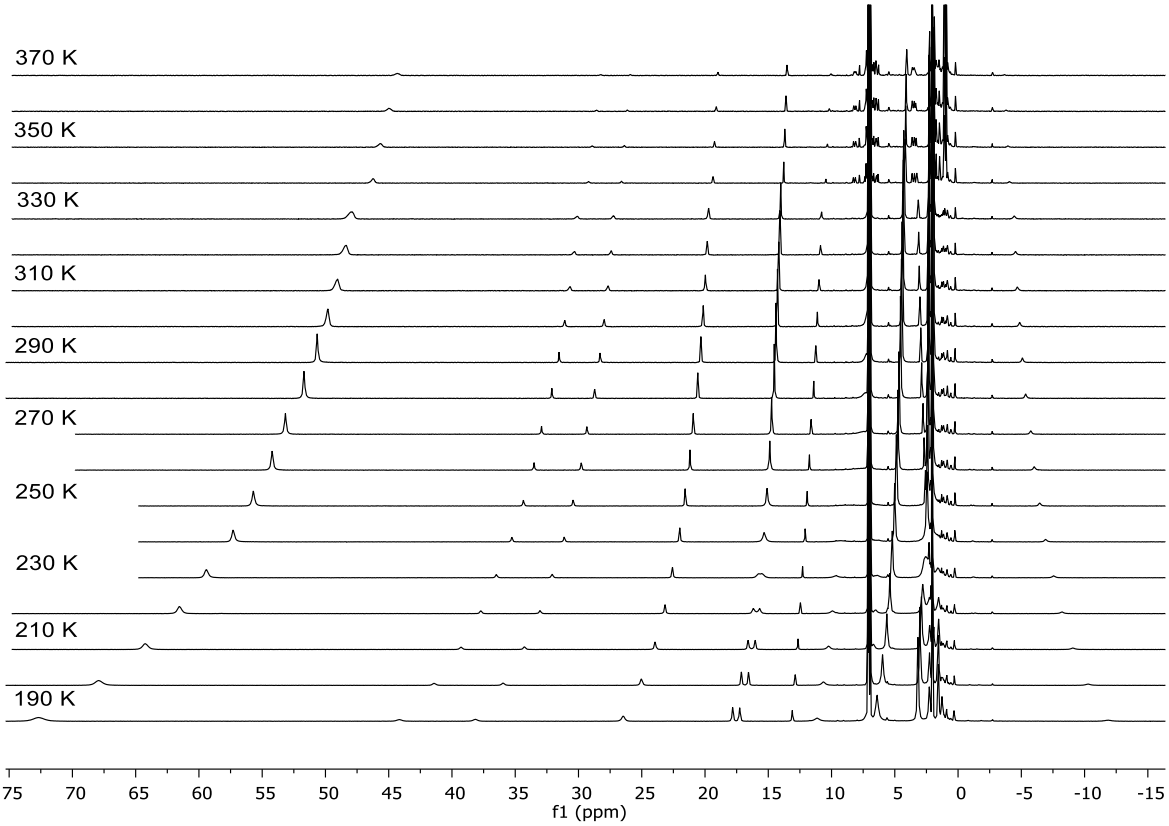

Figure S72. Variable temperature ^{1}H NMR spectrum overlay (toluene-d_8) showing selected peaks of **33** as a function of temperature.

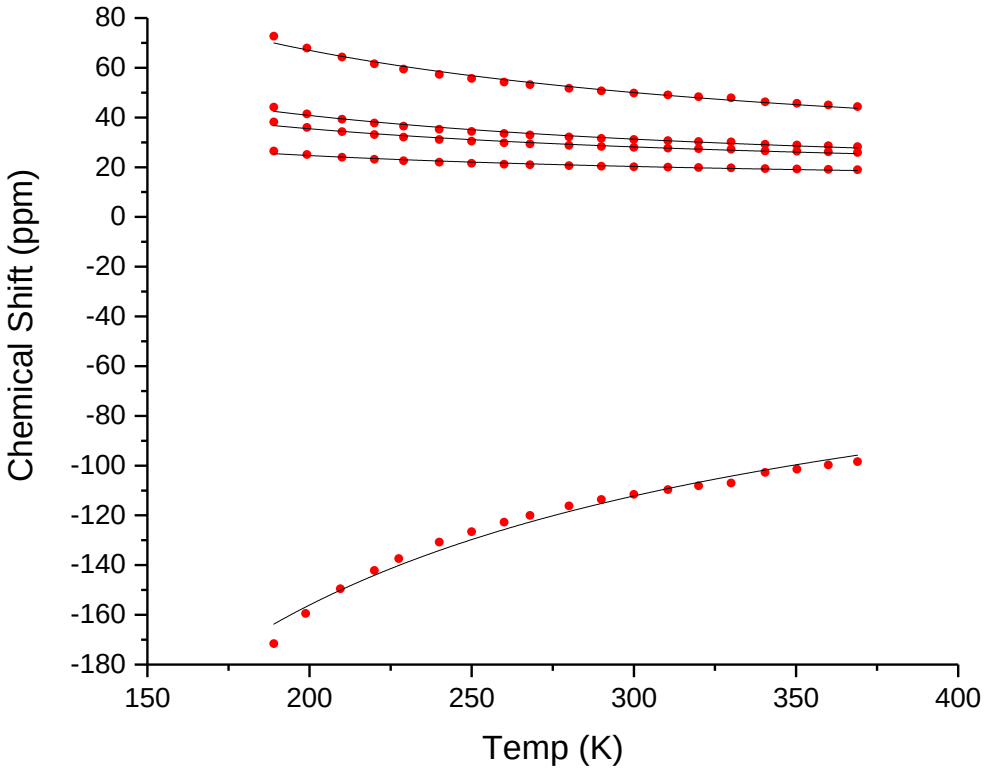

Figure S73. Selected ^{1}H NMR peaks for **33** are plotted as a function of temperature (red points), and each set of points was fit (black lines) to simple Curie behavior according to the equation below.

$$chemical\ shift = a + b * \frac{1}{T}$$

Curve	Adj. R^2	a	b
1	0.984	16 ± 1	10200 ± 300
2	0.979	12.2 ± 0.7	5700 ± 200
3	0.974	13.6 ± 0.6	4400 ± 200
4	0.965	11.5 ± 0.5	2600 ± 100
5	0.980	-24 ± 3	-26300 ± 900

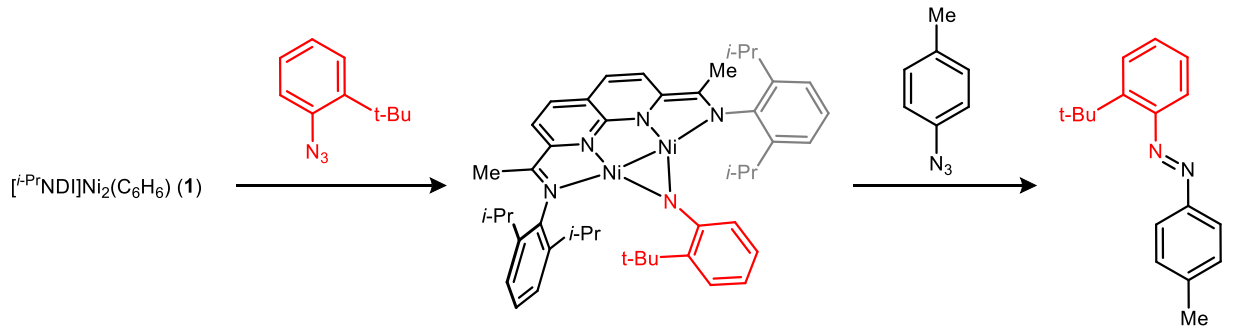

Reaction of 1 with 2-tert-butylphenyl azide and cross-azoarene formation with 4-tolyl azide. Under an atmosphere of N_2, an NMR tube equipped with a J. Young valve was charged with 2-*tert*-butylphenyl azide (50 µL of a 0.28 M solution in C_6D_6, 0.0137 mmol, 1.0 equiv), **1** (10.0 mg, 0.0137 mmol, 1.0 equiv), and C_6D_6 (600 µL). Immediate gas evolution was observed, and the clean formation of **33** was confirmed by ^{1}H NMR. 4-Tolyl azide was then added to the reaction mixture (250 µL of a 0.28 M solution in C_6D_6, 0.067 mmol, 5.0 equiv) along with 1,3,5-trimethoxybenzene (2.6 mg, 0.017 mmol) as an internal standard. Full consumption of the **33** was observed by ^{1}H NMR, and the solution was then filtered through a short plug of silica. The yield of the cross-azoarene product was determined by ^{1}H NMR integration (89% yield). The yield of the homocoupled 4-azotoluene product was 81%. The material was run through a silical column (hexanes) to remove the free NDI ligand and most of the 1,3,5-trimethoxybenzene. This material was then analyzed by ^{1}H NMR, COSY, and GC-MS, confirming the identity of the cross-coupled product.

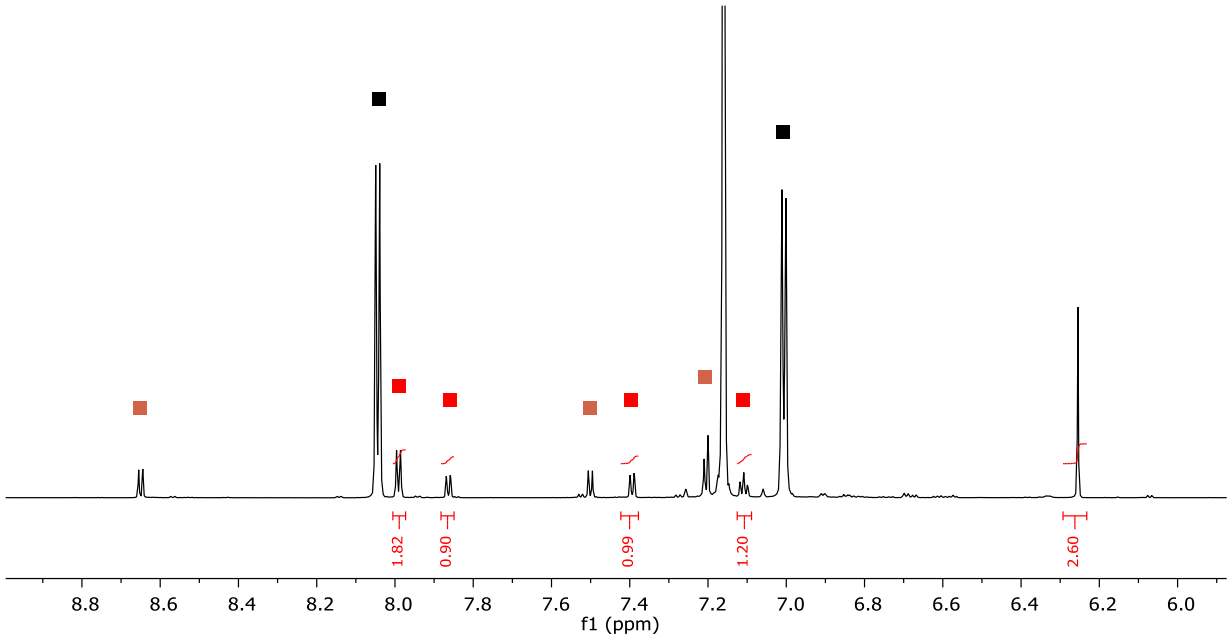

Figure S74. ^{1}H NMR spectrum (C_6H_6) of the product mixture after reaction of the imido intermediate with 4-tolylazide and running through a silica plug. Black, red, and blue squares correspond to 4-azotoluene (**9**), the cross-coupled product (**34**), and free NDI ligand respectively.

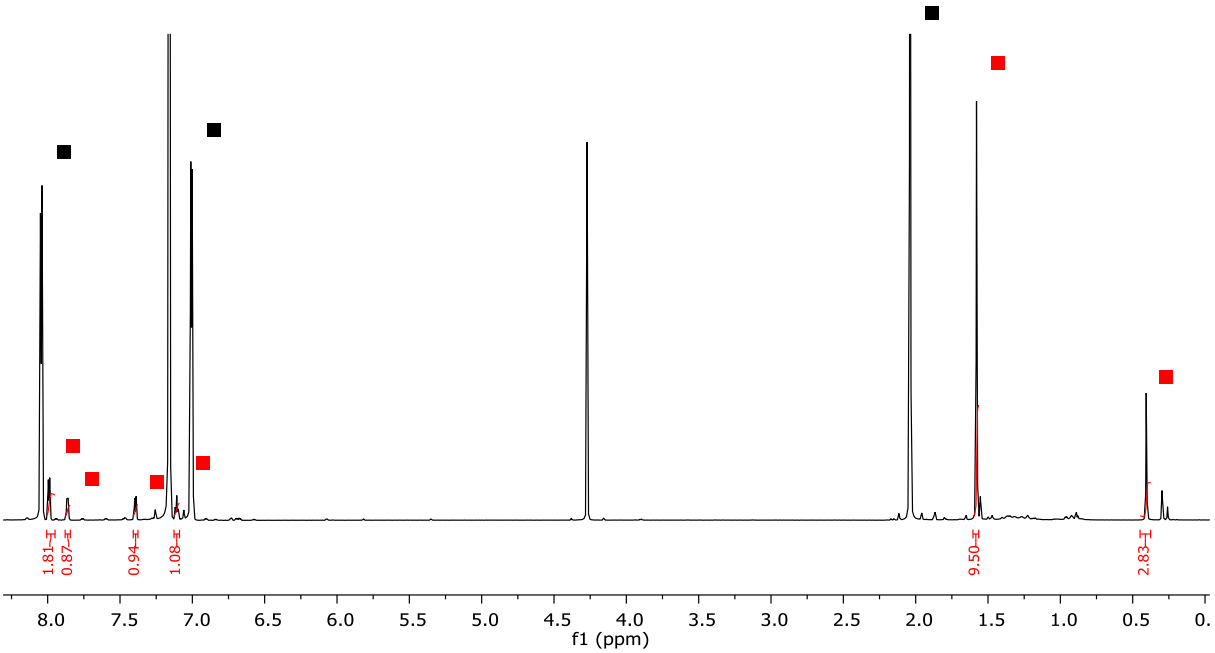

Figure S75. ^{1}H NMR spectrum (C_6H_6) of the product mixture after running through a column to remove the $^{i\text{-Pr}}$NDI ligand and 1,3,5-trimethoxybenzene. Black and red squares correspond to 4-azotoluene (**9**) and the cross-coupled product (**34**) respectively.

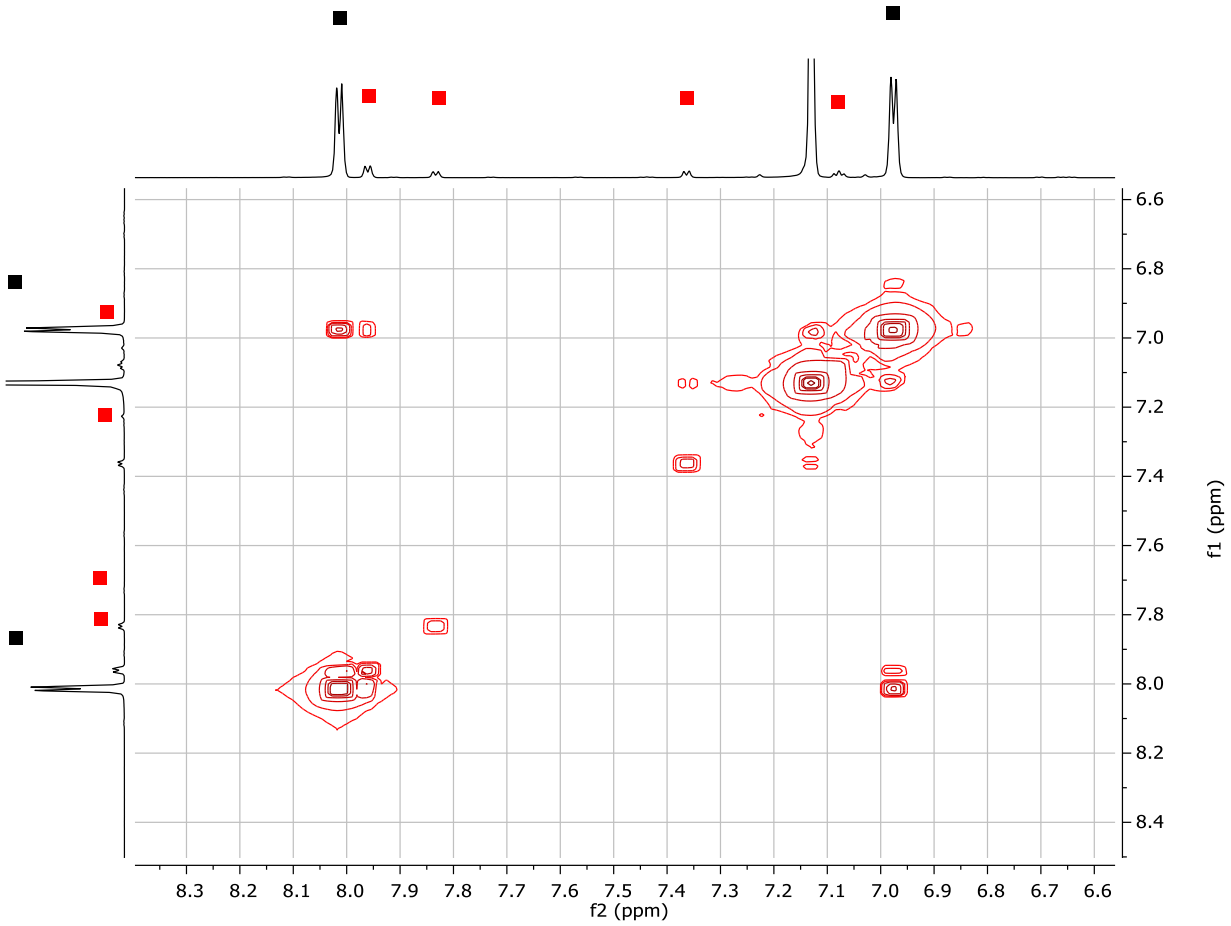

Figure S76. COSY spectrum of product mixture after column. Black and red squares correspond to 4-azotoluene (**9**) and the cross-coupled product (**34**) respectively.

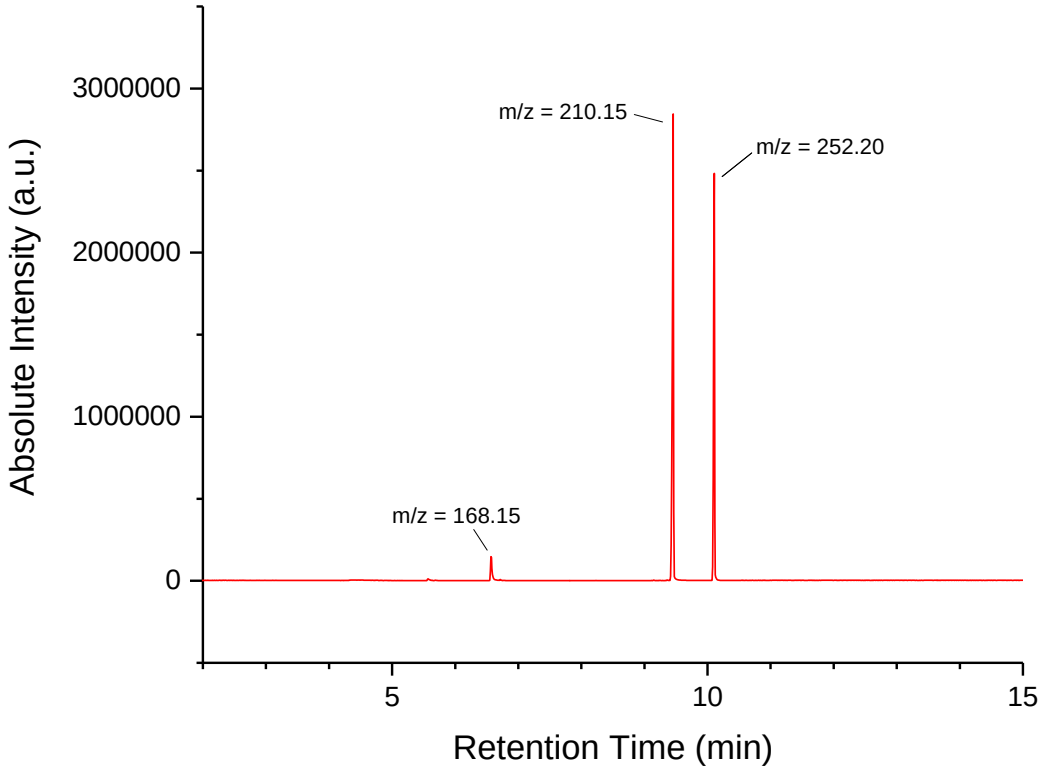

Figure S77. GCMS trace of the cross-coupling reaction following a silica plug. The masses at m/z = 168.15, 210.15, and 252.20 correspond to the masses of 1,3,5-trimethoxybenzene, 4-azotoluene (**9**), and the cross-coupled product (**34**) respectively.

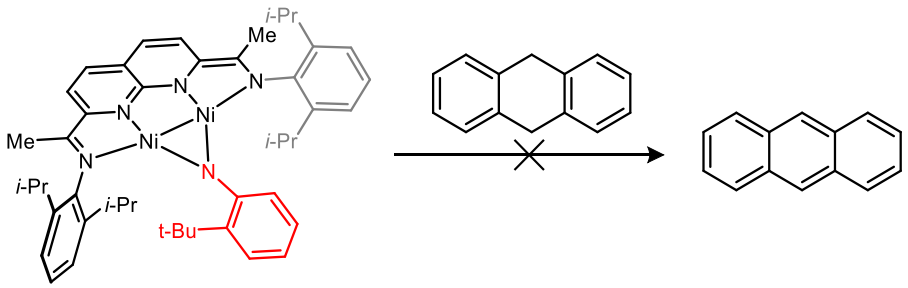

Comparison of the decomposition of 33 in the presence and absence of 9,10-dihydroanthracene. Under an atmosphere of N_2, a 20-mL vial was charged with 2-*tert*-butylphenyl azide (2.5 mg, 0.014 mmol, 1.0 equiv), **1** (10.0 mg, 0.014 mmol, 1.0 equiv), 1,3,5-trimethoxybenzene (2.5 mg, 0.015 mmol) as an internal standard, and C_6D_6 (1200 µL). This solution was then divided equally between two J. Young NMR tubes. To the first tube was added a solution of 9,10-dihydroanthracene (0.0068 mmol, 1.0 equiv) in C_6D_6 (150 µL). To the second was added C_6D_6 (150 µL). The decomposition of **33** in each solution was the monitored over several hours: over the time period of the catalytic N–N coupling reaction (2 h), a 13% decomposition of **33** in the solution without 9,10-dihydroanthracene was observed; the solution containing dihydroanthracene showed 14% decomposition of **33**. Measurement of the decomposition over a longer period showed minimal difference in the rate of decomposition between the two solutions. For the solution containing dihydroanthracene, no measurable amount of anthracene was formed by ^{1}H NMR.

Time	% Remaining **33**	% Remaining **33** (DHA)	% Remaining DHA
1 h	88%	89%	>95%
2 h	87%	86%	>95%
3 h	75%	74%	>95%
4 h	64%	72%	>95%
6 h	48%	51%	>95%
20 h	<5%	<5%	>95%

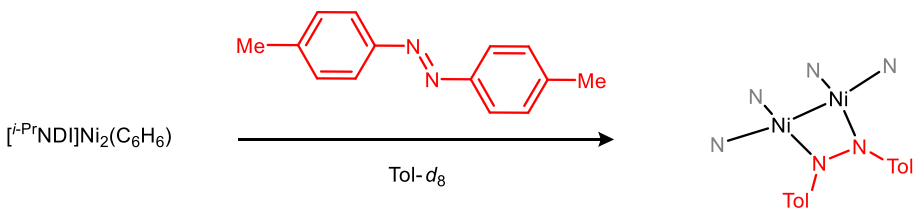

Variable-temperature NMR data for 1 + 4-tolylazobenzene. Under an atmosphere of N_2, a J-Young NMR tube was charged with 4-tolyl azide (2.8 mg, 0.014 mmol, 1.0 equiv), **1** (10.0 mg, 0.014 mmol, 1.0 equiv), and toluene-d_8 (600 µL). This lead to the formation of a new set up broad peaks observed by ^{1}H NMR. The spectrum was then taken over a range of temperatures from 200 to 350K, leading to a sharp set of diamagnetic peaks at low temperature, which broadened at high temperature.

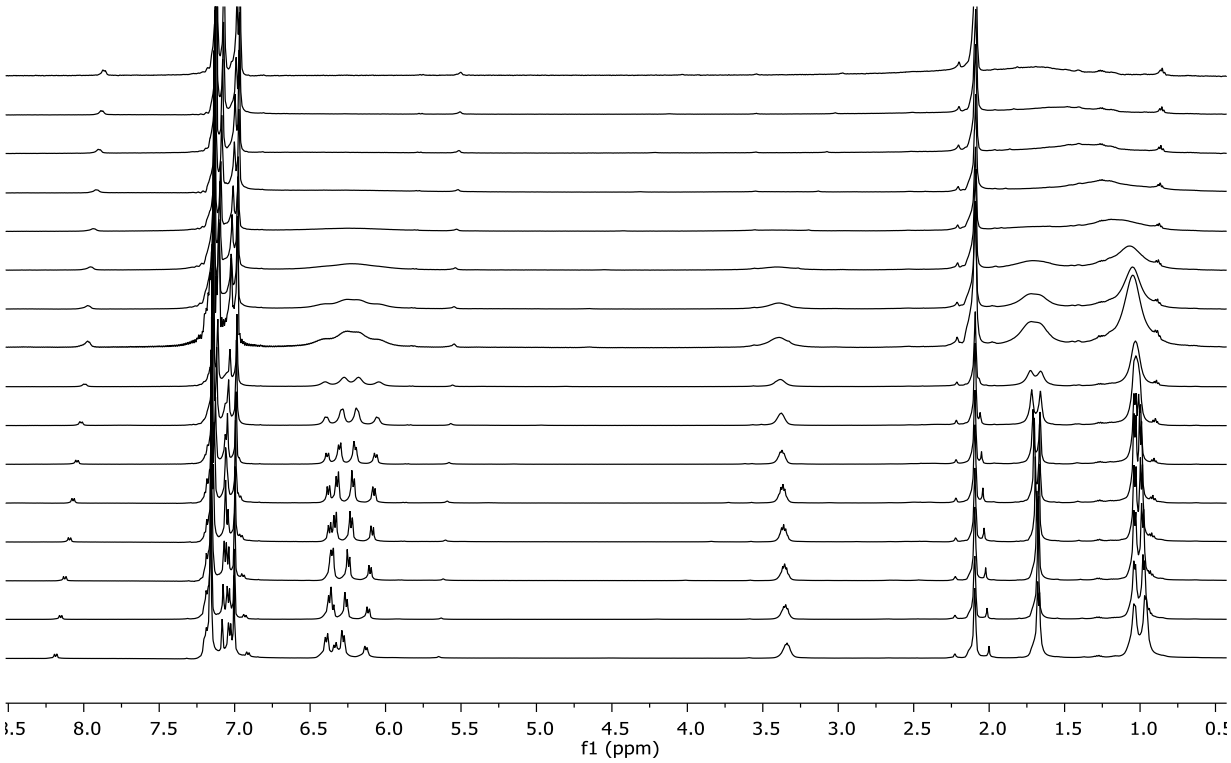

Figure S78. Variable-temperature ^{1}H NMR spectrum of the azoarene adduct formed on reaction of 4-azotoluene with **1** (200 to 350 K).

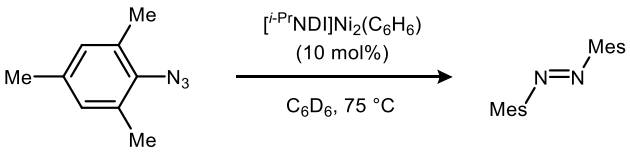

NMR kinetics studies for mesitylazide homocoupling. Under an atmosphere of N_2, an NMR tube equipped with a J. Young valve was charged with mesityl azide (103 µL of a 0.29 M solution in C_6D_6, 0.30 mmol, 1.0 equiv), **1** (400 µL of a 7.5 mM solution in C_6D_6, 0.03 mmol, 10 mol%) and C_6D_6 (97 µL). The reaction was then placed in an NMR spectrometer and heated at 75 °C. Data points were collected in 3-min intervals over 8 h.

The reaction rate was found to be zero order in [mesityl azide] ($k = 7.86 \pm 0.08$ mM/min).

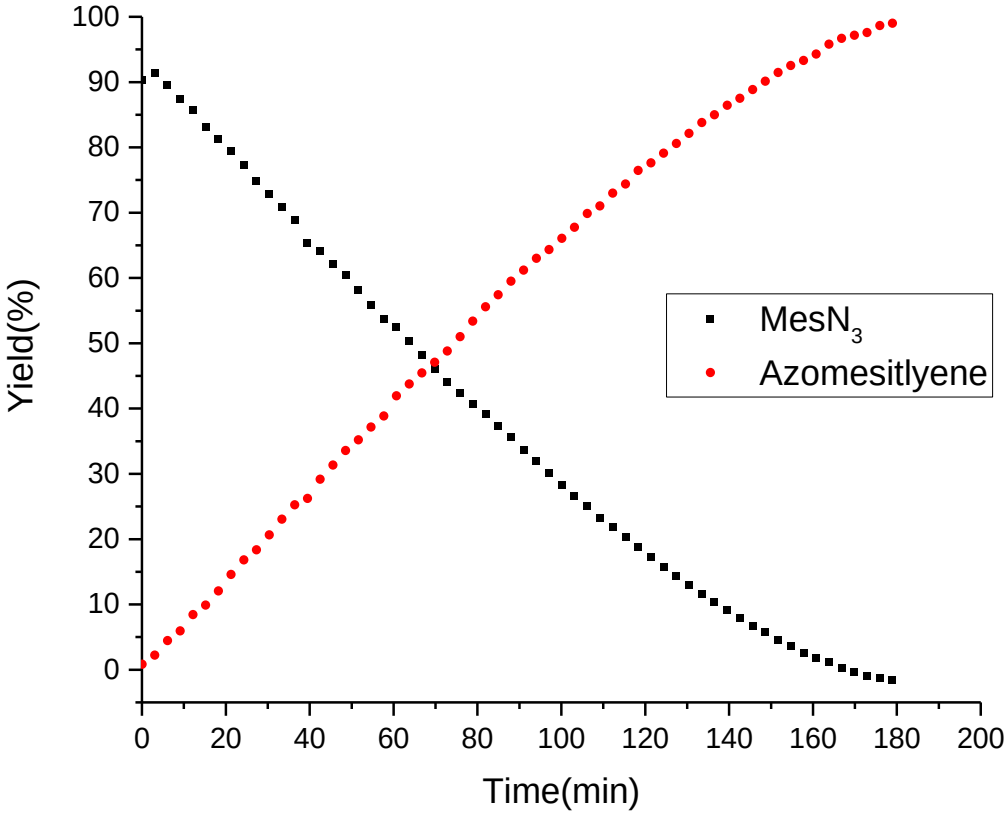

Figure S79. NMR kinetics plot of the formation of azomesitlyene catalyzed by **1**.

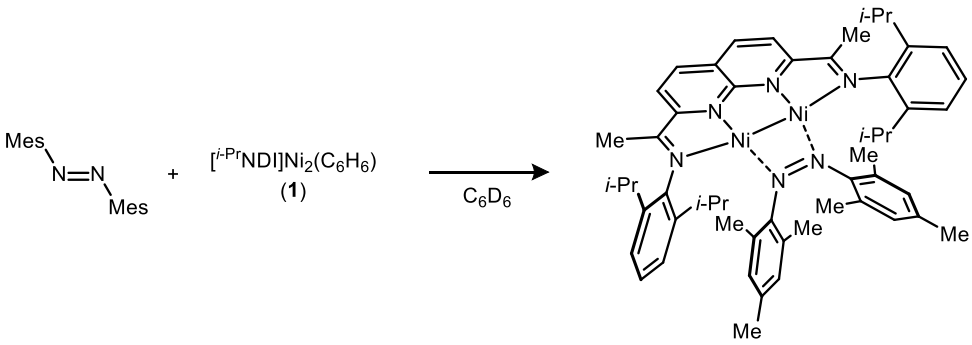

Azomesitylene binding under thermal conditions. Under an atmosphere of N_2, an NMR tube equipped with a J. Young valve was charged with **1** (3.9 mg, 0.005 mmol, 1.0 equiv), azomesitylene (10.6 mg, 0.040 mmol, 8.0 equiv), and C_6D_6 (600 µL). The NMR tube was placed in an oil bath and heated at 80 °C. Full conversion of **1** to the azomesitylene complex was observed after 30 days.

Azomesitylene binding under photolytic conditions. Under an atmosphere of N_2, an NMR tube equipped with a J. Young valve was charged with **1** (5.0 mg, 0.0069 mmol, 1.0 equiv), azomesitylene (1.8 mg, 0.0069 mmol, 1 equiv), and C_6D_6 (600 µL). The NMR tube was placed in a photobox and irradiated with 254 nm UV light[23] for 1.5 h. Full conversion to the azoarene complex was observed after 1.5 h.

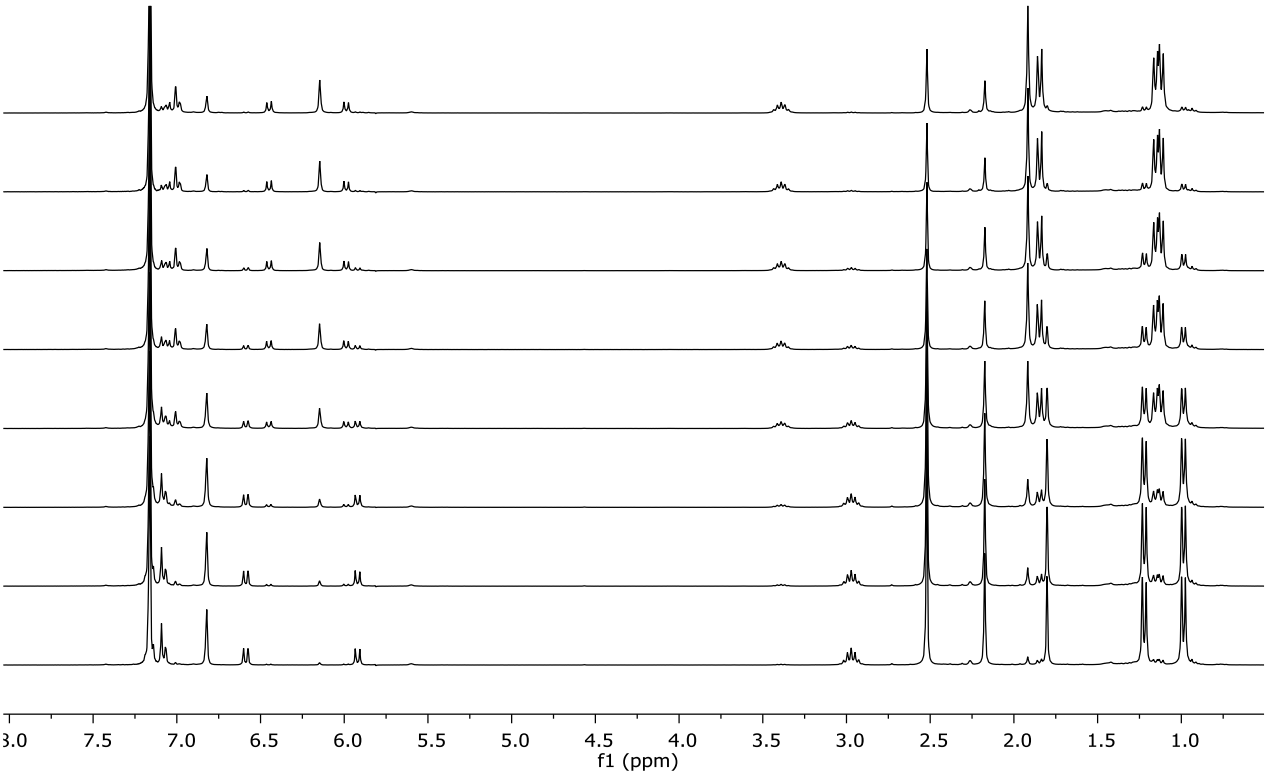

Figure S80. ^{1}H NMR spectrum of the azomesitylene binding experiment under thermal conditions.

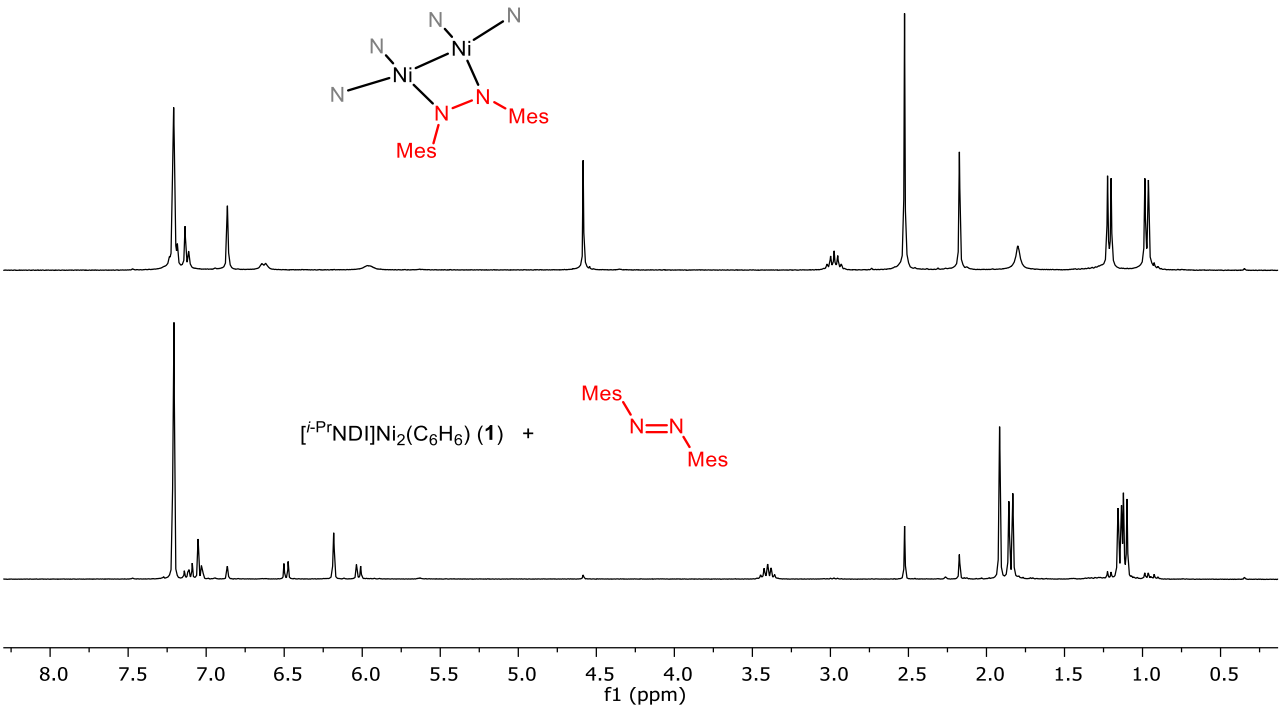

Figure S81. ^{1}H NMR spectrum of the asomesitylene binding experiment under photolytic conditions just after mixing (top) and after irradiation with UV light for 1.5 h (bottom).

8. X-Ray Diffraction Data

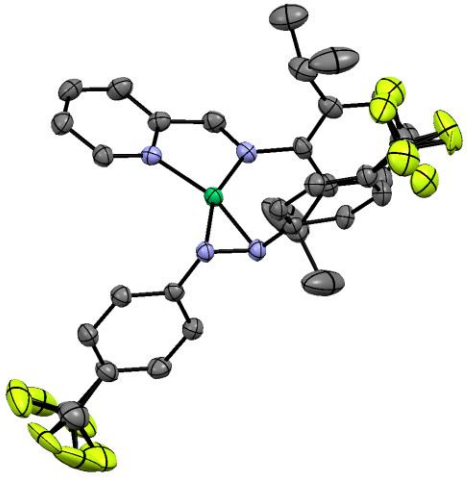

Compound 7

Crystal data	
Chemical formula	$C_{32}H_{30}F_6N_4Ni \cdot 0.146(C_7H_8) \cdot 0.104(C_5H_{12})$
M_r	664.24
Crystal system, space group	Orthorhombic, *Pbca*
Temperature (K)	150
a, *b*, *c* (Å)	16.3481 (3), 22.1973 (4), 35.0360 (7)
V (Å^3)	12714.0 (4)
Z	16
Radiation type	Cu $K\alpha$
μ (mm^{-1})	1.44
Crystal size (mm)	0.12 × 0.08 × 0.06
Data collection	
Diffractometer	Bruker AXS D8 Quest CMOS diffractometer
Absorption correction	Multi-scan *SADABS* 2016/2: Krause, L., Herbst-Irmer, R., Sheldrick G.M. & Stalke D., J. Appl. Cryst. 48 (2015) 3-10
T_{min}, T_{max}	0.650, 0.753
No. of measured, independent and observed [$I > 2\sigma(I)$] reflections	40453, 11767, 9216
R_{int}	0.040
$(\sin \theta/\lambda)_{max}$ (Å^{-1})	0.610
Refinement	
$R[F^2 > 2\sigma(F^2)]$, $wR(F^2)$, S	0.044, 0.118, 1.01
No. of reflections	11767
No. of parameters	1052
No. of restraints	1070

H-atom treatment	H-atom parameters constrained
$\Delta\rangle_{max}$, $\Delta\rangle_{min}$ (e Å^{-3})	0.54, -0.37

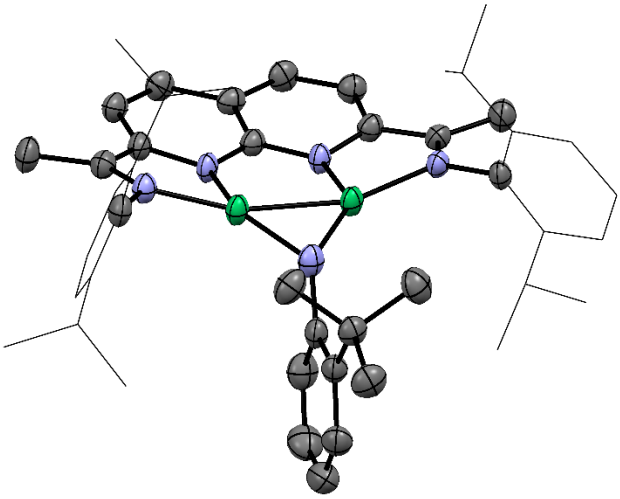

Compound 33

Crystal data	
Chemical formula	$2(C_{46}H_{57}N_5Ni_2)\cdot C_7H_8$
M_r	1686.90
Crystal system, space group	Monoclinic, $P2_1/n$
Temperature (K)	150
a, b, c (Å)	8.6475 (7), 22.8313 (17), 22.7875 (16)
β (°)	98.535 (3)
V (Å^3)	4449.2 (6)
Z	2
Radiation type	Cu $K\alpha$
μ (mm^{-1})	1.34
Crystal size (mm)	0.30 × 0.20 × 0.20
Data collection	
Diffractometer	Bruker AXS D8 Quest CMOS diffractometer
Absorption correction	Multi-scan TWINABS 2012/1: Krause, L., Herbst-Irmer, R., Sheldrick G.M. & Stalke D., J. Appl. Cryst. 48 (2015) 3-10
T_{min}, T_{max}	0.300, 0.754
No. of measured, independent and observed [$I > 2\sigma(I)$] reflections	73107, 8851, 7121
R_{int}	0.150
$(\sin \theta/\lambda)_{max}$ (Å^{-1})	0.619
Refinement	
$R[F^2 > 2\sigma(F^2)]$, $wR(F^2)$, S	0.069, 0.177, 1.03
No. of reflections	8851
No. of parameters	544
No. of restraints	46
H-atom treatment	H-atom parameters constrained

$\Delta\rangle_{max}$, $\Delta\rangle_{min}$ (e Å^{-3})	0.75, -0.68

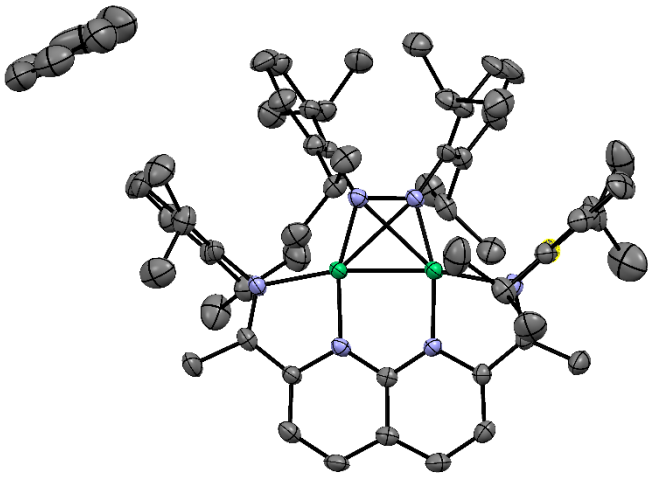

Compound 36

Crystal data	
Chemical formula	$C_{66}H_{84}N_6Ni_2$
M_r	1078.81
Crystal system, space group	Monoclinic, $P2_1/n$
Temperature (K)	123
a, b, c (Å)	12.0220 (5), 26.4576 (8), 18.2600 (6)
β (°)	97.465 (3)
V (Å^3)	5758.8 (4)
Z	4
Radiation type	Cu $K\alpha$
μ (mm^{-1})	1.15
Crystal size (mm)	0.30 × 0.20 × 0.16
Data collection	
Diffractometer	Rigaku Rapid II curved image plate diffractometer
Absorption correction	Multi-scan *SCALEPACK* (Otwinowski & Minor, 1997)
T_{min}, T_{max}	0.816, 1
No. of measured, independent and observed [$I > 2\sigma(I)$] reflections	40091, 10681, 9279
R_{int}	0.063

$(\sin \theta/\lambda)_{max}$ (Å^{-1})	0.618
Refinement	
$R[F^2 > 2\sigma(F^2)]$, $wR(F^2)$, S	0.054, 0.166, 1.08
No. of reflections	10681
No. of parameters	717
No. of restraints	186
H-atom treatment	H-atom parameters constrained
$\Delta\rho_{max}$, $\Delta\rho_{min}$ (e Å^{-3})	0.52, -0.47

9. DFT Calculations and Optimized Structures

Calculations addressing the thermodynamics of free nitrene release and comparison to imido formation. We were interested in the potential for free triplet nitrene release from a dinickel azide complex as an alternative mechanism to imido formation. We located a stable coordination mode for an $S = 1$ azide complex and found the formation of free triplet nitrene and a singlet N_2 complex to be endergonic by 16.3 kcal/mol (Figure S82). The subsequent substitution of N_2 for C_6H_6 is exergonic by 4.2 kcal/mol relative to the azide complex. By contrast, the formation of an imido species is much more energetically favorable, and the process is exergonic by 52.1 kcal/mol.

From the imido intermediate we considered the possibility of the formation of tetrazene intermediates upon addition of a second equivalent of azide. The formation of a 1,4-tetrazene complex is nearly energetically neutral from the imido complex. From this intermediate, the bis(imido) species is energetically accessible.

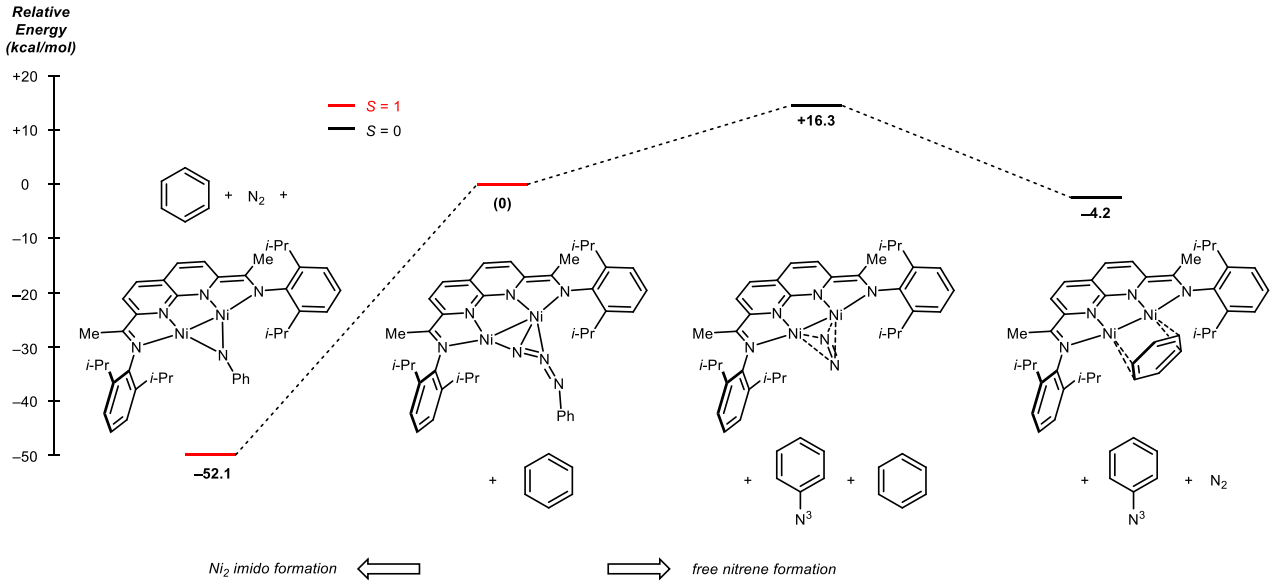

Figure S82. Thermodynamics of Ni_2(imido) formation (left pathway) vs. free triplet nitrene formation (right pathway) from an initial $Ni_2(N_3Ph)$ adduct. Energies are relative to: $Ni_2(N_3Ph)$ ($S = 1$) + C_6H_6. All structures are fully optimized and verified by frequency analysis.

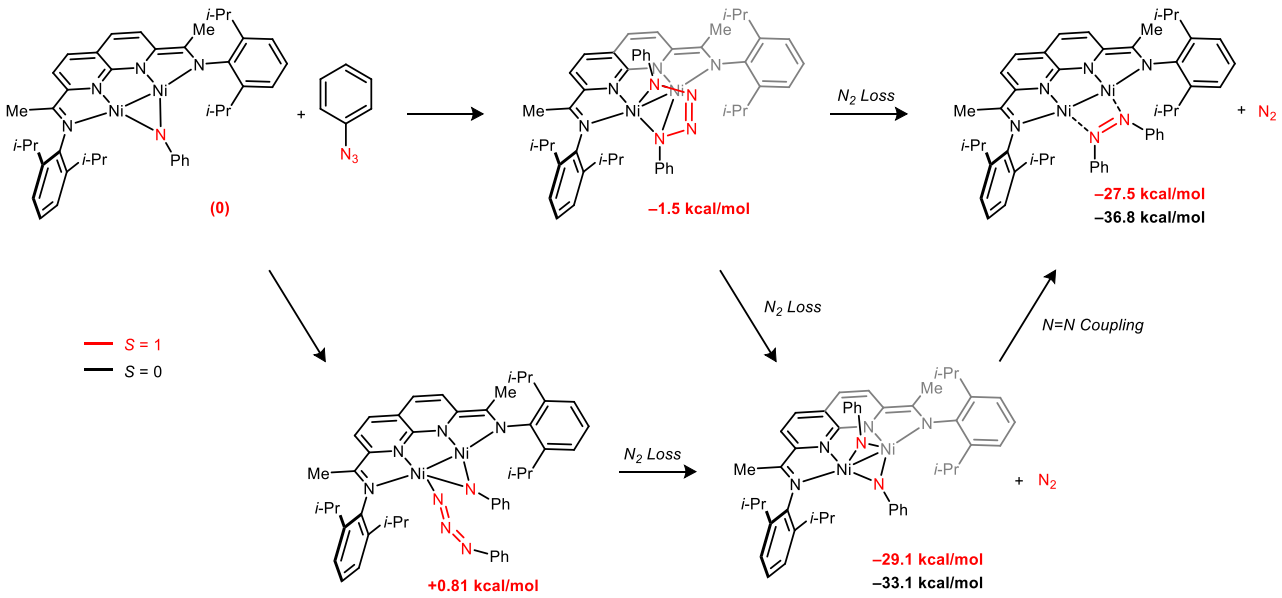

Figure S83. Calculated energies for possible intermediates leading from the Ni_2(imido) complex to the Ni_2(azoarene) product. Energies are relative to: Ni_2(imido) (S = 1) + PhN_3. All structures are fully optimized and verified by frequency analysis.

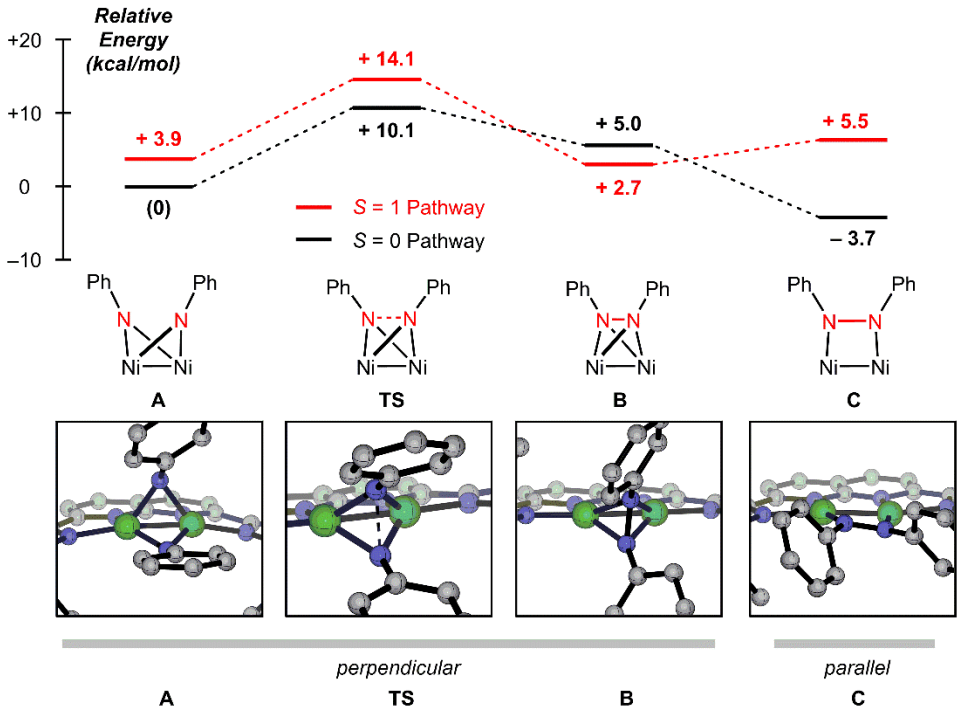

Figure S84. Energy profile for azoarene formation from a Ni_2 bis(imido) complex.

Computational Methods.[24] Geometry optimizations were performed using the Gaussian09 software package.[25] All geometries were fully optimized at the BP86/6-31G(d,p) level of DFT. Stationary points were verified by frequency analysis.

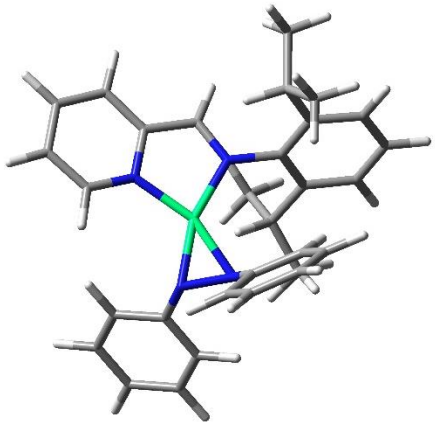

Charge: 0

Multiplicity: 1

Imaginary Frequencies: 0

Electronic Energy: -2889.91086561 Hartrees

Gibbs Free Energy (298.15 K): –2889.439275 Hartrees

Ni	0.5926660	0.3886680	-0.4362580
N	1.9741340	-0.6907440	-0.9781270
N	0.8922860	-1.4721310	-0.5512590
N	0.8712950	2.2301130	-0.7464130
N	-0.9190210	0.9401770	0.5010680
C	-1.4341860	-3.2060950	-3.6599600
C	-1.9206730	-3.1166050	-2.3424230
H	-2.9031310	-3.5315820	-2.0915230
C	-1.1511190	-2.5173610	-1.3385460
H	-1.5138420	-2.4643820	-0.3071160
C	0.1233180	-1.9792610	-1.6401180
C	0.6170250	-2.0862120	-2.9616890

H	1.6155610	-1.6971820	-3.1786960
C	-0.1618330	-2.6910020	-3.9575180
H	0.2350830	-2.7694660	-4.9760090
C	3.1207560	-0.8023280	-0.1536800
C	3.4143040	-1.9934300	0.5534050
H	2.6955800	-2.8152380	0.5067480
C	4.6059010	-2.1061290	1.2822000
H	4.8186350	-3.0369250	1.8199460
C	5.5299460	-1.0489580	1.3188320
C	5.2458620	0.1325540	0.6104230
H	5.9566010	0.9661320	0.6271120
C	4.0604790	0.2557100	-0.1220190
H	3.8459900	1.1770130	-0.6721320
C	-0.0455680	3.0321250	-0.0873050
C	-0.0421880	4.4314800	-0.2208540
H	-0.7749830	5.0271840	0.3316630
C	0.8866780	5.0325020	-1.0775320
H	0.9086010	6.1193600	-1.1982310
C	1.7800840	4.2122920	-1.7916610
H	2.5151710	4.6381430	-2.4795250
C	1.7362860	2.8265560	-1.6031830
H	2.4158210	2.1507080	-2.1293890
C	-0.9955270	2.2539760	0.6733400
H	-1.7394640	2.7135880	1.3346130
C	-1.8775250	0.1146860	1.1873700
C	-3.2313290	0.0960450	0.7579170
C	-4.1258200	-0.7348580	1.4622470
H	-5.1761020	-0.7653050	1.1526940
C	-3.7000900	-1.5260330	2.5340670
H	-4.4154800	-2.1631510	3.0643790
C	-2.3528140	-1.5087150	2.9212830

H	-2.0210180	-2.1367630	3.7537690
C	-1.4156870	-0.6971480	2.2598190
C	0.0466000	-0.6367370	2.6926480
H	0.6143180	-0.3618180	1.7822290
C	0.2669130	0.4717880	3.7472680
H	-0.0613220	1.4585890	3.3782270
H	1.3360220	0.5462420	4.0113670
H	-0.2994810	0.2539880	4.6703320
C	0.5961090	-1.9862930	3.1851890
H	1.6850340	-1.9113340	3.3398190
H	0.4133460	-2.7801690	2.4436080
H	0.1455620	-2.2919960	4.1467560
C	-3.7382730	0.9068090	-0.4378740
H	-2.8692120	1.3902060	-0.9163570
C	-4.7106380	2.0224400	0.0079570
H	-5.6052940	1.5984930	0.4966800
H	-5.0505130	2.6128770	-0.8607150
H	-4.2387340	2.7128450	0.7281450
C	-4.3931000	0.0022290	-1.5057250
H	-5.3039850	-0.4888500	-1.1205890
H	-3.6969330	-0.7830890	-1.8418870
H	-4.6876750	0.6019620	-2.3845350
H	6.4622810	-1.1452300	1.8840890
H	-2.0353050	-3.6836180	-4.4404070

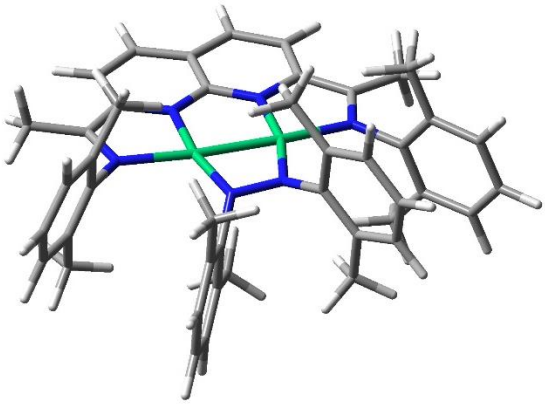

Charge: 0

Multiplicity: 1

Imaginary Frequencies: 0

Electronic Energy: –5049.84544543 Hartrees

Gibbs Free Energy (298.15 K): –5049.155070 Hartrees

Ni	1.09719700	0.82727600	0.09684800
Ni	-1.16945400	0.77999500	0.11863400
N	3.05013000	1.12072700	-0.02882400
N	-3.13432500	0.96492800	0.12889400
N	1.05414200	2.64968100	0.03410400
N	-1.22699600	2.60063800	0.12394800
N	0.68510900	-0.90195100	0.15432500
N	-0.69103000	-0.93954100	0.04376900
C	3.38716000	2.42012500	-0.06033400
C	-3.54330200	2.24275400	0.16129700
C	2.27230600	3.32586800	-0.01349400
C	2.29964800	4.73244700	-0.05514200
H	3.26206200	5.25100700	-0.09182800
C	1.11219100	5.46931400	-0.06552900
H	1.13605400	6.56246300	-0.10682800
C	-0.14162900	4.79722100	-0.02582100
C	-0.10499500	3.36034300	0.03616300

C	-1.42890800	5.40389300	-0.04467700
H	-1.50846700	6.49377400	-0.10138600
C	-2.57888600	4.61045300	0.00230700
H	-3.56561200	5.08176900	-0.02136000
C	-2.47941300	3.20872300	0.07821900
C	4.08281300	0.14164800	-0.16587600
C	4.63470400	-0.44570200	1.00114400
C	5.62280300	-1.43519800	0.85300100
H	6.05045000	-1.89454000	1.75123500
C	6.05702800	-1.83780600	-0.41720400
H	6.82430000	-2.61265700	-0.51593800
C	5.50352500	-1.24641400	-1.56112400
H	5.84126700	-1.55665500	-2.55694000
C	4.51301500	-0.25198500	-1.45961200
C	-4.09929300	-0.07173900	0.32999400
C	-4.25666200	-0.61124800	1.63246200
C	-5.19315400	-1.64261400	1.82539900
H	-5.32015600	-2.06205300	2.83018200
C	-5.95345300	-2.13608400	0.75618400
H	-6.67786500	-2.94030300	0.92124700
C	-5.77295700	-1.60456100	-0.52796400
H	-6.35327500	-1.99759500	-1.37049600
C	-4.84545000	-0.57378900	-0.76737600
C	1.37560000	-2.07615500	0.62246700
C	2.03839700	-2.95020800	-0.27363500
C	2.72605800	-4.05858400	0.25847100
H	3.24334500	-4.73608500	-0.43022900
C	2.76173000	-4.30080800	1.63585400
C	2.11320800	-3.42024500	2.51231100
H	2.14924100	-3.59489700	3.59395500
C	1.41491400	-2.29876200	2.02865600

C	0.72087500	-1.36091500	2.98931300
H	0.79116400	-0.31590700	2.63911500
C	2.00633100	-2.73656700	-1.76826200
H	1.90115300	-1.66964500	-2.01410800
C	-1.26679300	-1.97782700	-0.78530200
C	-1.85185600	-3.13559500	-0.21437300
C	-2.42783000	-4.08743200	-1.07677000
H	-2.88473800	-4.98304000	-0.64104300
C	-2.42978800	-3.90579800	-2.46561700
C	-1.85587600	-2.75306300	-3.01488800
H	-1.86156100	-2.60007300	-4.10058900
C	-1.26744300	-1.77172700	-2.19345100
C	-0.66058100	-0.53341300	-2.82171500
H	-0.28300700	0.16038700	-2.04905600
C	-1.86087800	-3.36732000	1.27789700
H	-2.13003000	-2.44642000	1.81797900
C	4.80796400	2.91421500	-0.17037500
H	5.51487600	2.17705300	0.23912600
H	4.93834200	3.86435200	0.37132600
H	5.09328200	3.09326900	-1.22370400
C	-4.97925500	2.66081100	0.35425400
H	-5.67649800	1.90322200	-0.03238300
H	-5.18612400	3.61925200	-0.14730700
H	-5.20616900	2.79570900	1.42831400
C	4.18087900	0.01844000	2.36475800
H	3.08192300	0.09926800	2.40127700
C	3.92543400	0.38888600	-2.69721200
H	4.29386500	1.42134900	-2.84212900
C	-3.41016800	-0.08436500	2.76818500
H	-3.72414300	0.92622900	3.08878100
C	-4.64905500	-0.01052600	-2.15598800

H	-3.58172500	-0.01543700	-2.43304200
H	1.15020700	-3.26413900	-2.22495900
H	2.92991100	-3.11561200	-2.23431800
H	-0.35722800	-1.58650600	3.06523900
H	1.15378800	-1.43711800	3.99985400
H	-2.58935300	-4.14936000	1.54551600
H	-0.86766700	-3.68672700	1.63847800
H	0.17986400	-0.79731900	-3.48792500
H	-1.40221100	0.00608200	-3.43744600
H	-5.20393200	-0.60250700	-2.90092600
H	-4.99264300	1.03722800	-2.23465200
H	-3.45993600	-0.74671400	3.64738200
H	-2.35967400	0.00591400	2.43483800
H	3.30494700	-5.16688900	2.02848000
H	-2.88532200	-4.65845700	-3.11783200
H	4.18874800	-0.18413800	-3.60075000
H	2.82564300	0.45776200	-2.63051600
H	4.51485400	-0.67454000	3.15288300
H	4.57829700	1.02213000	2.60587400

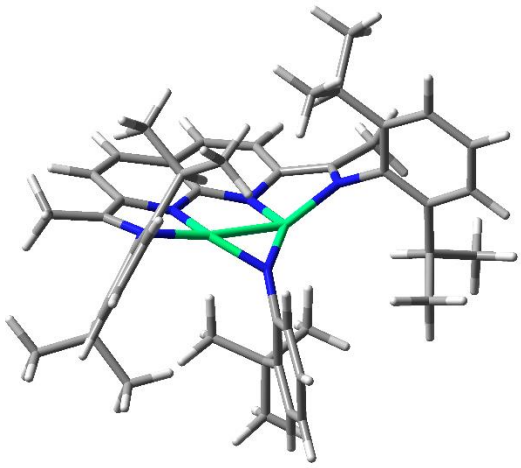

Charge: 0

Multiplicity: 1

Imaginary Frequencies: 0

Electronic Energy: –5077.92605368 Hartrees

Gibbs Free Energy (298.15 K): –5077.109486 Hartrees

Ni	1.1505560	0.5471040	-0.1204060
Ni	-1.1501240	0.5472220	-0.1203270
N	-2.9920050	0.8765940	0.2111620
N	-1.1542260	2.3146450	-0.6991760
N	1.1548260	2.3145270	-0.6990770
N	2.9924570	0.8761600	0.2110470
N	0.0001490	-0.7369790	-0.4104430
C	-4.8776300	2.5098170	-0.1420500
H	-5.3886950	2.3406470	-1.1071250
H	-4.9646490	3.5832010	0.0903480
H	-5.4251050	1.9404340	0.6252020
C	-3.4331210	2.0897550	-0.1924890
C	-2.3807370	2.9757910	-0.6022050
C	-2.4412090	4.3676600	-0.7976210
H	-3.4078750	4.8790850	-0.7712650
C	-1.2677160	5.1058490	-0.9810460

H	-1.3114730	6.1917860	-1.1094580
C	0.0004490	4.4634380	-0.9250280
C	0.0003550	3.0301060	-0.7467050
C	1.2687300	5.1056400	-0.9812290
H	1.3126340	6.1915610	-1.1097430
C	2.4421250	4.3672990	-0.7979070
H	3.4088730	4.8785770	-0.7717930
C	2.3814710	2.9754460	-0.6023050
C	3.4337340	2.0892780	-0.1926100
C	4.8783060	2.5091290	-0.1420970
H	5.4254820	1.9401660	0.6256890
H	4.9654450	3.5826470	0.0896110
H	5.3896130	2.3392000	-1.1069030
C	-3.8889510	-0.1547760	0.6222500
C	-3.8243510	-0.5641480	1.9894870
C	-4.6954910	-1.5748280	2.4285180
H	-4.6680700	-1.8916940	3.4755550
C	-5.5891270	-2.1938680	1.5434880
H	-6.2627850	-2.9787990	1.9031010
C	-5.5993870	-1.8245470	0.1939920
H	-6.2728410	-2.3409560	-0.4986020
C	-4.7546470	-0.8112110	-0.2999930
C	-4.7327100	-0.5185980	-1.8015610
H	-4.1230050	0.3866750	-1.9650870
C	-6.1410820	-0.2528680	-2.3780640
H	-6.0712990	0.0441130	-3.4387810
H	-6.6681000	0.5469380	-1.8307850
H	-6.7741970	-1.1561860	-2.3337230
C	-4.0446570	-1.6744240	-2.5659880
H	-3.0151810	-1.8405100	-2.2095240
H	-3.9986810	-1.4504790	-3.6461030

H	-4.6046270	-2.6177020	-2.4386500
C	-2.8081110	0.0923350	2.9213930
H	-1.9216830	0.2848900	2.2786710
C	-3.3054590	1.4593080	3.4447490
H	-4.2142710	1.3335370	4.0601710
H	-3.5430270	2.1488970	2.6190950
H	-2.5333860	1.9380140	4.0724220
C	-2.3702100	-0.8043080	4.0919480
H	-2.0354310	-1.7948180	3.7429330
H	-3.1835490	-0.9547910	4.8246910
H	-1.5330460	-0.3316020	4.6331350
C	3.8891750	-0.1552960	0.6223300
C	4.7551370	-0.8117270	-0.2996670
C	5.5997760	-1.8250440	0.1945360
H	6.2734480	-2.3414080	-0.4978770
C	5.5890970	-2.1944220	1.5440080
H	6.2626570	-2.9793460	1.9038210
C	4.6951380	-1.5754610	2.4287770
H	4.6673770	-1.8924250	3.4757760
C	3.8241390	-0.5647640	1.9895380
C	2.8076580	0.0917110	2.9211790
H	1.9213740	0.2842530	2.2782140
C	3.3048890	1.4586850	3.4446320
H	4.2137580	1.3329390	4.0599790
H	2.5328080	1.9372390	4.0724120
H	3.5423390	2.1483780	2.6190380
C	2.3694450	-0.8049250	4.0916120
H	2.0347760	-1.7954480	3.7425270
H	1.5321200	-0.3322310	4.6325650
H	3.1825630	-0.9553970	4.8246130
C	4.7333970	-0.5192840	-1.8012650

H	4.1239730	0.3861370	-1.9649880
C	4.0449600	-1.6750510	-2.5654610
H	3.9989110	-1.4512700	-3.6456080
H	3.0154840	-1.8407960	-2.2088320
H	4.6046970	-2.6184520	-2.4380150
C	6.1418430	-0.2540770	-2.3778000
H	6.7746710	-1.1575920	-2.3334250
H	6.6691190	0.5455970	-1.8305770
H	6.0721440	0.0428620	-3.4385340
C	-0.0002250	-1.6715680	-1.4592790
C	0.0000250	-1.1819610	-2.7953210
H	0.0004900	-0.0963400	-2.9410060
C	-0.0004120	-2.0499400	-3.8891080
H	-0.0002410	-1.6430530	-4.9058990
C	-0.0010440	-3.4349420	-3.6702860
H	-0.0013890	-4.1339980	-4.5126780
C	-0.0012170	-3.9249560	-2.3551940
H	-0.0016730	-5.0081170	-2.2095660
C	-0.0008150	-3.0885710	-1.2205500
C	-0.0009010	-3.6753600	0.2080730
C	1.2698030	-3.2074150	0.9658610
H	1.2625490	-3.6081400	1.9958570
H	1.3214660	-2.1089560	1.0174700
H	2.1841180	-3.5704820	0.4662100
C	-1.2711980	-3.2066630	0.9660420
H	-1.2639410	-3.6072340	1.9960960
H	-2.1858170	-3.5693210	0.4666430
H	-1.3222910	-2.1081730	1.0174720
C	-0.0013540	-5.2214390	0.2074360
H	0.8941040	-5.6380550	-0.2860010
H	-0.8971690	-5.6375190	-0.2858040

H	-0.0013520	-5.5810620	1.2508420

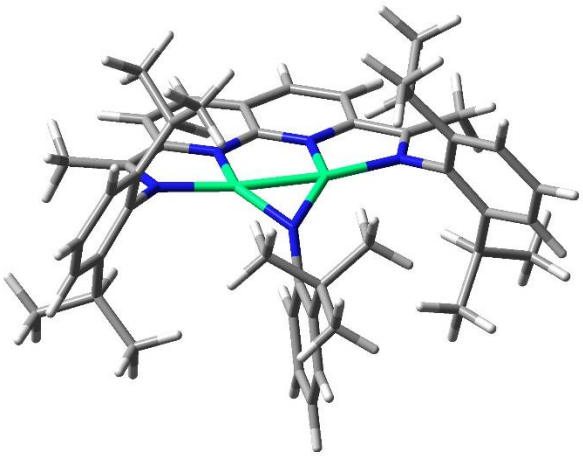

Charge: 0

Multiplicity: 3

Imaginary Frequencies: 0

Electronic Energy: –5077.92754475 Hartrees

Gibbs Free Energy (298.15 K): –5077.112786 Hartrees

Ni	1.1093600	0.6003990	0.0561330
Ni	-1.1093620	0.6002530	0.0559660
N	-3.0209030	0.8402980	0.1264300
N	-1.1400370	2.4134160	-0.3228530
N	1.1400740	2.4134870	-0.3224860
N	3.0208800	0.8401300	0.1262050
N	0.0001480	-0.7637350	-0.2663970
C	-4.8894040	2.5125010	-0.1441070
H	-5.3452690	2.4233890	-1.1473680
H	-4.9902860	3.5626460	0.1731640
H	-5.4779080	1.8805180	0.5389010
C	-3.4440940	2.0911590	-0.1509400
C	-2.3761070	3.0225930	-0.4247050
C	-2.4489210	4.3997690	-0.7349620
H	-3.4248780	4.8811740	-0.8457900
C	-1.2802630	5.1492810	-0.9060440

H	-1.3410540	6.2162110	-1.1426120
C	0.0000650	4.5335980	-0.7739180
C	0.0000150	3.1316880	-0.4722700
C	1.2804060	5.1491260	-0.9065040
H	1.3412170	6.2160120	-1.1432720
C	2.4490600	4.3995120	-0.7357600
H	3.4250360	4.8807200	-0.8472450
C	2.3761710	3.0224300	-0.4251120
C	3.4441420	2.0909250	-0.1514140
C	4.8894510	2.5122940	-0.1447410
H	5.4781360	1.8800540	0.5378630
H	4.9903210	3.5623130	0.1729630
H	5.3451010	2.4236480	-1.1481410
C	-3.9458660	-0.1880100	0.4904700
C	-3.9205850	-0.6422900	1.8438210
C	-4.8108820	-1.6598440	2.2248870
H	-4.8115730	-2.0139850	3.2602820
C	-5.6886060	-2.2381690	1.2971570
H	-6.3778360	-3.0287720	1.6118150
C	-5.6628760	-1.8191800	-0.0374350
H	-6.3253070	-2.3009130	-0.7649240
C	-4.7951430	-0.7989150	-0.4742020
C	-4.7322910	-0.4452620	-1.9611670
H	-4.1105750	0.4603690	-2.0694080
C	-6.1220750	-0.1399340	-2.5621010
H	-6.0217500	0.1965710	-3.6086040
H	-6.6529860	0.6454780	-1.9977890
H	-6.7677000	-1.0357580	-2.5691260
C	-4.0334630	-1.5741440	-2.7551790
H	-3.0164900	-1.7657230	-2.3766660
H	-3.9549410	-1.3047600	-3.8231510

H	-4.6058240	-2.5159460	-2.6846910
C	-2.9209540	-0.0273730	2.8210770
H	-2.0154560	0.1738470	2.2028720
C	-3.4140150	1.3280850	3.3770500
H	-4.3343450	1.1901670	3.9724350
H	-3.6336590	2.0468030	2.5715930
H	-2.6491750	1.7796070	4.0330660
C	-2.5192490	-0.9602960	3.9758590
H	-2.1902760	-1.9459830	3.6097180
H	-3.3516620	-1.1160600	4.6855770
H	-1.6886010	-0.5123470	4.5472210
C	3.9458990	-0.1880460	0.4905170
C	4.7954170	-0.7989210	-0.4739860
C	5.6634130	-1.8188220	-0.0369300
H	6.3260980	-2.3004760	-0.7642340
C	5.6891010	-2.2375680	1.2977530
H	6.3785620	-3.0278850	1.6126240
C	4.8110730	-1.6593800	2.2252600
H	4.8117150	-2.0133370	3.2607200
C	3.9205320	-0.6421230	1.8439100
C	2.9207060	-0.0272570	2.8210010
H	2.0152320	0.1737830	2.2027070
C	3.4135910	1.3283290	3.3768320
H	4.3339650	1.1905740	3.9721790
H	2.6487270	1.7798410	4.0328300
H	3.6331100	2.0469650	2.5712610
C	2.5190090	-0.9601050	3.9758560
H	2.1904920	-1.9459690	3.6097900
H	1.6880470	-0.5123350	4.5468900
H	3.3512820	-1.1154440	4.6858360
C	4.7323910	-0.4456800	-1.9610290

H	4.1106830	0.4599220	-2.0694850
C	4.0334100	-1.5748050	-2.7545810
H	3.9547350	-1.3057640	-3.8226250
H	3.0164880	-1.7662540	-2.3758670
H	4.6057880	-2.5165840	-2.6838570
C	6.1220680	-0.1405310	-2.5623090
H	6.7675150	-1.0364800	-2.5697200
H	6.6532740	0.6446840	-1.9980020
H	6.0214940	0.1961860	-3.6087200
C	0.0000160	-1.6831940	-1.3220590
C	0.0000210	-1.1767500	-2.6541510
H	0.0001540	-0.0882170	-2.7784080
C	-0.0001140	-2.0203950	-3.7670020
H	-0.0001160	-1.5943550	-4.7760490
C	-0.0002530	-3.4091810	-3.5741250
H	-0.0003640	-4.0924430	-4.4296550
C	-0.0002370	-3.9241380	-2.2685130
H	-0.0003410	-5.0101600	-2.1446500
C	-0.0000900	-3.1078960	-1.1194200
C	-0.0000810	-3.7234960	0.2948440
C	1.2701370	-3.2641470	1.0571290
H	1.2647620	-3.6777540	2.0822410
H	1.3138870	-2.1657710	1.1176760
H	2.1850190	-3.6178190	0.5518340
C	-1.2702270	-3.2640290	1.0571830
H	-1.2648060	-3.6775470	2.0823250
H	-2.1851490	-3.6176840	0.5519550
H	-1.3139140	-2.1656460	1.1176590
C	-0.0001550	-5.2690330	0.2685810
H	0.8953680	-5.6771510	-0.2319210
H	-0.8957250	-5.6770680	-0.2319000

H	-0.0001550	-5.6467780	1.3056810

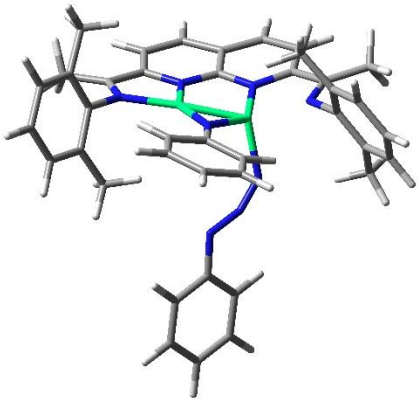

Charge: 0

Multiplicity: 3

Imaginary Frequencies: 0

Electronic Energy: –5002.06345819 Hartrees

Gibbs Free Energy (298.15 K): –5001.47561 Hartrees

Ni	-1.1194420	0.8882740	0.1354620
Ni	1.0468870	0.5894860	-0.0543640
N	2.9967560	1.1277200	0.2898650
N	1.1313270	2.2635490	-0.9983360
N	-1.1426180	2.2886380	-1.0620010
N	-3.0085530	1.1342010	0.0754150
N	-0.1425110	-0.2552670	1.0554280
C	4.8013190	2.7591680	-0.3525190
H	4.7900370	3.8230200	-0.0589670
H	5.2757990	2.7021700	-1.3486090
H	5.4283720	2.2062920	0.3613280
C	3.3993060	2.2026370	-0.3860920
C	2.3519320	2.8807930	-1.1325000
C	2.4600940	4.0780720	-1.8755360
H	3.4374950	4.5528130	-2.0004060
C	1.3210990	4.6640190	-2.4416700
H	1.4067770	5.5892000	-3.0202360

C	0.0345210	4.0914610	-2.2160770
C	0.0123110	2.8842890	-1.4447240
C	-1.2345070	4.5996180	-2.6304060
H	-1.2755960	5.5055570	-3.2433290
C	-2.4183710	3.9679940	-2.2299540
H	-3.3873240	4.3814070	-2.5249400
C	-2.3650810	2.8205170	-1.4076640
C	-3.4385500	2.0958040	-0.7672700
C	-4.8857180	2.4054950	-1.0435870
H	-5.0731130	2.4517350	-2.1301930
H	-5.1762730	3.3858910	-0.6227110
H	-5.5447350	1.6410650	-0.6070680
C	3.9060520	0.3650360	1.0801960
C	4.8384250	-0.5165230	0.4679180
C	5.6618290	-1.2968770	1.3019030
H	6.3805450	-1.9817220	0.8374710
C	5.5709060	-1.2173550	2.6977190
H	6.2203970	-1.8341860	3.3272100
C	4.6341910	-0.3545630	3.2835040
H	4.5483970	-0.2952010	4.3743320
C	3.7837060	0.4397460	2.4946170
C	2.7553900	1.3503080	3.1234610
H	1.7429790	1.1104840	2.7503890
C	4.9388410	-0.6340800	-1.0371730
H	3.9388010	-0.6884760	-1.4978870
C	-3.9425850	0.3562310	0.8279380
C	-4.5603730	0.9054330	1.9827240
C	-5.4329540	0.0849390	2.7222580
H	-5.9131980	0.4970500	3.6170390
C	-5.6834790	-1.2398950	2.3392750
H	-6.3658900	-1.8614880	2.9279870

C	-5.0416720	-1.7723200	1.2120690
H	-5.2155270	-2.8142670	0.9210660
C	-4.1569300	-0.9939040	0.4448730
C	-3.4046510	-1.5693080	-0.7288030
H	-2.3176130	-1.4194610	-0.5883160
C	-4.2630310	2.3196620	2.4278220
H	-4.7249480	3.0738770	1.7652350
C	-0.1180610	-1.2730650	1.9644670
C	-1.2939530	-1.6198550	2.6995480
H	-2.2151310	-1.0621600	2.5075180
C	-1.2613450	-2.6472780	3.6429560
H	-2.1733900	-2.8963070	4.1961660
C	-0.0727640	-3.3631150	3.8863090
H	-0.0558070	-4.1691250	4.6268110
C	1.0927440	-3.0345880	3.1673680
H	2.0214510	-3.5865350	3.3471900
C	1.0801100	-2.0076620	2.2227740
H	5.5013180	-1.5392530	-1.3170340
H	5.4645910	0.2281580	-1.4877880
H	1.9825070	-1.7492400	1.6607210
H	2.7573740	1.2492160	4.2201540
H	2.9388340	2.4111840	2.8757760
H	-4.6466590	2.4970510	3.4451790
H	-3.1769300	2.5172640	2.4259240
H	-3.5997190	-2.6467420	-0.8408680
H	-3.6699960	-1.0702440	-1.6778760
C	-0.0369030	-3.7765440	-2.4559390
C	0.8039980	-3.7942170	-3.5930690
C	-1.0075140	-4.7906600	-2.2978000
C	0.6678640	-4.8097460	-4.5471570
H	1.5578910	-3.0092950	-3.7155480

C	-1.1350710	-5.7984180	-3.2606650
H	-1.6451200	-4.7697000	-1.4090250
C	-0.3004450	-5.8164640	-4.3912160
H	1.3255410	-4.8135600	-5.4233200
H	-1.8913030	-6.5789170	-3.1247330
H	-0.4014790	-6.6065820	-5.1417060
N	1.4521150	-0.9227280	-1.1400970
N	0.9101600	-1.9056760	-1.5229160
N	0.0059090	-2.7985750	-1.4369230

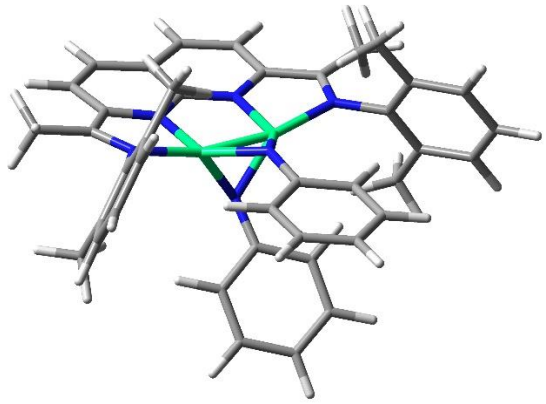

Charge: 0

Multiplicity: 1

Imaginary Frequencies: 0

Electronic Energy: –4892.57829958 Hartrees

Gibbs Free Energy (298.15 K): – 4891.989757 Hartrees

Ni	1.1058060	0.4884460	-0.0369120
Ni	-1.0675660	0.5093420	-0.0886400
N	3.0086090	0.7351880	-0.3576340
N	-2.9666680	0.8082180	-0.4245080
N	1.1835740	2.3634310	0.1090160
N	-1.0996510	2.3914960	0.0504030
N	0.0223710	-0.8453550	-0.7390280
N	-0.0309020	0.2489280	1.4537760
C	3.4555600	2.0006080	-0.1884610
C	-3.3766650	2.0895800	-0.2868720
C	2.4178340	2.9636610	0.0862670
C	2.5116730	4.3672800	0.2554900
H	3.4919610	4.8523570	0.2722310
C	1.3528580	5.1375820	0.3846370
H	1.4265830	6.2233580	0.5030070
C	0.0642560	4.5261770	0.3197690
C	0.0485850	3.0990570	0.1842690

C	-1.2090050	5.1715920	0.3301110
H	-1.2593960	6.2591120	0.4444550
C	-2.3808730	4.4296990	0.1590000
H	-3.3497420	4.9374240	0.1404360
C	-2.3163010	3.0243160	-0.0058930
C	3.9383040	-0.3148940	-0.6397050
C	4.7869160	-0.8388900	0.3717480
C	5.6407270	-1.9087860	0.0384510
H	6.2910660	-2.3248180	0.8165160
C	5.6674800	-2.4424470	-1.2549880
H	6.3401510	-3.2726560	-1.4934250
C	4.8186280	-1.9176740	-2.2409130
H	4.8259110	-2.3383830	-3.2525320
C	3.9375020	-0.8617340	-1.9538280
C	-3.9275680	-0.2267860	-0.6494140
C	-4.7656660	-0.6810590	0.4053520
C	-5.6493230	-1.7456070	0.1412960
H	-6.2925270	-2.1084770	0.9511270
C	-5.7153020	-2.3401590	-1.1247950
H	-6.4104930	-3.1655910	-1.3089080
C	-4.8793290	-1.8809610	-2.1529370
H	-4.9208690	-2.3469380	-3.1437820
C	-3.9698680	-0.8310500	-1.9362600
C	0.0183950	-2.2117840	-0.7180640
C	-1.2019980	-2.9518290	-0.7957780
C	-1.1900910	-4.3468120	-0.8676540
H	-2.1411550	-4.8869440	-0.9318470
C	0.0233300	-5.0573170	-0.8483200
C	1.2346010	-4.3457990	-0.7498110
H	2.1868500	-4.8866720	-0.7202190
C	1.2403020	-2.9525480	-0.6786100

C	-0.0813530	-0.9231200	2.1771310
C	1.0412910	-1.3157590	2.9694620
C	0.9567860	-2.3886750	3.8588400
H	1.8340710	-2.6603890	4.4567230
C	-0.2392750	-3.1182120	3.9955170
C	-1.3503850	-2.7598160	3.2138050
H	-2.2845140	-3.3263100	3.2971890
C	-1.2770970	-1.6921840	2.3143640
C	4.9012760	2.4023290	-0.3154790
H	5.4504420	1.7006870	-0.9617070
H	5.4082550	2.4125320	0.6671790
H	4.9887880	3.4143090	-0.7419540
C	-4.8040990	2.5430010	-0.4508050
H	-5.4081570	1.7788670	-0.9617300
H	-4.8477360	3.4744490	-1.0396160
H	-5.2801510	2.7526440	0.5247820
C	4.7923450	-0.2843490	1.7795760
H	3.8410980	0.2108130	2.0296210
C	2.9886250	-0.3299320	-3.0018400
H	3.1597730	0.7416090	-3.2073260
C	-4.7241670	-0.0512740	1.7810410
H	-3.7004900	0.2322200	2.0751910
C	-3.0436780	-0.3598720	-3.0329720
H	-1.9905300	-0.4264900	-2.7048200
H	-5.1201890	-0.7466010	2.5383820
H	-5.3414270	0.8648260	1.8292200
H	-3.1693350	-0.9685550	-3.9422080
H	-3.2249090	0.6970070	-3.2976860
H	3.0958390	-0.8842330	-3.9475110
H	1.9440720	-0.4214460	-2.6526060
H	5.5978660	0.4611300	1.9188810

H	4.9701270	-1.0870810	2.5138220
H	-2.1480090	-2.4033490	-0.8119880
H	0.0261840	-6.1507770	-0.8998490
H	2.1818620	-2.4021240	-0.5996040
H	1.9649660	-0.7365420	2.8795360
H	-0.3004480	-3.9568020	4.6961390
H	-2.1392060	-1.4168860	1.6998050

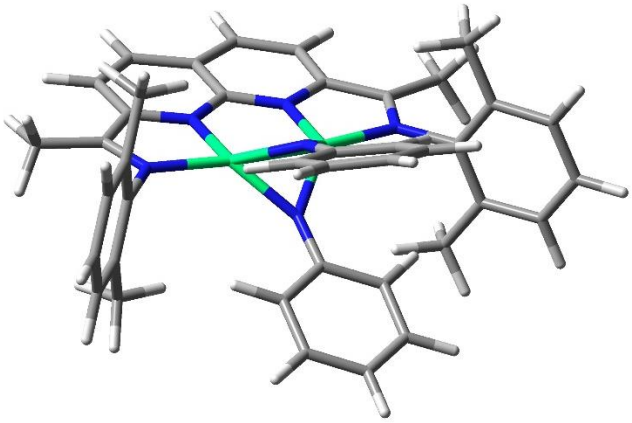

Charge: 0

Multiplicity: 1

Imaginary Frequencies: 1

Electronic Energy: – 4892.56156792 Hartrees

Gibbs Free Energy (298.15 K): – 4891.973713 Hartrees

Ni	-1.1206390	0.6317380	-0.0000320
Ni	1.1206180	0.6317260	-0.0000520
N	-3.0291450	0.8645590	0.0000990
N	3.0291190	0.8645290	0.0000160
N	-1.1426520	2.4807110	-0.0000510
N	1.1426500	2.4807020	-0.0000820
N	-0.0000060	-0.6082030	0.8962560
N	-0.0000250	-0.6080750	-0.8965230
C	-3.4457930	2.1501330	0.0000730
C	3.4457820	2.1501000	-0.0000130
C	-2.3804770	3.1099600	-0.0000220
C	-2.4445370	4.5226590	-0.0000680
H	-3.4180220	5.0215330	-0.0000530
C	-1.2775880	5.2871950	-0.0001330
H	-1.3338830	6.3802150	-0.0001640
C	0.0000080	4.6521550	-0.0001440
C	0.0000020	3.2198760	-0.0001000

C	1.2776100	5.2871850	-0.0001820
H	1.3339130	6.3802040	-0.0002240
C	2.4445510	4.5226400	-0.0001540
H	3.4180400	5.0215070	-0.0001930
C	2.3804820	3.1099410	-0.0000890
C	-4.0073870	-0.1762850	0.0002120
C	-4.4668390	-0.6986020	-1.2381720
C	-5.3960930	-1.7553310	-1.2126180
H	-5.7559570	-2.1663330	-2.1628400
C	-5.8607500	-2.2826450	0.0004640
H	-6.5805940	-3.1074980	0.0005620
C	-5.3957490	-1.7553430	1.2134220
H	-5.7553470	-2.1663520	2.1637420
C	-4.4664860	-0.6986190	1.2387240
C	4.0073930	-0.1762870	0.0001700
C	4.4668060	-0.6986840	-1.2381940
C	5.3960900	-1.7553850	-1.2126000
H	5.7559220	-2.1664510	-2.1628070
C	5.8608180	-2.2825910	0.0005020
H	6.5806850	-3.1074240	0.0006310
C	5.3958600	-1.7552070	1.2134400
H	5.7555140	-2.1661310	2.1637760
C	4.4665660	-0.6985080	1.2387020
C	-0.0000060	-1.8931270	1.4236000
C	1.2216950	-2.5515420	1.7199340
C	1.2145560	-3.8073840	2.3366500
H	2.1659440	-4.2996410	2.5648940
C	-0.0000030	-4.4396960	2.6542980
C	-1.2145610	-3.8074760	2.3364620
H	-2.1659470	-4.2998070	2.5645590
C	-1.2217030	-2.5516340	1.7197490

C	-0.0000220	-1.8929270	-1.4240390
C	-1.2217200	-2.5513140	-1.7204490
C	-1.2145780	-3.8070820	-2.3373130
H	-2.1659650	-4.2993200	-2.5656070
C	-0.0000180	-4.4393500	-2.6550460
C	1.2145380	-3.8071590	-2.3371440
H	2.1659240	-4.2994570	-2.5653080
C	1.2216760	-2.5513900	-1.7202810
C	-4.9033190	2.5293870	0.0001420
H	-5.4240910	2.1230240	0.8848630
H	-5.4241120	2.1232660	-0.8846700
H	-5.0325670	3.6212930	0.0002730
C	4.9033320	2.5292650	-0.0000210
H	5.0326370	3.6211540	0.0007730
H	5.4239320	2.1236810	-0.8852040
H	5.4242460	2.1223320	0.8843370
C	-3.9672250	-0.1223040	-2.5444240
H	-2.8677240	-0.0246330	-2.5388720
C	-3.9664590	-0.1223520	2.5448290
H	-4.3691960	0.8907180	2.7287760
C	3.9671130	-0.1225010	-2.5444670
H	2.8676010	-0.0249560	-2.5389090
C	3.9665770	-0.1221600	2.5447870
H	2.8670230	-0.0250600	2.5391360
H	4.2615540	-0.7578780	-3.3947640
H	4.3702120	0.8904010	-2.7285620
H	4.2612220	-0.7571860	3.3952740
H	4.3692360	0.8909630	2.7286190
H	-4.2609960	-0.7574810	3.3952770
H	-2.8669130	-0.0251660	2.5391120
H	-4.3704470	0.8905580	-2.7284720

H	-4.2615990	-0.7576780	-3.3947460
H	2.1628800	-2.0580130	1.4620290
H	-0.0000030	-5.4215140	3.1385360
H	-2.1628860	-2.0581720	1.4617110
H	-2.1629050	-2.0578210	-1.4624780
H	-0.0000160	-5.4211090	-3.1394020
H	2.1628560	-2.0579550	-1.4621860

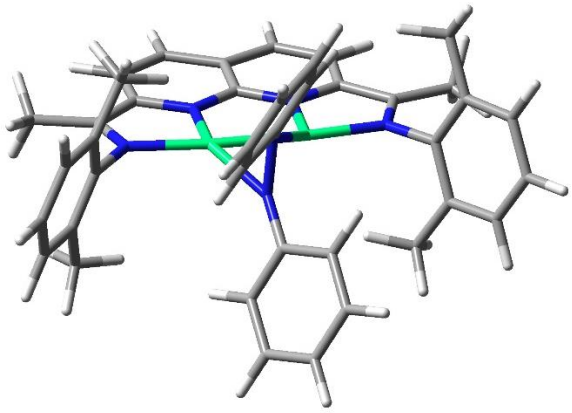

Charge: 0

Multiplicity: 1

Imaginary Frequencies: 0

Electronic Energy: – 4892.57068902 Hartrees

Gibbs Free Energy (298.15 K): – 4891.981767 Hartrees

Ni	-1.1248290	0.6441090	0.0214700
Ni	1.1246700	0.6442220	-0.0213740
N	-3.0245890	0.8548120	0.0755050
N	3.0243990	0.8550180	-0.0752170
N	-1.1413850	2.4658590	0.0310270
N	1.1411560	2.4659630	-0.0310120
N	0.0806970	-0.7738870	0.7127240
N	-0.0807540	-0.7738010	-0.7127850
C	-3.4488120	2.1372800	0.0973650
C	3.4485750	2.1375150	-0.0972110
C	-2.3803320	3.0943090	0.0758950
C	-2.4453690	4.5066250	0.0811850
H	-3.4223080	4.9986180	0.1091650
C	-1.2795670	5.2729440	0.0430170
H	-1.3363790	6.3659040	0.0444730
C	-0.0002180	4.6381970	0.0001020
C	-0.0001510	3.2091600	0.0000460

C	1.2790940	5.2730480	-0.0427520
H	1.3358160	6.3660130	-0.0441010
C	2.4449540	4.5068430	-0.0809770
H	3.4218340	4.9989560	-0.1088480
C	2.3800700	3.0945050	-0.0758000
C	-3.9486300	-0.2322780	0.0706070
C	-4.6062790	-0.6161900	-1.1286180
C	-5.4562000	-1.7373910	-1.0938310
H	-5.9651760	-2.0432340	-2.0152290
C	-5.6510510	-2.4648030	0.0882650
H	-6.3140050	-3.3361790	0.0932200
C	-4.9825180	-2.0816600	1.2597640
H	-5.1220340	-2.6527820	2.1845890
C	-4.1210940	-0.9706850	1.2723880
C	3.9486020	-0.2319300	-0.0704480
C	4.1216750	-0.9697670	-1.2724860
C	4.9833310	-2.0805690	-1.2600160
H	5.1233400	-2.6512490	-2.1850390
C	5.6514660	-2.4641000	-0.0884170
H	6.3146030	-3.3353370	-0.0935010
C	5.4559880	-1.7372660	1.0939340
H	5.9646560	-2.0434180	2.0153990
C	4.6058350	-0.6162510	1.1288710
C	-0.0432180	-1.9283470	1.5203540
C	0.7363880	-1.9728400	2.6980720
C	0.5995500	-3.0387600	3.5948140
H	1.2151380	-3.0644170	4.5001540
C	-0.3188130	-4.0706970	3.3362220
C	-1.1052660	-4.0201930	2.1720670
H	-1.8315230	-4.8137120	1.9666320
C	-0.9785050	-2.9607180	1.2651600

C	0.0434260	-1.9281120	-1.5205870
C	-0.7365170	-1.9728060	-2.6980800
C	-0.5995140	-3.0385700	-3.5949750
H	-1.2153680	-3.0643870	-4.5001310
C	0.3193520	-4.0701600	-3.3367660
C	1.1061230	-4.0194580	-2.1728350
H	1.8327610	-4.8127050	-1.9676940
C	0.9792070	-2.9601300	-1.2657800
C	-4.8980720	2.5443520	0.1507210
H	-5.5334720	1.7025530	0.4641810
H	-5.2616660	2.8923970	-0.8342620
H	-5.0442390	3.3748350	0.8617070
C	4.8978990	2.5443720	-0.1503730
H	5.5326300	1.7036550	-0.4681250
H	5.2628570	2.8878620	0.8357250
H	5.0435910	3.3778540	-0.8578880
C	-4.3909800	0.1517970	-2.4132970
H	-3.3269390	0.4096920	-2.5529700
C	-3.3802650	-0.5539680	2.5202400
H	-3.8192400	0.3546000	2.9723050
C	3.3812110	-0.5526440	-2.5204210
H	2.3364160	-0.3043270	-2.2650760
C	4.3897700	0.1511040	2.4137950
H	3.3255070	0.4081520	2.5533660
H	3.3892110	-1.3509100	-3.2782460
H	3.8199330	0.3564220	-2.9717350
H	4.7281500	-0.4356870	3.2828400
H	4.9478430	1.1054210	2.4247300
H	-3.3875260	-1.3527080	3.2775730
H	-2.3357180	-0.3049870	2.2645450
H	-4.9498170	1.1056760	-2.4238130

H	-4.7290590	-0.4349520	-3.2824890
H	1.4453330	-1.1606680	2.8861890
H	-0.4246030	-4.9046220	4.0372170
H	-1.6079160	-2.9198930	0.3729160
H	-1.4458730	-1.1609100	-2.8858530
H	0.4252830	-4.9039690	-4.0378760
H	1.6088720	-2.9191420	-0.3737190

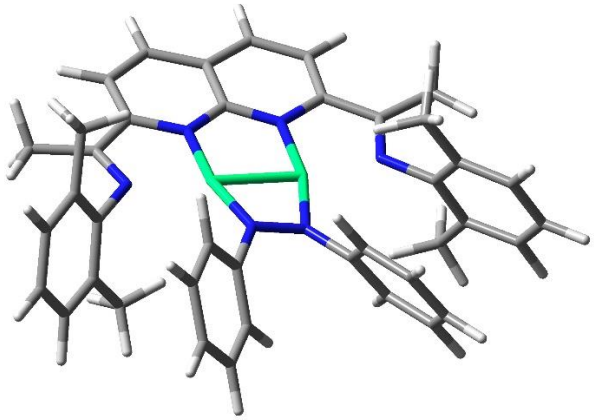

Charge: 0

Multiplicity: 1

Imaginary Frequencies: 0

Electronic Energy: – 4892.59061696 Hartrees

Gibbs Free Energy (298.15 K): – 4891.995589 Hartrees

Ni	-1.1315060	0.6856050	0.0652260
Ni	1.1315500	0.6856000	-0.0648270
N	-3.1058010	0.9314550	-0.0331540
N	3.1058650	0.9314700	0.0336190
N	-1.1404980	2.5028810	-0.0000420
N	1.1405310	2.5028800	-0.0000540
N	-0.6731360	-1.0432590	0.1240930
N	0.6731850	-1.0432220	-0.1238750
C	-3.4667910	2.2236310	-0.0962270
C	3.4668340	2.2236750	0.0962820
C	-2.3722350	3.1504580	-0.0464670
C	-2.4375490	4.5550170	-0.0659430
H	-3.4144970	5.0460400	-0.1015290
C	-1.2693700	5.3216100	-0.0332800
H	-1.3194840	6.4146500	-0.0381980
C	0.0000220	4.6797270	-0.0001830
C	0.0000160	3.2396780	-0.0000620

C	1.2694110	5.3216190	0.0328510
H	1.3195220	6.4146590	0.0376140
C	2.4375860	4.5550260	0.0656770
H	3.4145420	5.0460370	0.1012480
C	2.3722620	3.1504660	0.0464230
C	-4.1260940	-0.0655100	-0.0999310
C	-4.2721000	-0.7978890	-1.3058860
C	-5.2709390	-1.7839310	-1.3780440
H	-5.3869950	-2.3533660	-2.3069720
C	-6.1064270	-2.0460200	-0.2834890
H	-6.8816080	-2.8159720	-0.3552580
C	-5.9349110	-1.3307210	0.9098530
H	-6.5744220	-1.5451540	1.7741990
C	-4.9437720	-0.3387840	1.0286930
C	4.1261160	-0.0655230	0.1002640
C	4.9438780	-0.3387090	-1.0283340
C	5.9349440	-1.3307140	-0.9095180
H	6.5745110	-1.5450960	-1.7738360
C	6.1063310	-2.0461620	0.2837540
H	6.8814780	-2.8161510	0.3554860
C	5.2707550	-1.7841820	1.3782640
H	5.3867060	-2.3537510	2.3071230
C	4.2719560	-0.7980980	1.3061340
C	-1.4236380	-2.2487280	0.0366430
C	-2.3483460	-2.5411800	1.0594910
C	-3.1093530	-3.7158640	1.0081320
H	-3.8220290	-3.9312280	1.8102000
C	-2.9601090	-4.6108150	-0.0634530
C	-2.0469770	-4.3161160	-1.0901060
H	-1.9300130	-5.0034730	-1.9347290
C	-1.2810850	-3.1449740	-1.0474980

C	1.4236510	-2.2487590	-0.0368170
C	2.3482980	-2.5410010	-1.0597670
C	3.1092720	-3.7157260	-1.0086870
H	3.8219070	-3.9309420	-1.8108310
C	2.9600460	-4.6109020	0.0627100
C	2.0469650	-4.3164070	1.0894670
H	1.9300190	-5.0039440	1.9339450
C	1.2811130	-3.1452300	1.0471400
C	-4.8824430	2.7158540	-0.2786730
H	-5.6002380	1.8842650	-0.2876240
H	-4.9800480	3.2669780	-1.2308400
H	-5.1663570	3.4140130	0.5283150
C	4.8825400	2.7159930	0.2781140
H	5.6000520	1.8841850	0.2896600
H	4.9798200	3.2697620	1.2287600
H	5.1671460	3.4118030	-0.5306850
C	-3.3589790	-0.4988720	-2.4707590
H	-2.3416460	-0.2937180	-2.0926270
C	-4.7486330	0.4086000	2.3293540
H	-5.1139190	1.4503880	2.2732480
C	4.7487720	0.4086920	-2.3289790
H	3.6807520	0.4670610	-2.6026990
C	3.3587040	-0.4992180	2.4709360
H	2.3414660	-0.2938290	2.0926850
H	5.2937810	-0.0853830	-3.1495080
H	5.1135240	1.4506480	-2.2727100
H	3.3259330	-1.3384800	3.1830400
H	3.6778580	0.4053080	3.0216710
H	-5.2931970	-0.0857890	3.1499920
H	-3.6805700	0.4674530	2.6027680
H	-3.6780750	0.4058380	-3.0212280

H	-3.3264320	-1.3379690	-3.1830630
H	-2.4445190	-1.8429980	1.8962110
H	-3.5532370	-5.5300320	-0.1011230
H	-0.5722130	-2.9139540	-1.8467320
H	2.4444720	-1.8426410	-1.8963360
H	3.5531570	-5.5301390	0.1001510
H	0.5722850	-2.9143370	1.8464490

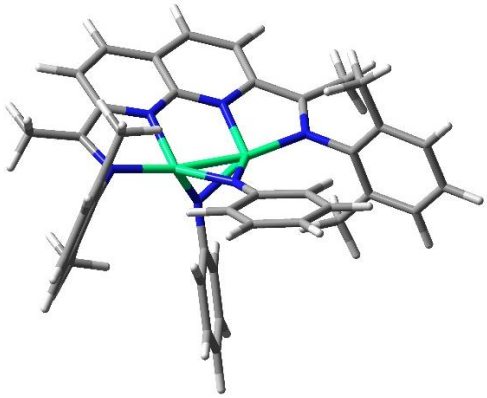

Charge: 0

Multiplicity: 3

Imaginary Frequencies: 0

Electronic Energy: – 4892.56655345 Hartrees

Gibbs Free Energy (298.15 K): – 4891.9835 Hartrees

Ni	1.0818440	0.3973800	-0.0577150
Ni	-1.1157420	0.4064160	-0.0022170
N	2.9963280	0.6342870	-0.2954770
N	-3.0085250	0.5863070	-0.2480530
N	1.0993610	2.2633280	-0.4640610
N	-1.1785130	2.2623090	-0.3173740
N	-0.0388850	-1.0015190	-0.5280510
N	0.0823250	0.5301940	1.5071980
C	3.3972990	1.9170240	-0.4710180
C	-3.4579560	1.8614670	-0.3221610
C	2.3307630	2.8823370	-0.4824690
C	2.3941210	4.3006990	-0.5023070
H	3.3650630	4.8041370	-0.5176340
C	1.2248600	5.0611220	-0.4947670
H	1.2802330	6.1540330	-0.5221380
C	-0.0534820	4.4245940	-0.4366910
C	-0.0406210	2.9935370	-0.3892280

C	-1.3393770	5.0437260	-0.4305850
H	-1.4084370	6.1358840	-0.4643700
C	-2.5030560	4.2725170	-0.3910450
H	-3.4803400	4.7632200	-0.3992210
C	-2.4164430	2.8573880	-0.3396420
C	3.9860920	-0.3997140	-0.3310820
C	4.5935800	-0.8292490	0.8779210
C	5.5358040	-1.8727900	0.8153550
H	6.0102990	-2.2105450	1.7437520
C	5.8697550	-2.4786070	-0.4034190
H	6.6031850	-3.2909720	-0.4306190
C	5.2613000	-2.0400870	-1.5875210
H	5.5193740	-2.5092100	-2.5438070
C	4.3149740	-0.9981220	-1.5771750
C	-3.9694460	-0.4756920	-0.2916050
C	-4.4375260	-1.0462720	0.9192960
C	-5.3630180	-2.1034920	0.8426960
H	-5.7288950	-2.5525260	1.7728740
C	-5.8140130	-2.5842020	-0.3937910
H	-6.5343440	-3.4076690	-0.4332500
C	-5.3316120	-2.0150150	-1.5805860
H	-5.6718950	-2.3959910	-2.5501490
C	-4.4010800	-0.9594990	-1.5555560
C	-0.0627000	-2.2196630	-1.1293450
C	-1.2958450	-2.8703070	-1.4519770
C	-1.3012830	-4.1320840	-2.0476750
H	-2.2600050	-4.6086290	-2.2804990
C	-0.0951060	-4.7953650	-2.3464220
C	1.1280030	-4.1742490	-2.0258510
H	2.0737330	-4.6837430	-2.2415700
C	1.1542080	-2.9153590	-1.4248170

C	0.1226810	-0.3856740	2.5302550
C	0.7992740	-1.6461530	2.4837200
C	0.8041070	-2.4950420	3.5939550
H	1.3225050	-3.4580010	3.5273860
C	0.1549040	-2.1297830	4.7876320
C	-0.5116200	-0.8915150	4.8562100
H	-1.0161620	-0.5915720	5.7815240
C	-0.5330330	-0.0335210	3.7549420
C	4.8452580	2.2923880	-0.6461430
H	5.4637510	1.9131610	0.1855250
H	4.9725250	3.3830790	-0.7051920
H	5.2603730	1.8531790	-1.5708780
C	-4.9231810	2.2031330	-0.3733650
H	-5.4568240	1.8041100	0.5069690
H	-5.4094170	1.7619340	-1.2609590
H	-5.0770480	3.2914640	-0.4054850
C	4.2345460	-0.1837610	2.1967630
H	3.1778800	-0.3692690	2.4602600
C	3.6532150	-0.5360690	-2.8564970
H	3.8432870	0.5323490	-3.0622180
C	-3.9495680	-0.5279110	2.2511550
H	-2.8465590	-0.5249990	2.3011590
C	-3.8439020	-0.3825440	-2.8375930
H	-2.7480050	-0.5167470	-2.8837130
H	-4.3312690	-1.1462670	3.0786170
H	-4.2728240	0.5138980	2.4306480
H	-4.2879950	-0.8787010	-3.7149800
H	-4.0297620	0.7019430	-2.9294270
H	4.0191960	-1.1171070	-3.7177860
H	2.5561270	-0.6537040	-2.8031000
H	4.3617990	0.9125570	2.1702550

H	4.8624080	-0.5811660	3.0100580
H	-2.2320990	-2.3623350	-1.2054680
H	-0.1080020	-5.7848390	-2.8140390
H	2.1037900	-2.4397140	-1.1601270
H	1.2897890	-1.9390380	1.5519190
H	0.1702530	-2.7991670	5.6534270
H	-1.0364240	0.9371730	3.8036600

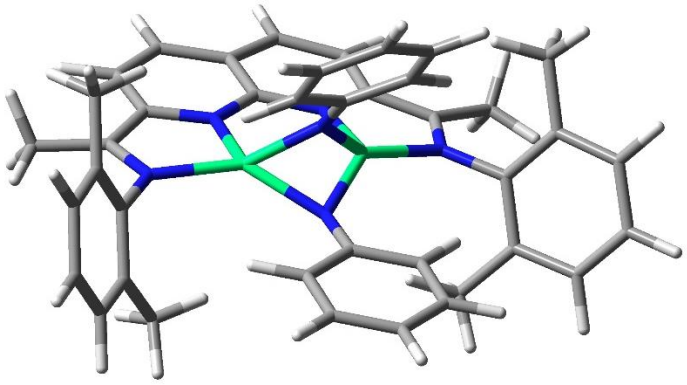

Charge: 0

Multiplicity: 3

Imaginary Frequencies: 1

Electronic Energy: – 4892.55222118 Hartrees

Gibbs Free Energy (298.15 K): – 4891.967319 Hartrees

Ni	1.2874080	0.4595140	-0.0523250
Ni	-1.2627740	0.4808470	-0.0895000
N	3.1481210	0.8127380	-0.3079810
N	-3.1202680	0.8589490	-0.3349080
N	1.1829800	2.3451600	0.0579540
N	-1.1362240	2.3628200	0.0411370
N	0.0032280	-0.8422080	-0.7078030
N	-0.0080590	-0.3245510	0.9961100
C	3.5070030	2.1107870	-0.2048380
C	-3.4628080	2.1605980	-0.2255710
C	2.4067400	3.0010550	0.0331470
C	2.4743510	4.4024920	0.1965580
H	3.4488090	4.8996530	0.1957510
C	1.3065030	5.1442990	0.3470130
H	1.3477870	6.2312860	0.4703980
C	0.0376690	4.4991350	0.2971080
C	0.0280350	3.0639440	0.1511490

C	-1.2220750	5.1623050	0.3392970
H	-1.2486390	6.2495350	0.4645740
C	-2.3995910	4.4372630	0.1820900
H	-3.3670580	4.9479080	0.1788090
C	-2.3507710	3.0356100	0.0147980
C	4.1221950	-0.2096030	-0.5058470
C	4.9581800	-0.6304170	0.5653730
C	5.8527180	-1.6933680	0.3382860
H	6.4956080	-2.0257890	1.1615700
C	5.9285760	-2.3274160	-0.9086900
H	6.6310560	-3.1525180	-1.0644770
C	5.0912050	-1.9076750	-1.9525350
H	5.1394270	-2.4040200	-2.9284510
C	4.1761890	-0.8555690	-1.7730020
C	-4.1059360	-0.1534720	-0.5223200
C	-4.9231630	-0.5746580	0.5634770
C	-5.8284490	-1.6309970	0.3484310
H	-6.4574220	-1.9635930	1.1823290
C	-5.9326980	-2.2580030	-0.9001870
H	-6.6431910	-3.0779770	-1.0463280
C	-5.1140820	-1.8373700	-1.9584890
H	-5.1856150	-2.3276240	-2.9360810
C	-4.1893440	-0.7914350	-1.7918430
C	-0.0003220	-2.2301990	-0.8595120
C	-1.2203730	-2.9381940	-1.0108050
C	-1.2136680	-4.3162730	-1.2557930
H	-2.1647430	-4.8458190	-1.3765190
C	0.0009730	-5.0184200	-1.3419620
C	1.2149810	-4.3283450	-1.1776710
H	2.1664760	-4.8673080	-1.2381690
C	1.2196370	-2.9506320	-0.9338300

C	-0.0535810	-1.3245790	1.9611020
C	1.1398890	-1.7884650	2.5691210
C	1.0854400	-2.7498460	3.5834380
H	2.0132200	-3.0962080	4.0508720
C	-0.1510110	-3.2760840	3.9982590
C	-1.3376510	-2.8357470	3.3856920
H	-2.3020700	-3.2504230	3.6972930
C	-1.2950100	-1.8723920	2.3725590
C	4.9186100	2.6154950	-0.3671270
H	5.5881730	1.8093370	-0.7013740
H	5.3191570	3.0186860	0.5813760
H	4.9628590	3.4312080	-1.1093650
C	-4.8690290	2.6825140	-0.3796280
H	-5.5527250	1.8817530	-0.6978420
H	-4.9101810	3.4903180	-1.1308520
H	-5.2539260	3.1022000	0.5681150
C	4.8926650	0.0376900	1.9210580
H	3.8550760	0.2837000	2.2039550
C	3.2530940	-0.4171330	-2.8851750
H	3.4930960	0.6010200	-3.2408950
C	-4.8250940	0.0870650	1.9205690
H	-3.7769030	0.2874680	2.2010880
C	-3.2882080	-0.3500490	-2.9209470
H	-2.2375080	-0.3238130	-2.5791670
H	-5.2800690	-0.5472780	2.6982730
H	-5.3505150	1.0593400	1.9435730
H	-3.3686110	-1.0302380	-3.7833990
H	-3.5307390	0.6716980	-3.2643790
H	3.3105640	-1.1038850	-3.7441960
H	2.2109410	-0.3832860	-2.5191690
H	5.4585370	0.9873180	1.9397110

H	5.3241530	-0.6128400	2.6988500
H	-2.1626110	-2.3841740	-0.9491380
H	0.0017050	-6.0964130	-1.5332810
H	2.1610440	-2.4048140	-0.8136690
H	2.0924380	-1.3692050	2.2302620
H	-0.1889230	-4.0298180	4.7911650
H	-2.2075960	-1.5193050	1.8817760

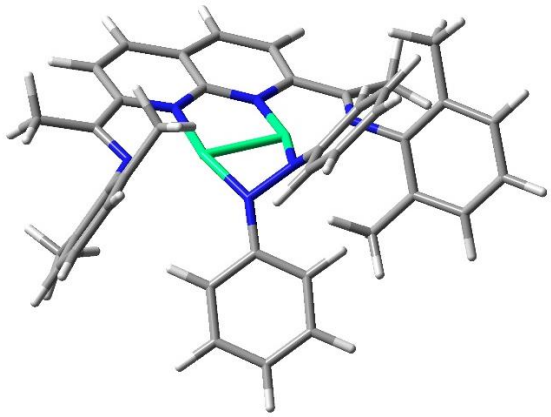

Charge: 0

Multiplicity: 3

Imaginary Frequencies: 0

Electronic Energy: – 4892.57464079 Hartrees

Gibbs Free Energy (298.15 K): – 4891.985531 Hartrees

Ni	-1.1329050	0.5903970	0.0338640
Ni	1.1088150	0.6026510	-0.0785620
N	-3.0653220	0.8516890	0.2640960
N	3.0372150	0.8443090	-0.3510620
N	-1.1225880	2.4279470	0.1898410
N	1.1128890	2.4344940	-0.2414300
N	0.6004070	-1.0843260	0.3597430
N	-0.6606950	-1.1554010	-0.2381900
C	-3.4254540	2.1298800	0.4816700
C	3.4085350	2.1207600	-0.5585220
C	-2.3382000	3.0647310	0.3757070
C	-2.4064020	4.4737880	0.4118190
H	-3.3740530	4.9610510	0.5617090
C	-1.2551290	5.2422370	0.2247440
H	-1.3077990	6.3352250	0.2392330
C	-0.0015530	4.6028270	-0.0049120
C	-0.0045520	3.1694320	-0.0179970

C	1.2542670	5.2409150	-0.2253760
H	1.3099250	6.3338750	-0.2187920
C	2.4041360	4.4742930	-0.4334980
H	3.3724500	4.9625190	-0.5759190
C	2.3300010	3.0655490	-0.4255850
C	-4.0508530	-0.1803650	0.3374940
C	-5.0060170	-0.3415390	-0.7036310
C	-5.9175700	-1.4106150	-0.6126630
H	-6.6527510	-1.5459980	-1.4142770
C	-5.8864400	-2.3023940	0.4676360
H	-6.5994590	-3.1316940	0.5157200
C	-4.9282840	-2.1375130	1.4771180
H	-4.8922350	-2.8375170	2.3194280
C	-3.9984680	-1.0842930	1.4314940
C	3.9973360	-0.2080420	-0.4656670
C	3.8743650	-1.1080610	-1.5589260
C	4.7733850	-2.1843770	-1.6490270
H	4.6824820	-2.8791540	-2.4916450
C	5.7718030	-2.3767530	-0.6838660
H	6.4592630	-3.2248970	-0.7644140
C	5.8768950	-1.4860880	0.3914630
H	6.6465100	-1.6403420	1.1565500
C	4.9999610	-0.3926470	0.5247860
C	0.9291680	-1.9672920	1.3928310
C	2.1032980	-1.7017180	2.1412030
C	2.4934010	-2.5515670	3.1776820
H	3.4057500	-2.3280410	3.7408770
C	1.7170640	-3.6770900	3.5099570
C	0.5348510	-3.9275610	2.7910790
H	-0.0884450	-4.7907580	3.0494950
C	0.1313330	-3.0881080	1.7465200

C	-0.9018810	-2.1559720	-1.1873880
C	-2.1579530	-2.1908510	-1.8439970
C	-2.4384350	-3.1836390	-2.7860470
H	-3.4190780	-3.1928440	-3.2739620
C	-1.4804510	-4.1617380	-3.1093320
C	-0.2278530	-4.1225820	-2.4726220
H	0.5348900	-4.8694590	-2.7195740
C	0.0701600	-3.1355680	-1.5264810
C	-4.8131120	2.5825060	0.8601880
H	-5.4780770	1.7236370	1.0290810
H	-5.2619660	3.2139480	0.0719910
H	-4.7842860	3.1888350	1.7820620
C	4.7940810	2.5640640	-0.9534420
H	5.4349640	1.7008770	-1.1834560
H	5.2786020	3.1446280	-0.1472120
H	4.7523500	3.2171010	-1.8420420
C	-5.0240420	0.5833630	-1.9014270
H	-4.0030900	0.7855060	-2.2688000
C	-2.9650830	-0.8949250	2.5148580
H	-3.2268620	-0.0591070	3.1897330
C	2.8081370	-0.8845400	-2.6042200
H	1.8609760	-0.5922940	-2.1158430
C	5.1321340	0.5433270	1.7072540
H	4.1517020	0.9125530	2.0519970
H	2.6336280	-1.7897170	-3.2055690
H	3.0766720	-0.0609980	-3.2916210
H	5.6291730	0.0366770	2.5502730
H	5.7398320	1.4339270	1.4617880
H	-2.8471770	-1.8030820	3.1257350
H	-1.9935600	-0.6418920	2.0550990
H	-5.4782910	1.5634350	-1.6675240

H	-5.6086310	0.1420360	-2.7244470
H	2.6791550	-0.8078680	1.8917560
H	2.0215630	-4.3409240	4.3249970
H	-0.7943420	-3.2878580	1.2027280
H	-2.9058170	-1.4367440	-1.5920440
H	-1.7041980	-4.9364420	-3.8492580
H	1.0519630	-3.1055450	-1.0485490

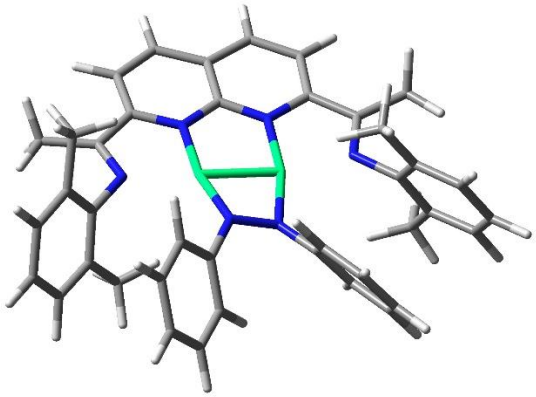

Charge: 0

Multiplicity: 3

Imaginary Frequencies: 0

Electronic Energy: – 4892.57170575 Hartrees

Gibbs Free Energy (298.15 K): – 4891.980935 Hartrees

Ni	-1.1061010	0.6811670	0.0893090
Ni	1.1061370	0.6811600	-0.0893820
N	-3.0810590	0.9347910	-0.0150790
N	3.0811300	0.9347980	0.0154680
N	-1.1357260	2.5228790	0.0145460
N	1.1357950	2.5229020	-0.0153230
N	-0.6651760	-1.0859210	0.1966040
N	0.6651500	-1.0859110	-0.1966640
C	-3.4551320	2.2238220	-0.0847700
C	3.4551870	2.2238640	0.0848730
C	-2.3638600	3.1584120	-0.0356490
C	-2.4389190	4.5650440	-0.0596970
H	-3.4175580	5.0517960	-0.0957860
C	-1.2721710	5.3350080	-0.0296500
H	-1.3265110	6.4280010	-0.0364380
C	0.0000200	4.6963980	-0.0002150
C	0.0000290	3.2599240	-0.0002820

C	1.2722110	5.3350250	0.0293700
H	1.3265440	6.4280150	0.0362670
C	2.4389520	4.5650600	0.0595110
H	3.4175750	5.0518280	0.0958440
C	2.3639270	3.1584300	0.0353640
C	-4.1013870	-0.0634100	-0.1020910
C	-4.2257390	-0.7896810	-1.3133010
C	-5.2309440	-1.7669740	-1.4094090
H	-5.3306130	-2.3336770	-2.3416980
C	-6.0907050	-2.0259960	-0.3334050
H	-6.8695140	-2.7901880	-0.4238330
C	-5.9383400	-1.3170270	0.8661060
H	-6.5958380	-1.5310560	1.7168270
C	-4.9423680	-0.3335030	1.0093580
C	4.1013770	-0.0634430	0.1025730
C	4.9426670	-0.3334170	-1.0086910
C	5.9385600	-1.3170000	-0.8652990
H	6.5962850	-1.5309290	-1.7158690
C	6.0905720	-2.0261590	0.3341440
H	6.8693280	-2.7903930	0.4246660
C	5.2305050	-1.7672850	1.4099360
H	5.3298860	-2.3341350	2.3421660
C	4.2253590	-0.7899450	1.3136870
C	-1.4386220	-2.2606690	0.0635660
C	-2.3938670	-2.5511280	1.0641680
C	-3.1667540	-3.7155160	0.9934820
H	-3.8983060	-3.9235620	1.7807630
C	-3.0024590	-4.6151070	-0.0732410
C	-2.0574980	-4.3299400	-1.0740200
H	-1.9235330	-5.0203800	-1.9140280
C	-1.2791220	-3.1684520	-1.0132450

C	1.4385950	-2.2606800	-0.0638750
C	2.3939250	-2.5508590	-1.0644790
C	3.1668380	-3.7152430	-0.9940370
H	3.8984490	-3.9230680	-1.7813200
C	3.0024990	-4.6151080	0.0724500
C	2.0574630	-4.3302170	1.0732360
H	1.9234650	-5.0208690	1.9130650
C	1.2790530	-3.1687390	1.0126990
C	-4.8719270	2.7086560	-0.2764340
H	-5.5827960	1.8720310	-0.3105600
H	-4.9621250	3.2781390	-1.2183770
H	-5.1725470	3.3876040	0.5411200
C	4.8719300	2.7087390	0.2768540
H	5.5827860	1.8721130	0.3112930
H	4.9618580	3.2783170	1.2187670
H	5.1728180	3.3875900	-0.5406820
C	-3.2869300	-0.4947720	-2.4586440
H	-2.2721660	-0.3117350	-2.0625320
C	-4.7668830	0.4059160	2.3174650
H	-5.1196250	1.4519270	2.2594770
C	4.7674990	0.4060340	-2.3168200
H	3.7055440	0.4493070	-2.6154620
C	3.2862460	-0.4951880	2.4588170
H	2.2716080	-0.3120110	2.0624430
H	5.3359360	-0.0861070	-3.1223480
H	5.1194910	1.4522730	-2.2585630
H	3.2527610	-1.3299400	3.1758540
H	3.5807670	0.4185000	3.0082440
H	-5.3345290	-0.0866540	3.1232890
H	-3.7047800	0.4498660	2.6154560
H	-3.5815610	0.4190250	-3.0078300

H	-3.2537050	-1.3293950	-3.1758420
H	-2.4964710	-1.8595970	1.9059230
H	-3.6021400	-5.5294450	-0.1236550
H	-0.5441260	-2.9516390	-1.7924470
H	2.4965750	-1.8591160	-1.9060560
H	3.6022070	-5.5294380	0.1226760
H	0.5440130	-2.9521470	1.7919210

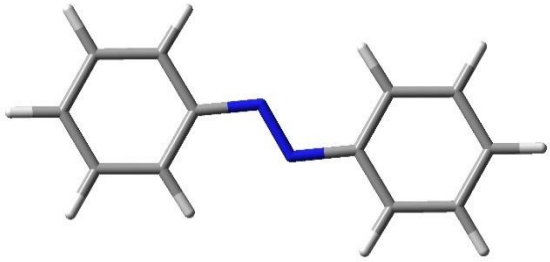

Charge: 0

Multiplicity: 1

Imaginary Frequencies: 0

Electronic Energy: –572.77189910 Hartrees

Gibbs Free Energy (298.15 K): –572.6256841 Hartrees

C	-3.6828550	-1.3128000	-0.0002940
C	-2.2988110	-1.1252990	-0.0002840
C	-1.7709460	0.1878230	-0.0000160
C	-2.6448630	1.2956590	0.0001430
C	-4.0319220	1.0995480	0.0002620
C	-4.5534580	-0.2042880	0.0000180
H	-4.0944880	-2.3277710	-0.0005940
H	-1.6009030	-1.9667500	-0.0004710
H	-2.2047460	2.2976630	0.0002290
H	-4.7064050	1.9617390	0.0004790
H	-5.6371160	-0.3610700	-0.0000230
C	1.7710750	-0.1882340	0.0003110
C	2.6453270	-1.2957740	0.0003240
C	2.2983300	1.1251090	0.0000080
C	4.0322790	-1.0991350	0.0001270
H	2.2053720	-2.2978600	0.0005990
C	3.6823260	1.3131100	-0.0002790
H	1.6001570	1.9663300	-0.0000830
C	4.5533190	0.2049110	-0.0002140
H	4.7070520	-1.9610980	0.0000690

H	4.0937050	2.3281920	-0.0005180
H	5.6368930	0.3622520	-0.0004160
N	-0.3866680	0.5090320	-0.0002290
N	0.3869050	-0.5098040	0.0002420

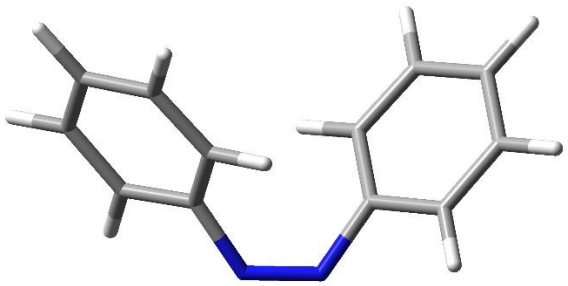

Charge: 0

Multiplicity: 1

Imaginary Frequencies: 0

Electronic Energy: –572.74987885 Hartrees

Gibbs Free Energy (298.15 K): –572.6034559 Hartrees

C	-2.2021330	-1.2664750	-1.1732570
C	-1.2613140	-0.2374410	-1.0435010
C	-1.4396740	0.7505020	-0.0490110
C	-2.5794320	0.7114830	0.7823620
C	-3.4897320	-0.3468600	0.6739080
C	-3.3070680	-1.3367440	-0.3070210
H	-2.0702450	-2.0219210	-1.9548780
H	-0.4010770	-0.1819960	-1.7161810
H	-2.7253830	1.5162800	1.5096020
H	-4.3575640	-0.3869870	1.3401330
H	-4.0327650	-2.1497330	-0.4090730
C	1.4399240	0.7512350	0.0477000
C	2.5782480	0.7096320	-0.7853560
C	1.2627590	-0.2338760	1.0452010
C	3.4884650	-0.3486700	-0.6750670
H	2.7235340	1.5120870	-1.5153200
C	2.2032850	-1.2629730	1.1763300
H	0.4034270	-0.1759670	1.7188560
C	3.3069950	-1.3358830	0.3087420

H	4.3552610	-0.3908740	-1.3425190
H	2.0722330	-2.0162690	1.9601670
H	4.0326220	-2.1487780	0.4119560
N	-0.6313810	1.9370080	0.0331410
N	0.6310990	1.9373610	-0.0344160

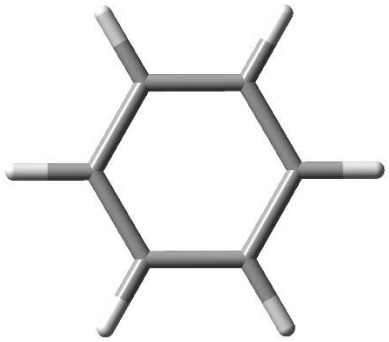

Charge: 0

Multiplicity: 1

Imaginary Frequencies: 0

Electronic Energy: –232.24708901 Hartrees

Gibbs Free Energy (298.15 K): –232.176951 Hartrees

C	-1.3908940	-0.1957900	0.0000010
C	-0.5257660	-1.3022380	0.0000590
C	0.8649700	-1.1064680	-0.0000310
C	1.3908860	0.1958420	0.0000110
C	0.5258150	1.3022180	0.0000330
C	-0.8650110	1.1064370	-0.0000440
H	-2.4752960	-0.3486330	-0.0000180
H	-0.9357410	-2.3177520	-0.0000200
H	1.5394110	-1.9692810	-0.0001060
H	2.4753080	0.3485340	-0.0000380
H	0.9356560	2.3177840	0.0000550
H	-1.5393340	1.9693440	-0.0000500

Charge: 0

Multiplicity: 1

Imaginary Frequencies: 0

Electronic Energy: –109.52669311 Hartrees

Gibbs Free Energy (298.15 K): –109.53981 Hartrees

N	0.0000000	0.0000000	0.5587680
N	0.0000000	0.0000000	-0.5587680

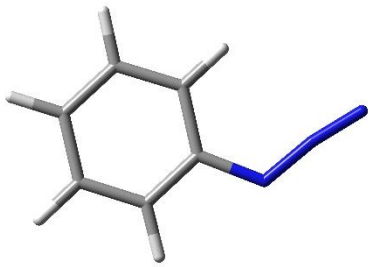

Charge: 0

Multiplicity: 1

Imaginary Frequencies: 0

Electronic Energy: -395.85954638 Hartrees

Gibbs Free Energy (298.15 K): -395.791068 Hartrees

C	0.1464350	-0.3599290	-0.0001210
C	-0.8867450	-1.3172800	-0.0001290
C	-0.1604020	1.0165440	0.0000370
C	-2.2218000	-0.8951930	-0.0000600
H	-0.6244430	-2.3789100	-0.0003560
C	-1.5010790	1.4231400	0.0000270
H	0.6444630	1.7591270	0.0000550
C	-2.5365350	0.4739790	0.0000250
H	-3.0212970	-1.6428470	-0.0001320
H	-1.7356550	2.4925230	0.0001180
H	-3.5809950	0.7998110	0.0001010
N	1.4734510	-0.8764850	0.0005140
N	2.4311190	-0.0821920	-0.0001320
N	3.4209560	0.5190660	-0.0001610

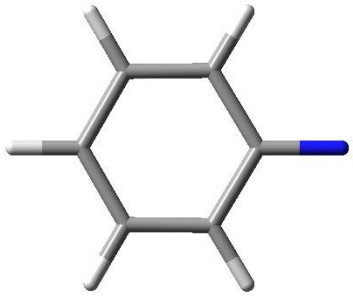

Charge: 0

Multiplicity: 3

Imaginary Frequencies: 0

Electronic Energy: -286.30615696 Hartrees

Gibbs Free Energy (298.15 K): -286.247434 Hartrees

C	1.0823430	-0.0000120	0.0000100
C	0.3379440	-1.2407910	-0.0000120
C	0.3379610	1.2407820	-0.0000190
C	-1.0524160	-1.2230580	0.0000000
H	0.8992170	-2.1790430	-0.0000250
C	-1.0523980	1.2230700	0.0000070
H	0.8992530	2.1790230	-0.0000390
C	-1.7577870	0.0000090	0.0000080
H	-1.6042000	-2.1688320	-0.0000130
H	-1.6041740	2.1688470	-0.0000010
H	-2.8519330	0.0000210	0.0000220
N	2.4125650	-0.0000020	0.0000130

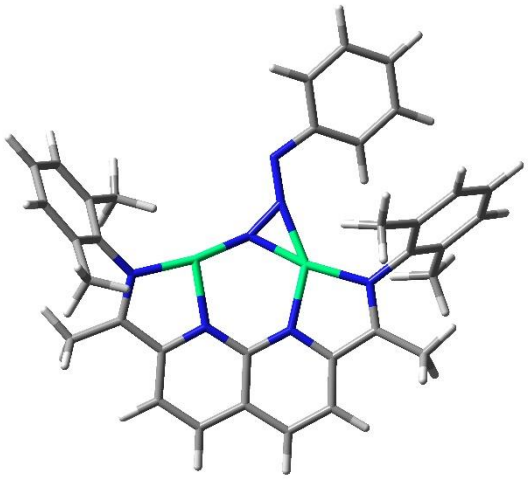

Charge: 0

Multiplicity: 3

Imaginary Frequencies: 0

Electronic Energy: -4715.65389915 Hartrees

Gibbs Free Energy (298.15 K): - 4715.14524 Hartrees

C	-5.7556480	1.3311260	0.5403860
H	-5.9253660	1.8181930	1.5168650
H	-6.3265260	0.3911890	0.5233920
H	-6.1745650	1.9998350	-0.2335020
C	-4.2881490	1.0627170	0.3227030
C	-3.3005680	2.1091060	0.4105810
C	-3.6369350	3.4658680	0.5872710
H	-4.6835140	3.7495570	0.7234130
C	-2.6392170	4.4261920	0.5571270
H	-2.8727430	5.4901250	0.6647560
C	-1.2882840	4.0377540	0.3555170
C	-0.9722020	2.6239300	0.2383240
C	-0.2460610	4.9941740	0.2399020
H	-0.4899900	6.0580400	0.3227560
C	1.0498450	4.5703690	-0.0013900

H	1.8639710	5.2898040	-0.1158820
C	1.3259030	3.1908780	-0.0753750
C	2.6431390	2.6658620	-0.3204380
C	3.7939260	3.5734200	-0.6755000
H	3.5097890	4.2624160	-1.4893130
H	4.6655540	2.9903640	-1.0047610
H	4.1058030	4.1960930	0.1830640
C	-4.5852690	-1.3065050	-0.1724210
C	-4.4867240	-2.4006610	0.7318790
C	-5.2327560	-3.5610950	0.4663180
H	-5.1628280	-4.4042330	1.1626400
C	-6.0459100	-3.6540790	-0.6717170
H	-6.6176040	-4.5671430	-0.8664500
C	-6.1013040	-2.5841130	-1.5743090
H	-6.7080160	-2.6659820	-2.4834150
C	-5.3734300	-1.3999750	-1.3534410
C	-3.5825940	-2.3070960	1.9371620
H	-2.6266690	-1.8232520	1.6471740
C	-5.4032500	-0.2875790	-2.3786480
H	-4.4059510	0.1639990	-2.5142320
C	3.9770940	0.6729860	-0.4744620
C	5.0060340	0.7463900	0.5015660
C	6.2233900	0.0903040	0.2338180
H	7.0261730	0.1445920	0.9781850
C	6.4151310	-0.6295890	-0.9529160
H	7.3696930	-1.1308440	-1.1426890
C	5.3703320	-0.7314500	-1.8815790
H	5.5022230	-1.3219760	-2.7948190
C	4.1372980	-0.0968630	-1.6563370
C	4.8062600	1.4852900	1.8071930
H	3.7862000	1.3406210	2.2010120

C	2.9899500	-0.2321270	-2.6272590
H	2.0650770	-0.4620390	-2.0673490
C	2.1188210	-3.2015660	0.5096610
C	3.3293090	-2.5562210	0.8574190
H	3.3171930	-1.4978760	1.1300240
C	4.5290980	-3.2778940	0.8729520
H	5.4564240	-2.7626290	1.1428070
C	4.5500630	-4.6451870	0.5489400
H	5.4923190	-5.2023620	0.5671390
C	3.3480060	-5.2936400	0.2139390
H	3.3495690	-6.3608280	-0.0330690
C	2.1431090	-4.5842630	0.2019200
H	1.1960620	-5.0741990	-0.0445430
N	-3.7780330	-0.1564160	0.0761720
N	-1.9749600	1.6876680	0.2653920
N	0.3364380	2.2188510	0.0832350
N	2.7219200	1.3265680	-0.2613620
N	-0.2494020	-0.5739260	0.6071960
N	0.7871840	-1.3234360	0.4458270
Ni	-1.9434930	-0.2290950	0.1702100
Ni	1.0982770	0.4923950	0.1341670
H	-5.7453840	-0.6715770	-3.3531040
H	-6.0897110	0.5297570	-2.0919630
H	-3.3675730	-3.3005390	2.3597830
H	-4.0151590	-1.6757800	2.7346130
H	3.1769490	-1.0317730	-3.3604670
H	2.7969310	0.7064650	-3.1776820
H	5.5238860	1.1325780	2.5651580
H	4.9572560	2.5748810	1.6985780
N	0.8434420	-2.6131170	0.5287680

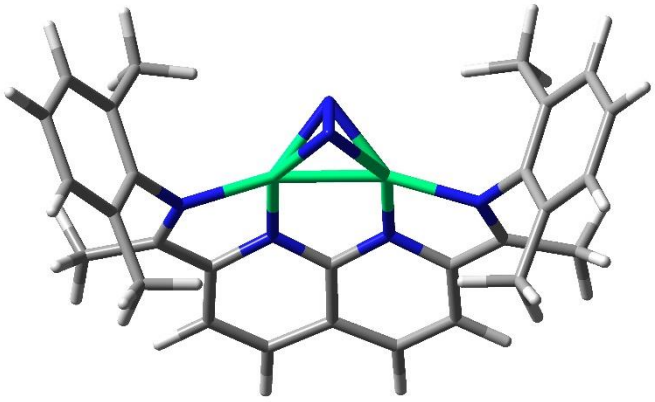

Charge: 0

Multiplicity: 1

Imaginary Frequencies: 0

Electronic Energy: -4429.29417922 Hartrees

Gibbs Free Energy (298.15 K): -4428.87177 Hartrees

Ni	1.1158880	-0.1712940	-0.4418070
Ni	-1.1158180	-0.1717840	-0.4411750
N	-2.9470540	-0.0004260	0.1071650
N	-1.1462980	1.6814140	-0.4069740
N	1.1466120	1.6816270	-0.4073090
N	2.9470700	-0.0004930	0.1066430
C	-4.8718140	1.6065720	0.1105810
H	-5.3581120	1.4168280	-0.8641890
H	-5.0294860	2.6669870	0.3577200
H	-5.3968980	0.9855530	0.8540520
C	-3.4077820	1.2646040	0.0455530
C	-2.3706120	2.2582680	-0.0849870
C	-2.4403130	3.6374670	0.1914890
H	-3.4089950	4.1030960	0.3948460
C	-1.2732850	4.4072880	0.2616100

H	-1.3291150	5.4724680	0.5059340
C	0.0001480	3.7936840	0.0973740
C	0.0001300	2.3888500	-0.2242810
C	1.2736200	4.4072950	0.2614710
H	1.3294400	5.4724710	0.5058210
C	2.4406760	3.6375290	0.1912560
H	3.4093390	4.1031900	0.3946440
C	2.3709890	2.2583380	-0.0853040
C	3.4079960	1.2645050	0.0452310
C	4.8720960	1.6061470	0.1105040
H	5.3590590	1.4134450	-0.8633410
H	5.3964250	0.9869620	0.8560510
H	5.0299840	2.6671690	0.3548470
C	-3.8616720	-1.0958120	0.2083460
C	-4.2539130	-1.5468030	1.4953260
C	-5.1230010	-2.6499840	1.5778750
H	-5.4354110	-3.0035120	2.5671210
C	-5.5742030	-3.3054010	0.4239060
H	-6.2432340	-4.1678100	0.5084260
C	-5.1486730	-2.8664610	-0.8375020
H	-5.4802530	-3.3895630	-1.7416940
C	-4.2897540	-1.7609210	-0.9694930
C	-3.7975430	-1.2994000	-2.3219150
H	-2.7062970	-1.1259770	-2.2905930
C	-3.7281340	-0.8695650	2.7407130
H	-2.6243870	-0.8321390	2.7306700
C	3.8614750	-1.0959800	0.2083090
C	4.2896080	-1.7615150	-0.9692690
C	5.1483060	-2.8671730	-0.8368400
H	5.4799300	-3.3905930	-1.7408330
C	5.5735790	-3.3058170	0.4247580

H	6.2424360	-4.1683260	0.5096300
C	5.1223230	-2.6499810	1.5784680
H	5.4345090	-3.0032910	2.5678630
C	4.2534380	-1.5466720	1.4954810
C	3.7274580	-0.8691370	2.7406260
H	2.6237020	-0.8319390	2.7304950
C	3.7977600	-1.3002270	-2.3219060
H	4.2606580	-0.3445510	-2.6303750
H	-4.0507370	-1.4081340	3.6459260
H	-4.0741880	0.1762500	2.8302880
H	-4.0140660	-2.0458780	-3.1019670
H	-4.2602260	-0.3435930	-2.6302940
H	4.0143630	-2.0469020	-3.1017470
H	2.7065360	-1.1266100	-2.2909080
H	4.0500920	-1.4073820	3.6460210
H	4.0732820	0.1767740	2.8299360
N	-0.0000600	-1.2887620	-1.4287700
N	0.0006270	-1.7643590	-0.2786310

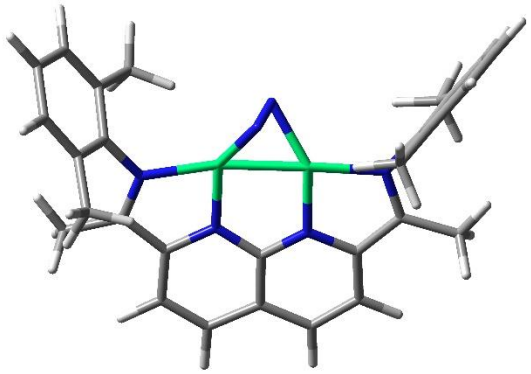

Charge: 0

Multiplicity: 3

Imaginary Frequencies: 0

Electronic Energy: -4429.27637992 Hartrees

Gibbs Free Energy (298.15 K: -4428.85774 Hartrees

Ni	1.1019100	-0.2191130	-0.1260400
Ni	-1.1018570	-0.2191870	0.1266690
N	-3.0306820	0.0098810	0.0764430
N	-1.1239320	1.6454840	0.1776910
N	1.1240610	1.6454790	-0.1767910
N	3.0307320	0.0098010	-0.0767460
C	-4.8703400	1.7131270	0.3908810
H	-5.2338580	2.2917540	-0.4784530
H	-4.9764910	2.3627390	1.2772610
H	-5.5269390	0.8397230	0.5154930
C	-3.4369290	1.2885900	0.2076930
C	-2.3615700	2.2545870	0.1809370
C	-2.4452550	3.6690720	0.1297990
H	-3.4261160	4.1530600	0.1243290
C	-1.2826640	4.4411450	0.0638990
H	-1.3486170	5.5336640	0.0382660

C	0.0000280	3.8138290	-0.0001640
C	0.0000480	2.3840340	0.0002260
C	1.2827330	4.4411320	-0.0646310
H	1.3486570	5.5336650	-0.0395720
C	2.4453340	3.6690780	-0.1303390
H	3.4261710	4.1531260	-0.1253820
C	2.3617120	2.2545550	-0.1807950
C	3.4370180	1.2885450	-0.2078850
C	4.8703580	1.7130880	-0.3916490
H	5.5274320	0.8396100	-0.5131390
H	5.2330640	2.2947770	0.4759600
H	4.9767080	2.3598630	-1.2801100
C	-3.9629100	-1.0709250	0.0704630
C	-4.0163200	-1.9258860	1.2037260
C	-4.8838150	-3.0311420	1.1724900
H	-4.9294440	-3.6917600	2.0456850
C	-5.6744620	-3.2983910	0.0463540
H	-6.3421080	-4.1658890	0.0355880
C	-5.5894420	-2.4621680	-1.0749720
H	-6.1860810	-2.6813720	-1.9679600
C	-4.7340050	-1.3450310	-1.0915310
C	-4.6128850	-0.4838040	-2.3286830
H	-3.5550460	-0.3223900	-2.5995630
C	-3.1399380	-1.6427610	2.4004590
H	-2.1277290	-1.3583860	2.0567800
C	3.9628370	-1.0710850	-0.0707670
C	4.0156730	-1.9264570	-1.2037580
C	4.8829980	-3.0318330	-1.1724880
H	4.9281700	-3.6927740	-2.0454630
C	5.6740850	-3.2988030	-0.0465870
H	6.3415800	-4.1664160	-0.0357910

C	5.5896970	-2.4621480	1.0744550
H	6.1866980	-2.6810990	1.9672620
C	4.7344240	-1.3448720	1.0909850
C	4.6140870	-0.4831270	2.3278530
H	3.5564170	-0.3209340	2.5989090
C	3.1389410	-1.6435550	-2.4002860
H	3.5163960	-0.7956990	-3.0011880
H	-3.0608840	-2.5210630	3.0599200
H	-3.5174040	-0.7946460	3.0009870
H	-5.1208930	-0.9579650	-3.1835220
H	-5.0619980	0.5165350	-2.1913010
H	3.0595090	-2.5220440	-3.0594520
H	2.1269000	-1.3588630	-2.0563870
H	5.1219930	-0.9572940	3.1827500
H	5.0638220	0.5168730	2.1899920
N	-0.2337090	-1.6975870	-0.5683060
N	0.2338140	-1.6969350	0.5700510

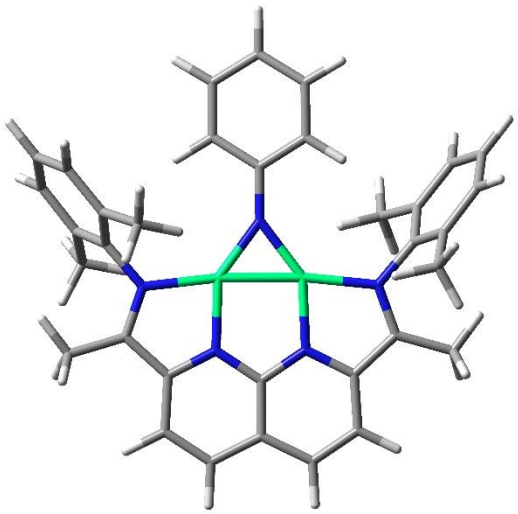

Charge: 0

Multiplicity: 1

Imaginary Frequencies: 0

Electronic Energy: -4606.18959433 Hartrees

Gibbs Free Energy (298.15 K): -4605.683989 Hartrees

Ni	-1.0690670	0.3255510	-0.0364870
Ni	1.0691340	0.3254460	0.0341410
N	2.9741230	0.5315910	0.1053030
N	1.1350600	2.1694830	0.0467710
N	-1.1349980	2.1695930	-0.0477930
N	-2.9740980	0.5317110	-0.1063940
N	0.0000380	-1.1106780	-0.0007570
C	4.8586510	2.2184690	0.3165550
H	4.9819060	2.8768470	1.1953840
H	5.2149080	2.7868270	-0.5628110
H	5.5128510	1.3443000	0.4461490
C	3.4202600	1.8041200	0.1622050
C	2.3529480	2.7812360	0.1132760
C	2.4399350	4.2102990	0.1294850
H	3.4212670	4.6899200	0.1823220

C	1.2858240	4.9768410	0.0701520
H	1.3458340	6.0700380	0.0753490
C	0.0000000	4.3405600	0.0014770
C	0.0000220	2.9257610	0.0001570
C	-1.2858410	4.9769050	-0.0658750
H	-1.3458870	6.0701090	-0.0691050
C	-2.4399840	4.2104570	-0.1261870
H	-3.4213360	4.6901770	-0.1777790
C	-2.3529460	2.7813840	-0.1124490
C	-3.4202710	1.8042810	-0.1619200
C	-4.8586870	2.2188570	-0.3153960
H	-4.9823210	2.8772740	-1.1941530
H	-5.2143070	2.7872880	0.5641740
H	-5.5131310	1.3448240	-0.4446540
C	3.9048420	-0.5535520	0.1145910
C	4.7029300	-0.8368970	-1.0266240
C	5.5646360	-1.9490630	-0.9735530
H	6.1815610	-2.1788970	-1.8498860
C	5.6335000	-2.7637060	0.1645770
H	6.3112040	-3.6233180	0.1840230
C	4.8104980	-2.4900850	1.2662320
H	4.8351330	-3.1416880	2.1467030
C	3.9277810	-1.3967760	1.2578140
C	2.9716280	-1.1329380	2.3939390
H	1.9770850	-0.9062720	1.9631570
C	4.6056770	0.0002550	-2.2829060
H	3.5544720	0.2172500	-2.5390260
C	-3.9047960	-0.5534590	-0.1160230
C	-4.7029240	-0.8371560	1.0250890
C	-5.5645650	-1.9493610	0.9716650
H	-6.1815120	-2.1794850	1.8479080

C	-5.6332910	-2.7637310	-0.1666640
H	-6.3109340	-3.6233850	-0.1863650
C	-4.8101650	-2.4898340	-1.2681550
H	-4.8346370	-3.1412670	-2.1487550
C	-3.9275150	-1.3964770	-1.2594030
C	-2.9711910	-1.1324340	-2.3953250
H	-1.9767270	-0.9058230	-1.9642980
C	-4.6057780	-0.0004660	2.2816960
H	-5.1205890	0.9724030	2.1806470
C	-0.0001330	-2.4813600	0.0007200
C	-1.1933880	-3.2186180	0.2619510
H	-2.1144760	-2.6656430	0.4690150
C	-1.1856880	-4.6155940	0.2614930
H	-2.1168350	-5.1555990	0.4668830
C	-0.0003990	-5.3294190	0.0037720
H	-0.0005050	-6.4241690	0.0049650
C	1.1850160	-4.6163780	-0.2555350
H	2.1160530	-5.1569940	-0.4598160
C	1.1929640	-3.2194080	-0.2590250
H	5.0676720	-0.5249370	-3.1341030
H	5.1192100	0.9737030	-2.1810120
H	2.1141310	-2.6670410	-0.4673640
H	2.8948710	-2.0007230	3.0667540
H	3.2638310	-0.2516560	2.9938540
H	-5.0665890	-0.5266210	3.1329430
H	-3.5546690	0.2176380	2.5372180
H	-2.8942990	-2.0001140	-3.0682600
H	-3.2632680	-0.2510460	-2.9951430

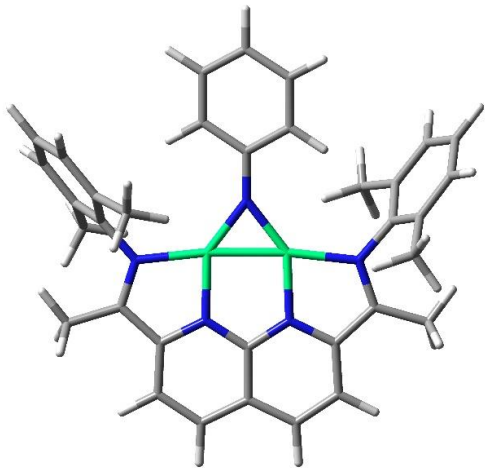

Charge: 0

Multiplicity: 3

Imaginary Frequencies: 0

Electronic Energy: -4606.19035728 Hartrees

Gibbs Free Energy (298.15 K): -4605.68853 Hartrees

Ni	-1.0832430	0.3040590	-0.0406100
Ni	1.0769070	0.3194590	0.0575880
N	3.0160600	0.5450520	0.1403940
N	1.1317140	2.1734810	-0.0484600
N	-1.1425610	2.1607350	-0.1374120
N	-3.0252380	0.5187260	-0.0523820
N	0.0084620	-1.1094980	0.0153710
C	4.8652320	2.2606760	0.2918490
H	4.9555020	3.0217420	1.0860040
H	5.2505900	2.7169440	-0.6382860
H	5.5124980	1.4095670	0.5483430
C	3.4308060	1.8257710	0.1411800
C	2.3588240	2.7931110	0.0404950
C	2.4305070	4.2024830	0.0455000
H	3.4039410	4.6983020	0.1056270
C	1.2598220	4.9701060	-0.0245420

H	1.3188230	6.0630520	-0.0245860
C	-0.0170520	4.3368510	-0.0866090
C	-0.0096900	2.9018840	-0.0872610
C	-1.3001640	4.9574750	-0.1414310
H	-1.3700910	6.0497600	-0.1469850
C	-2.4644480	4.1775100	-0.1767290
H	-3.4448350	4.6625700	-0.2031780
C	-2.3780810	2.7694120	-0.1596880
C	-3.4465970	1.7924620	-0.1526190
C	-4.8873090	2.2105170	-0.2931470
H	-5.0139530	2.8752140	-1.1651640
H	-5.2318030	2.7726420	0.5941080
H	-5.5440590	1.3379580	-0.4207860
C	3.9481640	-0.5319190	0.1916750
C	4.7941760	-0.8333320	-0.9114280
C	5.6490430	-1.9476840	-0.8086320
H	6.3015100	-2.1896640	-1.6555830
C	5.6660210	-2.7518750	0.3386780
H	6.3394070	-3.6132660	0.3955660
C	4.7957440	-2.4657760	1.4003870
H	4.7798980	-3.1086530	2.2875910
C	3.9209620	-1.3681820	1.3427120
C	2.9219100	-1.0832350	2.4356340
H	1.9515090	-0.8374340	1.9591880
C	4.7577400	-0.0181830	-2.1856810
H	3.7296370	0.2917630	-2.4369640
C	-3.9578990	-0.5610610	-0.0385620
C	-4.7570750	-0.8276960	1.1060750
C	-5.6198730	-1.9397410	1.0697520
H	-6.2383150	-2.1549380	1.9488050
C	-5.6875990	-2.7738910	-0.0544630

H	-6.3658340	-3.6333190	-0.0600420
C	-4.8638120	-2.5186010	-1.1602100
H	-4.8893030	-3.1834160	-2.0309070
C	-3.9834820	-1.4230590	-1.1687310
C	-3.0304040	-1.1681120	-2.3097560
H	-2.0404520	-0.9107600	-1.8818490
C	-4.6604900	0.0306000	2.3478390
H	-5.1756690	1.0012120	2.2291360
C	0.0288740	-2.4752070	-0.0836770
C	-1.1659550	-3.2392470	0.0788800
H	-2.1006960	-2.7084590	0.2826760
C	-1.1373060	-4.6322600	-0.0103240
H	-2.0657180	-5.1985730	0.1216540
C	0.0706200	-5.3095820	-0.2656590
H	0.0868260	-6.4020170	-0.3357320
C	1.2582860	-4.5700830	-0.4266720
H	2.2034870	-5.0877040	-0.6230820
C	1.2463600	-3.1770610	-0.3350380
H	5.1588960	-0.6029880	-3.0290900
H	5.3650390	0.9027140	-2.1126810
H	2.1667680	-2.5982130	-0.4567660
H	2.7976600	-1.9466690	3.1071160
H	3.2027530	-0.2044910	3.0443630
H	-5.1207570	-0.4799420	3.2088720
H	-3.6095830	0.2550260	2.5982550
H	-2.9335530	-2.0487950	-2.9630970
H	-3.3369220	-0.3055990	-2.9292500

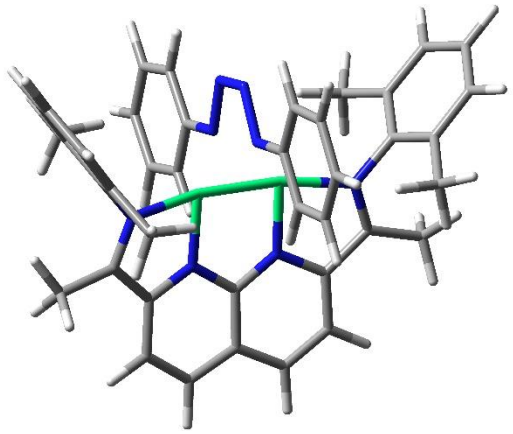

Charge: 0

Multiplicity: 3

Imaginary Frequencies: 0

Electronic Energy: -5002.07280163 Hartrees

Gibbs Free Energy (298.15 K): -5001.47934 Hartrees

Ni	-1.0961480	0.2078290	-0.0212110
Ni	1.0972000	0.1546250	-0.0529980
N	2.9820770	0.0330870	-0.4211610
N	1.1509670	1.3442950	-1.4988050
N	-1.1259520	1.3933570	-1.4696490
N	-2.9939760	0.1599230	-0.3555390
N	0.0375920	0.7203200	1.5711200
C	4.8868200	1.0169180	-1.7279670
H	5.3488760	1.7745970	-1.0678880
H	5.0290450	1.3519270	-2.7668290
H	5.4439540	0.0788530	-1.5797030
C	3.4279070	0.8420310	-1.4020590
C	2.3796050	1.5472670	-2.1004570
C	2.4544890	2.2985980	-3.2958550
H	3.4273100	2.4882810	-3.7584370
C	1.2917530	2.7754270	-3.9088500

H	1.3549920	3.3430490	-4.8424420
C	0.0114920	2.4899950	-3.3465990
C	0.0125000	1.7484960	-2.1196800
C	-1.2679990	2.8373520	-3.8729000
H	-1.3296900	3.4099730	-4.8035630
C	-2.4348650	2.4128360	-3.2278400
H	-3.4136290	2.6422660	-3.6594460
C	-2.3572980	1.6551240	-2.0384410
C	-3.4221740	0.9902380	-1.3245860
C	-4.8717250	1.2050960	-1.6737410
H	-5.5285130	0.7751920	-0.9037150
H	-5.1270200	0.7303370	-2.6391810
H	-5.0965880	2.2806460	-1.7703880
C	3.9104760	-0.7299110	0.3594670
C	4.3101790	-2.0127590	-0.1000560
C	5.1893400	-2.7624960	0.7027070
H	5.5040380	-3.7531690	0.3556760
C	5.6525420	-2.2685100	1.9294260
H	6.3313130	-2.8696560	2.5429510
C	5.2375850	-1.0051940	2.3707860
H	5.5904500	-0.6160230	3.3324790
C	4.3643310	-0.2150640	1.6014090
C	3.9011140	1.1359200	2.0940570
H	2.8099390	1.1446080	2.2630990
C	3.7970360	-2.5636360	-1.4110440
H	2.6963020	-2.6528910	-1.4050330
C	-3.9262340	-0.6003970	0.4226530
C	-4.2967370	-0.1285800	1.7090720
C	-5.1703130	-0.9148910	2.4818230
H	-5.4607920	-0.5568200	3.4758620
C	-5.6615560	-2.1365070	2.0030250

H	-6.3369920	-2.7375100	2.6203490
C	-5.2790650	-2.5892030	0.7333380
H	-5.6541120	-3.5474920	0.3566610
C	-4.4080610	-1.8389260	-0.0776180
C	-3.9858490	-2.3493020	-1.4364930
H	-2.8886660	-2.4533660	-1.5032090
C	-3.7546000	1.1798550	2.2335510
H	-4.0257900	2.0306940	1.5835530
C	0.0827210	2.0133610	2.1692020
C	0.0914640	3.1414260	1.3199140
H	0.0619340	2.9861550	0.2397170
C	0.1366510	4.4335800	1.8570990
H	0.1426560	5.2944230	1.1799480
C	0.1742650	4.6282060	3.2477160
H	0.2097920	5.6390690	3.6660310
C	0.1651650	3.5069530	4.0937630
H	0.1935020	3.6409530	5.1807110
C	0.1196920	2.2079180	3.5703080
H	4.2184740	-3.5627280	-1.6048880
H	4.0574550	-1.9154390	-2.2670020
H	0.1123570	1.3347050	4.2248160
H	4.3943850	1.3984900	3.0430600
H	4.1105110	1.9395380	1.3663680
H	-4.1362900	1.3876390	3.2452860
H	-2.6516580	1.1599530	2.2787220
H	-4.4331680	-3.3357540	-1.6369730
H	-4.2938810	-1.6704160	-2.2518260
C	-0.0832350	-2.6754820	-0.0455110
C	-0.1302790	-3.8976230	0.6615600
C	-0.0863680	-2.6964000	-1.4598040
C	-0.1795720	-5.1080870	-0.0424140

H	-0.1268990	-3.8750100	1.7528350
C	-0.1363860	-3.9142910	-2.1514580
H	-0.0470380	-1.7458050	-2.0050400
C	-0.1834980	-5.1292270	-1.4473760
H	-0.2159860	-6.0486890	0.5178740
H	-0.1373560	-3.9114700	-3.2466650
H	-0.2224580	-6.0805630	-1.9872830
N	0.0318340	-0.3151850	2.5167130
N	-0.0082080	-1.4751960	1.9875330
N	-0.0326340	-1.4074460	0.5913040

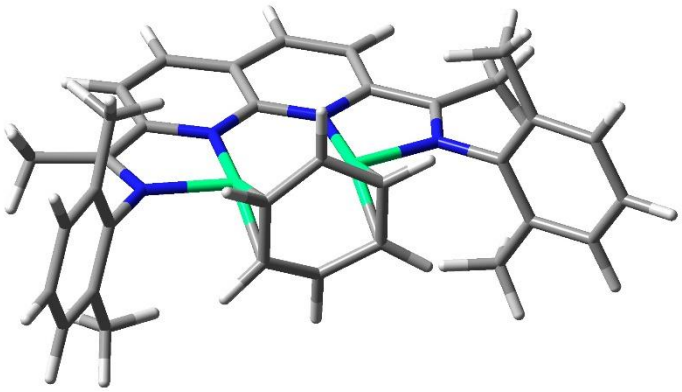

Charge: 0

Multiplicity: 1

Imaginary Frequencies: 0

Electronic Energy: –4552.05572180 Hartrees

Gibbs Free Energy (298.15 K): –4551.54164 Hartrees

Ni	1.2394110	-0.1417820	0.0024180
Ni	-1.2394390	-0.1417680	-0.0025480
N	3.1257200	0.1682600	0.0010620
N	-3.1257150	0.1682270	-0.0014090
N	1.1468710	1.7125410	0.0020860
N	-1.1469150	1.7125390	-0.0020650
C	1.2456540	-1.9851430	0.7141420
H	2.1475310	-2.2486550	1.2717760
C	1.2405620	-1.9809700	-0.7244960
H	2.1388120	-2.2409400	-1.2896090
C	-0.0053080	-1.7547750	-1.3901430
H	-0.0093110	-1.6914860	-2.4824050
C	-1.2454140	-1.9848800	-0.7157750
H	-2.1473690	-2.2481180	-1.2734400
C	-1.2404240	-1.9811360	0.7228680
H	-2.1385720	-2.2415420	1.2879350
C	0.0055150	-1.7541000	1.3883220

H	0.0095310	-1.6909090	2.4805930
C	3.4843410	1.4750640	0.0016940
C	-3.4843700	1.4750130	-0.0016790
C	2.3877480	2.3756280	0.0021760
C	2.4365820	3.7828770	0.0018990
H	3.4058660	4.2891170	0.0021310
C	1.2630320	4.5328890	0.0010860
H	1.2992900	5.6267440	0.0008970
C	-0.0000340	3.8795900	-0.0000600
C	-1.2630990	4.5328740	-0.0012430
H	-1.2993630	5.6267300	-0.0012170
C	-2.4366530	3.7828540	-0.0019640
H	-3.4059320	4.2890910	-0.0022030
C	-2.3877920	2.3756110	-0.0021120
C	-0.0000160	2.4378020	-0.0000110
C	4.1526650	-0.8242410	0.0000310
C	4.6400140	-1.3314240	1.2358460
C	5.6053180	-2.3558200	1.2106740
H	5.9821680	-2.7522470	2.1606020
C	6.0852220	-2.8689080	-0.0017070
H	6.8307730	-3.6707070	-0.0023930
C	5.6060400	-2.3530490	-1.2131730
H	5.9834930	-2.7472830	-2.1637740
C	4.6407840	-1.3285330	-1.2366540
C	-4.1526340	-0.8242960	0.0002370
C	-4.6401020	-1.3285940	1.2371530
C	-5.6054470	-2.3530460	1.2141520
H	-5.9823940	-2.7473190	2.1649390
C	-6.0853210	-2.8688370	0.0029330
H	-6.8309480	-3.6705660	0.0040200
C	-5.6060210	-2.3557600	-1.2096950

H	-5.9834030	-2.7521230	-2.1594360
C	-4.6406650	-1.3314320	-1.2353430
C	4.9270020	1.9090590	0.0019750
H	5.4645270	1.5216750	0.8856400
H	5.0179750	3.0044730	0.0043040
H	5.4639270	1.5255020	-0.8837160
C	-4.9270640	1.9088960	-0.0011760
H	-5.4653250	1.5205450	-0.8839440
H	-5.0181360	3.0042920	-0.0044810
H	-5.4631570	1.5261460	0.8853890
C	4.1623080	-0.7533300	2.5504050
H	3.0780350	-0.5526820	2.5351220
C	4.1644460	-0.7472840	-2.5503310
H	3.0805190	-0.5449180	-2.5352380
C	-4.1630450	-0.7474390	2.5506180
H	-3.0792320	-0.5445710	2.5347140
C	-4.1636540	-0.7532970	-2.5501390
H	-3.0793750	-0.5526540	-2.5354320
H	-4.3911550	-1.4244290	3.3897070
H	-4.6540300	0.2199840	2.7657050
H	-4.3939270	-1.4310660	-3.3879930
H	-4.6526300	0.2149260	-2.7661460
H	4.6550600	0.2204570	-2.7648100
H	4.3934850	-1.4239590	-3.3894190
H	4.3921180	-1.4311230	3.3883680
H	4.6511910	0.2148730	2.7666910

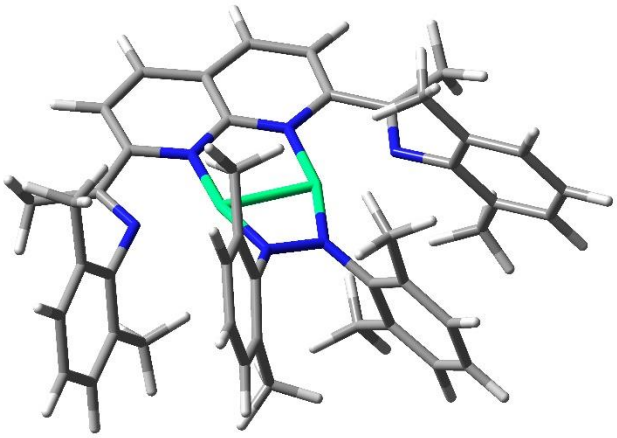

Charge: 0

Multiplicity: 1

Imaginary Frequencies: 0

Electronic Energy: -5049.84552013 Hartrees

Gibbs Free Energy (298.15 K): -5049.151627 Hartrees

Ni	-1.1221890	0.8434020	0.0555660
Ni	1.1328650	0.8326580	-0.0481760
N	-3.0787900	1.0783900	-0.0913570
N	3.1000990	1.0669950	0.0853710
N	-1.1339060	2.6627440	-0.0089500
N	1.1478540	2.6537000	0.0284130
N	-0.6790590	-0.8823550	0.1301530
N	0.6702910	-0.8934640	-0.1047670
C	-3.4550550	2.3705390	-0.1324600
C	3.4722330	2.3574570	0.1444200
C	-2.3720130	3.3067340	-0.0333010
C	-2.4287690	4.7131320	-0.0116210
H	-3.4007840	5.2147660	-0.0164540
C	-1.2569880	5.4747870	0.0232400
H	-1.3064640	6.5678140	0.0399010

C	0.0136600	4.8326500	0.0296320
C	0.0092190	3.3933360	0.0165460
C	1.2860280	5.4683420	0.0487970
H	1.3414090	6.5612150	0.0532250
C	2.4537920	4.6981790	0.0708140
H	3.4309630	5.1896070	0.0894710
C	2.3860680	3.2935680	0.0643270
C	-4.0615340	0.0704270	-0.3498270
C	-4.1416990	-0.4573270	-1.6690610
C	-5.0705380	-1.4767590	-1.9360190
H	-5.1362600	-1.8809600	-2.9528810
C	-5.9062030	-1.9750630	-0.9257010
H	-6.6206920	-2.7748940	-1.1462260
C	-5.8187690	-1.4460050	0.3664220
H	-6.4681600	-1.8321560	1.1608030
C	-4.9067810	-0.4185930	0.6782020
C	4.0853210	0.0498610	0.2892600
C	4.9112430	-0.3899360	-0.7769500
C	5.8264820	-1.4308070	-0.5304690
H	6.4603720	-1.7806910	-1.3534540
C	5.9365220	-2.0185460	0.7357790
H	6.6526530	-2.8291060	0.9057620
C	5.1229540	-1.5649600	1.7832930
H	5.2086760	-2.0136770	2.7797860
C	4.1897610	-0.5333750	1.5807620
C	-1.4002310	-2.0410480	0.5815010
C	-1.8108040	-2.0458540	1.9468160
C	-2.5203060	-3.1567450	2.4336960
H	-2.8259110	-3.1693300	3.4862460
C	-2.8371660	-4.2358260	1.5962370
C	-2.4698610	-4.1939820	0.2476880

H	-2.7495250	-5.0154900	-0.4216680
C	-1.7610850	-3.1004140	-0.2888870
C	1.3704830	-2.0752420	-0.5290810
C	1.7768650	-2.1217550	-1.8947010
C	2.4702490	-3.2538020	-2.3549720
H	2.7761420	-3.2953430	-3.4066030
C	2.7710800	-4.3169570	-1.4922330
C	2.4024460	-4.2385090	-0.1456790
H	2.6668120	-5.0496190	0.5423640
C	1.7115620	-3.1214760	0.3651850
C	-4.8880210	2.8043280	-0.3051150
H	-5.3955290	2.1788580	-1.0577060
H	-4.9563030	3.8552140	-0.6222560
H	-5.4572130	2.6943680	0.6360740
C	4.8974580	2.8195130	0.3213400
H	5.5245290	2.0149070	0.7331540
H	4.9508490	3.6879380	0.9974010
H	5.3414460	3.1267700	-0.6437280
C	-3.2554900	0.0968130	-2.7609440
H	-2.2136290	0.1861340	-2.4048520
C	-4.8669590	0.1496700	2.0801850
H	-5.7450390	0.7931580	2.2769600
C	4.8408970	0.2587150	-2.1410980
H	3.8074680	0.5214990	-2.4148890
C	3.3289390	-0.0212590	2.7124440
H	2.2832590	0.0986410	2.3770470
H	5.2498870	-0.4104110	-2.9153000
H	5.4294050	1.1947860	-2.1750270
H	3.3580640	-0.7027290	3.5774740
H	3.6586170	0.9765720	3.0565940
H	-4.8865030	-0.6572520	2.8319010

H	-3.9650400	0.7563870	2.2466080
H	-3.5646730	1.1148970	-3.0621670
H	-3.2803430	-0.5421470	-3.6580760
H	-3.3908430	-5.0946570	1.9898690
H	3.3122850	-5.1928660	-1.8649950
C	1.3904440	-3.0673460	1.8399510
H	1.2430680	-2.0310440	2.1781960
H	0.4696810	-3.6281100	2.0763320
H	2.2139410	-3.5083750	2.4259950
C	-1.4834930	-0.8898420	2.8628280
H	-1.6701950	0.0666090	2.3428100
H	-2.0868820	-0.9302720	3.7836160
H	-0.4178420	-0.8806150	3.1548030
C	-1.4467560	-3.0793250	-1.7657910
H	-1.2942240	-2.0503560	-2.1240830
H	-0.5315140	-3.6515270	-1.9960800
H	-2.2777120	-3.5241500	-2.3379460
C	1.4537700	-0.9903380	-2.8422690
H	1.6067370	-0.0202180	-2.3367280
H	2.0806390	-1.0389610	-3.7468080
H	0.3963090	-1.0086930	-3.1625440

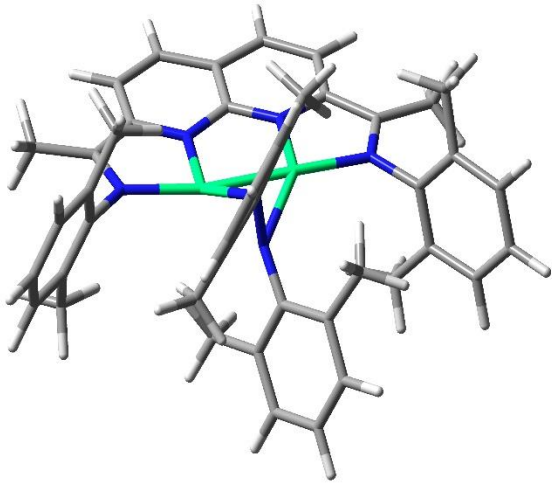

Charge: 0

Multiplicity: 1

Imaginary Frequencies: 0

Electronic Energy: -5049.82111491 Hartrees

Gibbs Free Energy (298.15 K): -5049.128763 Hartrees

Ni	-1.1252930	0.7215630	-0.1302420
Ni	1.1251470	0.7215460	0.1305590
N	-3.0475500	0.9538160	-0.1213030
N	3.0473890	0.9538040	0.1219880
N	-1.1384720	2.5550440	-0.1175500
N	1.1383250	2.5550410	0.1177730
N	-0.1220260	-0.7042360	0.7045450
N	0.1219600	-0.7039660	-0.7049230
C	-3.4507570	2.2461130	-0.1167010
C	3.4505950	2.2461070	0.1171120
C	-2.3770050	3.1910580	-0.1296930
C	-2.4396320	4.6036720	-0.1137980
H	-3.4142570	5.0995300	-0.1404280
C	-1.2740740	5.3661210	-0.0651620
H	-1.3260620	6.4593320	-0.0605350

C	-0.0000800	4.7259020	0.0000700
C	-0.0000720	3.2949560	0.0000940
C	1.2739150	5.3661280	0.0653190
H	1.3259010	6.4593390	0.0607000
C	2.4394670	4.6036870	0.1140100
H	3.4140760	5.0995730	0.1406660
C	2.3768670	3.1910640	0.1299460
C	-4.0353720	-0.0765280	-0.0137780
C	-4.7551500	-0.5246390	-1.1532350
C	-5.6642510	-1.5893970	-0.9959300
H	-6.2161400	-1.9453370	-1.8738690
C	-5.8747260	-2.1889460	0.2516760
H	-6.5856790	-3.0156740	0.3520800
C	-5.1714570	-1.7228670	1.3722860
H	-5.3356270	-2.1817390	2.3538290
C	-4.2466990	-0.6703250	1.2626710
C	4.0353430	-0.0764300	0.0145080
C	4.2472170	-0.6698220	-1.2620460
C	5.1721450	-1.7222090	-1.3716420
H	5.3367320	-2.1807720	-2.3532600
C	5.8750860	-2.1885140	-0.2509130
H	6.5861950	-3.0151090	-0.3513080
C	5.6641010	-1.5893420	0.9967810
H	6.2157560	-1.9454380	1.8748060
C	4.7547860	-0.5247580	1.1540760
C	-0.4215810	-1.8219120	1.5293100
C	0.1180960	-1.7409680	2.8515770
C	-0.1436110	-2.7787670	3.7580290
H	0.2936860	-2.7252080	4.7615200
C	-0.9543460	-3.8651370	3.3998610
C	-1.5309750	-3.8994550	2.1247420

H	-2.2026840	-4.7218610	1.8521720
C	-1.2935950	-2.8928920	1.1685790
C	0.4215920	-1.8212940	-1.5301200
C	-0.1179990	-1.7398020	-2.8524000
C	0.1438010	-2.7771890	-3.7592930
H	-0.2934220	-2.7231920	-4.7627930
C	0.9545510	-3.8636880	-3.4015540
C	1.5310910	-3.8985450	-2.1264110
H	2.2028170	-4.7210450	-1.8541640
C	1.2936090	-2.8924220	-1.1698120
C	-4.8993240	2.6566140	-0.0726900
H	-5.4828480	1.9734160	0.5653720
H	-5.3618100	2.6347350	-1.0769930
H	-5.0098820	3.6779380	0.3223040
C	4.8992080	2.6564070	0.0729290
H	5.4820930	1.9744620	-0.5670850
H	5.3624890	2.6321550	1.0768040
H	5.0097330	3.6785520	-0.3199120
C	-4.5959080	0.1284030	-2.5093930
H	-3.6440020	0.6724510	-2.5962300
C	-3.5064130	-0.1552160	2.4747330
H	-3.9058410	0.8211990	2.8067020
C	3.5073160	-0.1544190	-2.4742210
H	2.4420430	0.0056810	-2.2388080
C	4.5950450	0.1278890	2.5103770
H	3.6439760	0.6735310	2.5963220
H	3.5856840	-0.8585900	-3.3169390
H	3.9066130	0.8222500	-2.8056070
H	4.6406640	-0.6222100	3.3174520
H	5.4090460	0.8526270	2.7011840
H	-3.5842090	-0.8597670	3.3171860

H	-2.4412930	0.0052760	2.2388970
H	-5.4088380	0.8546900	-2.6988770
H	-4.6438010	-0.6212310	-3.3167580
H	-1.1528010	-4.6680730	4.1172220
H	1.1530920	-4.6662950	-4.1192590
C	2.0138210	-2.9856030	0.1572520
H	1.4633130	-3.6111380	0.8804130
H	3.0101920	-3.4327140	0.0101060
H	2.1611920	-1.9985730	0.6193070
C	0.9521420	-0.5550000	3.2717110
H	1.6183260	-0.2295580	2.4551830
H	0.3134290	0.3189310	3.4998860
H	1.5470010	-0.7853230	4.1700970
C	-2.0138570	-2.9855000	-0.1584990
H	-1.4633720	-3.6107080	-0.8819610
H	-3.0102190	-3.4326860	-0.0115070
H	-2.1612510	-1.9982660	-0.6201120
C	-0.9520430	-0.5536770	-3.2721010
H	-1.6184620	-0.2287470	-2.4555580
H	-0.3133670	0.3204440	-3.4996460
H	-1.5466670	-0.7835750	-4.1707530

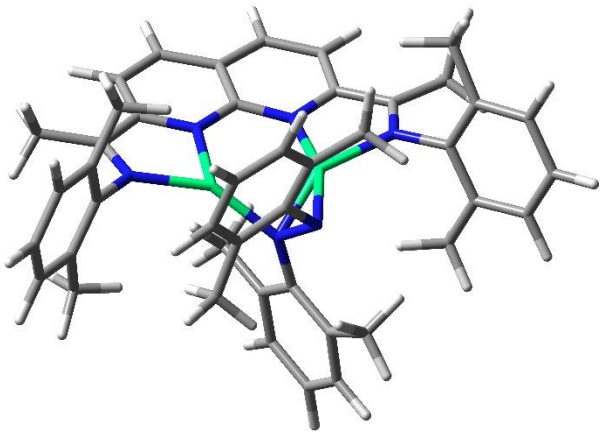

Charge: 0

Multiplicity: 3

Imaginary Frequencies: 0

Electronic Energy: -5049.81620498 Hartrees

Gibbs Free Energy (298.15 K): -5049.12748 Hartrees

Ni	-1.3132830	0.2406580	-0.0816570
Ni	1.2826640	0.2573250	0.0293080
N	-3.1798770	0.5261060	-0.5901670
N	3.1549970	0.6448480	-0.2691210
N	-1.2261810	2.1098740	-0.2361860
N	1.0885070	2.1384090	-0.2860950
N	-0.1043300	-0.6168170	1.0728580
N	-0.7270730	-1.5476490	0.2048000
C	-3.5447620	1.8198590	-0.5378930
C	3.4408820	1.9595080	-0.3554920
C	-2.4548290	2.7441630	-0.4030630
C	-2.5399920	4.1432920	-0.5127490
H	-3.5174580	4.6202530	-0.6257950
C	-1.3769980	4.9124160	-0.5168030
H	-1.4262620	6.0026820	-0.5994450
C	-0.1078510	4.2790080	-0.4478100
C	-0.0774740	2.8352990	-0.3324040

C	1.1381160	4.9594070	-0.4774010
H	1.1505960	6.0516740	-0.5449430
C	2.3261640	4.2350050	-0.4253480
H	3.2834410	4.7618400	-0.4501740
C	2.2999600	2.8285430	-0.3471900
C	-4.1921520	-0.4704150	-0.7746360
C	-4.6875810	-0.7577880	-2.0745170
C	-5.6149500	-1.8079780	-2.2194610
H	-5.9906320	-2.0442130	-3.2218570
C	-6.0596640	-2.5446680	-1.1146520
H	-6.7741680	-3.3630510	-1.2504730
C	-5.5931470	-2.2210590	0.1670210
H	-5.9556750	-2.7750490	1.0404410
C	-4.6663370	-1.1813910	0.3601950
C	4.2495750	-0.2717250	-0.3901510
C	4.6060100	-0.7389460	-1.6832630
C	5.6674430	-1.6548430	-1.7964520
H	5.9493080	-2.0168010	-2.7918740
C	6.3555530	-2.1110120	-0.6629620
H	7.1733410	-2.8314250	-0.7680920
C	5.9944870	-1.6368060	0.6050530
H	6.5354030	-1.9820720	1.4937470
C	4.9501330	-0.7054760	0.7654480
C	-0.5049150	-0.7009090	2.4546070
C	-0.1832250	0.4030360	3.3056760
C	-0.4459580	0.3210700	4.6829820
H	-0.1879410	1.1804350	5.3120850
C	-1.0215110	-0.8190480	5.2488670
C	-1.3377710	-1.8937160	4.4132500
H	-1.7867180	-2.7958480	4.8439880
C	-1.0998680	-1.8811780	3.0233440

C	0.2356850	-2.0247020	-0.7414420
C	-0.1925580	-2.2882330	-2.0807960
C	0.6878980	-2.8902510	-2.9891820
H	0.3441480	-3.0595620	-4.0163240
C	1.9751900	-3.2882080	-2.6007850
C	2.3697830	-3.0995420	-1.2735380
H	3.3528090	-3.4516680	-0.9442030
C	1.5299140	-2.4926040	-0.3155070
C	-4.9760780	2.2852450	-0.6353210
H	-5.6656980	1.5026820	-0.2844780
H	-5.2545140	2.5236030	-1.6784530
H	-5.1388320	3.1924480	-0.0326620
C	4.8534190	2.4668760	-0.5034180
H	5.2841200	2.1588040	-1.4731250
H	5.5111740	2.0478380	0.2761380
H	4.9061540	3.5626430	-0.4431720
C	-4.2745890	0.0560310	-3.2824550
H	-3.2465900	0.4394020	-3.1931460
C	-4.2192140	-0.7778110	1.7439540
H	-4.6913280	0.1725970	2.0560110
C	3.8574490	-0.2587160	-2.9051330
H	2.7901680	-0.5369060	-2.8492240
C	4.6253780	-0.1500580	2.1351420
H	3.5385660	-0.0765870	2.3065860
H	4.2791560	-0.7013590	-3.8216370
H	3.8943880	0.8402480	-3.0087990
H	5.0608670	-0.7785010	2.9283790
H	5.0285590	0.8717840	2.2663740
H	-4.4812420	-1.5421400	2.4919890
H	-3.1299820	-0.6103270	1.7766440
H	-4.9372020	0.9315120	-3.4192160

H	-4.3448720	-0.5448810	-4.2038360
H	-1.2181720	-0.8732170	6.3242700
H	2.6517430	-3.7639950	-3.3176640
C	0.4054310	1.6805470	2.7706500
H	1.2042300	1.4880110	2.0343040
H	-0.3577820	2.2791560	2.2415820
H	0.8121670	2.2943860	3.5900280
C	-1.5190390	-3.1371480	2.2757460
H	-2.3510730	-2.9508020	1.5801800
H	-0.7152160	-3.5708180	1.6617740
H	-1.8373520	-3.8986060	3.0089140
C	1.9859890	-2.5563230	1.1338880
H	2.2999530	-1.5797090	1.5343380
H	1.1893720	-2.9207330	1.8001440
H	2.8441940	-3.2416100	1.2183530
C	-1.5917080	-1.9369560	-2.4994140
H	-2.3253720	-2.6741540	-2.1253370
H	-1.8827870	-0.9720650	-2.0530040
H	-1.6856960	-1.8835930	-3.5956870

10. References

[1.]Zhou, Y.-Y.; Hartline, D. R.; Steiman, T. J.; Fanwick, P. E.; Uyeda, C. *Inorg. Chem.* **2014**, *53*, 11770-11777.

[2] Rigaku Corp., The Woodlands, Texas, USA.

[3] Otwinowski, Z.; Minor, W. *Methods Enzymol.* **1997**, *276*, 307-326.

[4] Bruker (2016). Apex3 v2016.9-0, Saint V8.34A, SAINT V8.37A, Bruker AXS Inc.: Madison (WI), USA, 2013/2014.

[5] (a) SHELXTL suite of programs, Version 6.14, 2000-2003, Bruker Advanced X-ray Solutions, Bruker AXS Inc., Madison, Wisconsin: USA; (b) Sheldrick, G. M. *Acta Crystallogr A.* **2008**, *64*, 112–122.

[6] (a) Sheldrick, G. M. University of Göttingen, Germany, **2016**; (b) Sheldrick, G. M. *Acta Crystallogr Sect C Struct Chem.* **2015**, *71*, 3-8.

[7] Hübschle, C. B.; Sheldrick, G. M.; Dittrich, B. *J. Appl. Crystallogr.* **2011**, *44*, 1281-1284.

[8] Harrity, K.; Jakobi, H.; Adams, H.; Foster, R.; *J. Org. Chem.* **2013**, *78*, 4049-4064.

[9] Grimes, K; Gupte, A.; Aldrich, C.; *Synthesis* **2010**, *9*, 1441-1448.

[10] Masuda, Y.; Watanabe, S.; Oyama, T.; Murata, M.; *J. Org. Chem.* **2000**, *65*, 164-168.

[11] Wang, L.; Ishida, A.; Hashidoko, Y.; Hashimoto, M. *Angew. Chem. Int. Ed.* **2017**, *56*, 870-873.

[12] Moneo, Á.; Justino, G. C.; Carvalho, M. F. N. N.; Oliveira, M. C.; Antunes, A. M. M.; Bléger, D.; Hecht, S.; Telo, J. P., *J. Phys. Chem. A.* **2013**, *117*, 14056-14064.

[13] Cai, S.; Rong, H.; Yu. X; Liu, X; Wang, D.; He, W; Li, Y. *ACS Catal.* **2013**, *3*, 478-486.

[14] Sakai, N.; Asama, S; Anai, S.; Konakahara, T.; *Tetrahedron* **2014**, *70*, 2027-2033.

[15] Moreno, C.; Arnanz, A.; Medina, R. M.; Macazaga, M. J.; Pascual, M.; García-Frutos, E. M.; Martínez-Gimeno, E.; Marcos, M. L., *Organometallics* **2015**, *34*, 2971-2984

[16] E. Busseron; J. Lux; M. Degardin; J. Rebek Jr., *Chem. Commun*., **2013**, *49*, 4842-4844.

[17] Zalesskaya, I. M.; Blakitnyi, A. N.; Saenko, E. P.; Fialkov, Yu. A.; Yagupol'skii, L. M. *Russ. J. Org. Chem.* **1980**, *16*, 1194-1202.

[18] Leyva, E.; Medina, C.; Moctezuma, E.; Leyva, S., *Can. J. Chem.* **2004**, *82*, 1712-1715.

[19] Zhang, C.; Jiao, N., *Angew. Chem. Int. Ed.* **2010**, *49*, 6174-6177.

[20] Bouchard, L.; Marcotte, I.; Chapuzet, J.; Lessard, J., *Can. J. Chem.* **2003**, *81*, 1108-1118.

[21] Nesmeyanov, A. N.; Perevalova, E. G.; Nikitina, T. V. *Dokl. Akad. Nauk USSR* **1961**, *138*, 118.

[22] Lemasson, F.; Berton, N.; Tittmann, J.; Hennrich, F.; Kappes, M. M.; Mayor, M. *Macromolecules* **2012**, *45*, 713-722.

[23] Rau, H.; Yu-Quan, S.; *J. Photochem. Photobiol. A.* **1988**, *42*, 321-327.

[24] John Towns, Timothy Cockerill, Maytal Dahan, Ian Foster, Kelly Gaither, Andrew Grimshaw, Victor Hazlewood, Scott Lathrop, Dave Lifka, Gregory D. Peterson, Ralph Roskies, J. Ray Scott, Nancy Wilkins-Diehr, "XSEDE: Accelerating Scientific Discovery", Computing in Science & Engineering, vol. 16, no. 5, pp. 62-74, Sept.-Oct. 2014, doi:10.1109/MCSE.2014.80

[25] Gaussian 09, Revision **D.01**, Frisch, M. J.; Trucks, G. W.; Schlegel, H. B.; Scuseria, G. E.; Robb, M. A.; Cheeseman, J. R.; Scalmani, G.; Barone, V.; Mennucci, B.; Petersson, G. A.; Nakatsuji, H.; Caricato, M.; Li, X.; Hratchian, H. P.; Izmaylov, A. F.; Bloino, J.; Zheng, G.; Sonnenberg, J. L.; Hada, M.; Ehara, M.; Toyota, K.; Fukuda, R.; Hasegawa, J.; Ishida, M.; Nakajima, T.; Honda, Y.; Kitao, O.; Nakai, H.; Vreven, T.; Montgomery, J. A., Jr.; Peralta, J. E.; Ogliaro, F.; Bearpark, M.; Heyd, J. J.; Brothers, E.; Kudin, K. N.; Staroverov, V. N.; Kobayashi, R.; Normand, J.; Raghavachari, K.; Rendell, A.; Burant, J. C.; Iyengar, S. S.; Tomasi, J.; Cossi, M.; Rega, N.; Millam, N. J.; Klene, M.; Knox, J. E.; Cross, J. B.; Bakken, V.; Adamo, C.; Jaramillo, J.; Gomperts, R.; Stratmann, R. E.; Yazyev, O.; Austin, A. J.; Cammi, R.; Pomelli, C.; Ochterski, J. W.; Martin, R. L.; Morokuma, K.; Zakrzewski, V. G.; Voth, G. A.; Salvador, P.; Dannenberg, J. J.; Dapprich, S.; Daniels, A. D.; Farkas, Ö.; Foresman, J. B.; Ortiz, J. V.; Cioslowski, J.; Fox, D. J. Gaussian, Inc., Wallingford CT, 2009.

APPENDIX C. SUPPORTING INFORMATION FOR CHAPTER 3.

1. General Information

General Considerations. All manipulations were carried out using standard Schlenk or glovebox techniques under an atmosphere of N_2. Solvents were dried and degassed by passing through a column of activated alumina and sparging with Ar gas. Deuterated solvents were purchased from Cambridge Isotope Laboratories, Inc., degassed, and stored over activated 3 Å molecular sieves prior to use. All other reagents and starting materials were purchased from commercial vendors and used without further purification unless otherwise noted. Liquid reagents were degassed and stored over activated 3 Å molecular sieves prior to use. The ($^{i\text{-Pr}}$NDI)$Ni_2(C_6H_6)$ complex (**1**), was prepared according to previously reported procedures.[1]

Physical Methods. ^{1}H NMR spectra were collected at room temperature on a Bruker Avance-III 800, Bruker AV-III-400-HD, Bruker DRX 500 MHz, or Varian Inova300 spectrometer. ^{1}H and ^{13}C NMR spectra are reported in parts per million relative to tetramethylsilane, using the residual solvent resonances as an internal standard. UV–vis measurements were acquired on an Agilent Cary 6000i UV-Vis-nIR spectrophotometer using a 1-cm two-window quartz cuvette. High-resolution mass data were obtained using a 6320 Ion Trap MS system. GPC data were obtained using a EcoSEC HLC-8321GPC/HT with a refractive index (RI) detector at 50 °C or a TOSOH ECOSEC HLC-8320 GPC run at 180 °C. IR data were collected on a Thermo Nicolet 6700 FT-IR spectrometer with an MCT-A detector and a KBr beam splitter with a range of 800–4500 cm^{-1}. Emission spectra were collected using an Edinburgh Instruments FLS980 Steady State Fluorescence Spectrometer with a xenon lamp. Thermogravimetric analysis was collected using a TA Instrument Q50 TGA instrument with a heating rate of 20 °C·min–1 under an N_2 atmosphere.

Spectroelectrochemistry Experiments. Spectroelectrochemistry data for **10** were obtained using a CHI 660E Potentiostat and a Flame Vis-NIR Fiber Optic Spectrometer Ocean Optics spectrometer. Electrochemical measurements of **15** were performed using a Gamry Interface 1000 Potentiostat. Cyclic voltammograms were acquired using a glassy carbon working

electrode (3 mm diameter disk) under an atmosphere of N_2. The potentials were internally referenced to the reversible Fc/Fc^+ couple.

Photoswitching Experiments. An in-house irradiation setup was built using a TENMA 72-2685 power supply, a 3D printed holder for a 1-cm UV-Vis cuvette bearing 3 unmounted LEDs. Two light sources were used: 395 nm (6 mW at 20mA) and 555 nm (1 mW at 20 mA) from Thorlabs, Newton, NJ, USA. The irradiance is 18 mW/cm² for the 395 nm LED unit and 3 mW/cm² for the 555 nm LED unit.

X-Ray Crystallography. Single Crystal XRD Data Collection. A single crystal of **17a** was coated with a trace of fomblin oil, affixed onto a MiTeGen micromesh mount and transferred to the goniometer head of a Bruker Quest diffractometer with kappa geometry, an I-μ-S microsource X-ray tube, laterally graded multilayer (Goebel) mirror single crystal for monochromatization, a Photon3 CMOS area detector and an Oxford Cryosystems low temperature device. Examination and data collection were performed with Cu Kα radiation (λ = 1.54178 Å) at 100 K. Data were collected, reflections were indexed and processed, and the files scaled and corrected for absorption using APEX3.[2]

The space group was assigned and the structure solved by direct methods using XPREP within the SHELXTL suite of programs[3] from an integration using only the major domain. The structure was refined using the hklf 5 routine by full matrix least squares against F^2 with all reflections of component 1 (including the overlapping ones), using Shelxl2016[4] using the graphical interface Shelxle[5] resulting in a BASF value of 0.392(1).

H atoms were positioned geometrically and constrained to ride on their parent atoms, with carbon hydrogen bond distances of 0.95 Å for aromatic C-H, 1.00, 0.99 and 0.98 Å for aliphatic C-H, CH_2 and CH_3 moieties, and 0.84 Å for O-H bonds, respectively. Methyl H and hydroxyl atoms were allowed to rotate but not to tip to best fit the experimental electron density. U_{iso}(H) values were set to a multiple of U_{eq}(C) with 1.5 for CH_3, and 1.2 for C-H units, respectively. Additional data collection and refinement details, including description of disorder and/or twinning (where present) can be found in Section **13**.

Complete crystallographic data, in CIF format, have been deposited with the Cambridge Crystallographic Data Centre. CCDC 2054149 contains the supplementary crystallographic data for this paper. These data can be obtained free of charge from The Cambridge Crystallographic Data Centre via www.ccdc.cam.ac.uk/data_request/cif.

2. Synthesis of Organoazides

SAFETY NOTE: Organoazides are high energy molecules, and they can be thermally unstable and shock sensitive. In order to minimize explosion hazards, care should be taken to avoid organoazides with low C-to-N ratios (generally C-to-N ratios >3 are recommended), limit scale to the extent possible, and store organoazides in solution. We did not encounter any specific safety concerns with the organoazides used in these studies. TGA studies were carried out using diazides **S10** and **2**.

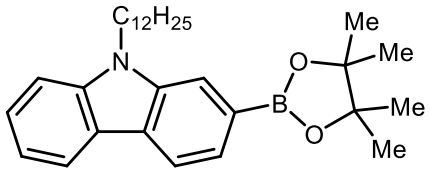

9-dodecyl-2-(4,4,5,5-tetramethyl-1,3,2-dioxaborolan-2-yl)-9H-carbazole (S1). This procedure is based on a modified literature procedure.[6] In an N_2 filled glovebox, a Schlenk tube was charged with 2-bromo-9-dodecyl-9H-carbazole[7], (0.50 g, 1.2 mmol, 1.0 equiv), Pd(dppf)Cl_2 (0.16 g, 0.22 mmol, 0.18 equiv), bis(pinacolato)diboron (0.37 g, 1.5 mmol, 1.2 equiv), KOAc (1.4 g, 15 mmol, 12 equiv), and 1,4-dioxane (33 mL). The reaction vessel was sealed, removed from the glovebox, and heated at 80 °C for 16 h. After cooling to room temperature, the reaction mixture was filtered through celite, and the filtrate was concentrated under reduced pressure. The residue was purified by column chromatography (SiO_2, 30% CH_2Cl_2/hexanes, R_f = 0.4). The product was isolated as a colorless oil (0.32 g, 57% yield).

^{1}H NMR (500 MHz, $CDCl_3$) δ 8.17 – 8.11 (m, 2H), 7.91 (s, 1H), 7.73 (d, *J* = 7.8 Hz, 1H), 7.50 (t, *J* = 7.6 Hz, 1H), 7.43 (d, *J* = 8.2 Hz, 1H), 7.27 – 7.22 (m, 1H), 4.36 (t, *J* = 7.4 Hz, 2H), 1.95 – 1.86 (m, 2H), 1.43 (s, 12H), 1.28 (m, 18H), 0.91 (t, *J* = 7.0 Hz, 3H).

^{13}C{^{1}H} NMR (126 MHz, $CDCl_3$) δ 141.0, 140.0, 126.2, 125.4, 125.1, 124.9, 122.6, 120.8, 119.6, 118.7, 115.1, 108.9, 83.8, 43.0, 32.0, 29.6, 29.1, 27.3, 25.2, 25.0, 24.9, 22.7, 14.1.

HRMS (APCI): calcd for $C_{30}H_{45}NO_2B^{10}$ $[M + H]^+$: 461.3574; found: 461.3562

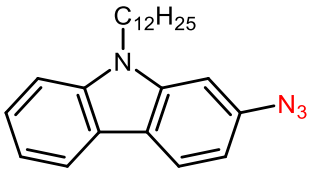

2-azido-9-dodecyl-9H-carbazole (4b). This procedure is based on a modified literature procedure.[8] NaN_3 (0.068 g, 1.0 mmol, 1.5 equiv) and $Cu(OAc)_2$ (0.013 g, 0.069 mmol, 0.10 equiv) were added to a solution of **S1** (0.32 g, 0.69 mmol, 1.0 equiv) in a mixture of $CHCl_3$ (5.7 mL) and MeOH (5.7 mL). The reaction was heated at 55 °C and stirred under air for 24 h. After cooling to room temperature, the reaction mixture was filtered and the filtrate was concentrated under reduced pressure. The residue was purified by column chromatography (SiO_2, 100% hexanes, R_f = 0.8). The product was isolated as an off-white solid (0.18 g, 70% yield).

^{1}H NMR (800 MHz, $CDCl_3$) δ 8.05 (d, J = 8.0 Hz, 2H), 7.46 (t, J = 7.6 Hz, 1H), 7.40 (d, J = 8.1 Hz, 1H), 7.25 (t, J = 7.3 Hz, 1H), 7.01 (s, 1H), 6.95 (d, 1H), 4.26 (t, J = 7.3 Hz, 2H), 1.90 – 1.84 (m, 2H), 1.39 – 1.24 (m, 18H), 0.89 (t, J = 7.2 Hz, 3H).

^{13}C{^{1}H} NMR (201 MHz, $CDCl_3$) δ 141.3, 140.8, 137.7, 125.5, 122.5, 121.4, 120.3, 120.0, 119.2, 110.2, 108.7, 99.0, 43.1, 31.8, 29.5, 29.5, 29.4, 29.3, 29.3, 28.8, 27.2, 22.6, 14.1.

HRMS (APCI): calcd for $C_{24}H_{32}N_4$ $[M + H]^+$: 377.2700; found: 377.2704

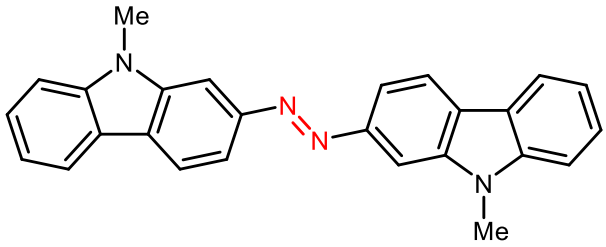

(E)-1,2-bis(9-methyl-9H-carbazol-2-yl)diazene (5a). This procedure is based on a modified literature procedure.[9] In an N_2 filled glovebox, a 20-mL vial was charged with **4a** (0.044 g, 0.20 mmol, 1.0 equiv), toluene (4.0 mL), and a magnetic stir bar. While stirring, **1** (7.0 mg, 0.010 mmol, 5 mol%) dissolved in toluene (1.0 mL) was added to the reaction vial. The vial was sealed, and the reaction mixture was stirred at room temperature. After 2 h, the reaction vial was opened to air, and the crude mixture was directly loaded onto a column (SiO_2, 5% EtOAc/hexanes, R_f = 0.3) for purification. The product was isolated as an orange solid. Run 1: 0.033 g, 44% yield; Run 2: 0.035 g, 44% yield.

^{1}H NMR (400 MHz, $CDCl_3$) δ 8.22 (d, J = 8.3 Hz, 2H), 8.14 (d, J = 7.8 Hz, 2H), 8.07 (s, 2H), 7.97 (d, J = 8.0 Hz, 2H), 7.53 (m, 2H), 7.44 (d, J = 8.2 Hz, 2H), 7.30 – 7.27 (m, 2H), 3.97 (s, 6H).

^{13}C{^{1}H} NMR (201 MHz, $CDCl_3$) δ 151.3, 142.5, 141.4, 126.6, 125.1, 122.4, 120.9, 120.6, 119.4, 115.3, 108.7, 102.8, 29.3.

HRMS (APCI): calcd for $C_{26}H_{21}N_4$ $[M + H]^+$: 389.1761; found: 389.1765

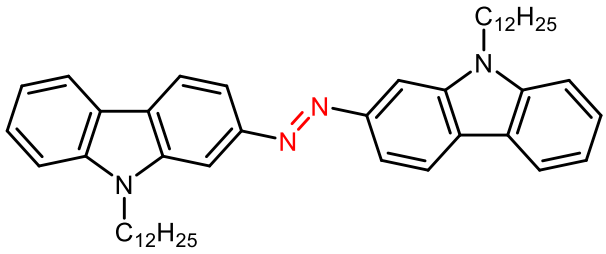

(E)-1,2-bis(9-dodecyl-9H-carbazol-2-yl)diazene (5b). This procedure is based on a modified literature procedure.[9] In an N_2 filled glovebox, a 20-mL vial was charged with **4b** (0.075 g, 0.20 mmol, 1.0 equiv), toluene (4.0 mL), and a magnetic stir bar. While stirring, **1** (7.0 mg, 0.010 mmol, 5 mol%) dissolved in toluene (1.0 mL) was added to the reaction vial. The vial was sealed, and the reaction mixture was stirred at room temperature. After 2 h, the reaction vial was opened to air, and the crude mixture was directly loaded onto a column (SiO_2, 2% EtOAc/hexanes, R_f = 0.2) for purification. The product was isolated as a yellow solid. Run 1: 0.066 g, 95% yield; Run 2: 0.066 g, 95% yield.

^{1}H NMR (400 MHz, $CDCl_3$) δ 8.23 (d, *J* = 8.3 Hz, 2H), 8.16 (d, *J* = 7.8 Hz, 2H), 8.09 (d, *J* = 1.6 Hz, 2H), 7.98 (d, *J* = 8.3 Hz, 2H), 7.57 – 7.49 (m, 2H), 7.45 (d, *J* = 8.2 Hz, 2H), 7.28 (t, *J* = 7.3 Hz, 2H), 4.41 (t, *J* = 7.3 Hz, 4H), 1.96 (p, *J* = 7.4 Hz, 4H), 1.50 – 1.42 (m, 4H), 1.41 – 1.34 (m, 4H), 1.33 – 1.22 (m, 28H), 0.89 (t, *J* = 6.8 Hz, 6H).

^{13}C{^{1}H} NMR (101 MHz, $CDCl_3$) δ 151.2, 141.8, 140.7, 126.4, 125.0, 122.4, 120.8, 120.5, 119.2, 114.1, 108.9, 104.0, 43.2, 31.8, 29.6, 29.5, 29.4, 29.3, 29.0, 27.3, 22.6, 14.1.

UV–Vis–NIR (C_6H_5Cl , 0.143 mM): λ_{max}, nm (ε, M^{-1} cm^{-1}): 302 (1800), 398 (4900).

HRMS (APCI): calcd for $C_{48}H_{65}N_4$ $[M + H]^+$: 697.5204 ; found: 697.5207

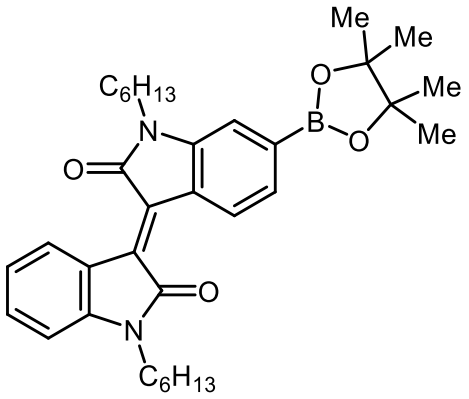

(E)-1,1'-dihexyl-6-(4,4,5,5-tetramethyl-1,3,2-dioxaborolan-2-yl)-[3,3'-biindolinylidene]-2,2'-dione (S2). This procedure is based on a modified literature procedure.[6] In an N_2 filled glovebox, a Schlenk tube was charged with (E)-6-bromo-1,1'-dihexyl-[3,3'-biindolinylidene]-2,2'-dione[10] (0.16 g, 0.31 mmol, 1.0 equiv), Pd(dppf)Cl_2 (0.041 g, 0.057 mmol, 0.18 equiv), bis(pinacolato)diboron (0.12 g, 0.47 mmol, 1.5 equiv), KOAc (0.092 g, 0.94 mmol, 3.0 equiv), and 1,4-dioxane (6.2 mL). The reaction vessel was sealed, removed from the glovebox, and heated at 80 °C for 16 h. After cooling to room temperature, the reaction mixture was filtered, and the filtrate was concentrated under reduced pressure. The residue was purified by column chromatography (SiO_2, 10% Et_2O/hexanes, R_f = 0.2). The product was isolated as a red solid (0.14 g, 81% yield).

^{1}H NMR (400 MHz, $CDCl_3$) δ 9.18 (d, 1H), 9.14 (d, *J* = 7.9 Hz, 1H), 7.49 (d, *J* = 7.9, 1.0 Hz, 1H), 7.34 (t, 1H), 7.16 (s, 1H), 7.03 (t, 1H), 6.77 (d, *J* = 7.8 Hz, 1H), 3.78 (p, *J* = 15.2, 7.4 Hz, 4H), 1.76 – 1.66 (m, 4H), 1.37 (s, 12H), 1.35 – 1.22 (m, 12H), 0.91 – 0.86 (m, 6H).

^{13}C{^{1}H} NMR (101 MHz, $CDCl_3$) δ 167.7, 167.6, 144.8, 143.8, 134.2, 133.4, 132.4, 130.0, 128.9, 128.7, 124.2, 122.0, 121.6, 113.0, 107.8, 84.0, 40.0, 39.9, 31.4, 27.4, 27.3, 26.6, 26.6, 24.8, 22.5, 13.9, 13.9.

HRMS (APCI): calcd for $C_{34}H_{45}B^{10}N_2O_4$ $[M + H]^+$: 556.3581; found: 556.3571

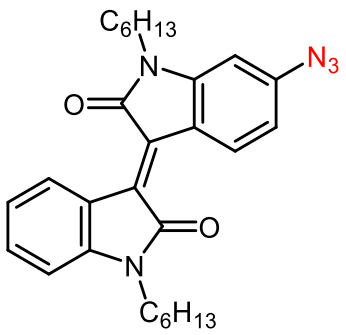

(E)-6-azido-1,1'-dihexyl-[3,3'-biindolinylidene]-2,2'-dione (S3). This procedure is based on a modified literature procedure.[8] NaN_3 (0.060 g, 0.93 mmol, 1.5 equiv) and $Cu(OAc)_2$ (0.011 g, 0.062 mmol, 0.10 equiv) were added to a solution of **S1** (0.34 g, 0.62 mmol, 1.0 equiv) in a mixture of $CHCl_3$ (5.0 mL) and MeOH (5.0 mL). The reaction was heated at 55 °C and stirred under air for 24 h. After cooling to room temperature, the reaction mixture was filtered, and the filtrate was concentrated under reduced pressure. The residue was purified by column chromatography (SiO_2, 10% Et_2O/hexanes, R_f = 0.3). The product was isolated as a deep red solid. (0.14 g, 48% yield). ^1H NMR (500 MHz, $CDCl_3$) δ 9.23 (d, *J* = 8.6 Hz, 1H), 9.14 (d, *J* = 8.0 Hz, 1H), 7.33 (t, 1H), 7.03 (t, *J* = 7.8 Hz, 1H), 6.77 (d, *J* = 7.8 Hz, 1H), 6.68 (dd, *J* = 8.6, 2.2 Hz, 1H), 6.36 (d, *J* = 2.2 Hz, 1H), 3.79 – 3.70 (m, 4H), 1.68 (m, 4H), 1.44 – 1.35 (m, 4H), 1.35 – 1.27 (m, 8H), 0.91 – 0.85 (m, 6H).

$^{13}C\{^1H\}$ NMR (126 MHz, $CDCl_3$) δ 168.2, 167.9, 146.5, 144.6, 143.8, 132.5, 132.2, 131.6, 129.8, 122.1, 121.7, 118.7, 111.9, 107.9, 99.1, 98.9, 40.2, 40.1, 31.5, 27.5, 26.7, 22.5, 14.0.

HRMS (APCI): calcd for $C_{28}H_{33}N_5O_2$ $[M + H]^+$: 472.2707 found: 472.2717

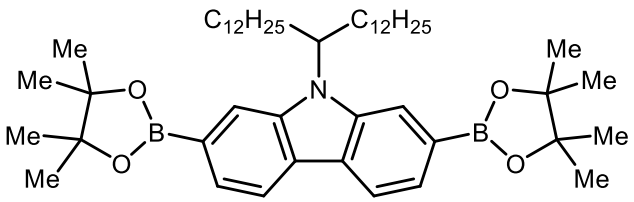

9-(pentacosan-13-yl)-2,7-bis(4,4,5,5-tetramethyl-1,3,2-dioxaborolan-2-yl)-9H-carbazole (S4). This procedure is based on a modified literature procedure.[6] In an N_2 filled glovebox, a Schlenk tube was charged with 2,7-dibromo-9-(pentacosan-13-yl)-9H-carbazole[11], (1.0 g, 1.5 mmol, 1.0 equiv), $Pd(dppf)Cl_2$ (0.39 mg, 0.53 mmol, 0.35 equiv), bis(pinacolato)diboron (0.90 mg, 3.6 mmol, 2.4 equiv), KOAc (1.7 g, 18 mmol, 12 equiv), and 1,4-dioxane (40 mL). The reaction vessel was sealed, removed from the glovebox, and heated at 80 °C for 16 h. After cooling to room temperature, the reaction mixture was filtered, and the filtrate was concentrated under reduced pressure. The residue was purified by column chromatography (SiO_2, 50% CH_2Cl_2/hexanes, R_f = 0.4). The product was isolated as a yellow oil (0.64 g, 56% yield).

^{1}H NMR (800 MHz, $CDCl_3$) δ 8.14 (d, J = 24.3, 2H), 8.04 (s, 1H), 7.90 (s, 1H), 7.74 – 7.63 (m, 2H), 4.75 – 4.67 (m, 1H), 2.40 – 2.30 (m, 2H), 2.00 – 1.93 (m, 2H), 1.41 (s, 24H), 1.33 – 1.09 (m, 38H), 1.02 – 0.97 (m, 2H), 0.88 (t, J = 7.2 Hz, 6H).

^{13}C{^{1}H} NMR (201 MHz, $CDCl_3$) δ 141.9, 138.6, 128.3, 126.0, 124.6, 124.5, 119.96, 119.65, 118.0, 115.4, 83.6, 56.3, 33.8, 31.8, 29.6, 29.5, 29.5, 29.4, 29.3, 29.3, 26.7, 24.9, 22.6, 14.0.

HRMS (APCI): calcd for $C_{49}H_{81}B^{10}{}_2NO_4$ [M + H]: 769.6461; found: 769.6446

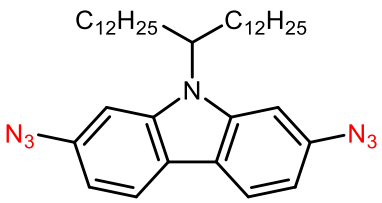

2,7-diazido-9-(pentacosan-13-yl)-9H-carbazole (2). This procedure is based on a modified literature procedure.[8] NaN_3 (0.13 g, 2.0 mmol, 3.0 equiv) and $Cu(OAc)_2$ (0.024 g, 0.13 mmol, 0.20 equiv) were added to a solution of **S4** (0.51 g, 0.66 mmol, 1.0 equiv) in a mixture of $CHCl_3$ (3.3 mL) and MeOH (3.3 mL). The reaction was heated at 55 °C and stirred under air for 24 h. After cooling to room temperature, the reaction mixture was filtered, and the filtrate was concentrated under reduced pressure. The residue was purified by column chromatography (SiO_2, 100% hexanes, R_f = 0.6). The product was isolated as a yellow oil (0.29 g, 73% yield).

^{1}H NMR (800 MHz, $CDCl_3$) δ 7.98 (dd, J = 28.7, 8.3 Hz, 2H), 7.12 (s, 1H), 6.97 – 6.90 (m, 3H), 4.45 – 4.38 (m, 1H), 2.25 – 2.14 (m, 2H), 1.93 – 1.82 (m, 2H), 1.30 – 1.08 (m, 38H), 1.01 – 0.94 (m, 2H), 0.87 (t, J = 7.2 Hz, 6H).

^{13}C{^{1}H} NMR (201 MHz, $CDCl_3$) δ 143.3, 139.7, 137.6, 137.0, 128.3, 121.0, 120.8, 119.7, 110.5, 110.4, 102.0, 99.4, 56.7, 33.4, 31.8, 29.5, 29.5, 29.4, 29.3, 29.2, 26.6, 22.6, 14.1.

HRMS (APCI): calcd for $C_{37}H_{58}N_7$ [M + H]: 600.4748; found: 600.4752

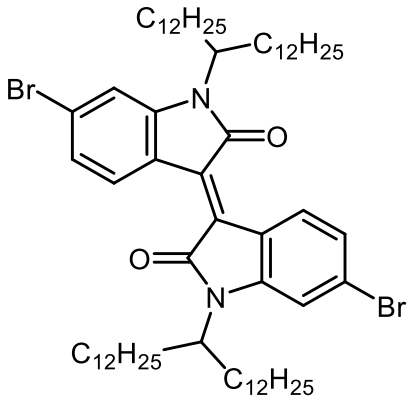

(E)-6,6'-dibromo-1,1'-di(pentacosan-13-yl)-[3,3'-biindolinylidene]-2,2'-dione (S5). This procedure is based on a modified literature procedure.[12] 6,6'-dibromoisoindigo[12] (0.42 g, 1.0 mmol, 1.0 equiv) and Cs_2CO_3 (0.98 g, 3.0 mmol, 3.0 equiv) were added to a reaction flask and sealed. The reaction vessel was sparged with N_2 to remove air. Anhydrous N,N-Dimethylformamide (10 mL) was added, and the mixture was heated at 70 °C. After 30 minutes of heating, pentacosan-13-yl 4-methylbenzenesulfonate[13] (1.2 g, 2.2 mmol, 2.2 equiv) dissolved in anhydrous N,N-dimethylformamide (10.0 mL) was added, and the reaction was allowed to stir for 16 h at 70 °C. After cooling to room temperature, the reaction mixture was filtered, and the filtrate was concentrated under reduced pressure. The residue was purified by column chromatography (SiO_2, hexanes, R_f = 0.2). The product was isolated as a deep red solid (0.56 g, 50% yield).

^{1}H NMR (800 MHz, $CDCl_3$) δ 9.06 (s, 2H), 7.23 – 6.90 (m, 4H), 4.64 (s, 1H), 3.69 (s, 1H), 2.26 (s, 1H), 1.92 (s, 3H), 1.75 (m, 4H), 1.38 – 1.13 (m, 80H), 0.89 (t, *J* = 7.2 Hz, 12H).

^{13}C{^{1}H} NMR (201 MHz, $CDCl_3$) δ 168.1, 144.6, 130.9, 126.4, 124.7, 120.5, 113.1, 52.5, 31.9, 31.9, 29.6, 29.6, 29.5, 29.5, 29.4, 29.3, 26.6, 22.6, 14.1.

HRMS (APCI): calcd for $C_{66}H_{109}Br_2N_2O_2$ $[M + H]^+$: 1119.6850; found: 1119.6866

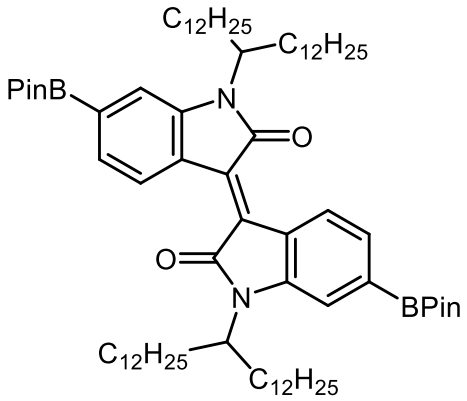

(E)-1,1'-di(pentacosan-13-yl)-6,6'-bis(4,4,5,5-tetramethyl-1,3,2-dioxaborolan-2-yl)-[3,3'-biindolinylidene]-2,2'-dione (S6). This procedure is based on a modified literature procedure.[6] In an N_2 filled glovebox, a Schlenk tube was charged with **S5** (0.56 g, 0.50 mmol, 1.0 equiv), $Pd(dppf)Cl_2$ (0.022 g, 0.030 mmol, 0.060 equiv), bis(pinacolato)diboron (0.38 g, 1.5 mmol, 3.0 equiv), KOAc (0.29 g, 3.0 mmol, 6.0 equiv), and 1,4-dioxane (10.0 mL). The reaction vessel was sealed, removed from the glovebox, and heated at 80 °C for 16 h. After cooling to room temperature, the reaction mixture was filtered, and the filtrate was concentrated under reduced pressure. The residue was purified by column chromatography (SiO_2, 20% CH_2Cl_2/hexanes, R_f = 0.25). The product was isolated as a deep red solid (0.49 g, 80% yield).

^{1}H NMR (400 MHz, $CDCl_3$) δ 9.09 (s, 2H), 7.45 (d, *J* = 8.0 Hz, 2H), 7.26 (s, 3H), 4.64 (s, 1H), 3.88 (s, 1H), 2.40 – 1.90 (m, 4H), 1.82 – 1.66 (m, 4H), 1.36 (s, 24H), 1.32 – 1.15 (m, 80H), 0.86 (t, *J* = 7.0 Hz, 12H).

^{13}C{^{1}H} NMR (201 MHz, $CDCl_3$) δ 168.0, 142.9, 133.6, 128.5, 124.3, 115.2, 83.9, 52.3, 32.0, 31.8, 29.6, 29.6, 29.5, 29.4, 29.3, 26.7, 24.8, 22.6, 14.1.

HRMS (APCI): calcd for $C_{78}H_{133}B^{10}{}_2N_2O_4$ $[M + H]^+$: 1215.0381; found: 1215.0417

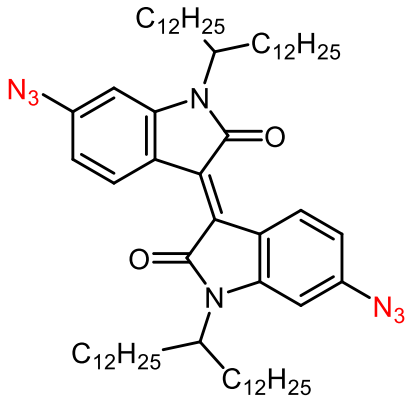

(E)-6,6'-diazido-1,1'-di(pentacosan-13-yl)-[3,3'-biindolinylidene]-2,2'-dione (S7). This procedure is based on a modified literature procedure.[8] NaN_3 (0.036 g, 0.56 mmol, 3.0 equiv) and $Cu(OAc)_2$ (7.0 mg, 0.037 mmol, 0.20 equiv) were added to a solution of **S6** (0.23 g, 0.19 mmol, 1.0 equiv) in a mixture of $CHCl_3$ (3.5 mL) and MeOH (3.5 mL). The reaction was heated at 55 °C and stirred under air for 16 h. After cooling to room temperature, the reaction mixture was filtered, and the filtrate was concentrated under reduced pressure. The residue was purified by column chromatography (SiO_2, 10% CH_2Cl_2/hexanes, R_f = 0.3). The product was isolated as a deep red solid (0.098 g, 50% yield).

^{1}H NMR (500 MHz, $CDCl_3$) δ 9.17 (s, 2H), 6.70 (d, *J* = 8.7 Hz, 2H), 6.55 (s, 2H), 4.64 (s, 1H), 3.68 (s, 1H), 2.26 (s, 1H), 1.90 (s, 3H), 1.78 – 1.67 (m, 4H), 1.37 – 1.14 (m, 80H), 0.87 (t, *J* = 6.9 Hz, 12H).

^{13}C{^{1}H} NMR (126 MHz, $CDCl_3$) δ 168.7, 145.2, 143.5, 131.1, 131.1, 118.8, 111.5, 101.1, 52.4, 31.9, 29.9, 29.6, 29.6, 29.5, 29.4, 26.7, 23.0, 22.7, 14.1.

HRMS (APCI): calcd for $C_{66}H_{109}N_8O_2$ $[M + H]^+$: 1045.8668; found: 1045.8696

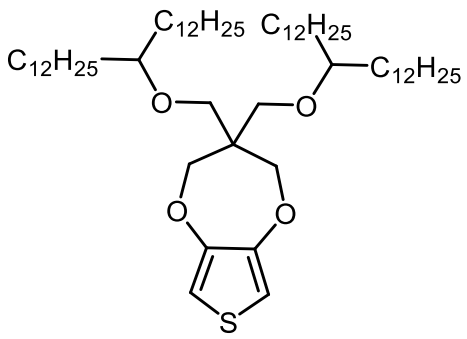

3,3-bis((pentacosan-13-yloxy)methyl)-3,4-dihydro-2H-thieno[3,4-b][1,4]dioxepine (S8). This procedure is based on a modified literature procedure.[14] A round-bottom flask was charged with NaH (0.11 g, 4.4 mmol, 3.0 equiv) and pentacosan-13-ol[13] (1.2 g, 3.2 mmol, 2.1 equiv). The solution was sparged with N_2 to remove air. Anhydrous N,N-dimethylformamide (6.0 mL) was added to the flask, and the reaction mixture was heated at 70 °C. After 6 h, 3,3-bis(bromomethyl)-3,4-dihydro-2H-thieno[3,4-b][1,4]dioxepine[14] (0.50 g, 1.5 mmol, 1.0 equiv) was added as a solid, and the reaction mixture was allowed to stir at 70 °C for 48 h. After cooling to room temperature, the reaction mixture was added to 200 mL of sat. NaCl (aq). The crude product was extracted with three portions of diethyl ether, and the combined organic phases were washed with three portions of water. The organic phase was dried using Na_2SO_4 then concentrated under reduced pressure. The residue was purified by column chromatography (SiO_2, 15% CH_2Cl_2/hexanes, R_f = 0.3). The product was isolated as a white solid (0.65 g, 48% yield).

^{1}H NMR (400 MHz, $CDCl_3$) δ 6.43 (s, 2H), 4.01 (s, 4H), 3.50 (s, 4H), 3.23 – 3.12 (m, 2H), 1.50 – 1.36 (m, 8H), 1.26 (s, 80H), 0.88 (t, *J* = 6.7 Hz, 12H).

^{13}C{^{1}H} NMR (201 MHz, $CDCl_3$) δ 149.7, 104.7, 67.7, 47.8, 34.1, 33.6, 31.9, 29.9, 29.7, 29.6, 29.6, 29.3, 25.3, 22.6, 22.3, 14.1, 14.0.

HRMS (APCI): calcd for $C_{59}H_{113}O_4S$ $[M + H]^+$: 917.8354; found: 917.8342

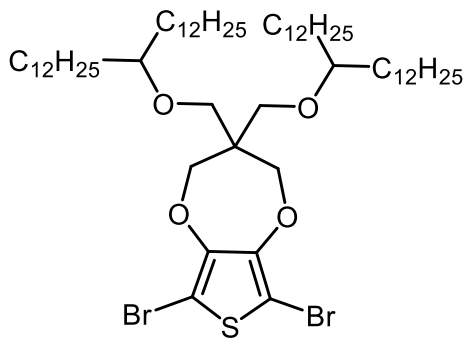

6,8-dibromo-3,3-bis((pentacosan-13-yloxy)methyl)-3,4-dihydro-2H-thieno[3,4-b][1,4]dioxepine (S9). This procedure is based on a modified literature procedure.[14] A round bottom flask was charged with **S8** (0.30 g, 0.33 mmol, 1.0 equiv) and NBS (0.17 g, 0.98 mmol, 3.0 equiv). The flask was sparged with N_2, and $CHCl_3$ (6.0 mL) was added under N_2. The reaction was allowed to stir at room temperature for 16 h. The reaction mixture was concentrated under reduced pressure, and the residue was purified by column chromatography (SiO_2, 10% CH_2Cl_2/hexanes, R_f = 0.4). The product was isolated as a white solid (0.33 g, 94% yield).

^{1}H NMR (500 MHz, $CDCl_3$) δ 4.09 (s, 4H), 3.53 (s, 4H), 3.21 – 3.15 (m, 2H), 1.49 – 1.23 (m, 88H), 0.88 (t, *J* = 6.9 Hz, 12H).

^{13}C{^{1}H} NMR (126 MHz, $CDCl_3$) δ 147.3, 90.9, 67.9, 48.2, 33.8, 32.1, 30.1, 29.9, 29.9, 29.6, 25.5, 22.9, 14.3.

HRMS (APCI): calcd for $C_{59}H_{110}Br_2O_4S$ $[M + H]^+$:1073.6564 ; found: 1073.6551

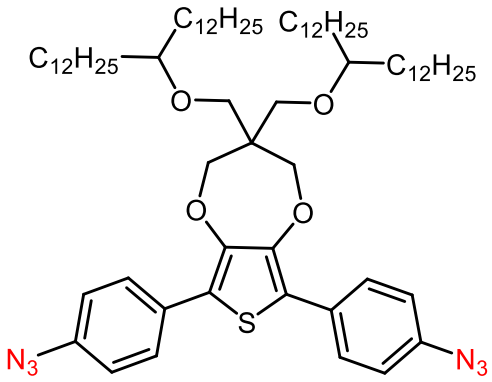

6,8-bis(4-azidophenyl)-3,3-bis((pentacosan-13-yloxy)methyl)-3,4-dihydro-2H-thieno[3,4-b][1,4]dioxepine (S10). This procedure is based on a modified literature procedure.[15] In an N_2 filled glovebox, a Schlenk tube was charged with **S9** (0.19 g, 0.18 mmol, 1.0 equiv), 2-(4-azidophenyl)-4,4,5,5-tetramethyl-1,3,2-dioxaborolane[16] (0.095 g, 0.39 mmol, 2.2 equiv), tris(o-methoxyphenyl)phosphine (0.015 g, 0.042 mmol, 0.24 equiv), K_3PO_4 (0.23 g, 1.1 mmol, 6.0 equiv), $Pd_2(dba)_3$ (0.019 g, 0.021 mmol, 0.12 equiv), Aliquat 336 (1 drop), and toluene (6.1 mL). The Schlenk tube was sealed and removed from the glovebox. Under N_2, degassed H_2O (0.90 mL) was added. The reaction was allowed to stir at room temperature for 4 h. The reaction mixture was then diluted with CH_2Cl_2 and washed with water (2 × 50 mL). The organic phase was dried over Na_2SO_4, filtered, and concentrated under reduced pressure. The residue was purified by column chromatography (SiO_2, 20% CH_2Cl_2/hexanes, R_f = 0.4). The product was isolated as an off-white solid. (0.12 g, 60% yield).

^{1}H NMR (400 MHz, $CDCl_3$) δ 7.72 (d, *J* = 8.8 Hz, 4H), 7.02 (d, *J* = 8.8 Hz, 4H), 4.16 (s, 4H), 3.58 (s, 4H), 3.26 – 3.16 (m, 2H), 1.43 (s, 8H), 1.26 (s, 80H), 0.87 (t, *J* = 6.8 Hz, 12H).

^{13}C{^{1}H} NMR (201 MHz, $CDCl_3$) δ 146.4, 138.2, 129.9, 127.8, 119.1, 118.3, 80.0, 73.9, 67.7, 47.9, 33.6, 31.9, 29.9, 29.7, 29.6, 29.3, 25.3, 22.6, 14.1.

HRMS (APCI): calcd for $C_{71}H_{118}N_6O_4S$ $[M + H]^+$: 1151.9008; found: 1151.8990

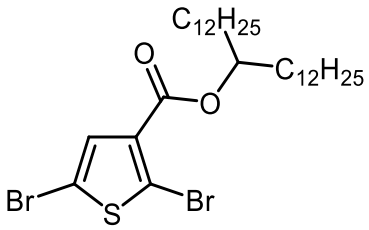

Pentacosan-13-yl 2,5-dibromothiophene-3-carboxylate (S11). This procedure is based on a modified literature procedure.[17] A round-bottom flask was charged with 2,5-dibromothiophene-3-carboxylic acid[17] (0.37 g, 1.0 mmol, 1.0 equiv), 4-Dimethylaminopyridine (0.37 g, 3.0 mmol, 3.0 equiv), pentacosan-13-ol[13] (0.86 g, 3.0 mmol, 3.0 equiv), and N,N'-dicyclohexylcarbodiimide (0.62 g, 3.0 mmol, 3.0 equiv). The reaction vessel was sparged with N_2, and CH_2Cl_2 (10 mL) was added to the reaction flask. The reaction was allowed to stir at room temperature for 48 h. The resulting mixture was filtered through celite, and the filtrate was concentrated under reduced pressure. The residue was purified by column chromatography (SiO_2, 10% Et_2O/hexanes). The product was isolated as a white semi-solid. (0.46 mg, 72% yield).

^{1}H NMR (400 MHz, $CDCl_3$) δ 7.33 (s, 1H), 5.13 – 5.01 (m, 1H), 1.68 – 1.57 (m, 4H), 1.26 (d, J = 6.5 Hz, 40H), 0.88 (m, 6H).

$^{13}C\{^1H\}$ NMR (101 MHz, $CDCl_3$) δ 160.7, 132.5, 131.9, 118.9, 111.3, 76.0, 34.8, 34.2, 32.1, 31.8, 29.8, 29.8, 29.7, 29.7, 29.5, 28.4, 25.5, 22.9, 22.8, 20.8, 14.3, 11.6.

HRMS (APCI): calcd for $C_{30}H_{52}Br_2O_2S$ $[M + H]^+$: 635.2128; found: 635.2123

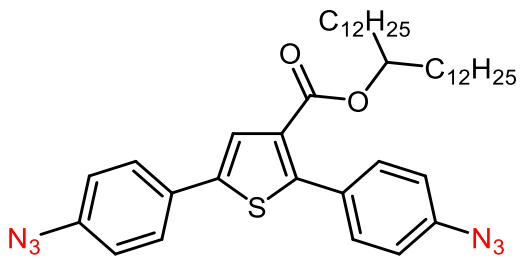

Pentacosan-13-yl 2,5-bis(4-azidophenyl)thiophene-3-carboxylate (S12). This procedure is based on a modified literature procedure.[15] In an N_2 filled glovebox, a Schlenk tube was charged with **S11** (0.20 g, 0.31 mmol, 1.0 equiv), 2-(4-azidophenyl)-4,4,5,5-tetramethyl-1,3,2-dioxaborolane[16] (0.17 g, 0.69 mmol, 2.2 equiv), tris(o-methoxyphenyl)phosphine (0.027 g, 0.075 mmol, 0.24 equiv), K_3PO_4 (0.40 g, 1.9 mmol, 6.0 equiv), $Pd_2(dba)_3$ (0.035 g, 0.038 mmol, 0.12 equiv), Aliquat 336 (1 drop), and toluene (11 mL). The Schlenk tube was sealed and removed from the glovebox. Under N_2, degassed H_2O (1.6 mL) was added. The reaction was allowed to stir at room temperature for 4 h. The reaction mixture was then diluted with CH_2Cl_2 and washed with water (2 × 50 mL). The organic phase was dried over Na_2SO_4, filtered, and concentrated under reduced pressure. The residue was purified by column chromatography (SiO_2, 10% CH_2Cl_2/hexanes, R_f = 0.2). The product was isolated as a yellow solid. (0.13 g, 57% yield).

^{1}H NMR (400 MHz, $CDCl_3$) δ 7.68 (s, 1H), 7.59 (d, *J* = 8.2 Hz, 2H), 7.52 (d, *J* = 8.2 Hz, 2H), 7.05 (d, *J* = 8.1 Hz, 4H), 5.00 (m, 1H), 1.51 (d, *J* = 6.5 Hz, 4H), 1.26 (s, 40H), 0.89 (t, *J* = 6.8 Hz, 6H).

^{13}C{^{1}H} NMR (101 MHz, $CDCl_3$) δ 162.9, 148.3, 141.5, 140.6, 139.9, 131.5, 130.3, 130.1, 129.9, 127.2, 125.6, 119.7, 118.6, 75.2, 34.1, 32.0, 29.8, 29.8, 29.7, 29.7, 29.5, 25.4, 22.8, 14.2.

HRMS (APCI): calcd for $C_{42}H_{60}N_6O_2S$ $[M + H]^+$: 712.4493; found: 712.4495

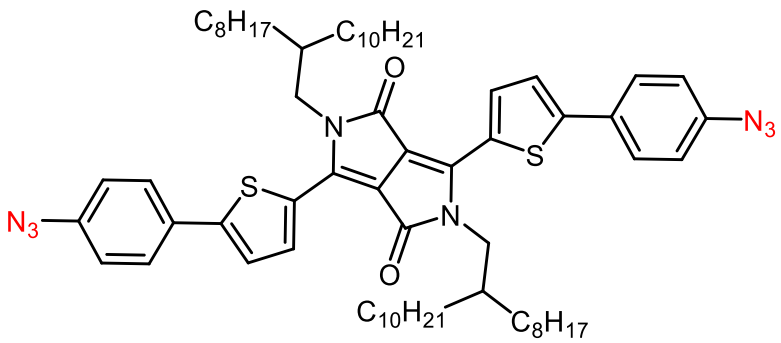

3,6-bis(5-(4-azidophenyl)thiophen-2-yl)-2,5-bis(2-octyldodecyl)-2,5-dihydropyrrolo[3,4-c]pyrrole-1,4-dione (S13). This procedure is based on a modified literature procedure.[15] In an N_2 filled glovebox, a Schlenk tube was charged with 3,6-bis(5-bromothiophen-2-yl)-2,5-bis(2-octyldodecyl)-2,5-dihydropyrrolo[3,4-c]pyrrole-1,4-dione[18] (0.25 g, 0.25 mmol, 1.0 equiv), 2-(4-azidophenyl)-4,4,5,5-tetramethyl-1,3,2-dioxaborolane[16] (0.13 g, 0.54 mmol, 2.2 equiv), tris(o-methoxyphenyl)phosphine (0.042 g, 0.12 mmol, 0.48 equiv), K_3PO_4 (0.63 g, 2.9 mmol, 12 .0 equiv.), $Pd_2(dba)_3$ (0.054 g, 0.059 mmol, 0.24 equiv), Aliquat 336 (1 drop), and toluene (8.5 mL). The Schlenk tube was sealed and removed from the glovebox. Under N_2, degassed H_2O (1.2 mL) was added. The reaction was allowed to stir at room temperature for 4 h. The reaction mixture was then diluted with CH_2Cl_2 and washed with water (2 × 50 mL). The organic phase was dried over Na_2SO_4, filtered, and concentrated under reduced pressure. The residue was purified by column chromatography (SiO_2, 30% CH_2Cl_2/hexanes, R_f = 0.1). The product was isolated as a deep blue oil. (0.15 g, 54% yield).

^{1}H NMR (300 MHz, $CDCl_3$) δ 8.92 (d, J = 4.1 Hz, 2H), 7.72 – 7.61 (m, 4H), 7.42 (d, J = 4.1 Hz, 2H), 7.08 (s, 4H), 4.06 (d, J = 7.7 Hz, 4H), 1.97 (s, 2H), 1.28 (m, 64H), 0.85 (s, 12H).

^{13}C{^{1}H} NMR (201 MHz, $CDCl_3$) δ 161.6, 148.4, 140.4, 139.6, 136.7, 130.0, 128.7, 127.4, 124.2, 119.6, 108.2, 46.2, 37.9, 31.9, 31.8, 31.3, 30.0, 29.6, 29.6, 29.5, 29.3, 29.3, 26.3, 22.6, 22.6, 14.0.

HRMS (APCI): calcd for $C_{66}H_{94}N_8O_2S_2$ $[M + H]^+$: 1095.7014; found: 1095.7001

3. Reaction Optimization Studies

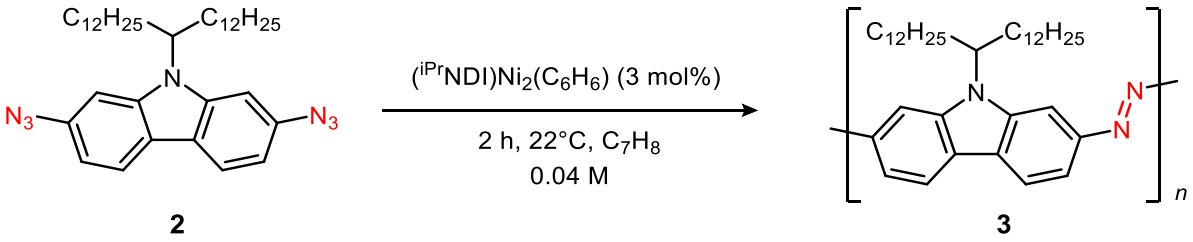

2 **3**

Standard procedure. This procedure is based on a modified literature procedure.[9] In an N_2 filled glovebox, a 2-dram vial equipped with a stir bar was charged with **2** (10.0 mg, 0.017 mmol, 1.0 equiv) and toluene (0.30 mL). Catalyst **1** (0.36 mg, 0.50 µmol, 3 mol %) dissolved in C_7H_8 (0.12 mL) was added to the stirring diazide solution. The reaction was allowed to stir for 2 h at room temperature. The reaction was quenched by exposure to air. MeOH (1.0 mL) and CH_2Cl_2 (1.0 mL) were added sequentially. The resulting suspension was sonicated and gravity filtered. The red solid was washed sequentially with Et_2O (20.0 mL) and CH_2Cl_2 (20.0 mL) to remove any low molecular weight material. The solid was allowed to air dry then collected and dried further under vacuum. Monomer conversions for entries 3 and 5 were determined by ^1H NMR. For entry 8 the polymer was purified using a Soxhlet apparatus. The product was washed sequentially with MeOH, hexanes, and $CHCl_3$ then extracted with C_6H_5Cl.

entry	deviation from Standard Conditions	conversion of **2**	M_n (kg/mol)	M_w (kg/mol)	$Đ_M$	X_n
1	none	>99%	20.5	58.7	2.9	37.7
2	purification by Soxhlet extraction (C_6H_5Cl)	>99%	42.1	92.5	2.2	77.6
3	1 mol% of **1**	31%	–	–	–	–
4	5 mol% of **1**	>99%	28.2	98.5	3.5	51.8
5	[**2**] = 0.02 M	79%	–	–	–	–
6	[**2**] = 0.08 M	>99%	35.2	104.2	3.0	64.7
7	60 °C	>99%	69.0	295.9	4.3	126.9
8	THF instead of toluene	>99%	8.6	18.6	2.1	15.8

4. Azopolymer Synthesis and Characterization

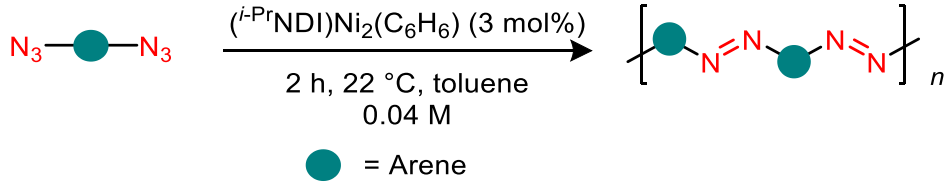

General procedure. In an N_2 filled glovebox, a microwave vial was charged with a solution of the diazide (1.0 equiv) dissolved in toluene and a magnetic stir bar. A solution of catalyst **1** (3 mol%) dissolved in toluene was added to the stirring diazide solution (0.04 M final concentration of the diazide). The vial was sealed, and the reaction mixture was stirred at room temperature. After 2 h, the reaction vial was opened to airm and methanol was added to precipitate the product. After sonication, the crude mixture was added to a thimble and purified in a Soxhlet apparatus (see below for wash and extraction solvents). Isolated polymers were obtained after drying under vacuum.

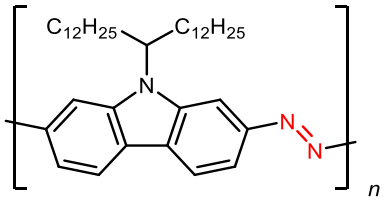

PolyAzoCarbazole (3).[19] Synthesized according to the general procedure using **2** (0.10 g, 0.17 mmol, 1.0 equiv), toluene (4.2 mL), and **1** (3.6 mg, 5.0 µmol, 3 mol%). Soxhlet wash solvents: MeOH, hexanes, then $CHCl_3$. Extraction solvent: C_6H_5Cl. PolyAzoCarbazole (**3**) was isolated as a red solid. (0.061 g, 61% yield).

^{1}H NMR (400 MHz, 100 °C, toluene-d_8) δ 8.47 (s, 2H), 8.16 (d, J = 8.4 Hz, 2H), 8.09 (d, J = 8.3 Hz, 2H), 4.70 (s, 1H), 2.52 – 2.36 (m, 2H), 1.97 – 1.83 (m, 2H), 1.32 – 1.09 (m, 40H), 0.86 (t, 6H).

UV–Vis–NIR (C_6H_5Cl, 0.0326 mM): λ_{max}, nm (ε, M^{-1} cm^{-1}): 440 (sh), 470 (sh), 503 (15,000), 538 (17,000).

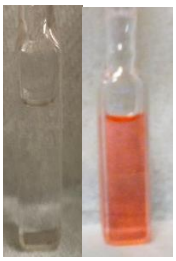

Figure S1. Photo of **2** (left) and **3** (right) in C_6H_5Cl.

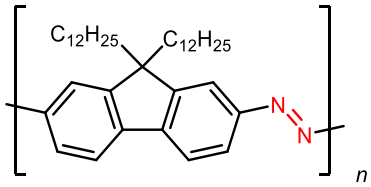

PolyAzoFluorene (6). Synthesized according to the general procedure using 2,7-diazido-9,9-didodecyl-9*H*-fluorene[9] (0.10 g, 0.17 mmol, 1.0 equiv), toluene (4.3 mL), and **1** (3.7 mg, 5.1 µmol, 3 mol%). Soxhlet wash solvents: MeOH then hexanes. Extraction solvent: $CHCl_3$. PolyAzoFluorene (**6**) was isolated as an orange solid. (0.082 g, 82% yield). Spectral match those previously reported.[9]

UV–Vis–NIR (C_6H_5Cl, 0.0566 mM): λ_{max}, nm (ε, $M^{-1}\,cm^{-1}$): 336 (1,700) 450 (sh), 484 (17,000) 520 (18,000)

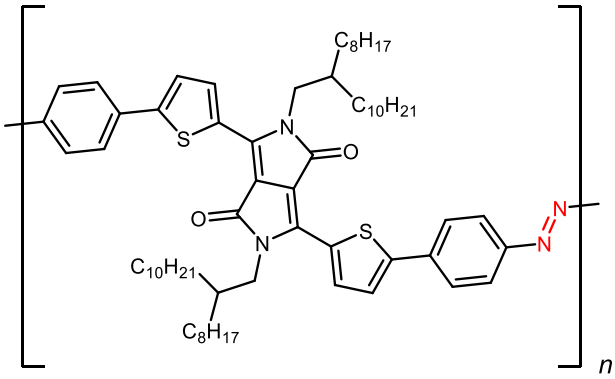

PolyAzoTDPP (7). Synthesized according to the general procedure using **S13** (0.10 g, 0.091 mmol, 1.0 equiv), toluene (2.3 mL), and **1** (2.0 mg, 2.7 µmol, 3 mol%). Soxhlet wash solvents: MeOH then hexanes. Extraction solvent: $CHCl_3$. PolyAzoTDPP (**7**) was isolated as a green solid. (0.077 g, 77% yield).

^{1}H NMR (400 MHz, toluene-d_8) δ 9.44 – 9.15 (m, 2H), 7.93 (d, J = 8.1 Hz, 3H), 7.62 (d, J = 8.4 Hz, 3H), 4.20 (s, 4H), 2.21 (s, 2H), 1.60 – 1.22 (m, 64H), 0.93 – 0.86 (m, 12H).

UV–Vis–NIR (C_6H_5Cl, 0.0385 mM): λ_{max}, nm (ε, M^{-1} cm^{-1}): 334 (1,300) 426 (3,500), 664 (8,600), 746 (sh)

Figure S2. Photo of **S13** (left) and **7** (right) in C_6H_5Cl.

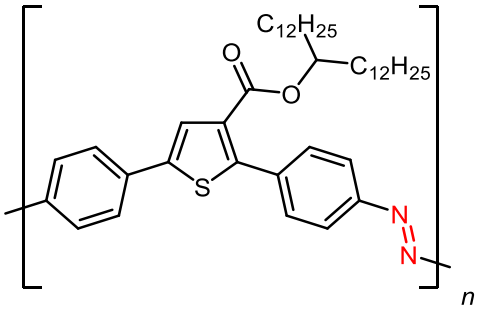

PolyAzoThiophene (8). Synthesized according to the general procedure using **S12** (0.10 g, 0.14 mmol, 1.0 equiv), toluene (3.5 mL), and **1** (3.1 mg, 4.2 µmol, 3 mol%). Soxhlet wash solvents: MeOH then hexanes. Extraction solvent: $CHCl_3$. PolyAzoThiophene (**8**) was isolated as an orange solid. (0.081 g, 81% yield).

^{1}H NMR (400 MHz, 100 °C, toluene-d_8) δ 8.05 (s, 2H), 7.97 (s, 3H), 7.72 (s, 2H), 7.58 (s, 2H), 5.23 (s, 1H), 1.68 – 1.44 (m, 4H), 1.31 (s, 40H), 0.90 (s, 6H).

UV–Vis–NIR (C_6H_5Cl, 0.0135 mM): λ_{max}, nm (ε, M^{-1} cm^{-1}): 427 (15,000)

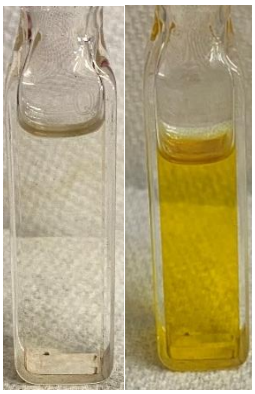

Figure S3. Photo of **S12** (left) and **8** (right) in C_6H_5Cl.

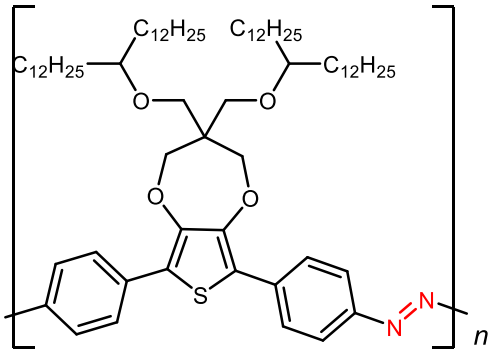

PolyAzoProDOT (9). Synthesized according to the general procedure using **S10** (0.10 g, 0.087 mmol, 1.0 equiv), toluene (2.2 mL), and **1** (1.9 mg, 2.6 µmol, 3 mol%). Soxhlet wash solvent: MeOH. Extraction solvent: hexanes. PolyAzoProDOT (**9**) was isolated as a red solid. (0.097 g, 97% yield).

^{1}H NMR (400 MHz, 50 °C, $CDCl_3$) δ 8.04 – 7.86 (m, 8H), 4.27 (s, 4H), 3.65 (s, 4H), 3.31 – 3.23 (m, 2H), 1.57 – 1.45 (m, 8H), 1.37 – 1.23 (m, 80H), 0.88 (t, 12H).

UV–Vis–NIR (C_6H_5Cl, 0.0456 mM): λ_{max}, nm (ε, M^{-1} cm^{-1}): 514 (20,000), 543 (sh)

Figure S4. Photo of **S10** (left) and **9** (right) in C_6H_5Cl.

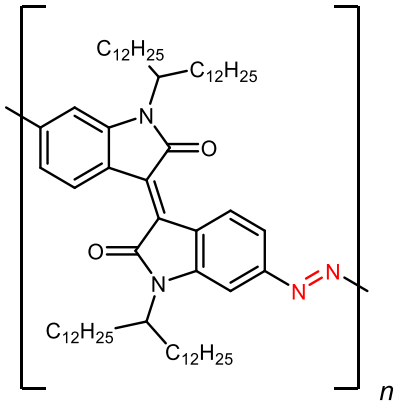

PolyAzoIsoindigo (10). Synthesized according to the general procedure using **S7** (0.098 g, 0.094 mmol, 1.0 equiv), toluene (2.3 mL), and **1** (6.8 mg, 9.4 µmol, 10 mol%). Soxhlet wash solvents: MeOH then hexanes. Extraction solvent: $CHCl_3$. PolyAzoIsoindigo (**10**) was isolated as a green solid. (0.091 g, 93% yield).

^{1}H NMR (400 MHz, 100 °C, toluene-d_8) δ 9.81 (s, 2H), 7.91 – 7.50 (m, 4H), 4.52 (s, 2H), 2.19 (s, 4H), 1.77 (s, 4H), 1.31 (s, 80H), 0.89 (s, 12H).

UV–Vis–NIR (C_6H_5Cl, 0.0606 mM): λ_{max}, nm (ε, M^{-1} cm^{-1}): 381 (sh), 481 (17,000), 664 (25,000), 709 (26,000).

Figure S5. Photo of **S7** (left) and **10** (right) in C_6H_5Cl.

Copolymerization Experiments

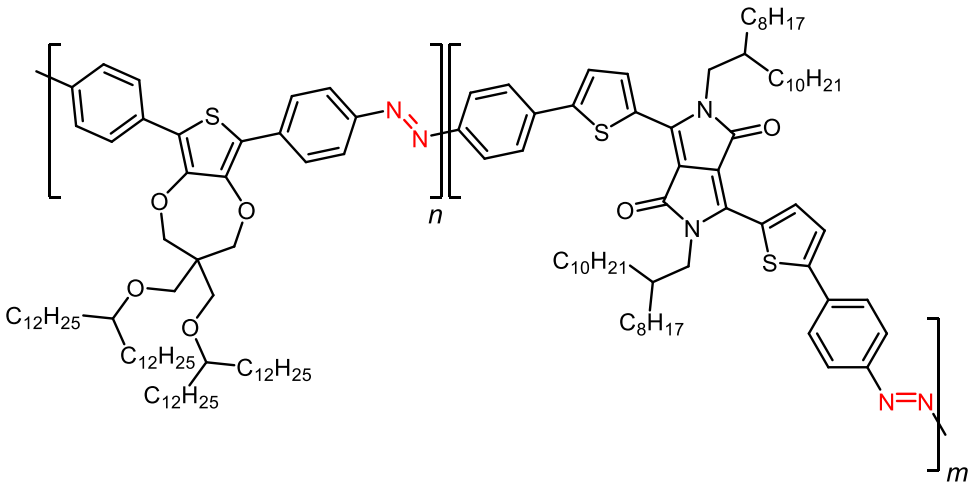

ProDOT/TDPP copolymerization at 1:1 (11). In an N_2 filled glovebox, a 2-dram vial was charged with a magnetic stir bar, **S10** (0.010 g, 8.7 µmol, 1.0 equiv), **S13** (0.010 g, 9.1 µmol, 1.0 equiv) and toluene (0.22 mL). Catalyst **1** (3.9 mg, 0.55 µmol, 3 mol% total) dissolved in toluene (0.22 mL) was added to the stirring solution of the diazides. The vial was sealed, and the reaction mixture was stirred at room temperature. After 2 h, the reaction vial was opened to air, and MeOH was added to precipitate the product. After sonication, the crude material was filtered, and the precipitate was washed with Et_2O (10.0 mL) and CH_2Cl_2 (10.0 mL). The solid was allowed to air dry then collected and dried further under vacuum to yield the product as a dark purple solid. (0.021 g, >99% yield). Ratio of ProDOT (**9**) to TDPP (**7**) by ^{1}H NMR integration (1:1.04).

UV–Vis–NIR (C_6H_5Cl, 0.0187 mM): λ_{max}, nm (ε, M^{-1} cm^{-1}): 327 (sh), 442 (sh), 534 (7,900), 659 (sh), 710 (13,000)

Figure S6. Photo of **11** in C_6H_5Cl.

ProDOT/TDPP copolymerization at 3:1 (12). In an N_2 filled glovebox, a 2-dram vial was charged with a magnetic stir bar, **S10** (0.015 g, 13.0 µmol, 1.0 equiv), **S13** (5.0 mg, 4.6 µmol, 0.35 equiv) and toluene (0.22 mL). Catalyst **1** (3.9 mg, 0.55 µmol, 3 mol% total) dissolved in toluene (0.22 mL) was added to the stirring solution of the diazides. The vial was sealed, and the reaction mixture was stirred at room temperature. After 2 h, the reaction vial was opened to air, and MeOH was added to precipitate the product. After sonication, the crude material was filtered, and the precipitate was washed with Et_2O (10.0 mL) and CH_2Cl_2 (10.0 mL). The solid was allowed to air dry then collected and dried further under vacuum to yield the product as a purple solid. (0.021 g, >99% yield). Ratio of ProDOT (**9**) to TDPP (**7**) by ^{1}H NMR integration (2.6:1).

UV–Vis–NIR (C_6H_5Cl, 0.0351 mM): λ_{max}, nm (ε, $M^{-1}\,cm^{-1}$): 521 (11,000), 644 (sh), 692 (6,300)

Figure S7. Photo of **12** in C_6H_5Cl.

5. Endcapping Experiments

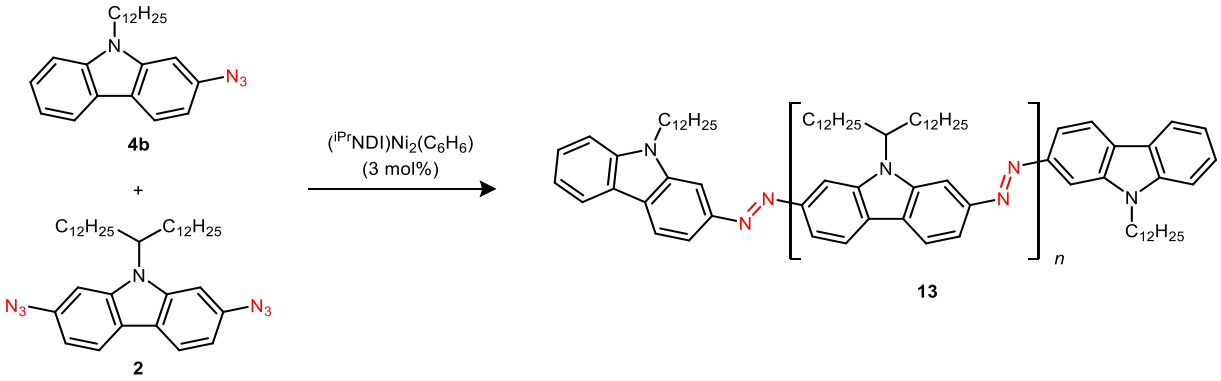

Carbazole end group incorporation (13). In an N_2 filled glovebox, a 2-dram vial was charged with a magnetic stir bar, **2** (0.015 g, 0.025 mmol, 1.0 equiv), **4b** (0.50 mg, 1.3 µmol, 0.050 equiv) and toluene (0.50 mL). Catalyst **1** (0.60 mg, 0.69 µmol, 3 mol %) dissolved in toluene (0.13 mL) was added to the stirring solution of the azides. The vial was sealed, and the reaction mixture was stirred at room temperature. After 2 h, the reaction vial was opened to air, and MeOH (3.0 mL) was added to precipitate the product. After sonication, the crude material was filtered, and the precipitate was washed with Et_2O (10.0 mL) and CH_2Cl_2 (10.0 mL). The solid was allowed to air dry then collected and dried further under vacuum to yield the product as a red solid (0.010 g, 67% yield). Ratio of repeat units to end groups by ^{1}H NMR integration (17:1).

^{1}H NMR of **13** end group (400 MHz, 100 °C, toluene-d_8) δ 7.97 (d, J = 7.9 Hz, 1H), 4.02 (br s, 2H).

^{1}H NMR of **13** repeat unit (400 MHz, 100 °C, toluene-d_8) δ 8.47 (s, 2H), 8.16 (d, J = 8.7 Hz, 2H), 8.09 (d, J = 8.8 Hz, 2H), 4.70 (s, 1H), 2.42 (s, 2H), 1.89 (s, 2H), 1.19 (d, J = 33.8 Hz, 40H), 0.86 (d, J = 7.2 Hz, 6H).

UV–Vis–NIR (C_6H_5Cl, 0.0428 mM): λ_{max}, nm (ε, M^{-1} cm^{-1}): 435 (sh), 465 (sh), 499 (21,000), 532 (22,000).

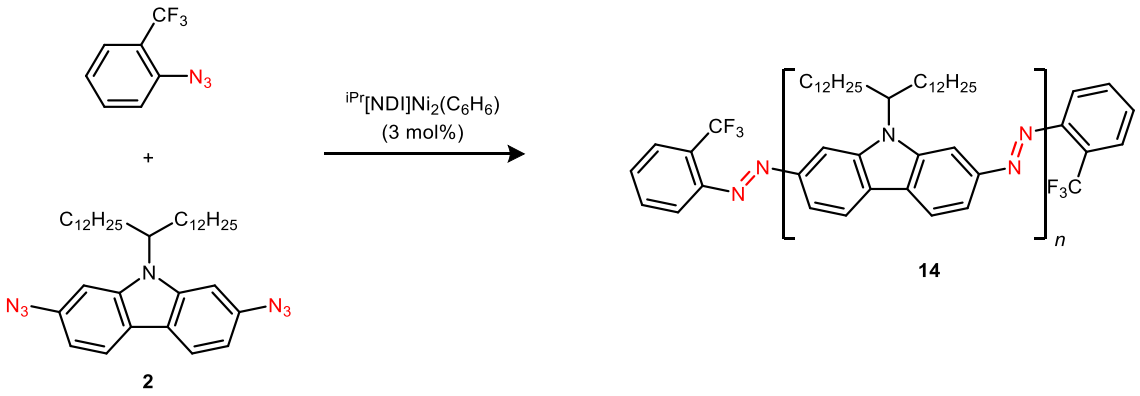

2-(trifluoromethyl)phenyl end group incorporation (14). In an N_2 filled glovebox, a 2-dram vial was charged with a magnetic stir bar, **2** (0.015 g, 0.025 mmol, 1.0 equiv), 2-(trifluoromethyl)phenyl azide[9] (0.20 mg, 1.3 µmol, 0.050 equiv) and toluene (0.50 mL). Catalyst **1** (0.60 mg, 0.69 µmol, 3 mol %) dissolved in toluene (0.13 mL) was added to the stirring solution of the azides. The vial was sealed, and the reaction mixture was stirred at room temperature. After 2 h, the reaction vial was opened to air, and MeOH (3.0 mL) was added to precipitate the product. After sonication, the crude material was filtered, and the precipitate was washed with Et_2O (10.0 mL) and CH_2Cl_2 (10.0 mL). The solid was allowed to air dry then collected and dried further under vacuum to yield the product as a red solid (8.9 mg, 60% yield). Ratio of repeat units to end groups by ^1H NMR integration (30:1).

^{1}H NMR of **14** end group (400 MHz, 100 °C, toluene-d_8) δ 7.79 (d, J = 8.2 Hz, 1H), 7.58 (d, J = 7.7 Hz, 1H)

^{1}H NMR of **14** repeat unit (400 MHz, 100 °C, toluene-d_8) δ 8.47 (s, 2H), 8.16 (d, J = 8.7 Hz, 2H), 8.09 (d, J = 8.8 Hz, 2H), 4.70 (s, 1H), 2.42 (s, 2H), 1.89 (s, 2H), 1.19 (d, J = 33.8 Hz, 40H), 0.86 (d, J = 7.2 Hz, 6H).

^{19}F NMR of **14** (376 MHz, 100 °C, toluene-d_8) δ –58.8.

UV–Vis–NIR (C_6H_5Cl, 0.0428 mM): λ_{max}, nm (ε, M^{-1} cm^{-1}): 435 (sh), 465 (sh), 499 (17,000), 532 (18,000).

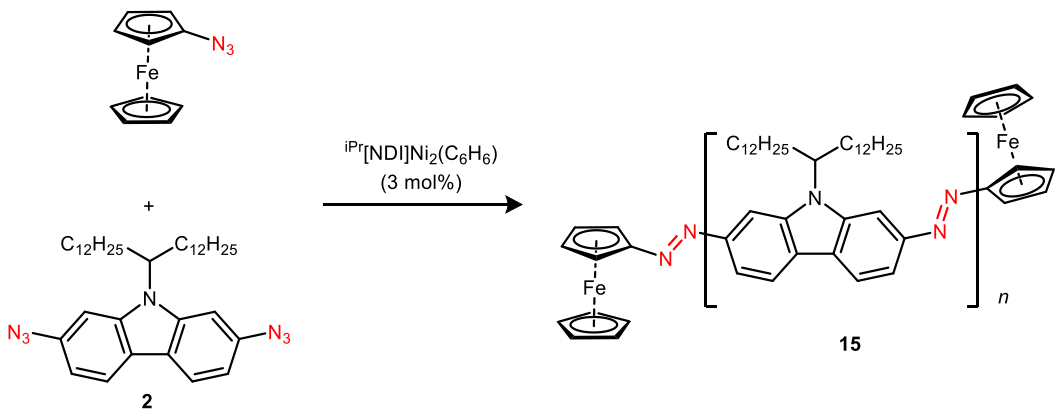

Ferrocene end group incorporation (15). In an N_2 filled glovebox, a 2-dram vial was charged with a magnetic stir bar, **2** (0.015 g, 0.025 mmol, 1.0 equiv.), azidoferrocene[9] (0.30 mg, 1.3 µmol, 0.050 equiv.) and toluene (0.50 mL). Catalyst **1** (0.60 mg, 0.69 µmol, 3 mol %) dissolved in toluene (0.13 mL) was added to the stirring solution of the azides. The vial was sealed, and the reaction mixture was stirred at room temperature. After 2 h, the reaction vial was opened to air, and MeOH (3.0 mL) was added to precipitate the product. After sonication, the crude material was filtered, and the precipitate was washed with Et_2O (10.0 mL) and CH_2Cl_2 (10.0 mL). The solid was allowed to air dry then collected and dried further under vacuum to yield the product as a red solid (9.1 mg, 60% yield). Ratio of repeat units to end groups by ^{1}H NMR integration (34:1).

^{1}H NMR of **15** end group (400 MHz, 100 °C, toluene-d_8) δ 5.15 (t, J = 2.0 Hz, 2H), 4.31 (t, J = 2.0 Hz, 2H), 4.10 (s, 5H).

^{1}H NMR of **15** repeat unit (400 MHz, 100 °C, toluene-d_8) δ 8.47 (s, 2H), 8.16 (d, J = 8.7 Hz, 2H), 8.09 (d, J = 8.8 Hz, 2H), 4.70 (s, 1H), 2.42 (s, 2H), 1.89 (s, 2H), 1.19 (d, J = 33.8 Hz, 40H), 0.86 (d, J = 7.2 Hz, 6H).

UV–Vis–NIR (C_6H_5Cl, 0.0551 mM): λ_{max}, nm (ε, M^{-1} cm^{-1}): 432 (sh), 468 (sh), 501 (6,200), 533 (7,200).

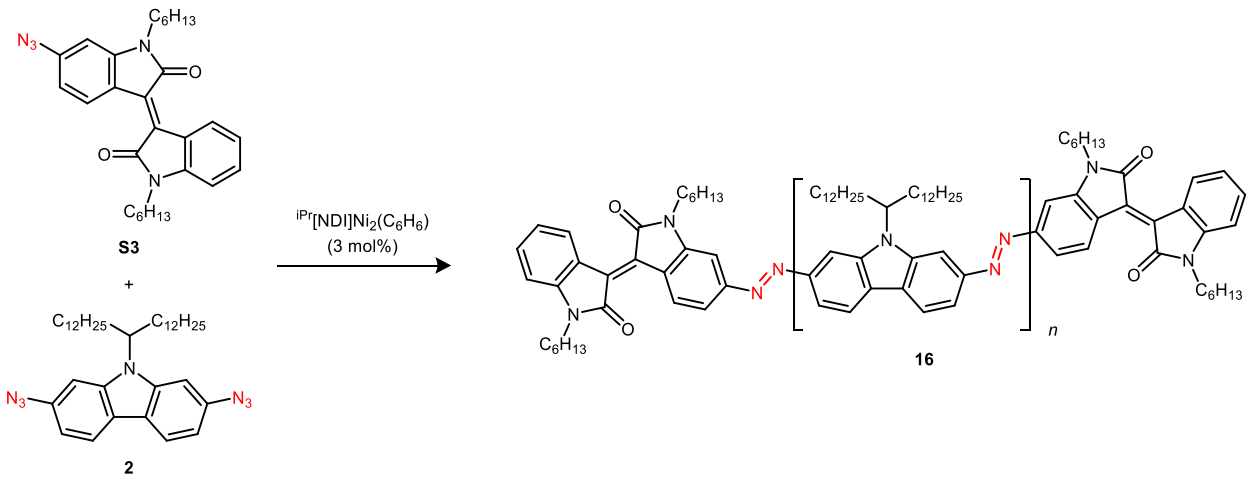

Isoindigo end group incorporation (16). In an N_2 filled glovebox, a 2-dram vial was charged with a magnetic stir bar, **2** (0.015 g, 0.025 mmol, 1.0 equiv.), **S3** (0.60 mg, 1.3 µmol, 0.050 equiv.) and toluene (0.50 mL). Catalyst **1** (0.60 mg, 0.69 µmol, 3 mol %) dissolved in toluene (0.13 mL) was added to the stirring solution of the azides. The vial was sealed, and the reaction mixture was stirred at room temperature. After 2 h, the reaction vial was opened to air, and MeOH (3.0 mL) was added to precipitate the product. After sonication, the crude material was filtered, and the precipitate was washed with Et_2O (10.0 mL) and CH_2Cl_2 (10.0 mL). The solid was allowed to air dry then collected and dried further under vacuum to yield the product as a red solid (11.0 mg, 73% yield). Ratio of repeat units to end groups by ^{1}H NMR integration (37:1).

^{1}H NMR of **16** end group (400 MHz, 100 °C, toluene-d_8) δ 9.83 (br s, 1H), 9.62 (br s, 1H), 3.65 (br s, 2H).

^{1}H NMR of **16** repeat unit (400 MHz, 100 °C, toluene-d_8) δ 8.47 (s, 2H), 8.16 (d, J = 8.7 Hz, 2H), 8.09 (d, J = 8.8 Hz, 2H), 4.70 (s, 1H), 2.42 (s, 2H), 1.89 (s, 2H), 1.19 (d, J = 33.8 Hz, 40H), 0.86 (d, J = 7.2 Hz, 6H).

UV–Vis–NIR (C_6H_5Cl, 0.0612 mM): λ_{max}, nm (ε, M^{-1} cm^{-1}): 432 (sh), 468 (sh), 501 (23,000), 534 (24,000)

6. Lewis Acid Experiments

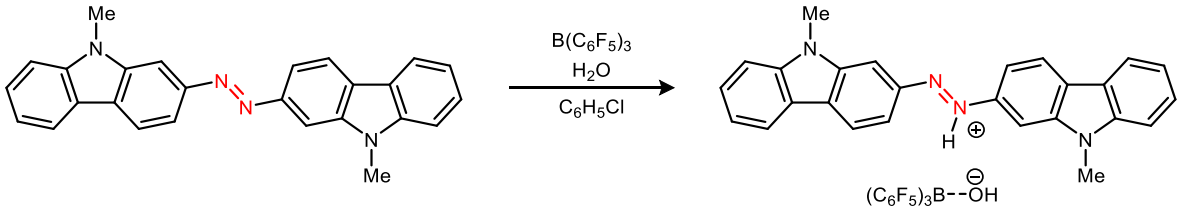

5a **17a**

Azocarbazole $B(C_6F_5)_3/H_2O$ adduct (17a). An NMR tube was charged with **5a** (2.0 mg, 5.2 µmol, 1.0 equiv) dissolved in C_6H_5Cl (0.40 mL). $B(C_6F_5)_3$ (10.0 mg, 0.020 mmol, 3.8 equiv) was added as a solid to solution, resulting in an immediate color change to deep blue. C_6H_5Cl (0.10 mL) was layered on top of the solution followed by pentane (0.70 mL). The solvents were allowed to mix for 7 days, and single crystals suitable for X-ray diffraction were obtained.

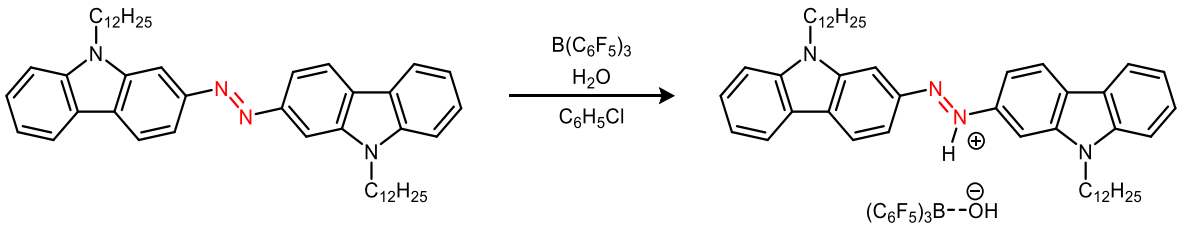

5b **17b**

Azocarbazole $B(C_6F_5)_3/H_2O$ adduct (17b). A vial was charged with **5b** (2.0 mg, 2.9 µmol, 1.0 equiv) and C_6H_5Cl (0.40 mL). $B(C_6F_5)_3$ (10.0 mg, 0.020 mmol, 3.8 equiv) was added as a solid to solution, resulting in a color change to deep blue.

^{1}H NMR (300 MHz, $CDCl_3$) δ 8.16 (t, *J* = 8.7 Hz, 4H), 8.08 (d, *J* = 1.7 Hz, 2H), 7.89 (d, *J* = 8.6, 2H), 7.61 (t, *J* = 7.7 Hz, 2H), 7.46 (d, *J* = 8.3 Hz, 2H), 7.33 (t, *J* = 7.5 Hz, 2H), 4.34 (t, *J* = 7.2 Hz, 4H), 1.91 (t, *J* = 7.3 Hz, 4H), 1.35 (s, 8H), 1.24 (d, *J* = 8.1 Hz, 28H), 0.85 (t, *J* = 6.6 Hz, 6H).

^{19}F NMR (282 MHz, $CDCl_3$) δ -136.98 (d), -159.12 (t, J = 20.3 Hz), -165.28 (t).

UV–Vis–NIR (C_6H_5Cl, 0.143mM): λ_{max}, nm (ε, M^{-1} cm^{-1}): 316 (3,200), 626 (11,000)

Figure S8. Photo of **5b** in C_6H_5Cl before (left) and after (right) addition of excess $B(C_6F_5)_3$.

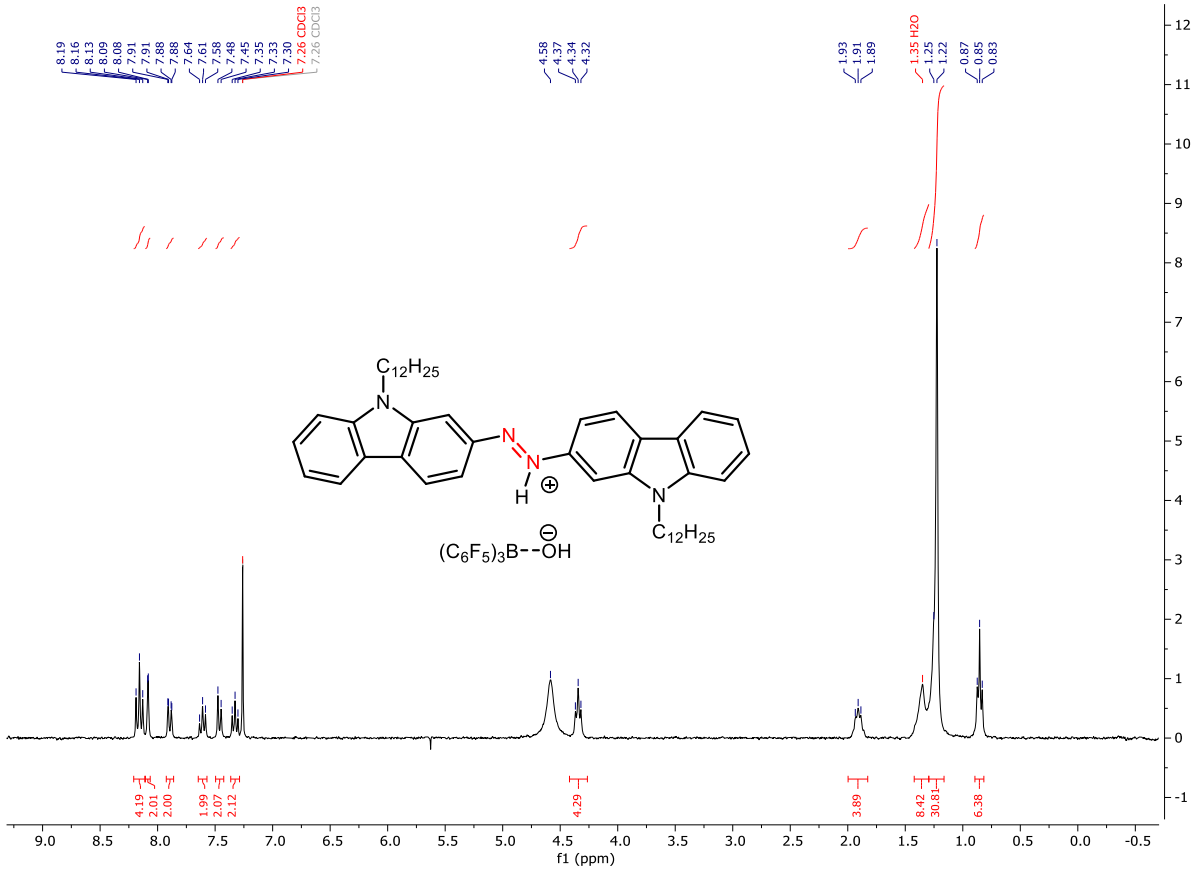

Figure S9. ^{1}H NMR spectrum of **17b** (300 MHz, $CDCl_3$).

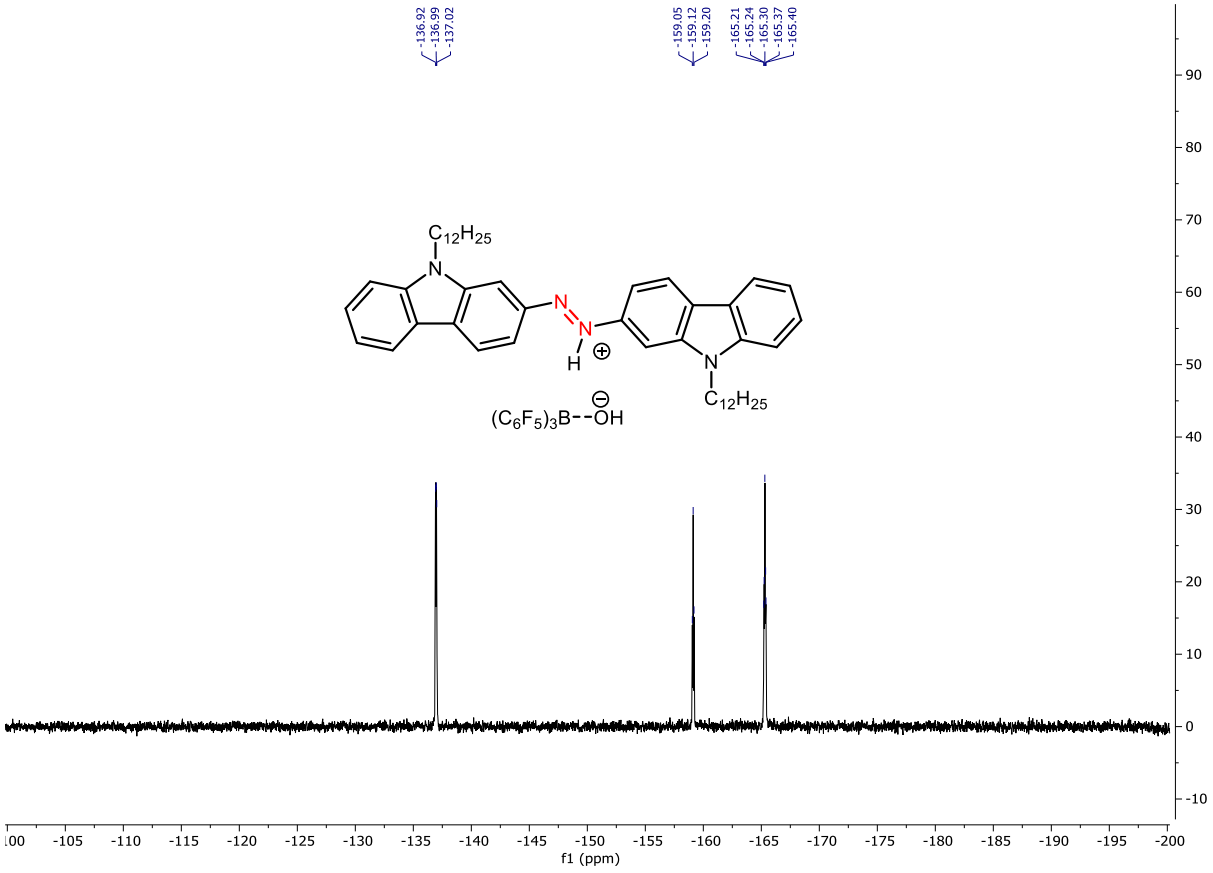

Figure S10. ^{19}F NMR spectrum of **17b** (282 MHz, $CDCl_3$).

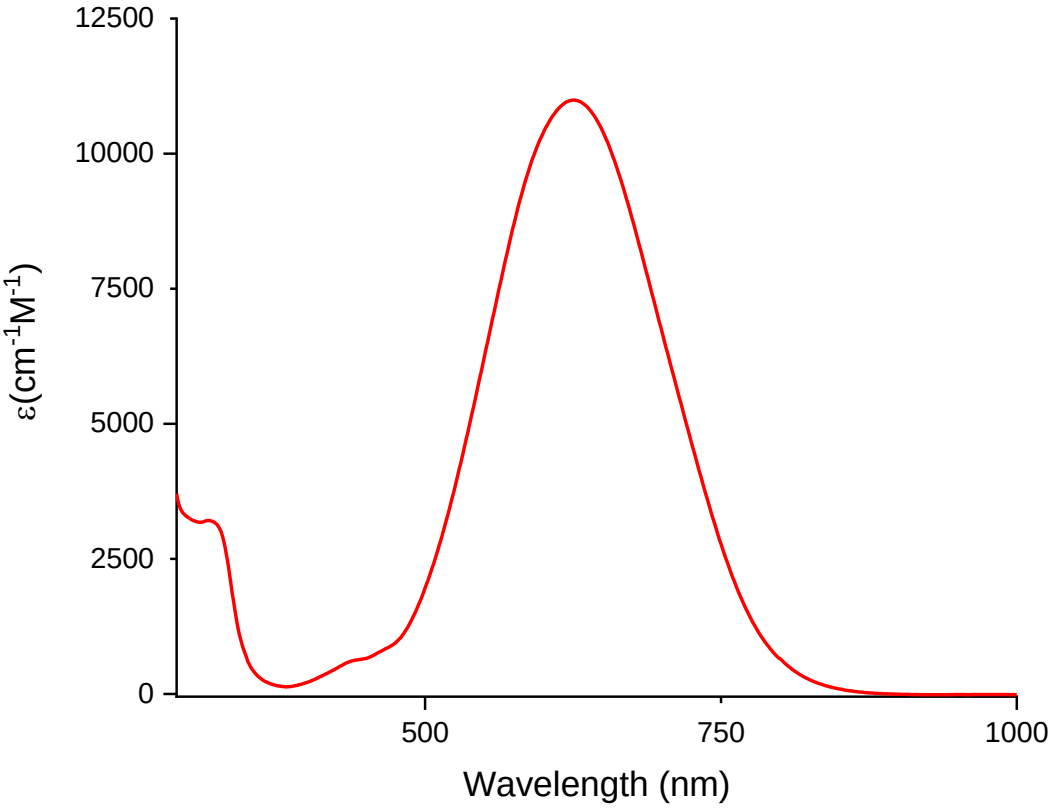

Figure S11. UV-Vis spectrum of **17b** (0.143mM) in C_6H_5Cl.

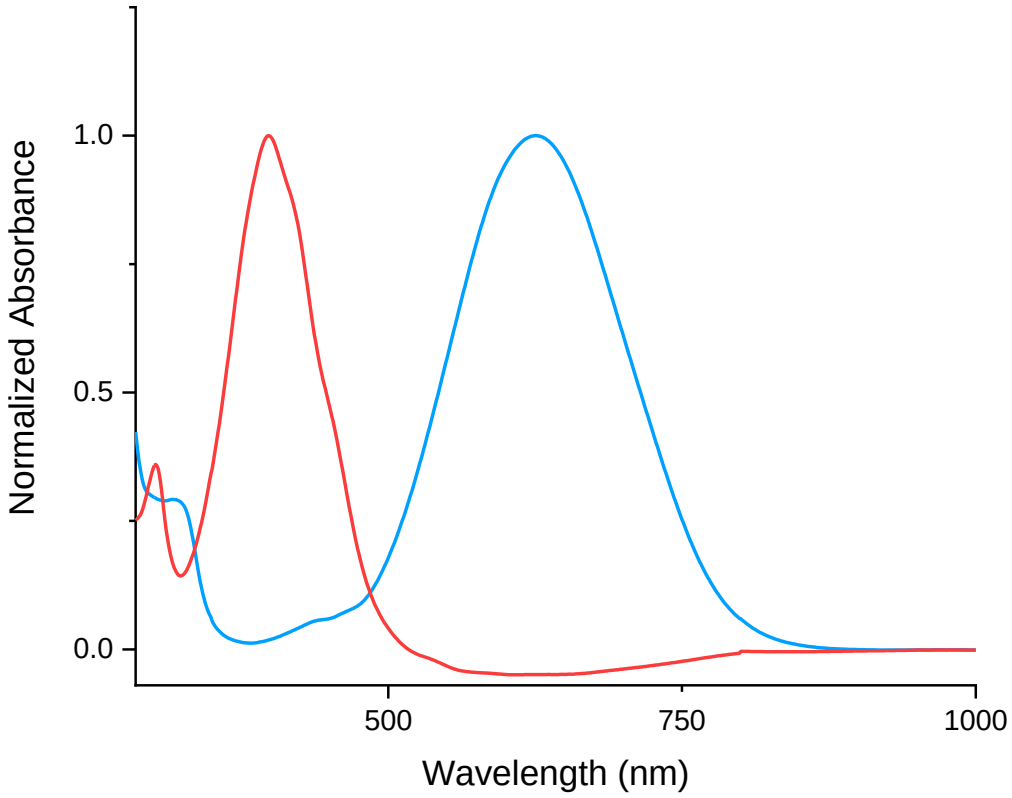

Figure S12. Normalized UV-Vis spectrum of **5b** (red) and **17b** (blue) in C_6H_5Cl.

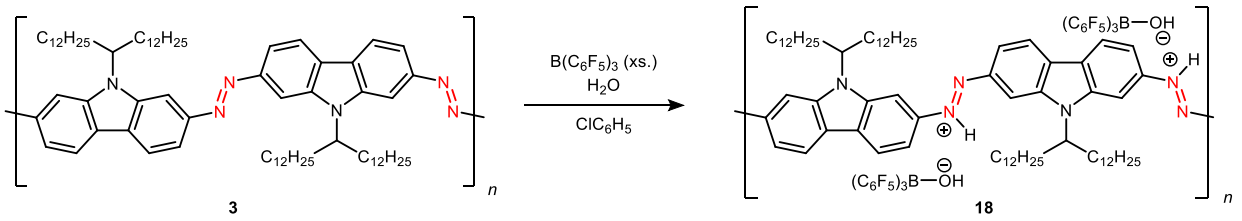

UV Vis titration of 3 using $B(C_6F_5)_3$ (18). A vial was charged with **3** (0.4 mg, 0.73 µmol, 1.0 equiv) and C_6H_5Cl (20 mL). An aliquot (3 mL) was taken, and $B(C_6F_5)_3$ (0.15 M in 1.0 mL) was titrated into the solution of **3**.

^{1}H NMR of **18** (400 MHz, 100 °C, toluene-d_8) δ 8.44 (s, 2H), 8.08 (q, J = 8.9 Hz, 4H), 6.03 (ddt, J = 14.2, 7.0, 3.6 Hz, 2H), 4.68 (s, 1H), 2.41 (s, 2H), 1.92 (s, 2H), 1.20 (d, J = 23.2 Hz, 40H), 0.91 – 0.82 (m, 6H).

UV–Vis–NIR of **18** (C_6H_5Cl, 0.0326 mM): λ_{max}, nm (ε, M^{-1} cm^{-1}): 411 (4,400), 748 (sh), 821 (18,000)

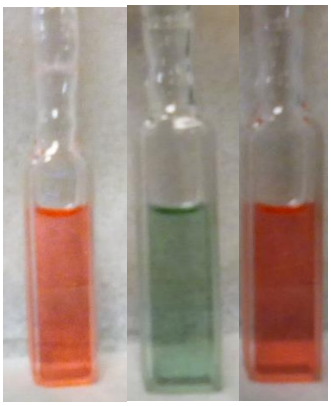

Figure S13. Pictures of (from left to right) **3, 18** (after 0.151 M addition of $B(C_6F_5)_3$) and **18** after 1 drop pyridine in C_6H_5Cl.

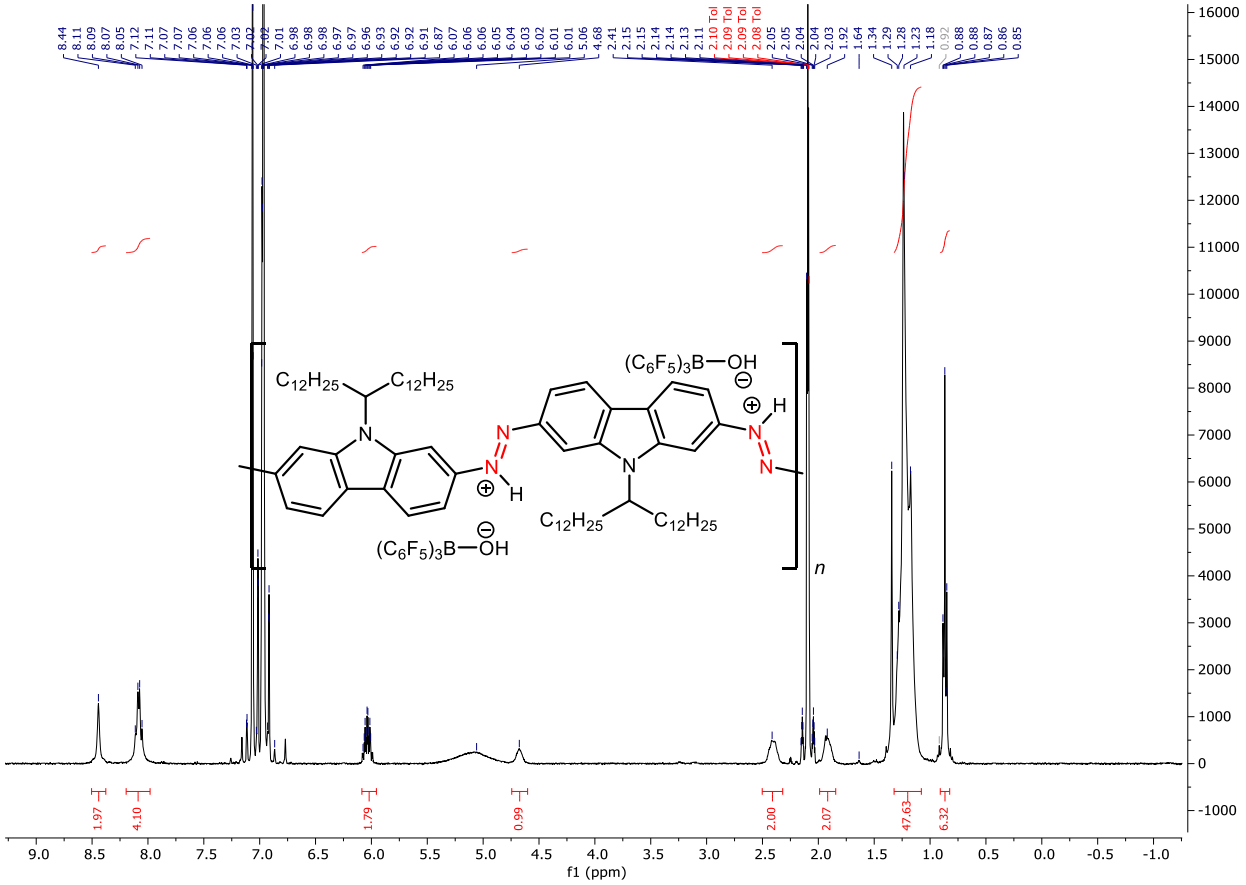

Figure S14. ^{1}H NMR spectrum of **18** (400 MHz, 100 °C, toluene-d_8).

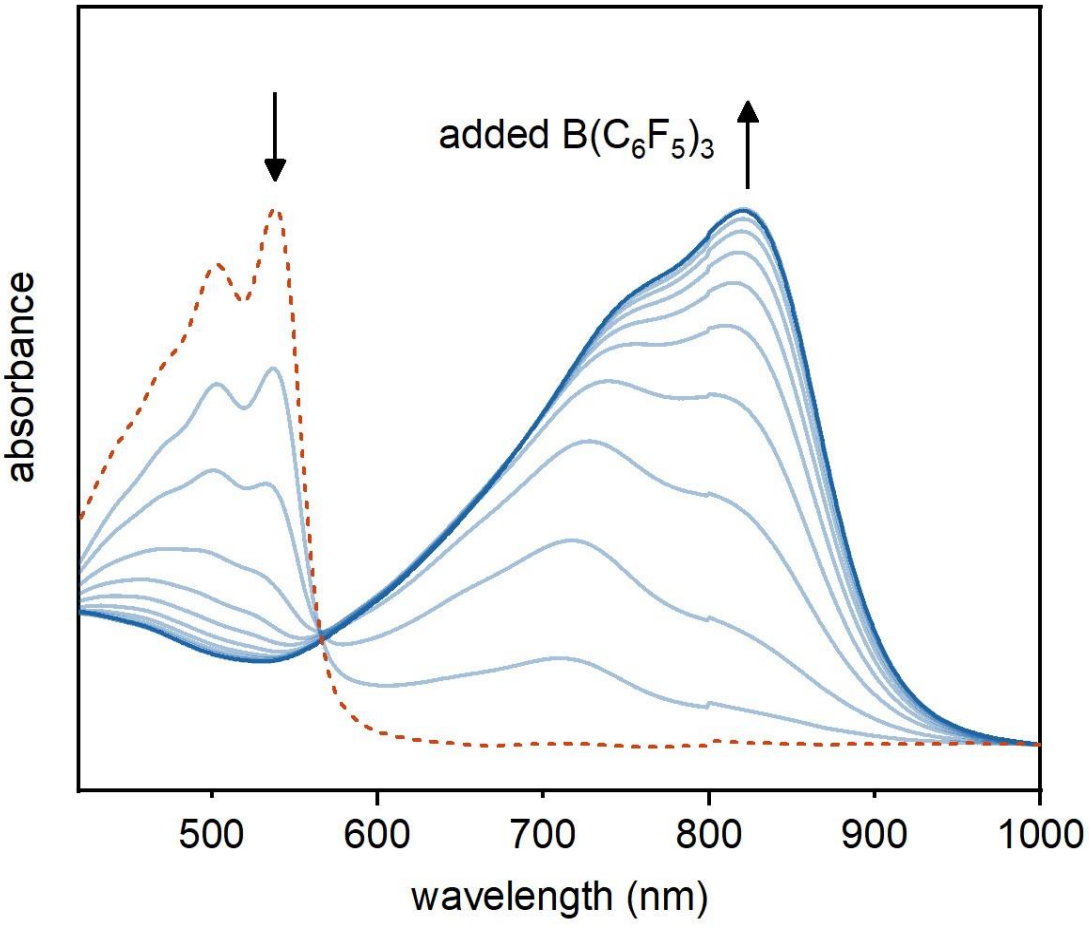

Figure S15. UV-Vis titration of $B(C_6F_5)_3$ (0.15 M) into **3** (0.0326 mM) in C_6H_5Cl.

7. Cyclic Voltammetry

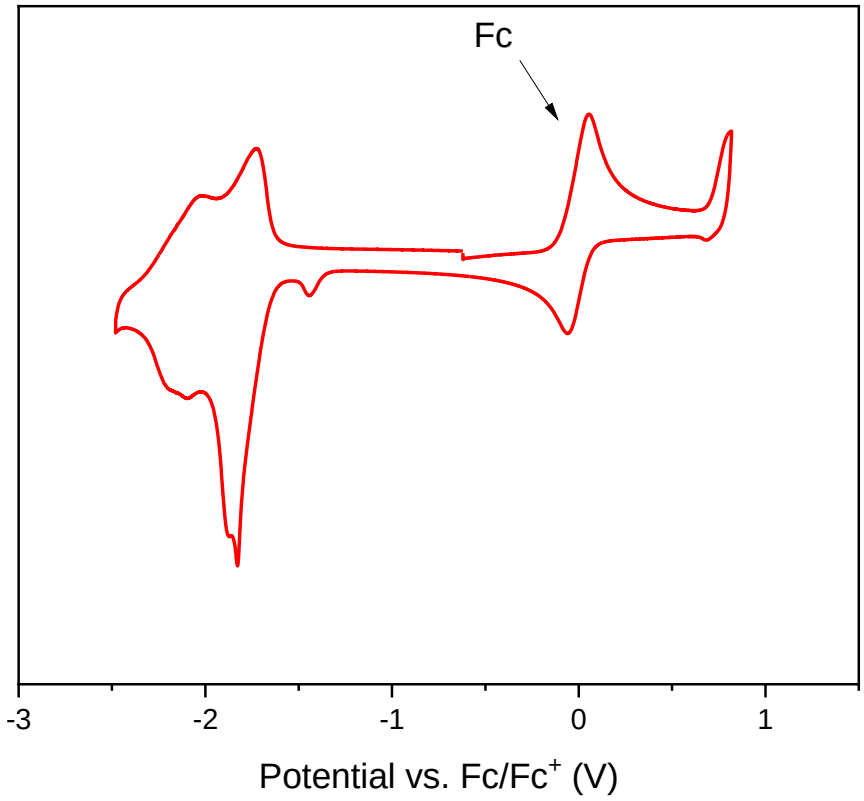

Figure S16. Cyclic voltammogram of **3**. The voltammogram was taken by heating a solution of **3** and dropping it onto a glassy carbon working electrode. Supporting electrolyte: 0.3 M $TBAPF_6$ in THF; 100 mV/s scan rate. Scans were started at the open-circuit potential and scanned in the anodic direction.

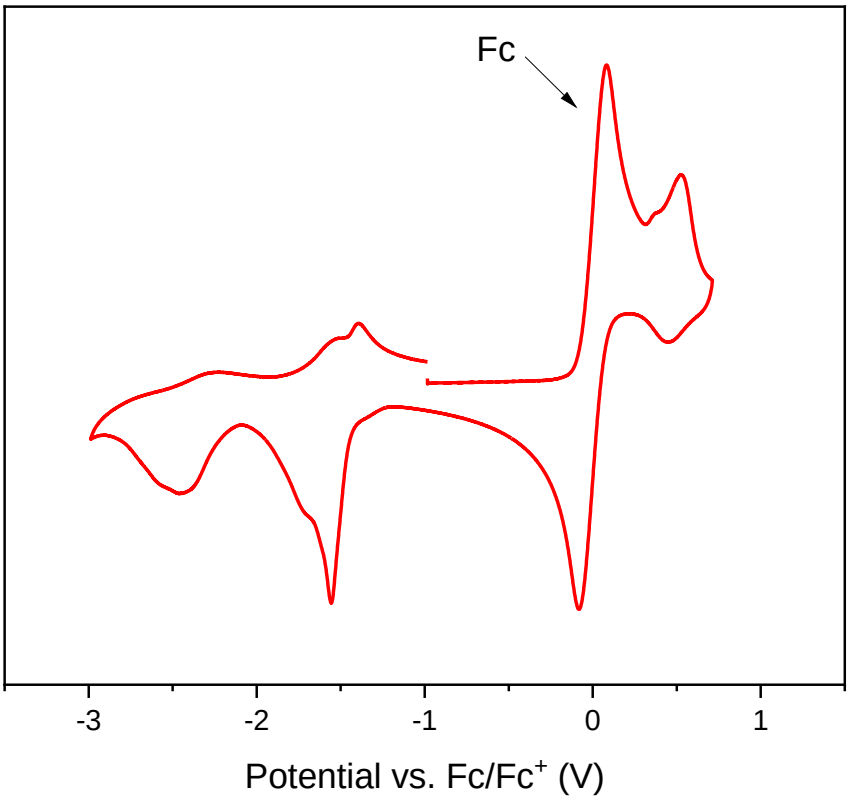

Figure S17. Cyclic voltammogram of **7**. The voltammogram was taken by heating a solution of **7** and dropping it onto a glassy carbon working electrode. Supporting electrolyte: 0.3 M $TBAPF_6$ in THF; 100 mV/s scan rate. Scans were started at the open-circuit potential and scanned in the anodic direction.

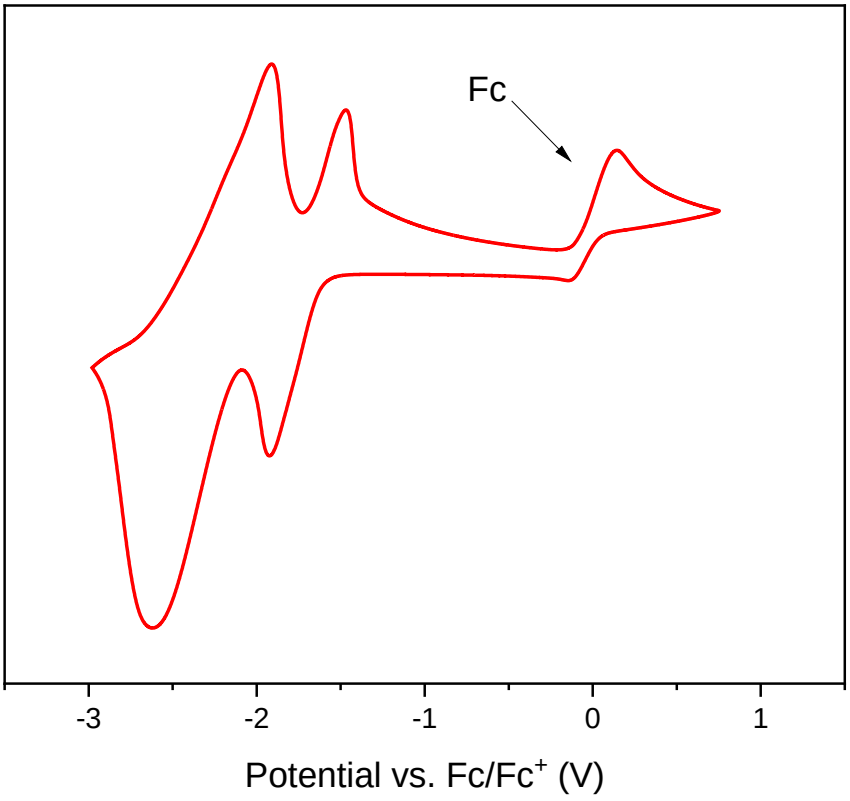

Figure S18. Cyclic voltammogram of **8**. The voltammogram was taken by heating a solution of **8** and dropping it onto a glassy carbon working electrode. Supporting electrolyte: 0.3 M $TBAPF_6$ in THF; 100 mV/s scan rate. Scans were started at the open-circuit potential and scanned in the anodic direction.

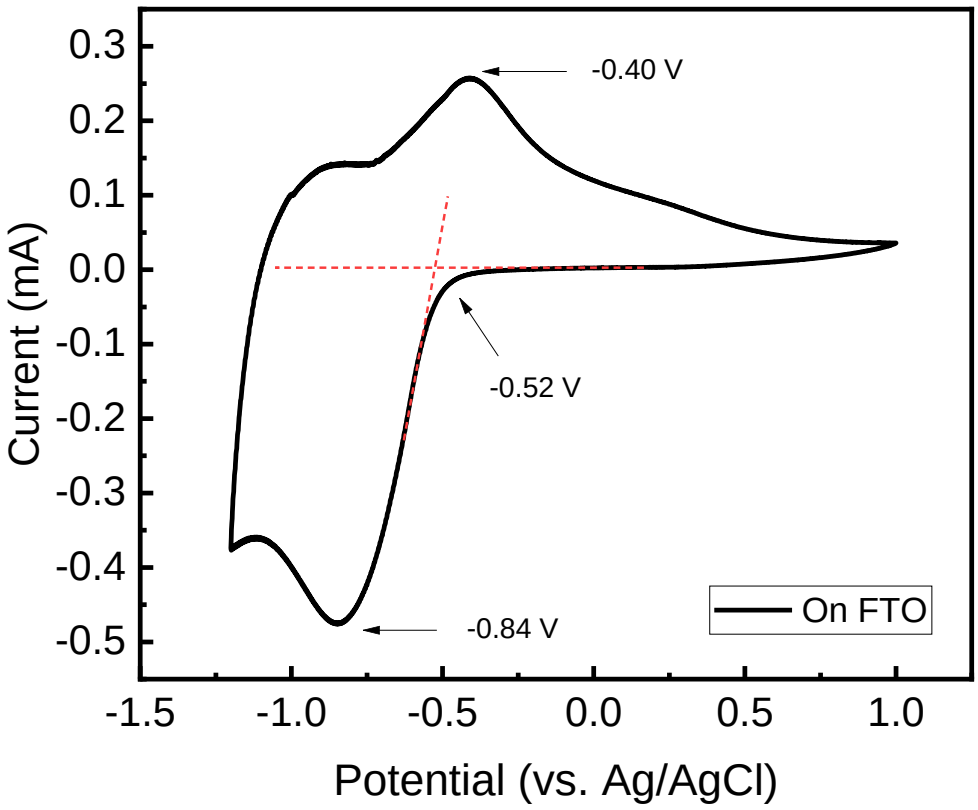

Figure S19. Cyclic voltammogram for a thin film of **10** spin coated on FTO/glass substrate. Voltammograms taken in a 0.2 M $TBAPF_6$ in propylene carbonate (PC) with a 50 mV/s scan rate. The $E_{1/2}$ value for **10** is -0.62V vs. Ag/AgCl.

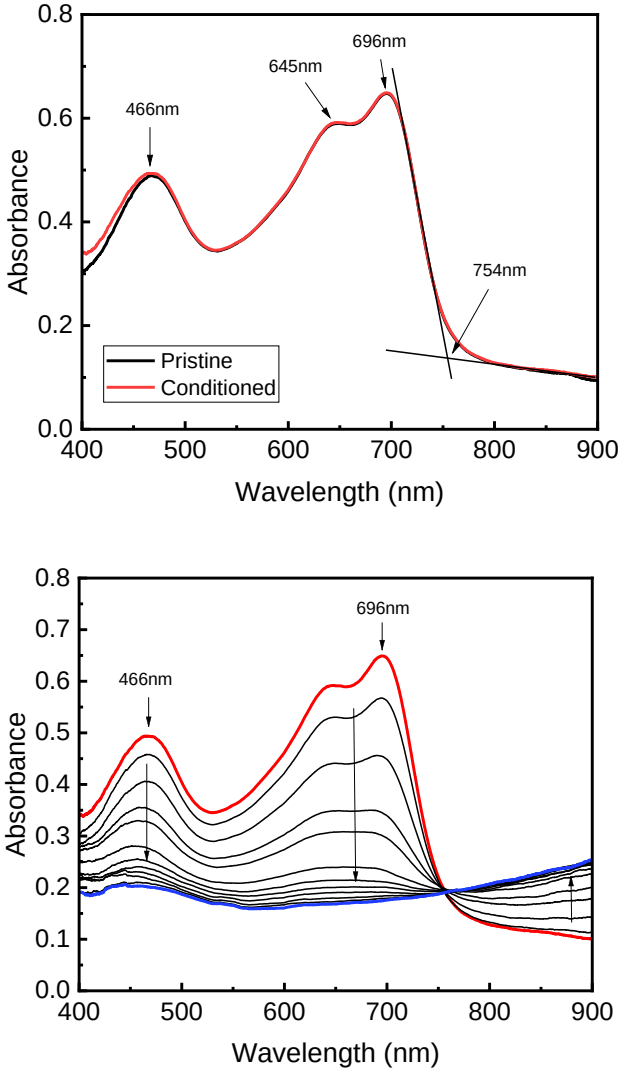

Figure S20. Spectroelectrochemistry for a thin film of **10** spin coated onto FTO/glass substrate in 0.2 M $TBAPF_6$/Propylene carbonate. UV-Vis Spectra of prisitine film and electrochemical conditioned film (left). Spectroelectrochemistry of **10** (red) subjected to 20 mV potential increments from -0.4 V to -0.7 V vs Ag/AgCl (right). The polymer film bleaches at -0.7 V (blue).

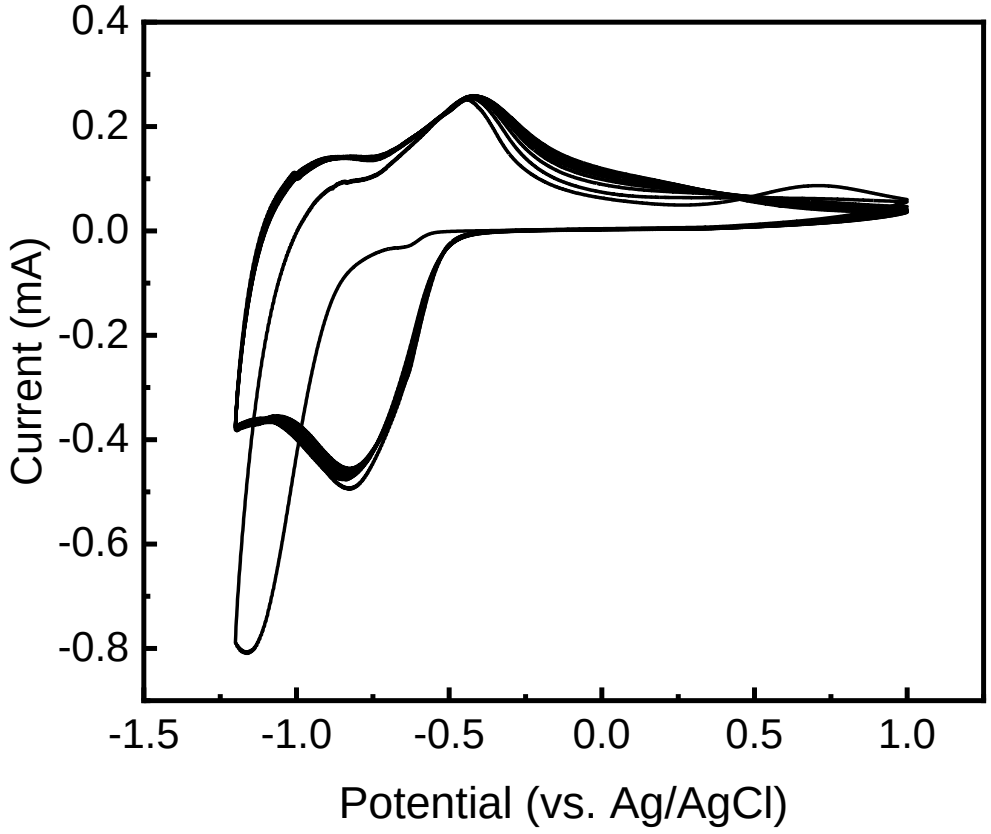

Figure S21. Cyclic voltammogram of **10** deposited on Fluorine-doped tin oxide (FTO) substrate after 10 continuous cycles under N_2 atmosphere. Voltammograms taken in a 0.2 M $TBAPF_6$ in propylene carbonate (PC) with a 50 mV/s scan rate. The $E_{1/2}$ value for **10** is -0.62V vs. Ag/AgCl.

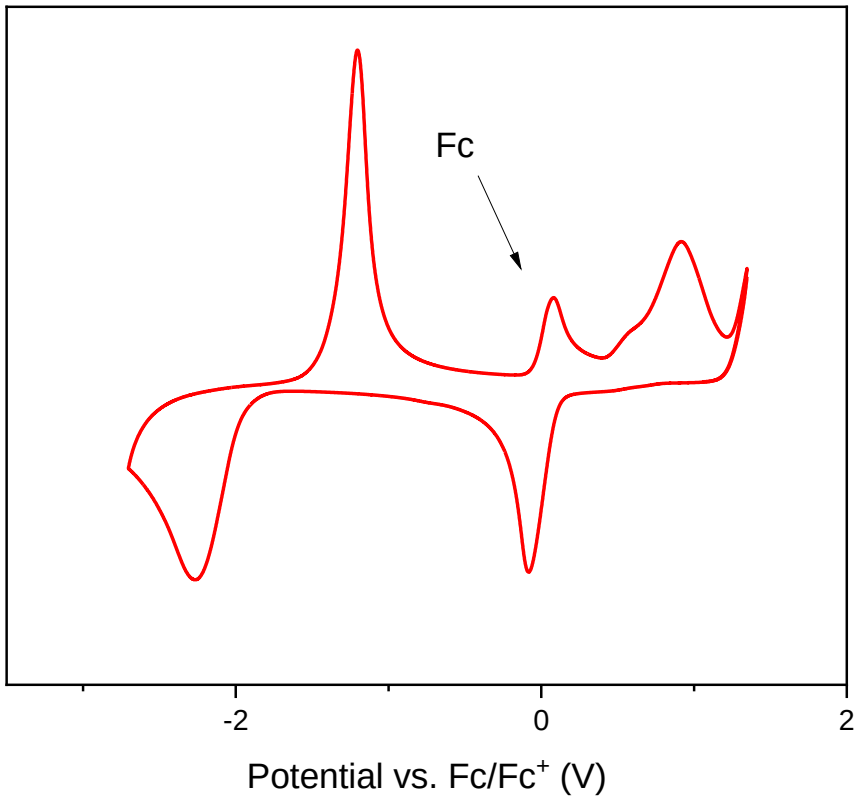

Figure S22. Cyclic voltammogram of **11**. The voltammogram was taken by heating a solution of **11** and dropping it onto a glassy carbon working electrode. Supporting electrolyte: 0.3 M $TBAPF_6$ in THF; 100 mV/s scan rate. Scans were started at the open-circuit potential and scanned in the anodic direction.

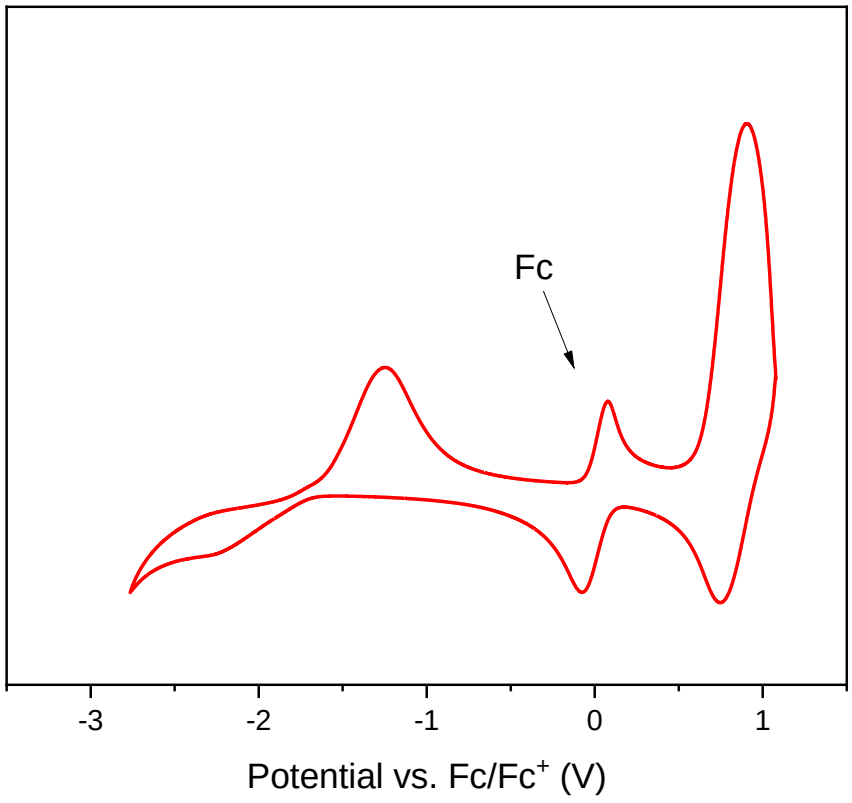

Figure S23. Cyclic voltammogram of **12**. The voltammogram was taken by heating a solution of **12** and dropping it onto a glassy carbon working electrode. Supporting electrolyte: 0.3 M $TBAPF_6$ in THF; 100 mV/s scan rate. Scans were started at the open-circuit potential and scanned in the anodic direction.

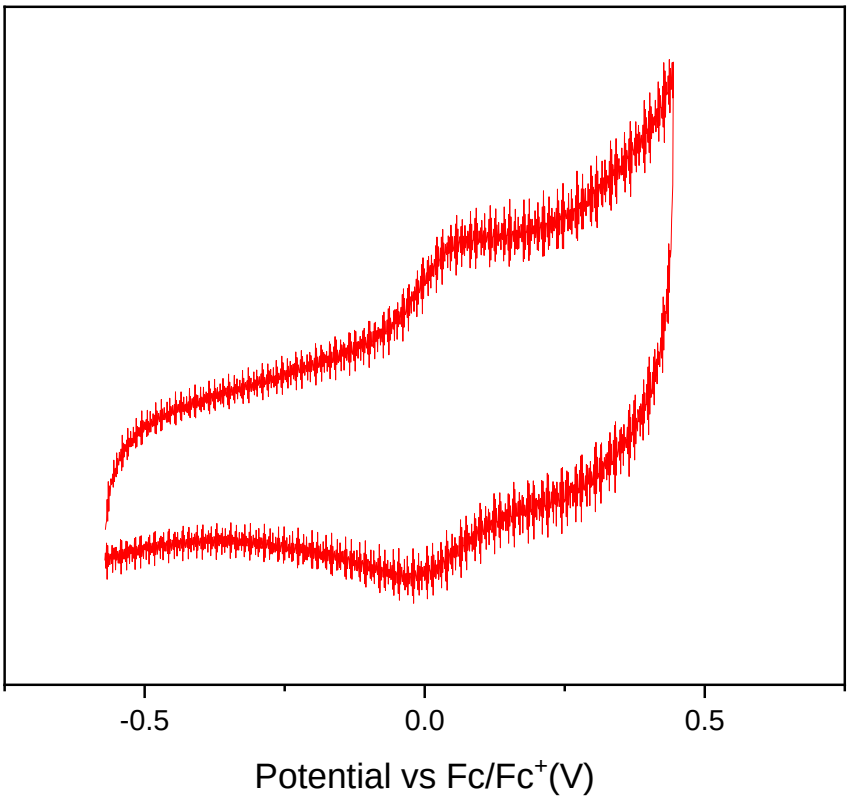

Figure S24. Cyclic voltammogram isolated in the ferrocene couple for **15**. The voltammogram was taken by heating a solution of **15** and dropping it onto a glassy carbon working electrode. Supporting electrolyte: 0.3 M $TBAPF_6$ in THF; 100mV/s scan rate. Scans were started at the open-circuit potential and scanned in the cathodic direction. The $E_{1/2}$ value for **15** is 0.02 V vs. Fc/Fc^+.

8. Photoswitching Experiments

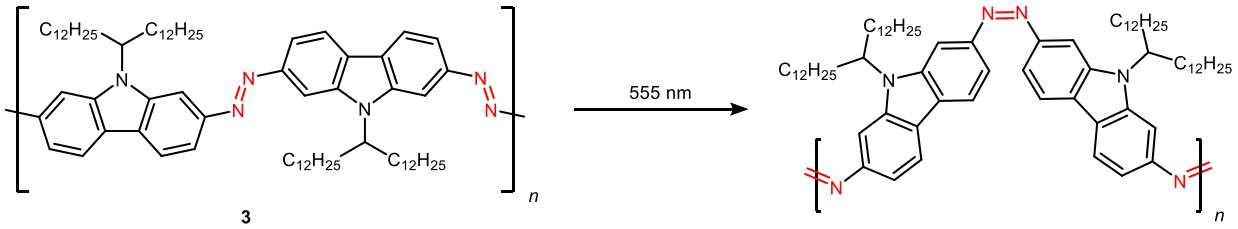

PolyAzoCarbazole (3). A vial was charged with **3** (0.4 mg) and C_6H_5Cl (20 mL). An aliquot (3 mL) was added to a cuvette, irradiated for 30 s at 555 nm, and quickly transferred to a UV-Vis instrument to obtain measurements.

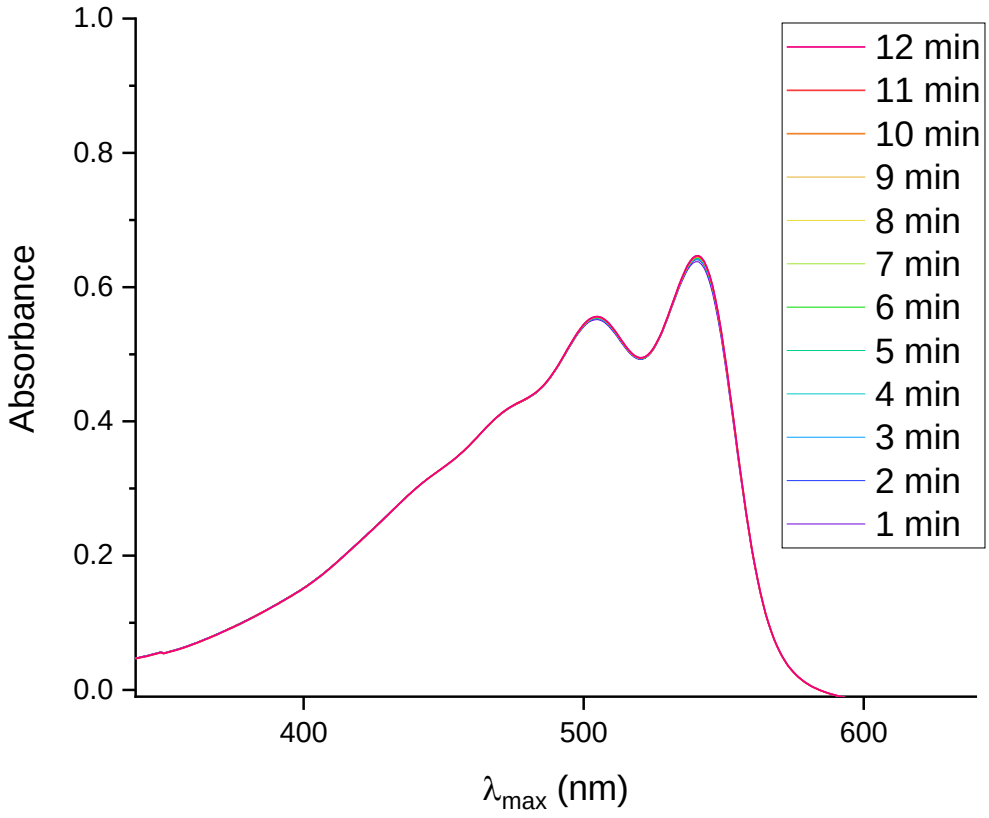

Figure S25. UV-Vis spectrum of photoisomerization of **3** (0.0326 mM) in C_6H_5Cl.

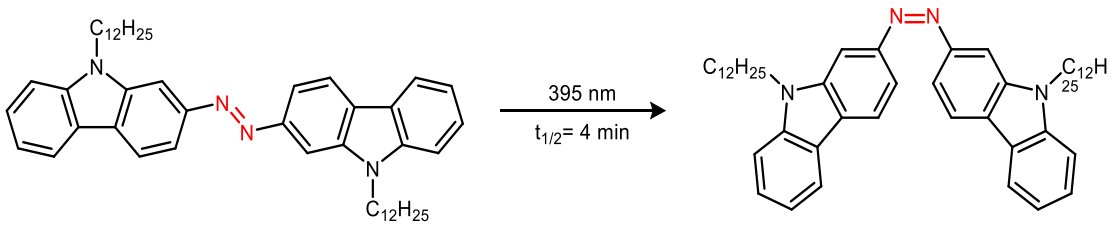

5b

Azocarbazole (5b). A vial was charged with **5b** (0.4 mg) and CH_2Cl_2 (20 mL). An aliquot (3 mL) was added to a cuvette, irradiated for 30 s at 395 nm, and quickly transferred to a UV-Vis instrument to obtain measurements.

UV–Vis–NIR (CH_2Cl_2, 0.028 mM): λ_{max}, nm (ε, M^{-1} cm^{-1}): 264 (62,000), 303 (25,000), 393 (18,000).

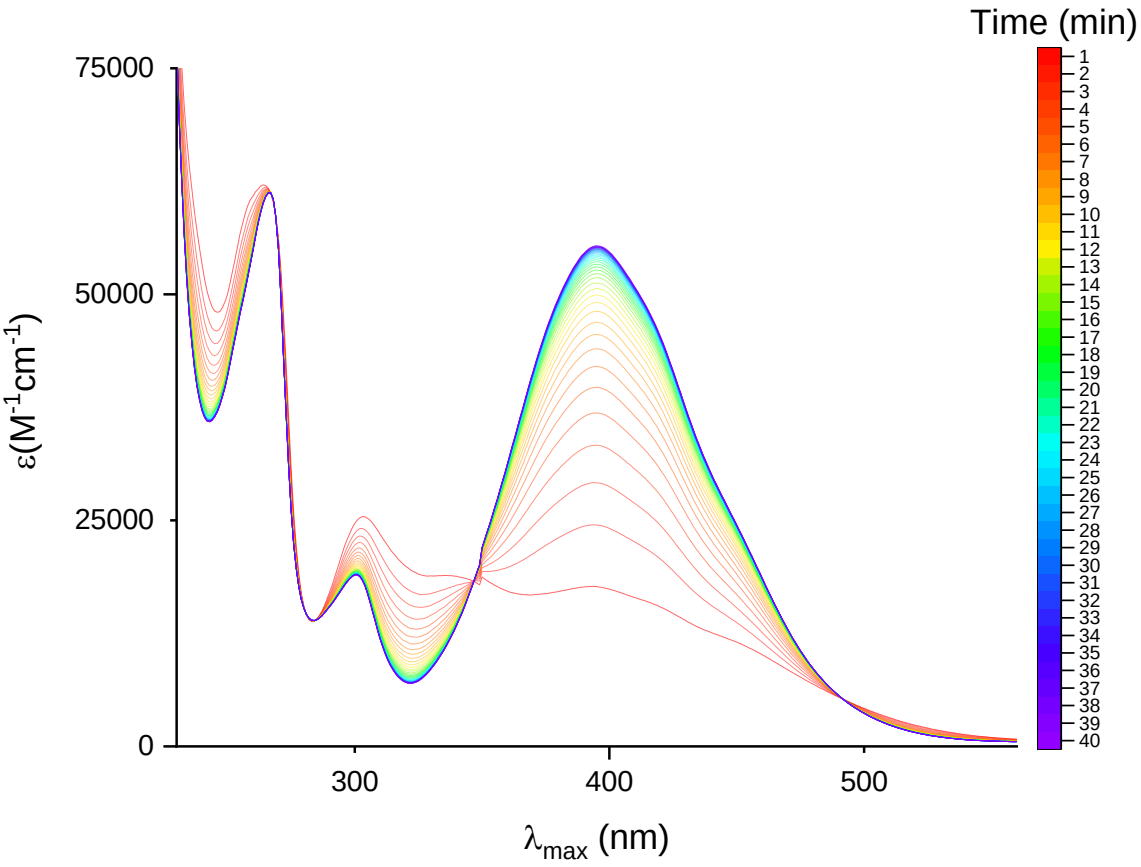

Figure S26. UV-Vis spectrum of photoisomerization of **5b** (0.028 mM) in CH_2Cl_2.

9. Thermogravimetric Analysis

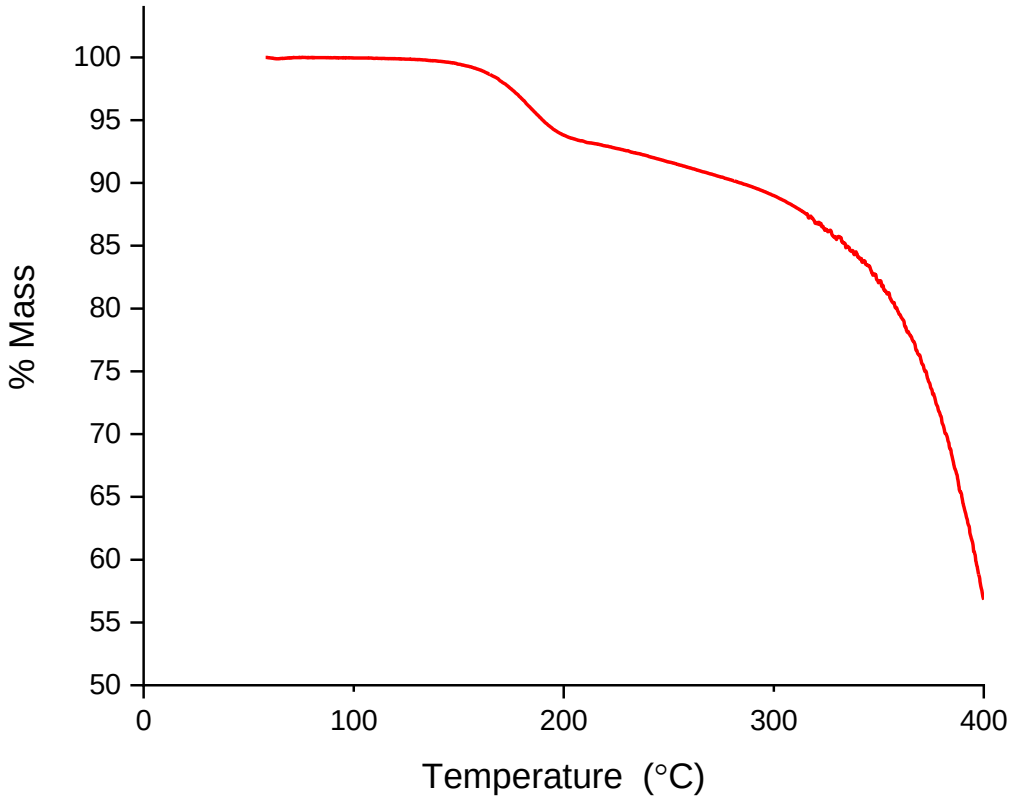

Figure S27. Thermogravimetric analysis of **S10** at 20°C per minute.

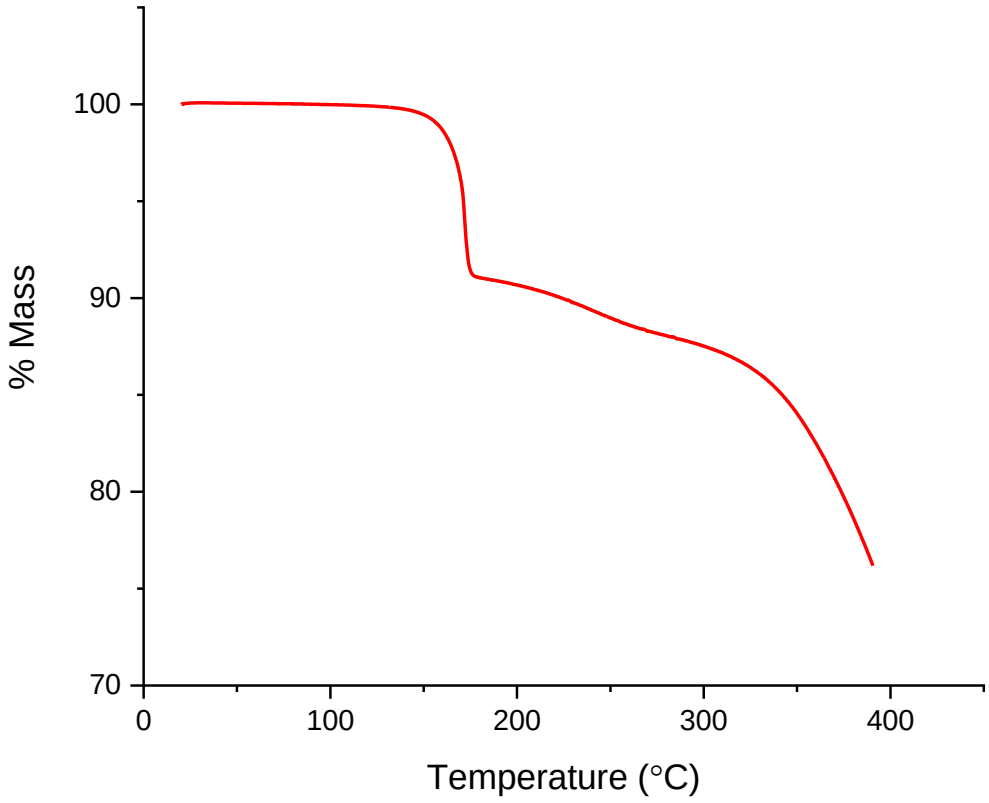

Figure S28. Thermogravimetric analysis of **2** at 20°C per minute.

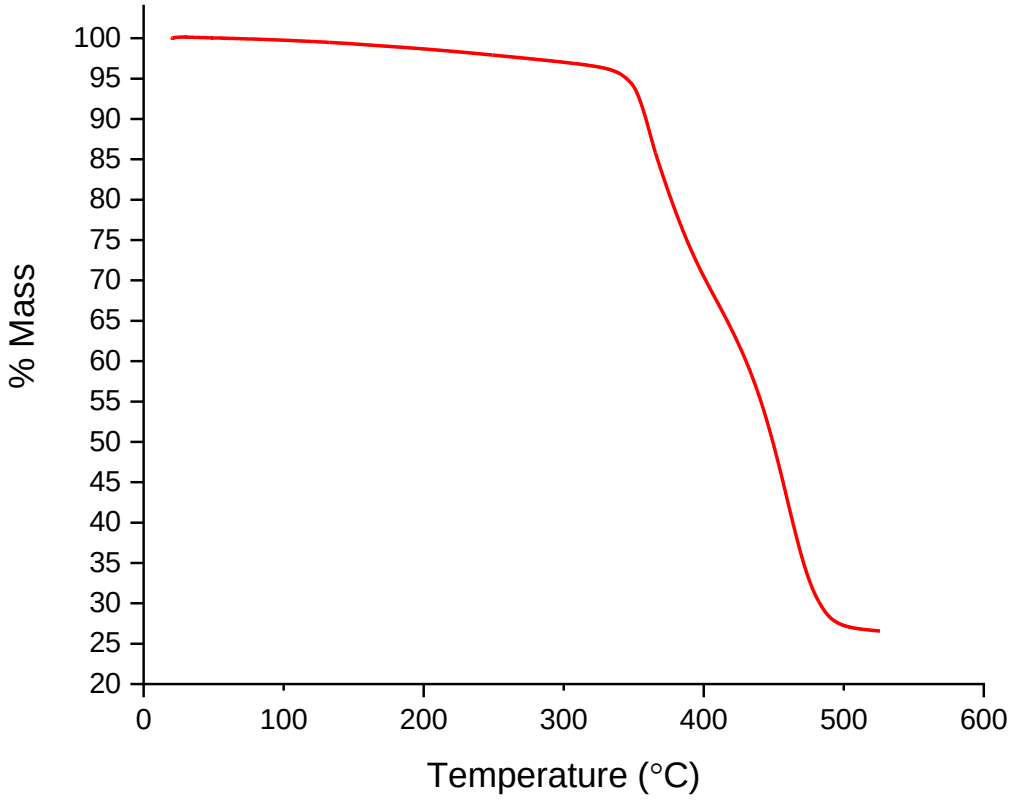

Figure S29. Thermogravimetric analysis of **3** at 20°C per minute.

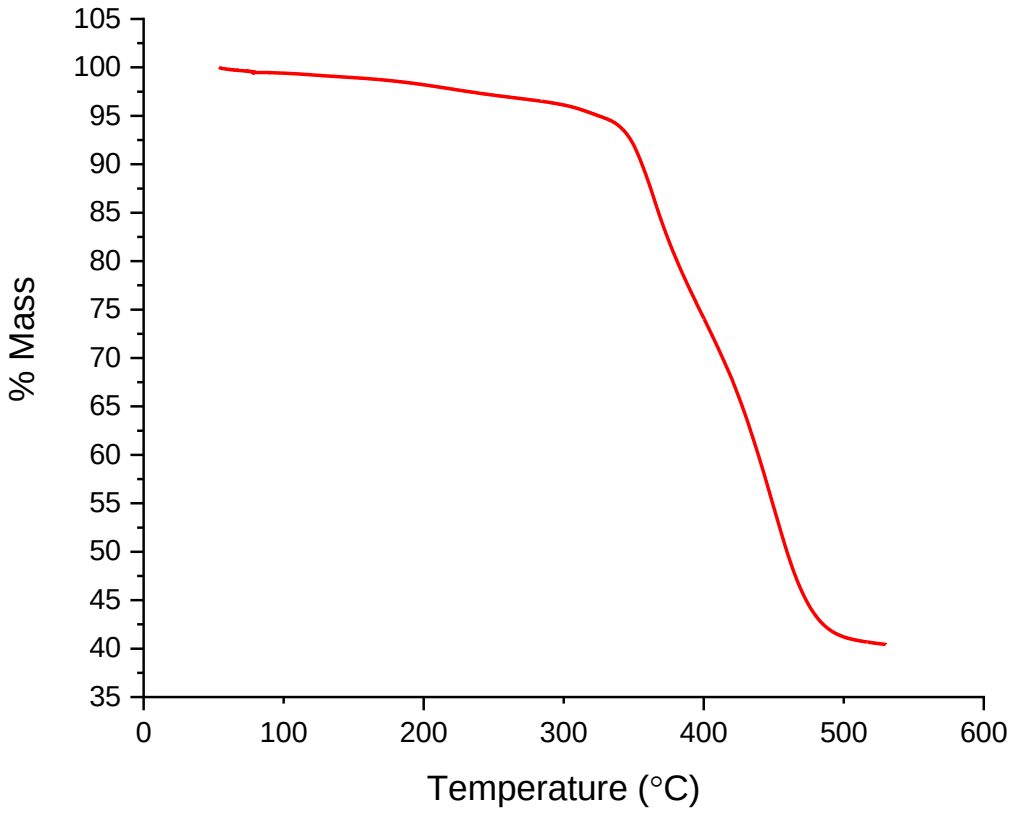

Figure S30. Thermogravimetric analysis of **10** at 20°C per minute.

10. Emission Spectra

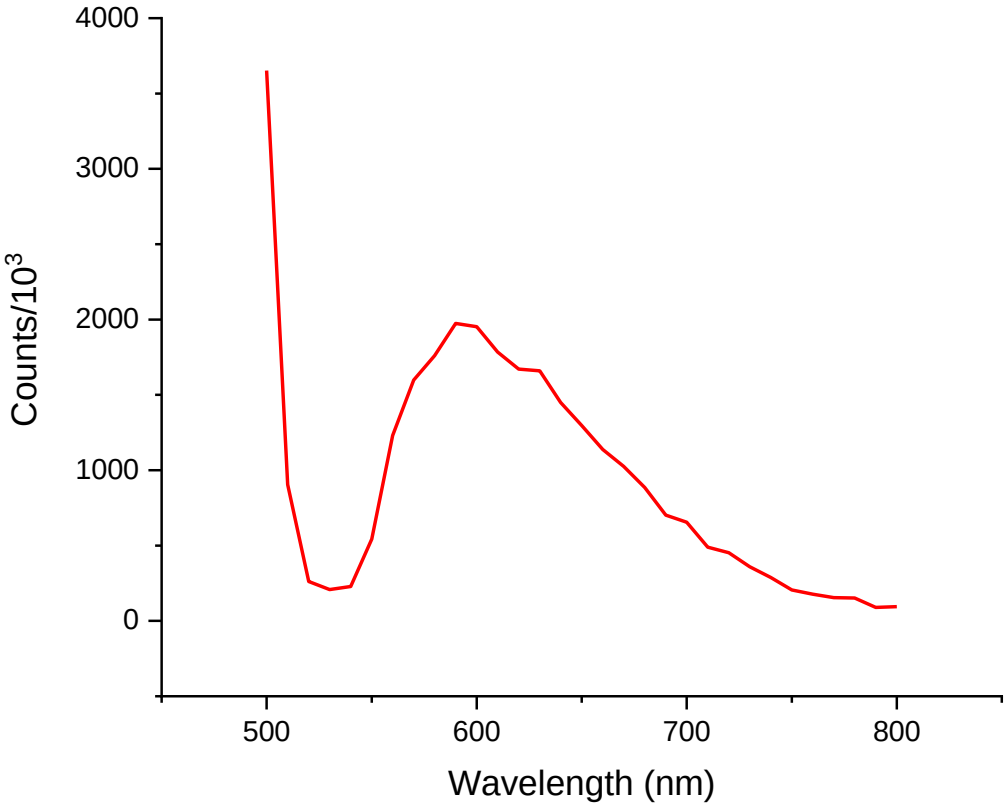

Figure S31. Emission spectrum of **3** (0.046 mM) at 503 nm in C_6H_5Cl.

11. NMR Spectra

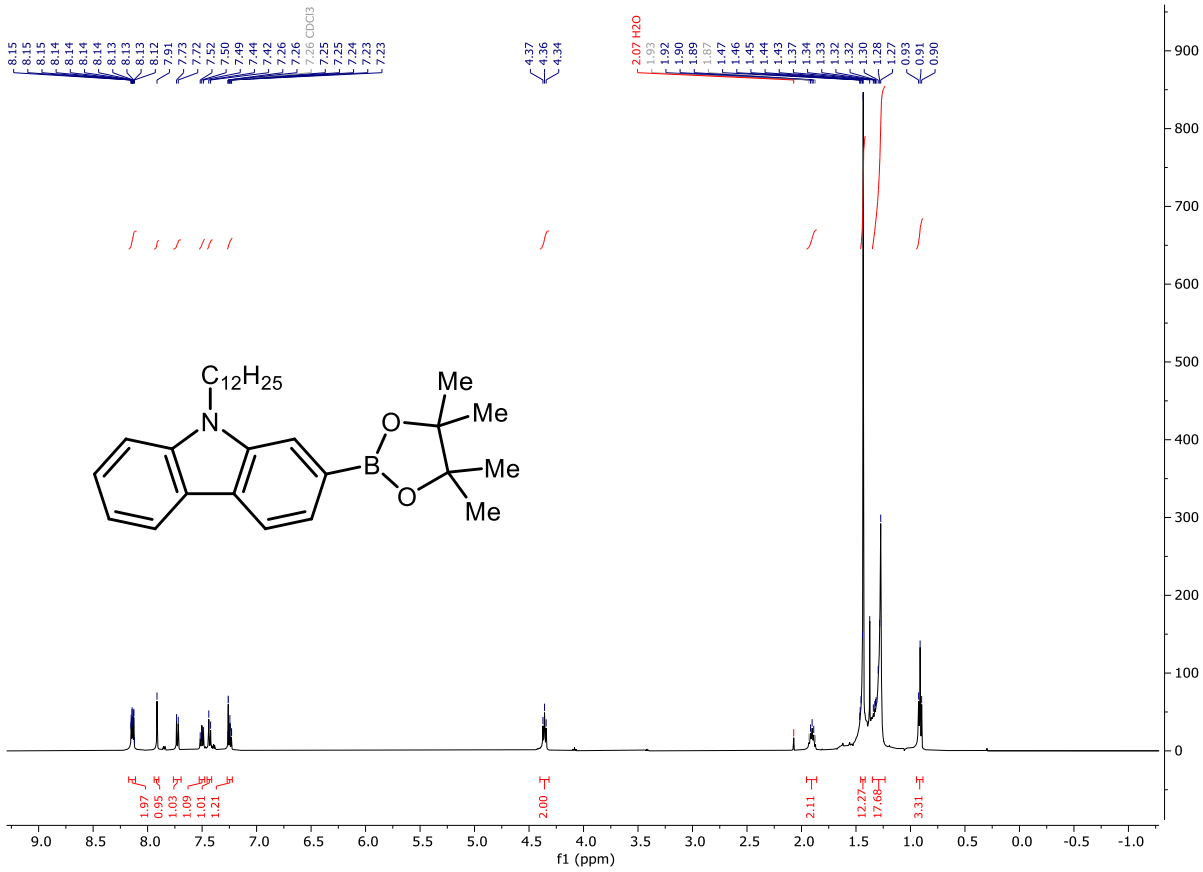

Figure S32. ^{1}H NMR spectrum of **S1** (500 MHz, $CDCl_3$).

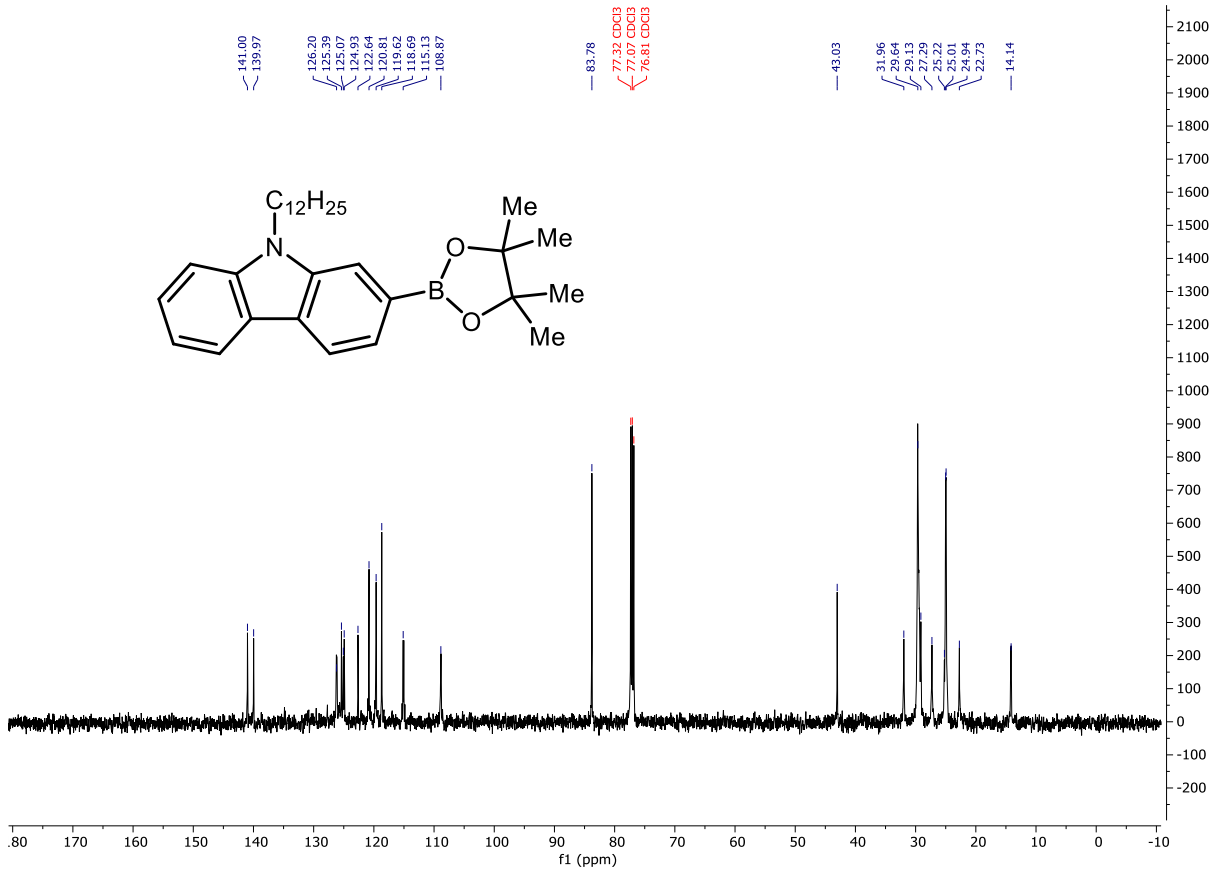

Figure S33. $^{13}C\{^{1}H\}$ NMR spectrum of **S1** (126 MHz, $CDCl_3$).

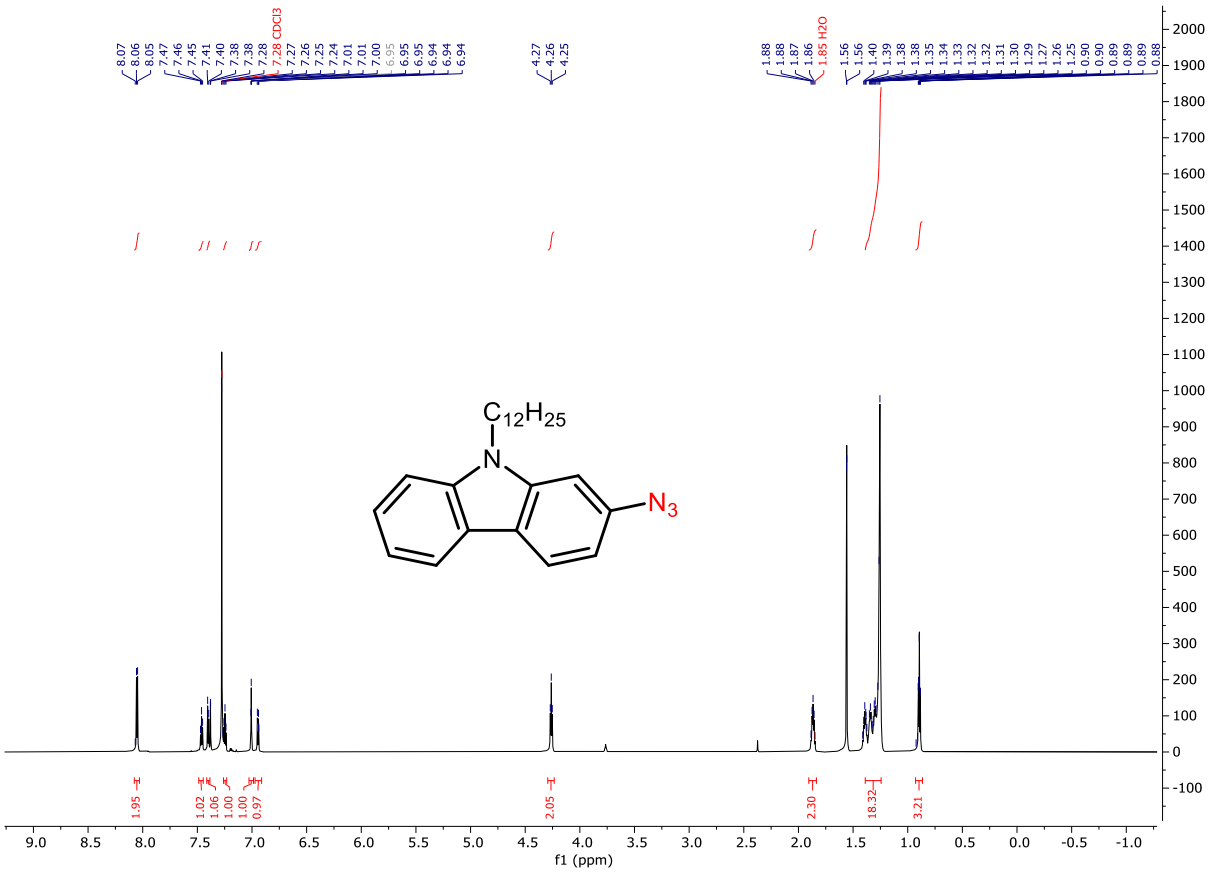

Figure S34. ^{1}H NMR spectrum of **4b** (800 MHz, $CDCl_3$).

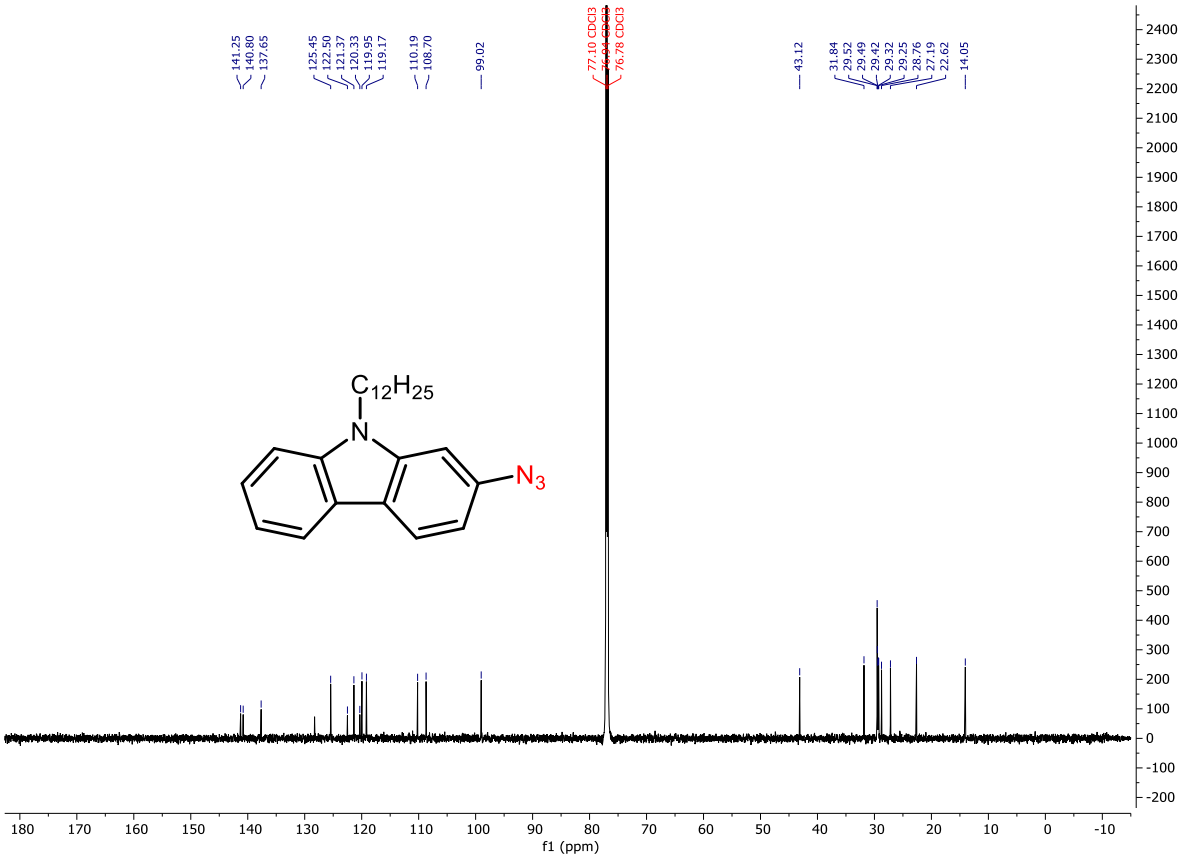

Figure S35. $^{13}C\{^{1}H\}$ NMR spectrum of **4b** (201 MHz, $CDCl_3$).

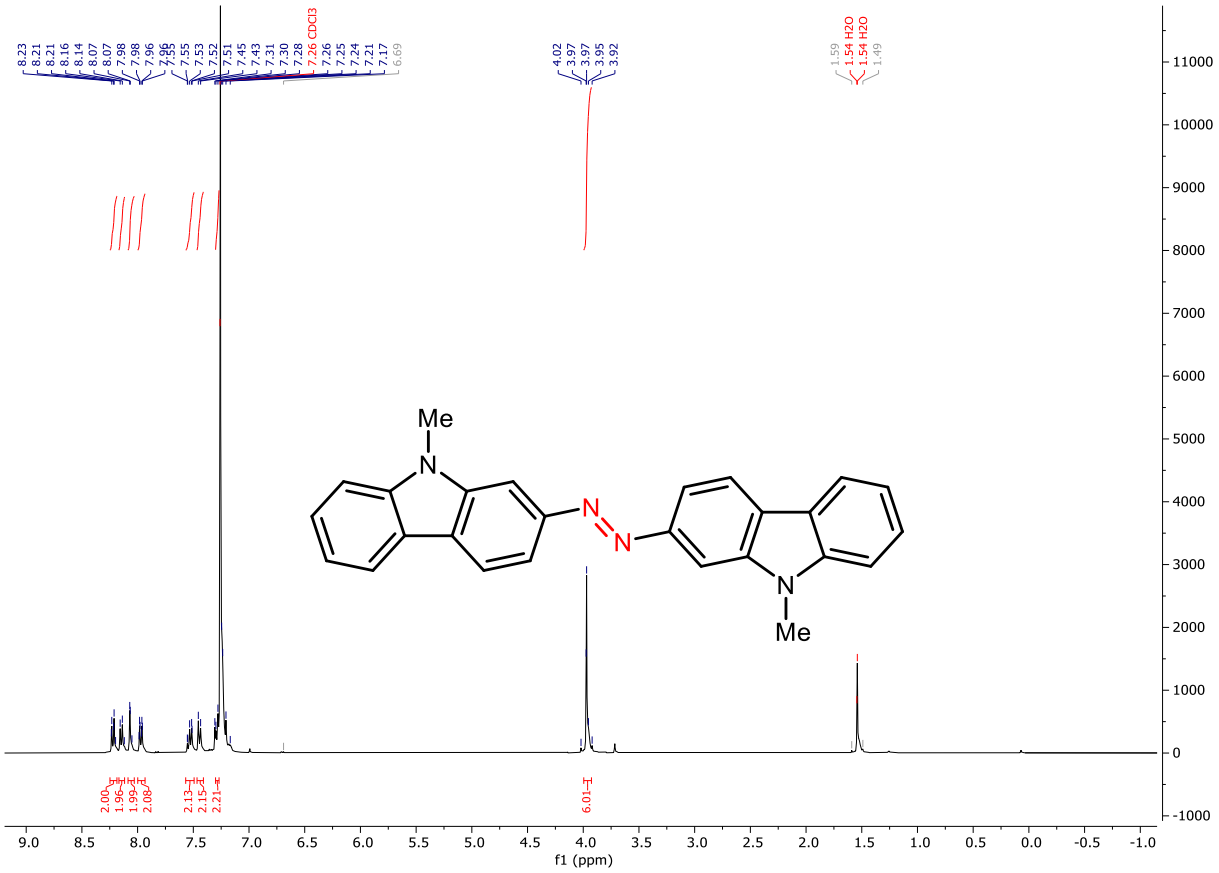

Figure S36. ^{1}H NMR spectrum of **5a** (400 MHz, $CDCl_3$).

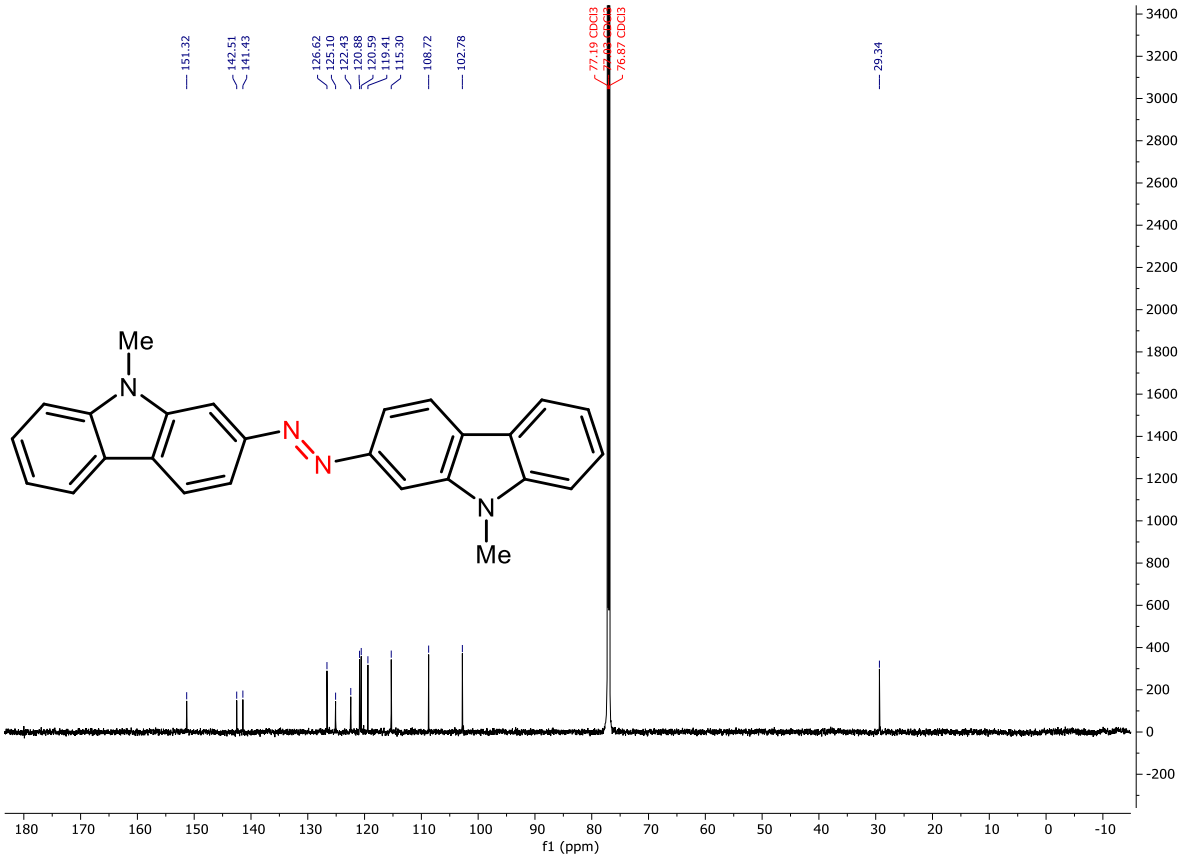

Figure S37. $^{13}C\{^{1}H\}$ NMR spectrum of **5a** (201 MHz, $CDCl_3$).

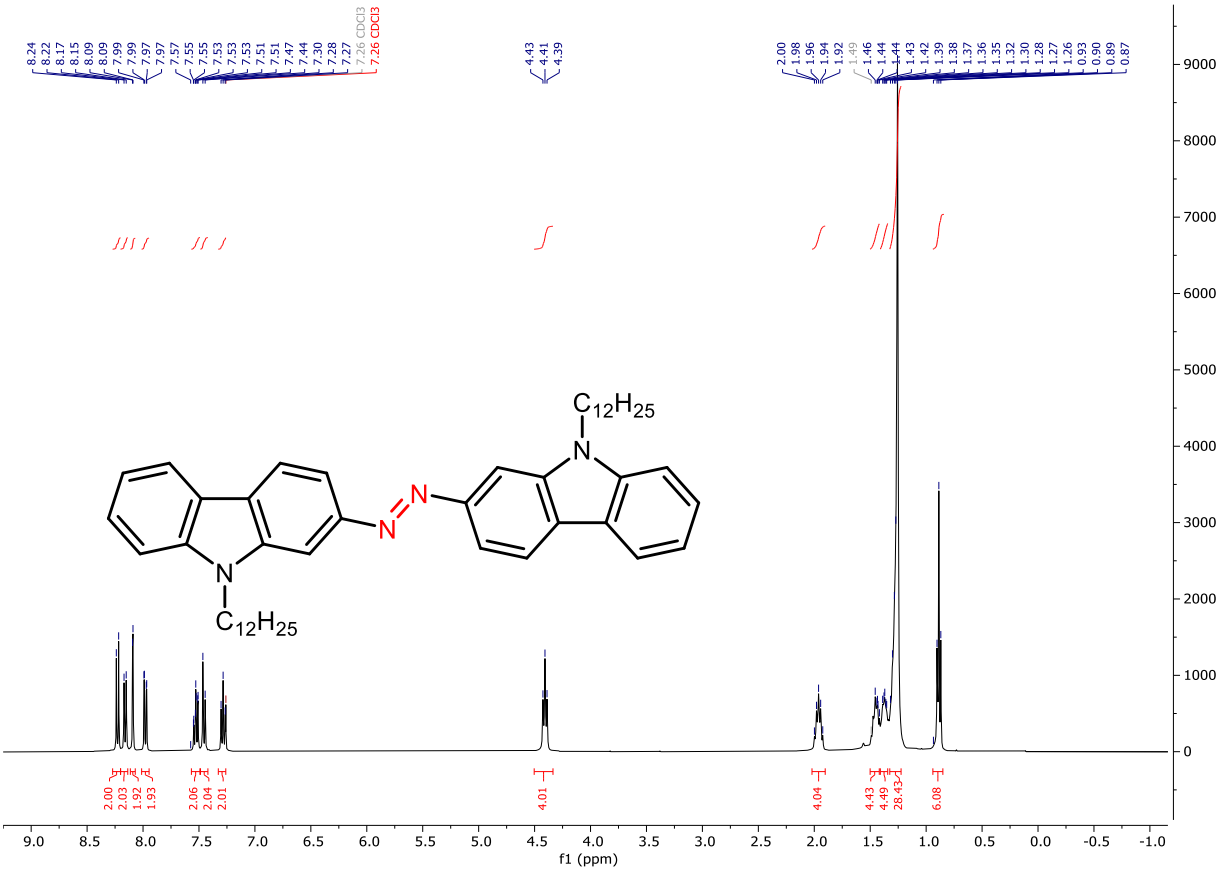

Figure S38. ^{1}H NMR spectrum of **5b** (400 MHz, $CDCl_3$).

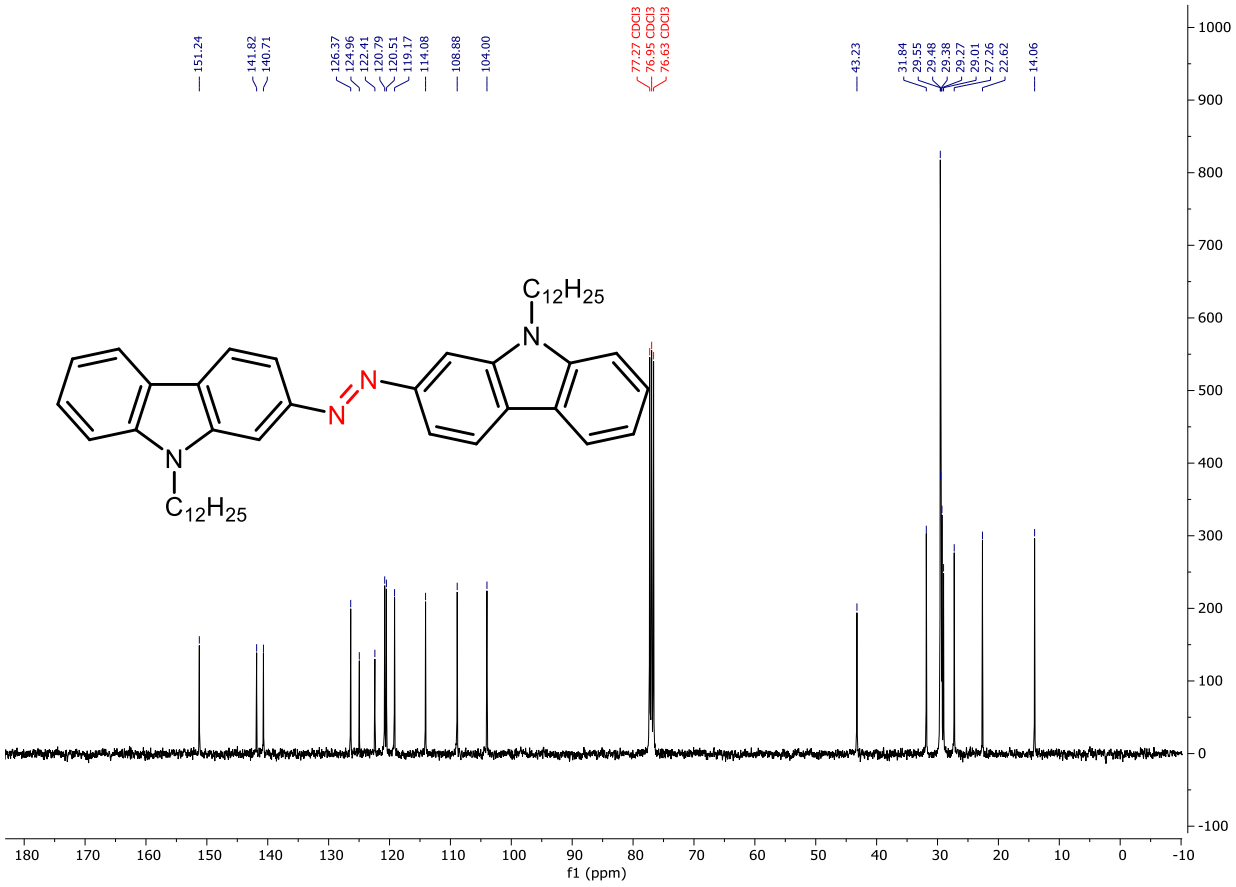

Figure S39. $^{13}C\{^{1}H\}$ NMR spectrum of **5b** (126 MHz, $CDCl_3$).

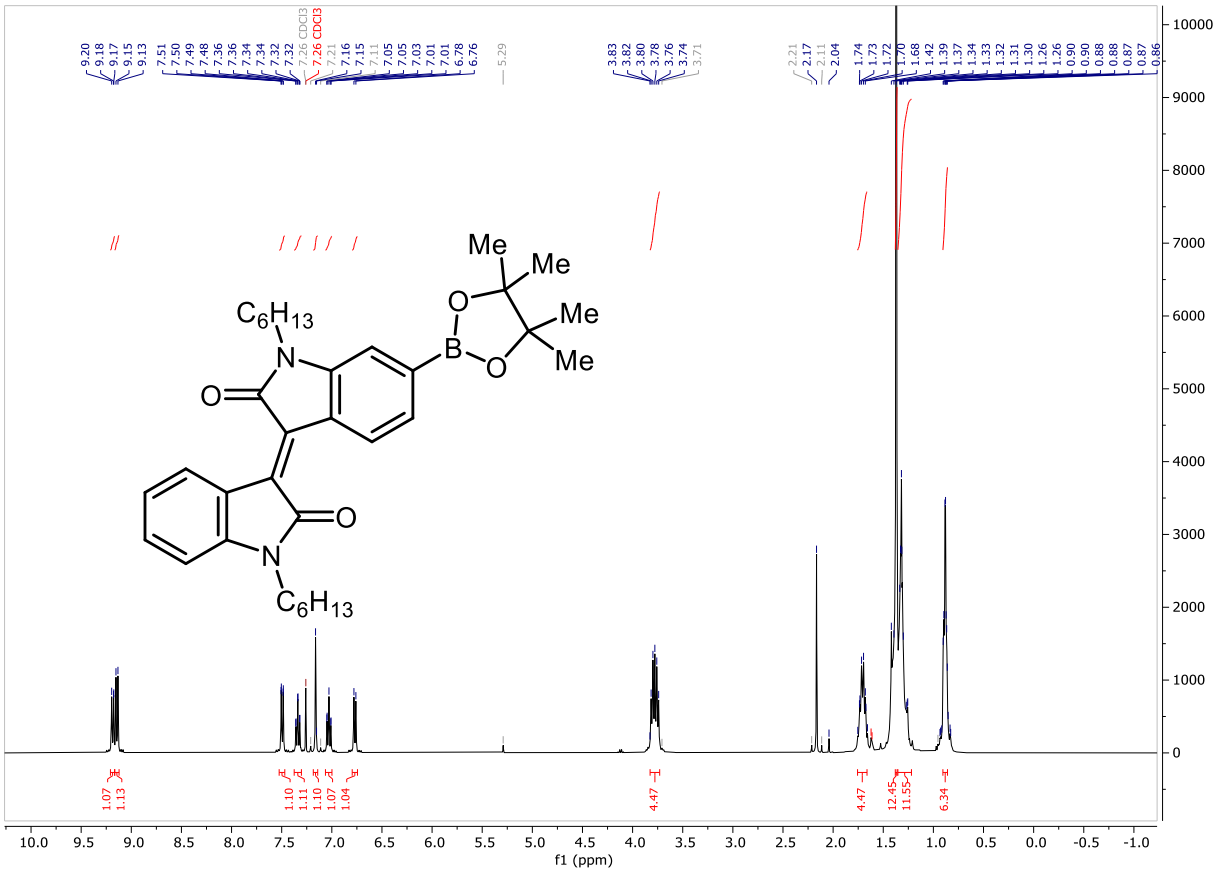

Figure S40. ^{1}H NMR spectrum of **S2** (400 MHz, $CDCl_3$).

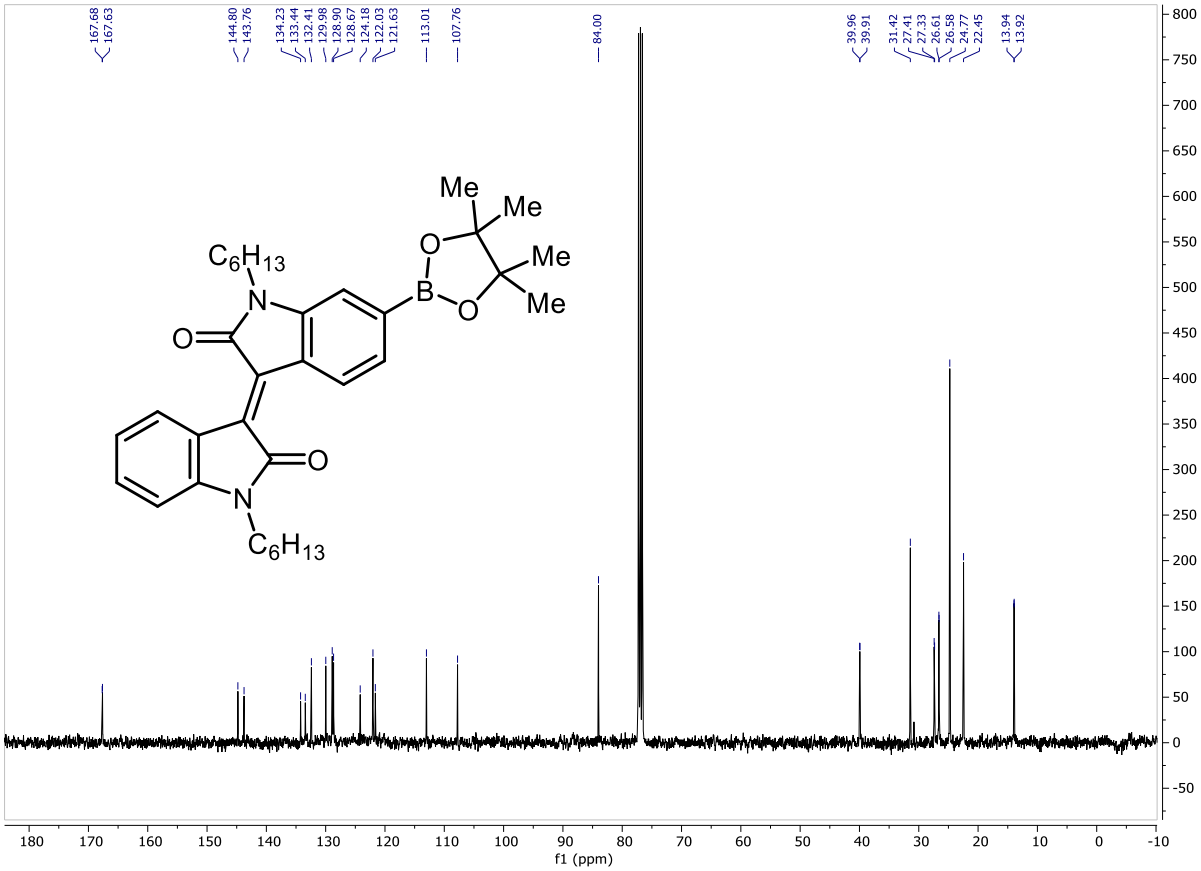

Figure S41. $^{13}C\{^{1}H\}$ NMR spectrum of **S2** (101 MHz, $CDCl_3$).

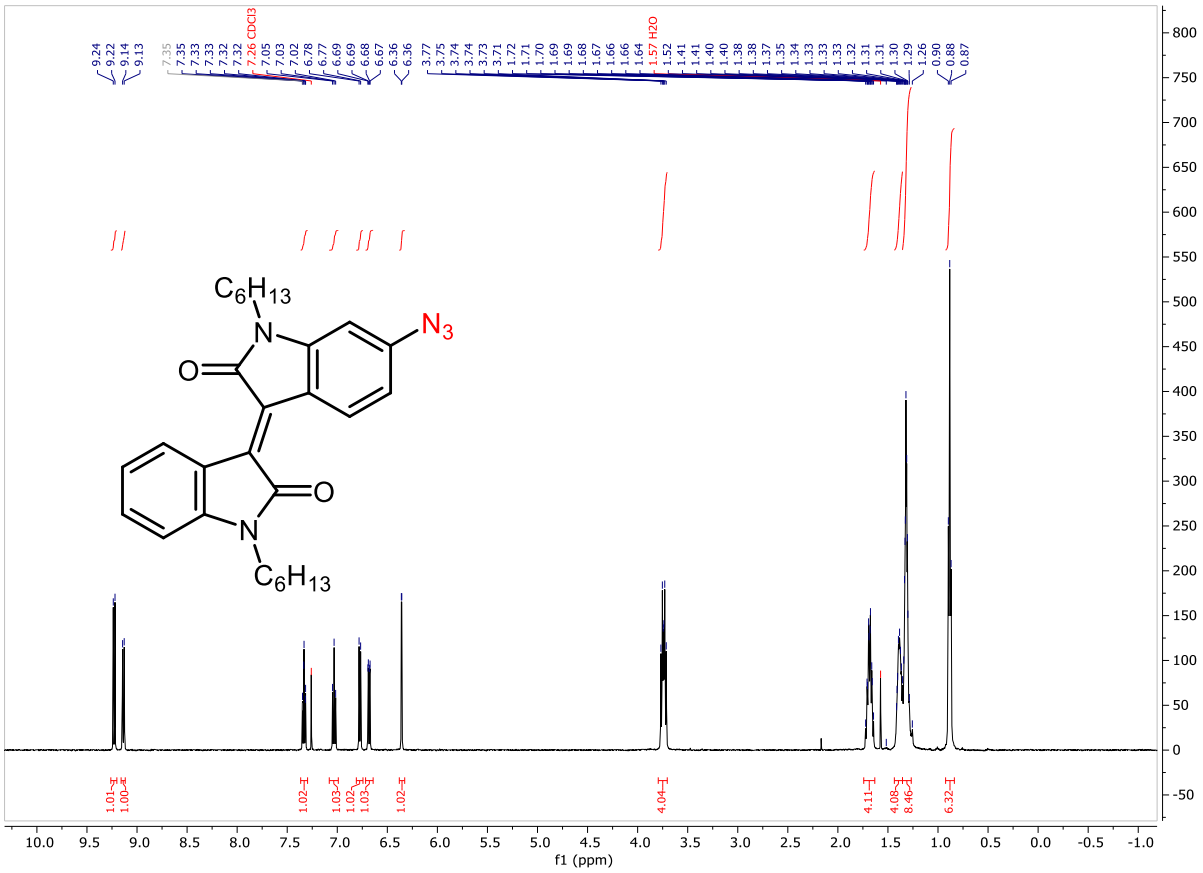

Figure S42. ^{1}H NMR spectrum of **S3** (500 MHz, $CDCl_3$).

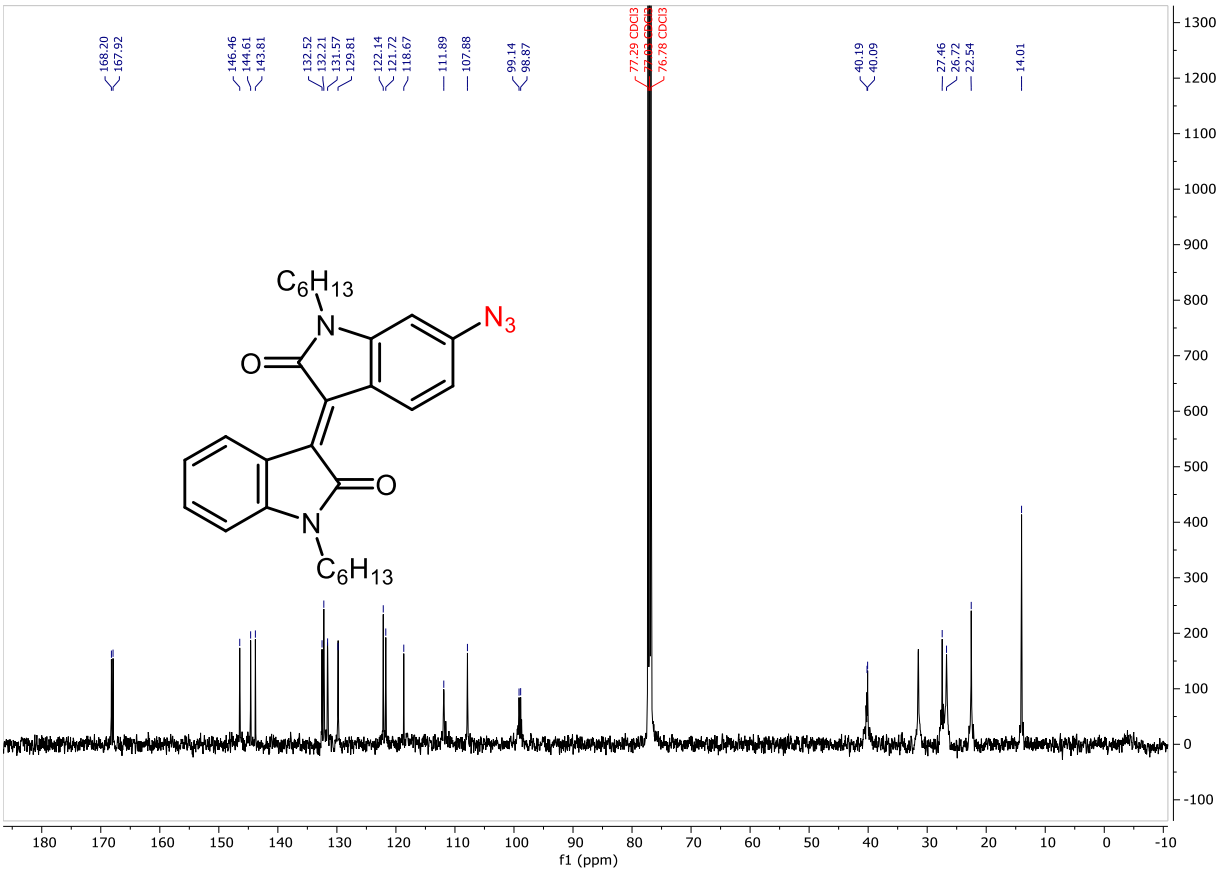

Figure S43. $^{13}C\{^{1}H\}$ NMR spectrum of **S3** (126 MHz, $CDCl_3$).

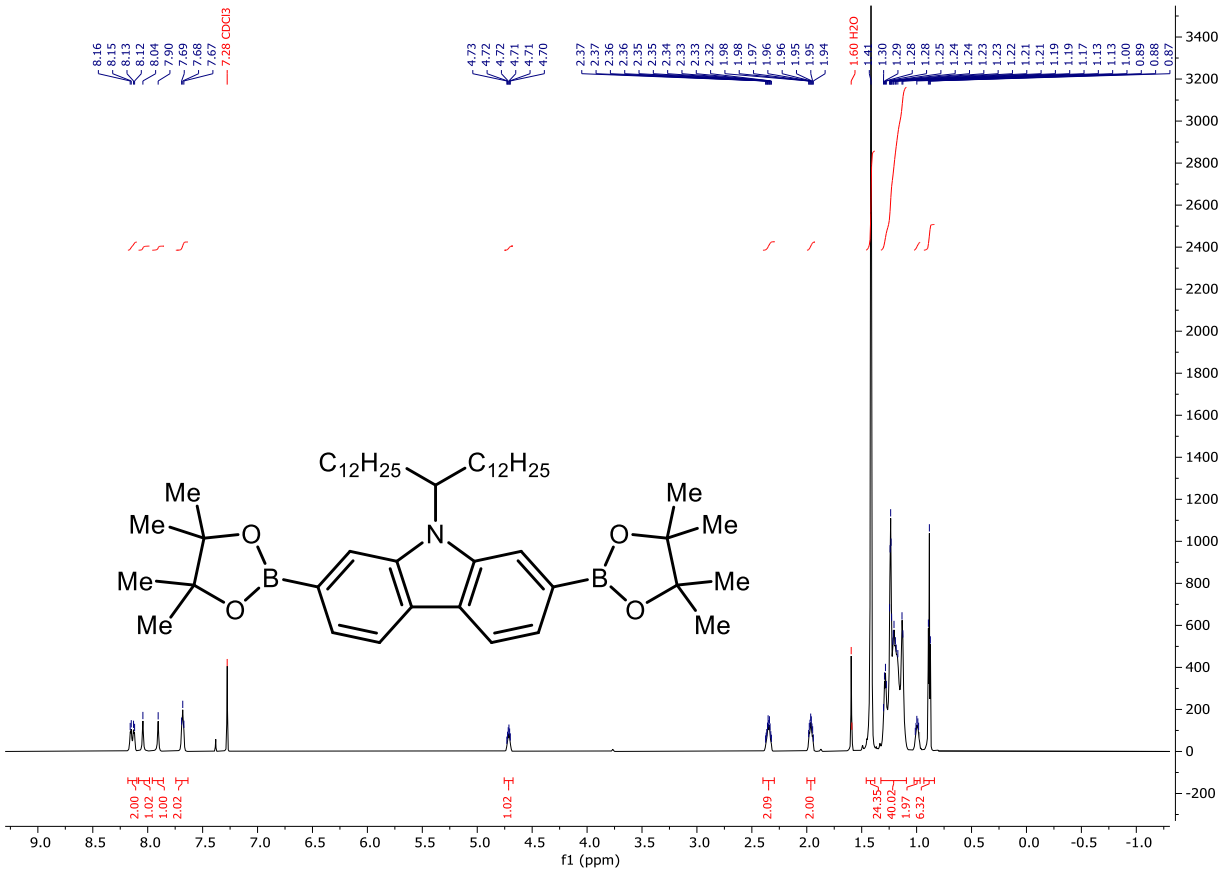

Figure S44. ^{1}H NMR spectrum of **S4** (800 MHz, $CDCl_3$).

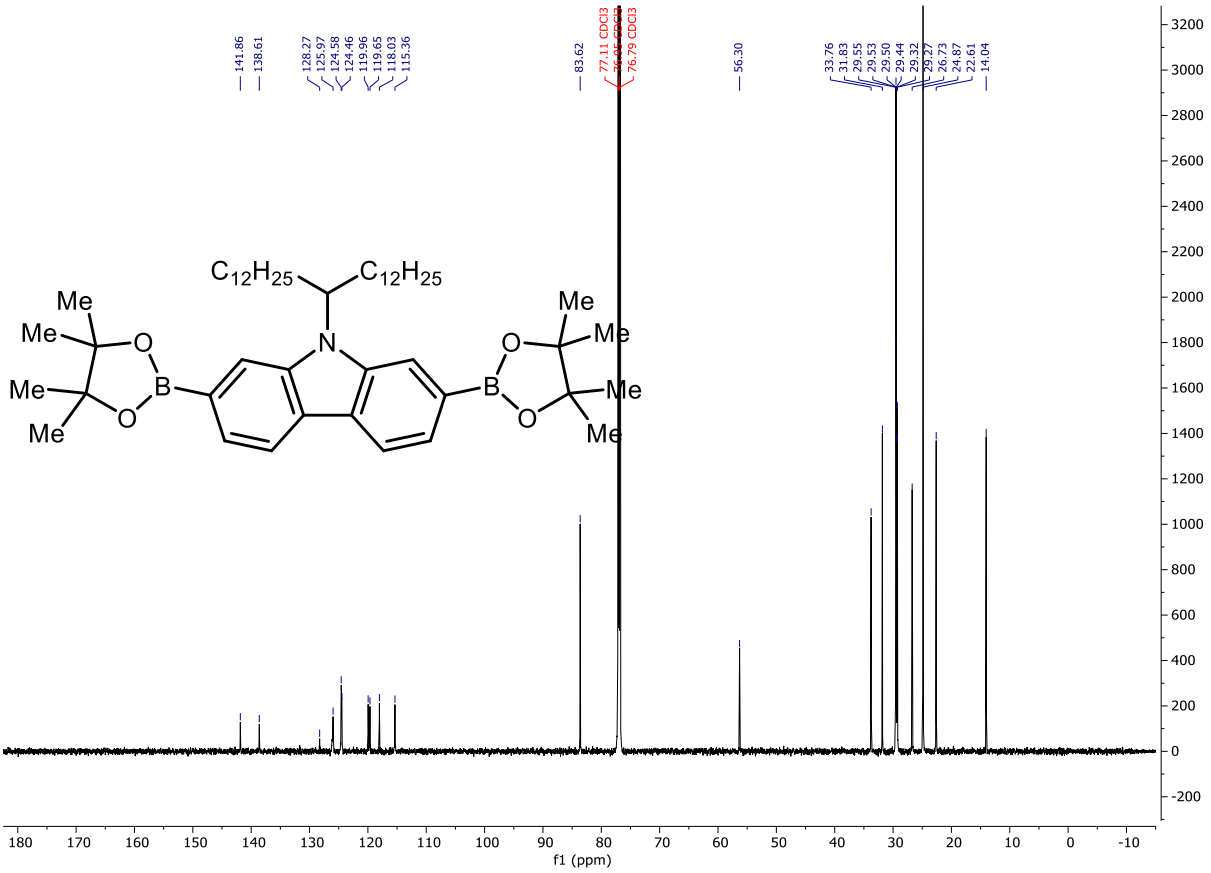

Figure S45. $^{13}C\{^{1}H\}$ NMR spectrum of **S4** (201 MHz, $CDCl_3$).

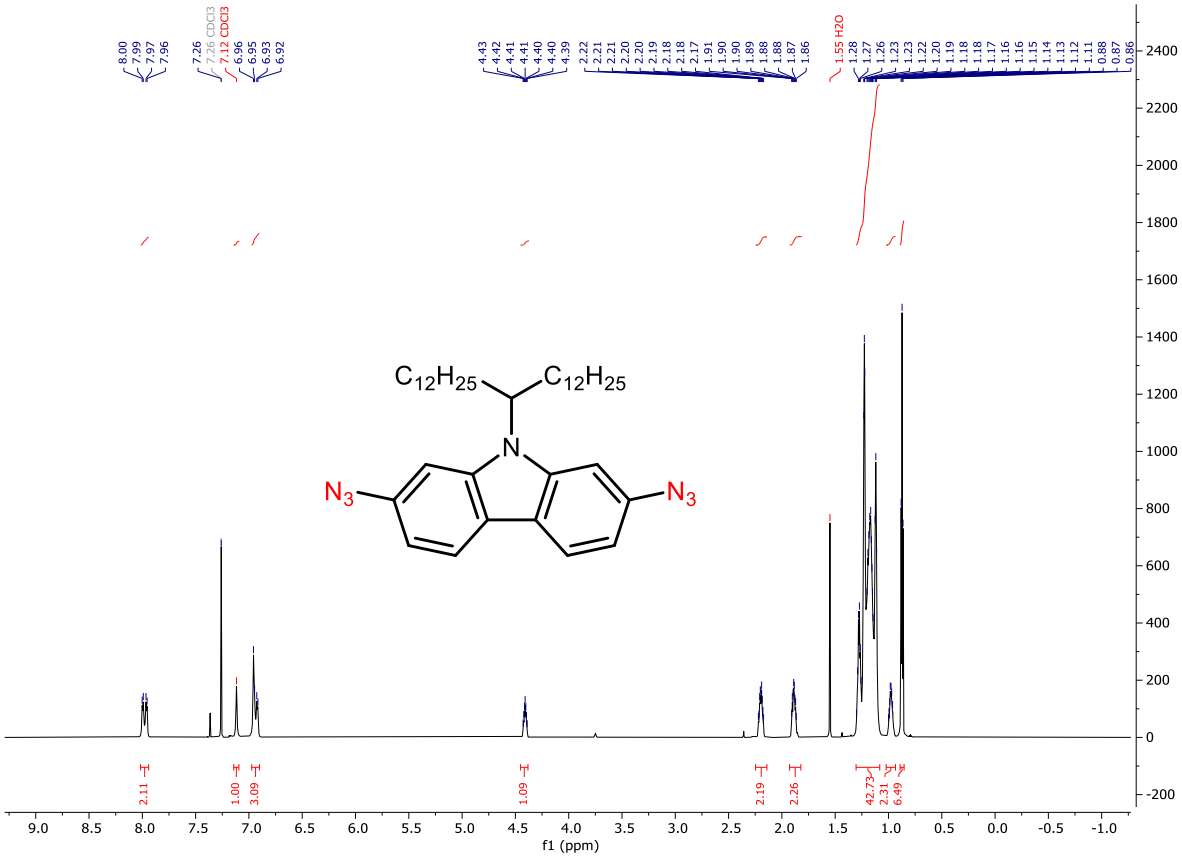

Figure S46. ^{1}H NMR spectrum of **2** (800 MHz, $CDCl_3$).

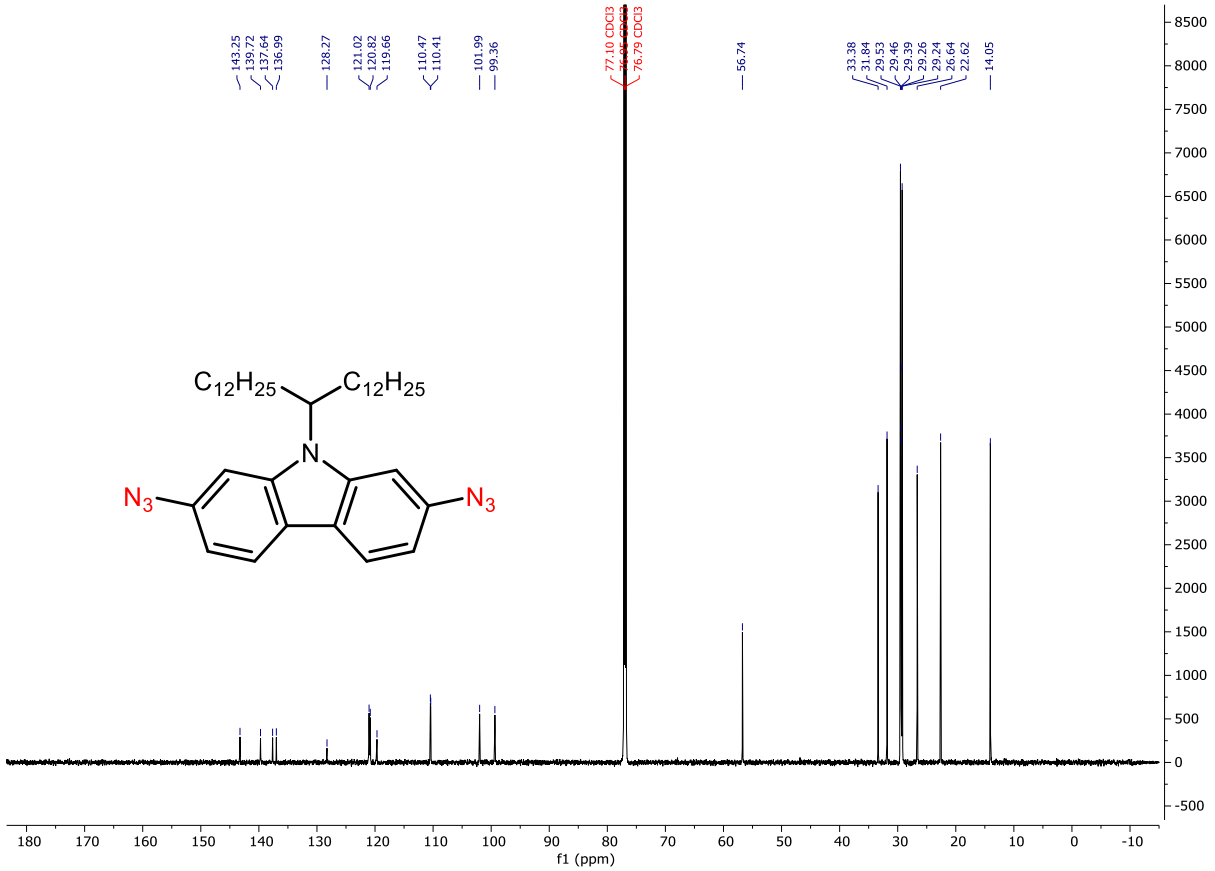

Figure S47. $^{13}C\{^{1}H\}$ NMR spectrum of **2** (201 MHz, $CDCl_3$).

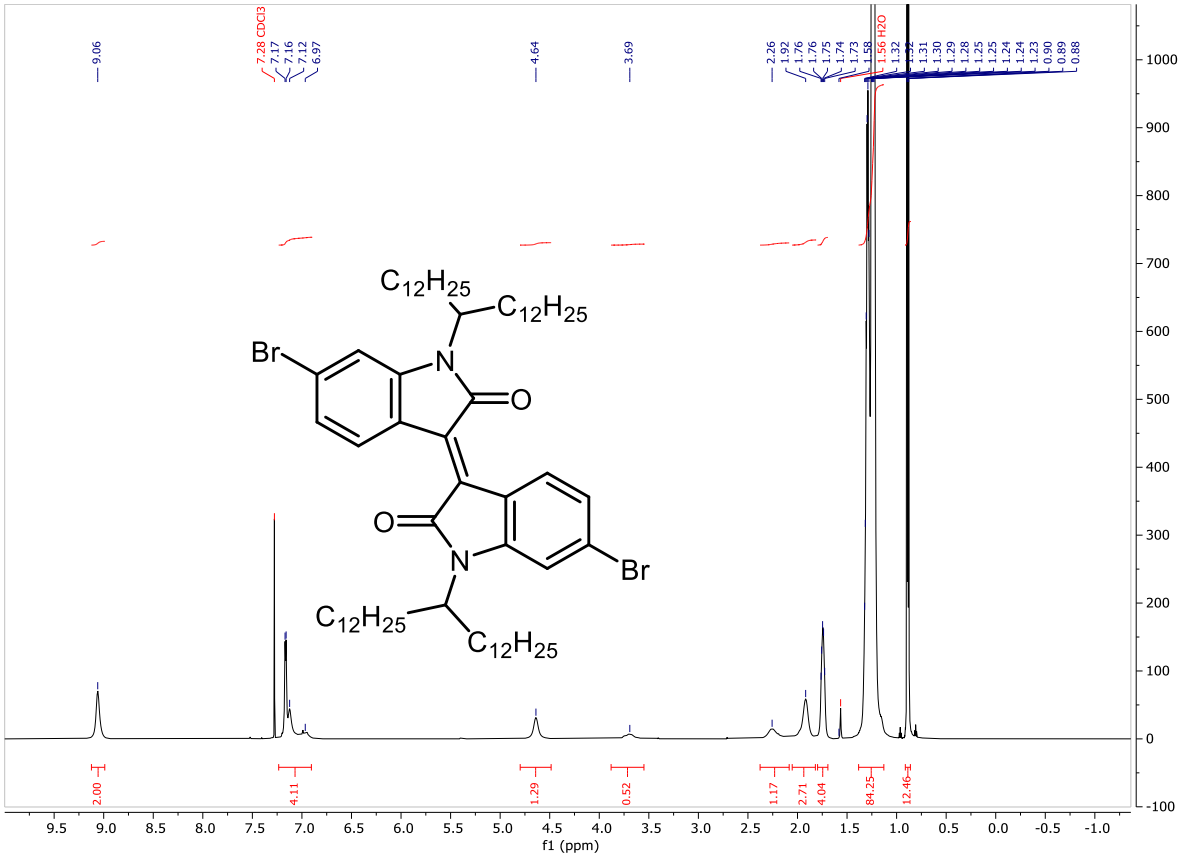

Figure S48. ^{1}H NMR spectrum of **S5** (300 MHz, $CDCl_3$).

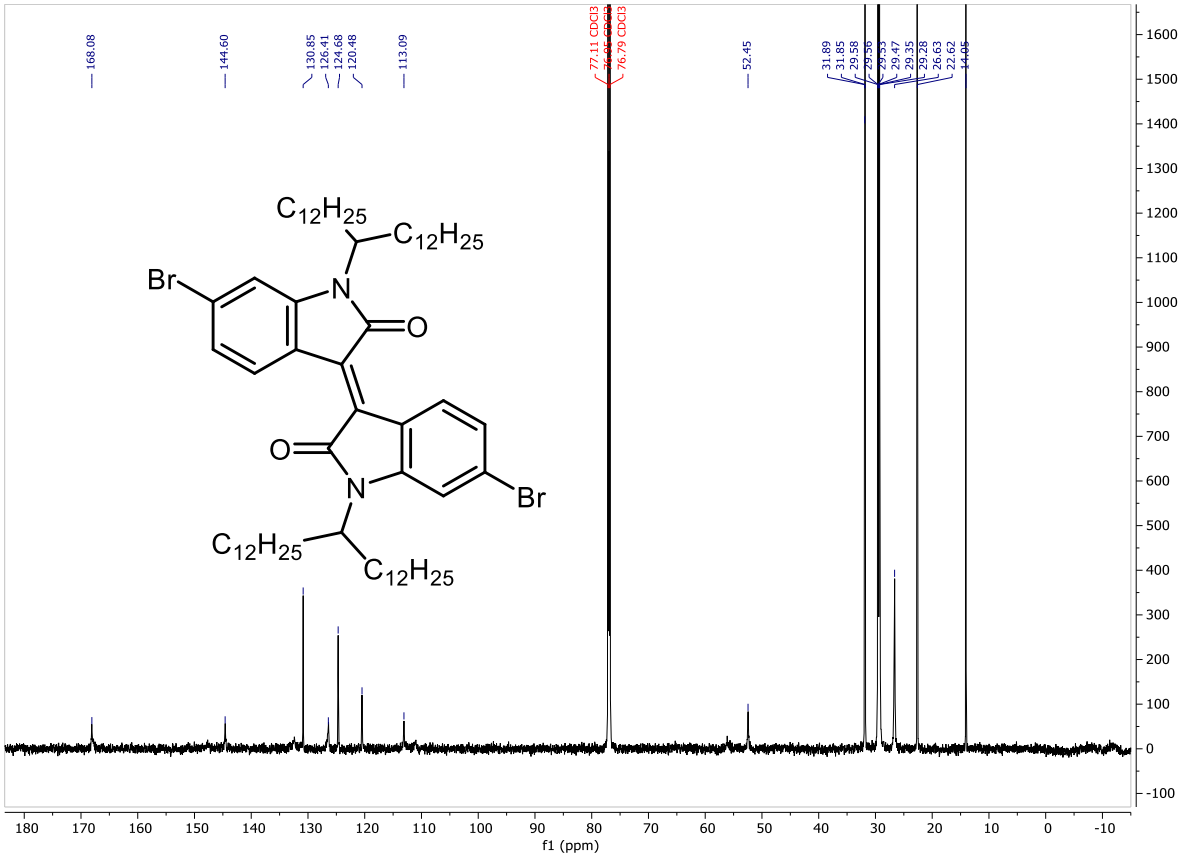

Figure S49. $^{13}C\{^{1}H\}$ NMR spectrum of **S5** (201 MHz, $CDCl_3$).

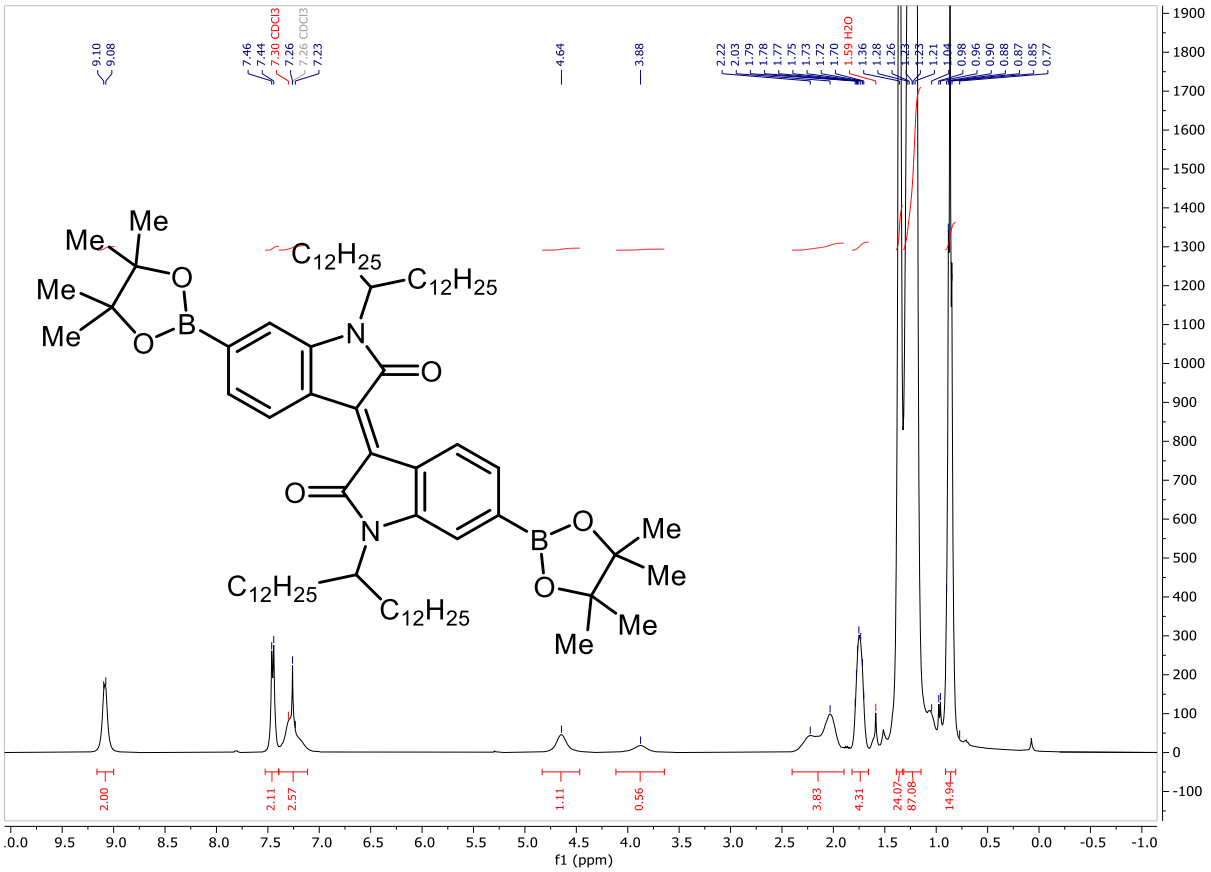

Figure S50. ^{1}H NMR spectrum of **S6** (400 MHz, $CDCl_3$).

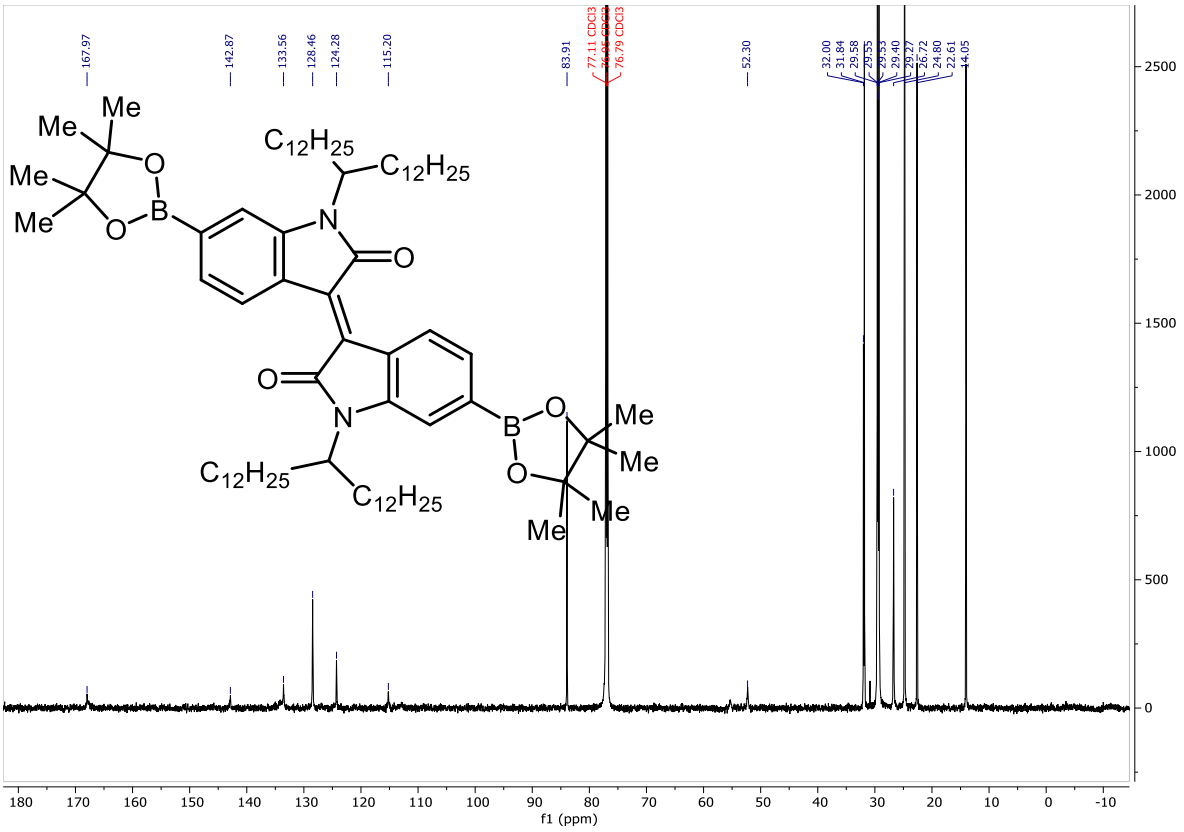

Figure S51. $^{13}C\{^{1}H\}$ NMR spectrum of **S6** (201 MHz, $CDCl_3$).

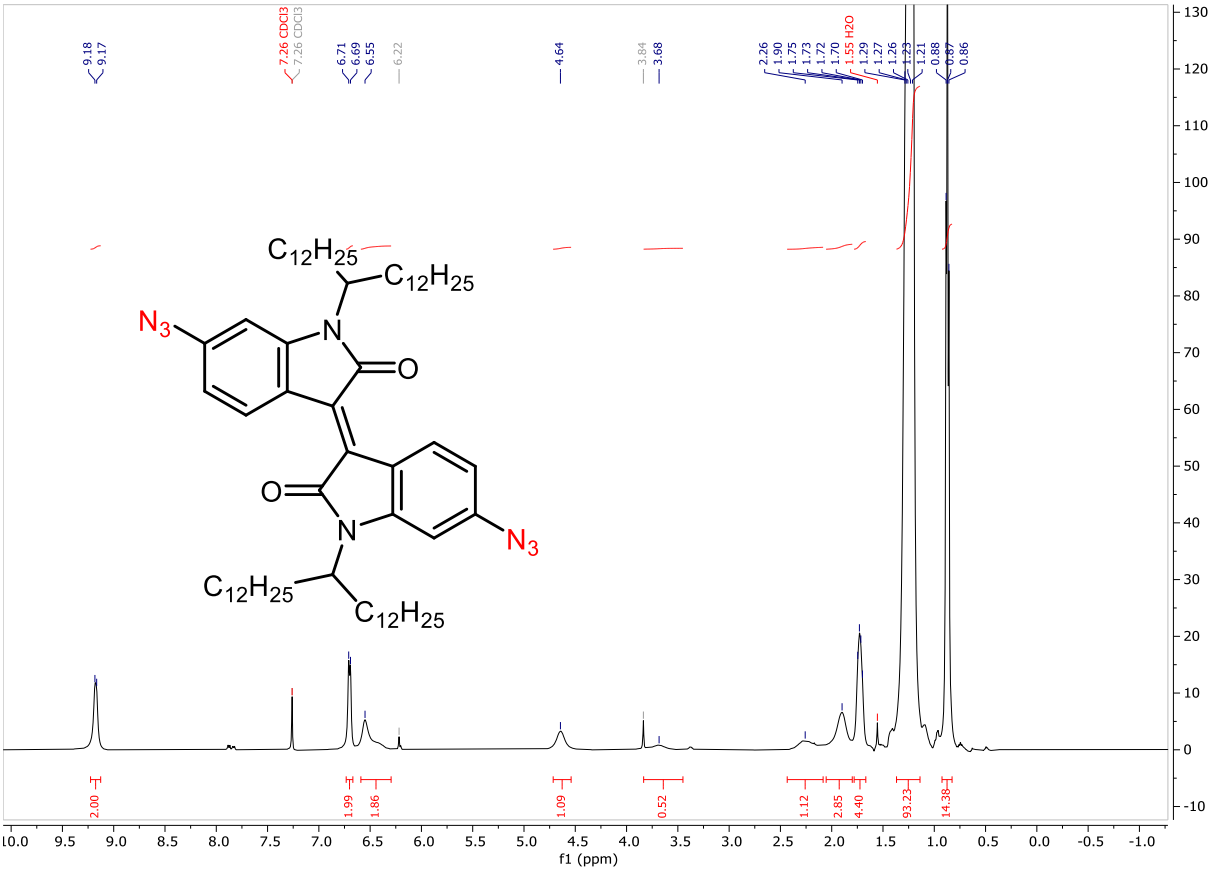

Figure S52. ^{1}H NMR spectrum of **S7** (500 MHz, $CDCl_3$).

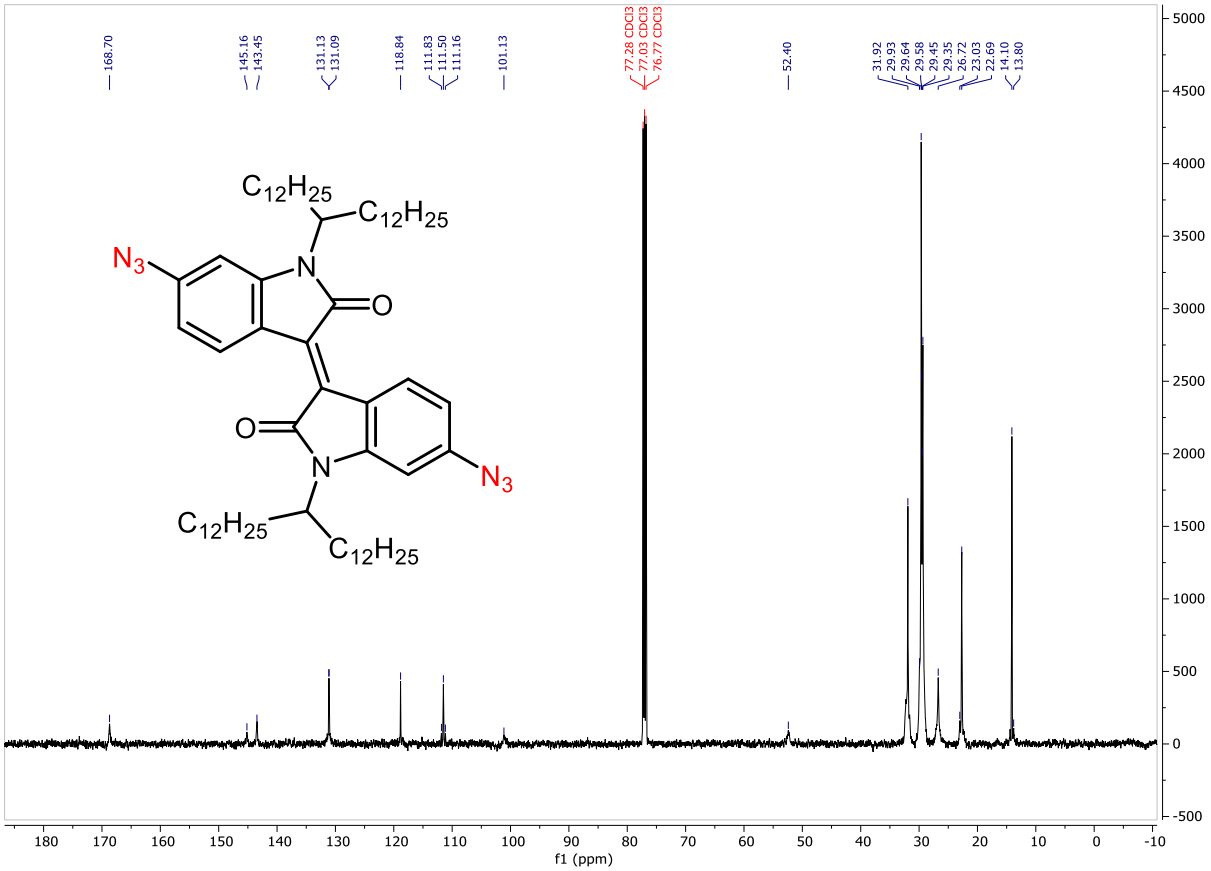

Figure S53. $^{13}C\{^{1}H\}$ NMR spectrum of **S7** (126 MHz, $CDCl_3$).

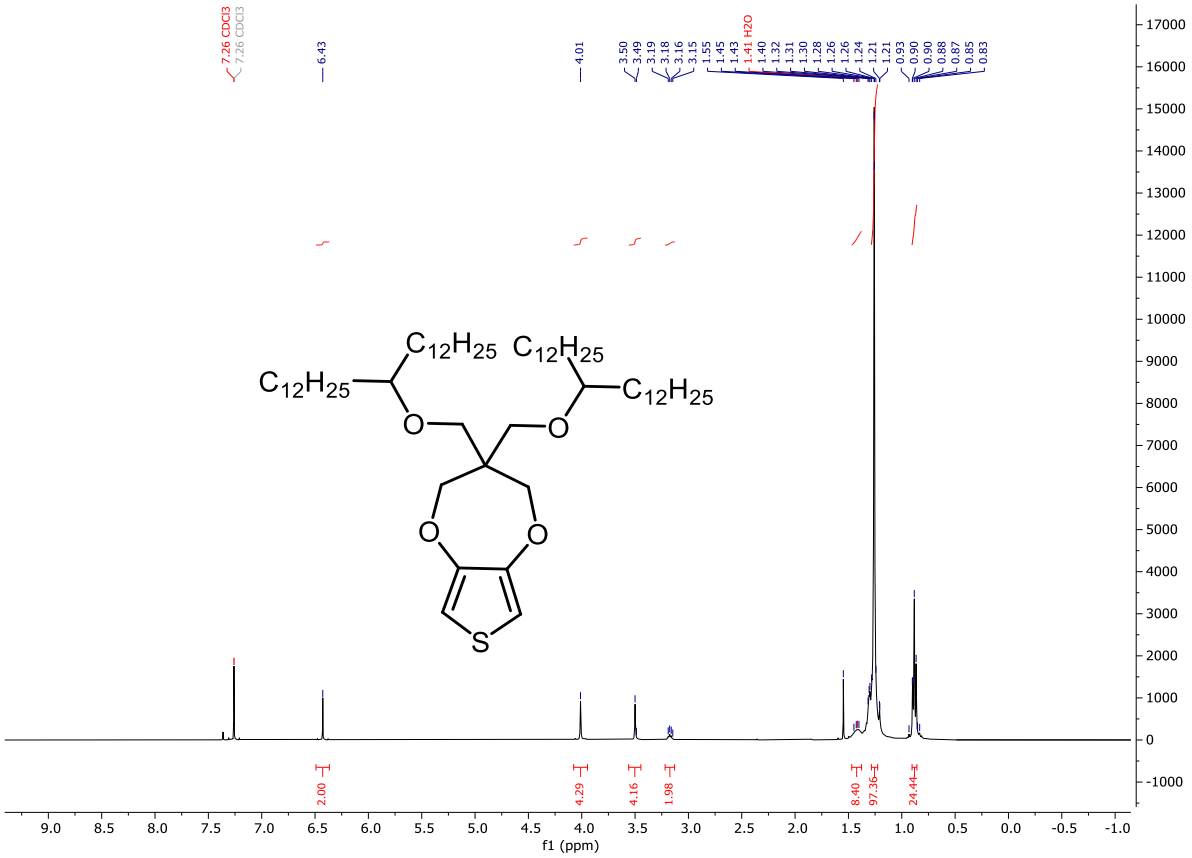

Figure S54. ^{1}H NMR spectrum of **S8** (400 MHz, $CDCl_3$).

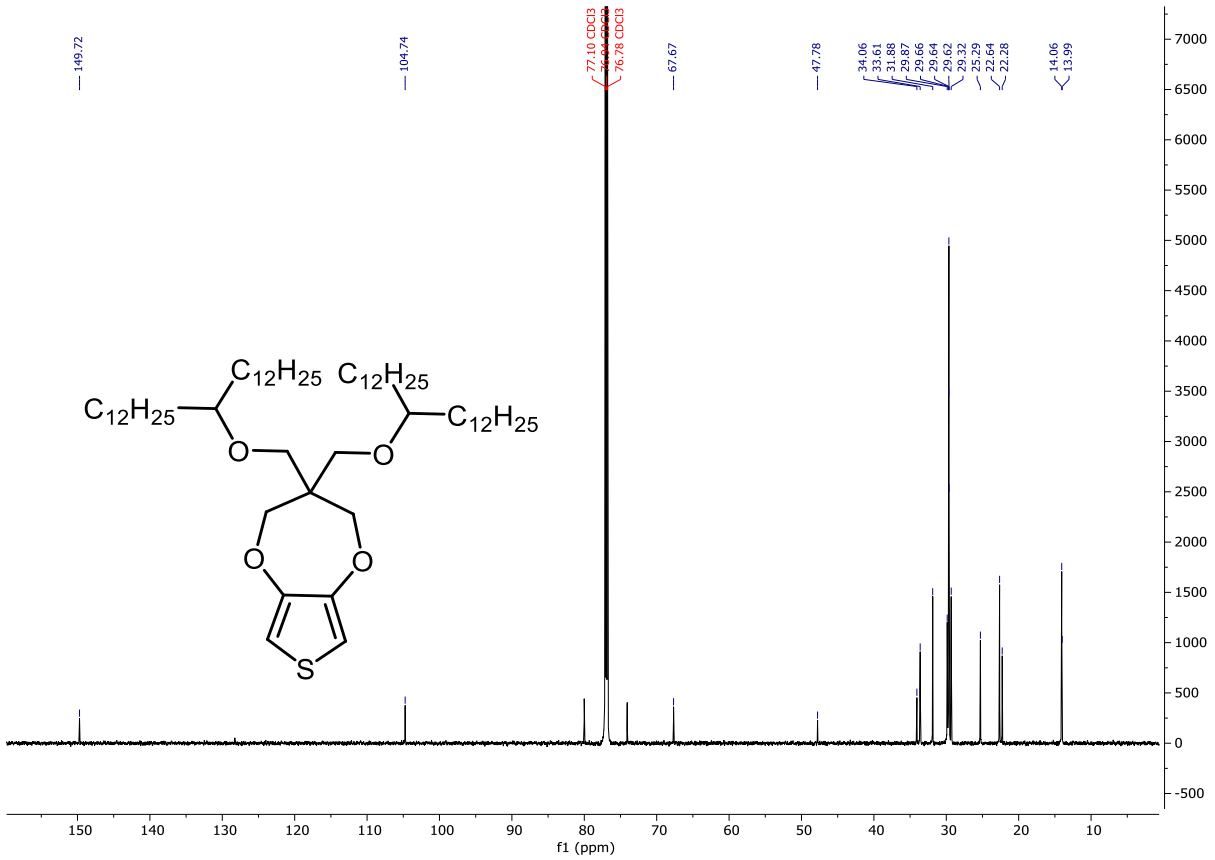

Figure S55. $^{13}C\{^{1}H\}$ NMR spectrum of **S8** (201 MHz, $CDCl_3$).

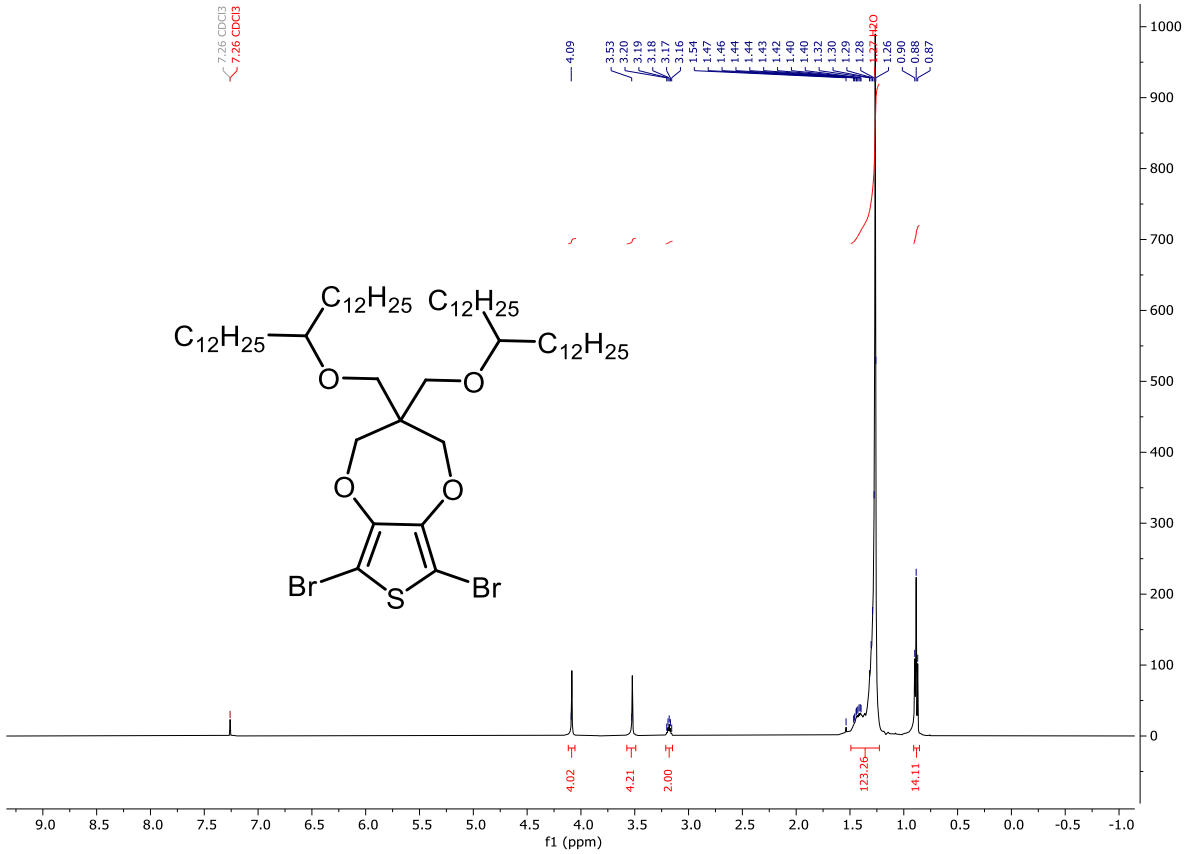

Figure S56. ^{1}H NMR spectrum of **S9** (400 MHz, $CDCl_3$).

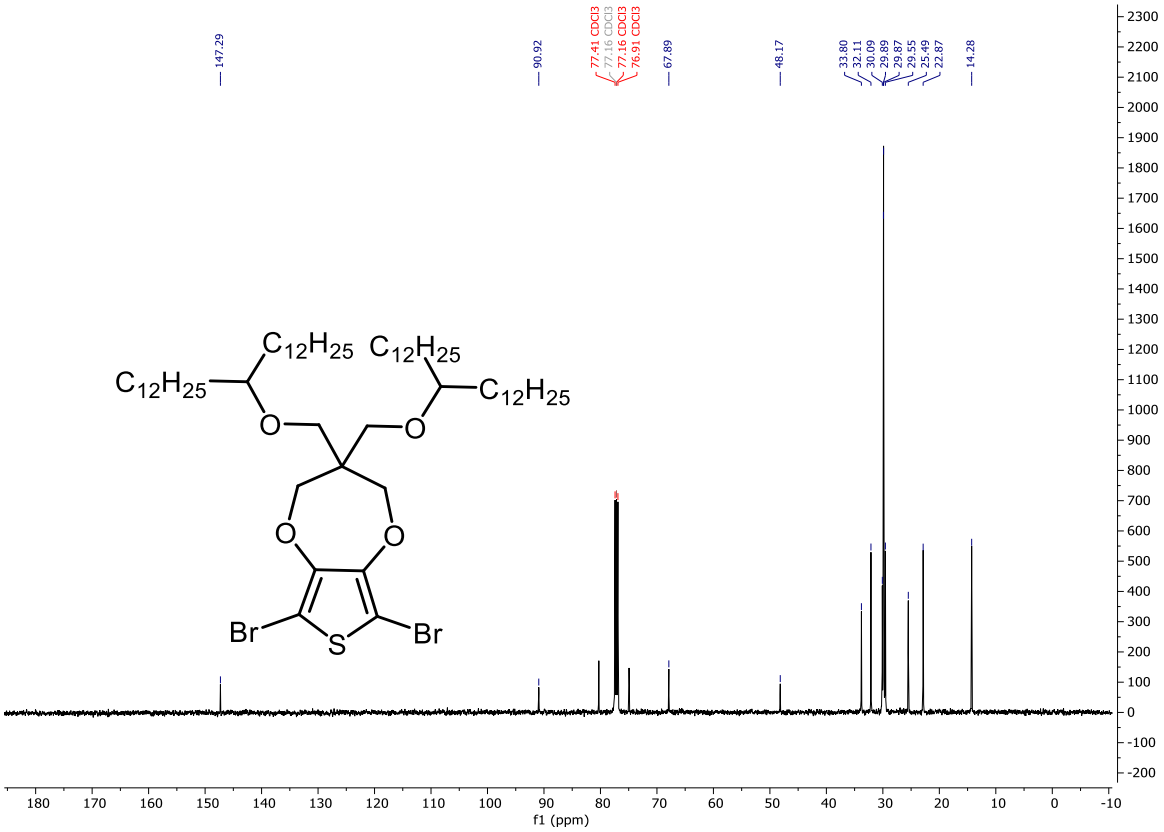

Figure S57. $^{13}C\{^{1}H\}$ NMR spectrum of **S9** (101 MHz, $CDCl_3$).

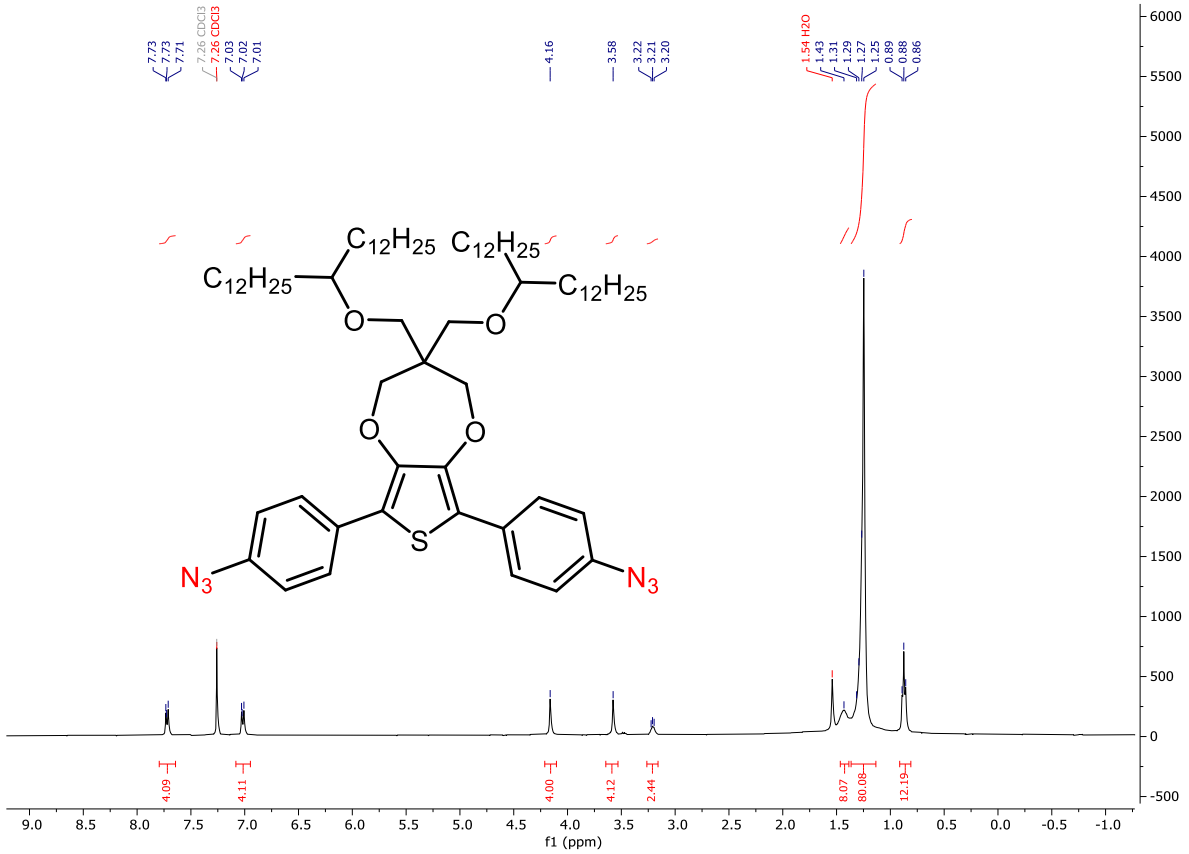

Figure S58. ^{1}H NMR spectrum of **S10** (400 MHz, $CDCl_3$).

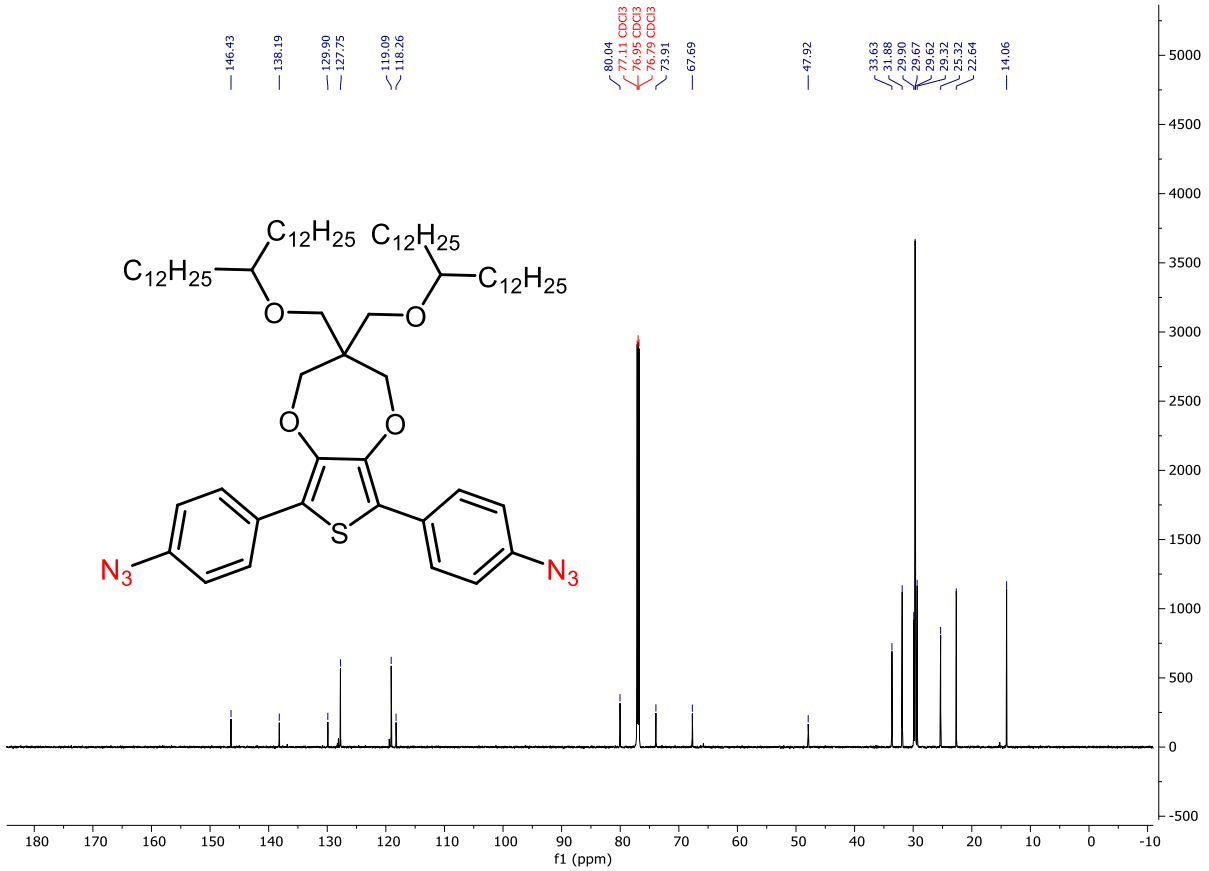

Figure S59. $^{13}C\{^{1}H\}$ NMR spectrum of **S10** (201 MHz, $CDCl_3$).

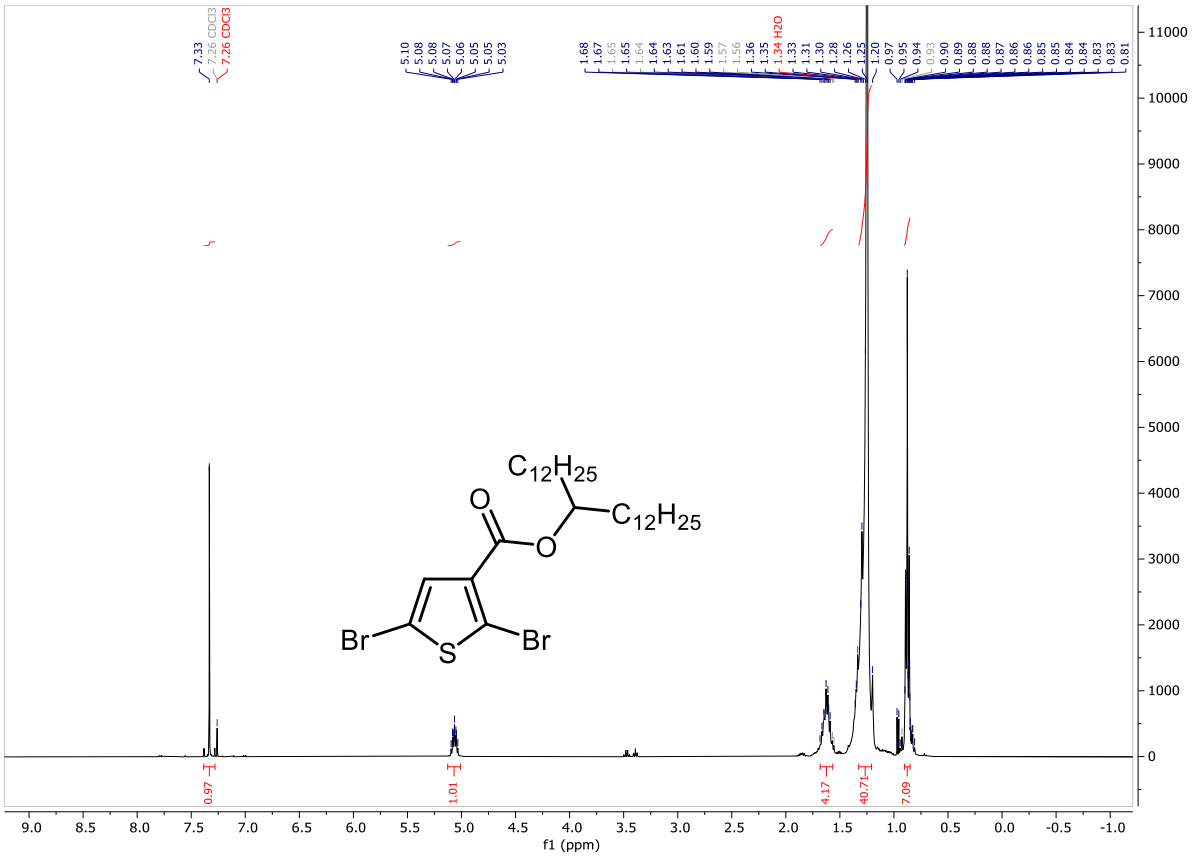

Figure S60. ^{1}H NMR spectrum of **S11** (400 MHz, $CDCl_3$).

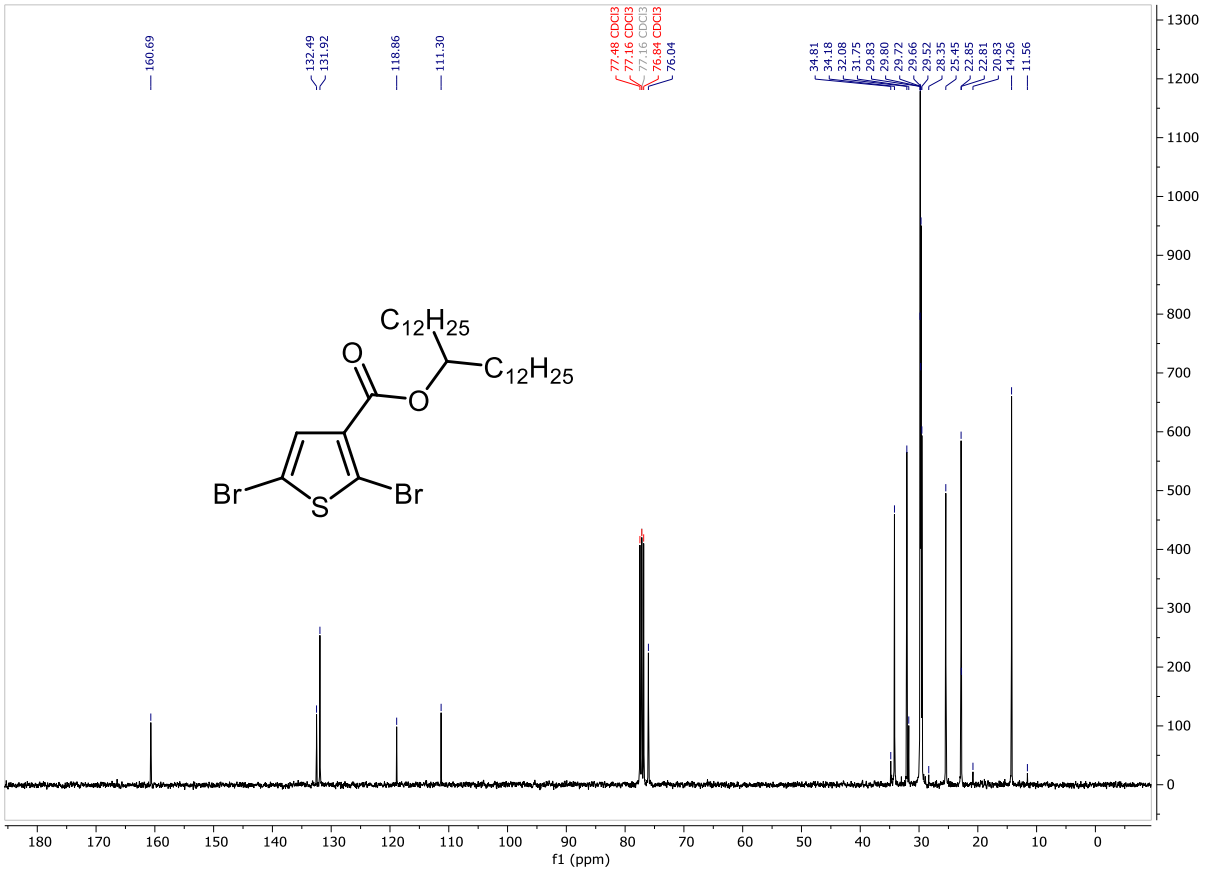

Figure S61. $^{13}C\{^{1}H\}$ NMR spectrum of **S11** (101 MHz, $CDCl_3$).

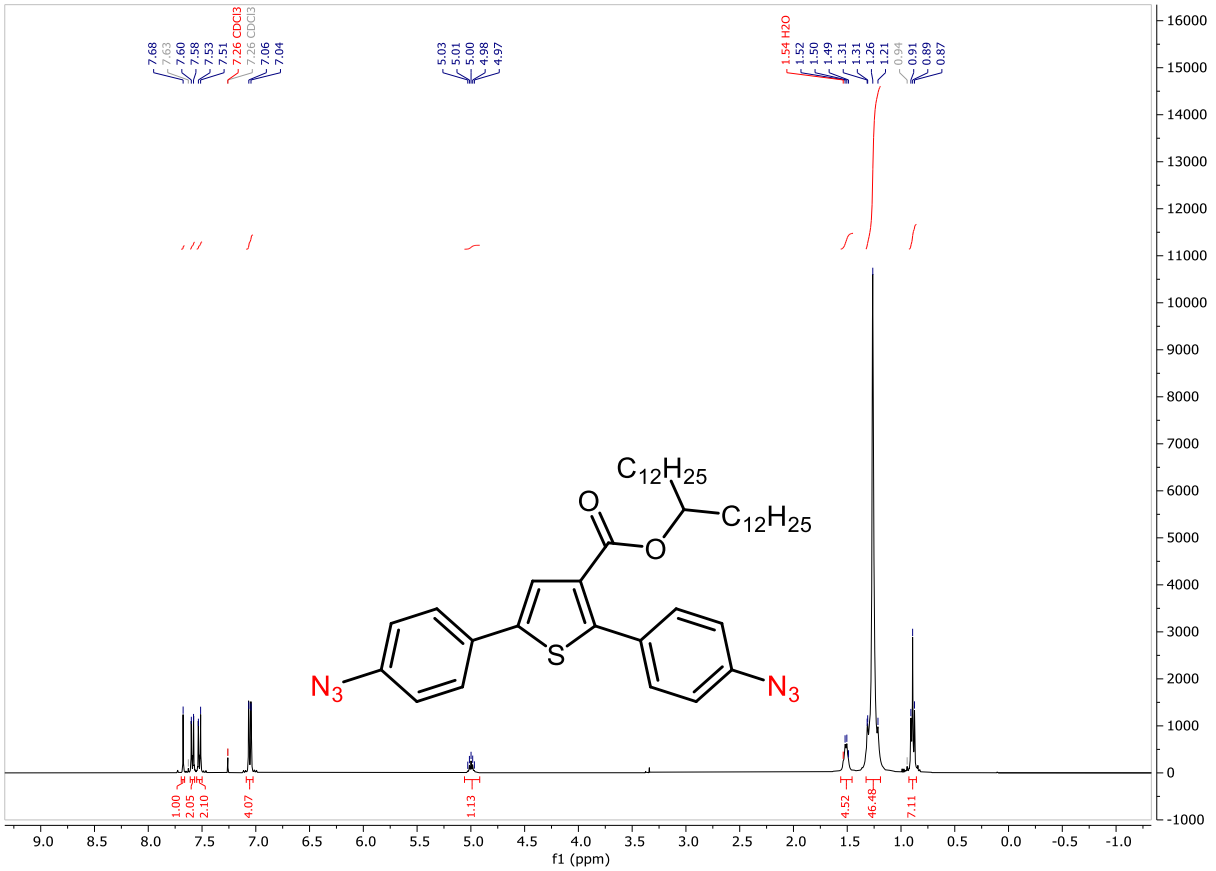

Figure S62. ^{1}H NMR spectrum of **S12** (400 MHz, $CDCl_3$).

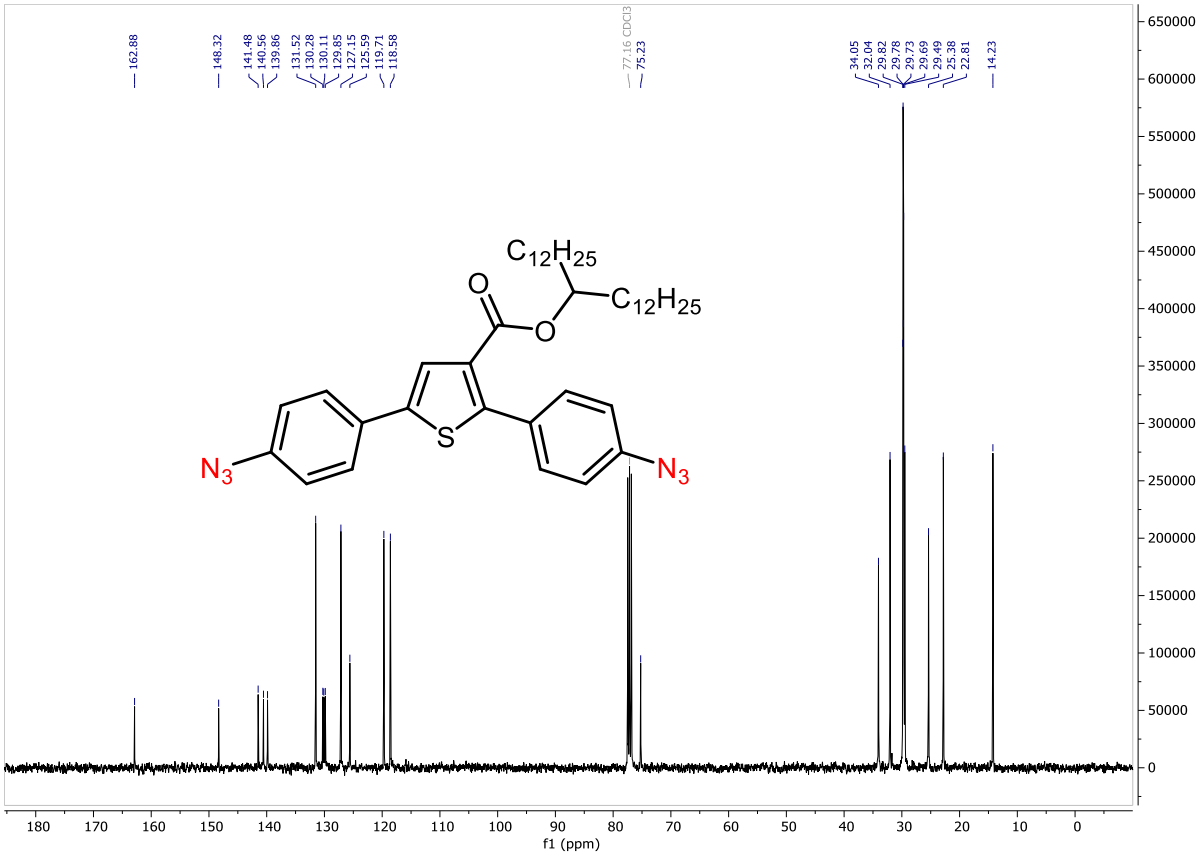

Figure S63. $^{13}C\{^{1}H\}$ NMR spectrum of **S12** (101 MHz, $CDCl_3$).

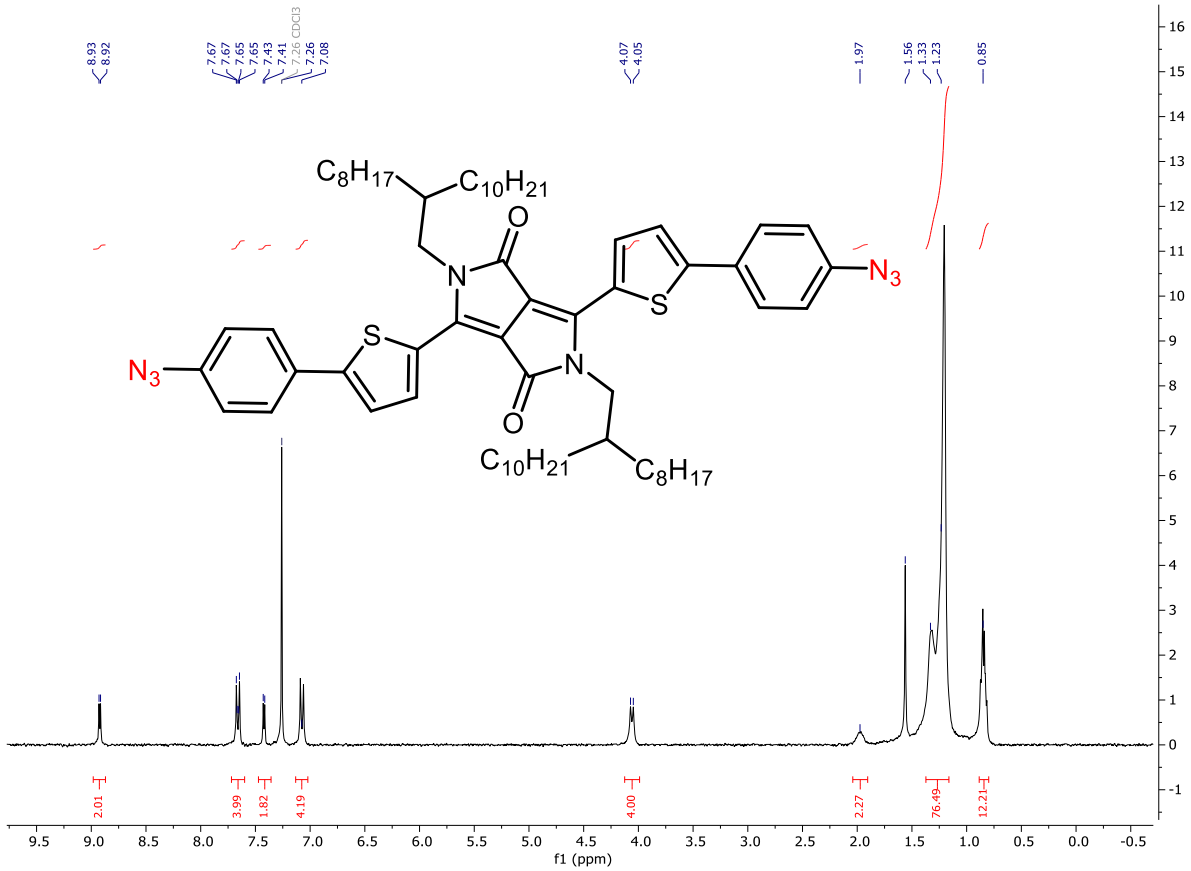

Figure S64. ^{1}H NMR spectrum of **S13** (300 MHz, $CDCl_3$).

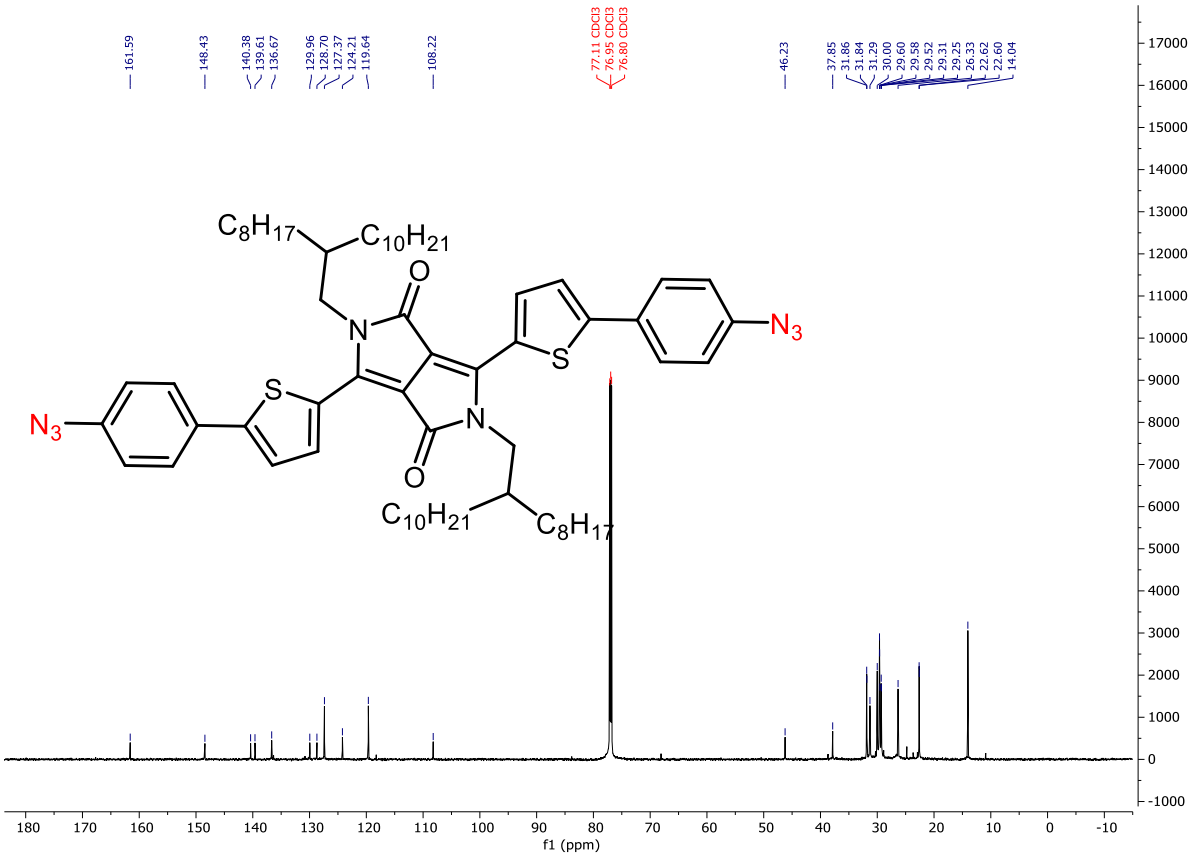

Figure S65. $^{13}C\{^{1}H\}$ NMR spectrum of **S13** (201 MHz, $CDCl_3$).

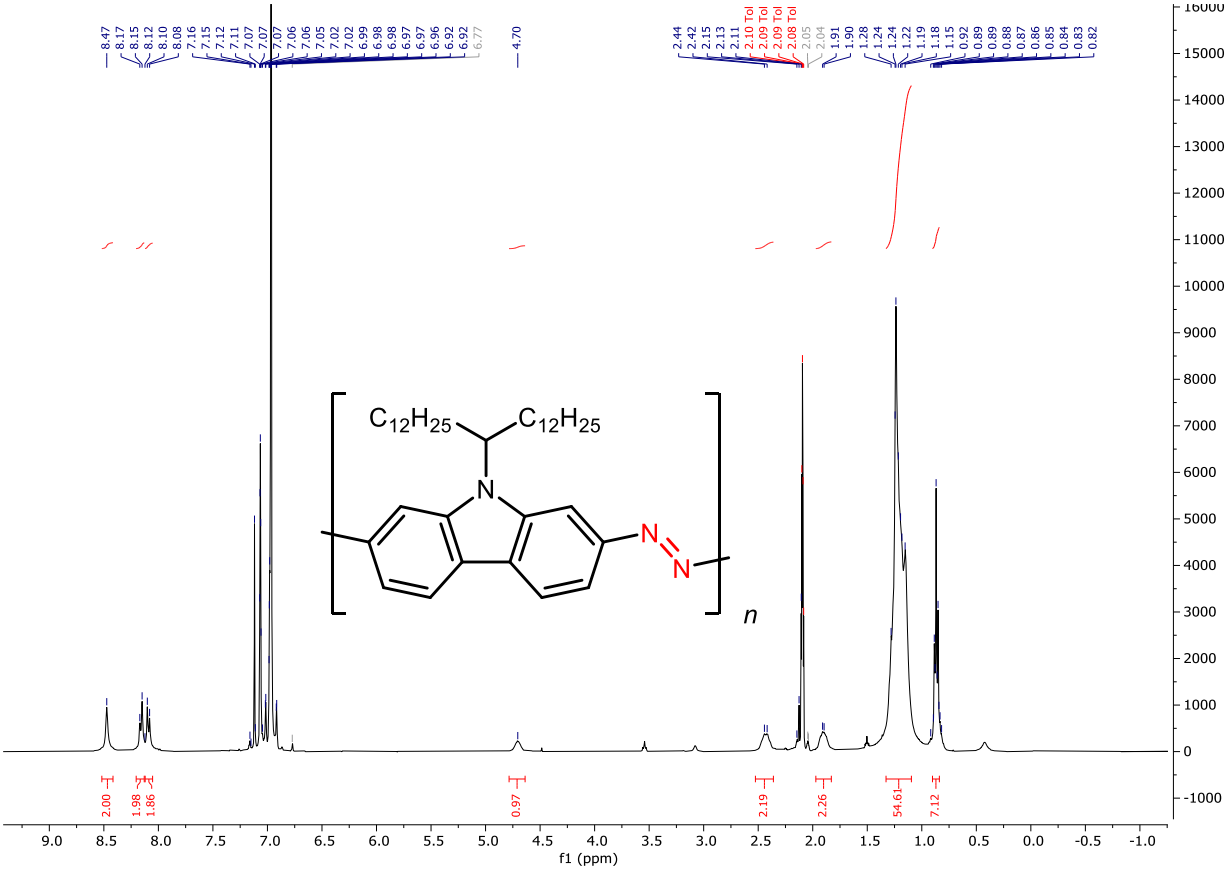

Figure S66. ^{1}H NMR spectrum of **3** (400 MHz, 100 °C, toluene-d_8).

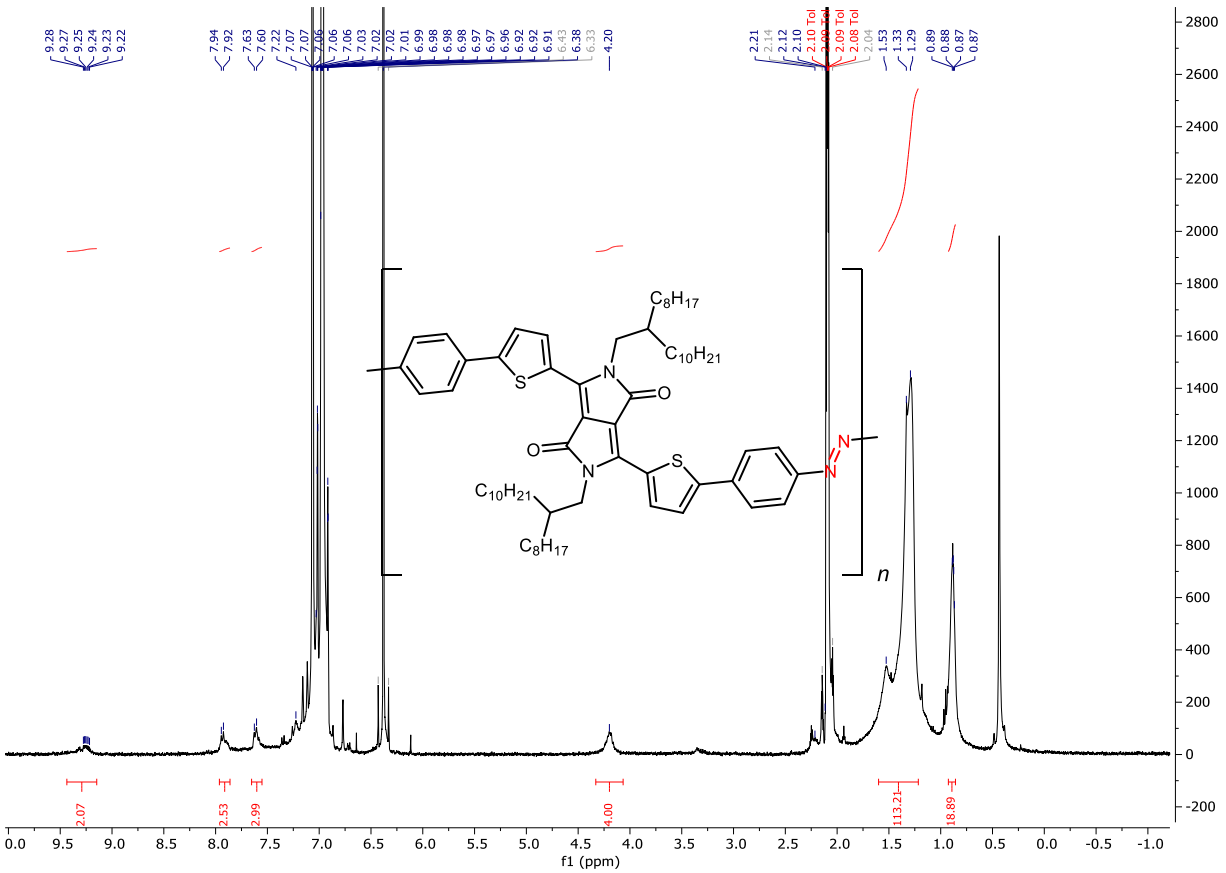

Figure S67. ^{1}H NMR spectrum of **7** (400 MHz, 100 °C, toluene-d_8).

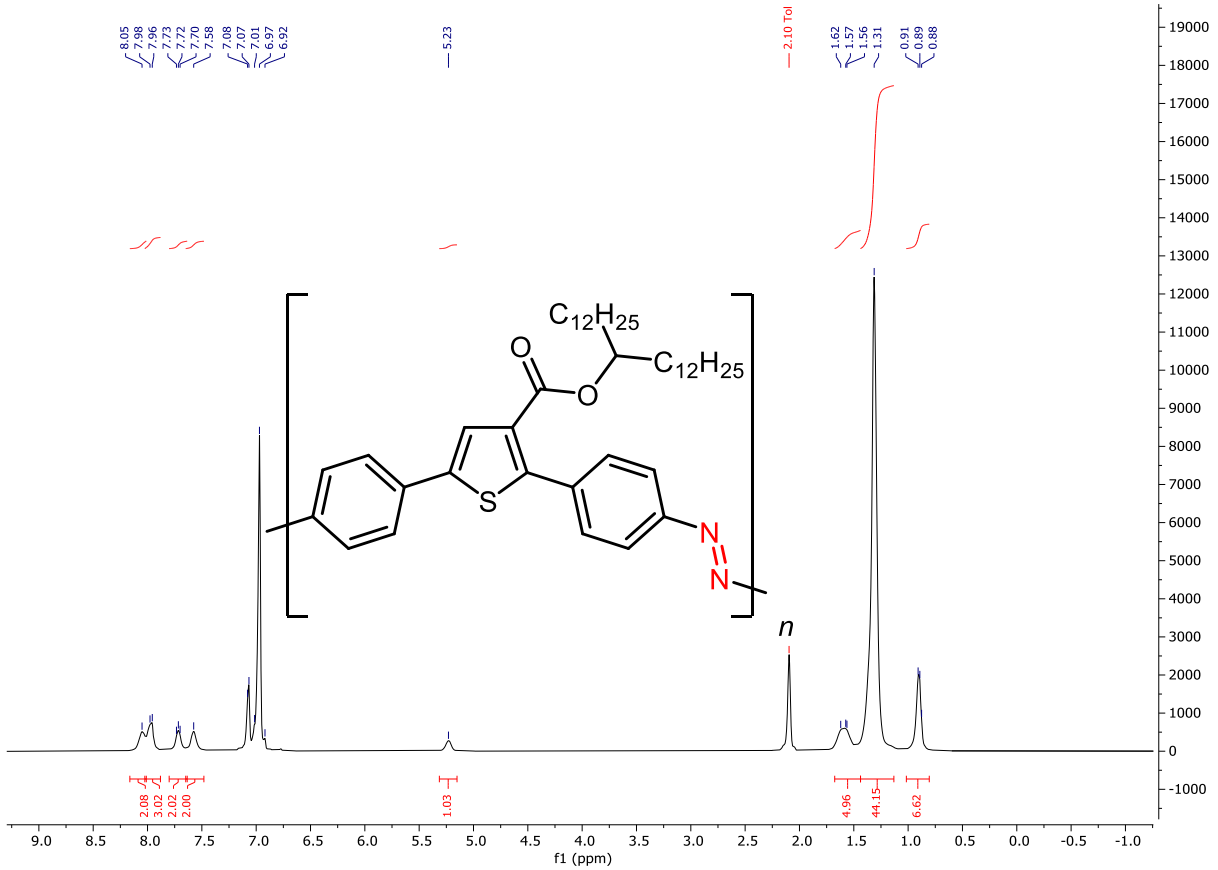

Figure S68. ^{1}H NMR spectrum of **8** (400 MHz, 100 °C, toluene-d_8).

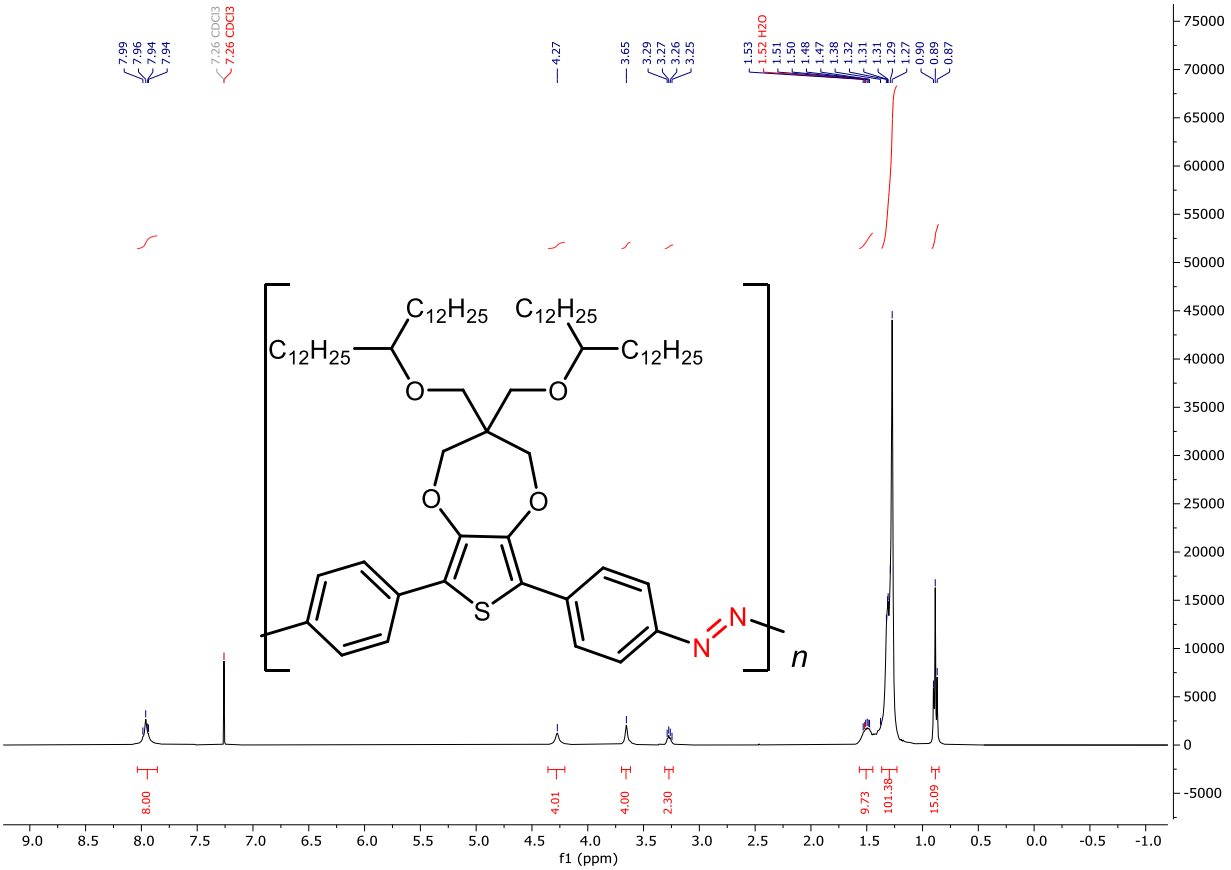

Figure S69. ^{1}H NMR spectrum of **9** (400 MHz, 50°C, $CDCl_3$).

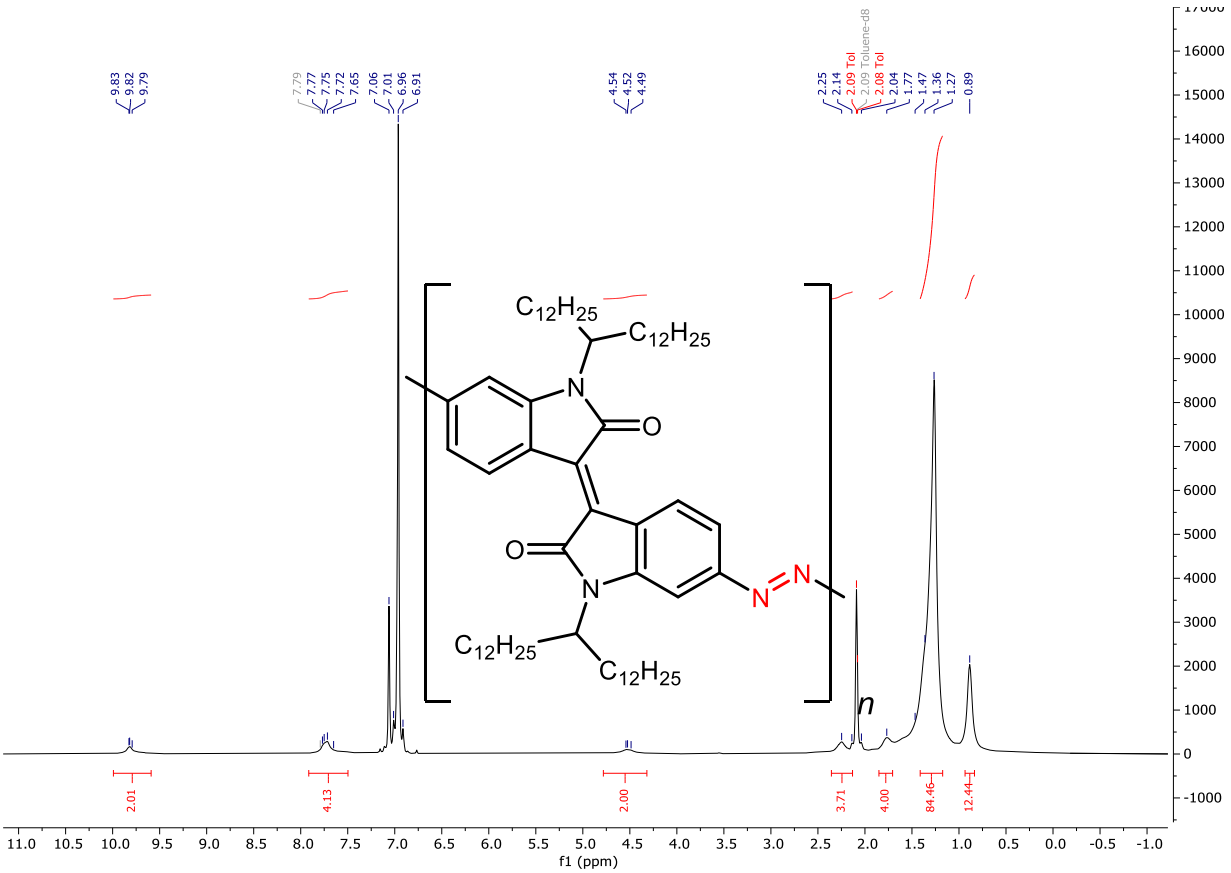

Figure S70. ^{1}H NMR spectrum of **10** (400 MHz, 100 °C, toluene-d_8).

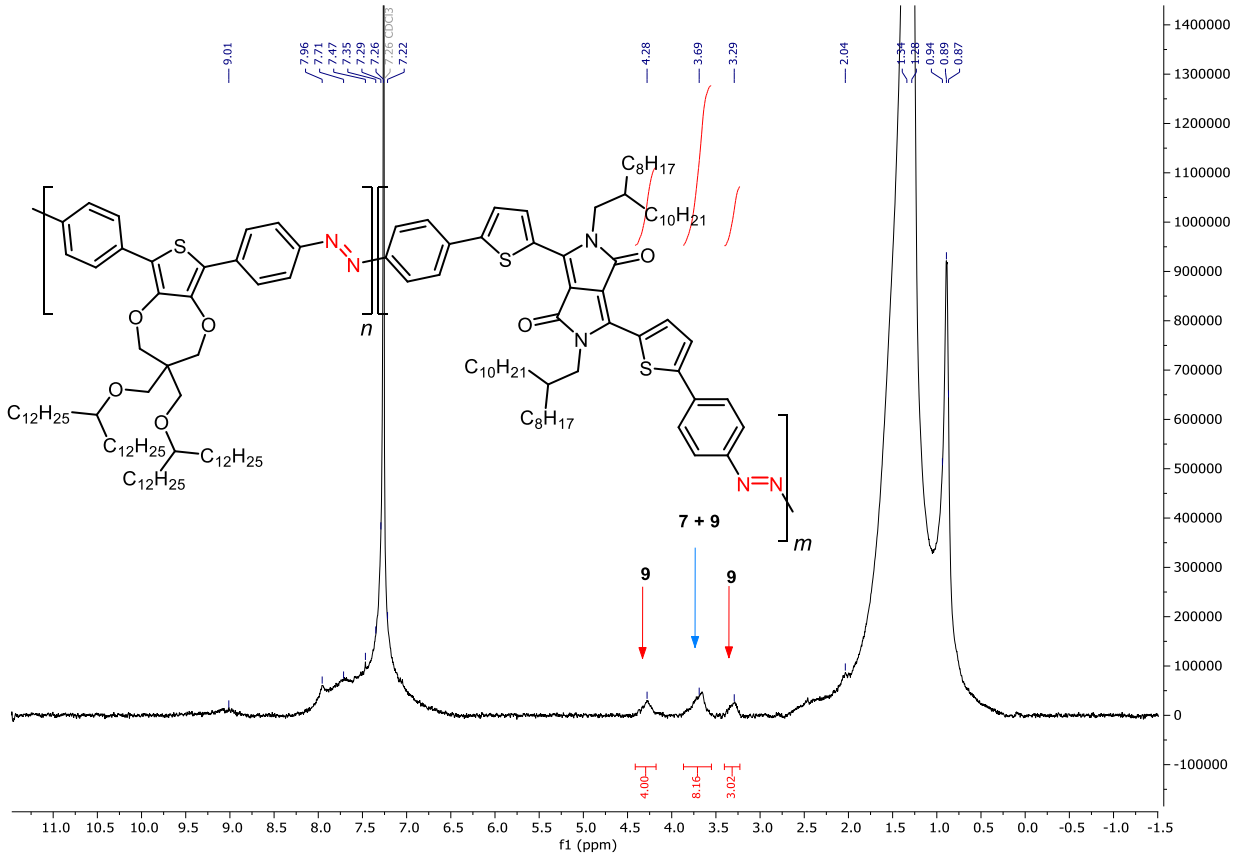

Figure S71. ^{1}H NMR spectrum of **11** (500 MHz, 50 °C, $CDCl_3$).

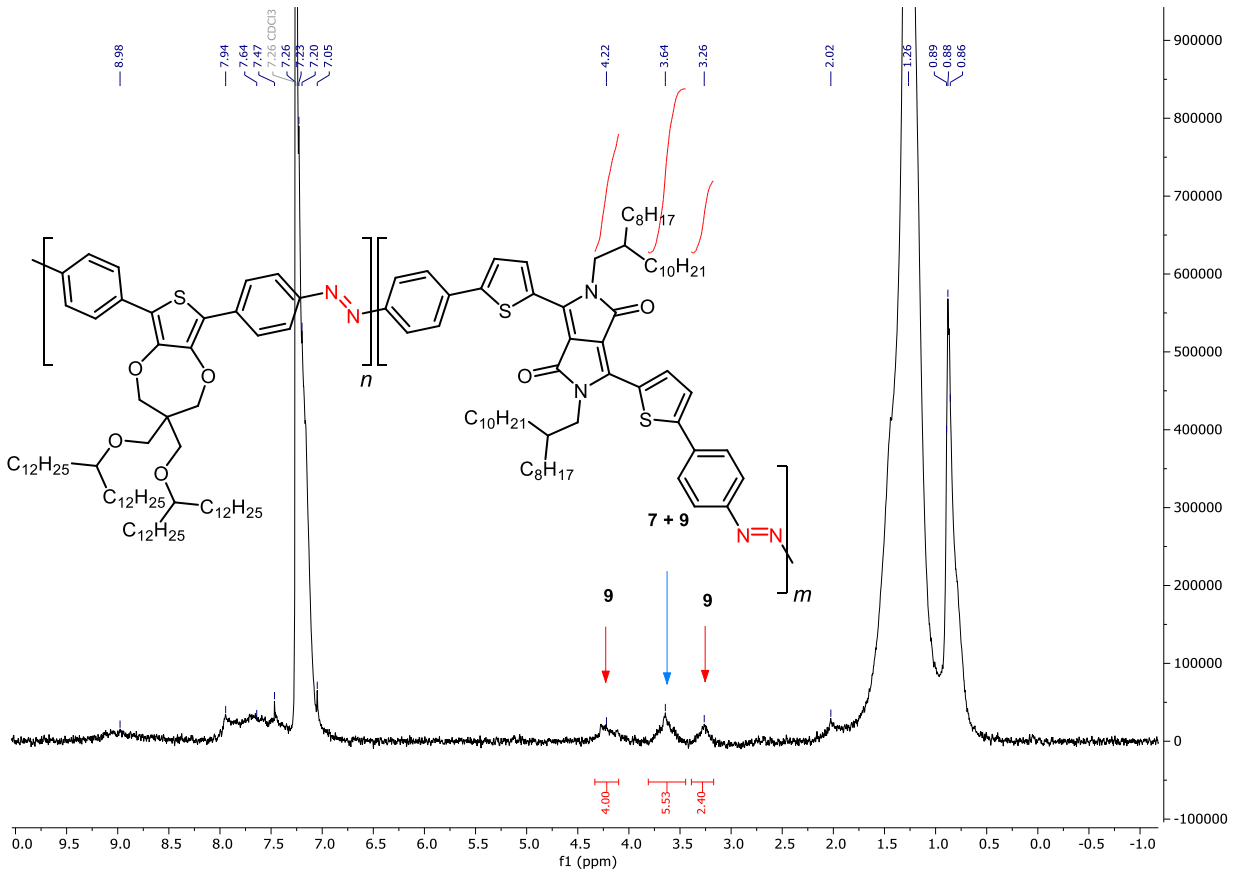

Figure S72. ^{1}H NMR spectrum of **12** (500 MHz, 50 °C, $CDCl_3$).

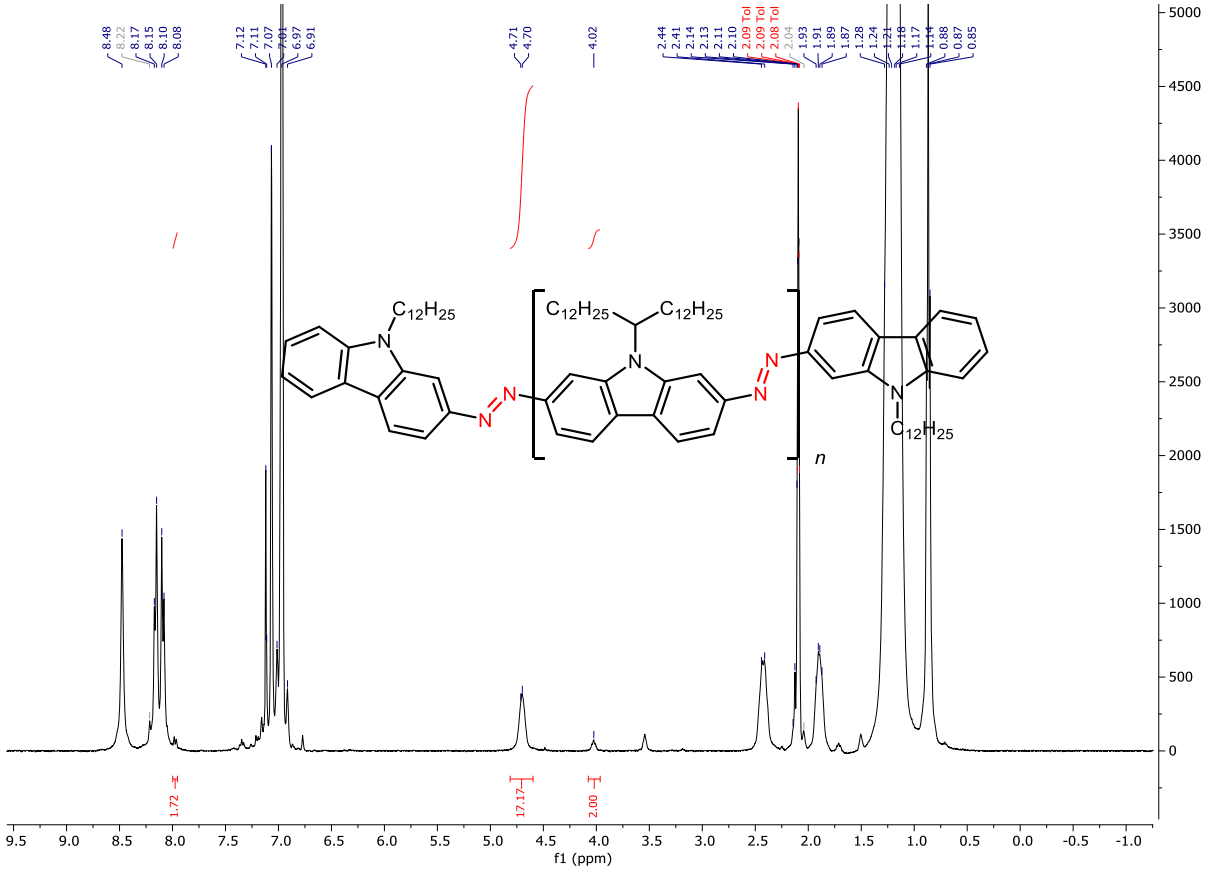

Figure S73. ^{1}H NMR spectrum of **13** (400 MHz, 100 °C, toluene-d_8).

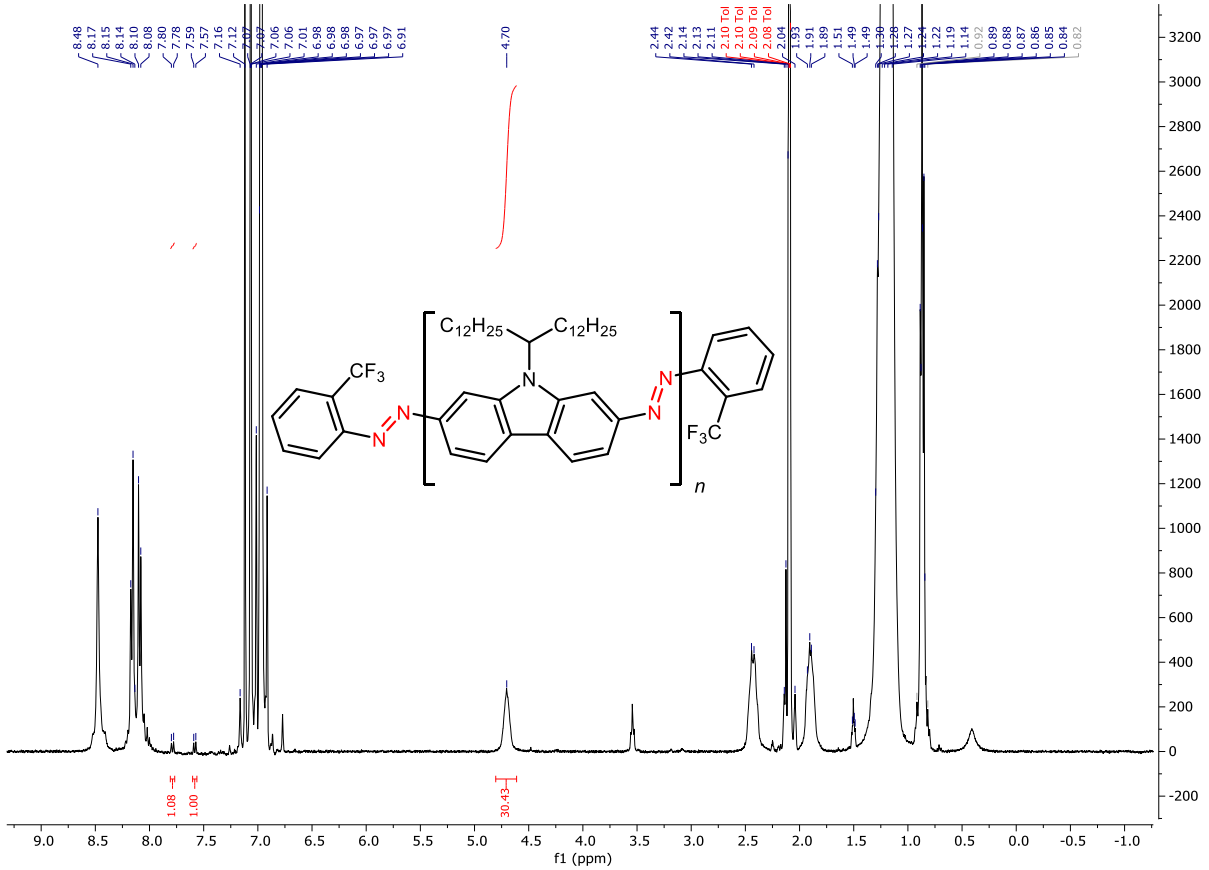

Figure S74. ^{1}H NMR spectrum of **14** (400 MHz, 100 °C, toluene-d_8).

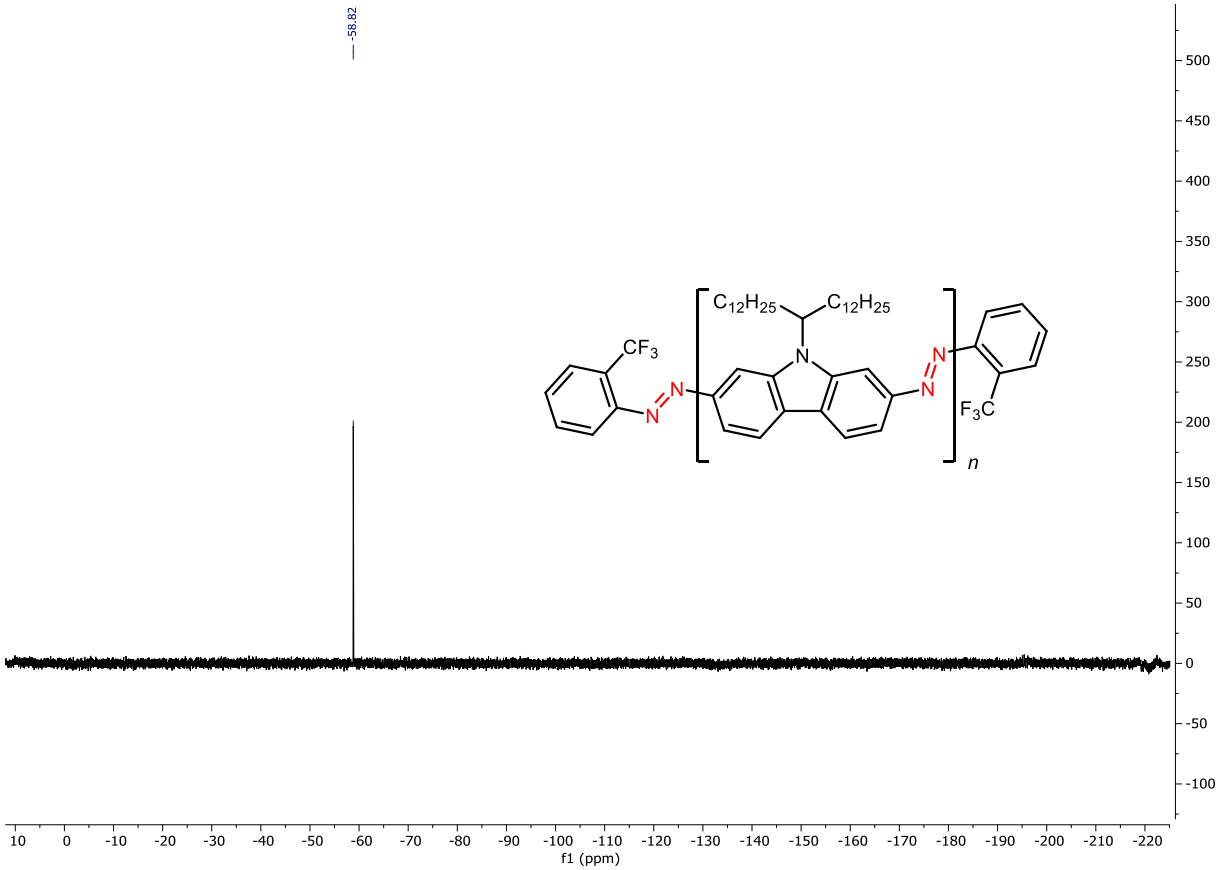

Figure S75. ^{19}F NMR spectrum of **14** (376 MHz, 100 °C, toluene-d_8).

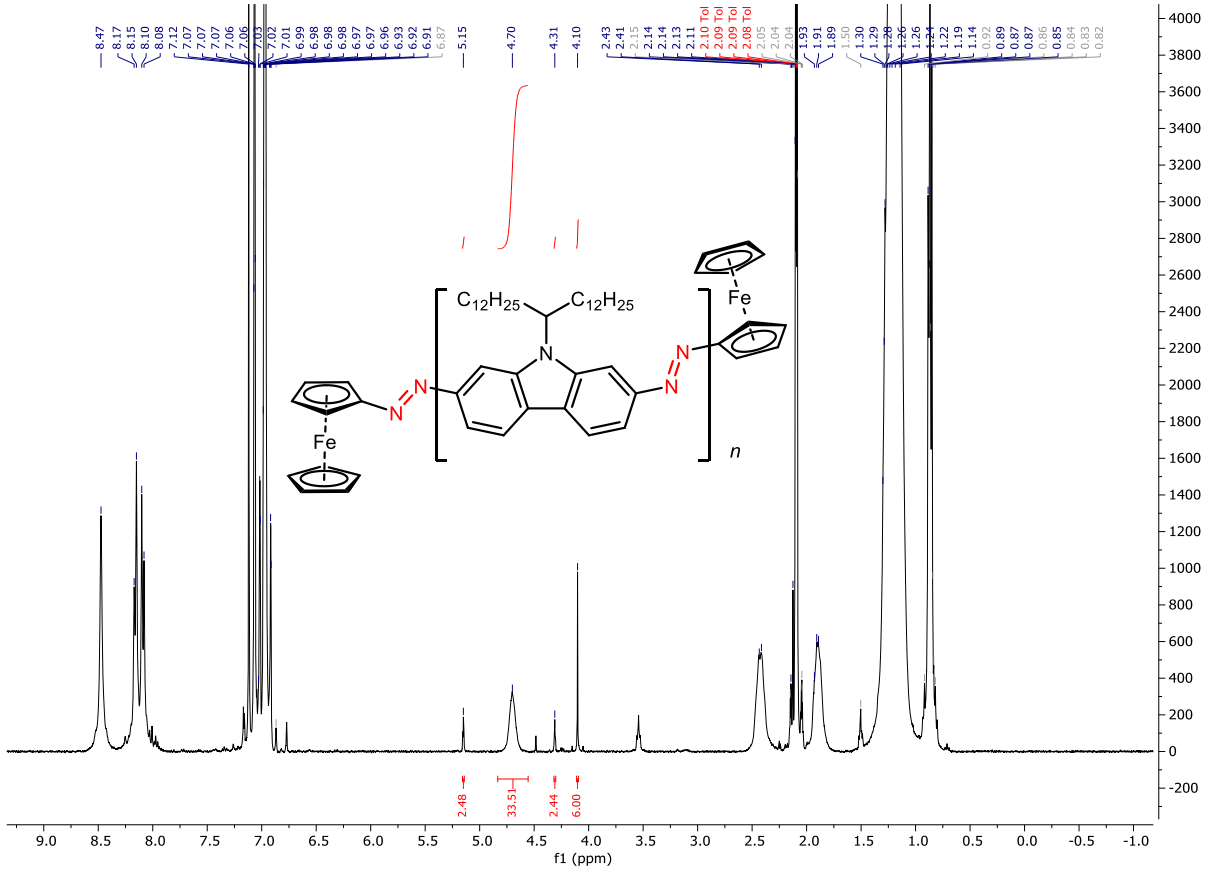

Figure S76. ^{1}H NMR spectrum of **15** (400 MHz, 100 °C, toluene-d_8).

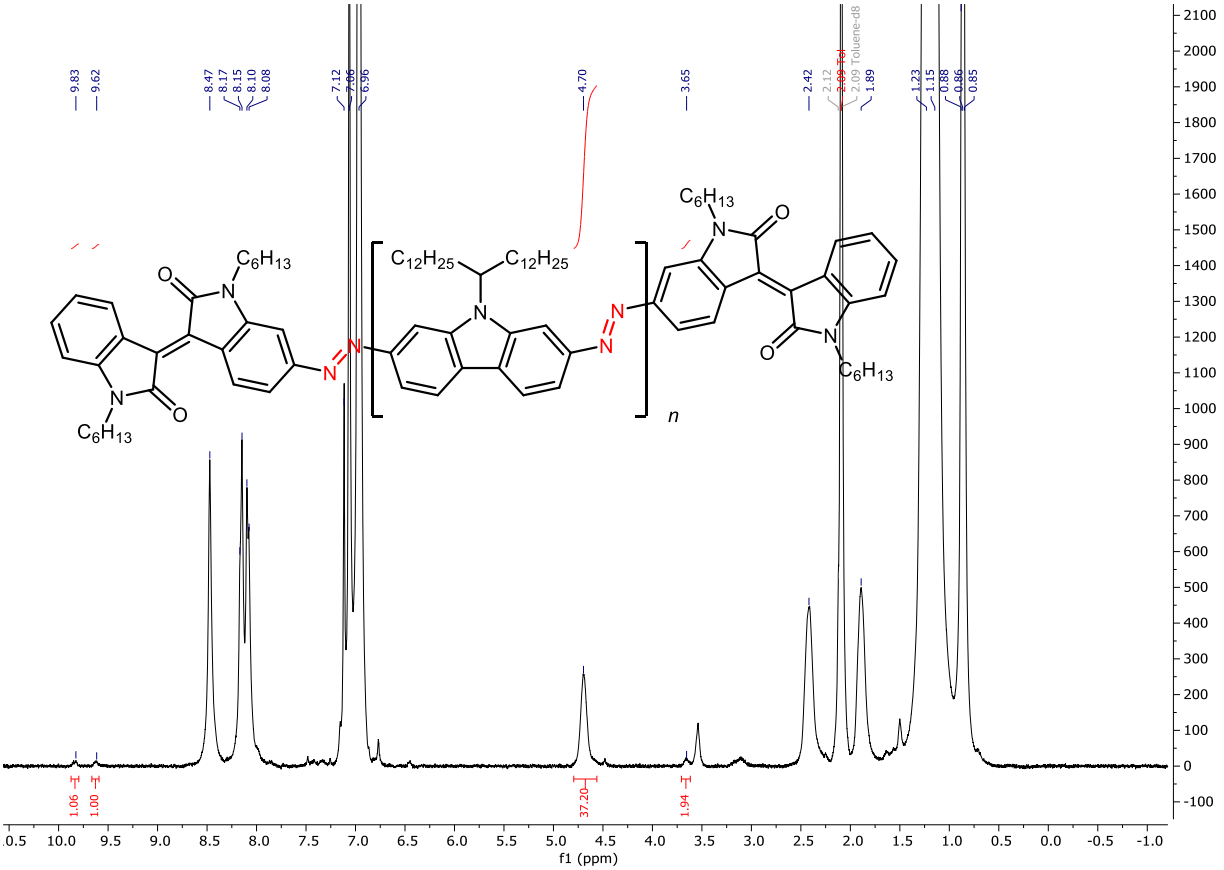

Figure S77. ^{1}H NMR spectrum of **16** (400 MHz, 100 °C, toluene-d_8).

12. UV–Vis Spectroscopy

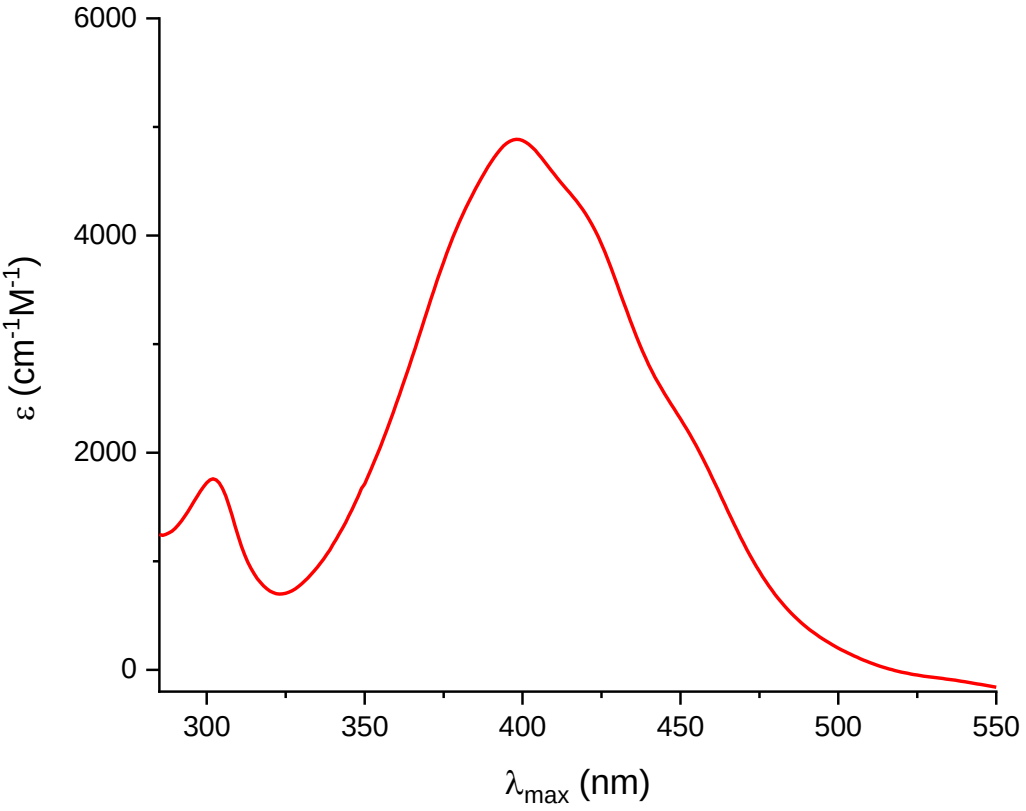

Figure S78. UV-Vis spectrum of **5b** (0.143 mM) in C_6H_5Cl.

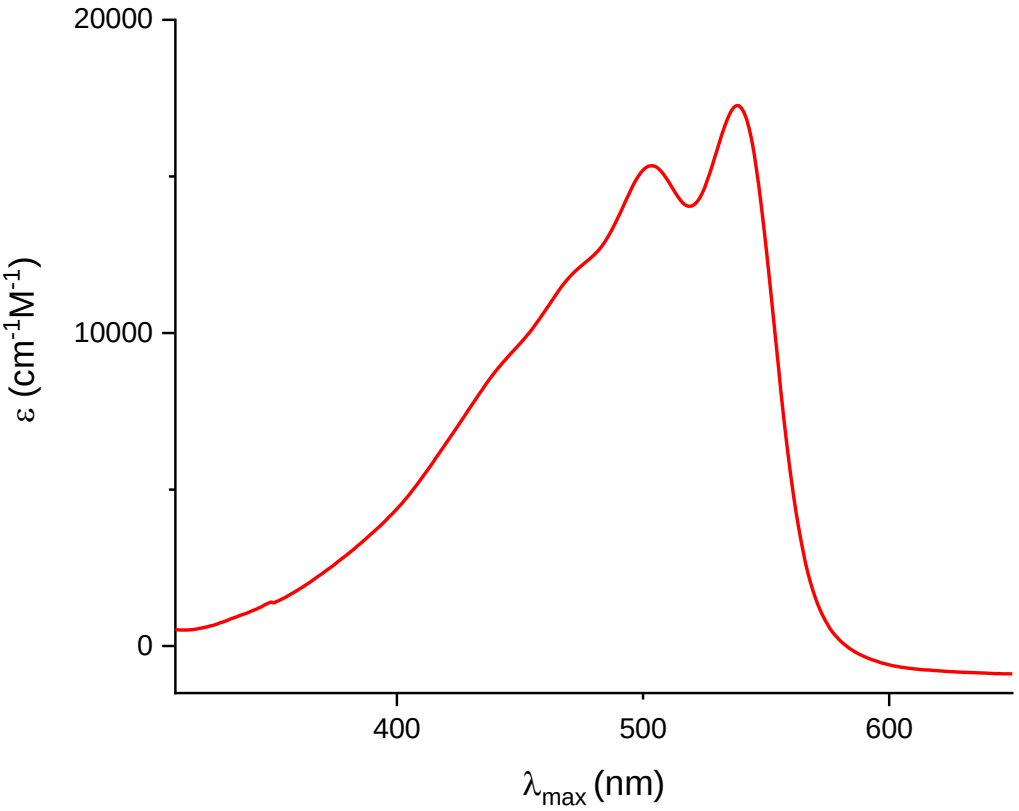

Figure S79. UV-Vis spectrum of **3** (0.0326 mM) in C_6H_5Cl.

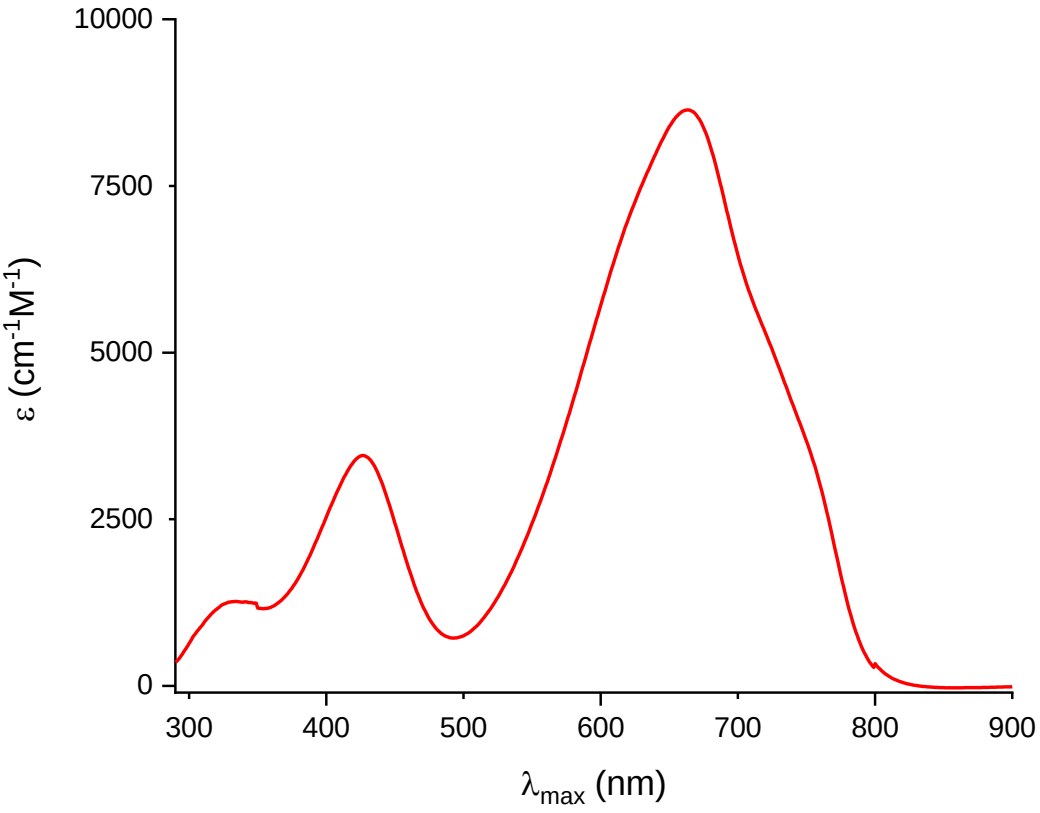

Figure S80. UV-Vis spectrum of **7** (0.0385 mM) in C_6H_5Cl.

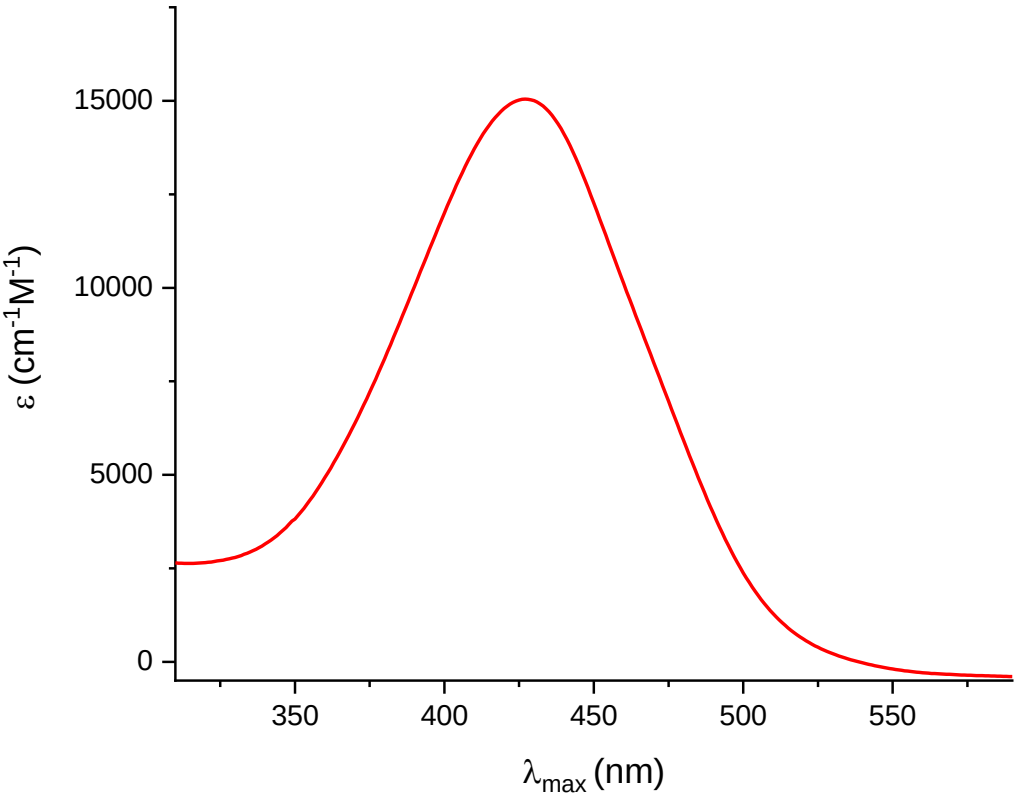

Figure S81. UV-Vis spectrum of **8** (0.0135 mM) in C_6H_5Cl.

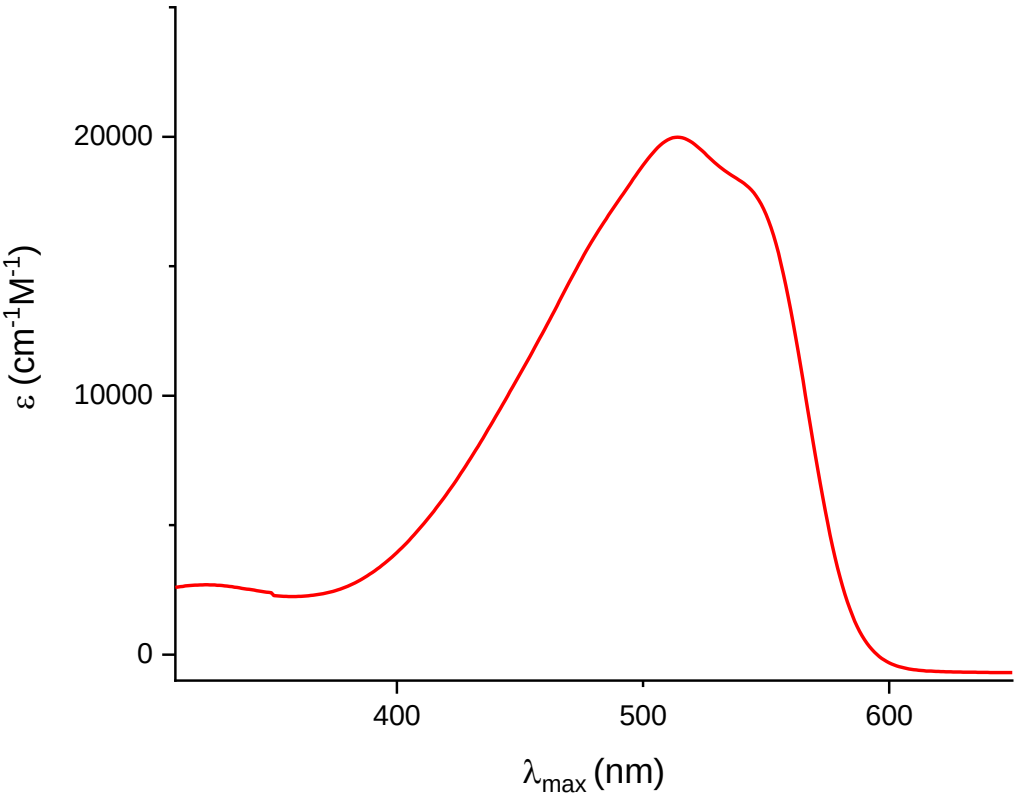

Figure S82. UV-Vis spectrum of **9** (0.0456 mM) in C_6H_5Cl.

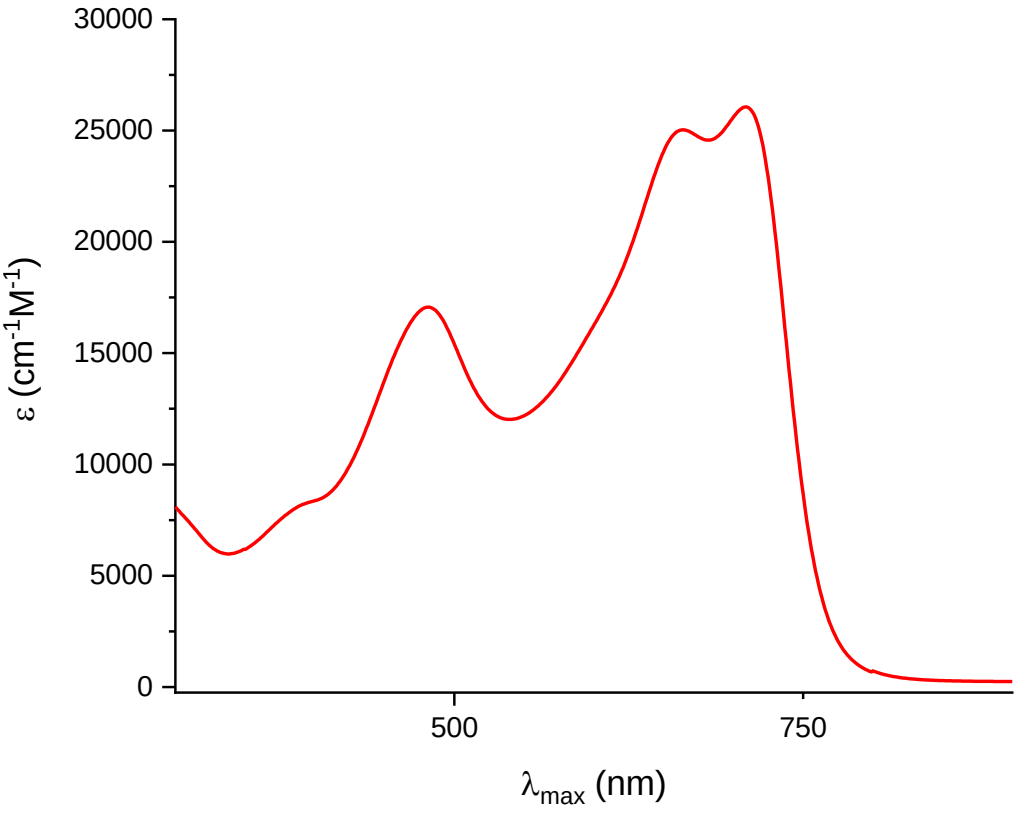

Figure S83. UV-Vis spectrum of **10** (0.0606 mM) in C_6H_5Cl.

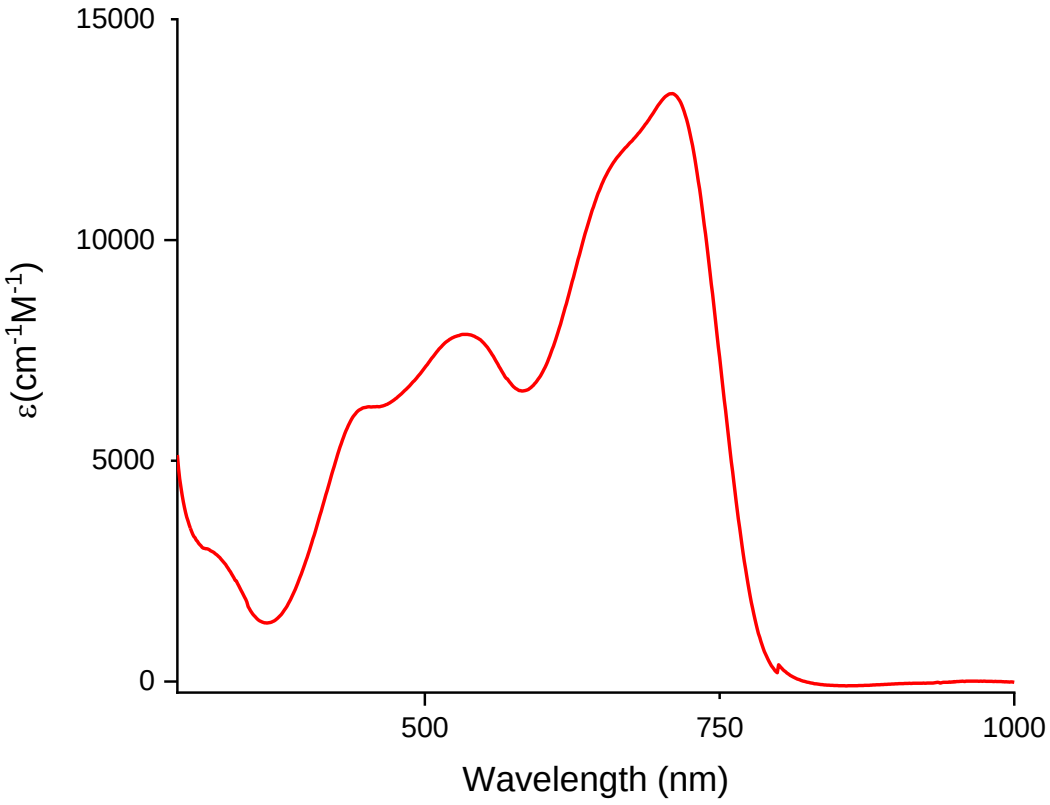

Figure S84. UV-Vis spectrum of **11** (0.0187 mM) in C_6H_5Cl.

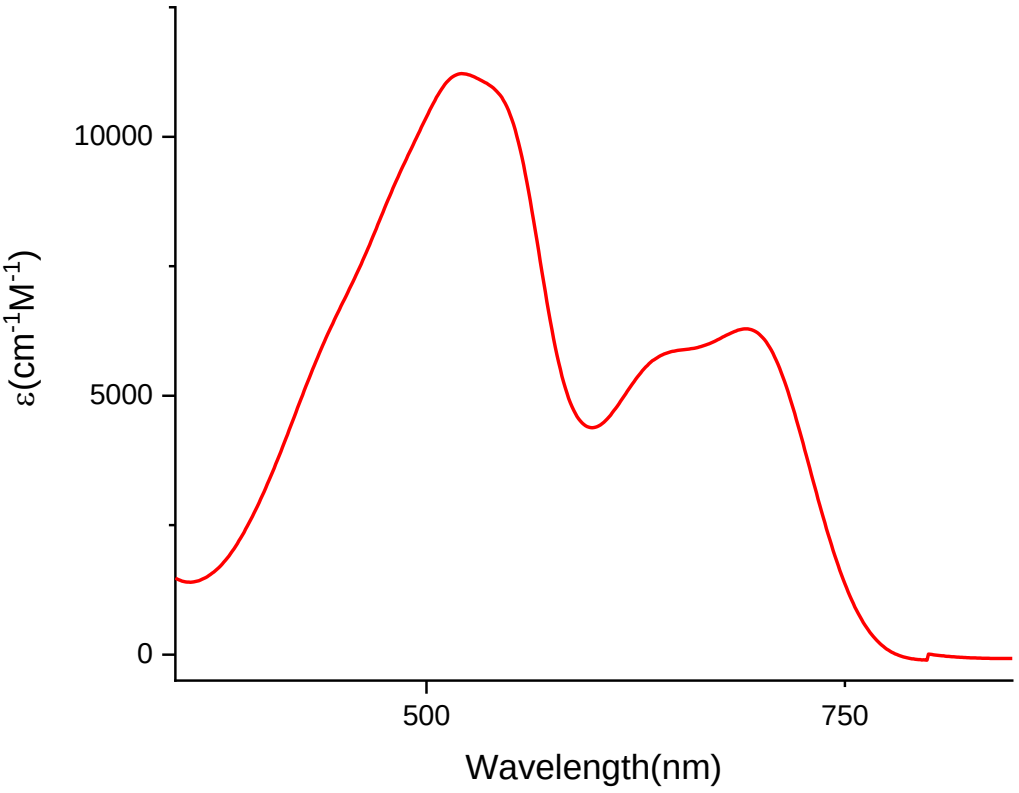

Figure S85. UV-Vis spectrum of **12** (0.0351 mM) in C_6H_5Cl.

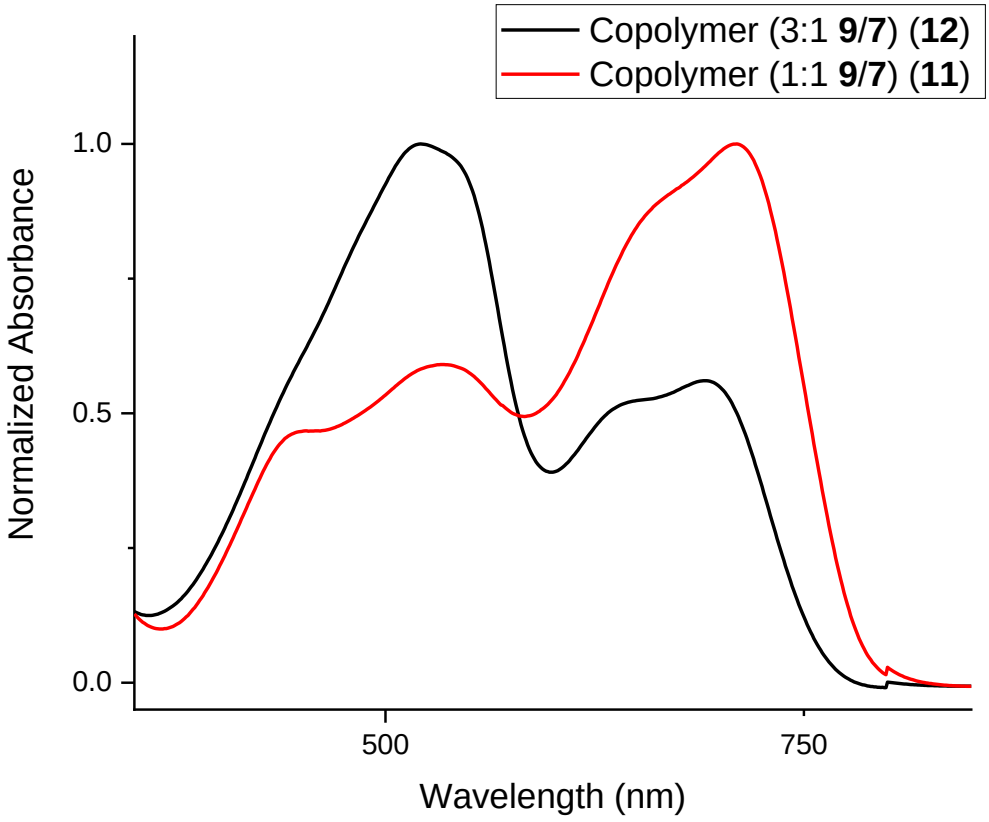

Figure S86. UV-Vis spectrum of **11** and **12** overlayed in C_6H_5Cl.

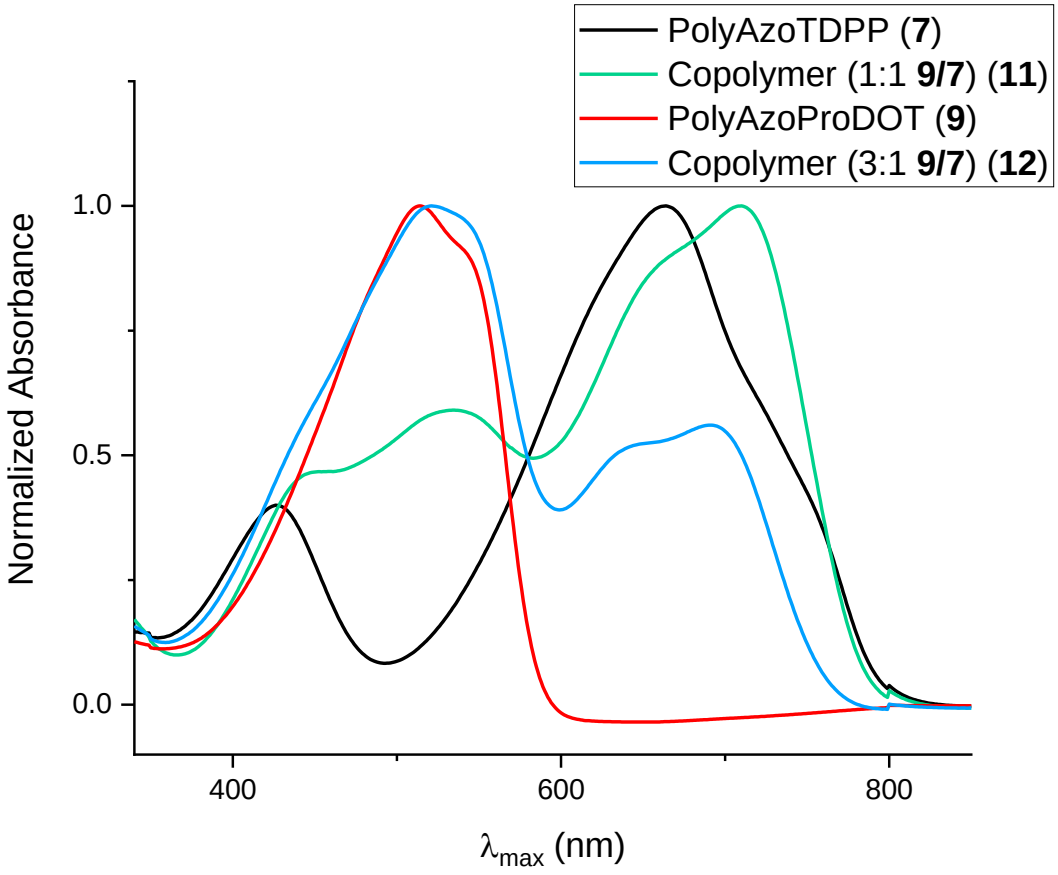

Figure S87. UV-Vis spectrum of **7**, **9**, **11** and **12** overlayed in C_6H_5Cl.

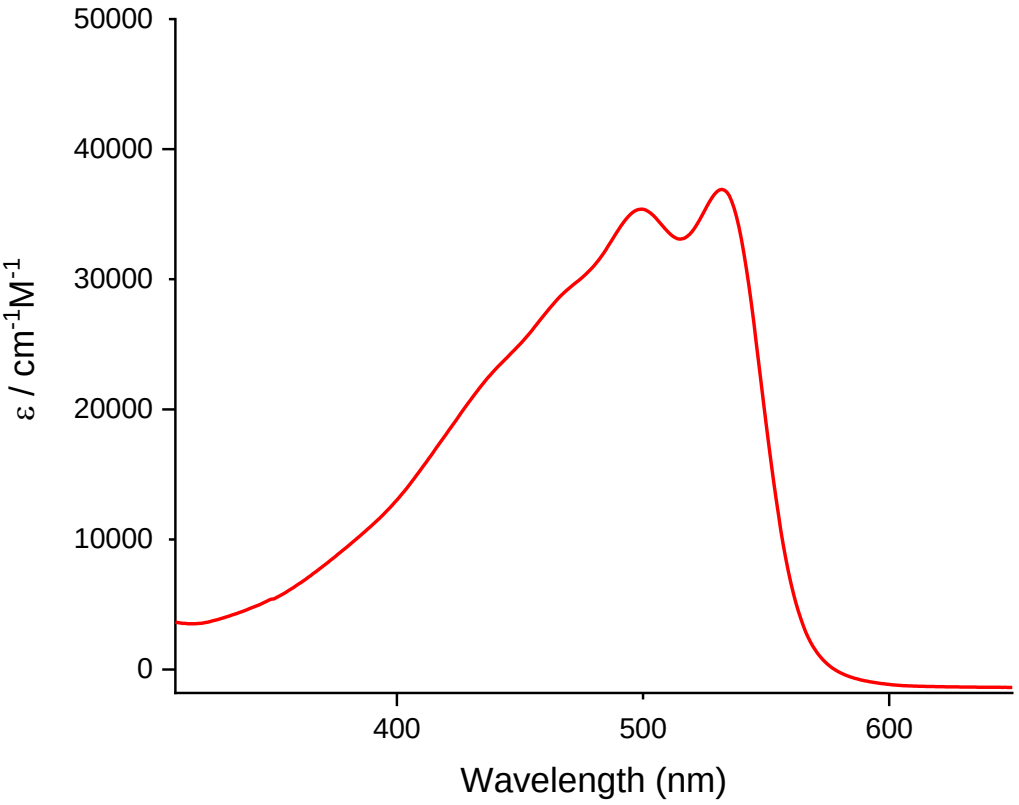

Figure S88. UV-Vis spectrum of **13** (0.0428 mM) in C_6H_5Cl.

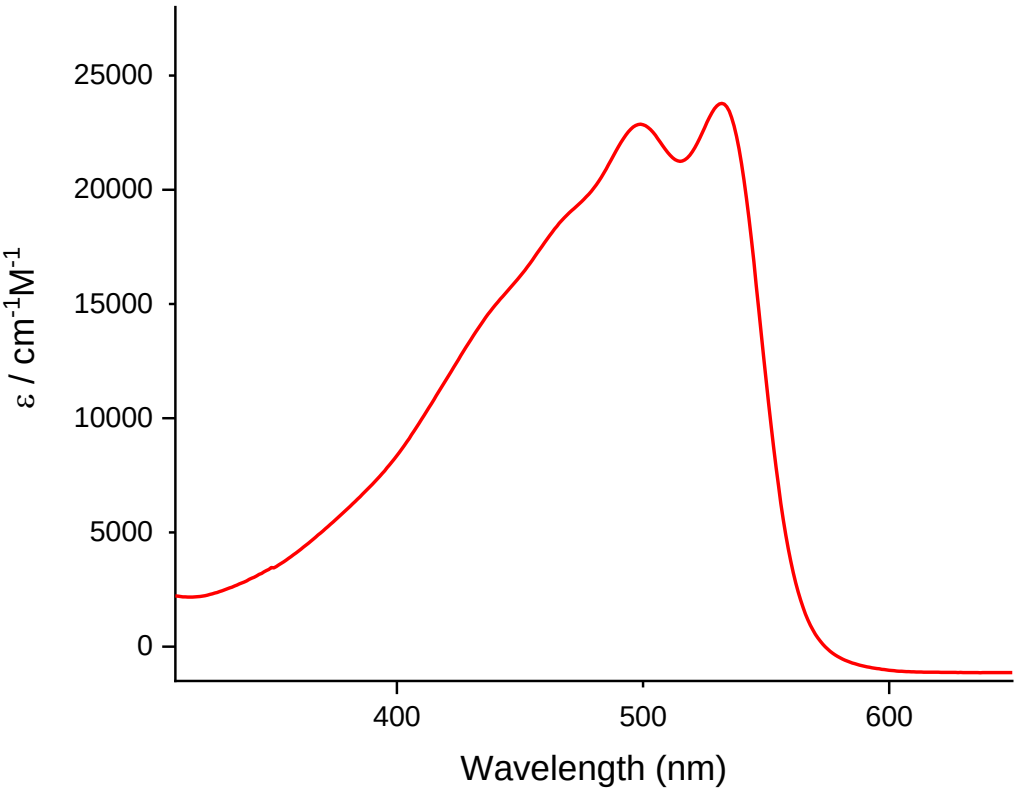

Figure S89. UV-Vis spectrum of **14** (0.0428 mM) in C_6H_5Cl.

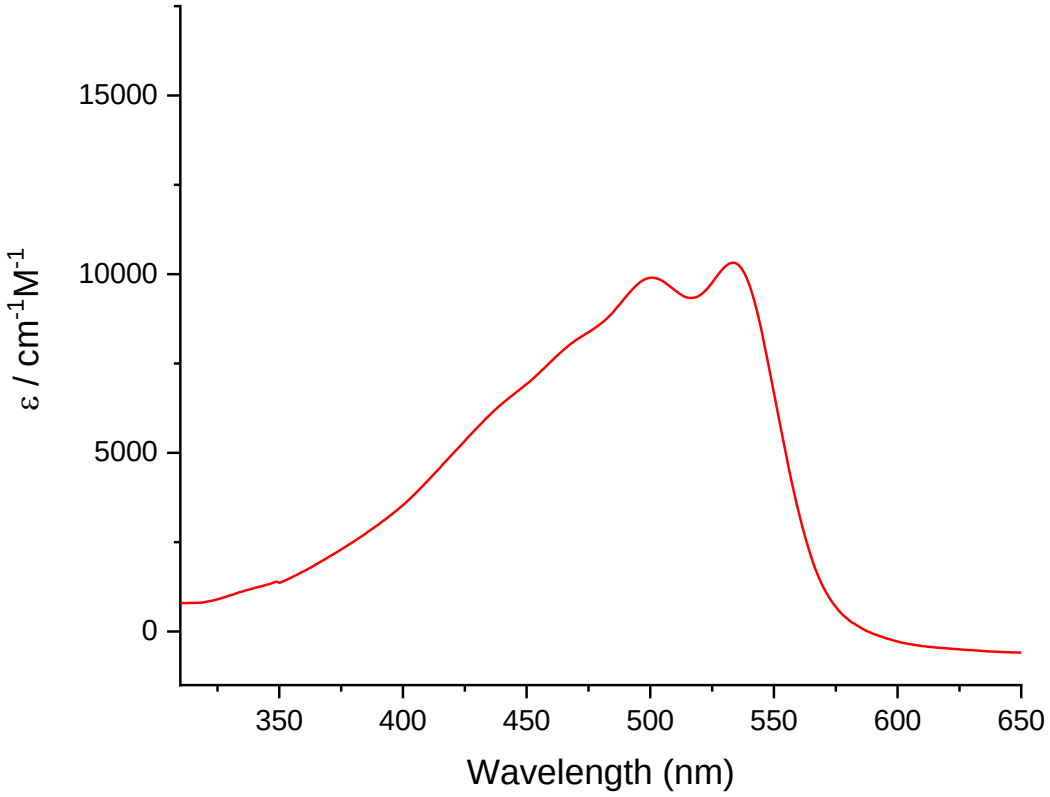

Figure S90. UV-Vis spectrum of **15** (0.0551 mM) in C_6H_5Cl.

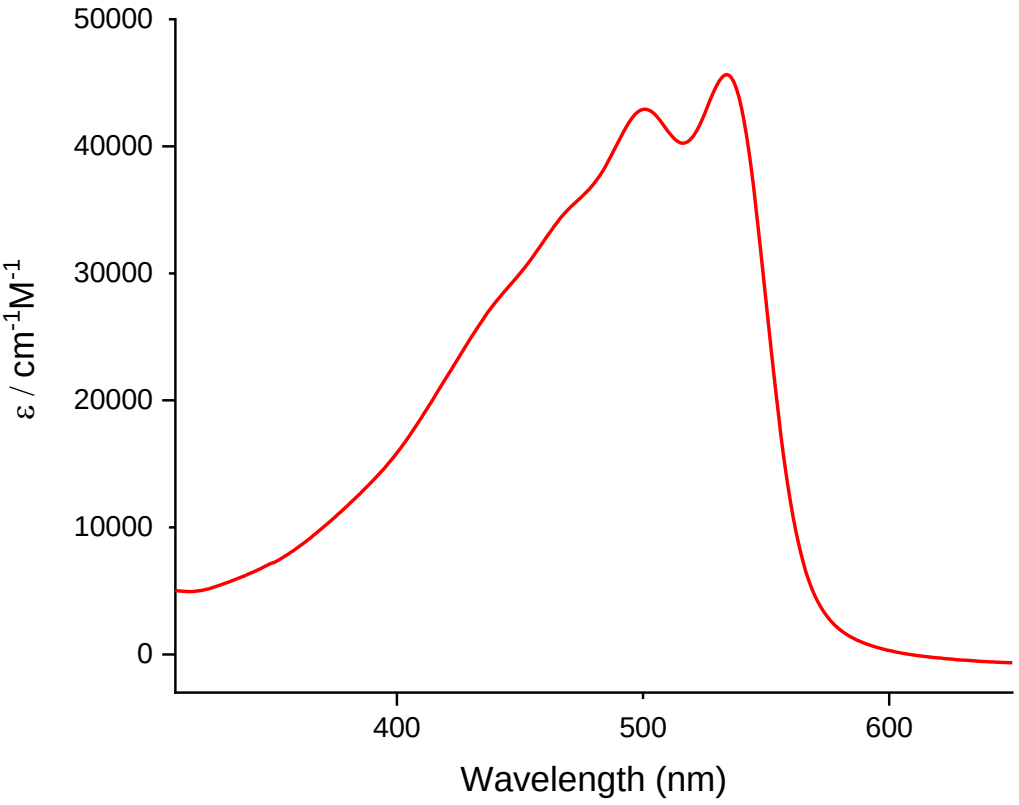

Figure S91. UV-Vis spectrum of **16** (0.0612 mM) in C_6H_5Cl.

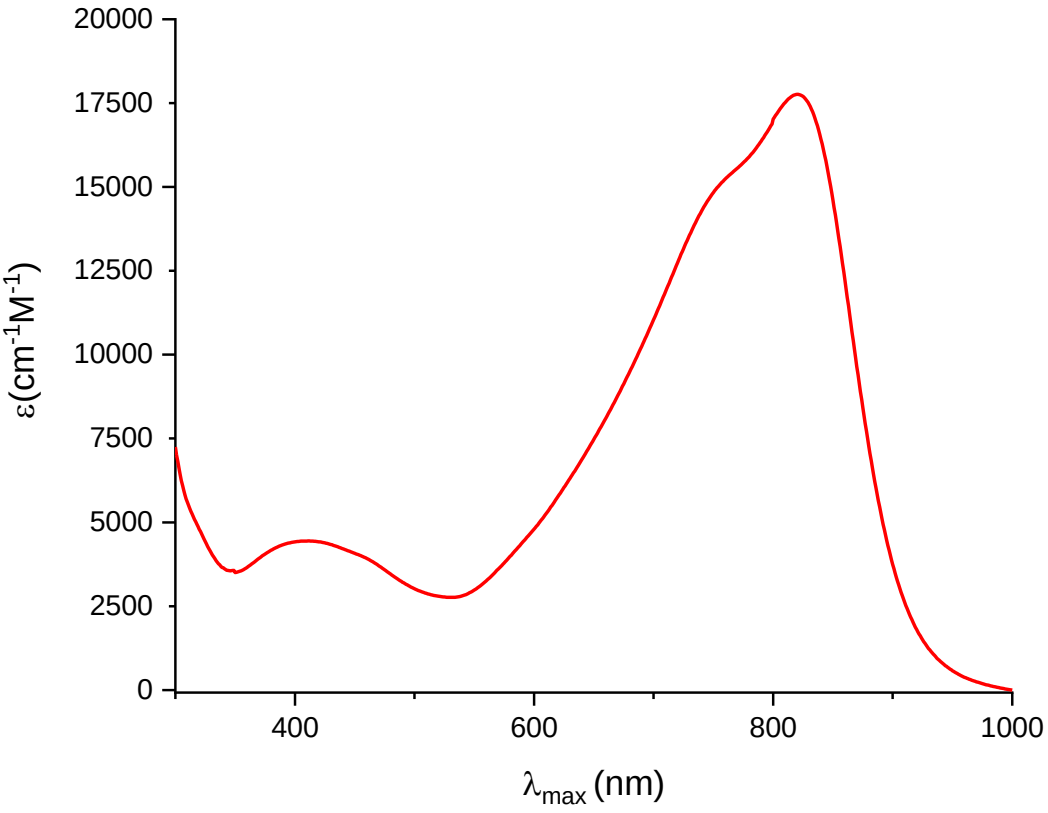

Figure S92. UV-Vis spectrum of **18** (0.0326 mM) in C_6H_5Cl.

13. IR Spectra

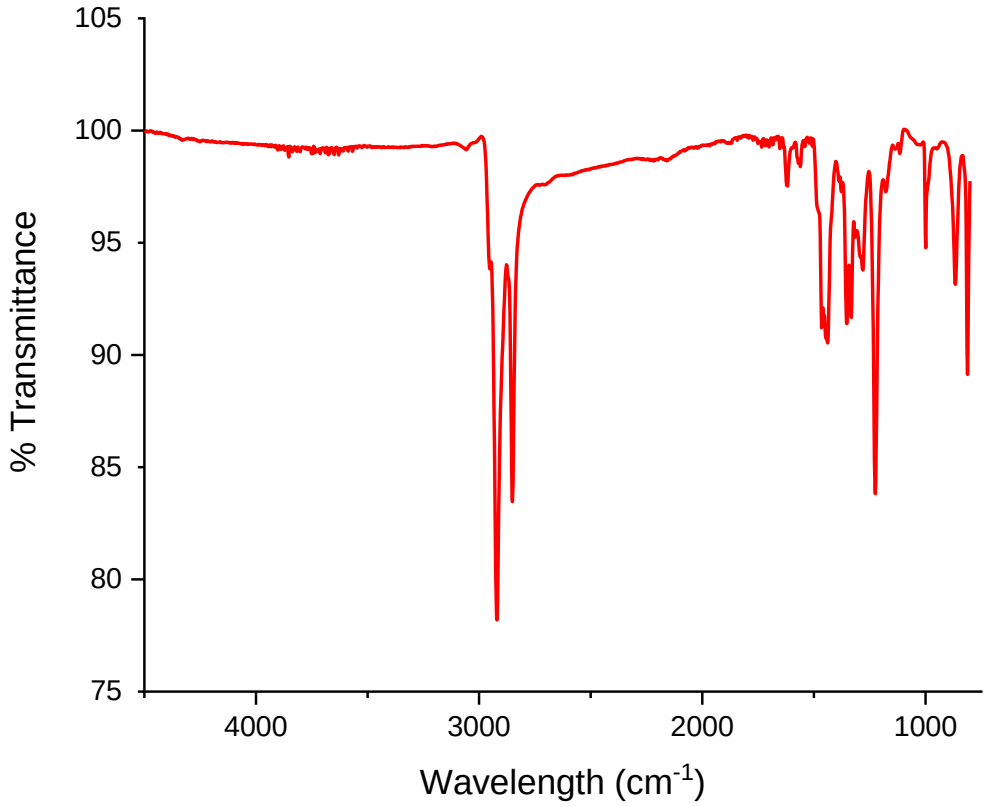

Figure S93. FT-IR spectrum of **3**.

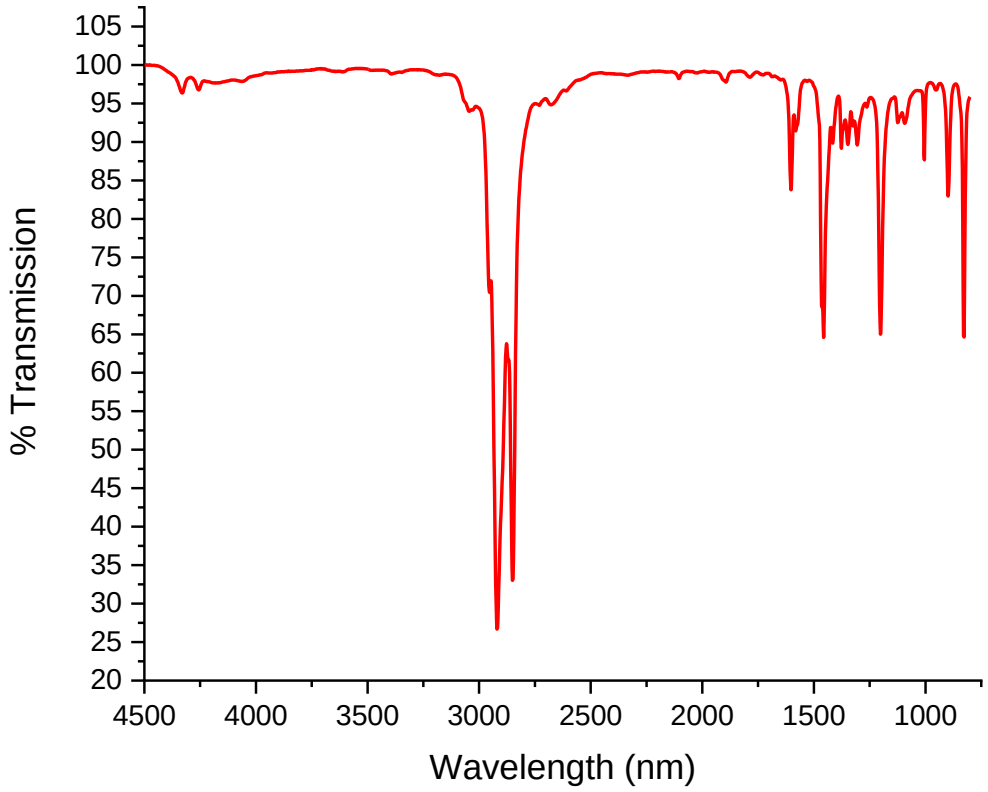

Figure S94. FT-IR spectrum of **6**.

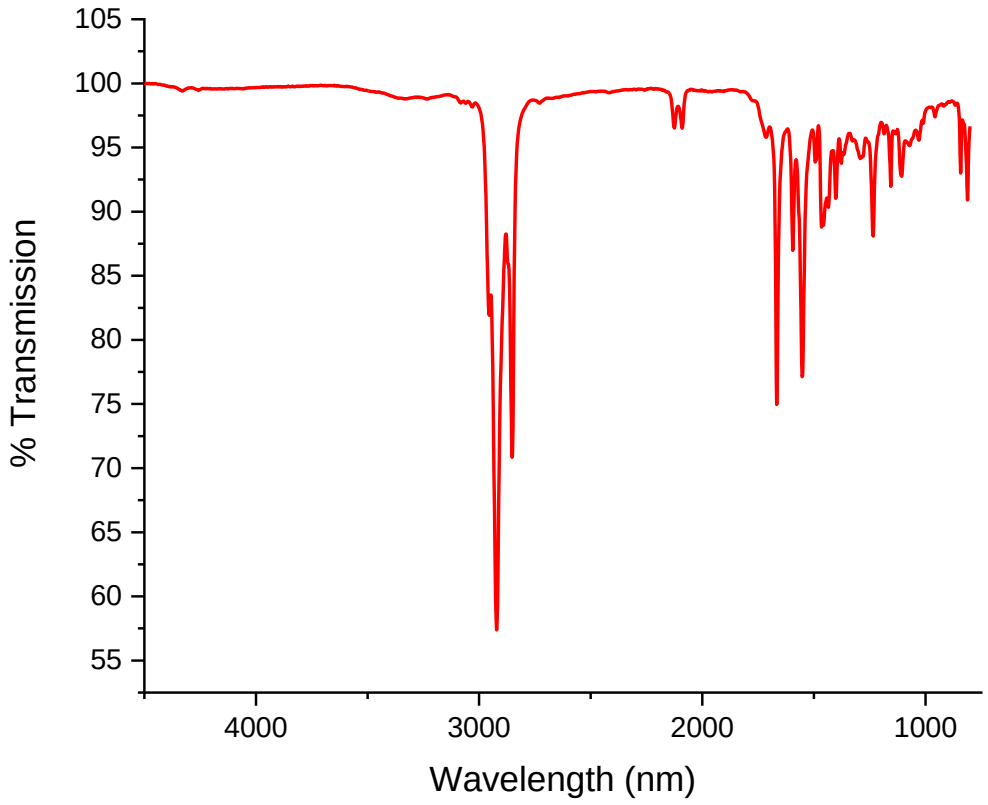

Figure S95. FT-IR spectrum of **7**.

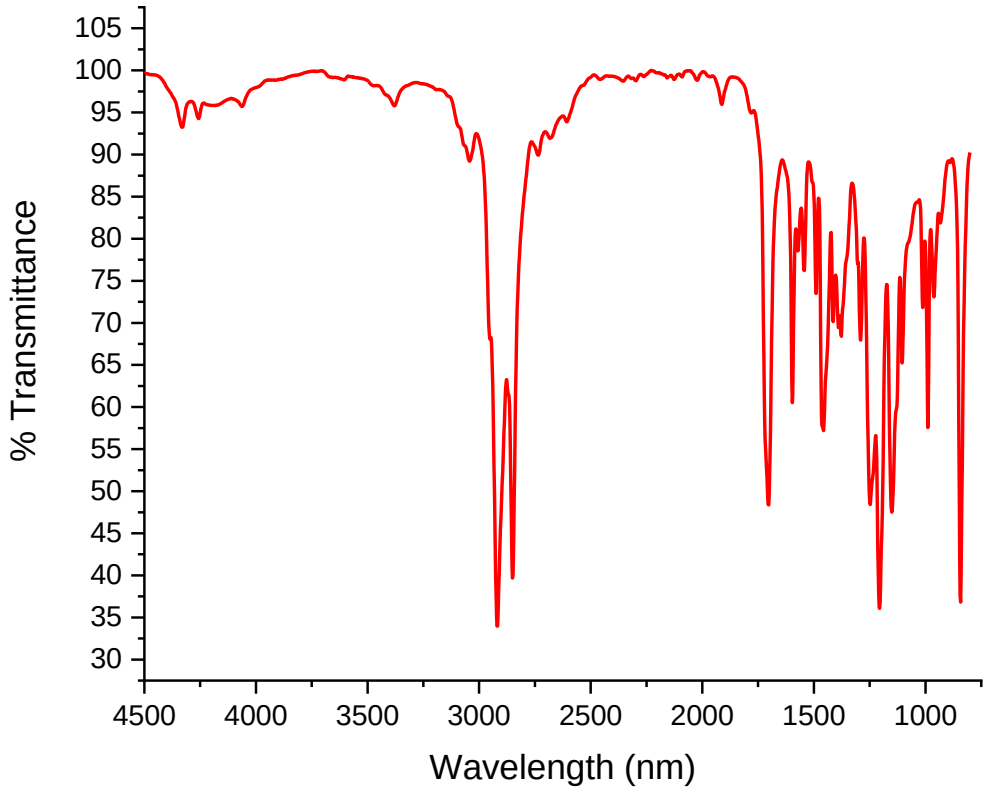

Figure S96. FT-IR spectrum of **8**.

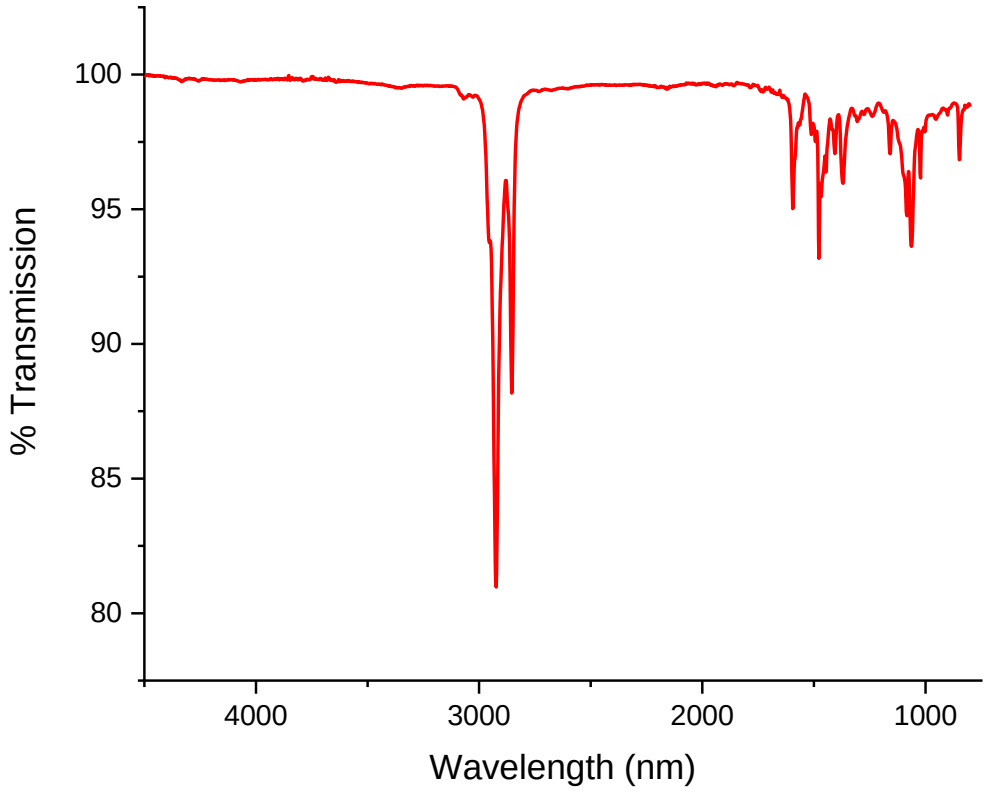

Figure S97. FT-IR spectrum of **9**.

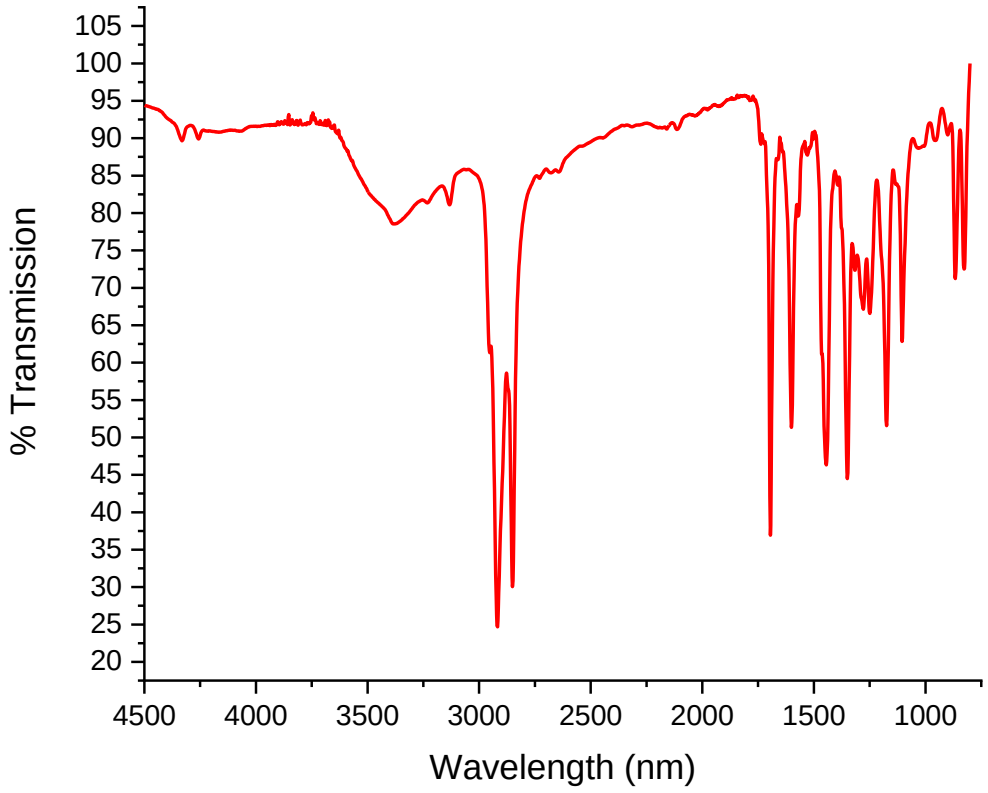

Figure S98. FT-IR spectrum of **10**.

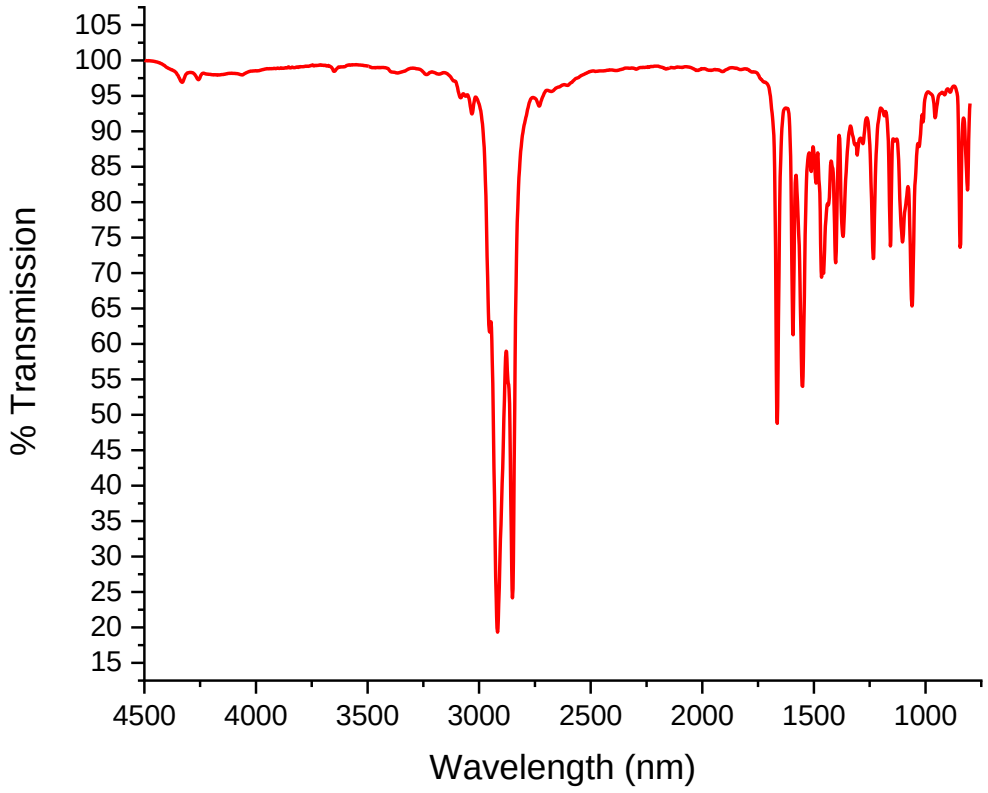

Figure S99. FT-IR spectrum of **11**.

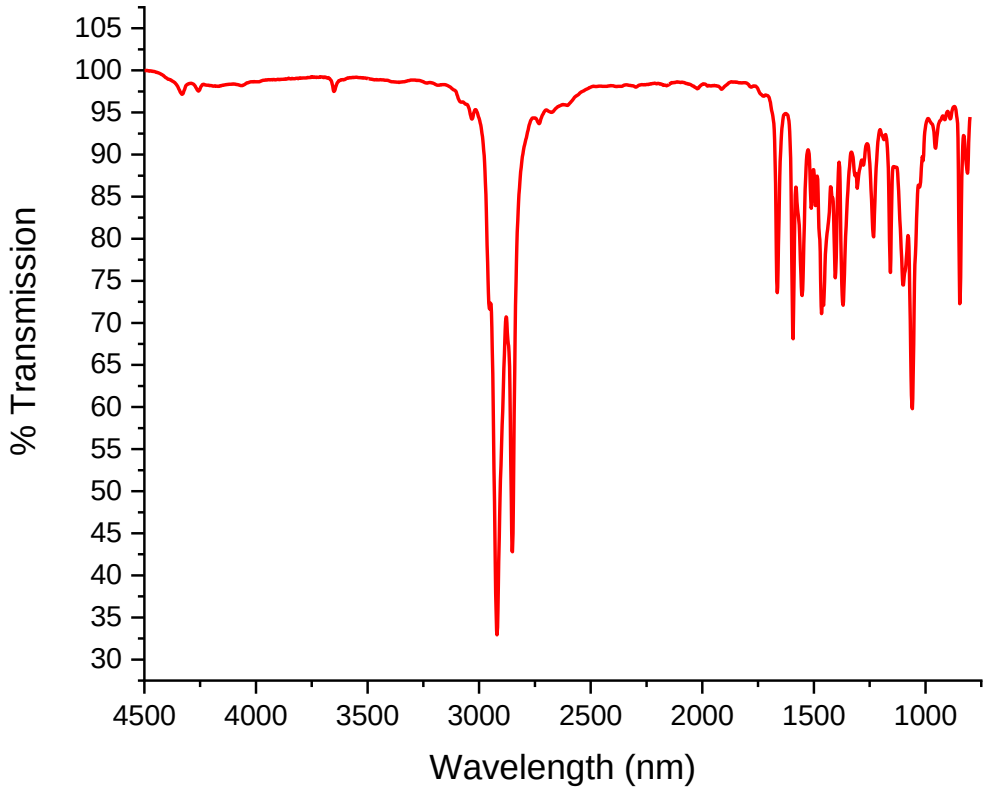

Figure S100. FT-IR spectrum of **12**.

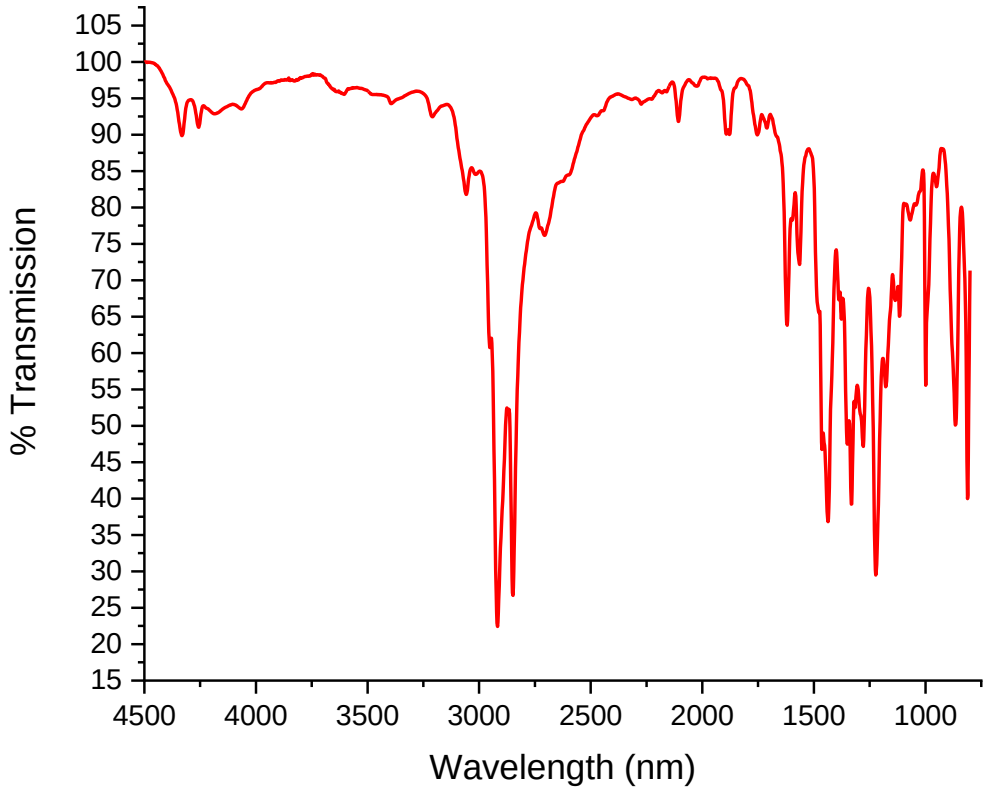

Figure S101. FT-IR spectrum of **13**.

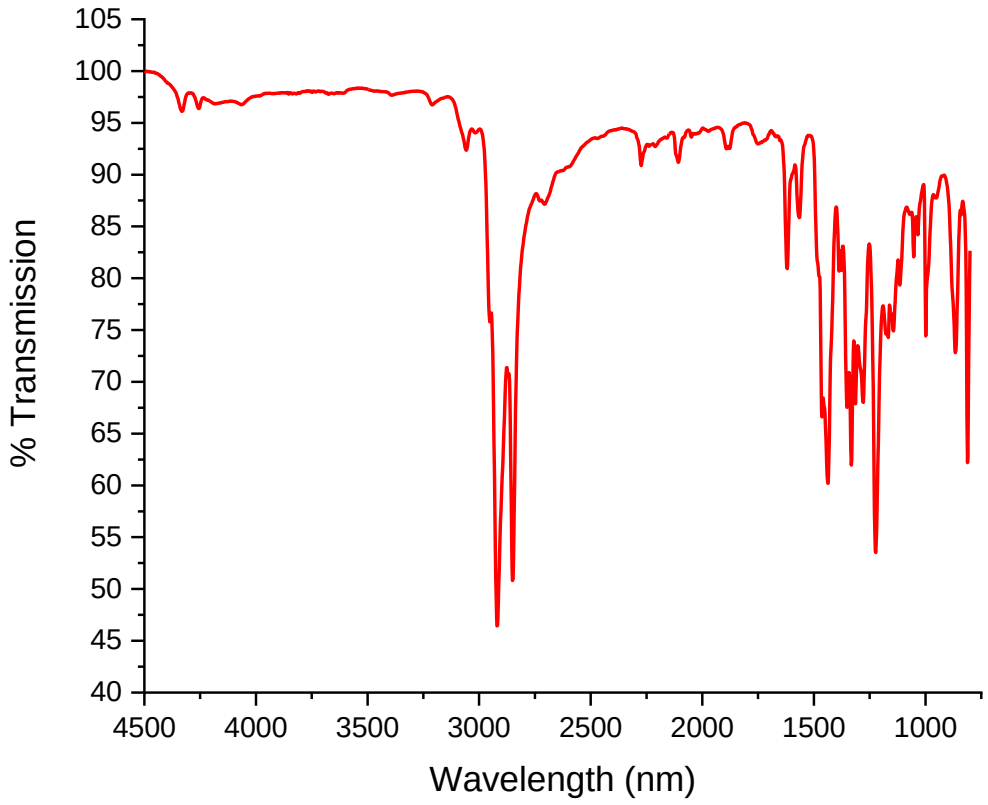

Figure S102. FT-IR spectrum of **14**.

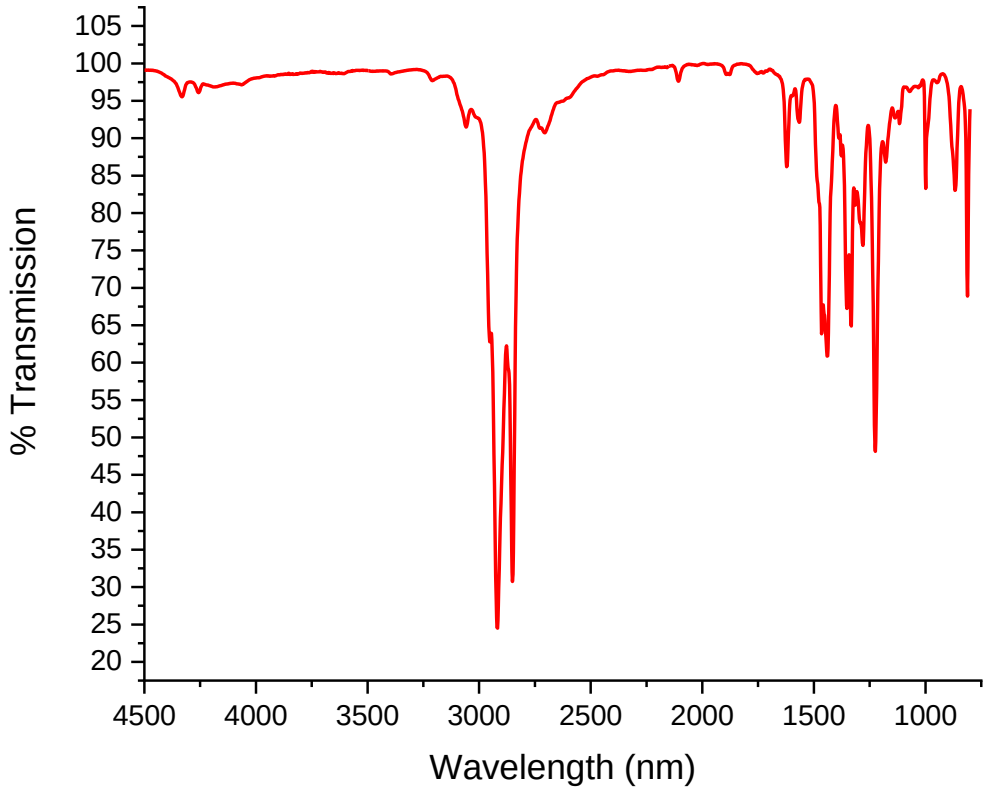

Figure S103. FT-IR spectrum of **15**.

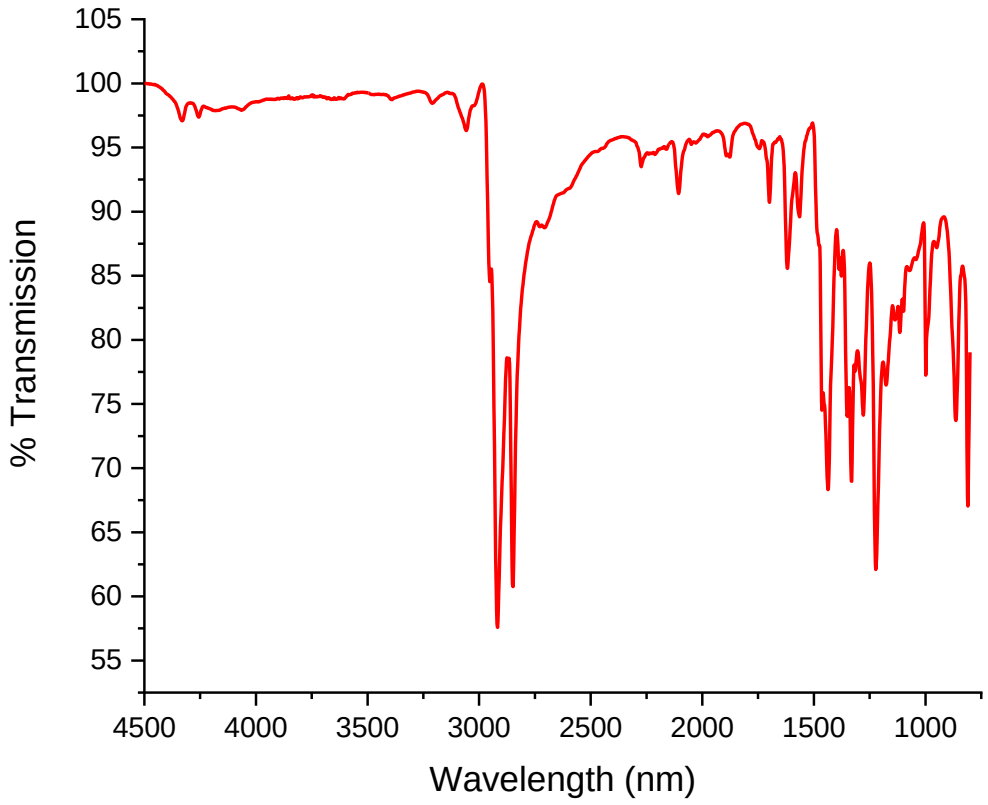

Figure S104. FT-IR spectrum of **16**.

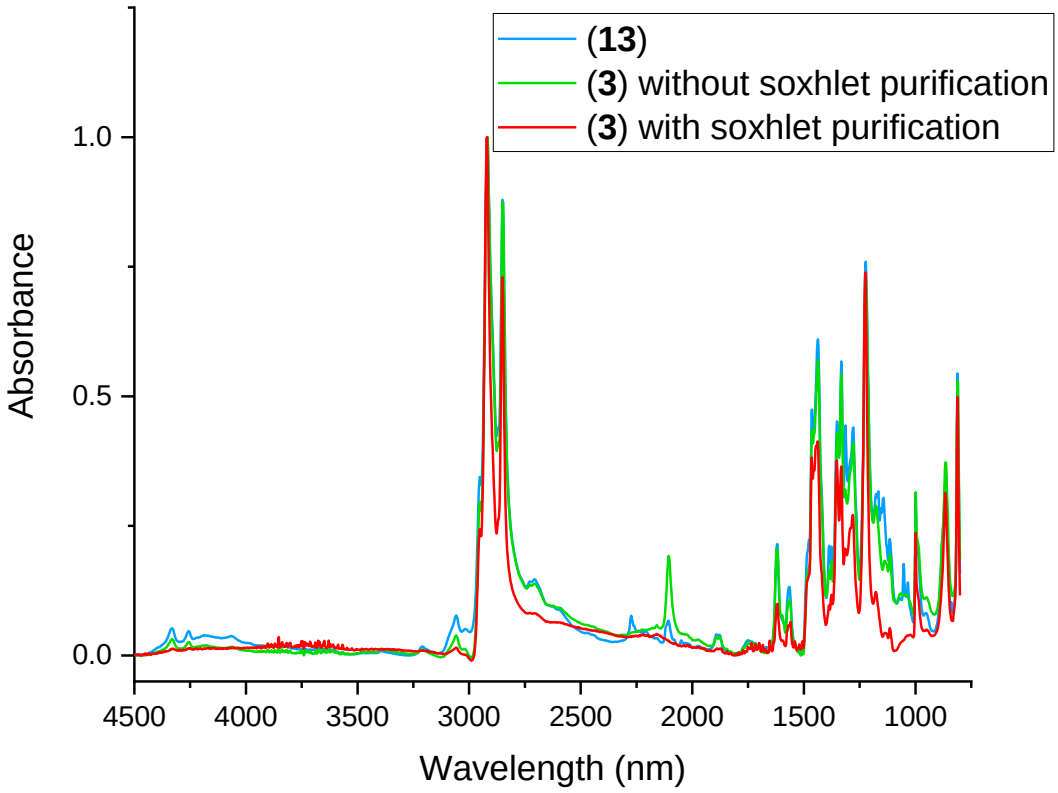

Figure S105. Normalized FT-IR spectrum of **3** (soxhlet purified), **3** (without soxhlet purification) and **13**.

14. High Temperature Gel Permeation Chromotography (HT-GPC) Data

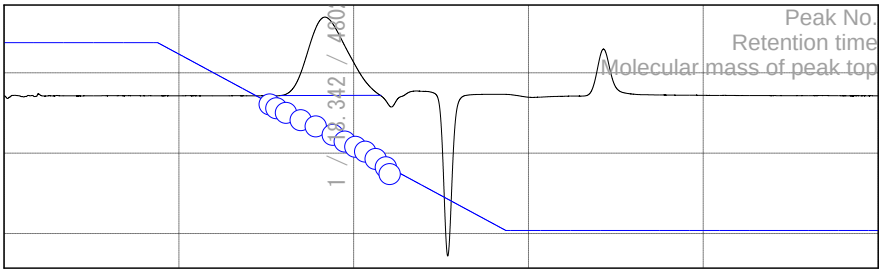

	[min]	[mV]	[mol]		
Peak start	15.795	-64.144	680,035	Mn	20,466
Peak top	18.342	-15.291	48,021	Mw	58,715
Peak end	21.522	-63.993	1,754	Mz	124,946
				Mz+1	203,599
				Mv	58,715
Height [mV]			48.786	Mp	48,021
Area [mV*s]			7608.918	Mz/Mw	2.128
Area% [%]			100.000	Mw/Mn	2.869
[eta]			58715.20917	Mz+1/Mw	3.468

Figure S106. HT-GPC data for optimization of **3** (entry 1).

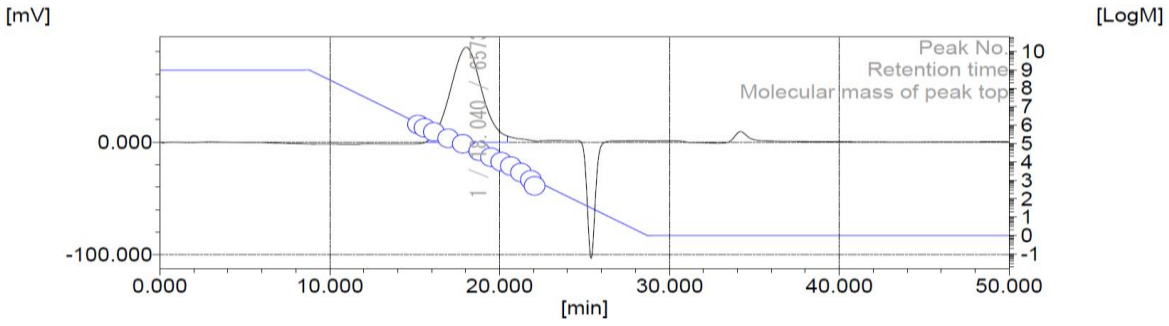

	[min]	[mV]	[mol]		
Peak start	15.680	0.179	766,499	Mn	42,067
Peak top	18.040	83.883	65,733	Mw	92,498
Peak end	20.445	5.361	5,379	Mz	176,486
				Mz+1	278,531
				Mv	92,498
Height [mV]			83,910	Mp	65,733
Area [mV*s]			10780.058	Mz/Mw	1.908
Area% [%]			100.000	Mw/Mn	2.199
[eta]			92497.57350	Mz+1/Mw	3.011

Figure S107. HT-GPC data for optimization of **3** (entry 2).

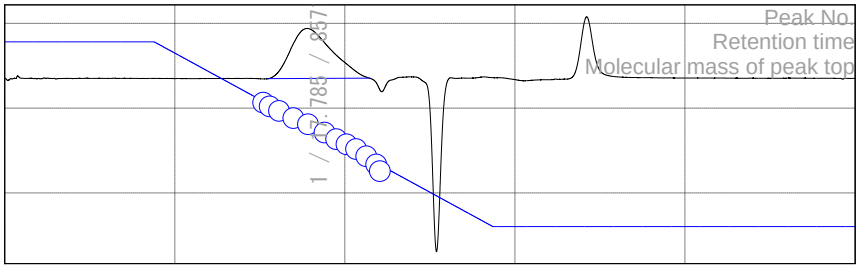

	[min]	[mV]	[mol]		
Peak start	15.488	-32.571	935,719	Mn	28,187
Peak top	17.785	-2.992	85,712	Mw	98,478
Peak end	21.445	-32.312	1,899	Mz	212,466
				Mz+1	328,444
				Mv	98,478
Height [mV]			29.479	Mp	85,713
Area [mV*s]			4953.753	Mz/Mw	2.157
Area% [%]			100.000	Mw/Mn	3.494
[eta]			98478.43174	Mz+1/Mw	3.335

Figure S108. HT-GPC data for optimization of **3** (entry 4).

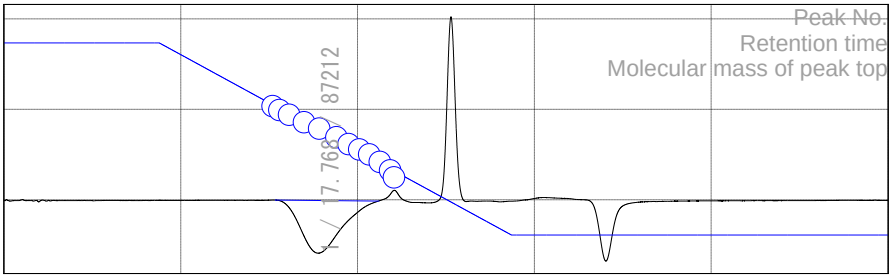

	[min]	[mV]	[mol]		
Peak start	15.335	49.880	1,097,621	Mn	35,167
Peak top	17.768	20.535	87,212	Mw	104,184
Peak end	21.177	49.352	2,511	Mz	213,256
				Mz+1	331,924
				Mv	104,184
Height [mV]			29.125	Mp	86,760
Area [mV*s]			4481.107	Mz/Mw	2.047
Area% [%]			100.000	Mw/Mn	2.963
[eta]			104183.85838	Mz+1/Mw	3.186

Figure S109. HT-GPC data for optimization of **3** (entry 6).

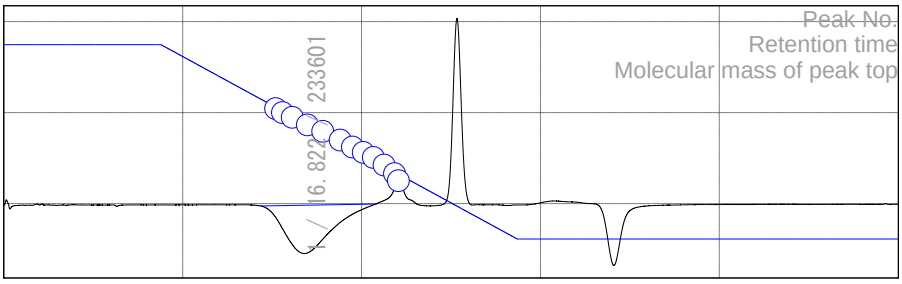

	[min]	[mV]	[mol]		
Peak start	14.373	48.679	2,986,265	Mn	68,976
Peak top	16.822	22.586	233,601	Mw	295,866
Peak end	20.792	49.778	3,749	Mz	681,896
				Mz+1	1,077,470
				Mv	295,866
Height [mV]			26.512	Mp	233,602
Area [mV*s]			4678.539	Mz/Mw	2.305
Area% [%]			100.000	Mw/Mn	4.289
[eta]			295865.63913	Mz+1/Mw	3.642

Figure S110. HT-GPC data for optimization of **3** (entry 7).

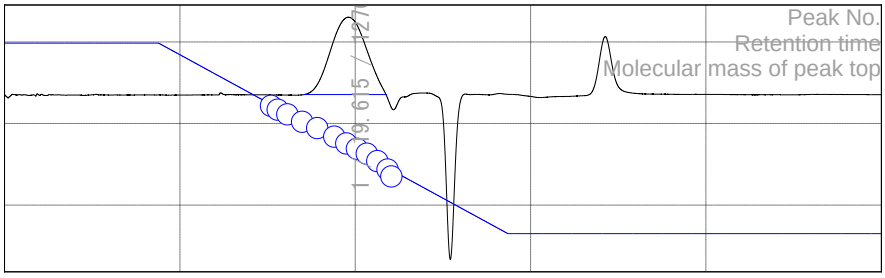

	[min]	[mV]	[mol]		
Peak start	17.063	-32.251	181,652	Mn	8,642
Peak top	19.615	15.180	12,760	Mw	18,556
Peak end	21.752	-32.253	1,380	Mz	36,147
				Mz+1	57,566
				Mv	18,556
Height [mV]			47.432	Mp	12,673
Area [mV*s]			6642.487	Mz/Mw	1.948
Area% [%]			100.000	Mw/Mn	2.147
[eta]			18556.27114	Mz+1/Mw	3.102

Figure S111. HT-GPC data for optimization of **3** (entry 8).

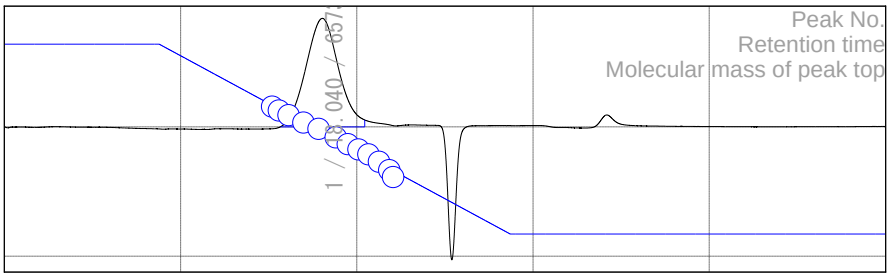

	[min]	[mV]	[mol]		
Peak start	15.680	0.179	766,499	Mn	42,067
Peak top	18.040	83.883	65,733	Mw	92,498
Peak end	20.445	5.361	5,379	Mz	176,486
				Mz+1	278,531
				Mv	92,498
Height [mV]			83.910	Mp	65,733
Area [mV*s]			10780.058	Mz/Mw	1.908
Area% [%]			100.000	Mw/Mn	2.199
[eta]			92497.57350	Mz+1/Mw	3.011

Figure S112. HT-GPC data of **3**.

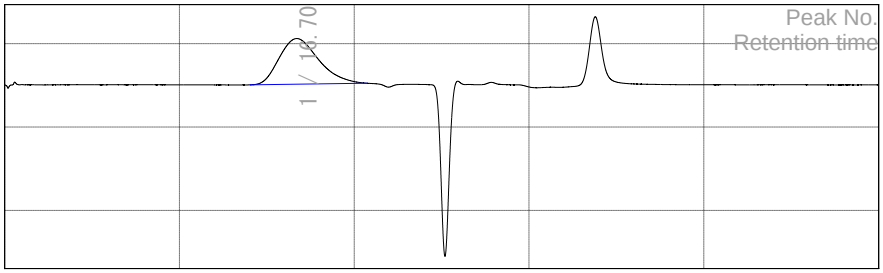

	[min]	[mV]	[mol]		
Peak start	14.028	-24.655	4,276,310	Mn	101,903
Peak top	16.705	3.141	263,760	Mw	336,931
Peak end	20.677	-23.646	4,226	Mz	711,511
				Mz+1	1,136,509
				Mv	336,931
Height [mV]			27.390	Mp	263,760
Area [mV*s]			4279.505	Mz/Mw	2.112
Area% [%]			100.000	Mw/Mn	3.306
[eta]			336931.47306	Mz+1/Mw	3.373

Figure S113. HT-GPC data of **6**.

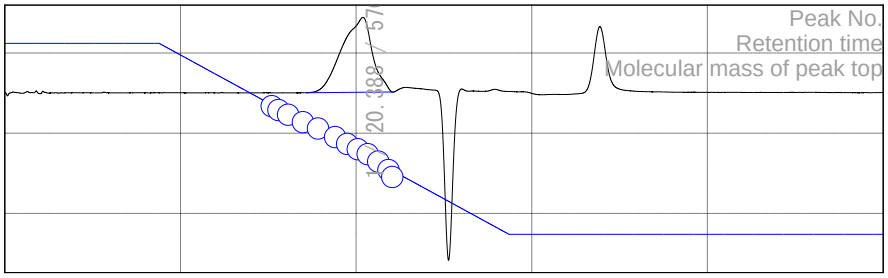

	[min]	[mV]	[mol]		
Peak start	17.178	-24.695	161,161	Mn	6,352
Peak top	20.388	22.266	5,706	Mw	12,490
Peak end	22.137	-24.281	924	Mz	24,366
				Mz+1	40,460
				Mv	12,490
Height [mV]			46.693	Mp	5,706
Area [mV*s]			5611.380	Mz/Mw	1.951
Area% [%]			100.000	Mw/Mn	1.966
[eta]			12490.00561	Mz+1/Mw	3.239

Figure S114. HT-GPC data of **7**.

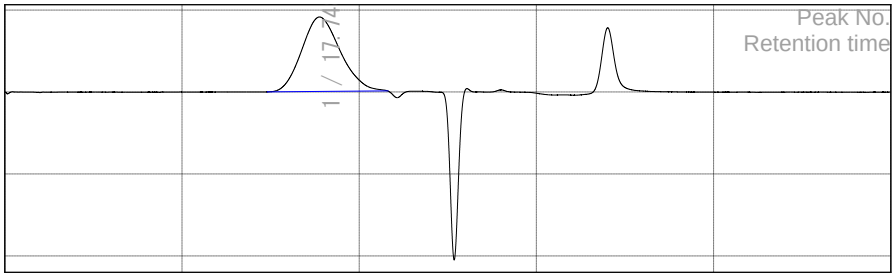

	[min]	[mV]	[mol]		
Peak start	14.797	0.067	1,922,120	Mn	39,430
Peak top	17.748	45.795	89,047	Mw	122,885
Peak end	21.598	0.703	1,619	Mz	277,144
				Mz+1	482,771
				Mv	122,885
Height [mV]			45.452	Mp	89,047
Area [mV*s]			6871.223	Mz/Mw	2.255
Area% [%]			100.000	Mw/Mn	3.117
[eta]			122884.55508	Mz+1/Mw	3.929

Figure S115. HT-GPC data of **8**.

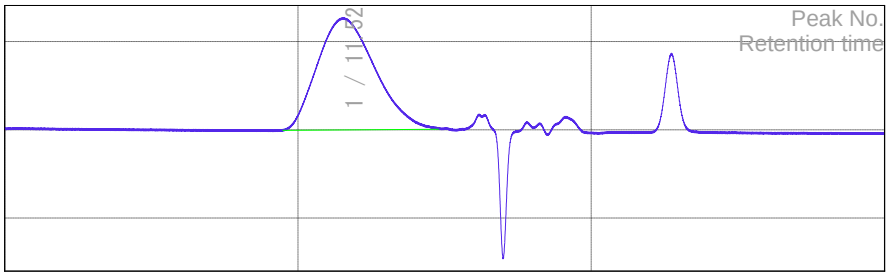

	[min]	[mV]	[mol]		
Peak start	9.475	-0.063	1,024,214	Mn	60,438
Peak top	11.522	12.712	121,984	Mw	143,312
Peak end	14.780	0.067	4,122	Mz	257,014
				Mz+1	372,197
				Mv	143,312
Height [mV]			12.725	Mp	121,985
Area [mV*sec]			1730.247	Mz/Mw	1.793
Height% [%]			100.000	Mw/Mn	2.371
[eta]			143311.58762	Mz+1/Mw	2.597

Figure S116. HT-GPC data of **9**.

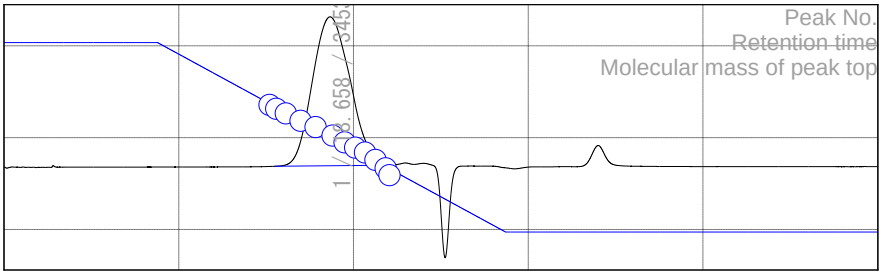

	[min]	[mV]	[mol]		
Peak start	15.488	-131.196	935,719	Mn	18,203
Peak top	18.658	31.599	34,538	Mw	48,122
Peak end	21.752	-130.023	1,380	Mz	104,763
				Mz+1	188,556
				Mv	48,122
Height [mV]			162.201	Mp	34,538
Area [mV*s]			24169.166	Mz/Mw	2.177
Area% [%]			100.000	Mw/Mn	2.644
[eta]			48121.88044	Mz+1/Mw	3.918

Figure S117. HT-GPC data of **10**.

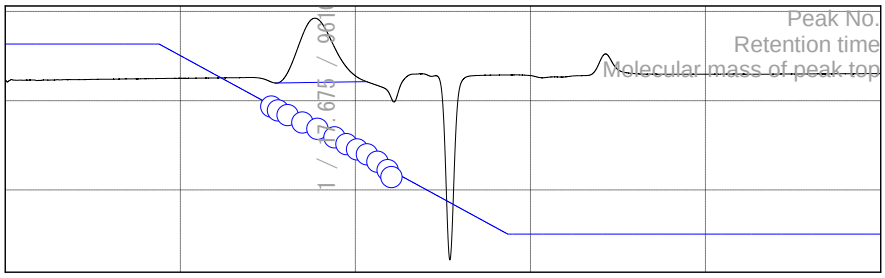

	[min]	[mV]	[mol]		
Peak start	15.412	-90.098	1,013,442	Mn	50,401
Peak top	17.675	-53.757	96,109	Mw	118,609
Peak end	20.638	-89.314	4,398	Mz	218,596
				Mz+1	322,260
				Mv	118,609
Height [mV]			36.002	Mp	96,110
Area [mV*s]			5036.410	Mz/Mw	1.843
Area% [%]			100.000	Mw/Mn	2.353
[eta]			118609.38304	Mz+1/Mw	2.717

Figure S118. HT-GPC data of **11**.

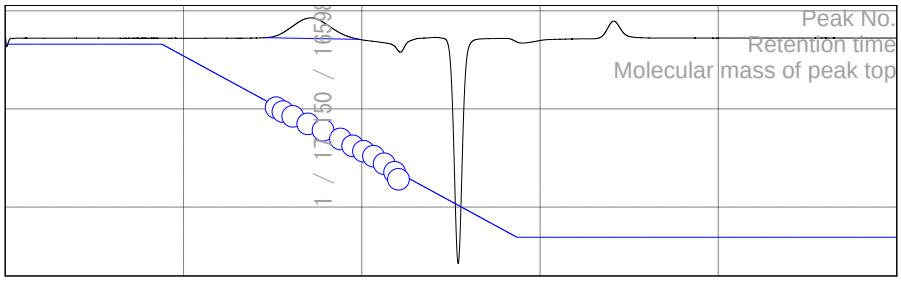

	[min]	[mV]	[mol]		
Peak start	14.488	-127.415	2,649,403	Mn	97,912
Peak top	17.150	-107.206	165,984	Mw	246,408
Peak end	19.832	-128.987	10,184	Mz	523,360
				Mz+1	865,928
				Mv	246,408
Height [mV]			20.992	Mp	165,985
Area [mV*s]			3098.102	Mz/Mw	2.124
Area% [%]			100.000	Mw/Mn	2.517
[eta]			246408.16930	Mz+1/Mw	3.514

Figure S119. HT-GPC data of **12**.

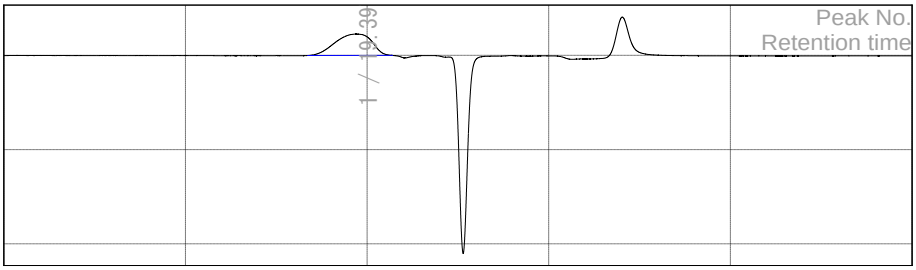

	[min]	[mV]	[mol]		
Peak start	16.718	-0.055	260,125	Mn	14,103
Peak top	19.397	11.360	16,016	Mw	28,468
Peak end	21.368	0.024	2,057	Mz	55,281
				Mz+1	87,673
				Mv	28,468
Height [mV]			11.369	Mp	16,017
Area [mV*s]			1586.423	Mz/Mw	1.942
Area% [%]			100.000	Mw/Mn	2.019
[eta]			28468.39072	Mz+1/Mw	3.080

Figure S120. HT-GPC data of **13**.

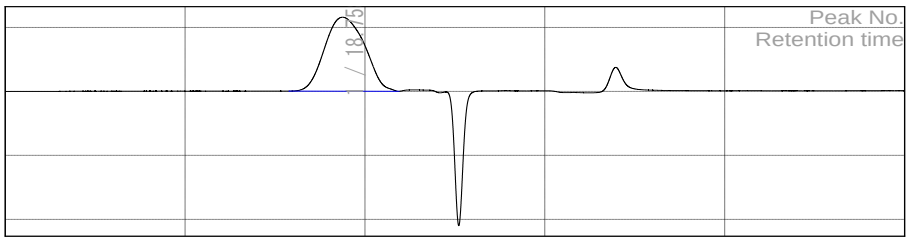

	[min]	[mV]	[mol]		
Peak start	15.757	0.228	707,714	Mn	16,459
Peak top	18.758	57.990	31,124	Mw	41,822
Peak end	21.868	0.061	1,222	Mz	89,640
				Mz+1	154,303
				Mv	41,822
Height [mV]			57.844	Mp	31,124
Area [mV*s]			8929.473	Mz/Mw	2.143
Area% [%]			100.000	Mw/Mn	2.541
[eta]			41822.39767	Mz+1/Mw	3.689

Figure S121. HT-GPC data of **14**.

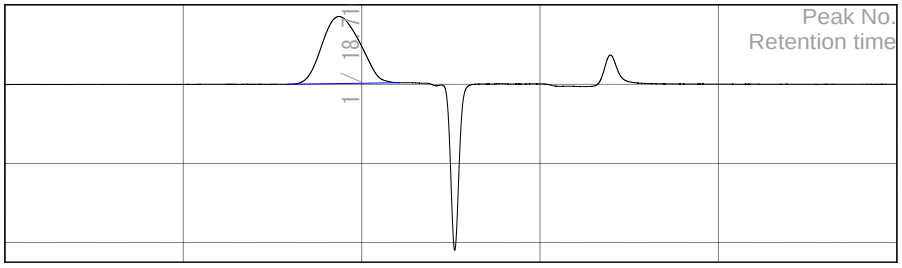

	[min]	[mV]	[mol]		
Peak start	15.872	0.128	627,881	Mn	16,957
Peak top	18.710	42.976	32,729	Mw	41,287
Peak end	22.098	1.101	962	Mz	83,579
				Mz+1	137,899
				Mv	41,287
Height [mV]			42.404	Mp	32,730
Area [mV*s]			6258.753	Mz/Mw	2.024
Area% [%]			100.000	Mw/Mn	2.435
[eta]			41287.32477	Mz+1/Mw	3.340

Figure S122. HT-GPC data of **15**.

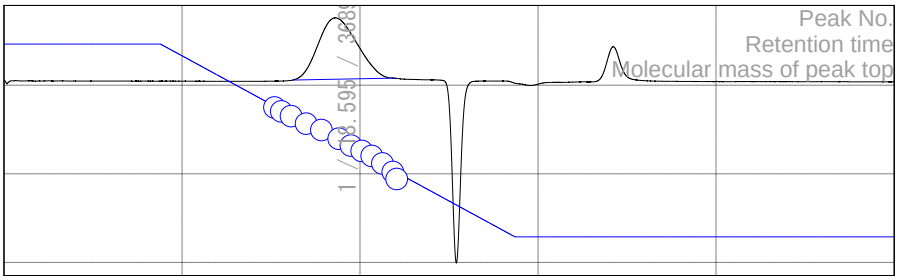

	[min]	[mV]	[mol]		
Peak start	16.218	-97.007	437,707	Mn	17,634
Peak top	18.595	-61.908	36,891	Mw	45,985
Peak end	21.907	-95.957	1,175	Mz	93,299
				Mz+1	146,892
				Mv	45,985
Height [mV]			34.660	Mp	36,891
Area [mV*s]			5230.977	Mz/Mw	2.029
Area% [%]			100.000	Mw/Mn	2.608
[eta]			45985.19891	Mz+1/Mw	3.194

Figure S123. HT-GPC data of **16**.

15. X-Ray Diffraction Data

AzoCarbazole $B(C_6F_5)_3/H_2O$ adduct (17a)

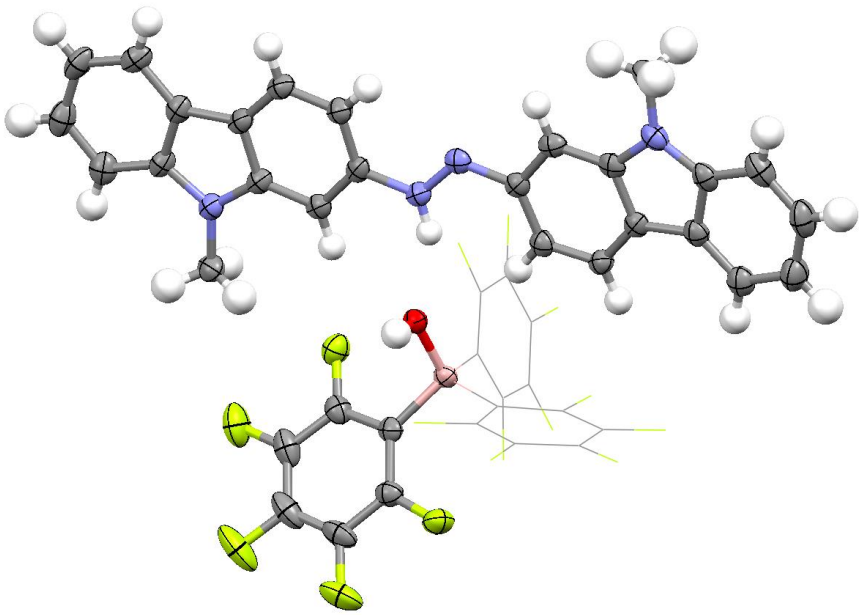

Crystal data	
Chemical formula	$2(C_{18}HBF_{15}O)\cdot C_{26}H_{20}N_4\cdot 2(C_{26}H_{21}N_4)$
M_r	2225.39
Crystal system, space group	Triclinic, *P-1*
Temperature (K)	150
a, *b*, *c* (Å)	15.0605 (16), 17.2367 (17), 20.238 (2)
α, β, γ (°)	67.095 (6), 88.512 (7), 88.113 (7)
V (Å^3)	4836.4 (9)
Z	2
Radiation type	Cu *K*α
μ (mm^{-1})	1.16

Crystal size (mm)	0.19 × 0.14 × 0.05
Data collection	
Diffractometer	Bruker AXS D8 Quest diffractometer with PhotonIII_C14 charge-integrating and photon counting pixel array detector
Absorption correction	Multi-scan, TWINABS 2012/1: Krause, L., Herbst-Irmer, R., Sheldrick G.M. & Stalke D. (2015). J. Appl. Cryst. 48 3-10.
T_{min}, T_{max}	0.589, 0.754
No. of measured, independent and observed [$I > 2\sigma(I)$] reflections	70344, 19498, 16118
R_{int}	0.065
$(\sin \theta/\lambda)_{max}$ (Å^{-1})	0.641
Refinement	
$R[F^2 > 2\sigma(F^2)]$, $wR(F^2)$, S	0.063, 0.173, 1.05
No. of reflections	19498
No. of parameters	1451
H-atom treatment	H-atom parameters constrained
$\Delta\rho_{max}$, $\Delta\rho_{min}$ (e Å^{-3})	0.49, -0.31

Structure Solution and Refinement. The crystals under investigation were multi-component with multiple domains. Most crystals screened did not diffract to sufficient resolution. The crystal chosen for data collection featured one dominant major domain with sufficient medium and high angle data for collection of acceptable resolution data, and several smaller domains. Transformation matrices identified using the program Cell_Now were ambiguous, suggesting that minor domains were not related to the major domain by a typical twin relationship. Analysis of

data using only the major domain did however indicate presence of twinning, with apparent difference densities of one to two electrons pert cubic Angstrom in positions incompatible with disorder, ill-defined ADPs, and higher than expected R values. Application of the Cell_Now suggested transformation matrices and integration of the data as two component did not result in reduction of these effects. The possibility of twinning was instead investigated using the program Rotax (Cooper et al., 2001) as embedded in WinGX (Farrugia, 2012), which identified the most likely type of twinning present to be a 180 degree rotation around the reciprocal [1 0 0] reciprocal lattice direction, with a twin transformation matrix of 1 -0.047 -0.023, 0 -1 0, 0 0 -1. Application of the approximate matrix 1 0 0, 0 -1 0, 0 0 -1 using a TWIN command in Shelx resulted in some reduction of effects from twinning. The exact twinning matrix as obtained from Rotax was applied to the major component and the data were subsequently integrated using SAINT using both components and corrected for absorption using twinabs, resulting in the following statistics:

41682 data (13063 unique) involve domain 1 only, mean I/sigma 11.1
41549 data (13057 unique) involve domain 2 only, mean I/sigma 7.9
28815 data (11803 unique) involve 2 domains, mean I/sigma 18.2
23 data (23 unique) involve 3 domains, mean I/sigma 23.2

The exact twin matrix identified by the integration program was found to be:

1.00082 -0.03854 -0.01864
0.02951 -0.99920 -0.00326
0.02744 0.00358 -1.00161

The Rint value given is for all reflections and is based on agreement between observed single and composite intensities and those calculated from refined unique intensities and twin fractions (TWINABS (Sheldrick, 2012)).

16. DFT Calculations and Optimized Structures

Computational Methods. Geometry optimizations were performed using the Gaussian16 software package.[20] All geometries were fully optimized at the B3LYP/6-31G(d,p) level of DFT. A polarizable continuum model (PCM) was used to apply solvent corrections for all compounds in C_6H_5Cl.

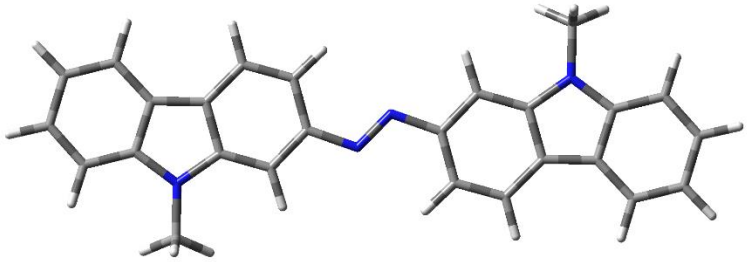

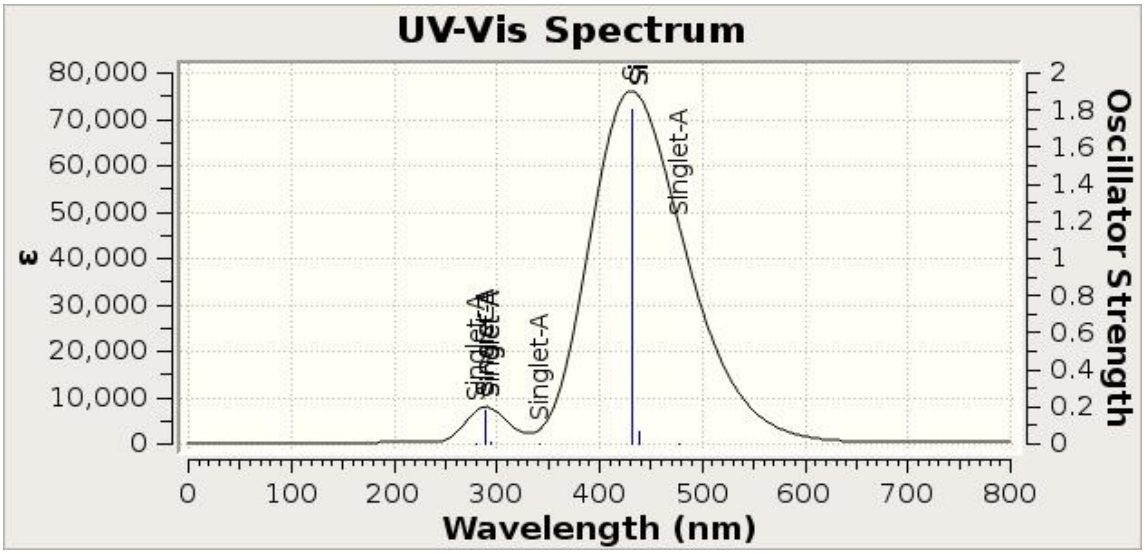

TD State	Wavelength (nm)	Oscillator Strength	ε
1	479.66	0.00080	2673
2	437.44	0.076	253888
3	436.62	0	0
4	433.17	1.8321	6120375
5	341.12	0	0

6	294.32	0	0
7	292.98	0.0090	30066
8	289.12	0.1796	599978
9	288.60	0	0
10	279.95	0	0

Functional and Basis Set: B3LYP/6-31G(d,p)

Charge: 0

Multiplicity: 1

Imaginary Frequencies: 0

Sum of electronic and thermal Free Energies: -1221.527517 Hartrees

Cartesian Coordinates:

C	5.91622800	-0.78649700	0.01062200
C	4.47352500	-0.76159500	0.00173500
C	4.09130800	0.60849000	-0.02312300
C	2.74985200	0.98806200	-0.02282100
C	3.48023500	-1.75533800	0.01352600
C	1.77721500	-0.02054700	-0.01059900
C	2.14470600	-1.38921000	0.00672400
H	3.75872400	-2.80519100	0.03054100
H	1.35902400	-2.13435200	0.01766800
H	2.42845900	2.02348000	-0.02735800
N	0.44428900	0.45049200	-0.01176500
C	-2.14470600	1.38921000	0.00671300
C	-3.48023500	1.75533800	0.01351500
C	-1.77721500	0.02054700	-0.01059400
C	-4.47352500	0.76159500	0.00173900
H	-3.75872400	2.80519100	0.03051900
C	-2.74985300	-0.98806300	-0.02280200

C	-4.09130800	-0.60849000	-0.02310500
H	-2.42845900	-2.02348000	-0.02732800
C	-6.34436600	-0.57089800	-0.00966200
C	-5.91622800	0.78649700	0.01063000
C	-7.70250000	-0.90892000	0.00618300
C	-6.87055300	1.81299600	0.03502700
C	-8.62789000	0.13174800	0.03056600
H	-8.03081400	-1.94292800	0.00519900
C	-8.22114700	1.47958500	0.04397100
H	-6.55829500	2.85333400	0.04941400
H	-9.68780300	-0.10453900	0.04315300
H	-8.97126700	2.26398400	0.06430700
C	6.34436600	0.57089800	-0.00968700
C	7.70250000	0.90892000	0.00615100
C	6.87055300	-1.81299600	0.03502800
C	8.62789000	-0.13174700	0.03054300
H	8.03081400	1.94292800	0.00515400
C	8.22114700	-1.47958400	0.04396400
H	6.55829500	-2.85333400	0.04942700
H	9.68780300	0.10453900	0.04312400
H	8.97126800	-2.26398300	0.06430700
C	-5.25943000	-2.85003200	-0.02703200
H	-6.12475800	-3.20824600	-0.58854500
H	-4.36174800	-3.23854000	-0.51091400
H	-5.31081800	-3.24517200	0.99411300
C	5.25943000	2.85003100	-0.02707900
H	5.31082000	3.24518300	0.99406200
H	6.12475700	3.20823900	-0.58859900
H	4.36174700	3.23853500	-0.51096300
N	-5.23210800	-1.39973200	-0.04648900

N	5.23210800	1.39973200	-0.04652000
N	-0.44428900	-0.45049200	-0.01175900
H	-1.35902400	2.13435300	0.01764700

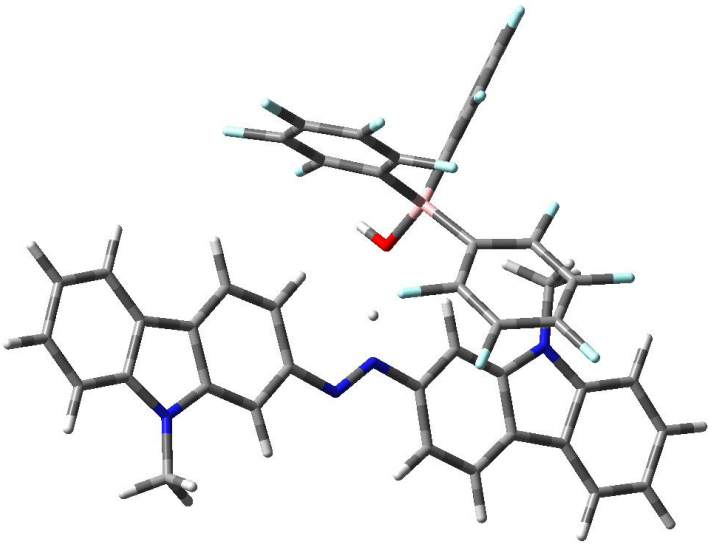

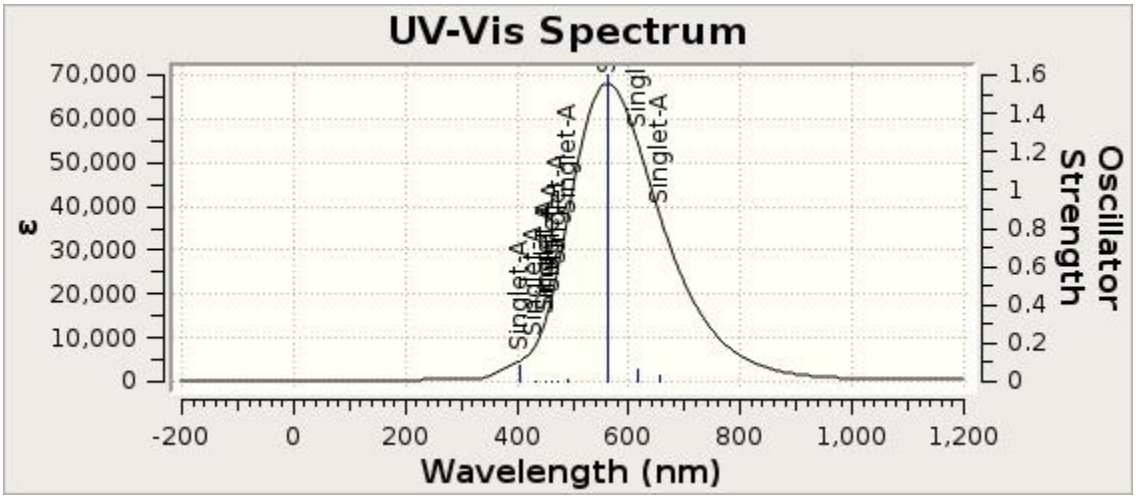

TD State	Wavelength (nm)	Oscillator Strength	ε
1	657.02	0.033	216835
2	614.90	0.061	396986
3	561.60	1.60	10453955
4	489.95	0.012	79266
5	472.62	0.00020	1310
6	461.18	0.0021	13756.93
7	452.21	0.00050	3275

8	450.62	0.0028	18343
9	432.02	0.00020	1310
10	406.70	0.082	537175

Functional and Basis Set: B3LYP/6-31G(d,p)

Charge: 0

Multiplicity: 1

Imaginary Frequencies: 0

Sum of electronic and thermal Free Energies: -3506.094310

Cartesian Coordinates:

C	-5.12884800	4.06127200	-0.56282600
C	-3.70408300	3.86734500	-0.57776100
C	-3.48828100	2.48756700	-0.86056800
C	-2.21257800	1.94287600	-0.93330700
C	-2.59637200	4.70865100	-0.37334300
C	-1.13408200	2.81362800	-0.70964800
C	-1.31519100	4.18958100	-0.43654000
H	-2.74186100	5.76239100	-0.15665100
H	-0.44650300	4.81327100	-0.27113400
H	-2.02827000	0.89818000	-1.15158400
N	0.14637200	2.23689100	-0.76967600
C	2.73375700	1.02955600	-1.10898100
C	4.04034900	0.59466500	-1.20038300
C	2.44913000	2.37775200	-0.74752700
C	5.09227800	1.48598800	-0.92311700
H	4.24695900	-0.43299400	-1.48115200
C	3.49483300	3.29443100	-0.48677800
C	4.80013300	2.83895800	-0.57256800
H	3.23489400	4.31123200	-0.21717600

C	7.04225200	2.63194500	-0.54960400
C	6.52111900	1.35608400	-0.90807100
C	8.41935700	2.84767000	-0.42702300
C	7.39773500	0.28763600	-1.15536400
C	9.26320100	1.77118300	-0.67983400
H	8.82259000	3.81241700	-0.13862800
C	8.76332300	0.50340600	-1.04072000
H	7.00970700	-0.69004400	-1.42461400
H	10.33627400	1.91134500	-0.59100900
H	9.45705700	-0.31023400	-1.22489200
C	-5.71383600	2.78939800	-0.83048400
C	-7.10300700	2.62204800	-0.86762300
C	-5.95460900	5.17464400	-0.34534900
C	-7.89483000	3.74367000	-0.64771100
H	-7.55477600	1.65384800	-1.05380900
C	-7.33183000	5.00966400	-0.39040800
H	-5.52084400	6.14917800	-0.14136300
H	-8.97532200	3.63859600	-0.67116600
H	-7.98491900	5.85993200	-0.22247700
C	6.11775600	4.90009500	0.05831700
H	7.03026200	5.33078400	-0.35947700
H	5.27280400	5.47851100	-0.32058500
H	6.14921600	4.99152300	1.15048300
C	-4.88108000	0.42592400	-1.23883600
H	-4.78176000	-0.13742000	-0.30496300
H	-5.86765400	0.24360200	-1.66645200
H	-4.13305500	0.06089800	-1.94604600
N	5.99272400	3.52045000	-0.36796900
N	-4.70780500	1.85477000	-1.02597000
N	1.19789700	2.94707900	-0.64714100

H	1.93166800	0.33383300	-1.31039500
H	0.15068100	1.17464100	-0.87811600
B	-0.45082100	-1.52344700	-0.03389400
C	0.99759500	-2.26513700	0.32224700
C	1.38255400	-2.72936400	1.58328700
C	1.97081500	-2.43688600	-0.66109600
C	2.62863400	-3.29183300	1.85728900
C	3.23674000	-2.96766800	-0.43378900
C	3.57263300	-3.40303800	0.84188700
C	-1.47854200	-2.64936900	-0.68664800
C	-2.20133300	-2.48176000	-1.86884000
C	-1.69572800	-3.88519700	-0.06760100
C	-3.05262500	-3.44175900	-2.41374200
C	-2.52989300	-4.87884800	-0.57190700
C	-3.21548200	-4.65744200	-1.76233500
C	-1.07871300	-0.72989600	1.27193500
C	-0.28725200	0.18819100	1.96846000
C	-2.39153600	-0.81055800	1.73668700
C	-0.72736300	0.94879200	3.04635600
C	-2.88337600	-0.06774300	2.81077500
C	-2.04351900	0.81440700	3.47818800
O	-0.19141700	-0.41860000	-1.03219800
H	-0.02352400	-0.79143200	-1.90499900
F	4.78578500	-3.91548600	1.08896300
F	2.93346600	-3.71020200	3.09460400
F	4.14835100	-3.01414000	-1.42724600
F	1.73609100	-2.03671100	-1.94655300
F	0.54427800	-2.63764900	2.63359700
F	0.99739400	0.39808400	1.58333900
F	0.09532500	1.81124000	3.66410800

F	-2.49674600	1.53887500	4.50898600
F	-4.16480700	-0.18944200	3.19107300
F	-3.30529400	-1.60774600	1.13116700
F	-1.09856500	-4.16120300	1.10953500
F	-2.68554700	-6.04010700	0.07993800
F	-4.02588700	-5.59678600	-2.26649400
F	-3.71645200	-3.19599700	-3.55563300
F	-2.13447500	-1.31756500	-2.58072300

17. References

1. Zhou, Y.-Y.; Hartline, D. R.; Steiman, T. J.; Fanwick, P. E.; Uyeda, C. Dinuclear Nickel Complexes in Five States of Oxidation Using a Redox-Active Ligand. *Inorg. Chem.* **2014**, *53* (21), 11770–11777.

2. Bruker (2016). Apex3 v2016.9-0, Saint V8.34A, SAINT V8.37A, Bruker AXS Inc.: Madison (WI), USA, 2013/2014.

3. (a) SHELXTL suite of programs, Version 6.14, 2000-2003, Bruker Advanced X-ray Solutions, Bruker AXS Inc., Madison, Wisconsin: USA; (b) Sheldrick, G. M. *Acta Crystallogr A.* **2008**, *64*, 112–122.

4. (a) Sheldrick, G. M. University of Göttingen, Germany, 2016; (b) Sheldrick, G. M. *Acta Crystallogr Sect C Struct Chem.* **2015**, *71*, 3–8.

5. Hübschle, C. B.; Sheldrick, G. M.; Dittrich, B. *J. Appl. Crystallogr.* **2011**, *44*, 1281–1284.

6. Miao, J.; Meng, B.; Liu, J.; Wang, L. An A–D–A′–D–A Type Small Molecule Acceptor with a Broad Absorption Spectrum for Organic Solar Cells. *Chem. Commun.* **2018**, *54* (3), 303–306.

7. Bu, L.; Li, Y.; Wang, J.; Sun, M.; Zheng, M.; Liu, W.; Xue, S.; Yang, W. Synthesis and Piezochromic Luminescence of Aggregation-Enhanced Emission 9,10-Bis(N-Alkylcarbazol-2-Yl-Vinyl-2)Anthracenes. *Dyes and Pigments* **2013**, *99*, 833–838.

8. Grimes, K; Gupte, A.; Aldrich, C.; Copper(II)-Catalyzed Conversion of Aryl/Heteroaryl Boronic Acids, Boronates, and Trifluoroborates into the Corresponding Azides: Substrate Scope and Limitations. *Synthesis* **2010**, *9*, 1441-1448.

9. Powers, I. G.; Andjaba, J. M.; Luo, X.; Mei, J.; Uyeda, C. Catalytic azoarene synthesis from aryl azides enabled by a dinuclear ni complex. *J. Am. Chem. Soc.* **2018**, *140*, 4110-4118.

10. Karakawa, M.; Aso, Y. Narrow-Optical-Gap π-Conjugated Small Molecules Based on Terminal Isoindigo and Thienoisoindigo Acceptor Units for Photovoltaic Application. *RSC Adv.* **2013**, *3*, 16259–16263.

11. Cartwright, L.; Yi, H.; Iraqi, A. Effect of Fluorination Pattern and Extent on the Properties of PCDTBT Derivatives. *New J. Chem.* **2016**, *40*, 1655–1662.

12. Mei, J.; Graham, K. R.; Stalder, R.; Reynolds, J. R. Synthesis of Isoindigo-Based Oligothiophenes for Molecular Bulk Heterojunction Solar Cells. *Org. Lett.* **2010**, *12*, 660–663.

13. Zhou, E.; Yamakawa, S.; Tajima, K.; Yang, C.; Hashimoto, K. Synthesis and Photovoltaic Properties of Diketopyrrolopyrrole-Based Donor−Acceptor Copolymers. *Chem. Mater.* **2009**, *21*, 4055–4061.

14. Reeves, B. D.; Grenier, C. R. G.; Argun, A. A.; Cirpan, A.; McCarley, T. D.; Reynolds, J. R. Spray Coatable Electrochromic Dioxythiophene Polymers with High Coloration Efficiencies. *Macromol.* **2004**, *37*, 7559–7569.

15. Hendriks, K. H.; Li, W.; Heintges, G. H. L.; van Pruissen, G. W. P.; Wienk, M. M.; Janssen, R. A. J. Homocoupling Defects in Diketopyrrolopyrrole-Based Copolymers and Their Effect on Photovoltaic Performance. *J. Am. Chem. Soc.* **2014**, *136*, 11128–11133.

16. Stéen, E. J. L.; Shalgunov, V.; Denk, C.; Mikula, H.; Kjær, A.; Kristensen, J. L.; Herth, M. M. Convenient Entry to 18F-Labeled Amines through the Staudinger Reduction. *Eur. J. Org. Chem.* **2019**, (8), 1722–1725.

17. Cianga, L.; Bendrea, A.-D.; Fifere, N.; Nita, L. E.; Doroftei, F.; Ag, D.; Seleci, M.; Timur, S.; Cianga, I. Fluorescent Micellar Nanoparticles by Self-Assembly of Amphiphilic, Nonionic and Water Self-Dispersible Polythiophenes with "Hairy Rod" Architecture. RSC Adv. 2014, 4, 56385–56405.

18. Ni, Z.; Wang, H.; Dong, H.; Dang, Y.; Zhao, Q.; Zhang, X.; Hu, W. Mesopolymer Synthesis by Ligand-Modulated Direct Arylation Polycondensation towards n-Type and Ambipolar Conjugated Systems. *Nat. Chem.* **2019**, *11*, 271–277.

19. Wang, L.; Pan, X.; Zhao, Y.; Chen, Y.; Zhang, W.; Tu, Y.; Zhang, Z.; Zhu, J.; Zhou, N.; Zhu, X. A Straightforward Protocol for the Highly Efficient Preparation of Main-Chain Azo Polymers Directly from Bisnitroaromatic Compounds by the Photocatalytic Process. *Macromol.* **2015**, *48* (5), 1289–1295.

20. Gaussian 16, Revision A.03, Frisch, M. J.; Trucks, G. W.; Schlegel, H. B.; Scuseria, G. E.; Robb, M. A.; Cheeseman, J. R.; Scalmani, G.; Barone, V.; Petersson, G. A.; Nakatsuji, H.; Li, X.; Caricato, M.; Marenich, A. V.; Bloino, J.; Janesko, B. G.; Gomperts, R.; Mennucci, B.; Hratchian, H. P.; Ortiz, J. V.; Izmaylov, A. F.; Sonnenberg, J. L.; Williams-Young, D.; Ding, F.; Lipparini, F.; Egidi, F.; Goings, J.; Peng, B.; Petrone, A.; Henderson, T.; Ranasinghe, D.; Zakrzewski, V. G.; Gao, J.; Rega, N.; Zheng, G.; Liang, W.; Hada, M.; Ehara, M.; Toyota, K.; Fukuda, R.; Hasegawa, J.; Ishida, M.; Nakajima, T.; Honda, Y.; Kitao, O.; Nakai, H.; Vreven, T.; Throssell, K.; Montgomery, J. A., Jr.; Peralta, J. E.; Ogliaro, F.; Bearpark, M. J.; Heyd, J. J.; Brothers, E. N.; Kudin, K. N.; Staroverov, V. N.; Keith, T. A.; Kobayashi, R.; Normand, J.; Raghavachari, K.; Rendell, A. P.; Burant, J. C.; Iyengar, S. S.; Tomasi, J.; Cossi, M.; Millam, J. M.; Klene, M.; Adamo, C.; Cammi, R.; Ochterski, J. W.; Martin, R. L.; Morokuma, K.; Farkas, O.; Foresman, J. B.; Fox, D. J. Gaussian, Inc., Wallingford CT, 2016.

VITA

John M. Andjaba was born on October 6th, 1994, in Windhoek, Namibia to Oshiwambo parents. He moved to Larchmont, New York with his parents in 1996 where they lived until moving back to Namibia in 2006. John finished primary school then continued his secondary education at St. Paul's High Secondary School. In 2010 he moved back to the United States where he finished his secondary education at St. Paul's College High School in Washington, D.C. Here, John cultivated his strong appreciation for STEM disciplines and his love for Hip-Hop and Breaking (breakdancing).

He then decided to attend Mount St. Mary's University (The Mount) in Emmitsburg, Maryland. After earning a whopping 50% on his first general chemistry exam, John decided to, rightfully so, hire a general chemistry tutor: Megan Whelan. Through tutoring Megan suggested John start chemistry research with Dr. Christopher A. Bradley as a means to getting into medical school. John started research with Dr. Bradley working on synthesizing piano stool cobalt complexes for small molecule activation. Through spending many hours in the lab, John was convinced by Dr. Bradley along with Dr. Christine McCauslin, Dr. Dana Ward, Dr. Danny Miles and Dr. Garth Patterson to pursue a career in chemistry and get his Ph.D. after graduating in 2016 with his B.S. in Biochemistry and Chemistry.

In 2016 John began his Ph.D. working in Christopher H. Uyeda's lab where he developed his synthetic, critical thinking, writing, and presenting skills. In his spare time during graduate school John also spent his time developing his breaking skills and deepened his love for music and dance. In the fall of 2021 John will begin his postdoctoral research at the Massachusetts Institute of Technology in Alex Radosevich's lab studying main group chemistry and catalysis.

LIST OF PUBLICATIONS

1. Powers, I.G.; Andjaba, J.M.; Luo, X.; Mei, J.; Uyeda, C. "Catalytic Azoarene Formation from Aryl Azides Enabled by a Dinuclear Nickel Imido Complex" *J. Am. Chem. Soc.*, **2018**, 140, 4110.

2. I. G. Powers, J. M. Andjaba; M. Zeller; C. Uyeda. "Catalytic C(sp^2)–H Amination Reactions Using Dinickel Imides" *Organometallics.* **2020**. 39, 3794.

3. J. M. Andjaba; C. J. Rybak; Z. Wang; J. Ling; J. Mei; C. Uyeda, "Catalytic Azopolymer Synthesis Enabled by a Dinuclear Nickel Catalyst" *J. Am. Chem. Soc.* **2021**, *143*, 3975.